Journal of ATMOSPHERIC and TERRESTRIAL PHYSICS

EDITORIAL ADVISORY BOARD

H. O. G. ALFVÉN-STOCKHOLM · **J. BARTELS**-GÖTTINGEN · **W. J. G. BEYNON**-ABERYSTWYTH · **P. M. S. BLACKETT**-LONDON · **H. G. BOOKER**-ITHACA, N.Y. **E. G. BOWEN**-SYDNEY · **SIR DAVID BRUNT**-LONDON · **R. BUREAU**-BAGNEUX **S. CHAPMAN**-ALASKA · **J. EGEDAL**-COPENHAGEN · **V. F. HESS**-NEW YORK · **E. O. HULBURT**-WASHINGTON, D.C. · **H. ISRAEL**-AACHEN · **D. K. MENZEL**-CAMBRIDGE, MASS. · **S. K. MITRA**-CALCUTTA · **M. NICOLET**-UCCLE · **E. H. NORINDER**-UPSALA · **N. V. PUSHKOV**-MOSCOW · **J. A. RATCLIFFE**-CAMBRIDGE · **O. E. H. RYDBECK**-GOTHENBURG · **J. C. W. SCOTT**-OTTAWA · **SIR GEORGE SIMPSON**-LONDON · **H. SOLBERG**-OSLO · **J. VELDKAMP**-DE BILT · **M. WALDMEIER**-ZÜRICH

VOL.
18
1960

EDITOR-IN-CHIEF

SIR EDWARD APPLETON, F.R.S.

EDINBURGH

VOLUME 18

1960

PERGAMON PRESS

LONDON · NEW YORK · PARIS · LOS ANGELES

VOL
18
196

CONTENTS

No. 1

W. C. HOFFMAN: Conditions for the persistence of purely longitudinal or purely transverse propagation 1
R. L. DOWDEN: Ionospheric thermal radiation at radio-frequencies in the auroral zone . 8
G. R. A. ELLIS: Gyro splitting of ionospheric echoes 20
E. D. R. SHEARMAN and J. HARWOOD: Sporadic-*E* as observed by back-scatter techniques in United Kingdom 29
V. MARASIGAN, S. J.: Spread-*F* in Baguio through half a solar cycle 43
J. E. C. GLIDDON and P. C. KENDALL: Theoretical world curves of maximum ion density in a quiet *F*-region 48
J. A. GLEDHILL and A. D. M. WALKER: The "valley effect" in the interpretation of ionospheric eclipse records 61
D. R. BATES and M. NICOLET: Ion–atom interchange 65
Research Notes
A. HAUBERT: Les perturbations ionosphériques à début brusque et la propagation des ondes longues 71
V. A. W. HARRISON: An unusual ionospheric disturbance in the Antarctic on 30 June to 1 July 1957 72
J. FRIHAGEN and J. TRØIM: Scintillations of the 20 Mc/s signal from the earth satellite 1958 δ II 75
K. W. ERIKSEN, O. HOLT and B. LANDMARK: A note on the polar absorption event of 11–18 May 1959 78
J. M. WATTS: A further note on "sweepers" 81
K-indices of geomagnetic activity for July–October 1959 82
Book Review
"Optics and Spectroscopy". Optical Society of America. (Reviewed by Sir EDWARD APPLETON) 86
Errata
K-indices of geomagnetic activity for 16 April 1957 87
C. A. ONWUMECHILLI: A study of the equatorial electrojet—II 87
C. A. ONWUMECHILLI and N. S. ALEXANDER: Variations in the geomagnetic field at Ibadan, Nigeria—I 87
Papers to be published in future issues 88

Nos. 2/3

R. A. DUNCAN: The equatorial *F*-region of the ionosphere 89
TATSUZO OBAYASHI and YUKIO HAKURA: Enhanced ionization in the polar ionosphere associated with geomagnetic storms 101
S. R. KHASTGIR and R. N. SINGH: The size of the moving irregularities in the *F*-region and the spread angle of the radio waves scattered from them 123
P. BANDYOPADHYAY: Electron distribution in the *F*-layer of the ionosphere over Haringhata (Calcutta) on quiet and disturbed days 127
J. A. FEJER: Hydromagnetic wave propagation in the ionosphere 135
J. TAUBENHEIM: Incoherency of pulse echoes and the measurement of ionospheric absorption 147
D. LEPECHINSKY et C. TAIEB: Sur la détermination des hauteurs réelles de l'ionisation dans les hautes latitudes 152
SYUN-ICHI AKASOFU: On the ionospheric heating by hydromagnetic waves connected with geomagnetic micropulsations 160
J. S. GREENHOW, E. L. NEUFELD and C. D. WATKINS: The scattering of 36 Mc/s radio waves by weak auroral ionization 174
C. M. MINNIS and G. H. BAZZARD: The geographical distribution of ionization in the *F2*-layer 181
R. F. STEBBINGS, G. V. GROVES, R. L. F. BOYD and P. J. BOWEN: Low-altitude testing of the rocket-grenade experiment for upper atmosphere temperatures and winds . . 184
J. VELDKAMP and D. VAN SABBEN: On the current system of solar-flare effects . . 192
J. S. GREENHOW and J. E. HALL: Diurnal variations of density and scale height in the upper atmosphere 203
B. J. ROBINSON: Diurnal variation of the electron distribution in the ionospheric *E*-layer 215
H. RISHBETH and D. W. BARRON: Equilibrium electron distributions in the ionospheric *F2*-layer 234

Research Notes
G. UMLAUFT: Focusing of electromagnetic waves by E_s-clouds 253
V. A. BAILEY: A unified theory of terrestrial and solar magnetization, the outer Van Allen belt and high energy primary cosmic rays 256
V. MARASIGAN, S. J.: Geomagnetic and sunspot influences on spread-F in Baguio . 257
K-indices of geomagnetic activity for November 1959–March 1960 259
Papers to be published in future issues 264

No. 4

P. DASGUPTA and K. K. VIJ: Statistical analysis of fading of a single down-coming wave . 265
J. W. WRIGHT: Some magnetoionic phenomena of the Arctic E-region 276
G. H. BAZZARD: Short-term differences in the behaviour of two daily indices of solar activity during the IGY 290
C. M. MINNIS and G. H. BAZZARD: A monthly ionospheric index of solar activity based on $F2$-layer ionization at eleven stations 297
C. M. MINNIS and G. H. BAZZARD: A world-wide semi-annual cycle in the E-layer of the ionosphere 306
L. R. MEGILL, P. M. JAMNICK and J. E. CRUZ: Seasonal variations in the twilight enhancement of [OI] 5577 309
R. G. RASTOGI: A synoptic study of the $F2$-region of the ionosphere in the Asian zone . 315
Research Notes
M. GADSDEN and C. J. LOUGHNAN: Observations of non-field-aligned auroral rays . 332
A. DALGARNO and D. PARKINSON: Photoionization of atomic oxygen and atomic nitrogen 335
A. HAUBERT: A propos de la détermination de la hauteur vraie du maximum d'ionisation dans la méthode des dix points 337
W. A. CILLIERS: Changes in the fading speed of low-frequency radio waves . . 339
J. F. NOXON and A. VALLANCE JONES: An auroral emission in the 2·0–2·2μ region . 341
Letter to the Editor
J. MAWDSLEY: Fading of satellite transmissions and ionospheric irregularities . . 344
Book Reviews
"Electromagnetic Phenomena in Cosmical Physics". Edited by B. LEHNERT. (Reviewed by H. A. BRÜCK) 345
"The Exploration of the Solar System" by F. GODWIN. (Reviewed by Sir EDWARD APPLETON) 345
K-indices of geomagnetic activity for April 1960 346
Papers to be published in future issues 347

AUTHOR INDEX

(B.R.) denotes a book review

AKASOFU S. 160
ALEXANDER N. S. 87
APPLETON E. V. (B.R.'s) 86, 345
BAILEY V. A. 256
BANDYOPADHYAY P. 127
BARRON D. W. 234
BATES D. R. 65
BAZZARD G. H. 181, 290 297, 306
BOWEN P. J. 184
BOYD R. L. F. 184
BRÜCK H. A. (B.R.) 345
CILLIERS W. A. 339
CRUZ J. E. 309
DALGARNO A. 335
DASGUPTA P. 265
DOWDEN R. L. 8
DUNCAN R. A. 89
ELLIS G. R. A. 20
ERIKSEN K. W. 78
FEJER J. A. 135
FRIHAGEN J. 75
GADSDEN M. 332
GLEDHILL J. A. 61
GLIDDON J. E. C. 48
GREENHOW J. S. 174, 203
GROVES G. V. 184
HAKURA Y. 101
HALL J. E. 203
HARRISON V. A. W. 72
HARWOOD J. 29
HAUBERT A. 71, 337
HOFFMAN W. C. 1
HOLT O. 78
JAMNICK P. M. 309
KENDALL P. C. 48
KHASTGIR S. R. 123
LANDMARK B. 78
LEPECHINSKY D. 152
LOUGHNAN C. J. 332
MARASIGAN V., S.J. 43 257
MAWDSLEY J. 344
MEGILL L. R. 309
MINNIS C. M. 181, 297 306
NEUFELD E. L. 174
NICOLET M. 65
NOXON J. F. 341
OBAYASHI T. 101
ONWUMECHILLI O. 87
PARKINSON D. 335
RASTOGI R. G. 315
RISHBETH H. 234
ROBINSON B. J. 215
SABBEN D. VAN 192
SHEARMAN E. D. R. 29
SINGH R. N. 123
STEBBINGS R. F. 184
TAIEB C. 152
TAUBENHEIM J. 147
TRØIM J. 75
UMLAUFT G. 253
VALLANCE JONES A. 341
VELDKAMP J. 192
VIJ K. K. 265
WALKER A. D. M. 61
WATKINS C. D. 174
WRIGHT J. W. 276

Journal of Atmospheric and Terrestrial Physics, 1960, Vol. 18, pp. 1 to 7. Pergamon Press Ltd. Printed in Northern Ireland

Conditions for the persistence of purely longitudinal or purely transverse propagation

W. C. HOFFMAN
Hughes Research Laboratories, Reseda, California*

(*Received* 9 *June* 1959)

Abstract—The conditions for radio waves to propagate through the ionosphere exactly parallel or exactly transverse to the local direction of the centred-dipole-magnetic field are determined. The analysis is based on an appropriate form of the Haselgrove equations for ray-tracing in an inhomogeneous anisotropic medium, and the general forms of the refractive indices required for the persistence of purely longitudinal and purely transverse propagation are determined by integration of the Haselgrove equations. The resultant refractive indices do not appear to be appropriate to the ionosphere.

1. INTRODUCTION

THE special cases of quasi-longitudinal and quasi-transverse propagation, which emerge from the Appleton–Hartree equation when the wave-normal is either very nearly aligned with the geomagnetic field or very nearly perpendicular to it, have received exhaustive investigation over a period of many years. The wave behaviour in such cases is essentially local, i.e. is associated with a particular point in the medium, rather than "global" or "in the large", in the sense that certain relative directions of wave-normal and geomagnetic field are maintained over an appreciable portion of the path. The question of the latter sort of behaviour has especially arisen in recent years in connexion with the propagation of "whistlers", these being naturally-occurring v.l.f. signals which, in a sense, are guided by the lines of force of the geomagnetic field. In the classical theory of whistlers (STOREY, 1953), propagation is supposed to take place approximately along the field lines. HINES (1957) showed how the tendency to guidance disappears (for sufficiently low frequencies) when the medium is assumed to consist of electrons *and* protons in electrostatic equilibrium, and that, now, propagation across the field lines is even possible. In this context it becomes of interest to determine how long propagation (especially whistler propagation) can persist either exactly along or transverse to the lines of force, and it is to this end that the present investigation is directed. Use, for this purpose, will be made of the ray-tracing equations of HASELGROVE (1955). The Haselgrove equations are integrable in the "pure" cases of exactly longitudinal or exactly transverse propagation, provided certain conditions are imposed on the refractive index. It is to these conditions upon the refractive index that we shall direct our attention.

2. THE HASELGROVE EQUATIONS IN THE CENTRED DIPOLE FIELD

Ray-tracing in the ionosphere is subject to the fundamental difficulty pointed out by WESTFOLD (1949):

> "... according to the Appleton–Hartree formula, the refractive index is in general a function of the angle the direction of propagation makes with the direction of the magnetic

* Present address: Dept. of Physics, University of Queensland, Brisbane, Australia.

field as well as of the electron density, the magnetic field intensity and the frequency. The differential deviation of a ray at any point of its trajectory depends on all these parameters, so that the difference in refractive index at neighbouring points on a ray in the medium under consideration depends on the deviation as well as on the new value of the electron density. The refractive index structure of the medium is therefore an intrinsic property of the particular ray under consideration. It follows that surfaces of constant refractive index, independent of ray directions, cannot be realized in a magneto-ionic medium. This is the fundamental difficulty which besets all attempts at a ray treatment of the propagation of radio waves through the ionosphere . . ."

Recognition of the fact that the ray direction gives rise to an intrinsic type of geometry constitutes a crucial step in the attack on the problem. Thus HASELGROVE (1955) was able in a paper published subsequently to lay down a system of differential equations, based on Fermat's principle and the theory of Finsler spaces, which are suitable for ray-tracing in an inhomogeneous anisotropic medium. In the present calculations, we shall assume that the ray path is restricted to the plane of the magnetic meridian. This assumption enables us to use the Haselgrove equations in a less general, but considerably simpler, form. We further assume that we have to do with a curved earth and a curved ionosphere. Under these assumptions the Haselgrove equations (1955) can be put in the form:

$$\left.\begin{aligned} \frac{dr}{dt} &= n^{-1}\left(\cos\chi_1 + \frac{1}{2}\frac{\partial \ln n^2}{\partial \psi}\sin\chi_1\right) \\ \frac{d\theta}{dt} &= \frac{1}{nr}\left(\sin\chi_1 - \frac{1}{2}\frac{\partial \ln n^2}{\partial \psi}\cos\chi_1\right) \\ \frac{d\chi_1}{dt} &= \frac{1}{2}\frac{1}{nr}\left\{\frac{\partial \ln n^2}{\partial \theta}\cos\chi_1 - \left(2 + r\frac{\partial \ln n^2}{\partial r}\right)\sin\chi_1\right\}. \end{aligned}\right\} \tag{1}$$

In these equations:

r = radial distance from the centre of the earth;
θ = geomagnetic latitude (measured positive counterclockwise);
χ_1 = angle between the position vector and the wave-normal;
n = (real) refractive index;
ψ = angle between the magnetic field and the wave-normal.

The next step is the incorporation of the centred dipole approximation for the geomagnetic field into the Haselgrove equations. The magnetic lines of force will thus be given by the equation

$$r = a\frac{\cos^2\theta}{\cos^2\theta_0} \tag{2}$$

where a is the radius of the earth, and θ_0 is the geomagnetic latitude at that point where the field line re-enters the earth's surface. The relations among the various angles involved in this and the Haselgrove equations are depicted in Fig. 1, wherein $\mathbf{B}_0$ represents the local magnetic field vector, $\mathbf{n}$ the wave-normal, τ the angle between the positive polar axis (geomagnetic equator) and the vector $\mathbf{B}_0$, χ the angle between the polar axis and the wave-normal $\mathbf{n}$, and the other quantities are defined just after equations (1).

Since $$\chi = \chi_1 + \theta$$

and $$\psi = \chi - \tau \qquad (\text{mod } 2\pi),$$

it follows that $$\psi = \chi_1 + \arctan\,(\tfrac{1}{2}\cot\theta). \tag{3}$$

Longitudinal propagation (in the traditional sense) takes place when the wave-normal is parallel to the magnetic field vector, transverse propagation when the wave-normal is perpendicular to the magnetic field. These two cases will be referred to here as "purely longitudinal" and "purely transverse" to distinguish

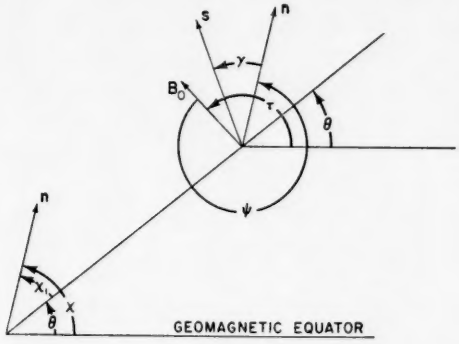

Fig. 1.

them precisely from quasi-longitudinal and quasi-transverse propagation which apply when the above conditions hold only approximately. The reason for so doing is that the Haselgrove equations are integrable in the "pure" cases, as will be shown below. This comes about from the fact that the term $\partial \ln n^2/\partial\psi$ vanishes when either $\psi = 0°$ or $\psi = 90°$, as may be readily seen either from the Appleton–Hartree formula (in the case of free electrons) or from HINES' formula for the refractive index (in the case of a proton-electron medium), since the factor $\sin 2\psi$ is involved.

The angle γ between the wave-normal and the ray direction is given by

$$\gamma = -\arctan\left(\frac{1}{2}\frac{\partial \ln n^2}{\partial\psi}\right) \tag{4}$$

and it is clear that γ vanishes when either $\psi = 0$ or $\psi = \pi/2$. Thus ray direction and wave-normal coincide for either purely longitudinal or purely transverse propagation.

3. Form of the Refractive Index Required for Purely Longitudinal Propagation to Persist

When $\psi = 0$, as noted above,

$$\frac{\partial \ln n^2}{\partial\psi} = 0 \tag{5}$$

and the first two of the Haselgrove equations (1) reduce to

$$\frac{d\theta}{dt} = \tan \chi_1 \frac{d \ln r}{dt}$$

or

$$\tan \theta \frac{d\theta}{dt} = -\frac{1}{2} \frac{d \ln r}{dt} . \tag{6}$$

For $\psi = 0$, this last equation has the solution

$$r = C \cos^2 \theta, \tag{7}$$

where $C = a/\cos^2 \theta_0$, in accordance with equation (2). That is, the ray coincides with the line of force through θ_0, provided the third Haselgrove equation, representing the effects of inhomogeneity in r and θ, remains satisfied.

The third Haselgrove equation becomes, for $\psi = 0$ and a dipole geomagnetic field,

$$3 \frac{1 + \sin^2 \theta}{1 + 3 \sin^2 \theta} \sin \chi_1 = \frac{1}{2} \frac{\partial \ln n^2}{\partial \theta} \cos \chi_1 - \frac{1}{2} \frac{\partial \ln n^2}{\partial r} \sin \chi_1$$

or

$$\tan \theta \frac{\partial \ln n^2}{\partial \theta} + \tfrac{1}{2} r \frac{\partial \ln n^2}{\partial r} = -3 \frac{1 + \sin^2 \theta}{1 + 3 \sin^2 \theta} . \tag{8}$$

This first-order linear partial differential equation in $\ln n^2$ has the general solution:

$$F\left(\ln \frac{\sin \theta}{r^2} , \ln \frac{n^2}{\dfrac{1 + 3 \sin^2 \theta}{\sin^3 \theta}} \right) = 0$$

or in equivalent form,

$$n^2 = \frac{1 + 3 \sin^2 \theta}{\sin^3 \theta} f\left(\frac{\sin \theta}{r^2} \right) \tag{9}$$

where f is an arbitrary function. Let

$$f\left(\frac{\sin \theta}{r^2} \right) = C_1 \left(\frac{\sin \theta}{r^2} \right)^3 g\left(\frac{\sin \theta}{r^2} \right). \tag{10}$$

Then (9) becomes

$$n^2 = C_1 G_e^2 g(\sin \theta / r^2) \tag{11}$$

where G_e is the angular electron gyro-frequency defined by

$$G_e = -5{\cdot}456 \times 10^6 \frac{\sqrt{(1 + 3 \sin^2 \theta)}}{(r/a)^3} \tag{12}$$

a being the radius of the earth (6380 km).

4. Form of the Refractive Index Required for Purely Transverse Propagation to Persist

In the purely transverse case $\psi = 90°$. Equation (5) again holds but the first two Haselgrove equations reduce to

$$\frac{d \ln r}{dt} = \tfrac{1}{2} \cot \theta \frac{d\theta}{dt} . \tag{13}$$

This equation has the integral

$$r = C' \sin^{1/2} \theta \tag{14}$$

which is the equation of the orthogonal trajectory to the geomagnetic field line (2). Thus purely transverse propagation will persist provided the third Haselgrove equation remains satisfied. As before, we shall see that this implies a special form for the refractive index.

When ψ becomes and remains equal to 90°, so that propagation is purely transverse, the third Haselgrove equation reduces to

$$\cot \theta \frac{\partial \ln n^2}{\partial \theta} - 2r \frac{\partial \ln n^2}{\partial r} = 12 \frac{1 + \sin^2 \theta}{1 + 3 \sin^2 \theta}. \tag{15}$$

This linear partial differential equation has the following general solution:

$$F_1 \left(\frac{\cos \theta}{\sqrt{r}}, \frac{(n/G_e)^2}{\cos^6 \theta} \right) = 0$$

or, what is equivalent,

$$n_T^2 = A_1 \cos^6 \theta \, G_e^2 f(\cos \theta / r^{1/2}) \tag{16}$$

5. Discussion and Conclusions

It is known from classical magneto-ionic theory that whenever purely longitudinal propagation takes place the refractive index will reduce to

$$n_{L(e)}^2 = 1 + \frac{\omega_e^2}{\omega(G_e - \omega)} \tag{17}$$

where ω_e is the angular electron plasma frequency, $\omega (= 2\pi f)$ is the angular wave frequency, and G_e is the electron gyro-frequency, defined by equation (12). When protons as well as electrons must be taken into account, it can be shown, based on Hines' (1957) formulas that the refractive index for purely longitudinal propagation reduces to

$$n_{L(ep)}^2 = 1 + \frac{\omega_e^2}{\omega(G_e - \omega)} + \frac{\omega_p^2}{\omega(G_p - \omega)}. \tag{18}$$

Whenever propagation becomes and remains purely longitudinal both (18) and (11) must hold. This implies the following relation for each point of the path, if purely longitudinal propagation is to persist:

$$C_1 G_e^2 g(\sin \theta / r^2) = 1 + \frac{\omega_e^2}{\omega G_e} \left(\frac{1}{1 - \omega/G_e} + \frac{(\omega_p/\omega_e)^2}{G_p/G_e - \omega/G_e} \right). \tag{19}$$

If we adopt the convention (usual in whistler propagation) that $\omega \ll \omega_e^2/|G_e|$, then the above expression becomes, approximately,

$$C_1 g(\sin \theta / r^2) \doteq \frac{\omega_e^2}{\omega G_e^3} \left(\frac{1}{1 - w/G_e} + \frac{(\omega_p/\omega_e)^2}{G_p/G_e - \omega/G_e} \right). \tag{20}$$

The gyro-frequency G_e is defined by (12), so that the only parameters at our

disposal are ω_e and ω_p (G_p being essentially a multiple, with opposite sign, of G_e). The electron and proton plasma frequencies are essentially multiples of the corresponding numerical electron and proton densities per cubic metre, N_e and N_p. Thus, to satisfy the $\sin\theta/r^2$ dependence required by the left-hand side of (19), or (20), N_e and N_p must be functions not only of that argument but also of some power of G_e and G_p. In the simplest case, when protons are not present in appreciable numbers and $-\omega/G_e \ll 1$, (20) reduces to

$$C_1 g(\sin\theta/r^2) \doteq \frac{{\omega_e}^2}{\omega {G_e}^3}. \tag{21}$$

This equation is satisfied only if

$$N_e(r, \theta) \doteq -\frac{(r/a)^9}{(5{\cdot}456 \times 10^6)^3} \cdot \frac{g(\sin\theta/r^2)}{[1 + 3\sin^2\theta]^3}. \tag{22}$$

We note that the $\sin\theta$ dependence required in (19), (20) or (21) does not exhibit equatorial symmetry, while the geomagnetic field lines do show a north–south symmetry. However, the $\sin\theta$ dependence does express the decrease of electron density on the dark side of the earth (in the northern hemisphere).

In the case of purely transverse propagation the local value of the refractive index is given by

$$n_T^2 = 1 + \left\{\left[\frac{X_e(1-X_e)}{{Y_e}^2-1} + \frac{X_p(1-X_p)}{{Y_p}^2-1} - 2\frac{X_eX_p(Y_eY_p-1)}{({Y_e}^2-1)({Y_p}^2-1)}\right]\Big/ \left[1 + \frac{X_e}{{Y_e}^2-1} + \frac{X_p}{{Y_p}^2-1}\right]\right\} \tag{23}$$

where

$$X_{e,p} = \omega^2_{e,p}/\omega^2, \qquad Y_{e,p} = G_{e,p}/\omega.$$

If protons can be neglected, (23) reduces to the usual transverse case of magneto-ionic theory. If transverse propagation persists, not only will (23) hold, but so also must (16). This yields the condition

$$A_1\cos^6\theta\, {G_e}^2 f(\cos\theta/r^{1/2}) = 1 + \left\{\left[\frac{X_e(1-X_e)}{{Y_e}^2-1} + \frac{X_p(1-X_p)}{{Y_p}^2-1} - 2\frac{X_eX_p(Y_eY_p-1)}{({Y_e}^2-1)({Y_p}^2-1)}\right] \div \left[1 + \frac{X_e}{{Y_e}^2-1} + \frac{X_p}{{Y_p}^2-1}\right]\right\}. \tag{24}$$

This expression also implies that N_e and N_p must be functions not only of $\cos\theta/r^{1/2}$ but also of the electron and proton gyro-frequencies, in a rather complicated way. Even in the case when only free electrons need be considered, so that (23) reduces to

$$A_1\cos^6\theta\, {G_e}^2 f(\cos\theta/r^{1/2}) = 1 - \frac{X_e}{1 - [{Y_e}^2/(1-X_e)]}, \tag{25}$$

the condition is not capable of any simple interpretation. However, letting $\Lambda = A_1\cos^6\theta\, {G_e}^2 f(\cos\theta/r^{1/2})$, we have the following expression for the electron density per cubic metre as a function of r, θ and G_e:

$$N_e \propto 1 - \tfrac{1}{2}\Lambda[1 + \sqrt{\{1 + 4(1-\Lambda){Y_e}^2/\Lambda^2\}}]. \tag{26}$$

VOL
18
196

The cosine θ dependence required by (25) is consistent with equatorial symmetry, but is not appropriate to the vicinity of the north geomagnetic pole.

The severe requirements for purely longitudinal and purely transverse propagation imposed upon the electron density and/or proton density profiles by the above conditions appear to be seldom, if ever, met in nature. It must be noted, however, that these are extreme cases, and the intermediate situations of quasi-longitudinal and quasi-transverse propagation may not impose such severe constraints upon the electron and/or proton density profiles. In any case tracing of the actual ray path appears necessary, if any more than a rough approximation to the full curve is desired. For this reason, further determination of the behaviour of the Haselgrove equations "in the large" appears particularly desirable.

Acknowledgements—The writer wishes to express his gratitude to C. O. HINES, in particular, for several valuable discussions, and to I. YABROFF for enlightenment on certain subtle points in connexion with the Haselgrove equations.

REFERENCES

HASELGROVE J.	1955	*Physics of the Ionosphere* pp. 355–364. Physical Society, London.
HINES C. O.	1957	*J. Atmosph. Terr. Phys.* **11,** 36.
STOREY L. R. O.	1953	*Phil. Trans. Roy. Soc.* A **246,** 113.
WESTFOLD K. C.	1949	*Aust. J. Sci. Res.* A **2,** 169.

VOL. 18 1960

Journal of Atmospheric and Terrestrial Physics, 1960, Vol. 18, pp. 8 to 19. Pergamon Press Ltd. Printed in Northern Ireland

Ionospheric thermal radiation at radio-frequencies in the auroral zone

R. L. Dowden
Ionospheric Prediction Service, Hobart, Tasmania

(*Received* 11 *August* 1959)

Abstract—Measurements of the temperature of the ionospheric *D*-region in the auroral zone from observations of 2 Mc/s radio noise are described and compared with measurements similarly made in the temperate region. The temperatures of the undisturbed and disturbed ionospheres at the two latitudes are found to be essentially similar, but the disturbing influence in the auroral zone is probably corpuscular rather than ultra-violet radiation.

1. Introduction

In the absence of man-made interference and atmospherics, it has been found possible to measure radio-frequency radiation from the ionosphere at medium frequencies.

The temperature of the ionospheric *D*-region has been previously measured by this method at 2 Mc/s in temperate latitudes (Pawsey *et al.*, 1951; Gardner, 1954). In a companion paper (Gardner and Pawsey, 1953), the absorbing structure of the lower ionosphere was determined from *D*-region echoes to find the heights to which the temperature applied. However, it was felt that conditions might be very different in an auroral zone.

Noise level and echo experiments were carried out by the writer at the Australian National Antarctic Research Station at Macquarie Island as a member of the 1956 party. The apparent *D*-region echoes were found to be not from the ionosphere, however, but from sea waves (Dowden, 1957). The present paper describes the radio noise level experiments at 2 Mc/s using a half-wave dipole aerial to provide a direct comparison with Gardner's (1954) observations in a temperate latitude (30°S).

2. Experimental Procedure

2.1. *Site and aerial*

The site of the experiment was near Hurd Point, Macquarie Island (55°S, 159°E, geomagnetic lat. −62°), on peat slopes at the foot of the plateau which forms most of the island. The nearest source of man-made interference of any kind was the Station, 20 miles north. Its noise was completely negligible at this distance. The nearest broadcast stations and atmospherics were several hundred miles to the north.

The aerial used for this part of the experiment was a half-wave dipole (2 Mc/s) suspended from wires attached to various crags. The aerial itself was about 20° off horizontal, about a quarter-wave above the ground (120 ft) and more than a wavelength from the cliffs of the plateau. The aerial passed directly over the recording hut from which it was fed by an 80 Ω shielded twin line. Far less trouble

TOT. 18 960

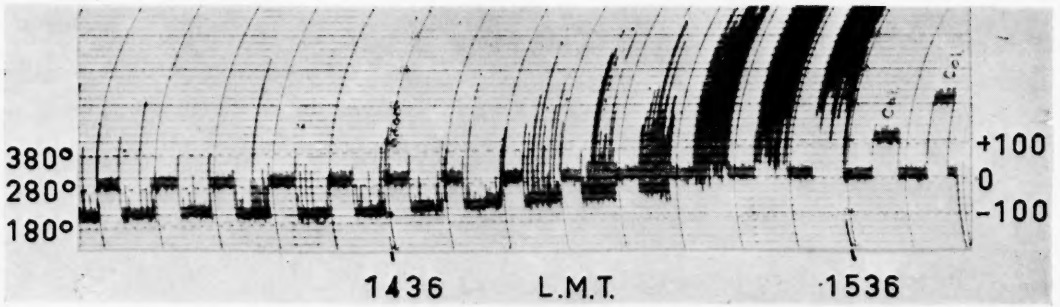

Fig. 1. Typical record showing onset of atmospherics (June observations).

VOL
18
196

from winds was encountered than expected, the mean wind velocity at the site being only about half that recorded at the Main Station.

2.2. *Determination of ionospheric temperature*

The equipment used and the recording technique was similar to that described by GARDNER (1954). The receiver was automatically connected to a dummy aerial for 3 min every 7·5 min by a chronometer operated relay. The sensitivity of the recording system was checked with a diode noise generator three times a day. The impedance of the aerial was accurately rematched to that of the dummy usually once a day.

The difference t between the noise level produced by the aerial and that by the dummy was read from the record in arbitrary units. A typical record showing this difference is in Fig. 1. The temperature T_i of the relevant part of the ionosphere can be found from this by an expression of the form: $T_i = At + T_d$. The scale factor A is the reciprocal of the product of the sensitivity of the receiving system (in recorder units per degree K), the attenuation of the aerial feed and matching unit, and the "efficiency" of the aerial. T_d is the ambient temperature of the dummy aerial, provided this is not greatly different from that of the matching unit, feed and ground. It was found that the temperature in the recording hut was usually within a degree Kelvin of that of the outside air and ground.

The efficiency of the half wire dipole was calculated from the SOMMERFELD and RENNER (1942) analysis using measured values of ground conductivity and aerial height. The figure obtained was also checked by the impedance method (GARDNER, 1954). Fortunately, for an aerial height of about a quarter wavelength, the efficiency is nearly unity and varies only slowly with height and ground constants. The adopted value was $0{\cdot}90 \pm 0{\cdot}05$. The total attenuation of matching unit and aerial feed was easily measured by the noise generator.

The errors of reading, sensitivity calibration and matching and those due to errors in aerial efficiency and attenuation measurement could be expected to give both systematic errors and random errors of about 5°K.

3. OBSERVATIONS

3.1. *General*

The seven observing periods from May to November (1956) are shown in Table 1.

Table 1. Observing periods

Period	Interval	Duration (days)
May–June	30 May–15 June	17
June–July	26 June–16 July	21
July	20 July–30 July	11
August	23 Aug.–31 Aug.	9
Sept.–Oct.	26 Sept.–17 Oct.	22
Oct.–Nov.	24 Oct.–3 Nov.	11
November	13 Nov.–20 Nov.	8

VOL. 18 1960

The observations made in the second period (June–July), showed strong interference from natural sources and so were not used for temperature measurement. During daylight hours random thermal noise was usually the only component seen on the "aerial" trace—similar in all respects except level to the "dummy" trace.

Occasionally, local cloud discharges produced small isolated spikes. Atmospherics propagated by the ionosphere from tropical latitudes were usually not

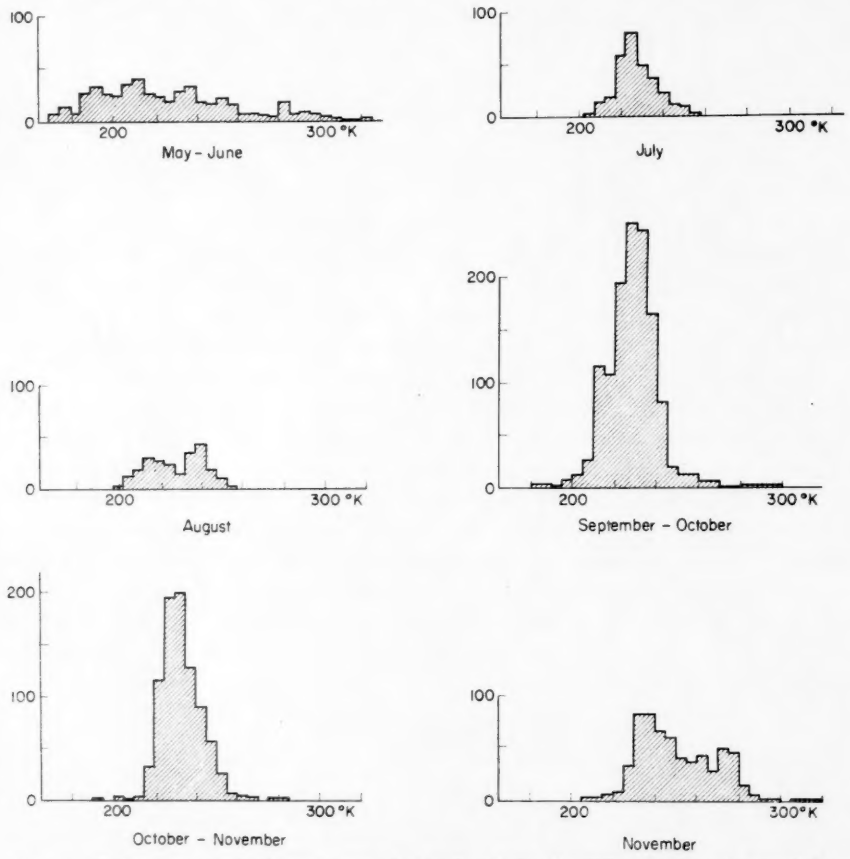

Fig. 2. Histograms of all observations of noise levels for the different observing periods. Only those obviously affected by atmospherics or precipation static were excluded. The average atmospheric free time (length of observing time) in a day was much larger in the summer months than in the winter (see Fig. 3).

observed until near sunset. Within an hour of their first appearance they were usually sufficiently strong to hold the recorder pen off scale continuously. A typical record showing this is Fig. 1. The length of observing time (about sunrise to sunset) varied from about 8 hr in May–June to 16 hr in November.

3.2. *Observed temperatures*

Histograms of the observed temperatures in each of the observing periods are shown in Fig. 2. All observed temperatures have been incorporated except those

obviously affected by atmospherics or precipitation static. These can be directly compared with temperate latitude observations (GARDNER, 1954). For the undisturbed months both sets of observations show distributions of temperatures starting from about 200°K, rising to a maximum around 220–230°K, then a slower tailing off to around 260–280°K. This undisturbed component of the distribution persists in most of the histograms. The temperatures of these first maxima (usually

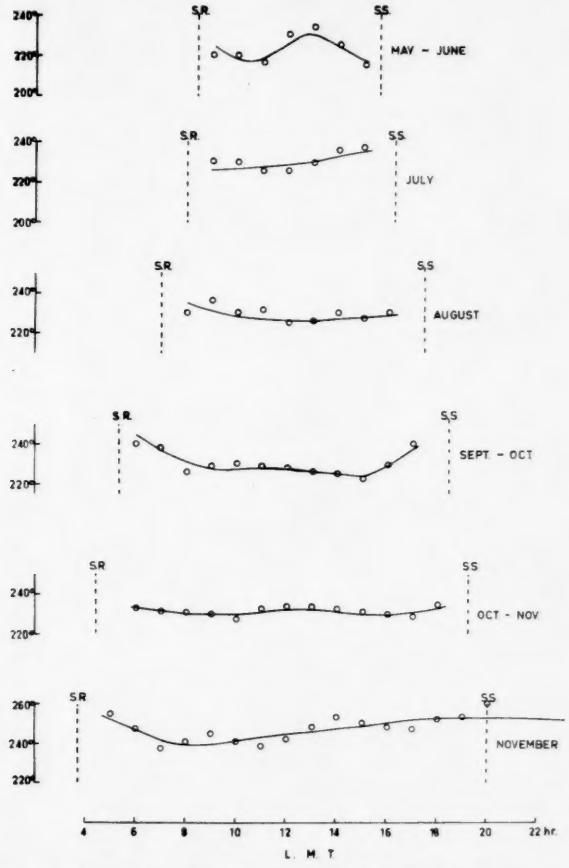

Fig. 3. Diurnal variation of ionospheric temperature for the different observing periods. Only observations unaffected by atmospherics have been considered. Times of sunrise and sunset are as indicated. The spread in observations can be gauged from the corresponding histograms (Fig. 2).

the modes), for each period in the Macquarie Island observations are usually within five or ten degrees of those for the corresponding periods in the Urisino (GARDNER, 1954) data. Again in agreement with lower latitude results, the temperatures observed in the winter periods are lower than those observed towards summer.

Hourly mean temperatures for each observing period are shown plotted in Fig. 3. Only observations unaffected by atmospherics, as gauged by the repetition rate and amplitude of the atmospherics, have been used in calculating these means.

VOL. 18 1960

The spread of observations in each period can be gauged from the corresponding histogram in Fig 2. The diurnal variations shown are on the verge of significance. This can also be judged from the corresponding histograms. The Sept.–Oct. and

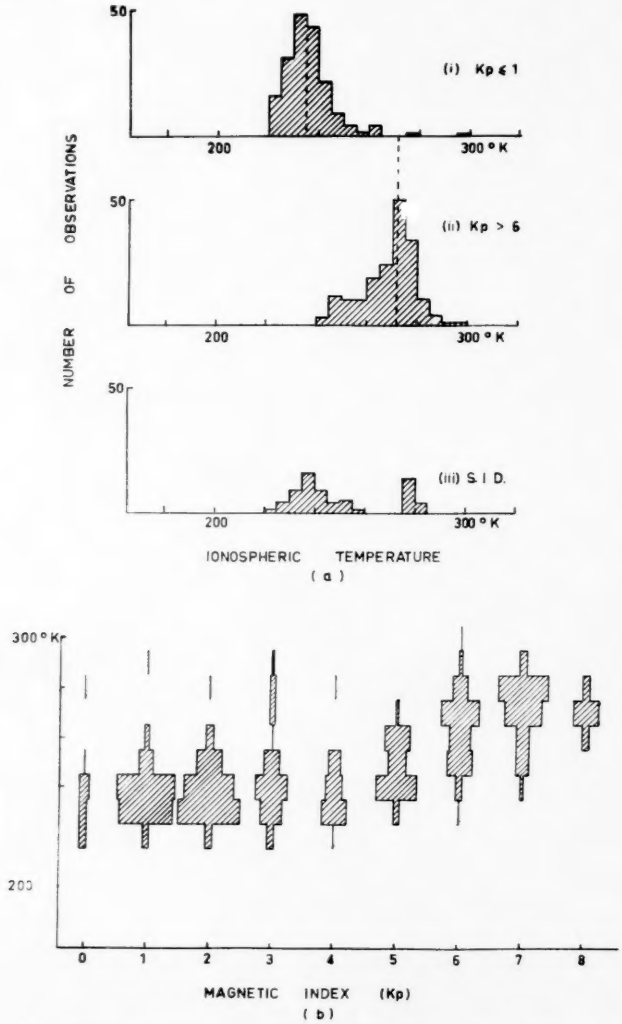

Fig. 4. (a). Histograms showing ionospheric temperatures during (i) three hourly periods for which $K_p < 1$, (ii) periods for which $K_p > 6$ and (iii) periods of s.i.d.s.
Fig. 4. (b). Histograms of temperatures for each value of K_p.

the Oct.–Nov. periods were fairly undisturbed and also a large number of observations were made and so the slight diurnal effect for these two periods is probably significant. A slight rise in temperature of about five degrees occurs about noon. The temperatures near sunrise and sunset appear higher than those during the day by some ten degrees. This may be due to an error in judgement of the effect of

weak atmospherics on temperature levels. Another possibility is that, as mentioned in a later section, on disturbed days, observed temperatures are higher and the absorption of the D-layer is higher so that the onset of atmospherics occurs later. Hence on these days values unaffected by atmospherics can be made nearer sunrise and sunset (as happens in the November period) so that at these times the means may not be truly representative.

A much larger effect of higher temperatures during early morning and late afternoon (about 50°) at Urisino and a still larger one at Rankin Springs (GARDNER, 1954) has been attributed to man-made interference propagated via the ionosphere. Consequently, the effect should be less at a site more remote from this interference as at Macquarie Island.

3.3. *Temperatures observed during disturbed periods*

During the November period some severe magnetic storms occurred. Two maxima are seen in the histogram (Fig. 2), suggesting a disturbed component. To separate this component histograms were computed of temperatures observed during quiet periods (three hourly periods for which the magnetic planetary index (K_p) was $\leqslant 1$), three hourly periods for which $K_p > 6$, and during sudden ionospheric disturbances (s.i.d.s). This is shown in Fig. 4(a). The correlation of observed ionospheric temperature with K_p is quite significant and sufficient to show up in a temperature–K_p plot as shown by the plotted histograms in Fig. 4(b). Up to about $K_p = 5$ the temperatures appear undisturbed but are increased by a further increase of K_p.

The effect of s.i.d.s, however, does not appear significant. This may partly be due to competition with magnetic disturbances occurring at about the same time. Also by an unhappy chance the equipment was not operating during many of the large s.i.d.s so that information is limited. At the Urisino site, GARDNER (1954) reported "a very definite rise of about 40°K during an s.i.d." This is not observed at Macquarie Island.

3.4. *Non-thermal noise*

As mentioned above, owing to the remoteness of the site, no trouble was experienced with man-made interference and comparatively little from atmospherics. The other forms of atmospheric noise listed by GARDNER were observed, viz. rain static, cloud static and wind static. In addition snow static was occasionally observed. This is aurally similar to rain static, but the intensity can be several orders of magnitude greater. The noise from sufficiently distant snow storms appeared quite random or "white" and at low enough intensities to appear as slowly varying increases of apparent temperatures (100°K) lasting for an hour or so.

The above spurious noise was easily recognized and ignored. A more serious type of non-thermal noise occurred in mid-winter. This produced an excess temperature of 50°K to 100°K or more for several days at a time. Because of this, the May–June histogram (Fig. 2) is strongly spread and shows temperatures above 300°K. In the June–July series (which was not used for temperature measurement for this reason) the apparent temperature was above ambient (280°K) all day for 10 days out of the 16 days observed.

VOL. 18 1960

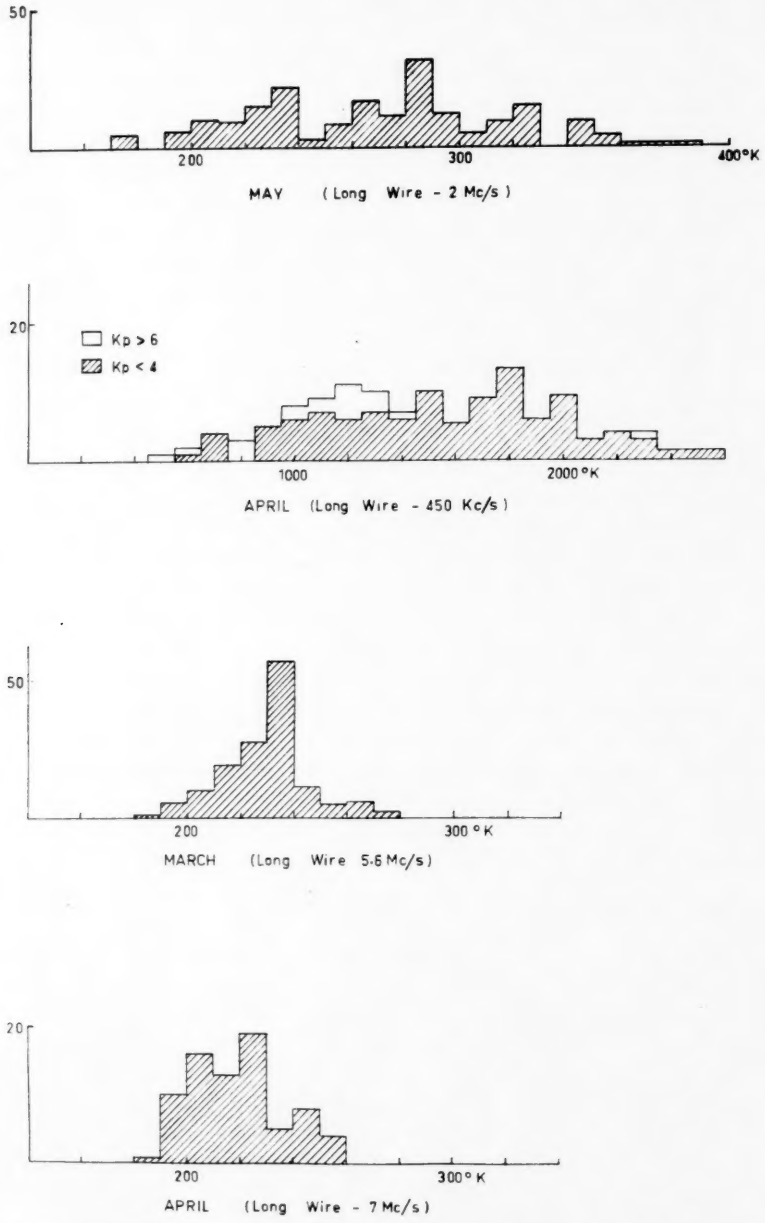

Fig. 5. Histograms of observations of apparent temperatures made using 400 m "long wire" aerial tilted 34° to the south.

Measurements carried out at 2·0 Mc/s and 450 kc/s using a southerly directed "long wire" aerial showed that this excess noise came from the south and that it was much stronger (2000°K) at 450 kc/s (Fig. 5). At 450 kc/s a weak negative

correlation with the magnetic index (K_p) was found indicating that the noise is *reduced* during disturbed periods. During mid-winter at Macquarie Island, the elevation of the sun is only 12° at noon. Consequently at this time of the year, the night side of the earth is never more than about 1250 km distant. It is suggested then that intense radiation incident on the night side of the earth might travel beneath the ionosphere to Macquarie Island with sufficiently weak attenuation to produce the observed noise levels. The stronger noise at 450 kc/s might be due to less attenuation at this frequency and the reduction of noise during disturbed conditions (high K_p) suggests increased attenuation.

At a frequency of 2 Mc/s the equivalent temperature of cosmic noise is of the order of 10^7 °K (Ellis, 1957). Near the edge of the night hemisphere the ionosphere would probably be transparent to this noise. For frequencies much below 1 Mc/s Ellis (1956) has shown that observations of cosmic noise are unlikely. However, Reber (1956) reports night-time temperatures of about 10^5 °K at 520 kc/s. Hence intense radiation is incident at night at both frequencies, so we now consider attenuation for propagation beneath the ionosphere. Ellis (1958) has considered such trapping of noise and its subsequent propagation by hop transmission for large horizontal distances. The attenuation with distance for several ionosphere power reflection coefficients is given in his Fig. 11. If we now take the reasonable reflection coefficients of 0·01 at 2 Mc/s and 0·5 at 450 kc/s and the initial noise temperatures of 10^7 °K we can expect excess noise at Macquarie Island during mid-winter days of about 10^2 °K at 2 Mc/s and 10^3 °K at 450 kc/s.

3.5. *Observations at 5·6 Mc/s and 7·0 Mc/s*

These measurements were made with the long wire aerial mentioned above. The 5·6 Mc/s histogram (Fig. 5) is not significantly different from the 2 Mc/s dipole one for Sept.–Oct. (Fig. 2). At 7 Mc/s the temperatures appear about ten degrees lower, which is barely significant. Cosmic noise was apparent at 7 Mc/s when the critical frequency of the F-layer (f_0F2) went below 7 Mc/s. The very high intensity of cosmic noise made it easily recognizable, so that it has not been included in the noise levels scaled for temperature measurement.

4. Discussion

Although a considerable volume of the ionosphere contributes to the measured temperature, it can be shown (Pawsey *et al.*, 1951) that only a small range of heights, about 10 km, contributes appreciably. Physically, the ionosphere is too opaque for the aerial to "see" beyond this range of heights and too transparent for it to "see" any ionosphere below it. To a first approximation, therefore, the measured temperature may be taken as that of a certain level of the ionosphere corresponding to the "optimum opaqueness" of the ionosphere which depends on the electron density N and collision frequency ν. If either N or ν is increased the optimum opaqueness will occur at a lower level. Rocket measurements (Rocket Panel, 1952) show that the temperature of the ionosphere varies with height so that we would expect a variation of N or ν to produce a variation in measured temperature.

The diurnal variation of the height of the D-region has been investigated by

BRACEWELL *et al.* (1951), with reflections of very long radio waves and found to fit the formula:

$$h_\chi = h_{\chi=0} + A(t) \ln \sec \chi$$

where χ is the altitude of the sun and $A(t)$ is a constant having the value of about six during the equinoxes. They also found a difference between the summer and winter noon heights and a sharp decrease in height during an s.i.d. (sudden phase anomaly). Using this, the expected diurnal height variation during an equinox at Macquarie Island together with summer and winter and s.i.d. effects is shown in Fig. 6. The temperature scale on the right was taken from the Rocket Panel (1952)

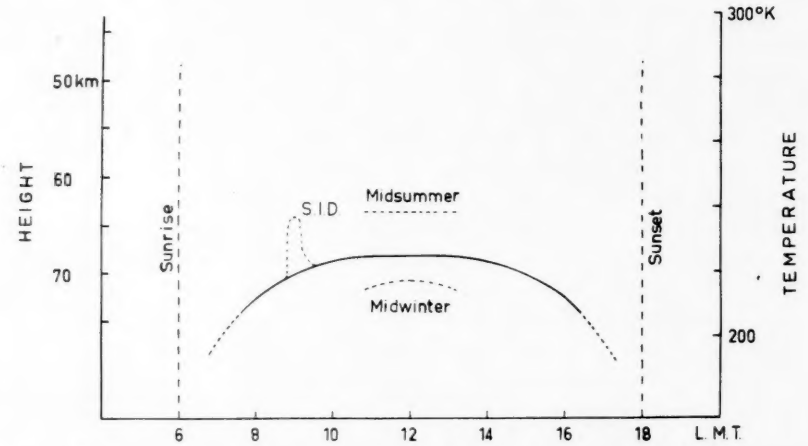

Fig. 6. Diurnal variation of the height of the *D*-layer at the equinoxes. Midday summer and winter heights are shown dotted. The temperature scale on the right was compiled from the Rocket Panel curve. The height decrease during a sudden phase anomaly indicates the temperature rise expected from an s.i.d.

temperature–height curve which is approximately linear in the height range 53 km to 74 km (210°K to 270°K).

Consider the possibility that all the variation of observed temperature is due to variation in electron density (as indicated by height measurements at very low frequencies) alone. The predictions of this hypothesis and the experimental results are compared in Table 2. The general agreement here is quite good. The predicted diurnal variation barely shows up probably owing to the atmospheric effect discussed in Section 3. A somewhat stronger temperature rise occurs during disturbed periods than that predicted. This was also the case during s.i.d.s at Urisino (40°K). For large increases of ionization, however, the optimum opaqueness level, being a function of N and ν, is depressed more than the isopyc* since the collision frequency ν increases exponentially with decrease in height, giving a stronger rise in measured temperature.

At 5·6 and 7 Mc/s the temperatures were much the same (within the expected error) as the 2 Mc/s measurements. However, at these frequencies the *D*-region

* *isopyc*: surface through points of equal electron density.

is much more transparent so that there is no longer a thin layer of "optimum opaqueness" responsible for most of the temperature contribution. This situation is apparent from the principle of detailed balancing. Suppose the aerial is radiating power towards the ionosphere. At 2 Mc/s the absorption is very high and most of the power will be absorbed in a relatively thin layer. At 7 Mc/s though, probably

Table 2

Fixed temperature–height hypothesis	Experiment
Mid-summer temp. : 240°K Equinox temp. : 225°K Mid-winter temp. : 215°K	November : 235°K Sept.–Oct. : 227°K July : 225°K
Noon temperatures, some 10–15° higher than early morning and late afternoon.	About 5° difference (Oct.–Nov. series)
Rise of 15–20° during an s.i.d.	40–50° during strong magnetic activity

VOL. 18 1960

only about half of this power would be absorbed on the ray's first trip through the D-region. If we assume that the reflection coefficients of the F-layer and "ground" (in this case the Southern Ocean) are both unity, then all the power will ultimately be absorbed in the D-region but the depth of ionosphere responsible for (say) 90 per cent of the absorption might include the entire D-region. The temperature measured would then represent an average one for the whole region.

Large increases in measured temperature and anomalously high absorption are strongly correlated with high K_p values. Both of these effects are probably due to large overall increases of D-region ionization produced by auroral particle bombardment. The apparent temperature increases have been explained above. If we make the simplifying assumptions that most of the absorption occurs in a relatively thin stratum, and that the various factors governing the absorption do not vary appreciably within this stratum, we find the total absorption ρ in nepers at frequencies greater than the collision frequency ν and the gyro-frequency f_L is given by:

$$\rho = CN_e\nu(f + f_L)^{-2}$$

where C is constant.

Since the absorption decreases rapidly with frequency it is often measured on ionospheric soundings in terms of the lowest frequency for which echoes are received ($f_{\min}$). During daylight hours $f_{\min}$ is around 2 Mc/s on undisturbed days but rises to around 10 Mc/s or more during highly disturbed conditions. Since the gyro-frequency f_L is about 1·5 Mc/s it is seen that at any given frequency the absorption and thus the product $N_e\nu$ must increase by a factor of about 10.

The collision frequency at any given height is unlikely to change by more than some per cent (since $\nu \propto T^{1/2}$), but as a function of height we find an exponential relation, so that at a height 20 km lower the collision frequency is some ten times higher. In order to explain increases of apparent temperature of from 40° to 50° during strong magnetic activity we required a height depression of isopycs of some 15 km (see Fig. 6). Owing to the limited region for which the slope of the temperature–height curve (Rocket Panel) is negative a further height decrease would not have given a further temperature increase. Hence during severe magnetic activity we might suppose that the overall ionization of the *D*-region is increased sufficiently to depress the lower isopycs by some 20 km. For each isopyc then, the collision frequency effectively increases some ten times so that the total absorption increases by about this amount.

5. CONCLUSIONS

The temperature of the lower ionosphere has been measured in an auroral zone, using similar techniques to those used by GARDNER (1954) in a temperate region. The temperature range and seasonal variation of temperatures have been found to be the same as in a temperate region. Owing to the much lower intensity of atmospherics and complete freedom from man-made noise temperatures have been measured from sunrise to sunset, and the higher temperatures during early morning and late afternoon in GARDNER's results were not apparent. The observed temperature variations can be similarly explained in terms of a fixed temperature height scale.

No large increases in temperature have been observed during s.i.d.s, but during strong magnetic activity temperatures have been found up to 50° above normal. This, and the very large increase in absorption ("polar blackout") experienced in auroral latitudes during magnetic storms is thought to be due to bombarding auroral particles causing a strong increase in ionization and thus a descent of the region of absorption to levels of much greater collision frequency rather than a direct heating effect caused by these particles producing higher collision frequencies.

For temperature measurements by this method the optimum frequency appears to be around 2 Mc/s. At much lower frequencies measurements can be contaminated by noise trapped from the night hemisphere and at much higher frequencies the *D*-region becomes too transparent for temperature measurements in a narrow height range.

Acknowledgements—The writer wishes to express thanks to the Radiophysics Division, CSIRO, for loan of the basic equipment; to the Antarctic Division, Department of External Affairs, for finance and auxiliary equipment; to Drs. J. L. PAWSEY and F. F. GARDNER of the Radiophysics Division, CSIRO, and Professor G. NEWSTEAD of the University of Tasmania for valuable criticisms and suggestions, and to the Australian National Antarctic Research Expedition members, particularly Mr. K. D. COLE, without whose co-operation this work would have been impossible.

VOL
18
196

References

Bracewell R. N., Budden K. G., Ratcliffe J. A., Straker T. W. and Weekes K.	1951	*Proc. Instn. Elect. Engrs.* III **98,** 221.
Dowden R. L.	1957	*J. Atmosph. Terr. Phys.* **11,** 111.
Ellis G. R.	1956	*J. Atmosph. Terr. Phys.* **9,** 51.
Ellis G. R.	1957	*J. Geophys. Res.* **62,** 229.
Ellis G. R.	1958	*J. Atmosph. Terr. Phys.* **13,** 61.
Gardner F. F.	1954	*J. Atmosph. Terr. Phys.* **5,** 298.
Gardner F. F. and Pawsey J. L.	1953	*J. Atmosph. Terr. Phys.* **3,** 321.
Pawsey J. L., McCready L. L. and Gardner F. F.	1951	*J. Atmosph. Terr. Phys.* **1,** 261.
Reber G.	1956	*Proc. Radio Astronomy Symposium,* 1956. CSIRO, Sydney.
Sommerfeld A. and Renner F.	1942	*Wireless Engr* **19,** 357, 409, 457.
The Rocket Panel	1952	*Phys. Rev.* **88,** 1027.

VOL. 18 1960

Journal of Atmospheric and Terrestrial Physics, 1960, Vol. 18, pp. 20 to 28. Pergamon Press Ltd. Printed in Northern Ireland

Gyro splitting of ionospheric echoes

G. R. A. Ellis
CSIRO Upper Atmosphere Section, Camden, N.S.W., Australia

(*Received* 11 *August* 1959)

Abstract—The propagation of extraordinarily polarized waves in the ionosphere is discussed. It is shown that the properties of highly retarded F-region echoes sometimes observed at frequencies just below the gyro-frequency may adequately be explained if they are caused by the reflection of the X-wave at the normal extraordinary reflection level.

Anomalous M-type multiple echoes and the mixed polarization of the echoes previously observed which had led to other explanations are interpreted in terms of mode change as a result of coupling in the E-region. The analysis shows that the zenith angle of arrival of the gyro echoes is not zero and increases as the gyro-frequency is approached.

Observations of gyro echoes at frequencies up to 1·51 Mc/s are described. It is found that there is a strong correlation between the occurrence of gyro echoes above 1·45 Mc/s and of sporadic-E echoes.

1. Introduction

It has long been known that it is possible to observe, occasionally, F-region ionospheric echoes with virtual heights which increase to large values in the vicinity of the gyro-frequency. The ionosonde record of Fig. 1 shows an example. Some uncertainty still exists concerning the mechanism responsible for these echoes (Ratcliffe, 1959) and, in the past, several conflicting explanations have been proposed.

Martyn and Munro (1938) have suggested that they result from the reflection of the ordinary wave at the "fourth level of reflection" where the refractive index becomes infinite ($X = (1 - Y^2)/(1 - Y_L^2)$ in Ratcliffe's notation). In these circumstances they expected that the virtual height of the echoes would increase to infinity as the wave frequency increased to $f_H \cos\theta_0$ where θ_0 is the zenith angle of the geomagnetic field. More recently, however, Budden (1954) has shown that reflection does not occur at a refractive index infinity.

Appleton, *et al.* (1938) proposed that the gyro echoes are produced by the reflection of the extraordinary wave at the level $X = 1 + Y$ where the X-mode refractive index is zero. The frequency of infinite virtual height should then approximate to the gyro-frequency in the F-region. Appleton *et al.* observed that the echoes were extraordinarily polarized although independent observations of Martyn and Munro showed that they had mixed ordinary and extraordinary polarization.

According to this latter hypothesis the major part of the total group delay should occur between the E-layer and the ordinary level of reflection in the F-layer. However, Booker and Berkner (1938) published an ionosonde record, obtained at Washington D.C., showing anomalous multiple echoes associated with gyro echoes where successive reflection at the F-layer after upward reflection of a downcoming gyro echo at an E_s-layer did not produce any additional large group delay. Booker and Berkner therefore considered that the region producing most

VOL.
18
1960

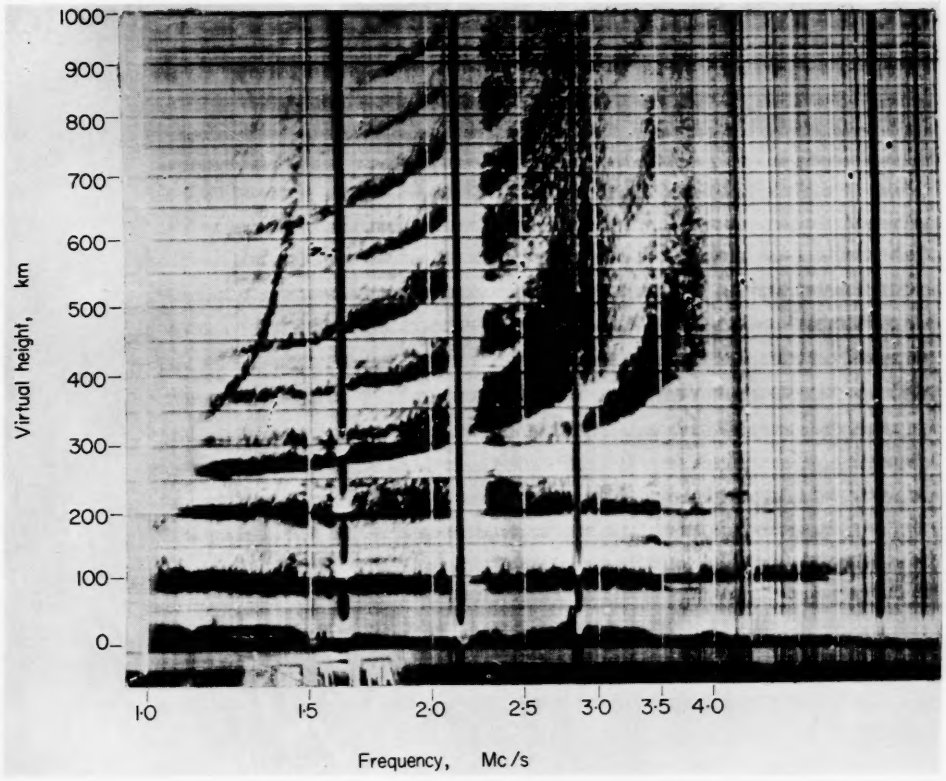

Fig. 1. Ionosonde record showing gyro echo up to 1·5 Mc/s.
Hobart, 0110 hours 17 May 1946.

VOL.
18
1960

of the group delay was below the E_s-layer. They observed that the greatest frequency of their gyro echoes was 1·38 Mc/s. Since at Washington the gyro-frequency at 100 km is about 1·55 Mc/s they proposed that the "Lorentz polarization term" should be used in deducing the Appleton–Hartree refractive index formula. When this term is included the virtual height of a gyro echo should increase to infinity at the so-called Lorentz frequency which at Washington is $0{\cdot}85\,f_H$ or 1·32 Mc/s at 100 km. BOOKER and BERKNER showed that an additional correction for the effect of heavy ions could increase the maximum frequency of the echoes to 1·38 Mc/s.

Subsequently MARTYN and MUNRO (1939) identified multiple echoes of the $F + E_s$ type which showed no additional large group delay and thus it appeared that the retarding region was not below the E_s-layer.

2. The Anomalous Multiple Echoes

If it could be shown that the anomalous multiple echoes and the mixed polarization of the gyro echoes result from extraordinary wave propagation, the main objection to the interpretation of APPLETON *et al.* would be removed and it would then be useful to examine in more detail how this interpretation agrees with the other observed properties of the echoes.

The M-type multiple echoes may be explained simply in terms of coupling in the E-layer. It is known (RYDBECK, 1951) that, with a high collision frequency and a strong electron gradient, mode coupling can occur at the ordinary level of reflection ($X = 1$). It is possible, therefore, for a down-coming extraordinary wave from the F-layer to be reflected back at the sporadic E-layer as an ordinary wave. The second reflection at the F-layer will be at the ordinary level and the total virtual height of the resulting multiple echo will be equal to the virtual height of the F_x echo plus the difference between the virtual heights of the F_0 and E_s echoes, as is actually observed.

Mixed ordinary and extraordinary multiple reflections between F- and E_s-layers of this type can only occur below the gyro-frequency. Above the gyro-frequency the extraordinary wave is reflected when $X = 1 - Y$ and cannot reach the coupling level $X = 1$ so that polarization reversal through reflection cannot occur. The different possible magneto-ionic components when coupling is included have been discussed by PFISTER (1953). These components are listed in Table 1, where D, A and B refer to reflection processes at the levels, $X = 1 - Y$, $X = 1$ and $X = 1 + Y$, respectively, and C refers to a coupling process of the $X = 1$ level. Fig. 2 illustrates the different possible refractive index paths. We may estimate the reflection coefficients of the different components for a given model, using the coupling transmission coefficient of RYDBECK.

$$T_{OX} = \exp\{-j\int(n_x - n_O)\,dz\} \qquad (X = 1)$$

where $n_x = x$-mode refractive index at $X = 1$;
$n_O = O$-mode refractive index;
$Z =$ complex height co-ordinate.

The reflection coefficient then is given by the attenuation into and out of the layer

together with the attenuation through the ordinary to extraordinary coupling process where there is a mode change.

The reflection coefficients of the different magneto-ionic components for a model of the E_s-layer are given in Table 2. It is interesting to note that an extraordinary wave is more likely to be reflected as an ordinary wave via a mode change than as an extraordinary wave. This is because with the assumed model, the

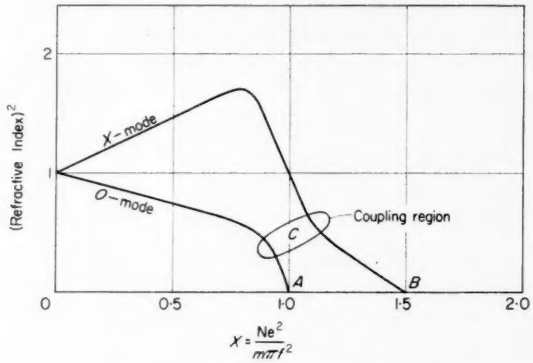

Fig. 2. Variation of refractive index with electron density below the gyro-frequency.

attenuation of the ordinary mode and of the coupling process is small while that of the extraordinary mode in the region between $X = 0$ and $X = 1$ is large. The reflection of an extraordinary wave without a mode change means that it travels twice through this highly attenuating region compared with only once if it is reflected as an ordinary wave.

Table 1. Reflection processes of the possible magneto-ionic components when coupling is included

$f < f_H$	$f > f_H$
$O \rightarrow A \rightarrow O$	$X \rightarrow D \rightarrow X$
$X \rightarrow B \rightarrow X$	$O \rightarrow A \rightarrow O$
$O \rightarrow A \rightarrow C \rightarrow X$	$O \rightarrow C \rightarrow B \rightarrow C \rightarrow O$
$X \rightarrow B \rightarrow C \rightarrow O$	
$O \rightarrow C \rightarrow B \rightarrow C \rightarrow O$	

3. Polarization

The possibility of mode change also provides an explanation of the mixed polarization of the echoes observed by Martyn and Munro. If the critical frequency of the E_s-layer is less than the wave frequency there will be no coupling level ($X = 1$) in the E_s. An extraordinary wave would then penetrate the E_s-layer without mode change and the polarization of the echoes would be extraordinary. Also there could be no anomalous M-type echoes. If the E_s critical frequency is

great enough to cause reflection of the X-mode $\{f_0E_s > \sqrt{(f^2 + ff_H)}\}$ then it is possible for transmission still to occur through gaps between E_s clouds, again without mode change. The polarization of the F-region gyro echoes would be extraordinary but mode change of downcoming waves reflected back at the E_s-layer could produce anomalous multiple echoes.

With the E_s critical frequency in the range $f < f_0E_s < \sqrt{(f^2 + ff_H)}$ transmission of the X-mode and reflection of the O-mode would occur and an extraordinary wave incident on the E_s-layer could be reflected or transmitted as either an extraordinary

Table 2. Reflection coefficients of the different magneto ionic components for the following model of E_s-layer: scale height, 1 km; gyro-frequency, 1·57 Mc/s; wave frequency, 1·35 Mc/s; collision frequency, 5×10^4/sec; plasma frequency, 3 Mc/s; inclination of geomagnetic field, 18°. (The mode coupling transmission coefficient $T_{OX} = 0{\cdot}618$.)

Reflection path	Reflection coefficient
$O \rightarrow A \rightarrow O$	0·496
$X \rightarrow B \rightarrow X$	0·0067
$O \rightarrow A \rightarrow C \rightarrow X$	0·058
$X \rightarrow B \rightarrow C \rightarrow O$	0·497

wave or an ordinary wave or both by coupling processes at the $X = 1$ levels. Anomalous M-echoes would still be produced and the normal gyro echo would have mixed ordinary and extraordinary polarization. Using the model of Table 2 the ordinary polarization would predominate. However, leakage of the extraordinary wave between E_s clouds could produce a net extraordinary polarization.

4. Extraordinary Wave Propagation near the Gyro-frequency

To see how well the X-mode hypothesis of Appleton *et al.* corresponds with the upper frequency limit of actual gyro echoes it is first necessary to analyse the propagation of extraordinary waves in typical circumstances, for wave frequencies near the gyro-frequency. The Lorentz polarization term will be omitted.

The condition for infinite extraordinary refractive index and therefore infinite group height (Budden, 1954) is

$$Y^2 = \frac{1 - X}{1 - X\cos^2\theta} \qquad (\theta = \text{propagation angle})$$

However, the situation is complicated by the variation of Y, θ and X along the ray path. Near the gyro-frequency small changes in the magnetic field intensity can produce large changes in the refractive index. As the wave travels upward into the ionosphere both the field intensity and the electron density will change, and since equipotential surfaces of the geomagnetic field are not in general parallel to surfaces of equal electron density the medium is doubly inhomogeneous.

The analysis of propagation in such a medium is complicated, and here we divide the propagation path into three height ranges in which the field intensity and the electron density do not both vary. If the wave frequency is in the vicinity of the gyro-frequency in the F-region, then in the E-region the variation in the geomagnetic field intensity will be unimportant and we can assume that only the electron density varies. Between the E- and the F-regions we assume the electron density to be constant and that the field intensity varies. In the F-region below the $X = 1$ level the direction of group propagation will be almost perpendicular

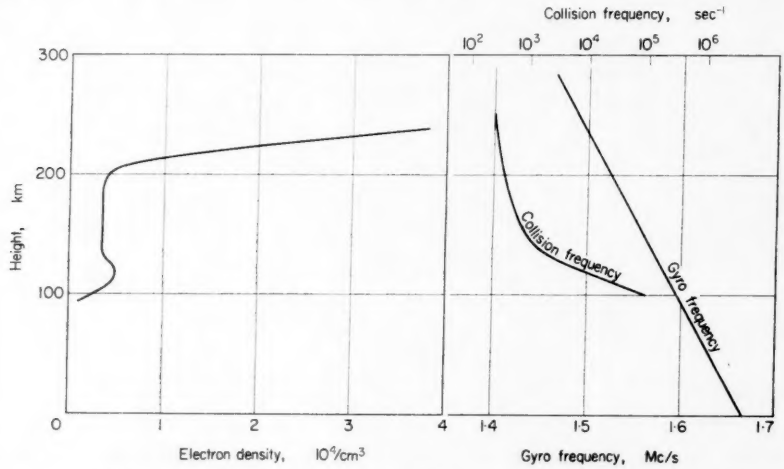

Fig. 3. Model of ionosphere assumed for calculation of extraordinary wave propagation. Inclination of geomagnetic field 18°.

to the field direction and the field intensity can again be considered to be constant. Above the $X = 1$ level the wave polarization will be ordinary and field variations will have a negligible effect on the refractive index.

Fig. 4 shows the ray paths calculated in this way from the model of Fig. 3 using the Appleton–Hartree refractive index theory (see, for example, Forsgren, 1951). As the frequency is increased the ray path for vertical incidence deviates more and more towards the nearer magnetic pole until it lies almost entirely in the magnetic equipotential plane passing through the zenith of the transmitter and the lower boundary of the ionosphere. Thus the rate of decrease in field strength along the ray path is much less than if the path in the ionosphere were vertical. This has the effect of permitting X-mode propagation to occur at all frequencies up to the gyro-frequency in the lower E-region.

A second property of the ray path results from the stratification of the medium in the E–F-region along the inclined equipotential planes of the geomagnetic field. A ray vertically incident at the E-layer will be obliquely incident at the E–F-region and after reflection in the F-layer, will not return to its point of origin. However, it is possible to find ray paths which do return, and in general they will have a non-vertical angle of arrival at the transmitter. The angle of arrival will increase as the frequency is increased (Fig. 5) and for the same vertical distribution

VOL
18
196

of ionization, will be greater if the inclination of the magnetic field is greater.

If the total group height is calculated it is found that most of the additional group delay compared with the *O*-mode occurs in the *E–F*-region and it has been

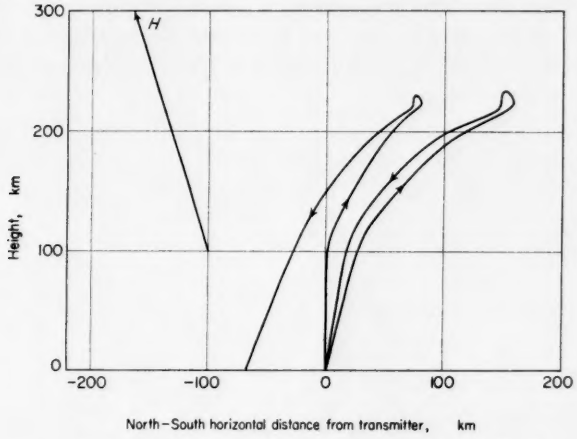

Fig. 4. Ray paths calculated using model of Fig. 3.
Wave frequency 1·50 Mc/s.

shown by J. M. WATTS (private communication) that the *X–O* virtual height difference provides a measure of the total electron content below the *F*-region. Although the group height increases rapidly with frequency it does not do so as rapidly as is the case, for example, with *O*-wave penetration of a parabolic layer.

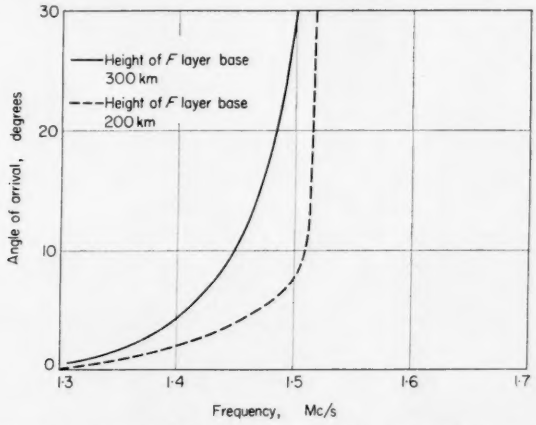

Fig. 5. Variation of angle of arrival of gyro echoes at the transmitter with wave frequency for two different heights of the base of the *F*-layer.

As a result the group height frequency curve still has a finite slope even for large group heights. In practice this means that the maximum frequency at which echoes are observed will depend on the height range of the particular pulse equipment used.

Fig. 6 shows the variation of group height and total attenuation with frequency

for the model of Fig. 2 and also the effect of increasing the thickness of the E–F-region. It can be seen that for a maximum virtual height of 1000 km the maximum observable frequency should be somewhat greater than 1·4 Mc/s. There should be marked reduction in the maximum frequency as the height of the base of the F-layer is increased and it is important to note that this results mainly from the increased virtual height of the gyro echoes rather than from the decrease in the gyro-frequency at the level of reflection.

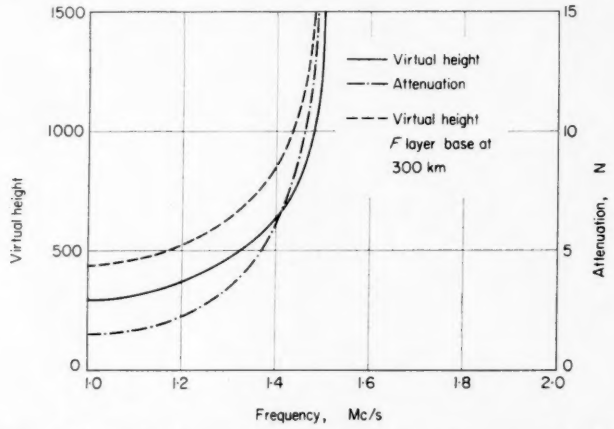

Fig. 6. Group height and attenuation of the X-mode vs. frequency calculated using the model of Fig. 3. The group height curve obtained with the F-layer base at 300 km is also known.

5. Observations

The parameters of the geomagnetic field chosen from the analysis of the previous section were those for Hobart, Tasmania, (geomagnetic latitude 51°) and a survey of Hobart ionosonde records showed that there were many examples of good gyro echoes which could be traced on the records up to virtual heights of 800 km to 1000 km and to frequencies of 1·5 Mc/s. All occurred during the early hours of the morning when broadcast stations in the Australian area were not transmitting. The best examples were found in the records for 1946 when the ionosonde was operating with large cage dipole antennae which had a natural resonance in the vicinity of 1·5 Mc/s.

Fig. 7 shows a plot of the observed maximum frequency of the echoes against the virtual height of the F-layer ordinary trace at 1 Mc/s together with the two theoretical points obtained from the 1000 km level of the $h'f$ curves of Fig. 5. It can be seen that the observed frequencies agree well with those expected from the analysis based on the assumption that the echoes are due to reflection of the extraordinary mode.

Nevertheless it is surprising that the echoes can be observed at all at the higher frequencies in view of the large attenuation (Fig. 5) and an inspection of Hobart ionosonde records shows in fact that the great majority of gyro echoes fade out at about 1·2 Mc/s. They are observed to extend to higher frequencies only when sporadic-E forms, a sequence of records taken every 10 min usually showing

VOL
18
196

the onset of higher frequency gyro echoes and sporadic-E on the same record.

Fig. 8 shows, for example, a histogram of the occurrence of gyro echoes above 1·45 Mc/s at Hobart in January 1946 with the critical frequency of the E_s-layer. No echoes extended to this frequency range in the absence of E_s or when f_0E_s exceeded 6 Mc/s.

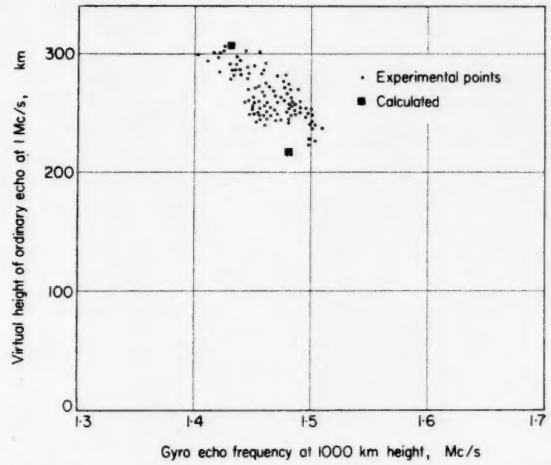

Fig. 7. Variation of the maximum wave frequency of gyro echoes with height of ordinary echoes at 1 Mc/s observed at Hobart during 1946.

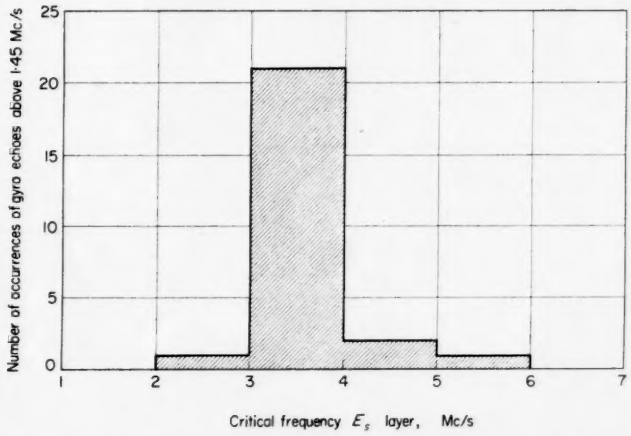

Fig. 8. Histogram showing the close association between gyro echoes above 1·45 Mc/s and the E_s critical frequency. Obtained from Hobart ionosonde records for January 1946 between the hours 0100 and 0500. The total number of records examined was 746.

The reason for this is not certain although it may be due to a rearrangement of electron density between the E–F-region and the E_s-layer. A sudden decrease in the density in the E–F-region would reduce the total attenuation of the gyro echoes while a moderate increase in f_0E_s need not increase it. Clearly if f_0E_s

increased sufficiently, blanketing of the F-layer would occur and no gyro echoes would be observed.

References

Appleton E. V., Farmer F. T. and Ratcliffe J. A.	1938	*Nature, Lond.* **141,** 409.
Booker H. G. and Berkner L. V.	1938	*Terr. Magn. Atmos. Elect.* **43,** 427.
Budden K. G.	1954	*Physics of the Ionosphere* p. 520. Physical Society, London.
Forsgren S. K. H.	1951	*Trans. Chalmers University of Tech., Gothenburg, Sweden* No. **17.**
Martyn D. F. and Munro G.	1938	*Nature, Lond.* **141,** 159.
Martyn D. F. and Munro G.	1939	*Terr. Magn. Atmos. Elect.* **44,** No. 1.
Pfister W.	1953	*J. Geophys. Res.* **58,** No. 1, 29.
Ratcliffe J. A.	1959	*The Magneto Ionic Theory and its Applications to the Ionosphere* p. 133. Cambridge University Press.
Rydbeck O.	1951	*J. Appl. Phys.* **21,** 1205.

VOL.
18
196(

Journal of Atmospheric and Terrestrial Physics, 1960, Vol. 18, pp. 29 to 42. Pergamon Press Ltd. Printed in Northern Ireland

Sporadic-*E* as observed by back-scatter techniques in United Kingdom*

E. D. R. Shearman and J. Harwood
DSIR, Radio Research Station, Slough

(*Received 7 September* 1959)

Abstract—Observation of sporadic-*E* clouds with a rotating-aerial back-scatter sounder enables a greater sample of E_s clouds to be studied than does the use of a vertical incidence sounder, and permits the size, location and movement of clouds to be estimated. Limitations are introduced by finite aerial beam-width and skip-distance effect. Multi-frequency operation eliminates the latter defect, and also permits ionization to be measured.

Results obtained during the IGY with a single-frequency rotating-aerial sounder are presented, showing the diurnal, seasonal and geographical characteristics of E_s occurrence. On particular occasions, movements have been tracked and under favourable conditions, the size and ionization of the clouds determined.

Earlier results obtained with a fixed-direction aerial and multi-frequency technique show similar diurnal and seasonal trends, and illustrate the possibilities of the variable-frequency facility for simultaneous measurement of cloud size and ionization.

1. Introduction

Most measurements of sporadic-*E* ionization have been made with vertical incidence sounders, and the spatial distribution has been obtained by correlating results from a number of these equipments distributed throughout the world (Smith, 1957). This paper, however, deals with observations at one site (Slough) using the back-scatter technique (Villard and Peterson, 1952; Shearman and Martin, 1956) which provides data on the occurrence of E_s within 600–700 km of the site.

The technique consists in transmitting, from a directional aerial, radio-frequency pulses which "illuminate" regions of the earth after reflection from the ionosphere; the signals scattered back along the outward path from the illuminated ground irregularities are received on the same aerial and displayed on cathode-ray tubes. The time delay between transmitted pulses and received echoes is a measure of the range of the illuminated ground area. This range enables propagation by way of E_s ionization to be distinguished from other modes of propagation, and, assuming that the reflection point on the E_s cloud lies half-way along the path to the ground, permits the range of the reflecting ionization to be deduced.

During the IGY continuous recordings of back-scatter were made at Slough on Regular World Days. A horizontal Yagi aerial was used for transmission and reception at 17 Mc/s, and rotated about a vertical axis in synchronism with the rotating time-base of a plan position indicator (P.P.I.). Records were obtained by photographing the P.P.I. display at intervals of 1 min on ciné film.

In this paper the interpretation of the records is discussed and the limited statistical data on geographical, seasonal and diurnal occurrence of E_s which they provide is summarized. The formation and movement of the E_s clouds on a few occasions is described in more detail, as the P.P.I. presentation is particularly adapted to this type of observation.

* Official communication.

The statistical information is amplified by a summary of some earlier back-scatter observations, in which a rhombic aerial was directed towards the east and the echoes studied as a function of time, range and frequency. These results, though lacking the directional information provided by the P.P.I., illustrate the potentialities of the multi-frequency technique for distinguishing between E_s and other modes of propagation, and for measuring simultaneously the range and critical frequency of an E_s cloud.

2. Equipment

In the both rotating and the fixed-aerial observations, pulses of 100 kW peak power and 100 μsec duration were transmitted at a rate of $12\frac{1}{2}$/sec. The back-scatter echoes were presented on a time-base calibrated in terms of the slant-range of the illuminated ground, free space velocity of propagation being assumed. Two forms of display were used: (a) the echoes were shown as vertical deflexions of a horizontal time-base trace (range–amplitude display); (b) when the rotating aerial was used, the echoes were also shown as blacked-out portions of a radial time-base rotating in synchronism with the aerial (P.P.I. display).

Sample records of the two displays are shown in Figs. 1 (a) and (b). In the rotating aerial observations, the range–amplitude records were used merely as an aid to the interpretation of the P.P.I. records,while in the fixed azimuth aerial experiments the range–amplitude records were the only source of information. The interpretation of the two types of records together with the results obtained from them are discussed separately in Sections 3 and 4.

Further details of the equipment used in these experiments has been published elsewhere (Shearman and Martin, 1956).

3. Rotating Aerial Observations

The echo-pattern produced on the plan position indicator when E_s echoes are being displayed is influenced by instrumental and propagation factors, and an analysis of these is necessary before information about the size and ionization of the E_s cloud can be deduced.

In the sample record of Fig. 1 (b), a dark area is shown covering bearings from 180° to 260° and extending from a radial distance of 400 km to 800 km. The azimuthal spread here is determined by the size of the E_s cloud and by the beam-width of the aerial; a typical correction for the latter would involve a reduction of about 100° in the azimuthal spread, the precise amount depending on the echo amplitude. Similarly the upper limit of radial distance which is observed will depend on the vertical radiation pattern of the aerial, on propagation factors, and on the scattering parameters of the ground. All these factors cause a rapid attenuation of echo amplitude with increasing range above, say, about 1500 km. To take account of these factors, a detailed examination of the echo amplitudes from range–amplitude records which correspond to the echo-patterns on the P.P.I. is required, and precise calibrations of the equipment are involved. For the purpose of this paper a simpler approach has been adopted, the centre bearing of the echo path, and the minimum and maximum ranges at this bearing being used in the analysis.

VOL.
18
196

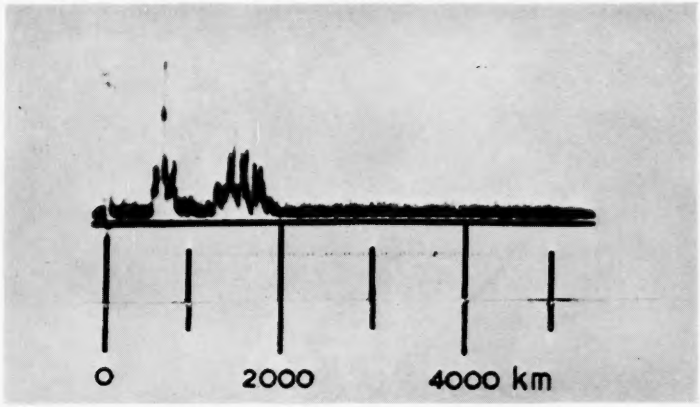

(a)

(b)

Fig. 1. (a) Example of range–amplitude display; (b) Example of P.P.I. display.

OL.
18
960

VOL
18
196

3.1. *Theoretical discussion*

The presence of a sufficiently dense cloud of E_s ionization within a few hundred kilometres of the observing site would be expected to produce a dark area on the P.P.I. display as shown in Fig. 1 (b). It will be useful to consider the form of display to be expected during the formation or movement of such a cloud, assuming it to be in the form of a thin layer. A simple relationship then holds between the minimum slant-range r observed (distance via reflecting layer to illuminated ground), the critical frequency f_c, and the operating frequency f, namely

$$\frac{f_c}{f} = \frac{r^2/4 + 2Rh + h^2}{r(R + h)} \tag{1}$$

where R = radius of earth;
h = height of reflecting region.

From this equation, the relationship between f_c and r for a frequency f of 17 Mc/s, and heights h of 100 and 120 km has been calculated and used in the analysis of the P.P.I. results.

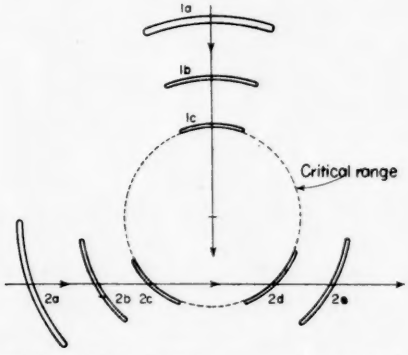

Fig. 2. Hypothetical echo movements—small cloud.

If a small E_s cloud were to form at a suitable distance, it would first show as a narrow arc on the P.P.I. display (the azimuthal spread being due to aerial beam-width). A movement towards the observer would show as a corresponding inward movement of the echo, until a certain minimum range were reached, when the echo would disappear as the critical angle of incidence for layer penetration was reached; this is shown in Fig. 2 by the sequence 1a, 1b, 1c. If the movement continued, the echo would appear again when its range exceeded the critical value in the reverse direction. A cloud moving from west to east but passing south of the observer would show as the sequence 2a, 2b, etc.

The formation of a larger E_s cloud would result in the growth of a correspondingly larger echo area, while movement towards the observer might give a sequence of echoes as in Fig. 3. As the angle subtended at the observing point and the echo amplitude increased, the azimuthal spread would increase, until eventually the echo would disappear at the critical range. It can be seen that an even larger cloud, as it crossed the critical range, might depending on the shape of the cloud, appear as two subsidiary echoes to either side; alternatively, the range of azimuths

over which it is observed may increase to 360°, giving an annular echo around the critical range.

The above examples have assumed the formation of a cloud with a fixed critical frequency, well outside the critical range corresponding to this frequency. If, however, a sufficiently large cloud forms gradually (increasing critical frequency) near to the observer, its observable range will extend from the critical range outwards, and this critical range will decrease with time. Thus an apparent inward movement will be observed, and may only be distinguishable from an actual movement by the constancy of range of the outer edge.

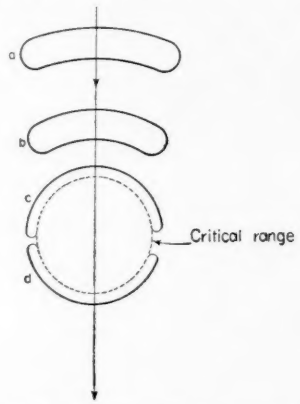

Fig. 3. Hypothetical echo movements—large cloud.

By applying the considerations described above to the observed echo patterns, it has been possible on particular occasions to estimate the size, critical frequency, and movements of regions of E_s ionization.

3.2. *Method of analysis*

P.P.I. displays were obtained at 1 min intervals throughout the Regular World Days of the IGY, with the primary object of recording as many modes of propagation as possible at 17 Mc/s. Some of the records showed echoes of range between 300 km and about 1500 km which appeared to be due to E_s propagation; the times of occurrence of these were noted. They were described by noting at intervals of a few minutes (i) the azimuthal extremes of each echo, (ii) the minimum and maximum slant-range at the centre azimuth. At the times of the experiments, the range–amplitude display was photographed hourly for north, south, east and west bearings of the aerial to provide data on echo amplitudes.

The range and azimuth data were plotted against time of day. The formation and movement of echoes were followed by examination of these graphs, and by ciné-projection of the P.P.I. displays to speed up the time-scale of events.

3.3. *Results*

Statistical data from P.P.I. displays. From August 1957 to December 1958 observations were made on fifty-eight days, and echoes due to sporadic-*E*

propagation were seen on twenty-seven of these. The dates and times (GMT = UT) of occurrence of the echoes are shown in Fig. 4; the seasonal distribution is evident, and echoes appear mostly in the day-time. The limited data suggest a more frequent occurrence in the mornings, but are obviously inadequate for providing detailed statistics.

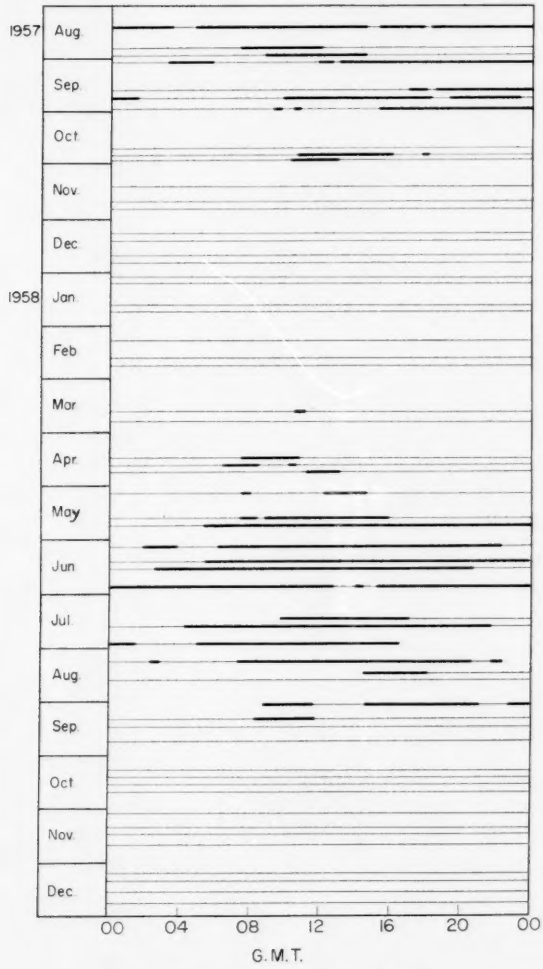

Fig. 4. Time of occurrence of E_s.

To demonstrate the distribution of echoes, and consequently of E_s ionization, in azimuth, a polar plot is shown in Fig. 5 for the months of May and June 1958. Each point corresponds to the minimum slant-range and the azimuth of echoes seen at $\frac{1}{2}$ hr intervals on 18, 19 May, and on 9, 17, 18 and 24 June. The greatest concentration of echoes is seen to be in the southern semicircle, with no significant bias to west or east.

The radial distance of the points from the origin will be determined partly by the critical frequency of the ionization, and partly by its actual distance from the observing site. The closest approach, however, should be determined by the maximum critical frequency, which, for an ionized region at a height of 100 km, is given by equation (1) as about 9 Mc/s.

A statistical estimate of the size of E_s clouds can be obtained most directly from the observed radial extent of the corresponding ground-scatter, the azimuthal extent being unreliable because of the wide aerial beam. The extent of each echo in range was noted at $\frac{1}{2}$ hr intervals on all the occasions during the IGY when E_s echoes were observed. The 744 observations thus obtained were classified to form

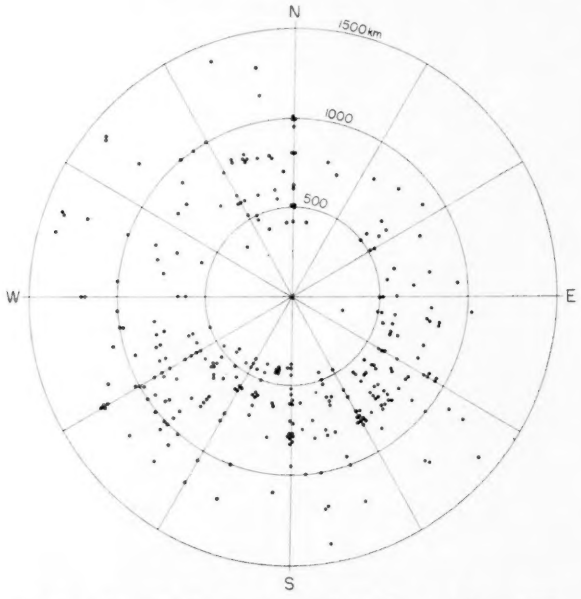

Fig. 5. Azimuthal distribution of E_s in May and June 1958.

the histogram shown in Fig. 6, the range scale being halved to give equivalent horizontal extents at the ionosphere. The mean size was 176 km. Because of the influence of skip distance effects on the observed minimum ranges and of echo sensitivity on the maxima, the true horizontal extent will be greater than this value.

3.4. *Formation and movement of echoes*

When the record of a day's variation of the P.P.I. display was studied it was usually found that the first echo patch would appear during daylight as a small arc, the range to the inner edge of the arc decreasing as the echo intensified. Frequently other echoes appeared in addition, as many as four simultaneous echoes being seen on occasion.

By speeding up the time-scale of events with ciné-projection, a search was made for movements of the echoes; such movements were only clear on one or two

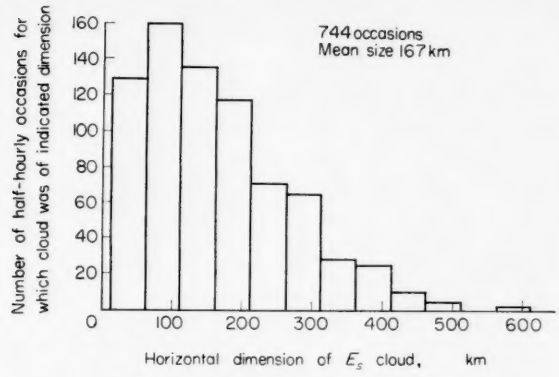

Fig. 6. Distribution of E_s cloud dimensions.

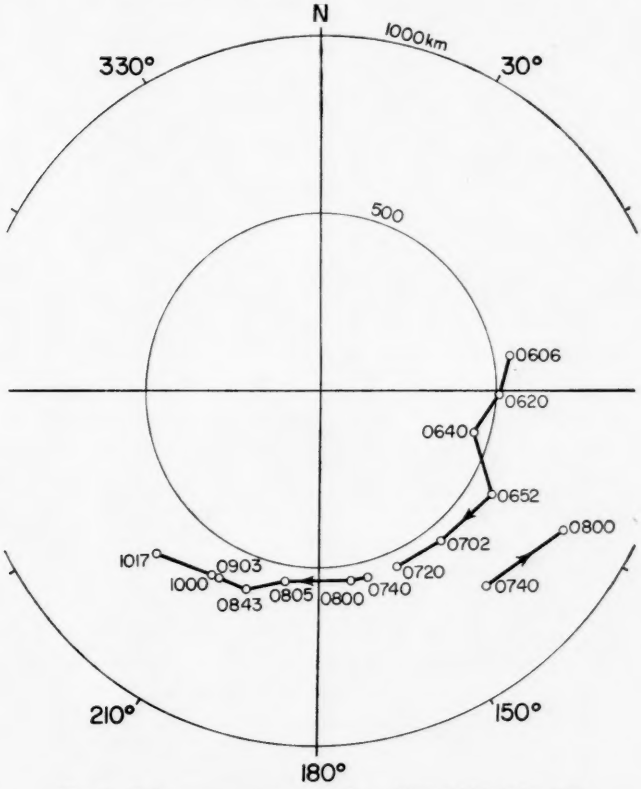

Fig. 7. Echo movement on 24 June 1958, 0606–1017 UT.

records, and the majority of echoes, although fluctuating in intensity and azimuth, appeared to be relatively stationary over long periods. Considering that the azimuthal spread might easily disguise some movements, plots were made of the centre bearing and minimum slant-range as a function of time. One such plot is shown for echoes on 24 June in polar form (Fig. 7). The lines show sequences of

echo movement which suggest a general trend in westerly direction. It is possible that different E_s clouds were being sampled during one trend, as the movement was not uniform and a particular echo occasionally faded out for a short time. The deduced speeds of movement of the E_s clouds are between 200 and 350 km/hr (55–100 m/sec).

The displays obtained on 19 May 1958, showed clear movement during the afternoon. A polar plot was prepared of the positions and movements of the echoes

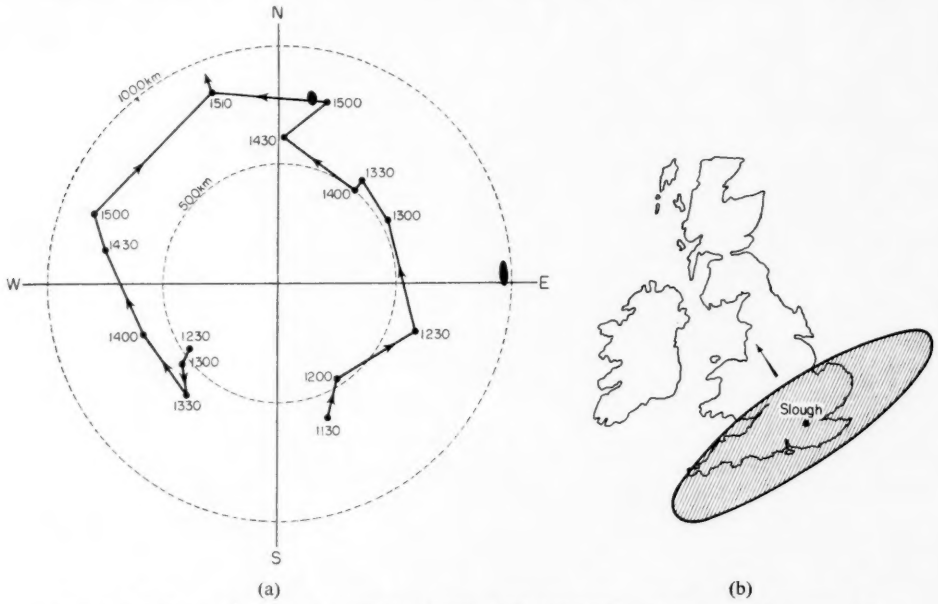

(a) (b)

Fig. 8. (a) Echo movement on 19 May 1958, 1130–1510 UT; (b) Shape and movement of E_s cloud deduced from (a).

throughout the day; a simplified form is shown in Fig. 8(a, b). Echoes first appeared at 0530 UT in a south-westerly direction and during the morning the minimum range decreased to about 500 km while echoes spread in azimuth to cover almost all bearings. The complex pattern clarified soon after noon. It was then possible to follow the movement of two simultaneous echoes until 1530 UT; these are shown in Fig. 8(a) with timing marks every $\frac{1}{2}$ hr. Between 1500 and 1530 hours the two echoes coalesced and faded out towards the north-west at a range of 820 km. No echoes were seen for about 1 hr afterwards, when a further complex pattern developed showing no significant trends.

It is of interest to compare the data with the simultaneous vertical incidence soundings at Slough. Ionization was shown at a height varying between 110 and 140 km during the morning. The corresponding critical frequencies were such that the minimum slant-ranges at 17 Mc/s would rarely fall below 1000 km until 0900 GMT. Between 0900 and noon, these ranges would be between 600 and 900 km. From about noon, however, the $\frac{1}{4}$ hr records showed ionization between 100 and 105 km with critical frequencies between 5·5 and 7·5 Mc/s. The corresponding

VOL. 18 196

slant-ranges would be between 500 and 700 km. After about 1445 UT the E ionization gradually disappeared.

The afternoon echo-pattern shown in Fig. 7 and the vertical incidence soundings might both be explained by the presence of a large region of E_s ionization drifting approximately from south-east to north-west. The vertical soundings show a maximum critical frequency between 1245 and 1330 UT. Between these times the polar display shows two echoes on a diameter through the origin, whose slant-ranges correspond to the critical frequencies observed overhead. As the region passes towards the north-west, the two echoes on the polar plot coalesce, while somewhat earlier the E_s ionization overhead decays.

The maximum ranges from which the two echoes were received were about 1000 km during the afternoon, and if the above explanation were valid, the NE–SW extent of the cloud would be approximately 1000 km with a considerably smaller extent along the direction of movement. The suggested configuration of the cloud is shown on a map in Fig. 8(b). The critical frequency would be about 7 Mc/s, and the speed of movement necessary to give the observed display would be about 150–200 km/hr (40–55 m/sec).

4. Fixed-Azimuth Observations

During the period August 1952–July 1953, daily back-scatter measurements were made at Slough on frequencies of 10, 11, 13, 15, 17, 19, 21, 23, 25 and 27 Mc/s using two rhombic aerials, directed 80° E of N and 289° E of N, respectively. Observations were made near noon UT throughout the whole period, with additional observations at 0900 and 1600 UT during July, August and September 1952. Some of the noon results have been discussed elsewhere (Shearman, 1956) but for the present purpose the data obtained with the 80° E of N aerial has been re-examined to obtain further statistical information about E_s occurrence. The information is perhaps of added interest because it refers to a year when E_s occurred more frequently than in 1957–1958.

A sample range–amplitude record obtained in this series of observations is shown in Fig. 1(a), in which the echoes are shown as vertical deflexions of the upper trace, and range markers displayed on the lower trace. The oblique ranges of the ground scattering sources can be measured by means of the 50 and 200 km markers, taking as reference the beginning of the transmitted pulse seen on the left.

Ground scatter propagated by way of sporadic-E is seen at between 550 and 900 km range, while the second group of echoes at 1250 to 1950 km is $F2$-layer propagated.

4.1. *Theoretical discussion*

When a directional aerial of fixed azimuth is employed for back-scatter E_s studies, the bearing of a cloud cannot be determined accurately. However, the amplitude of the observed echo is indicative of the bearing; the echo strength from a small cloud will be greatest when the cloud lies along the line of shoot of the aerial, and will decrease with deviation from this bearing in proportion to the squared voltage gain of the aerial. A complication is introduced, however, if the reflection coefficient at the E_s ionization varies from cloud to cloud. In the results given here,

no allowance has been made for echo amplitude, and the E_s clouds observed cannot therefore be assumed to lie along the great circle 80° E of N from Slough. However, a comparison of the individual observations in eastward and westward directions, and an examination of the time of day at which maximum occurrence of E_s is observed for the two directions shows that appreciable directivity is being maintained. From the calculated azimuthal polar diagram of the aerial, detection of clouds within $\pm 22°$ at 10 Mc/s and $\pm 12°$ at 25 Mc/s might be expected, while some clouds lying in the directions of the narrow first side lobes might also be detected.

Although directional information is lost, the multi-frequency technique enables the critical frequency of the ionization at a particular radial distance to be estimated by observing the frequency at which ground echoes from twice that distance disappear, and inserting the range and critical frequency in equation (1). Similarly the maximum critical frequency of the cloud can be estimated.

In applying this method, the angle of elevation for the range being studied should be compared with the vertical radiation pattern of the aerial at the frequency used to ensure that the echoes have not disappeared because of low aerial gain.

It should be stressed that these considerations are based on the assumption of a thin, dense layer for which the secant law is valid. A dependence of reflection coefficient on angle of incidence will modify the conclusions.

4.2. *Methods of analysis*

The records were analysed by noting, for each frequency, the occurrence of scattered echoes in each 100 km interval of range for all the records in 1 month. The resulting information for August 1952 is summarized in Fig. 9. The histograms show as a percentage of the total number of observing occasions, the echo occurrence plotted against range. A separate histogram is given for each transmitted frequency.

In the data presented in the former paper (Shearman and Martin, 1956) the histograms included short-range direct echoes from meteors and from persistent scattering centres in the *E*-layer. For the purposes of this paper the original records have been re-examined, and direct echoes, identifiable by pulse-like shape and short range, have been omitted from the statistics. Figs. 10 and 11, which show the seasonal and diurnal variation have been compiled from this new analysis.

4.3. *Variation of echoes with transmitted frequency*

Inspection of Fig. 9 shows that at the lowest frequency, 10 Mc/s, the E_s- and *F2*-propagated echoes overlap in range and cannot be distinguished; as the frequency is increased, however, the two modes become distinct as the *F2*-echoes increase in range up to the tangential-ray limit of 3000–4000 km. This behaviour is also apparent on a single day, and provides a method for identifying the modes of propagation.

It will be noticed that at the higher frequencies the percentage of occurrence of E_s echoes is lower than that at the lower frequencies, showing that penetration of some of the clouds is occurring between 10 and 25 Mc/s. Taking a fixed range of 1000 km (angle of incidence on the cloud of 76°), half the clouds appear to have been

VOL
18
196

penetrated at 17 Mc/s, indicating a median vertical incidence critical frequency of 17/(sec 76°) = 4 Mc/s. The corresponding measured vertical incidence median fE_s at Slough was 5·1 Mc/s.

On examining the records for particular days, it is found that the range of the leading edge of the E_s echo usually increases with frequency. This effect appears to

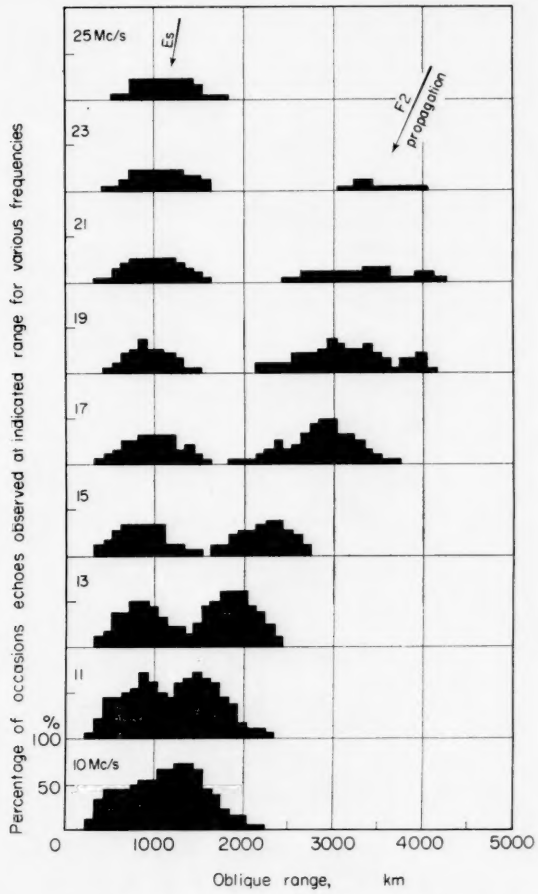

Fig. 9. Variation of occurrence of ground scatter with transmitted frequency, 1300 UT August 1952.

be due to properties of the clouds themselves, and not to be attributable to the reduction of the angle of elevation of the main lobe of the rhombic aerial. Assuming a thin, perfectly reflecting layer as in the model of Section 3.1, equation (1) can be used to determine the critical frequency of the cloud mid-way between the transmitter and the ground scattering point. In a particular example studied, the calculated critical frequency rose from 4·6 Mc/s at 225 km from Slough to 6·44 Mc/s at 475 km, the back edge of the echo indicating that the cloud extended to at least 875 km from Slough.

4.4. *Seasonal and diurnal changes*

To study seasonal and diurnal changes in E_s as seen by back-scatter, the histograms for 21 Mc/s have been selected from the data discussed in Section 4.3. At this frequency the *F2*-propagated echoes have increased in range sufficiently to be clearly distinguishable from the E_s echoes throughout the year.

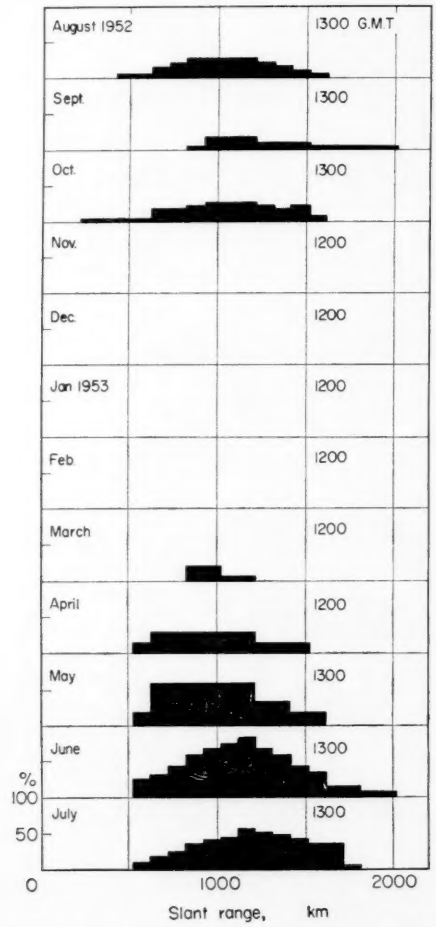

Fig. 10. Seasonal variation of E_s-propagated echoes. Percentage of occasions ground-scatter was observed at indicated range. Frequency 21 Mc/s, direction 80° E of N from Slough.

The histograms are presented in Fig. 10, from which it can be seen that no E_s propagation was observed between November 1952 and February 1953, while in May, June and July 1953, echoes were seen on over 50 per cent of the occasions.

The diurnal variation is shown in Fig. 11, which presents the histograms for 21 Mc/s at 0900, 1300 and 1600 UT in August and September 1952. A tendency for maximum E_s occurrence in the morning will be noticed; this is in agreement with

the P.P.I. results of Fig. 4. A time displacement of $\frac{1}{2}$ hr would be expected because the reflection points for the E_s seen by back-scatter are about 500 km to the east; this is much less than is required to explain the asymmetry about noon of the observations, as is also the difference between true noon and noon UT.

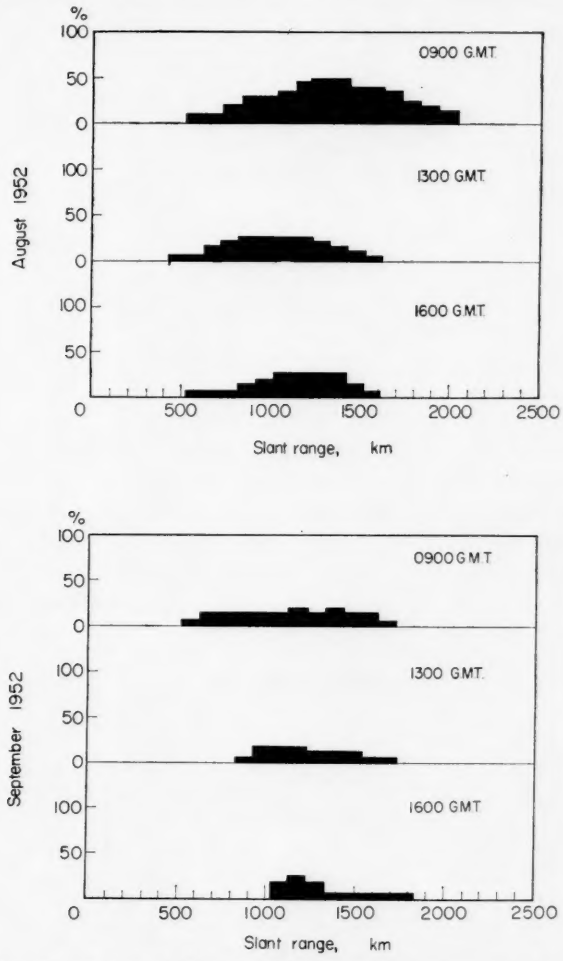

Fig. 11. Diurnal variation of E_s-propagated echoes. Percentage of occasions ground-scatter was observed at indicated range. Frequency 21 Mc/s, direction 80° E of N from Slough.

5. Conclusions

The back-scatter technique when applied to E_s studies, enables clouds within 600–700 km of the observing station to be detected, and enables a much larger sample of clouds to be observed than is possible with the vertical incidence technique. A rotating aerial and P.P.I. enables the geographical location of the clouds to be estimated and any movements followed.

There are two limitations at present. The finite aerial beam-width makes the estimation of the azimuthal extent of the cloud unreliable. Simultaneous amplitude measurement may enable this error to be reduced, but narrower beam-width would be a better solution. A second error arises from the skip-distance effect, and to overcome this, multi-frequency technique is required. The critical frequency of the ionization can then be measured as a function of radial distance from the sounder.

Results obtained at Slough, England, during the IGY with a 17 Mc/s rotating aerial and P.P.I. show the diurnal, seasonal and geographical variations of E_s occurrence. Tendencies for E_s to occur more frequently before noon and to the south of Slough are noted.

A detailed study of some individual days shows that under favourable conditions the size and critical frequency of clouds can be determined, even without multi-frequency observations. Some examples of cloud movements of 200–300 km/hr velocity have been identified.

A year's daily measurements obtained in 1952–1953 with fixed azimuth aerials and multi-frequency transmission show similar seasonal and diurnal trends, but reveal the advantages of the variable frequency facility for simultaneous measurement of critical frequency and range.

Acknowledgements—The work described above was carried out as part of the programme of the Radio Research Board and of the British National Committee of the International Geophysical Year. The paper was presented in September 1958, at a meeting on sporadic-*E* ionization held at Cambridge by the Ionospheric Research Committee of the NATO Advisory Group for Aeronautical Research and Development. It is published by permission of the Director of Radio Research of the Department of Scientific and Industrial Research.

References

Peterson A. M.	1957	*Annals of the IGY*. Vol. III, Part 4, p. 361. Pergamon Press, London.
Shearman E. D. R.	1956	*Proc. Instn Elect. Engrs* **103,** No. 8, 203.
Shearman E. D. R. and Martin L. T. J.	1956	*Wireless Engr* **33,** No. 8, 190.
Smith E. K., Jr.	1957	*A Study of Sporadic-*E *on a World-wide Basis.* National Bureau of Standards Circular 582.
Villard O. G., Jr. and Peterson A. M.	1952	*Transactions of the Institute of Radio Engineers* (*Professional Group on Antennas and Propagation*) PGAP-3, p. 186.

Journal of Atmospheric and Terrestrial Physics, 1960, Vol. 18, pp. 43 to 47. Pergamon Press Ltd. Printed in Northern Ireland

Spread-*F* in Baguio through half a solar cycle

V. Marasigan, S.J.
Manila Observatory, Baguio, Philippines

(*Received* 19 *September* 1959)

Abstract—A 6-year statistical survey is made of spread-*F* occurrence in Baguio. An attempt is made to explain the observed periodicity by the randomness of density–distribution introduced by the predominance of collision–detachment and by the random downward velocities.

Introduction

The phenomenon of spread echoes in the *F*-region has been the object of extensive investigations for the past two decades. Recent experiments by Bateman *et al.* (1959), positively establishing a correlation between spread-*F* and the Far East anomaly, have stimulated further study. With a view towards contributing to this aspect of the problem, a statistical survey is here made of the Baguio data on spread-*F*. It is hoped that such a survey may suggest additional clues with which to evaluate or supplement current theories.

VOL.
18
1960

Presentation of Data

Considered for this investigation are the nightly sequences of hourly ionograms at Baguio, from 1900 to 0800 hours (local time) inclusive, from January 1953 to December 1958. A count is made of those ionograms on which spread-*F* is present. (Spread-*F* is considered "present" when its intensity is sufficient to make the scaling of (*M*3000)*F*2 uncertain.) This count is divided by the number of ionograms in the group under consideration, and the quotient is the "percentage occurrence" for the group. Two groupings are made, an hourly grouping and a monthly grouping. The results of the first group are shown in Fig. 1. They clearly reveal a striking difference between the period 1953–1955 (years of low sunspot number) and the period 1956–1958 (high sunspot number). Consequently, both groups are further re-grouped and averaged according to their place in the solar-cycle, low and high. The graphs of these results are shown in Fig. 2. They have the following features: (1) maximum spread-*F* occurs at about 0100 hours and in summer of years of low sunspot count; (2) maximum spread-*F* occurs at about 2100 hours and in the equinoxes of years of high sunspot count; (3) spread-*F* occurs rarely in winter.

Theories of Spread-*F*

Any theory of spread-*F* must be consistent with the above trends. For instance, if the explaining mechanism is the *E*-region turbulence (Dagg, 1957), some parameter of this source and/or its ability to influence the *F*-region must vary with the periodicity described above. Alternatively, such periodicity must somehow fit in with the mechanism postulated by Martyn (1959) wherein the inhomogeneities are generated and dissipated by the tidal motions of the *F*-region under the influence of electrodynamic forces.

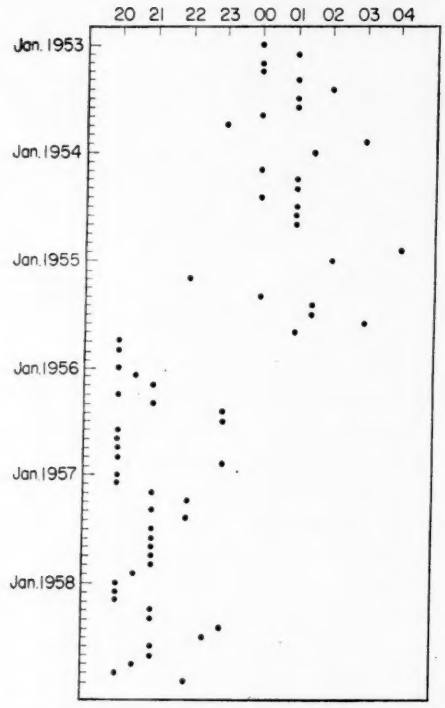

Fig. 1. Times of diurnal maxima of spread-F occurrence for each month.

If these and other current theories about spread-F should be found insufficient on this score, it would then be necessary to search for some subsidiary hypothesis with which to supplement them (but not necessarily to supplant them). Such a hypothesis is here proposed: it is suggested that inhomogeneities may result

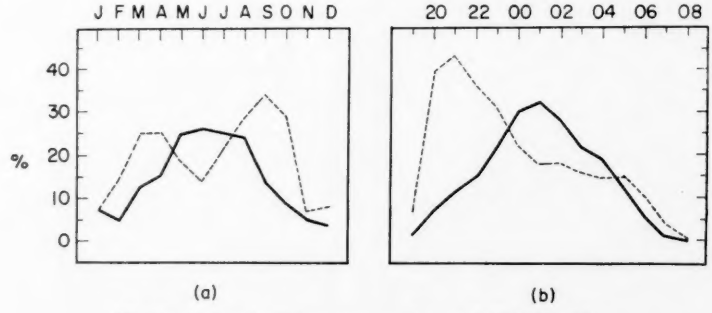

Fig. 2. Percentage occurrence of spread-F in Baguio.
(a) Seasonal variation. (b) Diurnal variation. Solid lines are for 1953–1955, years of low sunspot count. Broken lines are for 1956–1958, years of high sunspot count.

partly from randomness of the spatial distribution of electron-density due to the predominance of collision–detachment and to random drift of descending ionization.

Random Density–Distribution

A correlation is now sought between the periodicity in Fig. 2 and the periodicity of changes in $F2$ critical frequency and virtual height. The diurnal and seasonal maxima revealed in Fig. 2 suggest a basis for comparison with periods of increasing, decreasing or fairly steady values of f_0F2 and $h'F$. These periods are 2000–2200 hours and 0000–0200 hours for each of the four seasons of the year, for 1953–1955 (low sunspot count) and for 1956–1958 (high sunspot count). The results are compared with the corresponding percentage occurrence of spread-F and presented in Table 1.

Table 1. Comparison of spread-F occurrence with periods of increasing (+), decreasing (—) and steady (0) values of f_0F2 and $h'F$

Years	Sunspot count	Season	2000–2200 hours			0000–0200 hours		
			$\frac{d}{dt}(f_0F2)$	$\frac{d}{dt}(h'F)$	% spread	$\frac{d}{dt}(f_0F2)$	$\frac{d}{dt}(h'F)$	% spread
1953 to 1955	Low	Spring	—	+	10	—	—	20
		Summer	—	+	12	—	—	58
		Autumn	—	+	15	—	—	31
		Winter	—	0	6	—	0	8
1956 to 1958	High	Spring	+	—	50	—	—	20
		Summer	0	—	29	—	—	23
		Autumn	+	—	64	—	—	31
		Winter	0	—	22	—	0	8

In general, these figures indicate that spread-F occurs most frequently when the region is *descending* to lower levels, and even more so when its density is *increasing* at the same time (in spite of faster recombination and attachment at lower levels). From this and from the basic continuity equation applied to a given level z,

$$\left(\frac{\partial N}{\partial t}\right)_z = q - \alpha N^2 - \beta N + \frac{\partial}{\partial z}(Nv)$$

it can be shown that during the night hours, when photo-ionization $q = 0$ and the drift velocity v is downwards, spread-F occurs most frequently when

$$\frac{\partial}{\partial z}(Nv) > \alpha N^2 + \beta N$$

i.e. when, at each given level, electron-decay is overbalanced by electron-increase due to downward drift.

It will be recalled that the ionospheric layers are maintained in a dynamic equilibrium between production and decay of electrons, and that the main processes of production are solar photo-ionization and, to a less extent, detachment

of electrons from negative ions by collisions. During the night hours, with the cessation of solar radiation, collision–detachment predominates. Furthermore, when a region contracts, the mean free path decreases and the rate of collision–detachment increases. Since collisions are largely random, the resulting density should also be random. The range of randomness may be large or small compared with the average density of the region. When it is large, inhomogeneities result. Moreover, the downward drift velocity may itself be an average of widely random velocities, thus contributing further to an inhomogenous distribution.

The observed increase in average density of a descending region may then be explained as resulting from two connected processes: (1) because of the contraction resulting from downward drift, the ionization above the density-peak descends to lower levels and adds to the ionization therein; and (2) this contraction shortens the mean free path of ions and increases collision–detachment. Both are random processes.

Thus, when vertical drift contributes more electrons to a given level than can be removed by recombination and attachment, randomness predominates in the density–distribution of the region; the region is inhomogeneous.

It may reasonably be objected that empirical data require inhomogeneities with spatio-temporal dimensions larger than are possible with random density–distribution. This objection rests on two tacit assumptions: (1) that the inhomogeneities responsible for spread-F are themselves internally homogeneous; and (2) that they are relatively stable in time. These two assumptions may not be absolutely necessary. It may be possible to show from theoretical considerations: (1) that the overdense blob causing spread-F may be composed of many small blobs of unequal densities with a high average; and (2) that these small blobs may be appearing and disappearing in cycles of the order of milliseconds, such that probing signals pulsed at the rate of some microseconds are reflected or refracted. An alternative possibility is that a small blob of high density can, due to a density-dependent rate of collision–detachment, be self-amplifying in a chain-reacting fashion, and so will tend to expand until it is effectively moderated by recombination, attachment or cooling. If either alternative is correct, random density–distribution is a contributing factor in spread-F occurrence. Otherwise, the hypothesis is admittedly untenable.

VOL
18
196

Further Investigations

The preceding paragraph raises theoretical problems that may well be examined more analytically.

Also, the importance of magnetic activity in the study of spread-F at Ibadan has been convincingly shown by Lyon *et al.* (1958). It is hoped that a similar study of the Baguio data may be made in the near future.

Acknowledgements—This study arose out of detailed discussions with Father J. J. Hennessey, S.J., Director of the Manila Observatory, and with Father F. Glover, S.J., currently with the U.S. National Bureau of Standards, Boulder, Colorado.

References

Bateman R., Finney J. W., Smith E. K., Tveten L. H. and Watts J. M.	1959	*J. Geophys. Res.* **64,** 403.
Dagg M.	1957	*J. Atmosph. Terr. Phys.* **11,** 139.
Lyon A. J., Skinner N. J. and Wright R. W.	1958	*Nature, Lond.* **181,** 1724.
Martyn D. F.	1959	*Proc. Inst. Radio Engrs, N.Y.* **47,** 147.

OL.
18
960

Journal of Atmospheric and Terrestrial Physics, 1960, Vol. 18, pp. 48 to 60. Pergamon Press Ltd. Printed in Northern Ireland

Theoretical world curves of maximum ion density in a quiet *F*-region

J. E. C. Gliddon and P. C. Kendall*
Department of Mathematics, Queen Mary College, Mile End Road, London, E.1

(*Received* 20 *October* 1959)

Abstract—The global variation of electron density in the *F2*-region is investigated on the assumption of uniform temperature, uniform attachment-type law of recombination, a diffusion coefficient varying inversely as the density of neutral particles and a Chapman ionization law. Electron density is calculated as a function of altitude and of local time at a number of different latitudes for the equinox and solstices. World curves of maximum ion density are deduced and compared with Millington's curves. The curves presented here are "drawn out" in the east–west direction as appears to be the case with the corresponding curves obtained by ionosonde methods. Although the latter are plotted against the geomagnetic latitudes, this broad similarity seems to indicate that diffusion plays a sigificant part in the control of *F2*-ionization.

1. Introduction

This paper is the first of a series on the *F2*-region of the ionosphere. It is an extension of a recent paper by Ferraro and Özdogan (1958) in which the effect on the vertical distribution of ionization in an isothermal Chapman region was discussed. They assumed that electrons disappeared according to an attachment-type law of recombination, the attachment coefficient K being a constant and confined their investigation to the equator at the equinox. In the present paper we extend these results, with the same physical assumptions, to cover latitudes 30°, 60° and 75°, both at the equinox and at the solstice. Curves are drawn to show the diurnal variation of electron density at different altitudes and these have been used to construct curves to show the global variation of maximum electron density $N_E(\max)$.

2. Derivation of Equations

The electron density $N(z, t)$ at height z and time t (measured in seconds from sunrise) satisfies the equation (Ferraro and Özdogan)

$$\frac{\partial N}{\partial t} = q - KN + D\left(\frac{\partial^2 N}{\partial z^2} + \frac{3}{2H}\frac{\partial N}{\partial z} + \frac{N}{2H^2}\right). \tag{1}$$

The coefficient of diffusion D is assumed to be of the form b/n where b is a constant for the region considered and n, the density of neutral molecules, is assumed to be given by

$$n = n_0 \exp\left(-\frac{z - z_0}{H}\right). \tag{2}$$

Here, n_0 is the density of neutral molecules at height z_0, the height of maximum ion production, and H is the scale height for the region.

* Bedford College, Regent's Park, London, N.W.1.

The rate of ion-production q is given by the Chapman function:

$$q = q_0 \exp\left\{1 - \frac{z - z_0}{H} - \sec\chi \,.\, \exp\left(-\frac{z - z_0}{H}\right)\right\} \tag{3}$$

wherein χ denotes the zenith distance of the sun from the point of observation. This formula holds for $0 < |\chi| < \frac{1}{2}\pi$, which corresponds to hours of sunlight. When $\frac{1}{2}\pi < |\chi| < \pi$ (hours of darkness), q is assumed to be identically zero.

Consider an observer whose colatitude is $\theta(0 < \theta < \pi)$, and let the northern declination of the sun be δ. Then the local time ϕ', measured in radians from midday, is given in terms of χ by the equation

$$\cos\chi = \sin\delta\cos\theta + \cos\delta\sin\theta\cos\phi'. \tag{4}$$

The length of day ψ is then given by

$$0 = \sin\delta\cos\theta + \cos\delta\sin\theta\cos\tfrac{1}{2}\psi \tag{5}$$

and the day-time range of values of ϕ' is

$$\tfrac{1}{2}\psi > \phi' > -\tfrac{1}{2}\psi. \tag{6}$$

It is convenient to measure local time from sunrise. If ϕ is the local time measured in radians from sunrise and if t is the same time measured in seconds we have

$$t = 1{\cdot}37 \times 10^4\phi = k\phi \tag{7}$$

where

$$\phi = \tfrac{1}{2}\psi + \phi'. \tag{8}$$

The day-time range of values of ϕ is, from (6) and (8),

$$0 < \phi < \psi \tag{9}$$

while hours of darkness correspond to the range

$$\psi < \phi < 2\pi. \tag{10}$$

The rate of ion production q is now defined in terms of ϕ through the equations (3), (4), (8), (9) and (10).

3. Solution of the Equation

The periodic solution of (1) can be obtained conveniently (Gliddon, 1959) in terms of the appropriate Green's function. The substitution (7), together with

$$\zeta^2 = \exp\left(-\frac{z - z_0}{H}\right) \tag{11}$$

and

$$N = \zeta u \exp(-kK\phi) \tag{12}$$

transform (1) into

$$\frac{\partial^2 u}{\partial\zeta^2} - 4\gamma\frac{\partial u}{\partial\phi} = -4\gamma\, kq\,\zeta^{-1}\exp(kK\phi) \tag{13}$$

where

$$\gamma = n_0H^2/kb. \tag{14}$$

The Green's function for (13), satisfying the conditions of vanishing when $\zeta \to 0$ and when $\zeta \to \infty$ is shown to be

$$G(\zeta_0, \phi_0|\zeta, \phi) = \pi^{-1/2}\left(\frac{\gamma}{\phi - \phi_0}\right)^{1/2}\left[\exp\left\{-\frac{\gamma(\zeta_0 - \zeta)^2}{\phi - \phi_0}\right\} - \exp\left\{-\frac{\gamma(\zeta + \zeta_0)^2}{\phi - \phi_0}\right\}\right] \tag{15}$$

and the periodic solution of (13) takes the form

$$u = k\int_0^{\phi} \exp(kK\phi_0)\, d\phi_0 \int_0^{\infty} G(\zeta_0, \phi_0|\zeta, \phi) q\zeta_0^{-1}\, d\zeta_0 + \\ + k\sum_{m=1}^{\infty}\int_0^{2\pi} \exp\{kK(\phi_0 - 2m\pi)\}\, d\phi_0 \int_0^{\infty} G(\zeta_0, \phi_0 - 2m\pi|\zeta, \phi) q\zeta_0^{-1}\, d\,\zeta_0 \tag{16}$$

where, in the present case,

$$q = q_0 e\zeta_0^2 \exp(-\zeta_0^2 \sec\chi). \tag{17}$$

The integrations with respect to ζ_0 can be effected, to give

$$\int_0^{\infty} G(\zeta_0, \phi_0|\zeta, \phi) q\zeta_0^{-1}\, d\zeta_0 = q_0 e\zeta\{1 + [(\phi - \phi_0)/\gamma]\sec\chi\}^{-3/2} \times \\ \times \exp\left\{-\frac{\zeta^2 \sec\chi}{1 + \{(\phi - \phi_0)/\gamma\}\sec\chi}\right\}$$

and similar results are obtained by writing $\phi_0 - 2m\pi$ in place of ϕ_0. Thus the required solution can be written

$$N(\zeta, \phi) = kq_0 e\zeta^2 \int_0^{\phi}\left(\frac{\cos\chi}{\Delta_0}\right)^{3/2} \exp\left\{-kK(\phi - \phi_0) - \frac{\zeta^2}{\Delta_0}\right\} d\phi_0 + \\ + kq_0 e\zeta^2 \sum_{m=1}^{\infty}\int_0^{\psi}\left(\frac{\cos\chi}{\Delta_m}\right)^{3/2} \exp\left\{-kK(\phi + 2m\pi - \phi_0) - \frac{\zeta^2}{\Delta_m}\right\} \tag{18}$$

where
$$\Delta_m = \cos\chi + (\phi + 2m\pi - \phi_0)/\gamma, \qquad m = 0, 1, 2, \ldots \tag{19}$$

and the limits $(0, 2\pi)$ have been replaced by $(0, \psi)$ in virtue of (9) and (10).

4. The Density, Temperature and the Diffusion Coefficient in the *F2*-region

In our calculations we have taken z_0, the height of maximum ion-production, to be 300 km. The reason for this is that according to the theory presented here, the midday maximum of the electron density occurs at heights lying in the range $z_0 \pm 0{\cdot}25\, H$; and according to recent experimental evidence $h_m F2$ is believed to be in the region of 270 km in temperate latitudes. The density at 300 km, according to the interim atmosphere derived from satellite data (Harris and Jastrow, 1958), may be taken to be $7{\cdot}5 \times 10^{-14}$ g/cm^3. Assuming a mean molecular mass of $39{\cdot}8 \times 10^{-24}$ g, which implies that the oxygen is completely dissociated, we obtain a number density n_0 which is approximately 2×10^9/cm^3. The temperature of the layer is taken to be 1400°K, corresponding to a scale height of 54 km. This compares with about 80 km. quoted for the model atmosphere mentioned above. Presumably this higher figure was arrived at by assuming a smaller mean molecular

mass. Calculations on night-time N–h profiles (DUNCAN, 1958) gave a scale height of 55 km at the 300 km level.

With regard to the value of the diffusion coefficient, we have taken the parameter γ to be unity. From (14), we see that this implies $n_0 D = 4{\cdot}3 \times 10^{18}$. This may be compared with the value $n_0 D = 2 \times 10^{18}$ obtained by DALGARNO (1958) from results on the mobility of oxygen ions moving in atomic oxygen.

Lastly our calculations have been repeated for two different values of the attachment coefficient represented by $kK = \frac{1}{2}$ and $kK = 1$. The first of these represents an attachment coefficient $K = 0{\cdot}37 \times 10^{-4}\,\mathrm{sec}^{-1}$, which may be compared to the value $10^{-4}\,\mathrm{sec}^{-1}$ suggested for the 300 km. level by RATCLIFFE *et al.* (1956). The numbers of the diagrams relating to these two cases will be distinguished by the letters (a) and (b), respectively.

5. NUMERICAL ILLUSTRATIONS

For each of the values $\delta = 0°$ (equinox), $\delta = 23\frac{1}{2}°$ (solstice) of the sun's declination we have calculated the diurnal variation of N for latitudes given by $\theta = 15°$, $30°$, $60°$ $90°$, $120°$ and $150°$. Figs. 1(a) to 4(a) and Figs. 1(b) to 4(b)

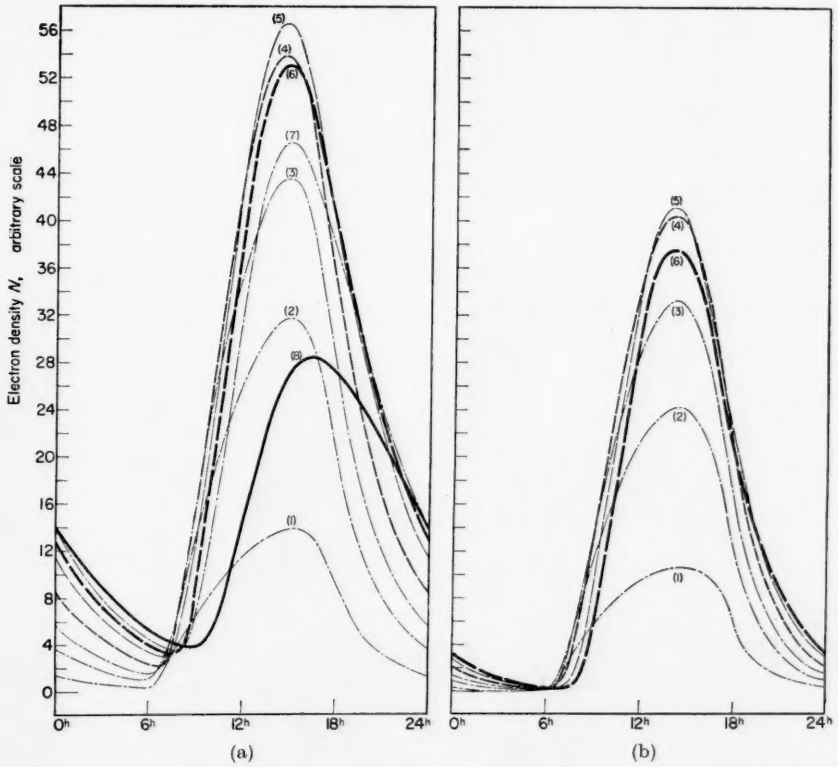

Fig. 1. Equinox at equator: (a) $kK = \frac{1}{2}$, $\delta = 0°$, $\theta = 90°$; (b) $kK = 1$, $\delta = 0°$, $\theta = 90°$. The curves represent values of $(z - z_0)/H$: (1) 2·0; (2) 1·0; (3) 0·5; (4) 0; (5) −0·5; (6) −0·75; (7) −1·0; (8) −1·5.

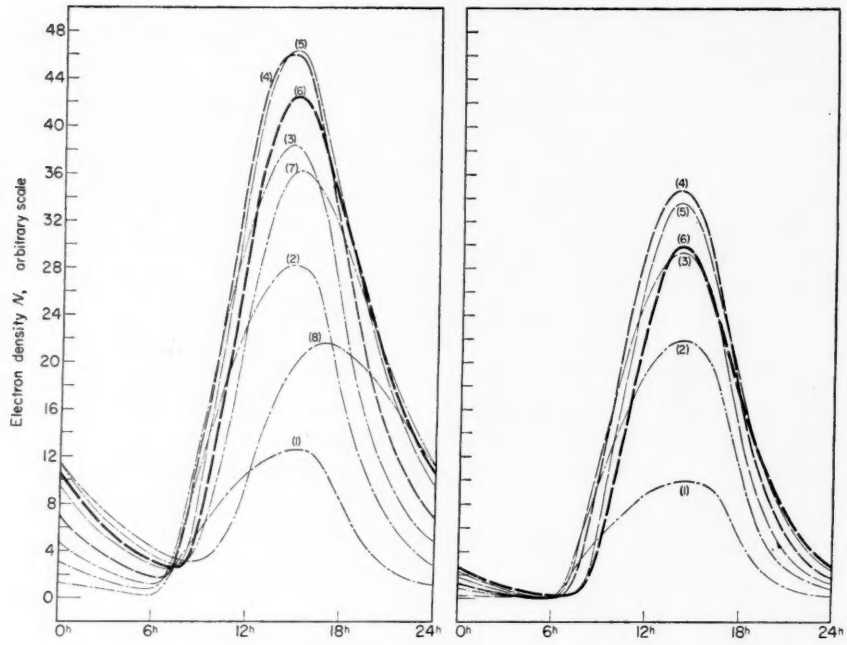

Fig. 2. Equinox at latitude 30°N: (a) $kK = \frac{1}{2}$, $\delta = 0°$, $\theta = 60°$; (b) $kK = 1$, $\delta = 0°$, $\theta = 60°$. The curves represent values of $(z - z_0)/H$: (1) 2·0; (2) 1·0; (3) 0·5; (4) 0; (5) −0·5; (6) −0·75; (7) −1·0; (8) −1·5.

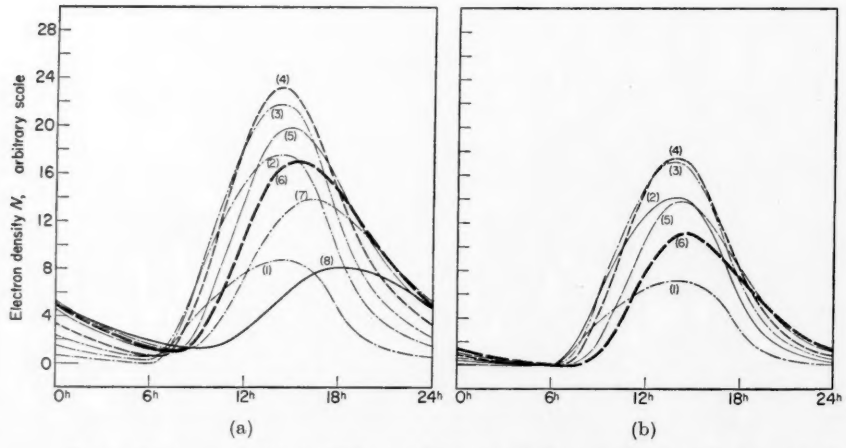

Fig. 3. Equinox at latitude 60°N: (a) $kK = \frac{1}{2}$, $\delta = 0°$, $\theta = 30°$; (b) $kK = 1$, $\delta = 0°$, $\theta = 30°$. The curves represent values of $(z - z_0)/H$: (1) 2·0; (2) 1·0; (3) 0·5; (4) 0; (5) −0·5; (6) −0·75; (7) −1·0; (8) −1·5.

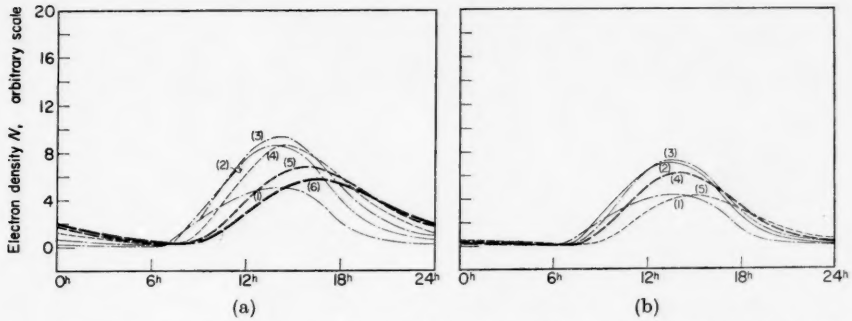

Fig. 4. Equinox at latitude 75°N: (a) $kK = \frac{1}{2}$, $\delta = 0°$, $\theta = 15°$; (b) $kK = 1$, $\delta = 0°$, $\theta = 15°$. The curves represent values of $(z - z_0)/H$: (1) 2·0; (2) 1·0; (3) 0·5; (4) 0; (5) −0·5; (6) −0·75.

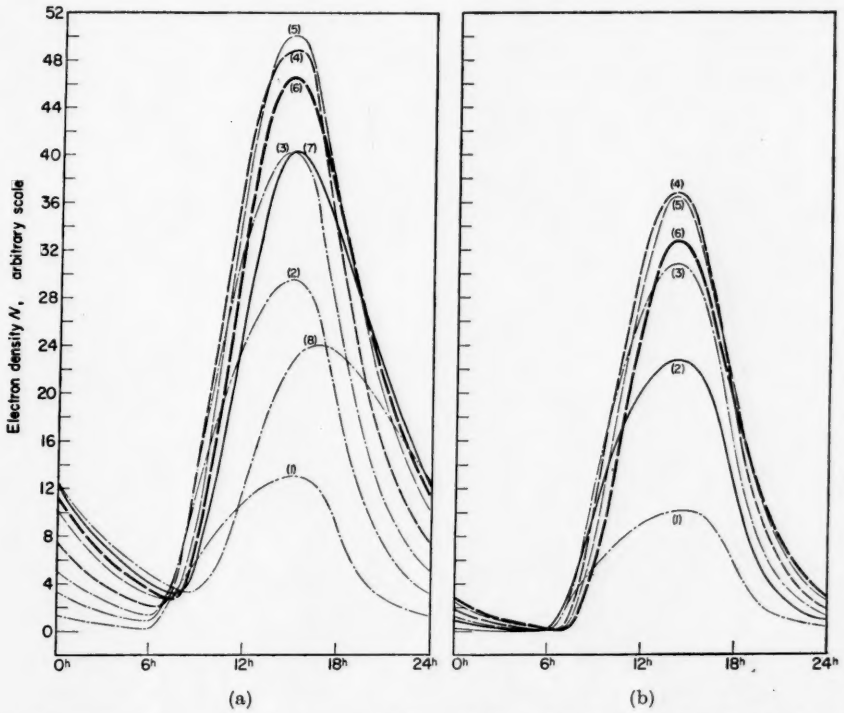

Fig. 5. Northern summer at equator: (a) $kK = \frac{1}{2}$, $\delta = 23{\cdot}5°$, $\theta = 90°$; (b) $kK = 1$, $\delta = 23{\cdot}5°$, $\theta = 90°$. The curves represent values of $(z - z_0)/H$: (1) 2·0; (2) 1·0; (3) 0·5; (4) 0; (5) −0·5; (6) −0·75; (7) −1·0; (8) −1·5.

show the diurnal variation of N for various heights at different latitudes at the equinox. (The scale chosen for N is the same in all diagrams but does not represent absolute values.) It will be noted that the peak electron density decreases steadily from the equator towards the poles. At the same time the level at which the peak

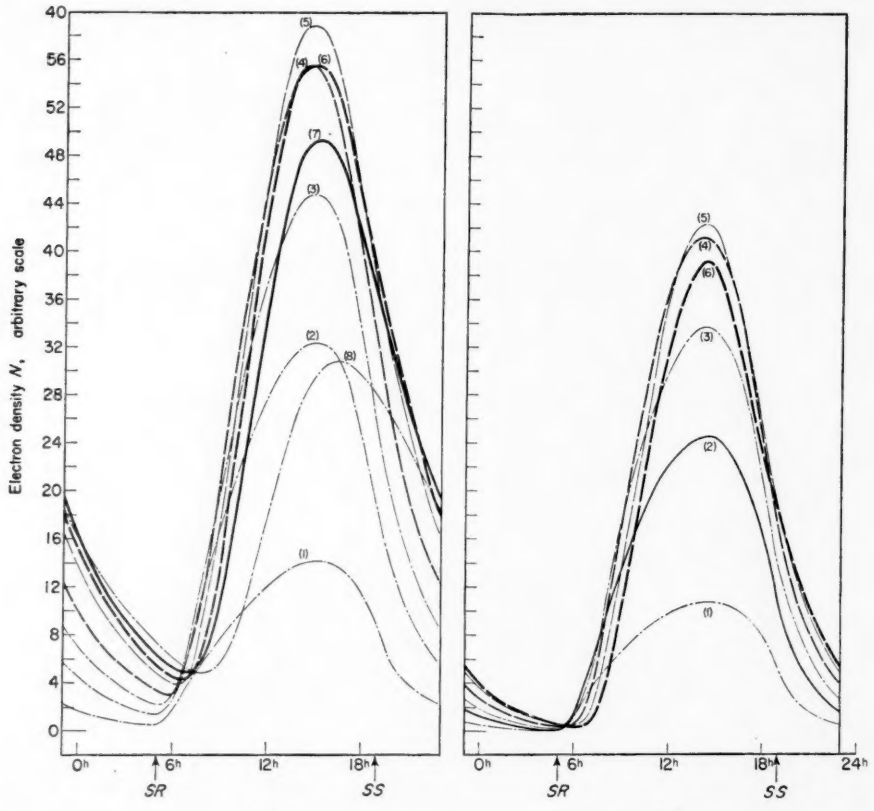

Fig. 6. Northern summer at latitude 30°N: (a) $kK = \frac{1}{2}$, $\delta = 23{\cdot}5°$, $\theta = 60°$; (b) $kK = 1$, $\delta = 23{\cdot}5°$, $\theta = 60°$. The curves represent values of $(z - z_0)/H$: (1) 2·0; (2) 1·0; (3) 0·5; (4) 0; (5) −0·5; (6) −0·75; (7) −1·0; (8) −1·5.

occurs rises from about one-half a scale height below to one-half a scale height above, the level of maximum ion production.

Figs. 5(a) to 10(a) and Figs. 5(b) to 10(b) are corresponding curves for the northern summer solstice. Peak electron density occurs, as may be expected, in the vicinity of the overhead sun. There is a slow decrease towards the north but a rapid decrease south of the equator. In summer the height of the peak remains about one-third of a scale height below the level of maximum ion production while in winter it rises above this level. In general, ionospheric observations of the *F2*-region show tendencies which are the reverse of these.

The world curves of maximum ionization, Figs. 11(a), 11(b), 12(a), 12(b), may be compared with the theoretical curves drawn by MILLINGTON (1932) and, with

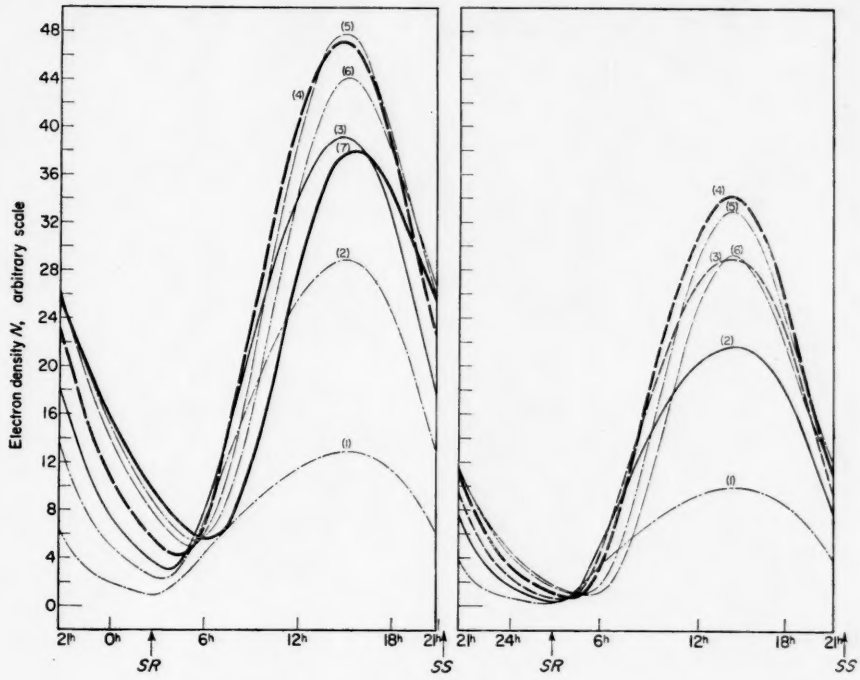

(a) (b)

Fig. 7. Northern summer at latitude 60°N: (a) $kK = \frac{1}{2}$, $\delta = 23{\cdot}5°$, $\theta = 30°$; (b) $kK = 1$, $\delta = 23{\cdot}5°$, $\theta = 30°$. The curves represent values of $(z - z_0)/H$: (1) 2·0; (2) 1·0; (3) 0·5; (4) 0; (5) −0·5; (6) −0·75; (7) −1·0.

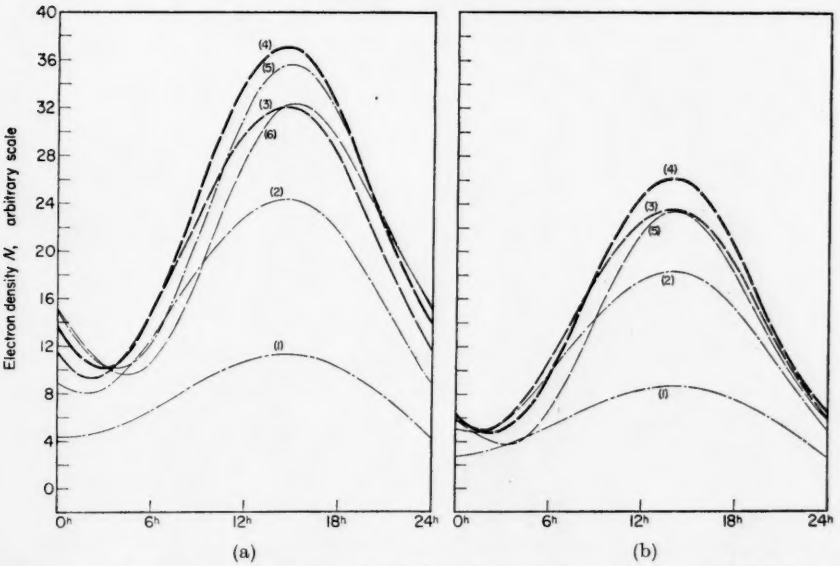

(a) (b)

Fig. 8. Northern summer at latitude 75°N: (a) $kK = \frac{1}{2}$, $\delta = 23{\cdot}5°$, $\theta = 15°$; (b) $kK = 1$, $\delta = 23{\cdot}5°$, $\theta = 15°$. The curves represent values of $(z - z_0)/H$: (1) 2·0; (2) 1·0; (3) 0·5; (4) 0; (5) −0·5; (6) −0·75.

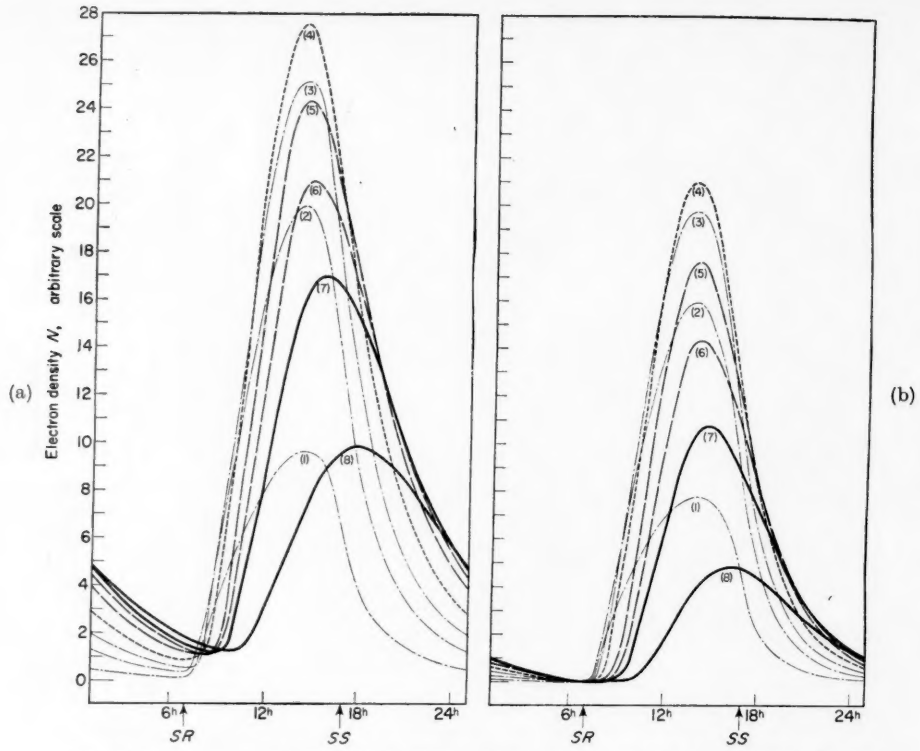

Fig. 9. Northern summer at latitude 30°S: (a) $kK = \frac{1}{2}$, $\delta = 23{\cdot}5°$, $\theta = 120°$; (b) $kK = 1$, $\delta = 23{\cdot}5°$, $\theta = 120°$. The curves represent values of $(z - z_0)/H$: (1) 2·0; (2) 1·0; (3) 0·5; (4) 0; (5) −0·5; (6) −0·75; (7) −1·0; (8) −1·5.

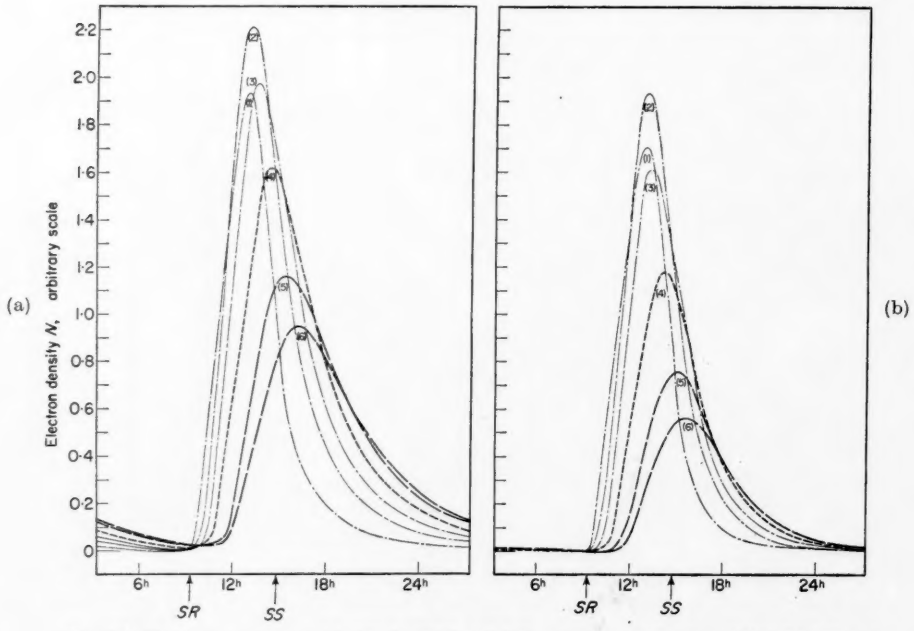

Fig. 10. Northern summer at latitude 60°S: (a) $kK = \frac{1}{2}$, $\delta = 23{\cdot}5°$, $\theta = 150°$; (b) $kK = 1$, $\delta = 23{\cdot}5°$, $\theta = 150°$. The curves represent values of $(z - z_0)/H$: (1) 2·0; (2) 1·0; (3) 0·5; (4) 0; (5) −0·5; (6) −0·75.

the curves of f_0F2 Figs. 13, 14 constructed by MARTYN (1959) from ionosonde data gathered from a number of observatories. MILLINGTON's curves may be considered applicable to the $F1$-region, since he assumes a quadratic law of electron *recombination* whereas we have assumed an attachment-type law. Also, his results ignore the effect of diffusion.

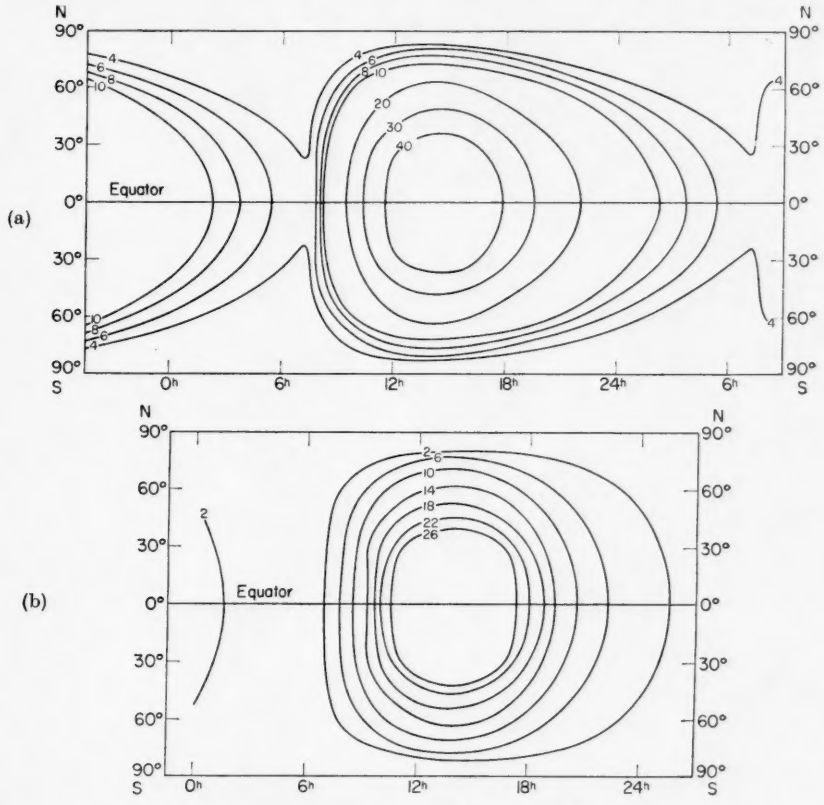

Fig. 11. Equinox: (a) $kK = \frac{1}{2}$; (b) $kK = 1$.

Figs. 11(a) and 11(b) show a general resemblance to MILLINGTON's curves for the equinox, the main feature being the system of closed contours surrounding a point near the overhead sun. The most noticeable difference is the drawing out of our curves in the longitudinal direction. In this respect our results are more in agreement with the curves drawn by MARTYN.

Our curves for the northern summer solstice (Figs. 12a and b), again show a general resemblance to the corresponding curves drawn by MILLINGTON. MARTYN's solstitial curves are dominated by the Appleton anomalous equatorial peaks of ionization. These are entirely absent from our results. However, the contours surrounding these peaks are very similar in shape to ours. In place of the tricorne which lies across the geomagnetic equator in MARTYN's curves we have a system of wedges. A rather similar wedge system exists in MILLINGTON's curves. The apex of a

wedge corresponds approximately to the local time of sunrise. A point in which all the theoretical curves differ from the practical curves is in the *range* of N_{max}. Where the practical curves show a threefold increase in N_{max}, the theoretical curves show a tenfold (or even greater) increase.

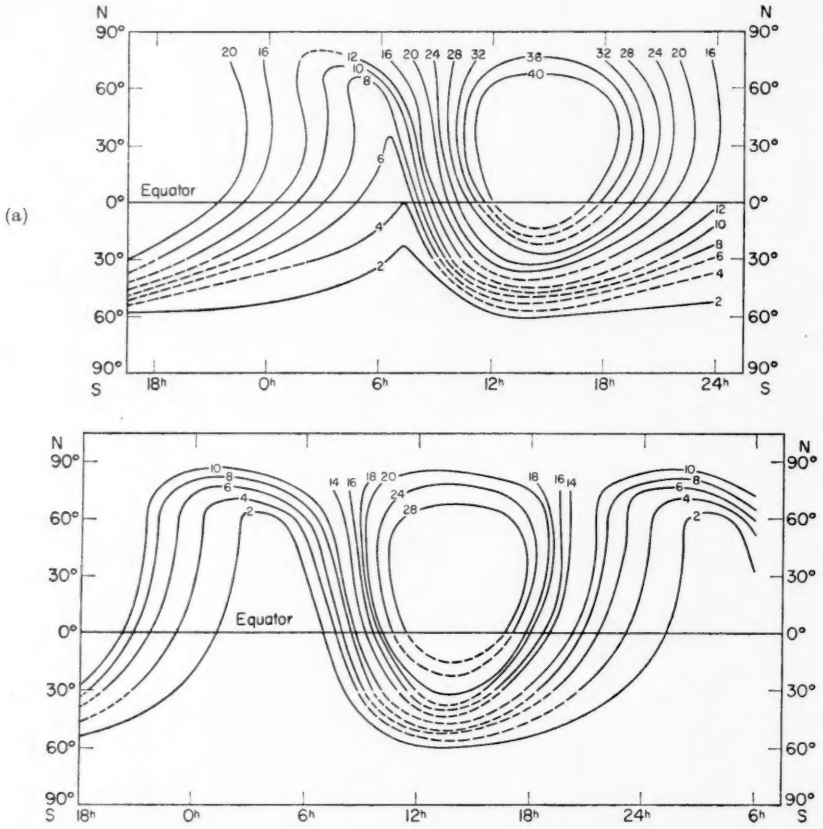

Fig. 12. Northern summer solstice: (a) $kK = \frac{1}{2}$; (b) $kK = 1$.

6. CONCLUSION

Our discussion has been restricted to consideration of the effect of diffusion on an ionized region in which the electrons disappear according to an attachment-type law. Since no account is taken of the geomagnetic control of ionization the results obtained serve to give a datum line from which the geomagnetic distortion may be measured.

The curves for the global distribution of N_{max} have been drawn and compared with MILLINGTON's curves. The curves presented here are drawn out in the east–west direction in a manner similar to the corresponding curves obtained by ionosonde methods plotted against geomagnetic latitude. The curves confirm that diffusion is an important controlling factor in the *F2*-region. Comparison

of the global distribution for the two cases $kK = \frac{1}{2}$ and $kK = 1$ suggests that the world distribution of N_{max} may be rather sensitive to the changes in the value chosen for K. It seems very likely that, as RATCLIFFE *et al.* (1956) have shown,

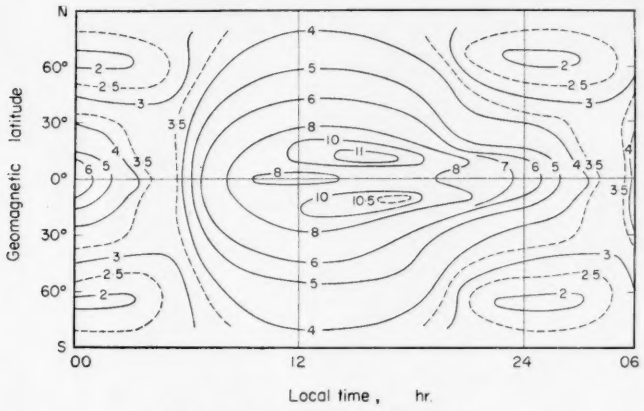

Fig. 13. Equinox f_0F2 1943–1944.

electrons in the $F2$-region disappear according to an attachment type of law with an attachment coefficient $K = 10^{-4} \exp\{(300 - z)/50\}$ sec^{-1}. If this is so, since we have assumed a constant coefficient of attachment, our results may be expected to differ from observed values on this account. In a later paper we hope

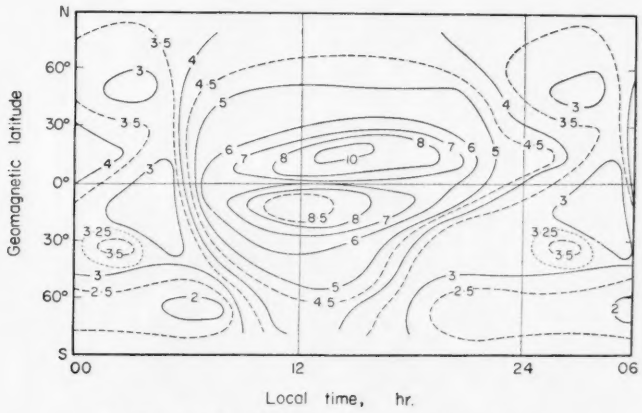

Fig. 14. Northern solstice f_0F2 1943–1944.

to consider the case of variable attachment coefficient, and also the effect of the geomagnetic field and transport terms.

Acknowledgements—We should like to thank Professor V. C. A. FERRARO, who suggested this investigation. Our thanks are also due to Mr. J. V. FALL who gave help and advice in preparing the programme for this work, which was carried out on a Ferranti "Pegasus" computer.

REFERENCES

DALGARNO A.	1958	*J. Atmosph. Terr. Phys.* **12,** 219.
DUNCAN R. A.	1958	*J. Geophys. Res.* 63, 491.
FERRARO V. C. A. and ÖZDOGAN I.	1958	*J. Atmosph. Terr. Phys.* **12,** 140.
GLIDDON J. E. C.	1959	*Quart. J. Mech.* **12,** No. 3, 347.
HARRIS J. and JASTROW R.	1958	*An Interim Atmosphere derived from Rocket and Satellite data.* U.S. Naval Research Laboratory, Washington, D.C.
MARTYN D. F.	1959	*Proc. Inst. Radio Engrs, N.Y.* **47,** 147.
MILLINGTON G.	1932	*Proc. Phys. Soc. Lond.* **44,** 580.
RATCLIFFE J. A., SCHMERLING E. R., SETTY C. S. G. K. and THOMAS J. O.	1956	*Phil. Trans.* A **248,** 621.

Journal of Atmospheric and Terrestrial Physics, 1960, Vol. 18, pp. 61 to 64. Pergamon Press Ltd. Printed in Northern Ireland

The "valley effect" in the interpretation of ionospheric eclipse records

J. A. GLEDHILL and A. D. M. WALKER
Dept. of Physics, Rhodes University, Grahamstown, South Africa

(*Received* 22 *November* 1959)

Abstract—It is shown that if a valley develops between the *F1*- and *F2*-layers during an eclipse it produces characteristic effects on the curves of electron density at fixed heights vs. time deduced from the ionograms. These curves show spurious maxima which are greatest at heights just above the valley and decrease with increasing height. The effects predicted correspond closely to those observed in South Africa during the eclipse of 25 December 1954.

VOL. 18 1960

IN A recent paper GLEDHILL (1959) has reported the results of a computation of the effects of a solar eclipse on a stratified model ionosphere. With reasonable assumptions as to the variation of the electron density and the recombination coefficient with height, he has shown that a minimum in the electron density may develop between the *F1*- and *F2*-layers during the second half of the eclipse. In the present paper we discuss the effect of this minimum, or valley, on the records taken with an ordinary swept-frequency ionosonde, and the errors which are produced when these records are interpreted in the normal way.

In the initial stages of the present work, the paths of rays which returned to the transmitter were plotted on the map described by GLEDHILL (1959) neglecting the effect of the earth's magnetic field. It was found that the points of reflection of such rays in the ionosphere deviated from the zenith only by a few kilometres, except very close to the critical frequency for the layer. The virtual heights and electron densities which would have been deduced from ionosonde records on the assumption that reflection took place at vertical incidence did not differ significantly from the actual conditions overhead. This lends some support to MINNIS's contention that errors due to non-vertical reflection are usually negligible (MINNIS 1958).

It was therefore possible to neglect the effects of deviation of the reflection point from the zenith, and to deduce the form of the ionogram which would be obtained at any time during the eclipse merely by evaluating numerically the time delay of the echo, using the curves of electron density vs. height given in Fig. 2 of GLEDHILL's (1959) paper. This was done by calculating the group propagation time $\Delta s/\mu$ for successive thin slabs Δs of the ionosphere, over each of which the refractive index μ was considered to be constant and equal to the value corresponding to the average electron density in the slab. By summing these times from the ground to the level in the ionosphere at which μ vanished the time delay of the returned pulse was found. By repeating the computation for a number of frequencies the form of the ionogram could be plotted.

The resulting "synthetic" ionograms were then scaled by the normal KELSO

(1952) technique, again neglecting the effect of the earth's magnetic field. It was necessary to scale the ionograms for a fairly large number of frequencies in order to eliminate scatter in the electron density vs. true height points due to the effect of sampling frequencies which fell near to cusps (PIGGOTT, 1954). The electron density vs. true height curves which would have been deduced by this method from the ionogram were thus found. These differed from the true curves of GLEDHILL's Fig. 2 because the ionograms gave no indication of the existence of the valley, and the Kelso method of scaling them assumes a monotonic increase of electron density with height. Fig. 1 shows the true electron distribution curve

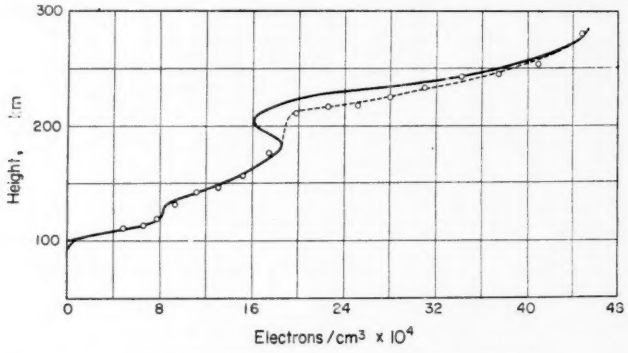

Fig. 1. Electron density profiles 130 min after first contact. Full line, true profile; dashed line, profile deduced by KELSO's method.

for 130 min after the start of the eclipse and also the distribution deduced from the corresponding ionogram by the Kelso method.

By reading off the electron densities at fixed heights from the electron distribution curves so deduced, graphs were plotted showing the apparent variation of electron density at these heights during the eclipse. The set of curves so obtained is shown in Fig. 2, together with the true variations at the same heights from Fig. 1 of GLEDHILL's paper. It will be seen that the effect of the valley is to cause the apparent electron density at all heights above it to increase shortly after the middle of the eclipse. The effect of the valley is naturally greatest for frequencies just above the critical frequency of the *F1*-layer, where the retardation produced by the ionization in the valley is greatest. This in turn means that the error in the curves of electron density vs. time is greatest for heights just above the valley where the plasma frequency just exceeds that at the *F1*-maximum, and decreases for greater heights, where the plasma frequency is higher. As Fig. 2 shows, this can produce a large apparent maximum in electron density in the lower *F2*-region during the second half of the eclipse, with a return to normal some time after the optical eclipse is over. At greater heights the effect is smaller, but still very noticeable. At 200 km, which falls in the valley, the apparent curve is very deceptive, looking rather like the true one but having much too rapid a recovery after the minimum. Below the valley, of course, the apparent curves would coincide with the true ones.

Comparison of these curves with those found experimentally by SZENDREI and

VOL. 18 196

McElhinny (1956) and shown in Figs. 6 and 7 of their paper, shows a remarkable similarity. The resemblance of the maxima found during the second half of the eclipse to those in our Fig. 2 is so striking as to leave little doubt that such a valley must have been formed between the *F1*- and *F2*-layers during the eclipse concerned. Szendrei and McElhinny's graphs show a maximum during the first part of the eclipse also. This might be explained if such a valley had been present near to the beginning of the eclipse, possibly as an effect of sunrise. During the first phase the valley would become less pronounced due to the faster rate of recombination at lower heights, and might even disappear altogether near the middle of the

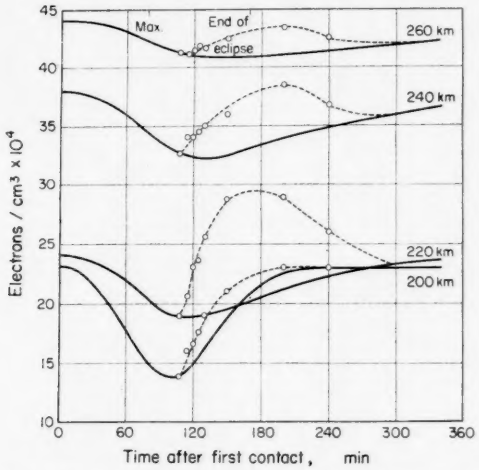

Fig. 2. Variation of electron density with time at fixed heights. Full line, true values; dashed line, apparent values.

eclipse. Thereafter the valley would re-form as suggested by Gledhill, and finally disappear long after the optical eclipse was over.

Owing to Szendrei and McElhinny's fortunate choice of comparison curves which passed through the *minima* of their experimental graphs, the values of recombination and attachment coefficients which they deduced are not as much affected by the presence of the valley as would have been the case had they chosen curves which gave the best overall fit.

It should thus be possible to infer the presence during eclipses of valleys, between the *F1*- and *F2*-layers or between the *E*- and *F1*-layers or both, by the occurrence of maxima of the type shown in Fig. 2. We believe that it will be better, by taking into account the effects of the earth's magnetic field, studying the behaviour of both the ordinary and the extraordinary rays, to deduce the existence and depth of such valleys and to allow for their effects in interpreting the ionograms (Titheridge, 1959). We are therefore examining this problem, and also re-evaluating the effects of deviation of the point of reflection from the zenith when magnetoionic phenomena are taken into account.

Acknowledgement—The authors wish to thank the South African Council for Scientific and Industrial Research for a bursary held by one of them (A. D. M. W.).

References

Gledhill J. A.	1959	*J. Atmosph. Terr. Phys.* **16,** 360.
Kelso J. M.	1952	*J. Geophys. Res.* **57,** 357.
Minnis C. M.	1958	*J. Atmosph. Terr. Phys.* **12,** 272.
Piggott W. R.	1954	*J. Atmosph. Terr. Phys.* **5,** 201.
Szendrei M. E. and McElhinny M. W.	1956	*J. Atmosph. Terr. Phys.* **9,** 118.
Titheridge J. E.	1959	*J. Atmosph. Terr. Phys.* **17,** 110.

VOL
18
196

Journal of Atmospheric and Terrestrial Physics, 1960, Vol. 18, pp. 65 to 70. Pergamon Press Ltd. Printed in Northern Ireland

Ion–atom interchange

D. R. Bates and M. Nicolet
Queen's University, Belfast, and Department of Radiation, R. Meteorological Institute, Brussels 18

(*Received* 3 *December* 1959)

Abstract—It is argued that the ion–atom interchange processes of importance in the upper atmosphere (e.g. $O^+ + N_2 \rightarrow NO^+ + N$ and $O^+ + O_2 \rightarrow O_2^+ + O$) are very much slower than simple collision theory has led some aeronomists to suppose. The rate coefficients involved are thought to be sensitive to the temperature. Ion–atom interchange does not, as has been suggested, exercise an appreciable direct influence on the degree of dissociation of the nitrogen.

1. Introduction

When attention was first drawn to the importance of ion–atom interchange

$$X^+ + YZ \rightarrow XY^+ + Z \tag{1}$$

in the upper atmosphere (Bates, 1955) it was pointed out that the rate coefficient is likely to be quite large in many instances since such interchange does not necessitate an electronic transition. Steric hindrance can scarcely be a major factor in simple rearrangements but it was thought that the activation energy might be significant in some instances and therefore quantitative estimations of rate coefficients were not attempted.

Several experimental studies of ion–atom interchange have now been made (Potter, 1955; Stevenson and Schissler, 1955, 1958; Lampe and Field, 1957). They relate mainly to cases involving the isotopes of hydrogen. For these rather special cases the interchange process is very fast indeed. Neither steric hindrance nor activation energy appear to be appreciable.

Following some early work by Eyring *et al.* (1936), Field *et al.* (1957) and Gioumousis and Stevenson (1958) have developed a theory based on the assumption that all close encounters lead to interchange. Account is taken of the long-range forces between the colliding systems. According to this theory the rate coefficient for process (1) is

$$k = 2\pi(e^2\mathscr{P}/\mu)^{\frac{1}{2}} \tag{2}$$

where e is the electronic charge, $\mathscr{P}$ is the polarizability of the neutral molecule and μ is the reduced mass. Comparisons which have been made demonstrate that the accord with the results of the experimental studies mentioned above is satisfactory.

Calculation using formula (2) gives the rate coefficient for any exothermic ion–atom interchange process between simple systems composed of only the main atmospheric constituents to be as large as about 1×10^{-9} cm^3/sec. This value has therefore been adopted by some aeronomists (e.g. Krasovsky, 1957). However, the absence of appreciable steric hindrance and activation energy for a process involving the isotopes of hydrogen should not be taken to imply their absence for

a similar process involving nitrogen and oxygen. It will be argued in Section 5 that certain of the interchange processes of interest to aeronomists must in fact be very slow.

2. Atmospheric Models

No attempt will be made here to survey current views on the structure of the thermosphere. However, information on a representative model constructed by Nicolet (1959) is presented in Table 1 for later reference. The model is in close accord with what has been learnt about the total air density from satellite drag

Table 1. Properties of thermosphere
(Nicolet, 1959)

Altitude (km)	Temperature (°K)	Number densities (particles/cm^3)			Total density (g/cm^3)
		O	N_2	O_2	
150	1186	$3{\cdot}3 \times 10^9$,	$2{\cdot}5 \times 10^{10}$	$5{\cdot}2 \times 10^9$	$1{\cdot}5 \times 10^{-12}$
200	1467	$1{\cdot}3 \times 10^9$,	$6{\cdot}2 \times 10^9$,	$1{\cdot}1 \times 10^9$	$3{\cdot}8 \times 10^{-13}$
250	1580	$7{\cdot}0 \times 10^8$,	$2{\cdot}0 \times 10^9$,	$3{\cdot}2 \times 10^8$	$1{\cdot}3 \times 10^{-13}$
300	1580	$4{\cdot}1 \times 10^8$,	$6{\cdot}5 \times 10^8$,	$1{\cdot}1 \times 10^8$	$4{\cdot}7 \times 10^{-14}$
400	1580	$1{\cdot}4 \times 10^8$,	$7{\cdot}7 \times 10^7$,	$1{\cdot}2 \times 10^7$	$7{\cdot}9 \times 10^{-15}$

data (Groves, 1959). This does not of course mean that its accuracy is high for the altitude distributions of the temperature and of the number-densities of the individual constituents.

3. Relative Abundance of the Ions in the Upper Atmosphere

Radio scientists have established that the effective recombination coefficient in the *E*- and *F1*-layers is large, and is almost independent of the gas or electron density, whereas the effective recombination in the *F2*-layer is moderate in magnitude, and is an increasing function of the gas density and a decreasing function of the electron density (Ratcliffe and Weekes, 1960). According to the theory which Bates and Massey (1947) put forward to explain the observations, the ions in the *E*- and *F1*-layers are mainly molecular. They disappear by dissociative recombination

$$XY^+ + e \rightarrow X' + Y' \qquad (3)$$

which is very rapid. As one ascends through the *F2*-layer the relative abundance of the slowly recombining atomic ions rises, due to the diminution in the frequency of the ion–atom interchange collisions* which convert them into molecular ions. Atomic ions predominate at and above the peak of the *F2*-layer.

The measurements carried out at Churchill by Johnson *et al.* (1958), using mass spectrometers mounted on rockets, support the general theoretical deductions on the ion composition. Table 2 shows some of their results. Similar results have been obtained in the Soviet Union (see Kellogg, 1959).

* The collision process operative was originally thought to be charge transfer.

4. Interchange Processes

The only ion–atom interchange processes which need be considered here are those which are exothermic and which do not involve an electronic transition. In the following the values given for the reaction energies have been computed with the relevant ionization and dissociation energies taken to be as recommended by Watanabe (1958). The symbol x denotes the excitation energy of the lowest state of NO^+ which can be formed from an N^+ ion and an O atom. This energy is doubtless great enough to render endothermic some of the processes leading to the excited state (designated below, by an asterisk).

Table 2. Observed ion composition
(Johnson *et al.*, 1958)

Altitude (km)	Day 1207 CST, 23 March 1958 Fractional abundance			Night 2321 CST, 20 November 1956 Fractional abundance		
	O^+	O_2^+	NO^+	O^+	O_2^+	NO^+
100	$0{\cdot}0_0$	$0{\cdot}4_0$	$0{\cdot}6_0$	$0{\cdot}0_0$	$0{\cdot}0_0$	$1{\cdot}0_0$
150	$0{\cdot}1_0$	$0{\cdot}2_5$	$0{\cdot}6_5$	$0{\cdot}0_5$	$0{\cdot}3_0$	$0{\cdot}6_5$
200	$0{\cdot}6_5$	$0{\cdot}1_0$	$0{\cdot}2_5$	$0{\cdot}3_5$	$0{\cdot}2_5$	$0{\cdot}4_0$
250				$0{\cdot}8_5$	$0{\cdot}0_5$	$0{\cdot}0_5$

Atomic oxygen ions may be transformed to molecular ions through

$$O^+ + N_2 \rightarrow NO^+ + N + 1{\cdot}0_9\ \text{eV} \qquad (4)\dagger$$

$$O^+ + O_2 \rightarrow O_2^+ + O + 1{\cdot}5_3\ \text{eV} \qquad (5)$$

$$O^+ + NO \rightarrow NO^+ + O + 4{\cdot}3_6\ \text{eV} \qquad (6)$$

or

$$\rightarrow O_2^+ + N + 0{\cdot}1_6\ \text{eV} \qquad (7)$$

and atomic nitrogen ions may be transformed similarly through

$$N^+ + O_2 \rightarrow NO^{+*} + O + (5{\cdot}7_6 - x)\ \text{eV} \qquad (8)$$

$$N^+ + NO \rightarrow NO^{+*} + N + (4{\cdot}3_6 - x)\ \text{eV} \qquad (9)$$

or

$$\rightarrow N_2^+ + O + 2{\cdot}2_4\ \text{eV}. \qquad (10)$$

If the colliding systems may be taken to be unexcited then the only interchange process transforming molecular ions into atomic ions is

$$N_2^+ + N \rightarrow N^+ + N_2 + 1{\cdot}0_3\ \text{eV} \qquad (11)$$

† Potter (1955) has inferred from mass-spectrometric investigations in the laboratory that k_4 is $1{\cdot}0 \times 10^{-8}$ cm³/sec. This can scarcely be accepted since the expected value of the rate coefficient describing all $O^+ - N_2$ close encounters is an order of magnitude smaller. It is to be doubted if (4) were responsible for the NO^+ ions observed and, therefore, if the investigations even provide evidence that the process is rapid.

and the only other interchange process suffered by molecular ions is

$$O_2^+ + N \rightarrow NO^+ + O + 4{\cdot}2_0 \text{ eV}. \qquad (12)\dagger$$

5. Discussion

By equating the rate at which O^+ ions are destroyed by (4) and (5) to the rate at which they are produced by the *inverse* of (7), which he believes has no reaction energy, Hertzberg (1958) obtained an expression purporting to give the equilibrium night value of the ratio $n(O^+)/n(O_2^+)$ in which n denotes the number-densities indicated. Using the data of Johnson *et al.* (1958) (Table 2) he hence deduced that the degree of dissociation of the nitrogen in the region of the F-layers is very high. He attributed this high degree of dissociation to (4) which, he argued, must be a much more important source of *odd* nitrogen atoms than

$$N_2^+ + e \rightarrow N' + N''. \qquad (13)$$

The reasoning is incorrect. It would be permissible to equate the rates of destruction and of production of O^+ ions if (5) and the inverse of (7) were the only processes operating; but it is not permissible to equate these rates in the presence of (6) since this process causes the *permanent* loss of O^+ ions. Equilibrium between the interchange processes listed clearly requires NO^+ to be the sole species of positive ion.

Provided no mechanisms of importance have been ignored the disappearance of O^+ ions during the night is determined by the equation

$$dn(O^+)/dt = -\gamma n(O^+) \qquad (14)$$

with

$$\gamma = k_4 n(N_2) + k_5 n(O_2) + [k_6 + k_7] n(NO) \qquad (15)$$

(from which terms due to recombination have been omitted as negligible). Letting $n_0(O^+)$ denote the number-density at sunset, the number-density t sec later is hence

$$n_t(O^+) = n_0(O^+) \exp(-\gamma t). \qquad (16)$$

For this relation to be consistent with the data of Johnson *et al.* (1958), given in Table 2, the numerical value of γ obviously must be extremely small compared with unity. Referring to Table 1 it may be seen that if k_4 and k_5 were indeed some 1×10^{-9} cm^3/sec as has been supposed (Section 1) then near the 200 km level γ would be at least about 3 sec^{-1}.

To explain why almost all the O^+ ions are not replaced by NO^+ ions within a few seconds of sunset, while retaining the supposition that k_4 and k_5 are some 1×10^{-9} cm^3/sec, it might be suggested that O^+ ions are continually being reformed from the NO^+ ions by

$$NO^+ + R \rightarrow O^+ + NR \qquad (17)$$

where R is some unidentified radicle. A systematic search has not revealed any species of radicle for which (17) is exothermic. The most favourable case appears

† It is assumed that

$$N_2^+ + O \rightarrow NO^{+*} + N + (2{\cdot}1_2 - x) \text{ eV}$$

is endothermic.

to be when R is an N atom. Even in this case the process is endothermic by $1{\cdot}0_9$ eV. The possibility that some of the NO^+ ions resulting from (4) may carry the requisite $1{\cdot}0_9$ eV does not appreciably affect the position: thus, since a considerable fraction of them must carry less energy, there would still be a rapid irreversible drain on the O^+ ions. It does not seem that the conclusion that k_4 and k_5 are very much smaller than 1×10^{-9} cm^3/sec can be avoided.

According to the theory of BATES and MASSEY (1947), outlined in Section 3, γ is to be identified with the coefficient describing the rate of loss of electrons in the *F2*-layer. Several groups have carried out determinations of this coefficient using radio data. The most thorough work is that of RATCLIFFE *et al.* (1956), who recognized in their analysis that there may be important vertical movements of the electrons. They derived values of $2{\cdot}7 \times 10^{-4}$, $1{\cdot}0 \times 10^{-4}$ and $3{\cdot}7 \times 10^{-5}$ sec^{-1} at the 250, 300 and 350 km levels, respectively (see also YONEZAWA *et al.*, 1959).

Information on the magnitude of γ may be obtained in another way. Denoting the rate coefficients for

$$NO^+ + e \rightarrow N' + O' \tag{18}$$

and

$$O_2^+ + e \rightarrow O' + O'' \tag{19}$$

by α_{18} and α_{19}, and assuming that these dissociative recombination processes and the ion–atom interchange processes (4) and (5) control the number-densities of the NO^+ and O_2^+ ions in the *F2*-layer during the night (which assumption should not cause serious error), it may be seen that

$$\gamma n(O^+) = \{\alpha_{18} n(NO^+) + \alpha_{19} n(O_2^+)\} n(e). \tag{20}$$

Since $n(O^+)$ and $n(e)$ are almost equal this reduces to.

$$\gamma = \alpha_{18} n(NO^+) + \alpha_{19} n(O_2^+). \tag{21}$$

Reliable laboratory measurements on the recombination coefficients have not yet been carried out, but the behaviour of the *E*-layer during the day and night (RATCLIFFE and WEEKES, 1960) when interpreted in conjunction with the data on the ion composition obtained by JOHNSON *et al.* (1958) suggests that perhaps α_{18} is about 3×10^{-9} cm^3/sec and α_{19} about 3×10^{-8} cm^3/sec*. Judging from their values relative to $n(O^+)$ it is likely that at 250 km both $n(NO^+)$ and $n(O_2^+)$ were some 1×10^4/cm^3 during the nocturnal flight on which part of Table 2 is based. Substitution of these two pairs of estimates in (21) gives γ to be 3×10^{-4} sec^{-1} at 250 km. The closeness of the agreement with the corresponding result in the preceding paragraph is of course fortuitous.

Accepting the deduced value of γ at 250 km and taking $n(N_2)$ and $n(O_2)$ to be as in Table 1 it is seen that

$$k_4 + 0{\cdot}1_6 k_5 = 1{\cdot}3 \times 10^{-13} \text{ cm}^3/\text{sec}. \tag{22}$$

Remembering that the rate coefficient for all close encounters is about 1×10^{-9} cm^3/sec it is hence apparent that (4) and (5) must be greatly inhibited by steric hindrance or, more probably, activation energy. An important consequence is

* The temperature dependence of neither coefficient is known.

that k_4 and k_5 are likely to be rapidly increasing functions of the temperature. Quantitative (as distinct from qualitative) prediction of how the effective recombination coefficient varies with altitude is not possible on present knowledge.

REFERENCES

BATES D. R.	1955	*Proc. Phys. Soc. Lond.* A **68,** 344.
BATES D. R. and MASSEY H. S. W.	1947	*Proc. Roy. Soc.* A **192,** 1.
EYRING H., HIRSCHFELDER J. O. and TAYLOR H. S.	1936	*J. Chem. Phys.* **4,** 479.
FIELD F. H., FRANKLIN J. L. and LAMPE F. W.	1957	*J. Amer. Chem. Soc.* **79,** 2419.
GIOUMOUSIS G. and STEVENSON D. P.	1958	*J. Chem. Phys.* **29,** 294.
GROVES G. V.	1959	*Nature, Lond.* **184,** 178.
HERTZBERG M.	1958	*J. Geophys. Res.* **63,** 856.
JOHNSON C. Y., MEADOWS E. B. and HOLMES J. C.	1958	*J. Geophys. Res.* **63,** 443.
KELLOGG W. W.	1959	*Planet. Space Sci.* **1,** 71.
KRASOVSKY V. I.	1957	*Izv. Akad. Nauk. SSSR, ser. geofiz.* **4,** 504.
LAMPE F. W. and FIELD F. H.	1957	*J. Amer. Chem. Soc.* **79,** 4244.
NICOLET M.	1959	*J. Geophys. Res.* **64,** in press.
POTTER R. F.	1955	*J. Chem. Phys.* **23,** 2462.
RATCLIFFE J. A., SCHMERLING E. R., SETTY C. S. G. K. and THOMAS J. O.	1956	*Phil. Trans.* A **248,** 621.
RATCLIFFE J. A. and WEEKS K.	1960	*Physics of the Upper Atmosphere* (Edited by RATCLIFFE J. A.). AcademicPress, New York.
STEVENSON D. P. and SCHISSLER D. O.	1955	*J. Chem. Phys.* **23,** 1353.
STEVENSON D. P. and SCHISSLER D. O.	1958	*J. Chem. Phys.* **29,** 282.
WATANABE K.	1958	*Adv. Geophys.* **5,** 153.
YONEZAWA T., TAKAHASHI H. and ARIMA Y.	1959	*J. Radio Res. Lab.* **6,** 21.

VOL.
18
1960

Journal of Atmospheric and Terrestrial Physics, 1960, Vol. 18, pp. 71 to 81. Pergamon Press Ltd. Printed in Northern Ireland

RESEARCH NOTES

Les perturbations ionosphériques à début brusque et la propagation des ondes longues

(*Received* 12 *September* 1959)

DANS une précédente note (HAUBERT, 1959) nous avons exposé qu'aux évanouissements en ondes courtes correspondaient des renforcements en ondes longues (200 kc/s). Nous avions en effet constaté le fait pendant plus de deux mois sans défaillance et nous avions cru pouvoir extrapoler dans le temps nos conclusions. Cependant, avec la fin de l'été, nous avons observé quelques évanouissements sur 200 kc/s et, pendant l'hiver, nous avons constaté que le nombre des évanouissements devenait beaucoup plus grand que celui des renforcements, cette situation tendant à s'inverser avec le retour de l'été.

Nous faisons donc amende honorable sur notre extrapolation hâtive et sur notre conclusion que la fréquence de transition, dont avait parlé R. Bureau, devait se trouver au dessus de 200 kc/s.

Ce qui nous parait important, c'est la mise en lumière d'un effet saisonnier sur la proportion de renforcements sur les évanouissements. Nous donnons ci-dessous le tableau de leurs nombres respectifs:

	1958						1959					
	J	A	S	O	N	D	J	F	M	A	M	J
Renforcements	35	36	29	17	5	9	8	2	3	7	16	10
Évanouissements	0	0	1	8	22	27	12	42	53	38	29	9

et un graphique représentant les pourcentages respectifs (Fig. 1). L'effet saisonnier est évident.

Entre temps, nous avons eu connaissance d'un article de LAUTER et SPRENGER (1958) qui nous a permis de comparer deux enregistrements de Droitwich reçu à Rabat avec ceux publiés par les auteurs, les 10 et 15 juillet 1958.

Le 10 juillet, LAUTER et SPRENGER observent à 0910 heures un évanouissement brusque sur 155, 209 et 281 kc/s, suivi, sur 155 et 209 kc/s seulement, d'une diminution du champ de longue durée. À Rabat, on note au même instant sur 200 kc/s un évanouissement brusque suivi d'abord d'une remontée immédiate au même niveau et ensuite d'une profonde crevasse d'une durée d'une heure environ.

Le 15 juillet, LAUTER et SPRENGER observent à 0920 heures une diminution brusque du champ sur 155 et 209 kc/s; sur 155 kc/s, la diminution du champ dure plus d'une heure et sur 209 kc/s moins d'une heure. À Rabat on note au même instant une diminution brusque suivie immédiatement d'un renforcement brusque important. La perturbation initiale est ensuite suivie d'une profonde crevasse d'une durée d'une heure et demie environ.

Ces différences de comportement, sous différentes latitudes et dans différentes directions (à peu près est–ouest en Allemagne et nord–sud au Maroc), indiquent nettement qu'une

telle étude doit être étendue dans l'espace et dans le temps avant de pouvoir déposer des conclusions.

Nous signalerons, entre autres particularités, qu'à Rabat, les renforcements ou évanouissements brusques apparaissent généralement au cours de périodes où le champ est en

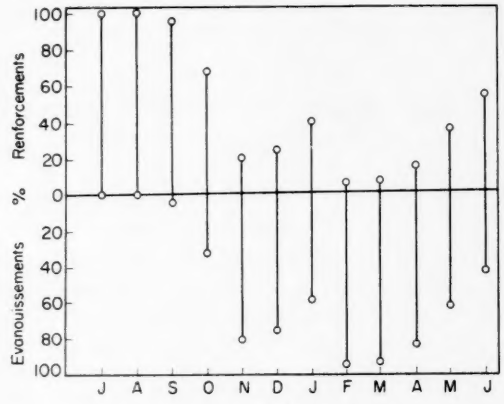

Fig. 1.

moyenne élevé, comme si une certaine activité solaire augmentait le coefficient de réflexion ionosphérique avant que ne se produise la rupture d'équilibre qui provoque la variation positive ou négative brusque qui caractérise le phénomène ionosphérique.

Notre étude n'est qu'une très minime contribution au travail sollicité par le voeu No. 43 du C.C.I.R.

A. Haubert

Centre D'Études Géophysiques
Garchy, Nièvre, France

Bibliographie

Haubert A. 1959 *J. Atmosph. Terr. Phys.* **13,** 379.
Lauter E. und Sprenger K. 1958 *Z. Meteorol.* **12,** 7.

An unusual ionospheric disturbance in the Antarctic on 30 June to 1 July 1957

(*Received* 30 *September* 1959)

Ionospheric disturbances of unusual type and magnitude were observed at the DSIR Radio Research Substation at Port Stanley in the Falkland Islands and at the Falkland Islands Dependencies Survey (FIDS) Base at Port Lockroy during the magnetic storm of 30 June to 1 July 1957. Recordings of changes in declination, *D*, of the earth's magnetic field were made at Port Stanley and also at the FIDS magnetic observatory in the Argentine Islands, a few miles from Port Lockroy, and it has therefore been possible to compare the ionospheric observations obtained at the two stations with magnetic recordings made nearby.

The magnetic storm started at 0245 UT on 30 June with slight fluctuations in *D*.

Large but slow variations in D then occurred between 0500 and 0600 UT and these were followed by a period of intense activity which lasted until 0900 UT on 1 July (Figs. 1a and 2a).

At Port Stanley, the first phase of the storm was associated with the presence of scattered reflections from the F-region, the critical frequency, f_0F2, also being depressed by about

Fig. 1(a). Magnetic changes (Port Stanley).
Mean declination 6° 30′ east.

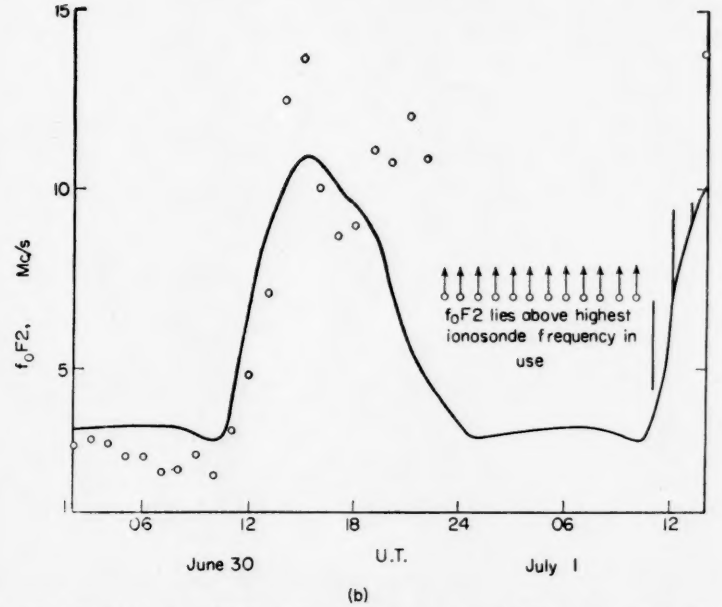

Fig. 1(b). Variation in f_0F2 (Port Stanley): ⊙ measured f_0F2; ~ median f_0F2 for June and July 1957; | range in which f_0F2 lies.

25 per cent. The absence of any marked changes in f_{min} on the ionograms shows that there were no significant abnormalities in the D-layer of the ionosphere during the period.

Up to about 1900 UT on 30 June the departures of f_0F2 from the median values for the period were fairly normal for storm conditions (about 25 per cent), but after this time quite unprecedented departures from typical storm behaviour were observed.

At Port Stanley (Fig. 1b), f_0F2 rose so that for 12 hr it exceeded the highest frequency being recorded (7 Mc/s), and was at least twice as high as the highest value ever recorded at the station in previous years at this time and season. Towards the end of this period the echoes showed an unusually large spread of about 2 Mc/s, the effect dying out shortly after 1400 UT on 1 July.

At Port Lockroy, comparable effects were observed (Fig. 2b), and for a similar period the F-layer was so disturbed and spread echoes so intense that no estimate of critical

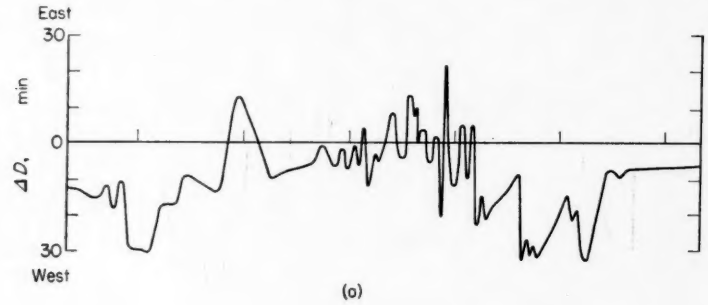

Fig. 2(a). Magnetic changes (Argentine Islands). Mean declination 17° 42′ 30″ east.

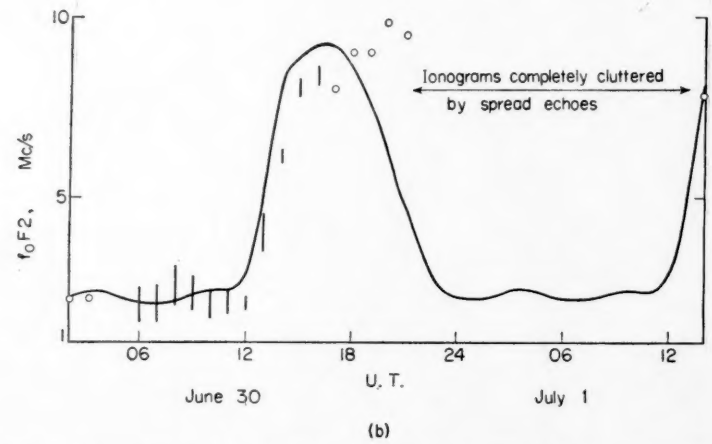

Fig. 2(b). Variations in f_0F2 (Port Lockroy): ⊙ measured f_0F2; ~ median f_0F2 for June and July 1957; | range in which f_0F2 lies.

frequencies or even of the ranges in which they might lie was possible. Here too, conditions returned to normal by 1400 UT on 1 July.

Only small magnetic and ionospheric disturbances were recorded at the Royal Society Base at Halley Bay, at a longitude 40° East of Graham Land but communications along the South American coast were disrupted, suggesting that the disturbance was confined to the longitudes of South America and the Graham Land peninsula.

Acknowledgements—The writer wishes to acknowledge the co-operation of Messrs. J. M. Smith and J. C. Farman who made the observations at Port Lockroy and the Argentine

VOL
18
196

Islands, respectively. This note is published by permission of the Director of Radio Research of the Department of Scientific and Industrial Research.

V. A. W. Harrison

DSIR, Radio Research Station
Slough, Bucks.

Scintillations of the 20 Mc/s signal from the earth satellite 1958 δ II

(*Received* 18 *December* 1959)

Introduction

This note gives some preliminary results which have been obtained at Kjeller 60°N 11°E in connexion with a study of scintillations of the signals from the earth satellite 1958 δ II.

It is well known that studies of the movements and structure of the diffraction pattern formed over the ground by radio signals either reflected from or transmitted through the ionosphere, may give information about the structure and movements of the irregularities of the electron density in the ionospheric layers. However, when use is made of the signals transmitted from a satellite like 1958 δ II, which itself moves with a velocity far greater than the velocity of the ionospheric irregularities, an amplitude pattern is produced over the ground which moves with a velocity determined by: (i) the velocity of the satellite and (ii) the height of the irregularities producing the scintillations as compared with the height of the satellite. It would therefore seem possible to obtain information on the height of the irregularities from observations of scintillations of satellite signals.

We shall divide our discussion in this note between the scintillations which are produced in the *F*-region and those which are produced in the *E*-region. Only 20 Mc/s recordings have so far been made.

Scintillations Produced in the *F*-Region

In order to determine the magnitude and direction of the drift of the amplitude pattern on the ground from observations of amplitude at three spaced receiving points, a full correlation analysis is necessary. However, it is also well known that if two antennae could be placed along the direction of the drift, the magnitude of the drift would be directly given from the observed time shifts on the amplitude recordings.

In our experiment we have set up our antennae in such a way that the two observing points are along the satellite path at its nearest approach. In some of the observations three observing points have been used. Fig. 1 shows a typical sample of a recording obtained for a transit which passed nearly overhead at Kjeller on 9 October at about 0410 GMT. The points (1) and (2) are along the direction of the satellite velocity, the distance between them being 150 m.

From Fig. 1 is seen that a systematic time shift between the amplitudes recorded at the points (1) and (2) can be obtained in spite of the satellite signal being keyed. In Fig. 2 we have plotted as a function of time the time shifts between the signals from (1) and (2).

The time of nearest approach has been marked on the figure. At this time the direction of the drift velocity is parallel to the direction of the line between the antennae, and the observed time shift will directly give the true drift velocity of the pattern.

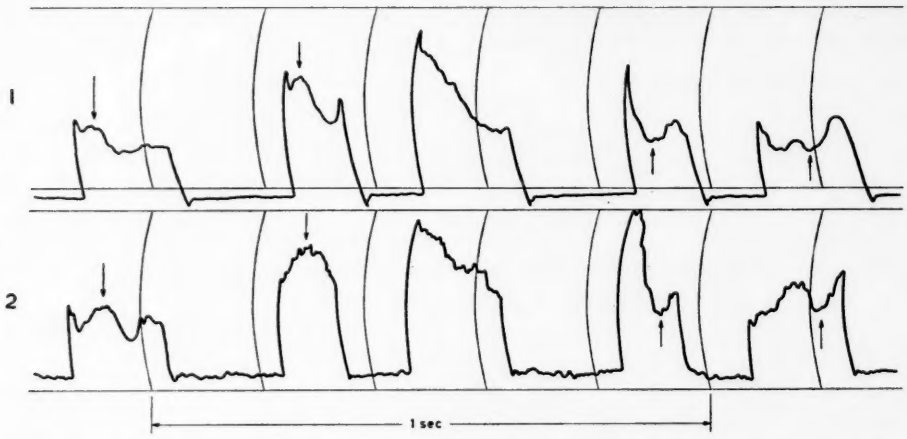

Fig. 1. Sample showing the signal strength recordings of 1958 δ II at two points separated by 150 m and lying on a line parallel to the motion of the satellite.

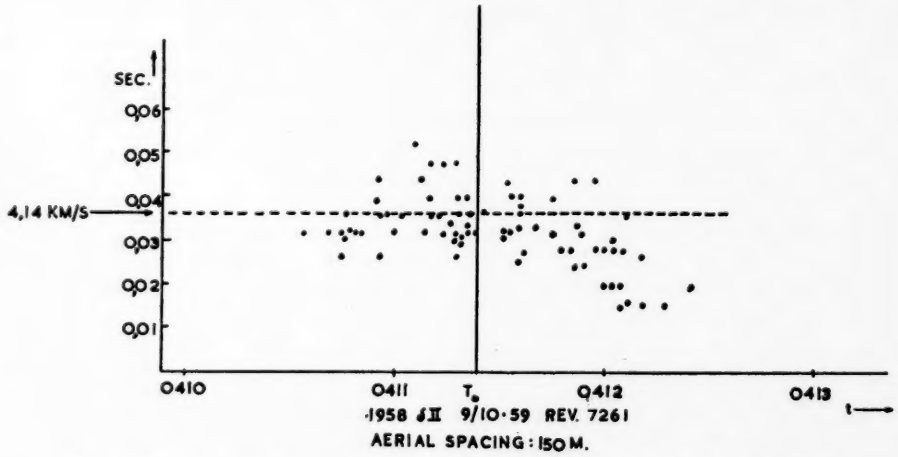

Fig. 2. The time shifts observed giving maximum correlation between recordings at two points.

The mean value of the observed time shift at the time of the nearest approach is 0·036 sec. This corresponds to a drift velocity of 4140 m/sec. If now the irregularities producing the scintillations are located within a limited slab at a height h above the ground, the height of the satellite above the ground is H, the observed velocity v is given as

$$v = V \frac{h}{H - h}$$

where V is the velocity of the satellite. Inserting the values of v, V and H, we obtain a value of 365 km for the height of the irregularities. Reliable observations have been obtained so far only in two cases, and the deduced values of h are 365 and 340 km. The spread of the observed time shifts in Fig. 2 can not be due only to experimental inaccuracy and they seem difficult to explain in terms of ionospheric movements. They can, however,

be explained if the scintillations are produced in a region of a considerably vertical extent rather than in a thin slab. The observed spread of the time shifts should therefore give information of the thickness of the active region. The observed variation with time of the time shifts can be qualitatively explained if the irregularities in the ionosphere are assumed to be stretched along the magnetic lines of force.

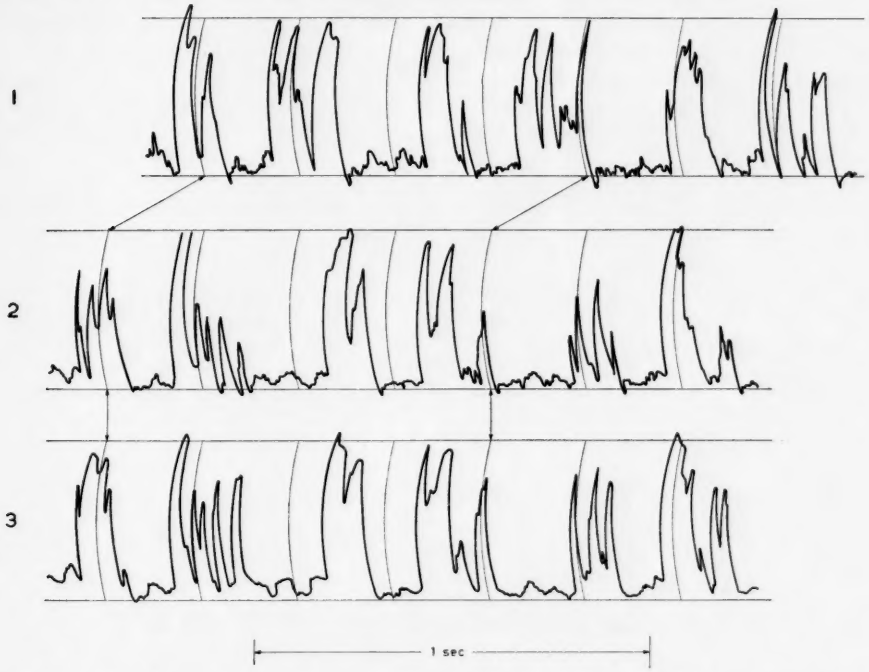

Fig. 3. Sample showing amplitude recordings at three points. (1) and (2) are separated by 200 m and lie on a line parallel to the satellite motion, (2) and (3) are separated by 135 m and lie on a line perpendicular to this direction and pointing towards magnetic north. The recording at point (1) has been shifted to obtain maximum correlation between (1) and (2).

VOL. 18 1960

Scintillations Produced in the *E*-Region

In Fig. 3 a sample of a record from 16 October 1959 at 0350 GMT is shown. The satellite was here passing north of Kjeller. During the passage the fading was extremely rapid and deep. In the sample shown in Fig. 3 the direction of the movement was almost along the direction between (1) and (2).

From the figure is seen that there is a very high correlation between the signals observed at the points (2) and (3). In the illustration we have shifted the amplitude recording obtained at point (1) with regard to that obtained at point (2) in order to get the best possible correlation between the two signals. We have found that a significant correlation can be obtained if a fairly large shift is made, the optimum shift being 0·24 sec, which corresponds to a height of 104 km for the active irregularities.

In the greater part of this recording the cross correlation between the recordings at (1) and (2) was found to be poor with any shift selected. However, if the amplitude pattern is made up of a superposition of a number of patterns produced at somewhat different heights, and consequently moving with different velocities, one should not expect to obtain a high

correlation even after shifting the recordings, if the spread of the corresponding time shifts are of the same order of magnitude as the speed of fading.

Although it has been possible only for selected periods of the recording to deduce reliable time shifts, it seems safe in view of the above arguments, to assume that the fading pattern is in fact moving with a velocity of this order of magnitude. It is thus possible from the observed speed of fading, to deduce the size of the irregularities in the fading pattern. By inspection of the recordings we have found that the correlation in the direction of the antennae (2) and (3) falls to a value of about 0·8 at a distance of 135 m. In the direction of the antennae (1) and (2) such a drop will be observed at a distance of less than 10 m. It is thus observed that the pattern over the ground is highly stretched, and this can again be explained if the irregularities in the ionosphere are stretched along the magnetic lines of force.

Acknowledgements—The research reported in this note has been sponsored by the Electronics Research Directorate of Cambridge Research Center, Air Research and Development Command, United States Air Force, through the European Office, ARDC, under contract AF 61(052)–08. We have benefited from discussions with Dr. B. H. Briggs of the Cavendish Laboratory, Cambridge. We would also like to express our thanks to our colleagues at the NDRE for help and advice.

J. Frihagen
J. Trøim

Norwegian Defence Research Establishment
Division of Telecommunication
Kjeller pr., Lillestrom, Norway

VOL
18
196(

A note on the polar absorption event of 11–18 May 1959

(*Received* 12 *January* 1960)

Introduction

A strong polar absorption event was observed on Norwegian galactic noise measuring stations in the period 11–18 May 1959. Observations were made at the following five stations: Longyearbyen (78°N, 16°E), Björnöya (74°N, 19°E), Skibotn near Tromsö (69°N, 20°E), Trondheim (63°N, 10°E) and Kjeller (60°N, 11°E). The method which is used in the recordings is similar to that used in Alaska by Little and Leinbach (1958), except that we have not used a frequency sweep technique. The measuring frequency is 28·6 Mc/s, and three-element yagis erected vertically are used.

Results

In Fig. 1 we have shown the observed absorption for the five stations in the period 11–16 May. The plotted values give the absorption referred to a quiet-day curve obtained for each month from selected magnetically quiet days. The event started in the early morning of the 11th. At the three northern-most stations, the absorption increased gradually to a value above the maximum recordable of 12 dB around noon, and stayed above this value for about 36 hr. Then the absorption gradually decreased towards a normal value. At Longyearbyen and Björnöya there was midnight sun at ground level, and at Skibotn a midnight sun at a height of about 6 km above the ground.

At Trondheim an increase of the absorption was also observed on the 11th, while at Kjeller no effect could be observed. In the evening of the 11th the absorption decreased at Trondheim after ground sunset, and the signal reached an almost normal value around midnight. Before ground sunrise in the morning of the 12th, however, the absorption again increased to a maximum recordable value. Similar effects were observed at Trondheim in the evening, and at Kjeller in the morning and evening of the 12th. Before ground sunset and after ground sunrise for these periods, the absorption was almost constant, except for the evening of the 12th at Kjeller where a deep additional absorption effect was observed.

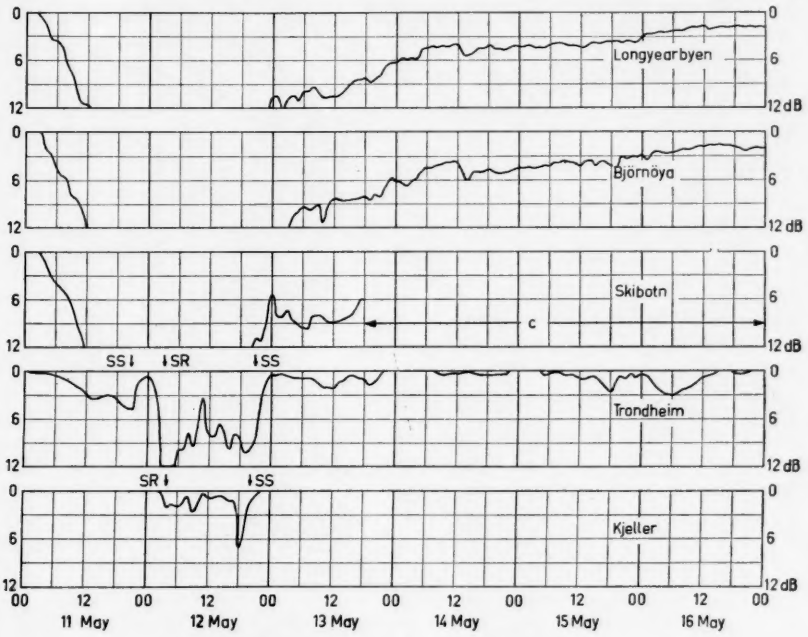

Fig. 1. Observed absorption for the five stations.

In order to study the solar control of the observed absorption in more detail, the "constant" absorption values in the periods before ground sunset and in the periods after ground sunrise were first deduced. Then the percentage absorption, referred to these values, was deduced for the periods after ground sunset and the period before ground sunrise. This percentage absorption was plotted for each of the five periods as a function of time, given by the height of the earth's shadow, i.e. the height of the transition between daylight and night. The results are shown in Fig. 2(a).

Fig. 2(b) shows the observed absorption in dB obtained at Kjeller with the galactic noise equipment in the sunrise period on the 12th, together with the $f_{\min}$ values observed at Kjeller in the same period. It can be seen that a similar effect to that observed for the v.h.f. waves is also observed on the h.f. waves, and that a full blackout is observed when the galactic noise absorption is about 0·4 dB. In the evening a similar effect was also observed on the $h'f$ recordings.

Discussion

Fig. 2 clearly demonstrates a marked solar control of the absorption. In the evening, before ground sunset, the absorption is approximately constant. Then, after ground

sunset, the absorption begins to decrease, and at the time of sunset at a height of about 55 km above the ground, the absorption is almost normal. In the morning, when sunrise occurs at this height, the absorption begins to increase, and increases until the time of sunrise at the ground.

It has been suggested that the solar control of the absorption, for the types of events here discussed, may be explained by a mechanism as follows. During the night, the free electrons produced by some primary source will attach to neutral molecules or atoms. Electrons will then be detached from the negative ions by the solar radiation. The electron affinity of the O_2 molecule, to which electrons mainly attach in the lower ionosphere is

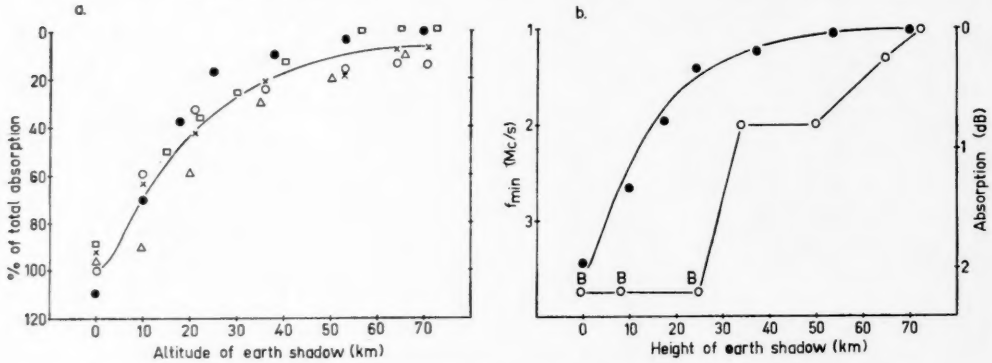

Fig. 2. The observed absorption plotted against the height above the ground of the earth's shadow. (a) ○ Trondheim—11 May SS. △ Trondheim—12 May SR. × Trondheim—12 May SS. ● Kjeller—12 May SR. □ Kjeller—12 May SS. (b) ○ $f$min. ● Galactic noise.

approximately 1 eV, so that the photons of almost the whole solar emission spectrum have sufficient energy for the photodetachment reaction. It has been argued (HULTQVIST and ORTNER, 1959) that for the suggested mechanism the absorption should be related to the shadow of the solid earth, and that this would lead to an upper boundary of the absorption layer at a height of about 55 km.

Our results seem not to be consistent with the suggested mechanism. Firstly, it would seem impossible to explain a blackout on the $h'f$ recordings for such a low layer, and secondly, it would also seem unreasonable to have a layer which extended right down to the ground

There can, however, be little doubt that the absorption is due to electrons produced by radiation from the sun, and it seems that the only explanation is that the active radiation becomes absorbed in a layer in the atmosphere, probably in the ozonosphere. The absorption of the radio waves should then be related to the shadow of this layer rather than to the shadow of the earth's surface.

If we put the upper boundary of the layer which absorbs the active radiation to 40 km, the heights of sunrise and sunset referred to this layer can be obtained approximately by adding 40 km to the heights given in Fig. 2. On this assumption, Fig. 2 would therefore give direct information on the height at which the absorption of the radio waves occur.

Acknowledgements—The galactic noise station at Longyearbyen was run by the Norwegian Telecommunication Administration, and the station at Björnöya by the Auroral Observatory. We are indebted to these organizations for their permission to use the results from these stations.

VOL. 18 1960

The research reported in this note has been sponsored by the Electronics Research Directorate of Cambridge Research Center, Air Research and Development Command, United States Air Force, through the European Office, ARDC, under contract AF 61(052)–08.

Norwegian Defence Research Establishment
Kjeller, Norway

K. W. Eriksen
O. Holt
B. Landmark

References

Little C. G. and Leinbach H. 1958 *Proc. IRE* **46,** 334.
Hultqvist B. and Ortner J. 1959 *Planet. Space Sci.* **1,** 193.

A further note on "sweepers"

(*Received* 18 *January* 1960)

The phenomenon reported recently by Gerson and Gossard (*J. Atmosph. Terr. Phys.* **17,** 82) was brought to my attention late in December, 1959. By using a conventional communications receiver and a rhombic antenna directed east from Boulder, Colorado, the signals could be readily identified. However, an interesting feature was noted that was not reported. Many of the signals, as they swept through the receiver pass-band, were observed to be modulated, having the characteristic sound of a poorly filtered plate supply. Analysis by a sound spectrograph of a few of them showed the modulation frequencies to be predominantly even harmonics of 60 c/s, which would be expected from a full-wave rectifier operating from a North American power line.

This additional feature of the observations puts an entirely different light on the phenomenon and, although it may still be a subject for investigation by those engaged in interference identification and suppression, it seems unlikely that it must be explained as a newly discovered natural phenomenon.

J. M. Watts

Ionospheric Research Section
Radio Propagation Physics Division
Boulder Laboratories
Boulder, Colorado, U.S.A.

Journal of Atmospheric and Terrestrial Physics, 1959, Vol. 18, pp. 82 to 85. Pergamon Press Ltd. Printed in Northern Ireland

Indices of geomagnetic activity

of the Observatories HARTLAND (*Ha*), ESKDALEMUIR (*Es*) and LERWICK (*Le*)
July to October 1959

The figures given on pages 82 to 85 represent the K-indices for three-hour intervals, beginning with 00–03 hrs for the first and ending with 21–24 hrs for the eighth figure.

July 1959

Day	*Ha* Range for $K = 9 : 500\gamma$			*Es* Range for $K = 9 : 750\gamma$			*Le* Range for $K = 9 : 1000\gamma$			*Day*
	K-Indices		*Sum*	*K-Indices*		*Sum*	*K-Indices*		*Sum*	
1	1011	2112	9	1111	1212	10	2111	1213	12	1
2	3422	1200	14	3432	1311	18	4452	3221	23	2
3	1211	2121	11	1221	3221	14	2222	3111	14	3
4	0012	3433	16	1013	3543	20	1113	3444	21	4
5	3332	3231	20	3333	3232	22	3322	3232	20	5
6	1112	3332	16	1122	4332	18	1122	3322	16	6
7	2433	3421	22	2333	3422	22	2333	3331	21	7
8	2333	4431	23	2333	4432	24	1323	3342	21	8
9	1332	2443	22	1332	3443	23	2332	2433	22	9
10	3433	2322	22	3333	2231	20	4333	1221	19	10
11	4431	3655	31	3432	3655	31	5432	3557	34	11
12	5223	3311	20	4333	4322	24	6322	4322	24	12
13	2222	3312	17	2222	3323	19	2321	3323	19	13
14	2333	3331	21	2332	4331	21	3332	5431	24	14
15	3499	7987	56	3477	6977	50	5599	9989	63	15
16	5434	3354	31	6543	4454	35	8543	4444	36	16
17	3333	3877	37	3433	3778	38	4543	3688	41	17
18	6654	4635	39	7765	4645	44	8884	4646	48	18
19	4334	4433	28	4334	4543	30	5533	4533	31	19
20	2223	3334	22	3333	3434	26	3323	3435	26	20
21	3222	3333	21	3323	4333	24	4322	4333	24	21
22	2222	2224	18	2222	3324	20	3322	3324	22	22
23	3331	3222	19	3333	3222	21	4332	3223	22	23
24	3124	3454	26	3134	4454	28	3224	3344	25	24
25	4444	3554	33	4444	4554	34	4334	3455	31	25
26	3333	4544	29	3334	4543	29	3533	4555	33	26
27	4333	3344	27	4333	3343	26	5433	2344	28	27
28	3223	3322	20	3222	4323	21	4322	3323	22	28
29	2321	3132	17	2322	3232	19	2332	2121	16	29
30	1111	1120	8	1112	2231	13	1101	1121	8	30
31	2322	3233	20	2323	3333	22	2322	3333	21	31

August 1959

Day	*Ha* Range for $K = 9 : 500\gamma$			*Es* Range for $K = 9 : 750\gamma$			*Le* Range for $K = 9 : 1000\gamma$			*Day*
	K-Indices		*Sum*	*K-Indices*		*Sum*	*K-Indices*		*Sum*	
1	3333	3332	23	3344	4432	27	4333	4432	26	1
2	4331	2341	21	3332	2342	22	4431	3331	22	2
3	3343	3432	25	3243	4431	24	4433	3321	23	3
4	2224	4424	24	2314	4433	24	2314	4334	24	4
5	2121	3432	18	2122	3432	19	1212	4432	19	5
6	0323	3453	23	1323	3553	25	1332	3654	27	6
7	3322	2332	20	3323	3432	23	5322	3433	25	7
8	2223	2314	19	2123	3314	19	3123	3323	20	8
9	4232	3442	24	4133	4452	26	4333	4443	28	9
10	2421	3332	20	3421	4432	23	3421	3333	22	10
11	3312	2212	16	3312	3312	18	3322	3311	18	11
12	1111	2202	10	2122	2212	14	1111	2212	11	12
13	1212	1221	12	1212	2232	15	2112	2221	13	13
14	2221	2231	15	2111	3331	15	1112	2221	12	14
15	2113	4535	24	2113	4535	24	3213	4435	25	15
16	4466	6646	42	4456	7766	45	5355	7777	46	16
17	6644	4644	38	7855	5655	46	8875	5745	49	17
18	2343	4443	27	2343	4443	27	3443	4443	29	18
19	3433	2443	26	3433	2343	25	4442	2342	25	19
20	3554	3243	29	2555	4343	31	3544	4333	29	20
21	5334	3444	30	5334	3454	31	4333	3455	30	21
22	3332	3454	27	4343	3454	30	5343	3443	29	22
23	3333	4434	27	3333	4543	28	4333	4545	31	23
24	3343	2322	22	3343	3322	23	4333	3313	23	24
25	3323	3313	21	2323	4413	22	3323	3423	23	25
26	2122	1222	14	2122	2222	15	3121	2122	14	26
27	3022	1010	9	2122	2100	10	3212	1100	10	27
28	0110	2102	7	0112	1212	10	0112	1211	9	28
29	3113	3333	20	3213	3433	22	3212	3333	20	29
30	3222	2321	17	3222	2321	17	3222	2321	17	30
31	1222	2322	16	1222	3332	18	1222	3233	18	31

OL.
18
960

September 1959

Day	*Ha* Range for $K = 9 : 500\gamma$			*Es* Range for $K = 9 : 750\gamma$			*Le* Range for $K = 9 : 1000\gamma$			*Day*
	K-Indices		*Sum*	*K-Indices*		*Sum*	*K-Indices*		*Sum*	
1	3222	3343	22	3223	3342	22	4323	3552	27	1
2	4443	2334	27	4444	3334	29	5544	2344	31	2
3	2333	3337	27	2233	3349	29	4222	3459	31	3
4	5654	4544	37	6755	5645	43	7855	6667	50	4
5	4333	3345	28	3334	4435	29	6433	4436	33	5
6	4232	2210	16	4333	3211	19	7332	2210	20	6
7	2012	3321	14	1122	3422	17	1122	3321	15	7
8	1123	2413	17	1123	2413	17	1123	2313	16	8
9	1022	1213	12	1123	2322	16	3122	1212	14	9
10	1011	2214	12	1112	2324	16	1112	2213	13	10
11	1233	3223	19	2233	3232	20	2333	3234	23	11
12	4232	2311	18	4222	3322	20	4322	2321	19	12
13	3122	2225	19	3122	3225	20	3121	2215	17	13
14	4333	3324	25	3233	4322	22	3233	3323	22	14
15	2133	3344	23	2123	4444	24	2122	3344	21	15
16	4422	2333	23	4423	2333	24	4322	3233	22	16
17	2122	3444	22	2212	3444	22	2212	3344	21	17
18	3224	3334	24	3234	4435	28	3223	3346	26	18
19	5424	4223	26	5435	4323	29	5634	4212	27	19
20	4444	5465	36	4443	5565	36	4433	5578	39	20
21	5563	5665	41	6563	5545	39	7663	6755	45	21
22	5554	4353	34	6555	5453	38	8754	5453	41	22
23	2233	2445	25	2233	2455	26	3123	3466	28	23
24	4333	4333	26	3333	4233	24	5333	4343	28	24
25	4333	3434	27	4333	3534	28	6533	4646	37	25
26	3223	3244	23	3223	4344	25	5332	4345	29	26
27	3333	3333	24	3333	3343	25	3223	3444	25	27
28	4223	3333	23	4323	4333	25	5322	3333	24	28
29	3023	2213	16	3123	2313	18	3212	2203	15	29
30	2123	3343	21	2223	3333	21	1112	3333	17	30

VOL
18
196

October 1959

Day	*Ha* Range for $K = 9 : 500\gamma$			*Es* Range for $K = 9 : 750\gamma$			*Le* Range for $K = 9 : 1000\gamma$			*Day*
	K-Indices		*Sum*	*K-Indices*		*Sum*	*K-Indices*		*Sum*	
1	5444	3344	31	4444	4344	31	4444	4457	36	1
2	2433	1322	20	1433	2222	19	3543	1222	22	2
3	0122	2466	23	2233	2567	30	1232	3687	32	3
4	4533	4243	28	4543	4343	30	5643	4344	33	4
5	5422	2466	31	4422	3455	29	5532	3687	39	5
6	4443	3555	33	4444	3554	33	6444	4454	35	6
7	3323	2124	20	3322	3225	22	3322	3224	21	7
8	3222	2211	15	2212	2211	13	3222	1211	14	8
9	3112	1230	13	3112	2231	15	3111	1131	12	9
10	1111	1322	12	1112	1321	12	1111	1321	11	10
11	1012	0022	8	1021	1122	10	1011	1132	10	11
12	1001	2233	12	1011	2333	14	1010	2233	12	12
13	1011	2211	9	1122	2211	12	1011	1111	7	13
14	1123	3233	18	1123	3333	19	1113	3233	17	14
15	3323	3344	25	3223	3344	24	2222	2244	20	15
16	1110	1121	8	1111	1221	10	1000	0131	6	16
17	0124	3344	21	1123	3333	19	1013	3243	17	17
18	3334	4445	30	3334	4444	29	5423	3444	29	18
19	3322	2134	20	3323	2233	21	3322	1133	18	19
20	4122	1100	11	4122	2101	13	3122	1111	12	20
21	0001	2313	10	0001	2323	11	0011	1213	9	21
22	3322	2433	22	3222	3333	21	2222	3333	20	22
23	3222	1110	12	3122	2010	11	4322	1100	13	23
24	0012	2112	9	0111	2222	11	0011	2213	10	24
25	3433	3324	25	3433	3324	25	3433	3324	25	25
26	4333	4334	27	3333	4424	26	3332	4534	27	26
27	2233	2301	16	2232	3311	17	2222	2211	14	27
28	0021	1000	4	1012	1100	6	1011	1001	5	28
29	0011	2103	8	0011	2103	8	0010	2112	7	29
30	6322	3245	27	5322	3345	27	5322	3258	30	30
31	5323	3456	31	3333	3455	29	5223	3677	35	31

VOL.
18
960

Journal of Atmospheric and Terrestrial Physics, 1960, Vol. 18, p. 86. Pergamon Press Ltd. Printed in Northern Ireland

BOOK REVIEW

Optics and Spectroscopy: An English translation of the Russian
Optika i Spectroscopiya. Optical Society of America, National Bureau of Standards, Washington.

WE draw the attention of our readers to the appearance of a scientific journal in English entitled *Optics and Spectroscopy*. This is a translation, made by the Optical Society of America, of the Russian journal *Optika i Spectroscopiya*. This monthly journal of the U.S.S.R. Academy of Sciences commenced publication in 1956, and publishes the work of leading Russian scientists in all branches of optics and spectroscopy, including X-ray, ultra-violet, visible, infra-red and microwave radiations, thin-layer optics, filters, detectors, diffraction gratings, electro-luminescence, thermal radiation backgrounds, infra-red polarizers, and their many other applications in science and industry. The English translation, which is being published with a grant-in-aid from the National Science Foundation, starts from Volume 6, January 1959, and it is the aim of the Society that *Optics and Spectroscopy* will appear within 4 months of the Russian original.

E. V. APPLETON

VOL
18
196

ERRATA

J. Atmosph. Terr. Phys. **11,** 75 (1957)

Indices of geomagnetic activity of the Observatory at LERWICK (*Le*).
16 April 1957: 09–12 hr, for "2" read "4"; and *Sum*, for "26" read "28".

Direction of variation in the geomagnetic vertical field at Ibadan, Nigeria

IN two papers published in this Journal the variation of the vertical component of the geomagnetic field (Z) has erroneously been regarded to have been in the direction of upward Z increasing to a maximum around noon. The true position is this: Z at Ibadan is upwards and therefore negative by the usual convention. Variation in Z a few hours before noon is in the direction of downward Z increasing so that Z reaches an algebraic maximum about noon; that is the numerical value is a minimum.

The error, which is very much regretted, necessitates the following errata.

Department of Physics
University College
Ibadan, Nigeria

N. S. ALEXANDER
C. A. ONWUMECHILLI

J. Atmosph. Terr. Phys. **13** (1959)

C. A. ONWUMECHILLI: A study of the equatorial electrojet—II. A model electrojet that fits H-observations.

Page 251, line 3: for "upward" read "downward".

J. Atmosph. Terr. Phys. **16** (1959)

C. A. ONWUMECHILLI and N. S. ALEXANDER: Variations in the geomagnetic field at Ibadan, Nigeria—I. Solar variations.

Page 108, Fig. 1: delete "up".

Page 110, line 8: for "upward" read "downward".

Papers to be published in future issues

C. M. Minnis and G. H. Bazzard: The geographical distribution of ionization in the *F2*-layer

T. Obayashi and Y. Hakura: Enhanced ionization in the polar ionosphere associated with geomagnetic storms

R. A. Duncan: The equatorial *F*-region of the ionosphere

R. F. Stebbings, G. V. Groves, R. L. F. Boyd and P. J. Bowen: Low-altitude testing of the rocket-grenade experiment for upper atmosphere temperatures and winds

J. Veldkamp and D. van Sabben: On the current system of solar-flare effects

P. Das Gupta and K. K. Vij: Statistical analysis of fading of a single down-coming wave

P. Bandyopadhyay: Electron distribution in the *F*-layer of the ionosphere over Haringhata (Calcutta) on quiet and disturbed days

J. Taubenheim: Incoherency of pulse echoes and the measurement of ionospheric absorption

J. A. Fejer: Hydromagnetic wave propagation in the ionosphere

J. S. Greenhow and J. E. Hall: Diurnal variations of density and scale height in the upper atmosphere

D. Lepechinsky et C. Taieb: La détermination des hauteurs réelles de l'ionisation dans les trés hautes latitudes

S. R. Khastgir and R. N. Singh: The size of the moving irregularities in the *F*-region and the spread angle of the radio waves scattered from them

Syun-Ichi Akasofu: On the ionospheric heating by hydromagnetic waves connected with geomagnetic micropulsations

J. S. Greenhow, E. L. Neufeld and C. D. Watkins: The scattering of 36 Mc/s radio waves by weak auroral ionization

G. H. Bazzard: Short-term differences in the behaviour of two daily indices of solar activity during the IGY

J. W. Wright: Some magnetoionic phenomena of the arctic *E*-region

B. J. Robinson: Diurnal variation of the electron distribution in the ionospheric *E*-layer

C. M. Minnis and G. H. Bazzard: A monthly ionospheric index of solar activity based on *F2*-layer ionization at eleven stations

C. M. Minnis and G. H. Bazzard: A world-wide semi-annual cycle in the *E*-layer of the ionosphere

H. Rishbeth and D. W. Barron: Equilibrium electron distributions in the ionospheric *F2*-layer

L. R. Megill, P. M. Jamnick and J. E. Cruz: Seasonal variations in the twilight enhancement of [OI] 5577

Syun-Ichi Akasofu: Large-scale auroral motions and polar magnetic disturbances—I. A polar disturbance at about 11 hr on 23 September 1957

C. D. Watkins: The height and geometry of auroral radio echoes

R. G. Rastogi: A synoptic study of the *F2*-region of the ionosphere in the Asian zone

I. L. Jones: Further observations of radio stellar scintillation

VOL.
18
196

Journal of Atmospheric and Terrestrial Physics, 1960, Vol. 18, pp. 89 to 100. Pergamon Press Ltd. Printed in Northern Ireland

The equatorial *F*-region of the ionosphere

R. A. Duncan

Upper Atmosphere Section, CSIRO, Camden, Australia

(*Received* 26 *October* 1959)

Abstract—A comparison of data from ionospheric sounders at Chimbote and Panama, shows that afternoon critical frequencies in the equatorial zone are negatively correlated with those on the same meridian in the sub-tropical belts. This supports Martyn's suggestion that ionization is transported from the equatorial zone to the sub-tropics.

The process suggested by Martyn, electrodynamic lift at the equator followed by diffusion under gravity along the geomagnetic field lines to the sub-tropical belts, is investigated quantitatively, and it is shown that the process can account for the high sub-tropical electron densities observed.

It is shown that the diurnal variation of the correlation between Chimbote and Panama critical frequencies, the diurnal variation in the height, thickness and electron density of the equatorial *F*-region, and the diurnal variation of electron density enhancement in the sub-tropics, can all be ascribed to the simple diurnal electrodynamic tide expected from the observed magnetic variations, in conjunction with diffusion along the geomagnetic field lines.

Introduction

During the second world war it was discovered (Appleton, 1946; Bailey, 1948; Rastogi, 1959) that the afternoon *F*-region electron density is less near the magnetic equator than in two sub-tropical belts at magnetic latitudes of $\pm 20°$ (Fig. 1). Mitra (1946) suggested that this might be because much of the ionization

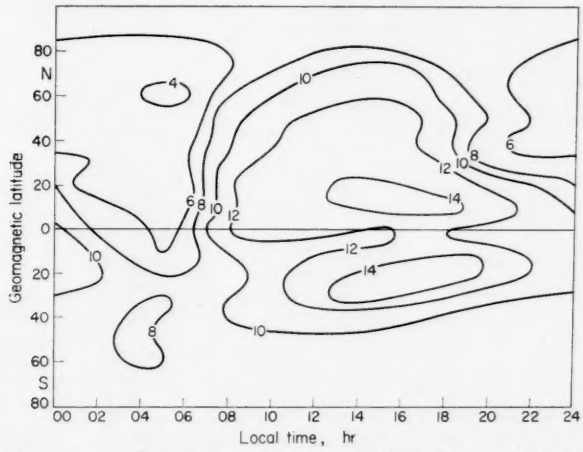

Fig. 1. World contours of *F*-region critical frequencies, February 1958. Contours at 2 Mc intervals (as predicted by the Australian Ionospheric Prediction Service for the west zone).

comprising the *F*-region is produced by ultra-violet light at heights up to 600 km, only subsequently diffusing down under gravity to normal *F*-region heights; diffusion can occur only along the geomagnetic field lines so that the *F*-region at the magnetic equator is robbed of this ionization which is instead guided to the two sub-tropical belts (Fig. 2).

Bailey (1948) (for recent work see Skinner *et al.*, 1954) noticed that the low

equatorial electron densities are associated with high, thick and multiple layer formation (Fig. 3). MARTYN (1954) suggested that this feature too, might be due to the inhibition of downward vertical diffusion under gravity. He repeated MITRA's suggestion that diffusion would instead take the ionization via the geomagnetic field lines to the two sub-tropical belts, but invoked electrodynamic

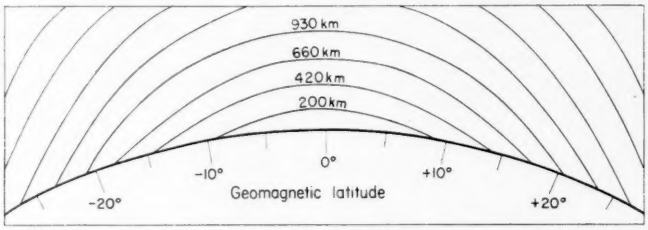

Fig. 2. The geomagnetic field above the equatorial zone.

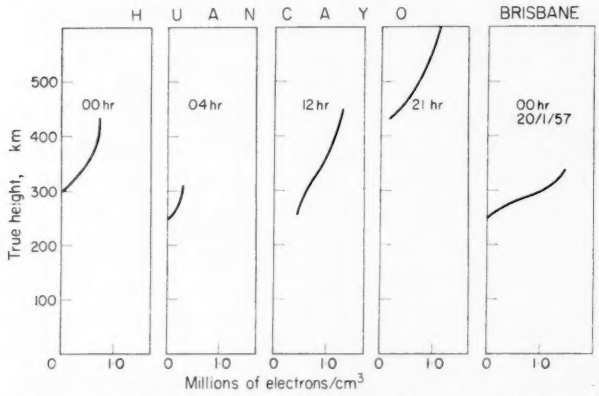

Fig. 3. Huancayo true height—electron density profiles. Mean of five magnetically quiet days, December 1938. A moderate latitude profile is shown for comparison (Huancayo profiles from SCHMERLING and THOMAS, 1955).

lift, rather than *in situ* production by solar radiation, as the source of the high equatorial ionization.

MITRA's and MARTYN's explanation of the anomalous equatorial *F*-region has been strengthened by the accumulating evidence that diffusive settling under gravity is indeed a controlling factor at more moderate latitudes. DUNCAN (1956a) suggested that the opposing forces of downward diffusion under gravity and a negative height gradient of electron decay should combine to stabilize the height of the middle latitude night-time *F2*-region. YONEZAWA (1956) developed a similar theory in some detail, for the more involved case of the day-time *F2*. Subsequently MARTYN (1956), DUNCAN (1956b) and DUNGEY (1956), put the theory for the night-time *F2*-region on a quantitative basis. They showed that under an attachment law of electron decay the electron density will assume a vertical distribution of the Chapman form centred at a height such that

$$v = \frac{g \sin^2 \chi}{2 H \beta} \tag{1}$$

where ν is the positive ion collision frequency;
g is the gravitational field strength;
χ is the geomagnetic dip;
H is the scale height;
β the attachment coefficient.

To account for the observed height of the $F2$-region at middle latitudes this theory requires a neutral particle density of about 10^{10} particles per cm^3 at 300 km (MARTYN, 1956) and this is much higher than the density adopted by the Rocket Panel (1952) and widely accepted at the time.

Recent true height analyses (DUNCAN, 1958) (see also BERKNER, 1940) have shown that the observed night-time electron distribution is indeed close to the Chapman form. Satellites (SCHILLING and STERNE, 1959) have found the high air densities required by the diffusion theory.

The critical frequency at a given hour and station fluctuates irregularly from day to day. WRIGHT *et al.* (1957) have mentioned, without published evidence, that unusually low critical frequencies in the equatorial zone are associated with unusually high critical frequencies in the sub-tropics. This negative correlation was evidently noticed by MCNISH and GAUTIER (1949) during their studies of equatorial lunar tides*. Such an inverse relation supports the idea of ion transport from one place to the other.

In this paper the correlation between critical frequencies at Chimbote near the magnetic equator, and Panama in the sub-tropics will be studied in some detail. It will be shown that the diurnal variation of this correlation, the diurnal variation of the height, thickness and electron density of the equatorial F-region, and the diurnal variation of electron density enhancement in the sub-tropics can all be ascribed to a simple diurnal electrodynamic tide and MARTYN's ion transport process. It will be suggested, however, that *in situ* ion production at great heights, as suggested by MITRA, may be important in the winter polar region. MARTYN's process; electrodynamic lift at the equator followed by diffusion under gravity down the geomagnetic field lines to the sub-tropics, will be analysed and it will be shown that it can account quantitatively for the high electron densities observed in the sub-tropical belts.

THE CO-VARIATION OF ELECTRON DENSITY AT THE EQUATOR AND SUB-TROPICS, AND OTHER EVIDENCE FOR ION TRANSPORT

In Fig. 4 we have compared the daily fluctuations of critical frequency at 1500 hours at two stations lying near the 75°W meridian, Chimbote, Peru, near the magnetic equator (magnetic dip 7°N) and Panama in the sub-tropical belt (dip 37°N). It will be seen that they are negatively correlated; above average critical frequencies are observed at Panama on afternoons when below average critical frequencies are observed at Chimbote, and vice versa.

This lends support to the picture of electron transport. We may suppose that the intensity of the electrojet and hence the magnitude of the F-region electrodynamic lift varies from day to day and that this variation in turn results in a variation of the quantity of ionization shifted from Chimbote to Panama.

* Private communication, J. W. WRIGHT.

Part of the variation of the electrojet is no doubt due to the ever-changing phase relationship of the solar and lunar atmospheric tide. This is the connexion between the present study and that of MCNISH and GAUTIER (1949).

It might be thought that the ideas advanced above could be best substantiated by a study of the daily values of the magnetic variation and the true height of the F-region. However, daily true $h_{\max}F$ data are not available; magnetic data are available, but it is believed that a great part of the magnetic variation observed

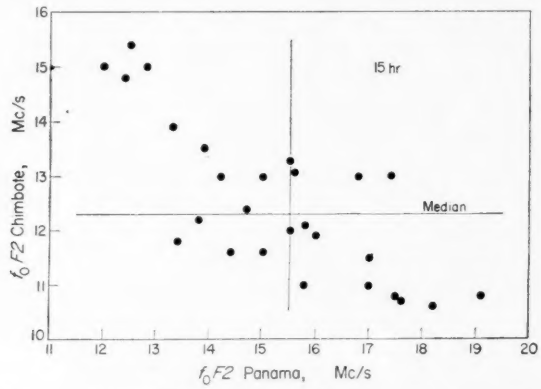

Fig. 4. Critical frequency at 1500 hours at Chimbote against that at Panama, February 1958.

at the ground is not due to ionospheric electric currents, but to something in the nature of CHAPMAN and FERRARO'S (1941) ring current much further out.

However, that part of the magnetic variation which shows a diurnal pattern should be of ionospheric origin and we shall see in a later section that this mean diurnal magnetic variation is in accord with the mean diurnal behaviour of the equatorial ionosphere and MARTYN'S ion transport process.

Another consideration favours MARTYN'S electrodynamic lift rather than MITRA'S *in situ* production as the source of ionization high above the equatorial zone. The moderate latitude F-region rises rapidly after sunset. This suggests that ion production occurs predominantly at low heights.

There is one part of the world where this is not true, the winter polar zone. Here the atmosphere is not illuminated below 450 km and the maintainence of the F-region (GATES, 1959) at about the same height, as the moderate latitude night-time F-region, 350 km, is probably due to diffusion from above.

TRANSPORT OF IONIZATION FROM THE EQUATOR TO THE SUB-TROPICS

We shall suppose that the ionosphere over a large part of the globe is lifted perpendicularly to the geomagnetic field by an eastward electric field and subsequently gravitates back along the magnetic field lines to normal F-region heights. It can be seen from Fig. 2 that this will cause a shift of ionization away from the equator. We wish to calculate the actual redistribution of ion density with latitude which will result.

We shall assume that the ionization gravitates to the height from which it was originally lifted. This is not quite true. As we have said ionization is produced predominantly at, and thus lifted from, a height of about 250 km, whereas it settles to a height of between 300 and 350 km. This means that from 50 to 100 km more lift will be needed to produce a given result than our theory will indicate. As we shall argue that lifts of the order of 800 km occur this is of little consequence.

Assuming a dipole field the equation of a geomagnetic line of force is

$$\frac{r}{\cos^2\theta} = K \tag{2}$$

where r is the radial distance from the centre of the earth;
θ is the geomagnetic latitude;
K is the radial distance of the field line at the equator.

Now at $F2$-heights an electric field (E) perpendicular to the geomagnetic field (H), causes a drift normal to the plane of E and H with a velocity

$$v = \frac{E}{H}. \tag{3}$$

That is, for a given electric field the drift velocity is inversely proportional to the geomagnetic field strength. The distance between adjacent geomagnetic field lines is also inversely proportional to the geomagnetic field strength so that an electric field which shifts the ionization from one geomagnetic line to the other at the equator will, in the same time, shift the ionization from one line to the other at any latitude.

Now if ionization on the geomagnetic field line

$$\frac{r_1}{\cos^2\theta_1} = K_1 \tag{4}$$

is moved electrodynamically onto the geomagnetic field line

$$\frac{r_2}{\cos^2\theta_2} = K_2 \tag{5}$$

and if it then gravitates along this line until it reaches its original height, we have

$$r_1 = r_2 \tag{6}$$

and hence

$$r\left\{\frac{1}{\cos^2\theta_2} - \frac{1}{\cos^2\theta_1}\right\} = K_2 - K_1 \tag{7}$$

and from (2)

$$K_2 - K_1 = h \tag{8}$$

where h is the height of line (2) above line (1) at the equator. Thus

$$\frac{1}{\cos^2\theta_2} - \frac{1}{\cos^2\theta_1} = \frac{h}{r} \tag{9}$$

i.e.

$$\tan^2\theta_2 - \tan^2\theta_1 = \frac{h}{r}. \tag{10}$$

This then is the expression giving the change in latitude of the ionization. We now derive the change in ion concentration.

Referring to Fig. 5, suppose that ionization above the element of area dA_1 is carried to the element dA_2, then if n_1 was the number of ions per vertical column

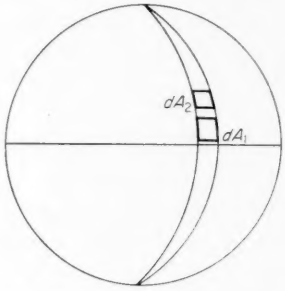

Fig. 5. Geometry of ion transport.

at dA_1 before transport, and n_2 is the corresponding areal density at dA_2 after transport

$$n_1\,dA_1 = n_2\,dA_2. \tag{11}$$

Let r be the radius of the earth, $d\phi$ the element of longitude, and $d\theta$ an element of latitude, then (11) becomes

$$n_1 r\,d\theta_1\, r\cos\theta_1\,d\phi = n_2 r\,d\theta_2 r\cos\theta_2\,d\phi \tag{12}$$

i.e.
$$n_2 = n_1\frac{\cos\theta_1}{\cos\theta_2}\frac{d\theta_1}{d\theta_2}. \tag{13}$$

Differentiating (10) with respect to θ_2

$$2\tan\theta_2\sec^2\theta_2 - 2\tan\theta_1\sec^2\theta_1\frac{d\theta_1}{d\theta_2} = 0 \tag{14}$$

i.e.
$$\frac{d\theta_1}{d\theta_2} = \frac{\tan\theta_2\sec^2\theta_2}{\tan\theta_1\sec^2\theta_1} \tag{15}$$

so that
$$n_2 = n_1\frac{\tan\theta_2\cos^3\theta_1}{\tan\theta_1\cos^3\theta_2}. \tag{16}$$

This is better expressed as a function of θ_2 only.

$$\frac{\cos^2\theta_2}{\cos^2\theta_1} = 1 - \frac{h}{r}\cos^2\theta_2 \tag{17}$$

and
$$\frac{\tan^2\theta_1}{\tan^2\theta_2} = 1 - \frac{h}{r}\cot^2\theta_2. \tag{18}$$

Hence
$$n_2 = \frac{n_1}{(1-(h/r)\cot^2\theta_2)^{1/2}(1-(h/r)\cos^2\theta_2)^{3/2}}. \tag{19}$$

To reiterate; if there were originally n_1 ions per vertical column at a latitude θ_1, an electrodynamic lift equivalent to a lift through a height h at the equator, followed by settling under gravity to the original height, will carry the ions to a

VOL.
18
196

latitude θ_2 determined by equation (10) and the number of ions per vertical column here will now be n_2 as given by equation (19).

It is a property of equations (10) and (19) that m operations with $h = h_1$, $h_2, \ldots . h_i \ldots . h_m$, respectively, produces the same result as a single operation with $h = \sum_{i=1}^{m} h_i$. Two 100 km lifts with settling after each lift produce the same effect as a single 200 km lift followed by settling. Hence lift and settling can occur concurrently without invalidating equations (10) and (19).

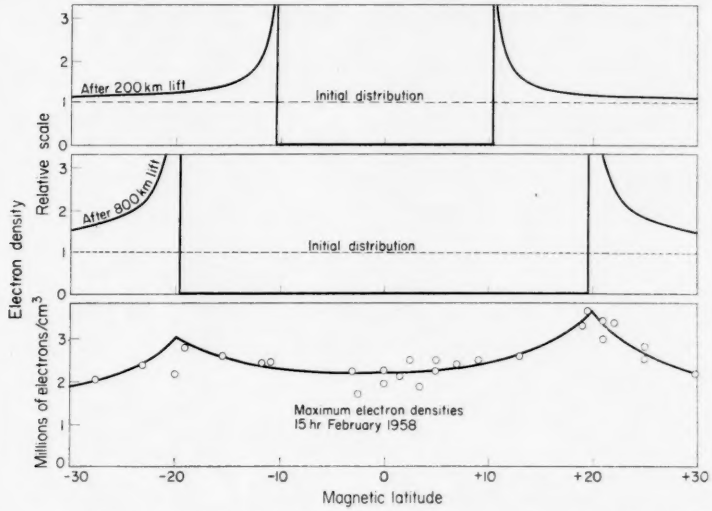

Fig. 6. The latitude distribution of electron content per vertical column, which would be produced from an initially uniform distribution by electrodynamic lift and subsequent settling down the geomagnetic field lines, compared with the mean maximum electron densities observed at 1500 hours during February 1958.

In Fig. 6 we have used equations (19) to determine the latitude redistribution, by lifts of 200 and 800 km, respectively, of an ion density initially uniform with latitude. The observed latitude variation of maximum electron density is shown for comparison. It can be seen that the transfer process can account for the high electron densities observed in the sub-tropics, if lifts as great as 800 km occur.

This is not improbable. The magnetic variations observed at Huancayo (Fig. 7) lead us to expect upward drift during the day and downward drift at night. Calculations analogous to those of DUNCAN (1956a) for the lunar tidal case, suggest velocities of about 85 km/hr. The height of maximum electron density above Huancayo is observed to fall through 300 km during the night (Fig. 8) and the actual downward drift of ionization must be greater, as downward movement of the layer profile is largely countered by preferential decay of the under surface. By day, ion production at a fixed height stabilizes the height of maximum electron density even more strongly, although the expected upward smearing of the layer is observed (Fig. 3). It will not even be the case that individual ions will reach heights of 1000 km because, as we shall show in the next

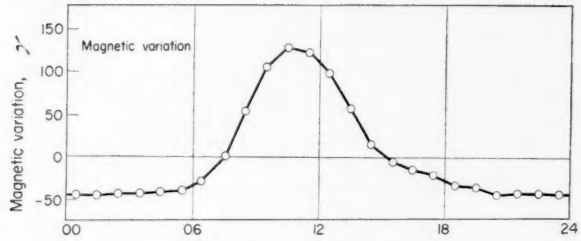

Fig. 7. The diurnal variation of the north–south geomagnetic field at Huancayo. Five quiet days, December 1938 (after JOHNSON *et al.*, 1948).

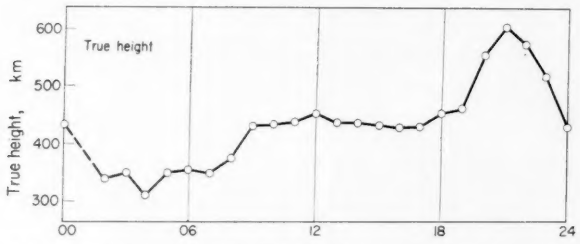

Fig. 8. The diurnal variation of the true height of the ionospheric electron density maximum at Huancayo. Five quiet days, December 1938 (after SCHMERLING and THOMAS, 1955).

VOL.
18
1960

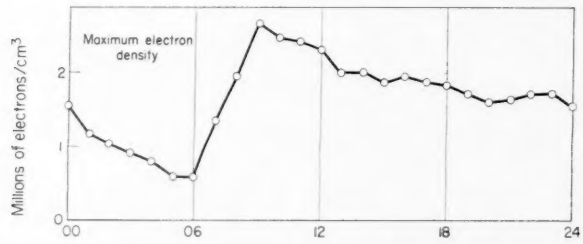

Fig. 9. The diurnal variation of maximum electron density, Chimbote, February 1958.

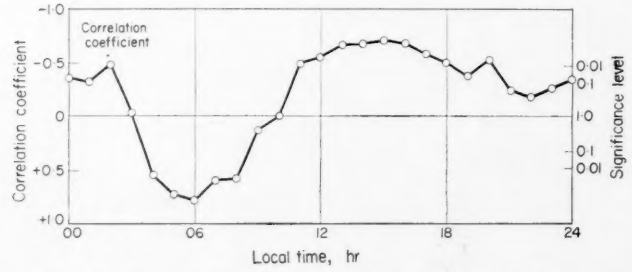

Fig. 10. The diurnal variation of the correlation between f_0F2, at Chimbote and Panama, February 1958. The ordinate has been reversed to bring out the relation of this variation to that of maximum electron density.

section; settling down along the field lines is prompt, and will occur concurrently with electrodynamic lift across them. A drift of 800 km across the geomagnetic field will not, then, result in an 800 km increase in height, but nevertheless there is every reason to believe that it occurs and that it is the cause of the enhanced electron densities observed in the sub-tropics.

The observed distribution of electron density with latitude (Fig. 6) is less extreme than the computed curves, but this is to be expected because of the mollifying effect of continuous ion production and decay.

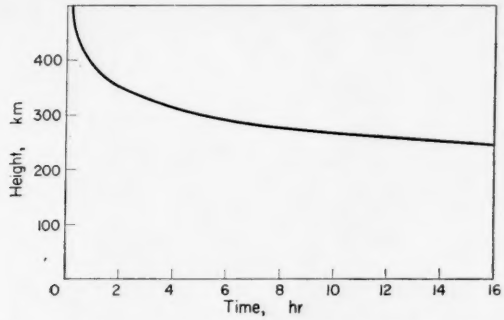

Fig. 11. Time for ionization to diffuse from the equator to various heights at a magnetic latitude of 20°.

OL.
18
960

Time Required for Ion Transport

It remains to be shown that ionization high above the equatorial zone will gravitate to the sub-tropics in an acceptable time.

The component of gravity along the geomagnetic field lines is $g \sin \chi$, where χ is the dip, and gas theory (Huxley, 1951) indicates that the ionization should gravitate down the field lines with a velocity

$$v = \frac{0{\cdot}85\, g \sin \chi}{\nu} \tag{20}$$

ν being the collision frequency of the positive ions with neutral molecules. The collision frequency term (ν) causes the settling velocity to increase exponentially with height and numerical substitution shows that this factor overwhelms the effect of the great length and low inclination of that part of the geomagnetic field line above the equatorial zone. Almost all the time for the journey is taken over the last hundred or so kilometres. The time for the journey thus depends, not on how far the ionization has travelled, but on the depth to which it settles.

The times needed for ionization at a magnetic latitude of 20° to settle to various heights is shown in Fig. 11. In calculating these Martyn's (1959) estimate of the collision frequency at 300 km, viz. 1·1 $\sec^{-1}$, was adopted and this was assumed to decrease exponentially with altitude with a scale height of 50 km, i.e.

$$\nu = 1{\cdot}1 \exp \frac{300 - h}{50} \sec^{-1}. \tag{21}$$

It will be seen that ionization settles to 350 km in about 2 hr.

The Mean Diurnal Behaviour of the Equatorial *F*-region

The diurnal variation of the geomagnetic field at Huancayo is shown in Fig. 7. An application of Ampere's law shows that if the currents responsible for this variation flow in the ionosphere they should cause an electrodynamic tide with maximum upward velocity at midday and maximum downward velocity at midnight. Keeping in mind the great resistance to movement of the height of maximum electron density ($h_{\max}F2$) conferred by ion production at a fixed height during the day, it can be seen that the magnetic variation and the observed variation of true $h_{\max}F2$ are in accord (Fig. 8).

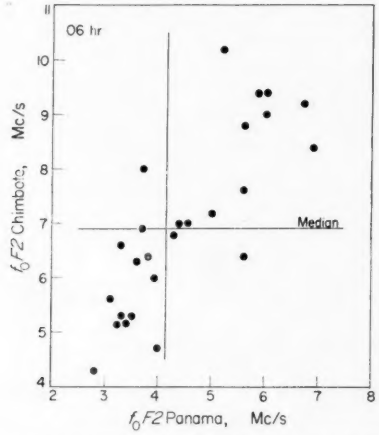

Fig. 12. Critical frequency at 0600 hours at Chimbote against that at Panama, February 1958.

Minimum $h_{\max}F2$ occurs at 0400 hours, naturally a little after the time of maximum downward velocity. Similarly the maximum effect from the day-time upward drift, which as we have said should be more in the nature of an upward smearing of the region than an outright increase in $h_{\max}F2$, should occur in the mid-afternoon.

Consider now the effect these tidal drifts will have on the critical frequency. The lowering of the ionosphere at 0400 hours should carry it into a region of high neutral particle density and consequent rapid electron decay. The critical frequency should therefore drop rapidly at this time and, as is well known, it does (Fig. 9). There is, naturally, a second time-lag here; minimum f_0F2 occurs at 0600 hours, a couple of hours after the time of most rapid decay.

The process just described will be effective at both Chimbote and Panama, so that if day to day fluctuations in f_0F2 are largely due to fluctuations in the amplitude of the electrodynamic tide, Chimbote and Panama f_0F2 should be positively correlated at dawn. Fig. 12 shows that they are.

Upward drift, occurring as it does during daylight, will also cause a decrease of the maximum electron density by spreading ionization upwards from the height of production. The total electron content of the ionosphere will, however,

VOL.
18
196

be increased as electrons are carried to the high regions of low decay. In the afternoon therefore, when, as we have said, the effects of upward drift will be at their maximum, we should expect the critical frequency in the equatorial zone to be perhaps slightly depressed but the layer should be high and thick. This store of electrons in the high regions of low decay should give it long life, and a relatively high electron density should therefore persist after sunset. The observed equatorial *F*-region (Fig. 9) has the expected behaviour.

The high ionization in the equatorial zone will tend to gravitate down the geomagnetic field lines to the sub-tropics. In the mid-afternoon therefore we should expect f_0F2 at Chimbote and Panama to be negatively correlated and the phenomena of high critical frequencies in the sub-tropical belts to be most pronounced. Figs. 1 and 10 show that such is the case.

Acknowledgements—This work forms part of the programme of the Upper Atmosphere Section of the Commonwealth Scientific and Industrial Research Organization. I am greatly indebted to Dr. D. F. MARTYN for careful criticism of the paper.

Data studied were circulated by the Cavendish Laboratory, the Carnegie Institution of Washington, the Central Radio Propagation Laboratory of the U.S. National Bureau of Standards, the Indian Council of Scientific and Industrial Research, the Belgian Bureau de Geophysique, and the French Institut pour la Recherche Scientifique en Afrique Centrale.

I am indebted to Dr. B. A. CHARTRES for advice on the use of Sydney University's Silliac computor, on which the correlation coefficients were calculated.

OL.
18
960

REFERENCES

APPLETON E. V.	1946	*Nature, Lond.* **157,** 691.
BAILEY D. K.	1948	*Terr. Magn. Atmos. Elect.* **53,** 35.
BERKNER L. V.	1940	*International Union of Geodesy and Geophysics, Transactions of Washington Meeting, 4–15 September* 1939. Bulletin No 11, p. 417.
CHAPMAN S. and FERRARO V. C. A.	1941	*Terr. Magn. Atmos. Elect.* **46,** 1.
DUNCAN R. A.	1956a	*Aust. J. Phys.* **9,** 112.
DUNCAN R. A.	1956b	*Aust. J. Phys.* **9,** 436.
DUNCAN R. A.	1958	*J. Geophys. Res.* **63,** 491.
DUNGEY J. W.	1956	*J. Atmosph. Terr. Phys.* **9,** 90.
GATES D. M.	1959	*J. Res. Nat. Bur. Stand.* D **63,** 1.
HUXLEY L. G. H.	1951	*Proc. Phys. Soc.* B **64,** 844.
JOHNSTON H. F., MCNISH A. G., THORBUSH S. E., SCOTT W. E., VALSAM E. and LEDIG P. G.	1948	*Magnetic Results from Huancayo Observatory, Peru,* 1936–1944. Carnegie Institution of Washington.
MARTYN D. F.	1954	*The Physics of the Ionosphere,* p. 259. Physical Society, London.
MARTYN D. F.	1956	*Aust. J. Phys.* **9,** 161.
MARTYN D. F.	1959	*Proc. Inst. Radio Engrs, N.Y.* **47,** 147.
MCNISH A. G. and GAUTIER T. N.	1949	*J. Geophys. Res.* **54,** 303.
MITRA S. K.	1946	*Nature, Lond.* **158,** 668.
RASTOGI R.G.	1959	*J. Atmosph. Terr. Phys.* **14,** 31.
ROCKET PANEL	1952	*Phys. Rev.* **88,** 1027.
SCHILLING G. F. and STERNE T. E.	1959	*J. Geophys. Res.* **64,** 1.

Schmerling E. R. and Thomas J. O.	1955	*Tables of* F2*-layer Electron Density on International Quiet Days.* Cavendish Laboratory, Cambridge.
Skinner N. J., Brown R. A. and Wright R. W.	1954	*J. Atmosph. Terr. Phys.* **5,** 92.
Wright J. W., Knecht R. W. and Davies K.	1957	*Annals IGY.* Vol. III, pt. I, p. 50. Pergamon Press, London.
Yonezawa T.	1956	*J. Radio Res. Lab.* **3,** 1.

VOL
18
196

Journal of Atmospheric and Terrestrial Physics, 1960, Vol. 18, pp. 101 to 122. Pergamon Press Ltd. Printed in Northern Ireland

Enhanced ionization in the polar ionosphere associated with geomagnetic storms

TATSUZO OBAYASHI and YUKIO HAKURA
Radio Research Laboratories, Kokubunji, Tokyo

(*Received* 29 *October* 1959)

Abstract—New evidence indicating the existence of energetic solar particles associated with solar flares has been found from the analysis of world-wide data of $f_{\min}$ in the ionograms. An outstanding enhancement of ionization in the lower ionosphere occurs in the polar region with the delay of several hours after a large solar flare accompanied with major radio outbursts of type IV. Radio blackouts due to enhanced ionizations develop, spreading inside the whole polar cap without inducing any marked geomagnetic activity. With the onset of a geomagnetic storm, however, the blackout region spreads from the polar cap up to the so-called auroral zone. As the D_{st} field of geomagnetic storm develops, it comes down to considerably low latitudes forming a spiral-shaped ionization pattern.

The radio blackouts, which precede the onset of geomagnetic storms, may be termed the polar cap blackouts because they are confined within the geomagnetic latitude of about $60 \sim 65°$, while those related to geomagnetic storms and auroral displays are the auroral zone blackouts. It is shown that the polar cap blackouts are caused by the invasion of energetic particles of the order of $10 \sim 100$ MeV, generated in an agitated solar coronal plasma bearing magnetic fields, and that those particles precipitate on the polar ionosphere following nearly the Störmer orbits. For the auroral zone blackouts, an improved version of the Störmer theory is applied, in which an interesting behaviour of a charged particle in the distorted geomagnetic field is revealed. The remarkable equatorward shifting of the auroral zone and some peculiar increases of cosmic ray intensity during the main phase of magnetic storms are explained consistently by the decrease of geomagnetic cut-off for incoming particles owing to the contraction of the geomagnetic cavity.

1. INTRODUCTION

SINCE the greatest solar activity was attained during the IGY 1957–1958, considerable interest has been stimulated on the research concerning solar disturbances and their effects on the terrestrial ionosphere. It has been discovered, recently, that an enhanced ionization in the ionosphere, which is indicated by the increase of $f_{\min}$ or the black-out of echoes in the ionograms, occurs in the polar cap several hours after great solar flares and, yet, well before the onset of geomagnetic storms (HAKURA *et al.*, 1958). Since it is thought that polar blackouts are caused by the abnormal ionization due to bombardment of energetic particles, this fact would suggest the invasion of solar particles of presumably higher energies than those producing geomagnetic storms. Incidentally, one occasion of such polar blackouts and an increase of absorption of v.h.f. waves has already been noted by SHAPLEY and KNECHT (1958) and BAILEY (1957, 1959) at the event associated with the great solar flare of 23 February 1956. Meanwhile, a new technique measuring the ionospheric absorption of v.h.f. cosmic radio noise has been developed during the IGY, and it has been revealed by these observations that an excess ionization in the polar ionosphere occurs frequently following great solar flares (REID and COLLINS, 1959; LEINBACH and REID, 1959). The effect is essentially identical with the above-mentioned polar blackouts, suggesting that such events are more frequent than ever has been suspected.

Precise global patterns of abnormal ionization in the lower ionosphere are revealed in this paper by examining world-wide data of $f_{\min}$ during the IGY. Two

characteristic types of ionization pattern are found: The one appears before the onset of geomagnetic storms, the enhanced ionization being confined within the polar cap region. In contrast to this, the other is accompanied with geomagnetic storms and aurorae, being formed along the so-called auroral zone, though the outer boundary of this zone shows considerable equatorward shifting at the main phase of geomagnetic storms.

Explanations for these phenomena are given in terms of the conditions of the outer geomagnetic field and behaviour of incoming charged particles from the sun. Some discussion about the statistical solar–terrestrial relationship and the nature of solar corpuscular clouds will also be given briefly.

2. Polar Blackouts Associated with Intense Solar Radio Outbursts and Geomagnetic Storms

It has been known that radio waves passing through the polar routes suffer severe attenuation during geomagnetic storms. Although a part of this is due to *F2*-region disturbances, the enhanced ionization in the lower ionosphere has an important effect. In order to investigate such abnormal ionization, data of $f_{\min}$ in the ionograms are very useful. The $f_{\min}$ is one of the elements of vertical ionospheric soundings defined as the minimum frequency of which ionospheric echoes are observable, and its time variation mainly depends on the electron density in the lower ionosphere. The value of $f_{\min}$ increases when an excess solar ultra-violet radiation (soft X-rays) is present and when corpuscles invade the lower ionosphere. The former is known as the "s.i.d. effect" and the latter is the "polar blackouts". Sometimes all ionospheric echoes are completely masked.

Using the data of about sixty ionospheric stations, world-wide variations of $f_{\min}$ associated with geomagnetic storms are examined. The location map of ionospheric stations whose data are used in the present analysis is shown in Fig. 1.

Although the analysis is made for all data during the period of the IGY, in order to show the general aspect of disturbances, a typical one associated with the severe magnetic storm of 13 September 1957 is described. A pattern of the storm-time variation of $f_{\min}$ vs. geomagnetic latitudes is illustrated in Fig. 2, with the geomagnetic record at Kakioka (geomagnetic latitude 26°). The upper one is for the pattern in the North America zone and the lower is in the Australia zone. The hatched regions indicate increased $f_{\min}$ or blackouts. The regions enclosed by dotted lines are those of increased $f_{\min}$ caused by s.i.d.s and they are confined in the middle and low latitudes of the sunlit hemisphere.

It is clear that an outstanding increase of $f_{\min}$ appeared at high latitudes both in the northern and southern hemispheres well before the onset of magnetic storm, and it was enhanced gradually up to the time of the s.c. of magnetic storm. Intense polar blackouts were observed along the auroral zones in the earlier stages of the storm, while in the last phase no systematic widespread blackout was observed. It was also remarkable that the pattern was almost symmetrical with respect to the geomagnetic equator and did not show any marked difference when the region was in the sunlit or dark hemispheres.

The original *f*-plot obtained at Tikhaya Bay ($\phi = 80°3'$ N, $\lambda = 52°8'$ E) is also reproduced in Fig. 3. It is noted that an abrupt increase of $f_{\min}$ was observed

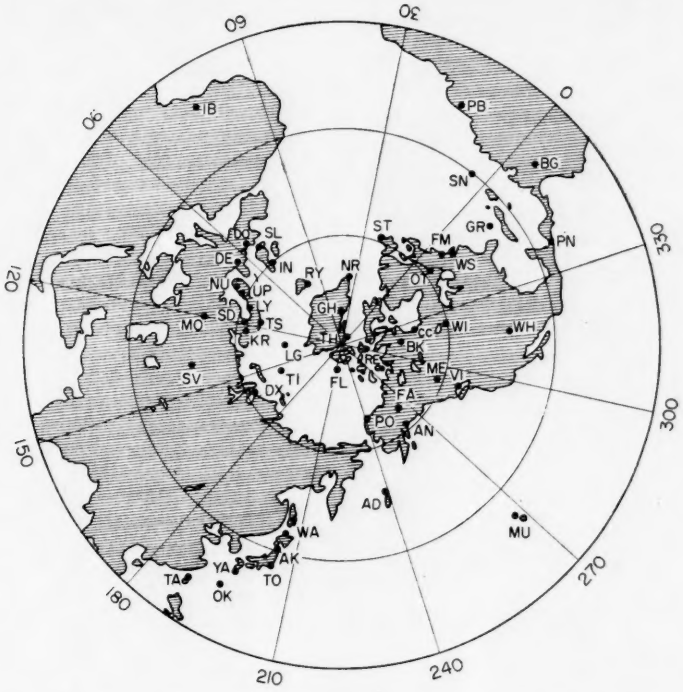

Fig. 1. Distribution of ionospheric stations whose data are used in the present study.

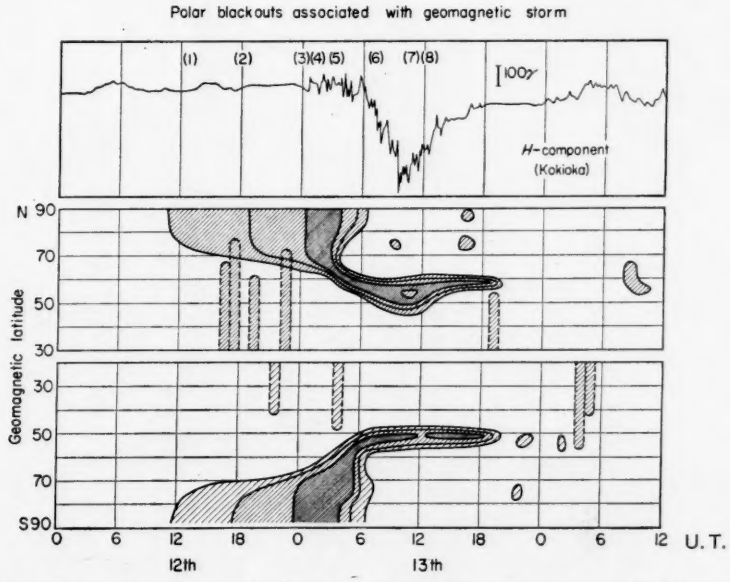

Fig. 2. Latitude effect of polar blackouts associated with a severe magnetic storm on 13 September 1957. The hatched regions show abnormal increase of f_{min} and complete blackouts (dense hatching).

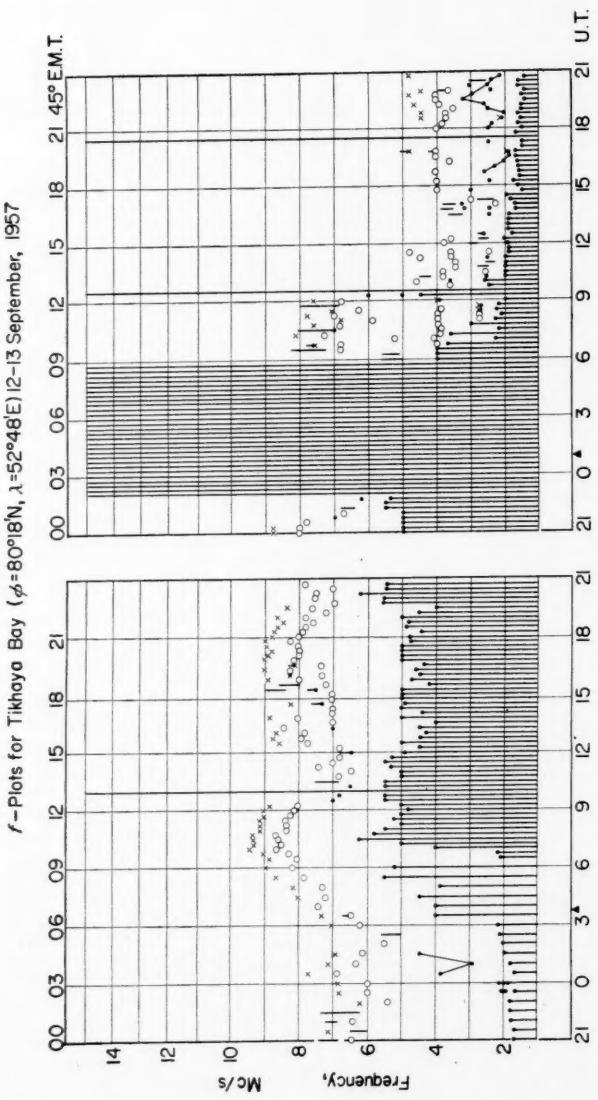

Fig. 3. *f*-Plots for Tikhaya Bay. (a) 12 September 1957; ▲ indicates onset of abnormal ionization. (b) 13 September 1957; ▲ indicates s.c. of magnetic storm.

clearly at 0330 hours on 12 September, which was about 21 hr earlier than the time of s.c. of magnetic storm. Since it is generally believed that polar blackouts are caused by the spontaneous ionization due to the invasion of energetic particles from the outer space, the present result suggests that some corpuscles, which have probably originated from the sun, are impinging on the earth well before the

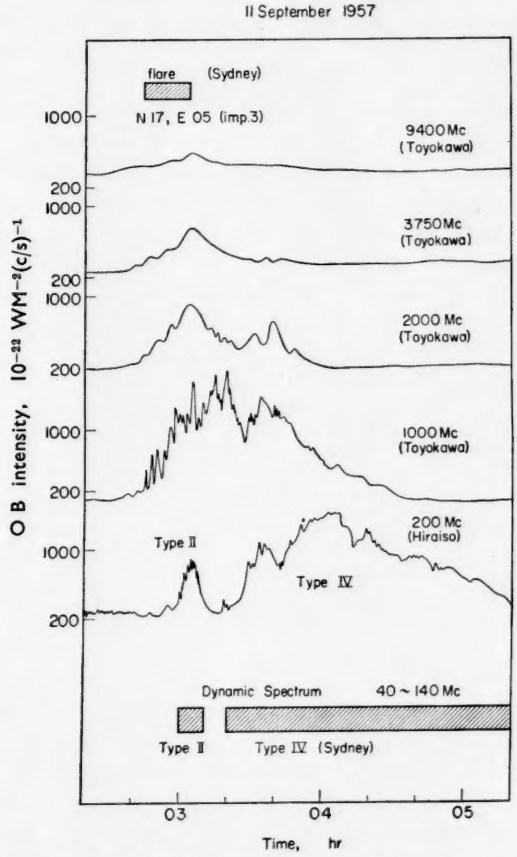

Fig. 4. A solar flare at 0245 hours 11 September 1957 and accompanied solar radio outbursts (data observed at Sydney are by the courtesy of J. P. WILD).

onset of geomagnetic storm. In fact, according to SINNO (1958), an important solar flare accompanied by major radio outbursts of type IV was observed at 0245 hours on 11 September (Fig. 4), and this would possibly be the source of the disturbance described above.

This fact may be very important, and a further confirmation is required. As shown elsewhere (HAKURA and GOH, 1959), a statistical investigation was made to find out the solar–terrestrial relationship responsible for those polar ionospheric disturbances: During the period July 1957 to December 1958, there were fifty-nine s.c. magnetic storms of which twenty were followed by major radio outbursts

with type IV. It has been found that prolonged severe polar blackouts which preceded geomagnetic storms were always associated with those of the type IV outbursts except in three rather doubtful cases. The occurrence probability of such polar blackout following type IV outburst is about 75 per cent whereas without type IV it is only 8 per cent. Since the type IV outburst is caused by synchrotron radiation of relativistic electrons in a violently agitated plasma bearing magnetic fields (BOISCHOT and DENISSE, 1957), the generation of high-energy particles may also be expected. Therefore, the early invasion of energetic particles into the polar cap could be explained on this basis. The discussion of this will be given later.

In order to investigate details of particle precipitation on the upper atmosphere, world-wide patterns of polar blackouts are examined using simultaneous values of $\Delta f_{\min}$ (deviation from the quiet-day values) at all stations. The progresses of polar blackouts for various stages of magnetic storm are drawn on the map viewed from above the geomagnetic north pole. They are shown in Fig. 5, in which numbers (1)–(8) show the respective stages of the magnetic storm indicated in Fig. 2, contour lines are at 2 Mc/s intervals, and hatched regions are complete blackouts.

Important characteristics of disturbances for respective stages are described briefly as follows: In the pre-s.c. stage (1)–(3), an area of increased $f_{\min}$ appears somewhere in the polar region well before the s.c. of magnetic storm. Polar blackouts are then enhanced gradually and at the time of s.c. (4), the disturbance is induced in the whole polar cap within the geomagnetic latitude of 60°. Since it is likely that the conductivity in the polar cap is greatly enhanced at this time, this would possibly be attributed to the observed geomagnetic current system of s.c.s in the polar regions which has been found previously by one of the writers (OBAYASHI and JACOBS, 1957).

In the initial to the main phase of the storm (5)–(7), the region of blackouts starts to elongate towards lower latitudes in the morning hemisphere. Then it moves to concentrate along the so-called auroral zone, forming rather like a right-hand spiral pattern. During the main phase of the storm, the outer edge of the disturbed region shows considerable southward shifting as the magnetic storm progresses. It is quite remarkable that the tail of the disturbed region comes down well south of the usual auroral zone to about 40° N of geomagnetic latitude at the end of the main phase. In the last phase (8), however, all systematic disturbance suddenly disappears and only some remnants of abnormal ionization are observed in the polar regions.

The most important feature discovered in the present analysis is that there are two distinct patterns of enhanced ionizations in the polar ionosphere. The polar cap blackouts, which are confined within the geomagnetic latitude of about 60–65°, are observed before the onset of geomagnetic storm. On the other hand, during the progress of storm, blackouts spread along the so-called auroral zone, and may be termed the auroral zone blackouts. This has been confirmed by the independent discovery in the study of abnormal absorption of cosmic noise at v.h.f. band by REID and COLLINS (1959), in which they showed two types of absorption event other than the s.i.d.s; one is closely connected with great solar flares and occurs only at high latitudes, while the other is for the most part a night-time effect

VOL.
18
196

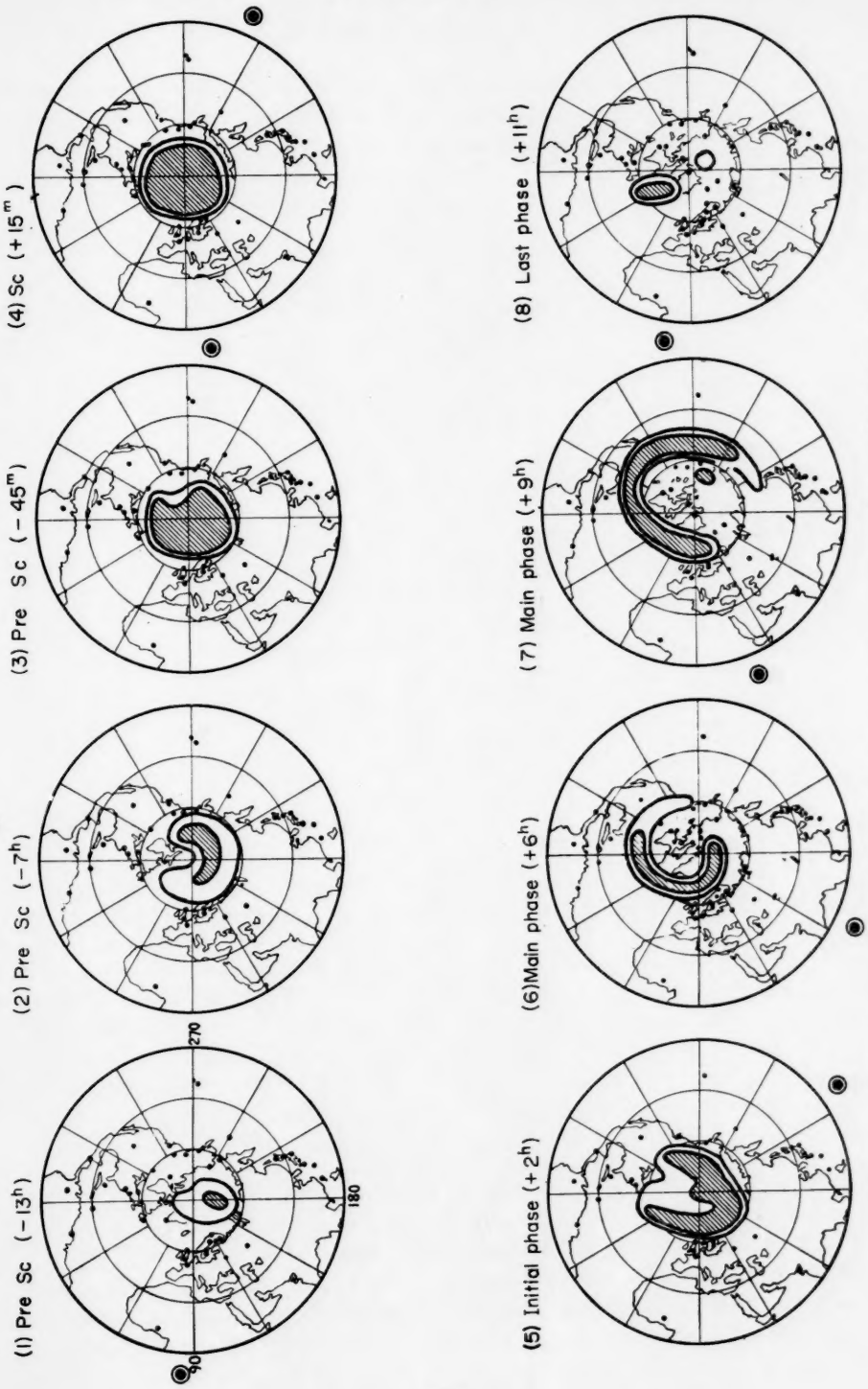

Fig. 5. The world-wide patterns of $\Delta f_{\min}$ (contour lines every 2 Mc/s, and hatched regions are complete blackouts) for various stages of the geomagnetic storm of 13 September 1957.

and its occurrence is correlated with that of visible aurorae and local geomagnetic disturbances.

Auroral zone blackouts have a remarkable characteristic. The zone of enhanced ionization shows considerable equatorward shifting during the main phase of magnetic storm. In Fig. 6, the storm-time changes of the latitude of the southern-most extent of enhanced ionization and that of visible aurora in the North America

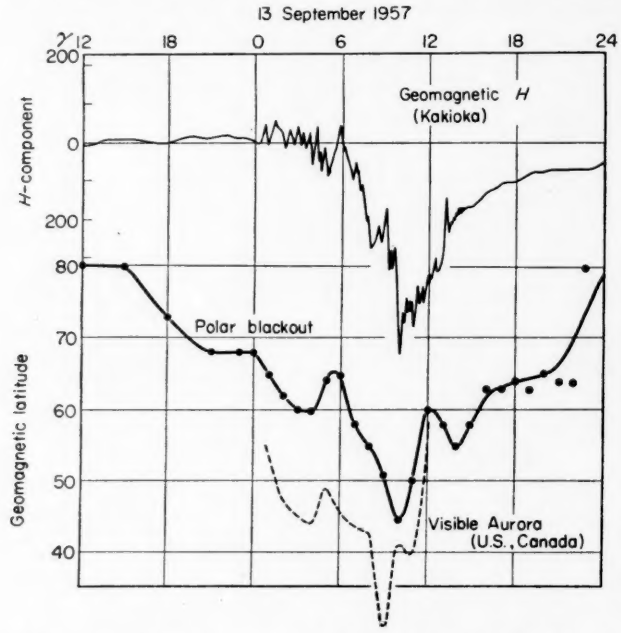

Fig. 6. Southwards shifting of the outer boundary of polar blackouts and southern-most extent of visible aurorae.

zone (supplied by P. MILLMAN, N.R.C. Canada) are illustrated with the record of geomagnetic horizontal intensity at Kakioka. There is an outstanding correlation between the enhanced ionization and visible aurorae. A slight discrepancy will be removed if it is presumed that aurorae can be seen well in the northern horizon, while radio blackouts indicate the condition overhead. The difference is estimated to be about 10° and this accords well with the observed result. It is also evident that the equatorward shifting of the auroral zone is proportional to the depression of the geomagnetic field intensity, viz. the D_{st} field of the geomagnetic storm. Since the D_{st} field is believed to be of the external origin, this fact may suggest that the precipitation of charged particles is controlled by the distorted outer geomagnetic field during the storm. A theoretical discussion of this geomagnetic storm effect is given in the following sections.

3. GEOMAGNETIC STORM EFFECTS FOR INCOMING SOLAR PARTICLES

Enhanced ionizations in the polar ionosphere associated with geomagnetic storms are of special importance for understanding the behaviour of solar corpuscles precipitated on the earth's upper atmosphere. The problem involved is to solve the

motion of charged particles in the geomagnetic field, and to reveal the precipitation pattern of particles so that the observed results can be compared. However, the present results indicate rather complicated situations for the invasion of charged particles and they can not simply be explained by the Störmer theory. NAGATA (1950), some years ago, pointed out the importance of the effect of an existing ring current, and he showed that the observed southward shifting of the auroral zone could be explained by the development of the D_{st} part of geomagnetic storms. It has been revealed by recent investigations, however, that the outer atmosphere at distances greater than several earth radii is drastically disturbed during magnetic storms, and that the geomagnetic field is confined within a cavity surrounded by corpuscular streams (OBAYASHI, 1958; PARKER, 1958). Therefore, the field due to the ring current no longer exists outside the cavity but is replaced by the disordered magnetic fields due to violent agitations in the corpuscular clouds. In fact, the earth is immersed in interplanetary gas.

Even under undisturbed conditions there must be a relative motion between the interplanetary gas and the earth with a velocity which is at least comparable with the orbital velocity of the earth. As might be expected, the gas stream interacts with the geomagnetic field and it can only penetrate up to the distance where the hydrodynamic pressure of the stream is balanced by the geomagnetic pressure; since the geomagnetic field behaves in such a way to prevent the gas stream coming nearer the earth thus the stream flows round the surface of the cavity. Assuming that interplanetary gas consists of protons and electrons and has the bulk speed V, the equation of hydromagnetic balance is given approximately as

$$\frac{H^2}{8\pi} = nmV^2 \tag{1}$$

where n and m are the particle density and the proton mass, respectively, H is the total magnetic field at the surface of the stream, and twice the original geomagnetic field at that point when the gas stream is perfectly conducting. Namely

$$H = \frac{2H_0}{R^3};\ H_0 = 0{\cdot}3 \text{ gauss}. \tag{2}$$

The size of the cavity, forbidden space for the gas-stream, formed in this way can be approximated to a sphere of its radius of

$$R_0 = \left[\frac{{H_0}^2}{2\pi nmV^2}\right]^{1/6}. \tag{3}$$

Since $n \sim 10^3/\text{cm}^3$ and $V \sim 30$ km/sec, under undisturbed condition, the distance of the cavity boundary is about ten earth radii. Such a cavity formation surrounding the earth may also be expected for the impact of solar corpuscular clouds, which is identified by the onset of geomagnetic storms. Corpuscular clouds must have much stronger energy than usual solar streams, and hence they penetrate deeper into the outer atmosphere forming a distinct and much contracted cavity. Since the particle density of the clouds is about 10^3–10^4 protons/cm^3 and their invading velocity is of the order of 1000 km/sec, the distance of cavity is reduced to a few earth radii at the equatorial plane.

Furthermore, it is noted that during geomagnetic storms the field inside the cavity may not be a simple dipole field, but it will be distorted considerably. The observed world-wide change of the field during magnetic storms indicates the existence of an impressed field parallel to the geomagnetic axis. An interesting situation is that, though low energy particles in the cloud will flow round the surface of the cavity, some high energy particles penetrate through the distorted geomagnetic field into the earth. As will be shown elsewhere (OBAYASHI and HAKURA, 1960), the density of those high energy particles entering to the polar ionosphere would be sufficiently low allowing to be treated as a single charged particle, though the bulk of low energy particles behaves like a conductive plasma because the mutual interaction of particles is important.

With these considerations, an improved version of the Störmer theory is attempted. A general theoretical computation of the entry of charged particles under the condition of the distorted geomagnetic field is described in the Appendix. The result seems to be very encouraging, and this is applied to the observed precipitation patterns of particles at various stages of geomagnetic storms.

The polar cap blackouts occur well before the onset of geomagnetic storms. Since the distortion of the geomagnetic field may be slight at this stage, those particles causing blackouts will enter into the earth, following nearly Störmerian orbits. The observed outer boundary of the precipitation of particles is the geomagnetic latitudes of 60–65°. Therefore, from Fig. 6A in Appendix, it is found that the energy of incoming particles would be of the order of 10–100 MeV assuming that the cavity is situated at about ten earth radii before the onset of geomagnetic storms. Unlike ordinary auroral zone ionizations, the observed pattern of abnormal ionizations indicates that the precipitation of particles occurs in the whole polar cap. This effect seems to suggest an apparent isotropy of incoming particles, arriving essentially uniformly from all directions.

The early invasion of solar corpuscles before the onset of geomagnetic storms, however, requires further discussion. Although the nature of the acceleration process of particles in the solar corona remains a field for lively speculation, there is some good reason to suppose that the sun ejects particles of considerably wide energy spectrum at the time of solar eruptions (OBAYASHI and HAKURA, 1960). The low-energy particles then form a corpuscular cloud and flow outwards into interplanetary space with the velocity of the order of 1000–2000 km/sec, while high-energy particles are also trapped inside, owing to the existence of weak magnetic fields in the cloud. Since the magnetic trapping may not be strong enough for high-energy particles, they might escape gradually from the cloud, and hence arrive at the earth earlier than the onset of geomagnetic storms.

Since the corpuscular cloud is responsible for geomagnetic distortions, a geomagnetic storm starts immediately after the arrival of the cloud at the earth. Beams of high-energy particles inside the cloud then impinge on the upper atmosphere in the polar regions through the distorted geomagnetic field. This is the situation of the auroral zone blackouts. Since the outer boundary of the auroral zone mainly depends on the size of the geomagnetic cavity, a remarkable equatorward shifting of the auroral zone during the main phase of magnetic storms, shown in Fig. 6, could be explainable on this basis.

VOL.
18
196

In order to compare the observed result with the theoretical computation, a diagram, giving the relation between ΔH, the depression of the geomagnetic field, viz. the D_{st} part of magnetic storms, and the latitude Φ of southern-most extent of particle precipitation, is constructed using the equations in Appendix. The cut-off rigidity of a particle P is given by

$$P = \frac{M \cos^4 \Phi \, (1 + a^3/2R_0^3)}{4a^2\gamma^2} \tag{4}$$

and

$$\Delta H = -\frac{M}{R_0^3} \tag{5}$$

where R_0 = radius of the geomagnetic cavity, and M, a and γ are the geomagnetic moment, radius of the earth and the numerical integration constant, respectively.

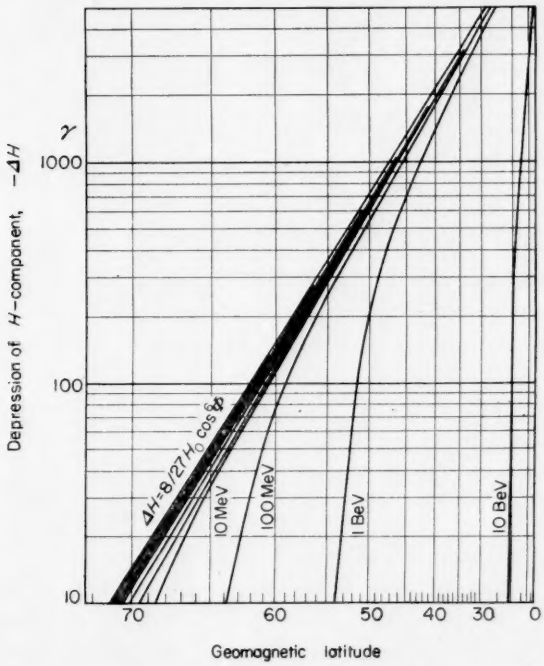

Fig. 7. The relation between the depression of the geomagnetic field and the minimum geomagnetic latitude of particle precipitation for various cut-off energies of solar particles. Cut-off energy–latitude curves for distorted geomagnetic field.

Fig. 7 shows the relation of ΔH and Φ for various cut-off energies of solar particles. For low-energy particles ΔH is proportional to $(\cos \Phi)^6$, while high-energy particles do not exhibit any appreciable latitude shift with respect to the change of ΔH. From this diagram it is possible to predict the change of the latitude of precipitation zone by using the observed D_{st} field of the magnetic storm.

To carry this out, the energy of incoming particles must be specified. The energy of particles responsible for auroral zone blackouts may be somewhat less

than that of polar cap blackouts. It is probably 1 MeV or less because of their late arrival and also of evidence from auroral observations (MEINEL, 1950; CHAMBERLAIN, 1954). Using this value, the observed southern-most extent of auroral blackouts shown in Fig. 6 is compared with the theoretically expected one in Fig. 8. Agreement between the two curves is very good except for some minor discrepancies, justifying the theory and the model of the outer atmosphere during geomagnetic storms.

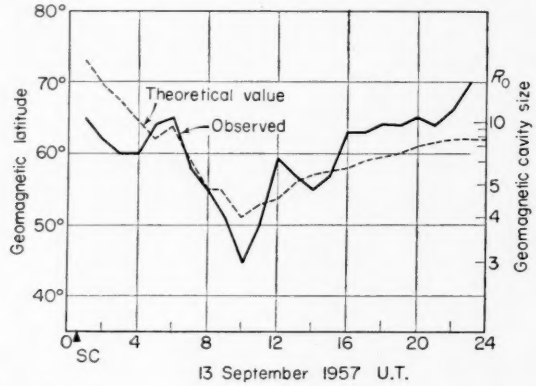

Fig. 8. Observed southern-most extent of auroral blackouts and the theoretically estimated one from the D_{st} field of the magnetic storm.

The curve of precipitation is also of special interest. The pattern of auroral blackouts shows a rather spiral-like shape, which is very similar to that of the spiral curve of precipitation predicted by STÖRMER (1955) providing that the particles are protons. According to STÖRMER, the orbit of $\gamma \leqslant \gamma^*$ will strike the earth at points which define the curve of precipitation forming a spiral round the geomagnetic axis. The point is approximately given by the formulae

$$\cos \Phi_\gamma = \sqrt{\frac{2\gamma a}{s_0}} \qquad [\gamma \leqslant \gamma^*] \tag{6}$$

and it is evident that the tail of the spiral corresponding to the value $\gamma = \gamma^*$ is the theoretical outer boundary of the auroral zone. The present result indicates that the particles are mostly protons and, unlike the polar cap blackouts, the invading particles are coming from a fixed direction and are essentially anisotropic. The importance of the fact that the high-energy particles causing polar cap blackouts or auroral zone blackouts follow essentially the Störmerian orbits must be emphasized.

There is another interesting fact, lending further support to the theory of distortion of the outer geomagnetic field during geomagnetic storms. This is the effect found by YOSHIDA and WADA (1959) in their analysis of world-wide cosmic ray storms. They have shown that the world-wide increases of cosmic ray intensity occur associated with severe geomagnetic storms, though they are usually superposed on the Forbush type decreases. The event of 13 September 1957 was an especially typical one; the cosmic-ray intensities observed by neutron monitors at middle and low latitudes show marked increases, coinciding with the maximum depression of

the geomagnetic field. KONDO *et al.* (1960) have given an explanation of this effect as due to decrease of cut-off rigidities of incoming cosmic rays caused by depression of the geomagnetic field during the geomagnetic storm. This is exactly the same line of thought mentioned in the discussion of the auroral zone blackouts. Therefore, the present theory could predict the nature of such cosmic ray disturbances consistently.

As has been shown in equation (4), the cut-off rigidity of an incoming particle P can approximately be expressed by

$$P = \frac{M \cos^4 \Phi}{4a^2\gamma^2} \qquad [a \ll R_0]. \tag{7}$$

If P_0 denotes the cut-off rigidity when $R_0 \to \infty$, viz. an undisturbed geomagnetic dipole field, and hence $\gamma = 1$, then

$$P = P_0/\gamma^2 \tag{8}$$

where

$$P_0 = \frac{M \cos^4 \Phi}{4a^2} \tag{9}$$

γ is a numerical constant which is specified by P_0 and ΔH (or the size of cavity R_0). The change of geomagnetic cut-off rigidity ΔP is given by differentiating the equation (8),

$$\frac{\Delta P}{P_0} = \frac{P_0 - P}{P_0} = 1 - \frac{1}{\gamma^2} \tag{10}$$

and this is shown in Fig. 9 with a parameter of the depression of geomagnetic field ΔH (cf. equations (4), (5) and (10)).

To calculate the intensity increase from the estimated $\Delta P/P_0$, one may utilize the observed latitude curves of cosmic-ray neutron intensity (KONDO *et al.*, 1960), or else it can be obtained by the following way. Since the intensity of integral rigidity spectrum of cosmic-ray I can be written as

$$I = \int_{P_0}^{\infty} m(P, x) i(P)\, dP \tag{11}$$

where $m(P,x)$ is the overall multiplicity at P and atmospheric depth x g cm^{-2},

$$m(P,x) = m_0(x) P_0^{\alpha(x)} \tag{12}$$

and

$$i(P) = i_0 P^{-(n+1)}\, dP \tag{13}$$

then

$$I = m_0 i_0 \int_{P_0}^{\infty} P^{-(n-\alpha+1)}\, dP \tag{14}$$

the increment of cosmic-ray intensity is given by

$$\frac{\Delta I}{I_0} = -(n - \alpha)\frac{\Delta P}{P_0}. \tag{15}$$

The expected rigidity spectrum of the increment of cosmic-ray intensity is obtained from equations (10) and (15), and is compared with the observed increments for

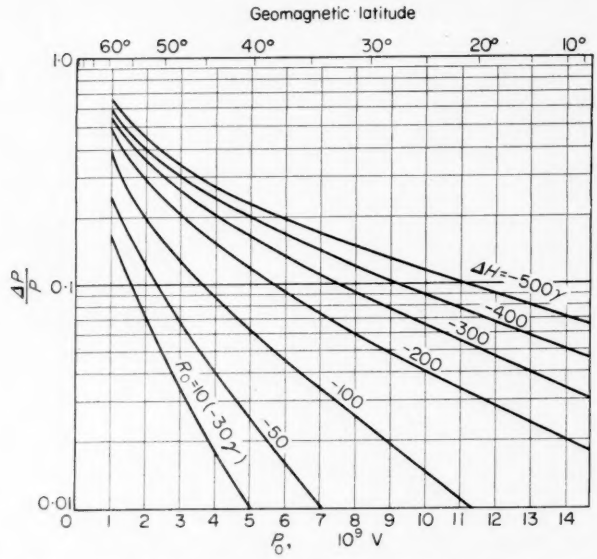

Fig. 9. Change of magnetic cut-off rigidity due to the depression of the geomagnetic field during storms.

$$P = \frac{P_0}{\gamma^2} = \frac{M \cos^4 \Phi}{4a^2\gamma^2} \qquad \frac{\Delta P}{P_0} = 1 - \frac{1}{\gamma^2(\Delta H, P_0)}$$

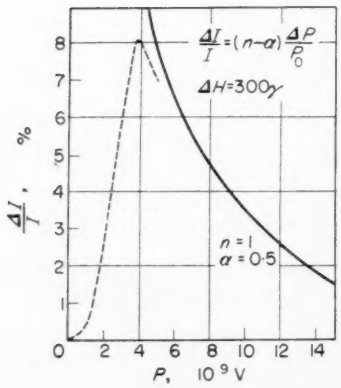

Fig. 10. Expected increment of cosmic ray intensity caused by the change of cut-off rigidity(- - - - due to atmospheric absorption).

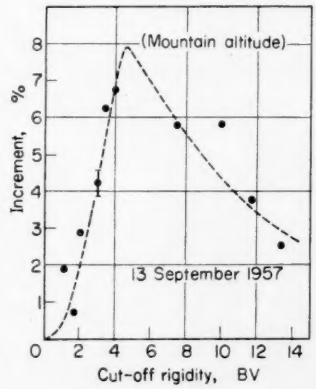

Fig. 11. Observed increments of cosmic ray intensity for stations at various latitudes during the main phase of the magnetic storm of 13 September 1957 (after KONDO *et al.*, 1960).

stations at various latitudes. Since the value of n is not known precisely near a few billion-volt range and the effect due to atmospheric absorption is appreciable, a good agreement may not be expected between the theoretical curve in Fig. 10 and the experimental one shown in Fig. 11. Nevertheless, it seems to be likely that the storm-time increases of cosmic rays associated with geomagnetic storms

VOL. 18 1960

can also be explained by the same effect of the induced D_{st} field for incoming charged particles. The changes in precipitation of cosmic ray particles into the earth are partly due to the distortion in the outer geomagnetic field during storms. Thus, independent observed facts concerning the polar blackouts and the storm-time increase of cosmic ray intensity both substantiate the theory followed in the present analysis.

4. Conclusion

New evidence has been shown in the present paper indicating that energetic charged particles of 10–100 MeV reach the earth with some delay after a large solar flare, yet well before the onset of the geomagnetic storm. They impinge on the polar regions and cause an enhanced ionization in the lower ionosphere. During a geomagnetic storm, however, the particles are precipitated along the auroral zone. The former is observed as the polar cap blackouts, which are confined within the geomagnetic latitude of about 60–65°, while the latter, the auroral zone blackouts, are closely related to the auroral displays and polar magnetic storms.

It has been found that the polar cap blackouts are closely related to the type IV solar radio outbursts. Since the type IV outburst originates from violently-agitated solar plasma bearing magnetic fields, the production of high-energy particles (solar cosmic rays) may also be expected. Those high-energy particles invade into the polar ionosphere following nearly Störmerian orbits and cause prolonged polar cap blackouts. In fact, during severe polar cap blackouts, an incidence of high-energy protons has been confirmed by the high altitude observation with cosmic ray counter flown in a balloon at Churchill (Winckler *et al.*, 1959), and also by the satellite observation (*Explorer* IV) during the events of August 1958 (Rothwell and McIlwain, 1959). The estimated energy of particles is of the order of 100 MeV, considerably higher than that of particles producing geomagnetic storms or aurorae.

Besides such high-energy particles, corpuscular clouds consisting mainly of low-energy particles are ejected from the sun. The cloud arrives after a day or so, corresponding to a speed of the order of 1000 km/sec. The particle density of the cloud is very high and hence the cloud behaves like a conducting fluid. Therefore, owing to the interaction of such a conducting cloud with the geomagnetic field, the latter is confined within a cavity surrounding the earth, and the outside of this is exposed to a violently agitated solar plasma. The size of cavity is variable according to the kinetic energy density of the incoming corpuscular cloud, and the D_{st} field of geomagnetic storms may in some way be related to this cavity formation.

Since it is likely that the corpuscular cloud retains a considerable amount of high-energy particles, which are trapped by the magnetic fields in the cloud, they enter the earth after the arrival of the cloud, viz. after the onset of a geomagnetic storm. Those particles, which are called the auroral particles, invade the polar ionosphere through the outer geomagnetic field and cause auroral zone blackouts, aurorae and polar magnetic storms. An equatorward shifting of the auroral zone during the main phase of magnetic storms has been explained by the effect due to the distortion of the outer geomagnetic field and subsequent decrease of the geomagnetic cut-off rigidity for incoming particles.

Acknowledgements—The writers wish to express their thanks to Professor T. NAGATA for his encouragement of this study, and also to the members of the Ionosphere Research Committee for their valuable discussions.

REFERENCES

BAILEY D. K.	1957	*J. Geophys. Res.* **62,** 431.
BAILEY D. K.	1959	*Proc. Inst. Radio. Engrs, N.Y.* **47,** 255.
BOISCHOT A. and DENISSE J. F.	1957	*C.R. Acad. Sci., Paris* **245,** 2194.
CHAMBERLAIN J. W.	1954	*Astrophys. J.* **120,** 360.
HAKURA Y., TAKENOSHITA Y. and OTSUKI T.	1958	*Rep. Ionos. Res. Japan* **12,** 459.
HAKURA Y. and GOH T.	1959	*J. Radio. Res. Lab.* **6,** 635.
KONDO I., NAGASHIMA K., YOSHIDA S. and WADA M.	1960	*Planet. Space Sci.* In press.
LEINBACH H. and REID G. C.	1959	Private communication.
MEINEL A. B.	1950	*Phys. Rev.* **80,** 1096.
NAGATA T.	1950	*J. Geophys. Res.* **55,** 127.
OBAYASHI T.	1958	*Rep. Ionos. Res. Japan* **12,** 301.
OBAYASHI T. and HAKURA Y.	1960	*Planet. Space Sci.* In press.
OBAYASHI T. and JACOBS J. A.	1957	*J. Geophys. Res.* **62,** 589.
PARKER E. N.	1958	*Physics of Fluids* **1,** 171.
REID G. C. and COLLINS C.	1959	*J. Atmosph. Terr. Phys.* **14,** 63.
ROTHWELL P. and MCILWAIN C.	1959	*Nature, Lond.* **184,** 138.
SHAPLEY A. H. and KNECHT R. W.	1958	NBS Report, Boulder U.S.A.
SINNO K.	1958	*Rep. Ionos. Res. Japan* **12,** 6.
STÖRMER C.	1955	*The Polar Aurora.* Clarendon Press, Oxford.
YOSHIDA S. and WADA M.	1959	*Nature, Lond.* **183,** 381.
WINCKLER J. R., ARNOLDY R., HOFFMAN R., PETERSON L. and ANDERSON K. A.	1959	*Bull. Amer. Phys. Soc.* **4,** 238.

APPENDIX

Motion of Charged Particles in the Distorted Geomagnetic Field

Following STÖRMER's investigation (1955), consider a charged particles moving with the velocity $\boldsymbol{v}$ in a magnetic field $\boldsymbol{H}$, the equation of motion is given

$$m\frac{d\boldsymbol{v}}{dt} = e\,[\boldsymbol{v} \times \boldsymbol{H}]. \tag{1A}$$

Assuming that the magnetic field has a potential $\Omega = MU$, where M is the geomagnetic moment, then

$$\boldsymbol{H} = -\text{grad}\,\Omega. \tag{2A}$$

Using a cylindrical co-ordinate (r,z,ϕ) and position vector $\boldsymbol{R}$, shown in Fig. 1A, the equation (1) can be reduced to

$$\frac{d^2\boldsymbol{R}}{ds^2} = -\frac{eM}{mv}\left(\frac{d\boldsymbol{R}}{ds} \times \text{grad}\,U\right) \tag{3A}$$

where s denotes the distance measured along the trajectory of a moving particle.

If the function U satisfies Laplace's equation, and has an axial symmetry, there must be a function V related to U by the equations

$$\frac{\partial V}{\partial z} = r\frac{\partial U}{\partial r}, \quad \frac{\partial V}{\partial r} = -r\frac{\partial U}{\partial z}. \tag{4A}$$

Since the curves U = constant are equipotentials, the curves V = constant, must be the lines of force. Now, substituting from (4A) in (3A) and $s_0 = \sqrt{eM/mv}$ being

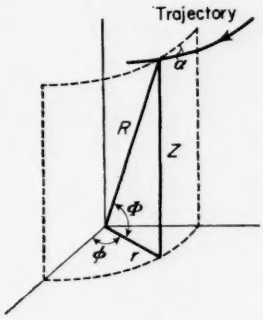

Fig. 1A. Cylindrical polar co-ordinates and the geometry of a particle trajectory.

taken as the unit of length (Störmer's unit length), it can be shown that the equation (3A) becomes

$$\frac{d}{ds}\left(r^2\frac{d\phi}{ds}\right) = -\frac{dV}{ds} \tag{5A}$$

of which the integral is

$$r^2\frac{d\phi}{ds} + V = \text{constant}. \tag{6A}$$

Let α denote the angle between the direction of motion of a particle at any instance and the line (r = const., z = const.) at the point of intersection, then

$$\left| r\frac{d\phi}{ds} \right| = |\cos\alpha| \leqslant 1. \tag{7A}$$

STÖRMER showed that the whole space can be divided into allowed and forbidden regions, and the equation (7A) provides a means of determining the region to which the trajectories are allowed.

STÖRMER's works are mostly concerned with trajectories of particles in an ideal dipole field, while in the present study a distorted geomagnetic field which is appropriate during magnetic storms is considered. It is known that during magnetic storms the field intensity is enhanced at the initial phase and this is followed by a remarkable decrease at the main phase. Since the impressed field is almost uniform with the direction of the geomagnetic axis, a potential of the distorted geomagnetic field can be approximated as the sum of a dipole field and an additional uniform field. Namely,

$$\Omega = M\left[\frac{1}{R^2} + AR\right]\sin\Phi \tag{8A}$$

where $M = 8{\cdot}1 \times 10^{25}$ gauss cm^3 and Φ is geomagnetic latitude. On the other hand, the geomagnetic field is confined within a cavity of the size of R_0, and the field beyond this is considerably disordered by the agitated cloud. Therefore, one may postulate a condition that the geomagnetic field vanishes at the distance $R = R_0$.

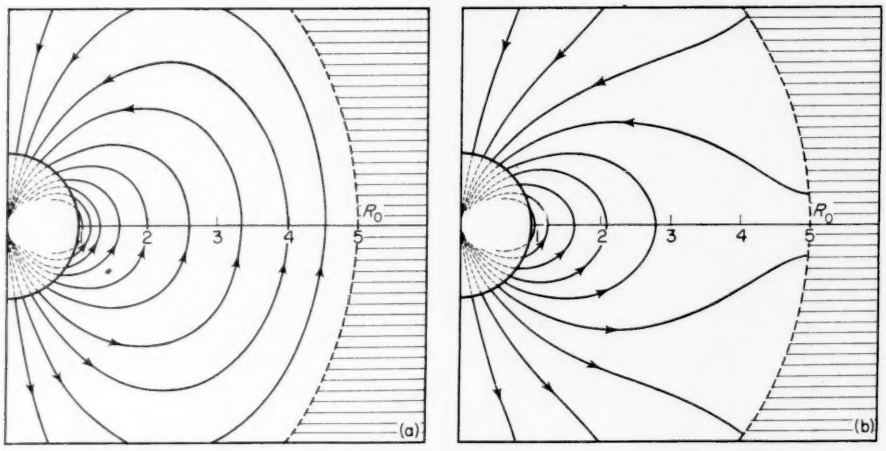

Fig. 2A. Geomagnetic lines of force for two kinds of the distorted geomagnetic field (R_0 is the boundary of the geomagnetic cavity).

(a) Geomagnetic potential $U = \left(\frac{1}{R^2} + \frac{2R}{R_0^3}\right) \sin \Phi$.

(b) Geomagnetic potential $U = \left(\frac{1}{R^2} - \frac{R}{R_0^3}\right) \sin \Phi$.

The potential field which might be set is the one satisfying the condition $H_R = -(\partial\Omega/\partial R) = 0$, or else $H_\Phi = -1/R(\partial\Omega/\partial\Phi) = 0$ at the boundary. These two potential fields can be determined from (8A), and given

$$\Omega_1 = M\left[\frac{1}{R^2} + \frac{2R}{R_0^3}\right] \sin \Phi \tag{9A}$$

and

$$\Omega_2 = M\left[\frac{1}{R^2} - \frac{R}{R_0^3}\right] \sin \Phi. \tag{10A}$$

The horizontal intensities of the additional fields are given, respectively,

$$\Delta H_1 = \frac{2M}{R_0^3} \cos \Phi \tag{11A}$$

and

$$\Delta H_2 = -\frac{M}{R_0^3} \cos \Phi. \tag{12A}$$

The former potential field gives the compression of the geomagnetic field since there is no line of force across the spherical surface $R = R_0$, and so may represent

the initial phase of a geomagnetic storm. On the other hand, the latter is opposite to the primary geomagnetic field, and can be regarded as the field during the main phase of geomagnetic storms, which shows an effect of dissipation of the geomagnetic field if it is allowed to expand outward and thereby reduce the horizontal component at the earth's surface (PARKER, 1958).

The lines of force for these potentials can be obtained using relation (6A)

$$V_1 = \frac{r^2}{R^3} - \frac{r^2}{R_0{}^3} + \text{constant} \tag{13A}$$

$$V_2 = \frac{r^2}{R^3} + \frac{r^2}{2R_0{}^3} + \text{constant} \tag{14A}$$

Geomagnetic lines of force for these cases are illustrated in Fig. 2A, where the boundary of the cavity is indicated by dotted lines.

The condition of allowed trajectories under the effect of such fields should follow the relation (7A) and can be replaced by the equations

$$\left| \frac{r}{R^3} - \frac{r}{R_0{}^3} - \frac{2\gamma_1}{r} \right| \leqslant 1 \tag{15A}$$

and

$$\left| \frac{r}{R^3} + \frac{r}{2R_0{}^3} - \frac{2\gamma_2}{r} \right| \leqslant 1 \tag{16A}$$

where γ_1 and γ_2 denote arbitrary constants of integration. Since the trajectory of particle should be continuously on a line from the cavity boundary to the earth's upper atmosphere, (15A) and (16A) must hold, at least, in some range of Φ during the whole range of R from R_0 to the earth's surface. The range of geomagnetic latitude Φ, within which charged particles are precipitating on the earth's atmosphere, is determined from (15A) and (16A). Remembering that $r = R \cos \Phi$, the zone of particle precipitation is given approximately by the following equations, provided that $a \ll s_0$, where a is the radius of the earth. This can be justified for all particles with $E < 15$ BeV.

$$\cos \Phi_1 \leqslant \sqrt{\left\{ \frac{2a\gamma_1}{s_0(1 - a^3/R_0{}^3)} \right\}} \tag{17A}$$

and

$$\cos \Phi_2 \leqslant \sqrt{\left\{ \frac{2a\gamma_2}{s_0(1 + a^3/2R_0{}^3)} \right\}}. \tag{18A}$$

The outer boundary, minimum latitude at which the particle can enter, is given by the largest possible values of γ_1 or γ_2, which satisfy the conditions (15A) or (16A), respectively. Those values are computed numerically for various R_0 (in Störmer unit) and shown in Fig. 3A. It is clear that when R_0 becomes infinity, both γ_1 and γ_2 tend to unity, and this is identical with the Störmer calculation for an ideal geomagnetic dipole field. It can be shown also that, when $R_0 \ll s_0$, γ_1 and γ_2 approach to the values

$$\gamma_1 = \frac{R_0}{2s_0} \quad \text{and} \quad \gamma_2 = \frac{3s_0}{4R_0} \tag{19A}$$

respectively. Allowed and forbidden regions for different cavity size are illustrated schematically in Fig. 4A. As the size of the geomagnetic cavity is reduced, the precipitating zone shifts towards the equator, for the case of the distorted geomagnetic field given by the equation (10A).

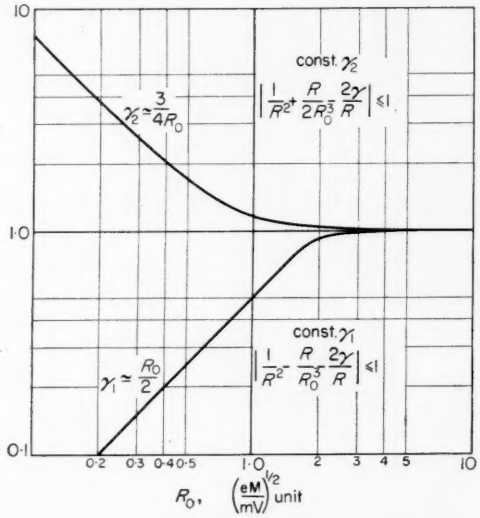

Fig. 3A. The largest possible values of the numerical integration constants γ_1 and γ_2 with respect to R_0.

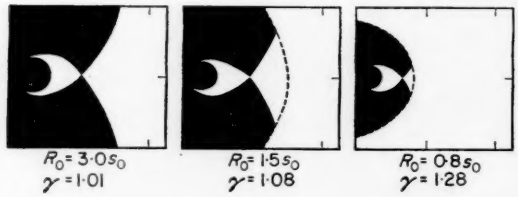

Fig. 4A. Forbidden and allowed regions for charged particles.

From the equations (17A) and (18A), now it is possible to find out the geomagnetic cut-off rigidity for a charged particle at various geomagnetic latitude. Magnetic rigidity of a particle P is given

$$P = \frac{m_0 v}{e\sqrt{(1-\beta^2)}} = \frac{M}{{s_0}^2} \tag{20A}$$

where m_0 is the rest mass of a proton and $\beta = v/c$. Then, the equations (17A) and (18A) can be written in the forms

$$P_1 \geqslant \frac{M \cos^4 \Phi (1 - a^3/{R_0}^3)}{4a^2 {\gamma_1}^2} \tag{21A}$$

and

$$P_2 \geqslant \frac{M \cos^4 \Phi(1 + a^3/2R_0^3)}{4a^2\gamma_2^2}. \tag{22A}$$

The cut-off rigidity of a particle P_c is given as the minimum value of P, indicating

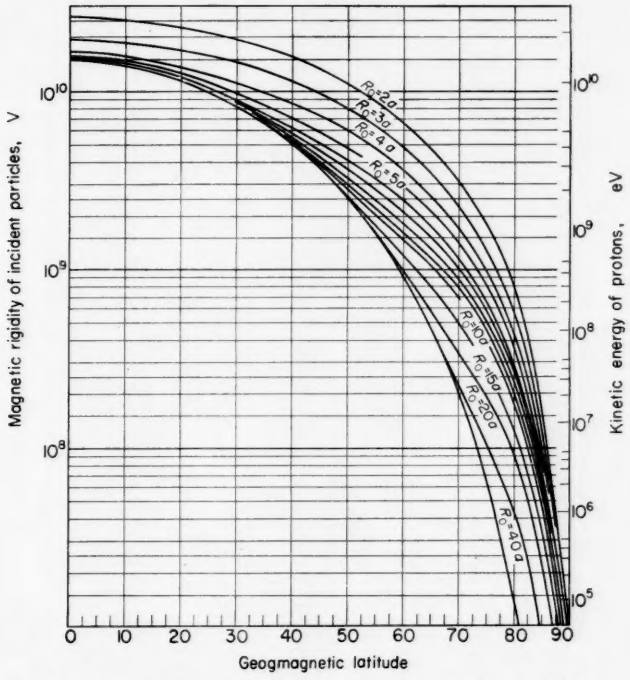

Fig. 5A. Geomagnetic cut-off rigidity of particles P_1 vs. geomagnetic latitude for various R_0.
Geomagnetic potential:

$$\Omega = M\left(\frac{1}{R^2} + \frac{2R}{R_0^3}\right)\sin\Phi$$

$$\cos\Phi = \frac{2a\gamma}{(eM/mv)^{1/2}[1 - (a^3/R_0^3)]}$$

the possible lowest rigidity which can enter at the geomagnetic latitude Φ. These results are shown in Figs. 5A and 6A with parameters of R_0.

For the case of an enhanced geomagnetic field, the cut-off rigidity is shifted towards higher values with decreasing value of R_0. The relation between ΔH, and Φ, for low rigidity particles ($P < 10^8$ V) is given approximately by

$$\Delta H_1 = \frac{2M}{R_0^3} \simeq 2\left\{\sqrt{\left(\frac{M}{aP_1}\right)}\cos\Phi_1\right\}^{-6}. \tag{23A}$$

On the other hand, for a depressed geomagnetic field, the cut-off rigidity decreases with decreasing value of R_0. In other words, the zone of particle precipitation shifts towards lower latitudes as the boundary of the cavity approaches to the

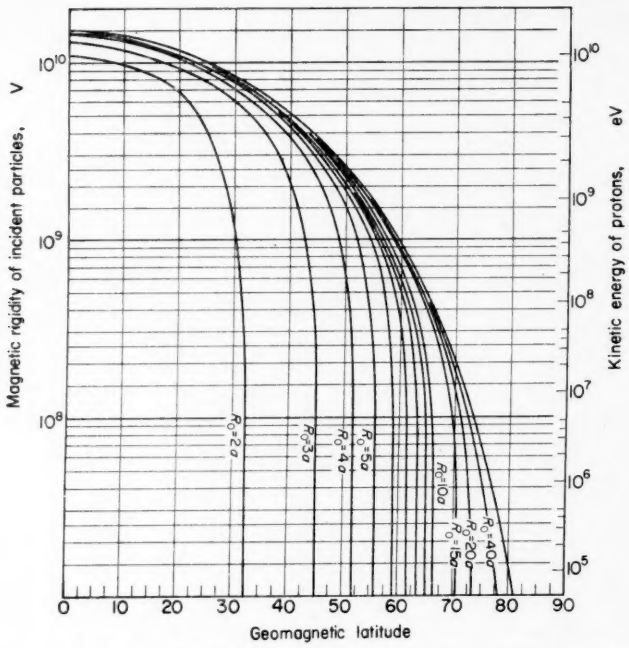

Fig. 6A. Geomagnetic cut-off rigidity of particles P_2 vs. geomagnetic latitude for various R_0.

Geomagnetic potential:

$$\Omega = M\left(\frac{1}{R^2} - \frac{R}{R_0^3}\right)\sin\Phi$$

$$\cos^2\Phi_0 = \frac{2a\gamma}{(eM/mv)^{1/2}[1 + (a^3/2R_0^3)]}$$

earth. For low rigidity particles ($P < 10^8$ V), however, the minimum geomagnetic latitude, at which charged particles can enter, does not change appreciably with the magnetic rigidity of particles, but only depends on the cavity size. The relation between the depression of the geomagnetic field ΔH_2 and Φ_2 can be written approximately by

$$\Delta H_2 = -\frac{M}{R_0^3} \simeq -\frac{8}{27}\frac{M}{a^3}\cos^6\Phi_2. \tag{24A}$$

Journal of Atmospheric and Terrestrial Physics, 1960, Vol. 18, pp. 123 to 126. Pergamon Press Ltd. Printed in Northern Ireland

The size of the moving irregularities in the *F*-region and the spread angle of the radio waves scattered from them

S. R. Khastgir and R. N. Singh
Calcutta University and Banaras Hindu University, India

(*Received* 25 *November* 1959)

Abstract—The three-spaced receiver fading records of the *F*-echo at 3·8 Mc/s, taken at Banaras during the period from November 1956 to September 1958 show certain characteristic patterns. The fading patterns which were considered as due entirely to the movement of large ionospheric irregularities are analysed by the method of Briggs and Phillips (1950). As a result of this analysis the average characteristic length of the irregularities is found to be 270 m and the average angular spread is found to be 6°. The variations of these parameters are shown with the help of histograms. The records show some diurnal and seasonal variations, but no definite conclusion can be made regarding such variations.

1. Introduction

The short-duration radio-frequency pulses incident on an ionospheric layer are reflected back to the ground in the form of a cone of rays. In the idealized case of a stationary ionosphere and plane wave illumination, the cone angle is very small but in the case of moving irregularities, the angle of spread is considerable. If these irregularities are of great size and move with certain velocity, they produce characteristic fading patterns which vary almost periodically without much change in their details. In the present paper some results are given concerning the size of the moving irregularities in the *F*-region and the angle of spread. These results are obtained from the analysis of those fading patterns which are considered to be due entirely to the movement of large irregularities in the ionospheric region.

The fading records were taken during 1956–1958 at Banaras by the three-spaced receiver method of Mitra (1949). The apparatus consisted of a pulse transmitter giving a pulse width of 200 μsec at 50 c/s, and three receiving horizontal dipole aerials situated at the corners of a right-angled triangle with two arms in the E–W and N–S directions and each arm of length 100 m. The recording unit consisted of three communication receivers, the detector output of which was connected to three DuMont Oscillographs operated with a common time base. The simultaneous fading records at the three spaced points were taken by a ciné-camera. Those patterns which were not found to change in their details, and which could be regarded as due entirely to the movement of large irregularities were analysed by the method of Briggs and Phillips (1950). Such fading patterns are shown in Fig. 1.

2. Theoretical Considerations

It is assumed that the irregularities scatter in such a way that the power received per unit solid angle by an aerial varies with θ in a manner given by the function

$$W(\theta) = \cos^n \theta \qquad (1)$$

where n depends on the mode of reflection, and the polar diagrams of the transmitting and the receiving aerials. It may be mentioned that the polar diagrams (for power) from the transmitting and the receiving aerials can be represented by $\cos^t \theta$ and $\cos^r \theta$ respectively. When the irregularities regarded as a random screen are illuminated by a plane wave, the scatter power received per unit solid angle by a detector can be represented by $\cos^q \theta$. Assuming that the scatter power polar diagram is turned through an angle θ, so that its maximum lies in the direction of the geometrically reflected ray, BRIGGS and PHILLIPS (1950) have shown that the response is given by $\cos^q 2\theta$ which is approximately equal to $\cos^{4q} \theta$ which is in the range $-\pi/2 < \theta < +\pi/4$, falling off to zero when θ lies outside this range. They have also shown that the power received from the elementary area of the screen within the solid angle $d\Omega$ can be written as

$$dW \propto \cos^n \theta \, d\Omega$$

where
$$n = t + r + 4q + 3 \tag{2}$$

The spread of the function $\cos^n \theta$ is taken as the angle θ_0 at which the amplitude falls to $\frac{1}{2}$ and the function $\cos^n \theta$ to $\frac{1}{4}$. The spread of the function plotted against n is shown in Fig. 2.

In the case of irregularities moving with velocity V the space auto-correlation function is given by

$$\rho_R(\xi) \propto \left[\int_{-1}^{+1} (1 - u^2)^{n/2} \cos(2\pi u \xi) \, du\right]^2 \tag{3}$$

where ξ is the distance between the two points in terms of the wavelength as unit, $u = 1/k$ times the Doppler frequency shift of the power scattered from the elementary area of the irregularities, $k = 2V/\lambda$, V = velocity of the irregularities and λ the wavelength under the stationary condition. The spacing is then given by $\lambda\xi = V\tau$, where τ is a small time-interval within which the amplitude change is considered. The variation of the space auto-correlation function $\rho_R(\xi)$ for different spacings of the receivers is shown in Fig. 3.

Denoting $\overline{|R(x) - R(x + \xi)|}$ which is the mean value of the amplitude-change over an interval ξ by $\Delta(\xi)$, we get, following MCNICOL (1949), the following relation connecting the average amplitude-difference $\Delta(\xi)$ with the space autocorrelation function $\rho_R(\xi)$:

$$\frac{\Delta(\xi)}{\bar{R}} = 0{\cdot}59\,[1 - \rho_R(\xi)]^{1/2} \tag{4}$$

where $\bar{R}$ is the average amplitude. The value of $\Delta(\xi)/\bar{R}$ corresponding to the variation of the space autocorrelation function $\rho_R(\xi)$ is plotted against the spacing $\lambda\xi$ for different values of n and is shown in Fig. 4. If fading patterns are due entirely to the motion of an unchanging irregularity, then the average shift $\Delta(\tau)$ will be the same as the average amplitude difference $\Delta(\xi)$, subject to the transformation $\lambda\xi = 2V\tau$.

VOL.
18
196

J. GEOPHYS. RES. 1960

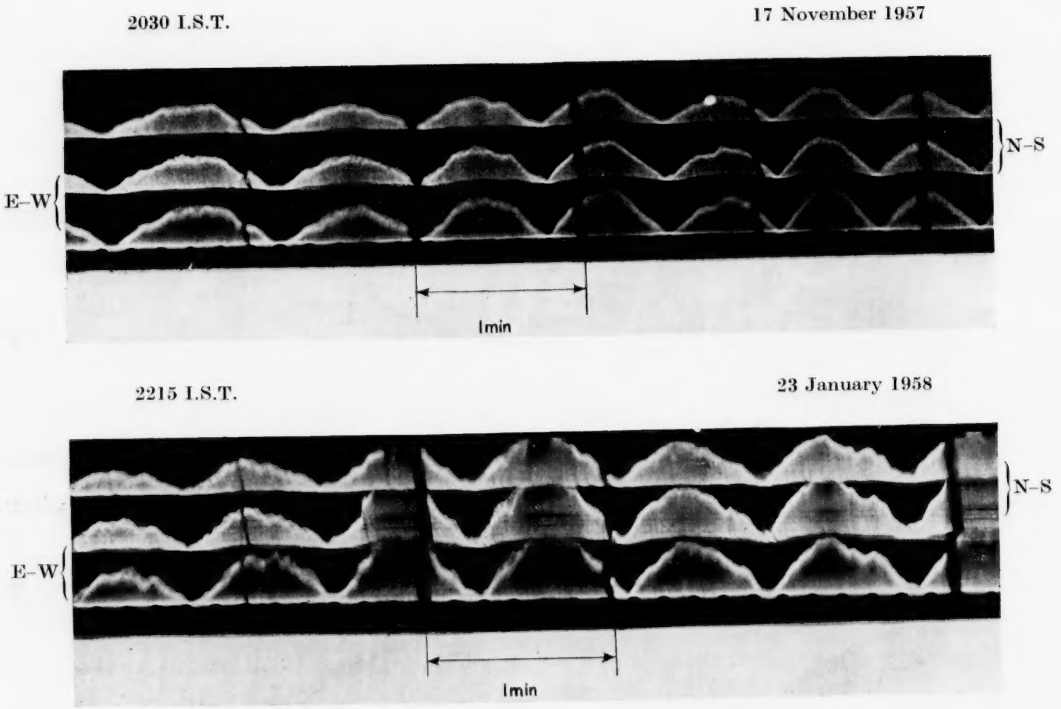

Fig. 1. Typical three-spaced receiver fading records.

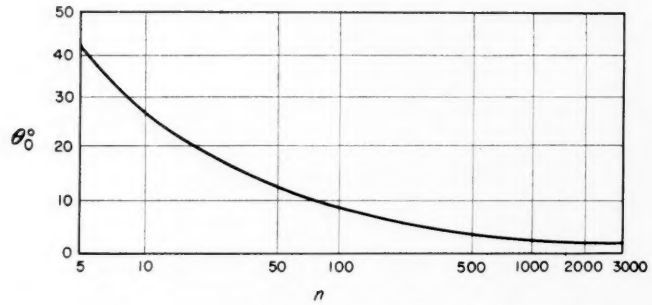

Fig. 2. Variation of the spread-angle θ_0 of the function $\cos^n \theta$ with different values of n.

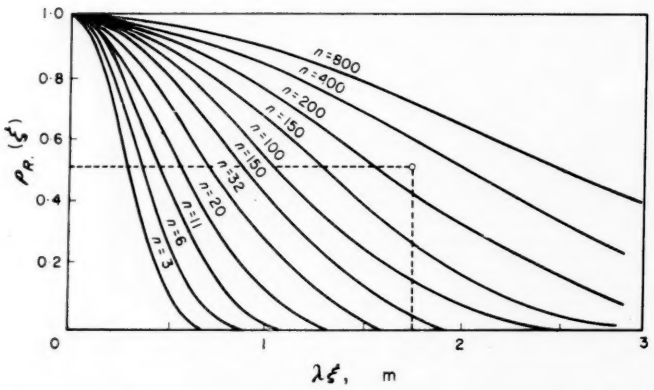

Fig. 3. Variation of the theoretical space-autocorrelation function $\rho_R(\xi)$ for different receiver spacings.

VOL.
18
196(

3. Procedure for the Analysis

In practice $\Delta(\tau)$ was computed by making two tracings of a fading record on graph paper with the desired time-shift. The included area between the original and the shifted curve was measured from the graph paper. This area divided by the length of the fading record would give $\Delta(\tau)$. The area underneath one of the fading records was also measured and $\bar{R}$ was obtained by dividing this area by the total length of the record. The values of $\Delta(\tau)/\bar{R}$ for the records shown in Fig. 1, plotted against τ on the graph are shown in Fig. 4. The value of n which best

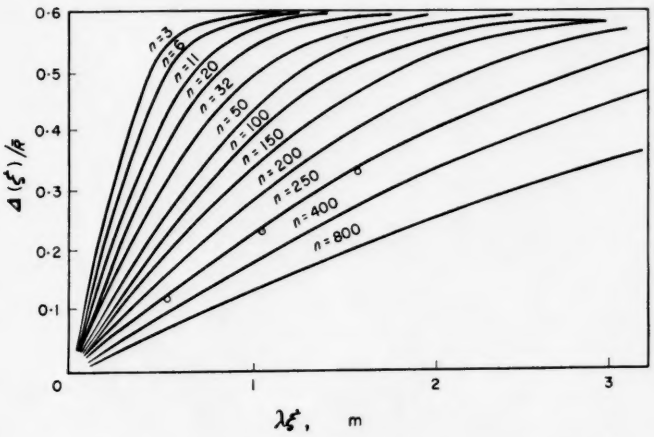

Fig. 4. Variation of $\Delta(\xi)/\bar{R}$ for different receiver spacings.

fitted the experimental points was determined. To obtain the amount of scattering by the ionosphere in a form independent of aerial properties, it is necessary to correct for the effect of aerial polar diagrams. For this correction we have to find the value of q from equation (2). Thus

$$q = \frac{n - t - r - 3}{4}.$$

In the case of dipole aerials, $t = r = 3$, so that $q = (n - 9)/4$.

The size of the irregularity was determined from its definition according to which the size of the irregularity is equal to the distance at which the autocorrelation function falls to 0·5 in the case of plane wave illumination. Corresponding to the different values of n the characteristic length of the irregularity L was found from Fig. 3. The corresponding values of the angular spread θ_0 is also directly determined from Fig. 2.

4. Results of the Analysis

A number of records taken mostly in night hours during the period from November 1956 to September 1958 were analysed as described above. The average value of the characteristic length L of the irregularities was found to be

270 m and the average value of the spread angle for radio waves scattered from the irregularity was found to be approximately 6°. The variation of the size and spread angle is shown by histograms in Fig. 5 (a) and (b). The results obtained in this paper are in fair agreement with the results of BRIGGS and PHILLIPS (1950), and others. Abnormal values of characteristic length L and their spread angle obtained as a result of such analyses are due either to unusual disturbances in the reflecting layer or to the wrong selection of the proper records. Such values were discarded in averaging and were not shown in the histograms. The observations were made on a number of special days in the IGY Calendar. Records taken

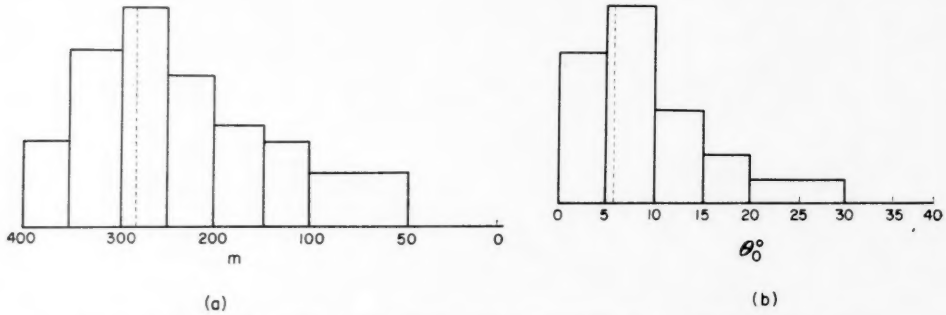

Fig. 5(a). Histograms showing the frequency of occurrence for different values of characteristic size of irregularities L.
(b). Histograms showing the frequency of occurrence for different values of the spread-angle θ_0.

during the quiet days and the Regular World Days gave the same order of magnitude of the characteristic length L and the angle of spread. Results could not be obtained during magnetically-disturbed days as these gave complicated amplitude patterns which could not be regarded due entirely to the movement of the ionospheric irregularities. The results showed some diurnal and seasonal variations but no definite conclusions cquld be made regarding such variations.

Acknowledgement—The writers are grateful to the Council of Scientific and Industrial Research for sponsoring a Research Scheme on the "study of fading of radio waves".

REFERENCES

MITRA S. N.	1949	*Proc. Instn Elect. Engrs* **96,** 441.
BRIGGS B. H. and PHILLIPS G. J.	1950	*Proc. Phys. Soc. Lond.* B **63,** 907.
MCNICHOL R. E. W.	1949	*Proc. Instn Elect. Engrs* **96,** 517.

Journal of Atmospheric and Terrestrial Physics, 1960, Vol. 18, pp. 127 to 134. Pergamon Press Ltd. Printed in Northern Ireland

Electron distribution in the *F*-layer of the ionosphere over Haringhata (Calcutta) on quiet and disturbed days

P. Bandyopadhyay
Institute of Radiophysics and Electronics,
University of Calcutta, Calcutta, India

(*Received* 3 *December* 1959)

Abstract—The paper presents the results of a study of the behaviour of the *F*-layer of the ionosphere over Haringhata (Calcutta) on quiet and disturbed days. The study is made from "mean quiet *F*-layers" and "mean disturbed *F*-layers" constructed for this place following the method of the Cambridge group of workers. The quiet-day results are further examined with a view to verifying the model of the coefficient of electron loss in the layer, as derived by the above workers.

1. Introduction

In many theoretical studies of the *F2*-layer of the ionosphere values of parameters like electron density, rate of electron production, coefficient of electron loss, etc., at different (true) heights of the layer are needed. The routine parameters such as f_0F2 and $h'F2$, that are scaled directly from the virtual height curves (ionograms), are not of much significance in this respect since the former refers to a height that is constantly changing, while the latter suffers much from group retardation in the regions below. It has, therefore, been stressed of late, that for better description and understanding of the morphology of the layer, the different ionospheric parameters and their variations should be studied from true height profiles on a world-wide basis. The present paper describes the results of such a study made separately from the records of the Internationally Quiet Days (i.q.d.s) and of the Internationally Disturbed Days (i.d.d.s) at Haringhata (28 miles from Calcutta). These results have been compared with those of similar studies made of records at other places. Besides examining the characteristic true-height variation of the *F*-layer parameters on quiet and disturbed days, there has also been another object of this study. This is outlined below.

The *F2*-layer of the ionosphere is the seat of many important movements—some regular, some irregular. These movements obscure, what may be called, the "basic behaviour" of the layer, i.e. its behaviour under essentially simple conditions, unperturbed by movements, so that the continuity equation contains only the production and the loss terms. A method of studying the "basic behaviour" of the layer, particularly with regard to the coefficient of electron loss and its height variation in the layer, has very recently been developed by the Cambridge group of workers (Schmerling and Thomas, 1956; Ratcliffe *et al.*, 1956). In this method the hourly h'–f records obtained for the i.q.d.s in any one month are normalized and averaged and are then reduced to true-height electron density profiles (N_e–h curves). These hourly N_e–h curves define a kind of "mean quiet *F*-layer" for the month and for the station concerned. When the variations of electron density at different heights were studied from the "mean quiet *F*-layers" it was found that not only were the effects of irregular movements eliminated but,

on many occasions, the night-time electron density values, at all levels, were found to decrease uniformly as though controlled by the loss processes only and that regular movements had negligible effect. The mean "quiet *F*-layers" could then be analysed to yield values of the coefficient of electron loss at different heights in the layer. When this was done for such different places as Slough, Watheroo and Huancayo, and for different seasons, it was found that the results for all those places conformed to a particular loss coefficient model. Since movements, regular or irregular, cannot have the same effect in different seasons at all these places, having widely different geographic locations, it has been claimed that the above loss-coefficient model is a true feature of the "basic behaviour" of the layer. It should be noted, however, that this loss-coefficient claim is based on data principally from a few selected places, these being Slough, Watheroo and Huancayo. It is therefore desirable that the proposed loss-coefficient model be checked against data from other places also. To do this with our data for Haringhata (Calcutta) has also been an aim of the present work.

Our results unfortunately show that the "mean quiet *F*-layer" here is not so free from the effects of movements as one might expect from the results for Slough or Watheroo. Although random fluctuations are reduced, the effects of regular movements appear prominently in our results. Consequently, our object of verifying the loss-coefficient model has not been fulfilled. An attempt has, nevertheless, been made in this direction by using our data for comparatively undisturbed hours during the night, with some success.

VOL.
18
196(

2. Data and the Method of Analysis

The ionograms analysed in this study were selected from those obtained regularly at our Ionosphere Field Station at Haringhata (28 miles from Calcutta) since the beginning of 1955. For the purpose of this study, however, we could not go much beyond the beginning of 1956, as then, owing to the approach to the maximum of the sunspot cycle, the critical frequency of the *F2*-layer around midday rose above the upper limit of the recorder (13·0 Mc/s). For the purpose of studying the quiet-day behaviour of the *F*-layer and also of verifying the loss-coefficient model "mean quiet *F*-layers" were constructed with data obtained for the five i.q.d.s during each of the months May 1955, September 1955 and February 1956 for which good records were available. (The months represent approximately summer, equinox and winter conditions, respectively, and the period of study belongs mainly to the sunspot-minimum epoch.) The "mean quiet *F*-layers" so constructed showed certain irregular fluctuations and some unexpected variations (to be discussed later). So it was thought advisable to derive the "mean quiet *F*-layer" for a year instead of for the individual months selected. This has been done by taking the data obtained for three i.q.d.s. for each month during the 1 year period March 1955 to February 1956. The study of the disturbed-day behaviour of the layer has been made from "mean disturbed *F*-layer" constructed with data obtained on two i.d.d.s for each month during the above period (March 1955 to February 1956).

The method adopted for constructing the "mean *F*-layers" as noted above followed closely that given by Schmerling and Thomas (1956) which is as follows:

The h'–f records for a given hour for the selected group of days are first taken and the average value of f_0F2 for the hour is determined. The ordinary trace of the F-layer echo in each record is then normalized and an average normalized curve is obtained from all the records for the hour. This is done by using a card to be set along the frequency scale of the h'–f records. It is marked at a suitable index frequency and at a set of fractional values (like 0·9, 0·8, etc.) of this frequency. These markings are on the same logarithmic scale as that of the ionograms. The card is set along the frequency scale of a given hourly curve with the index $\downarrow$ frequency mark corresponding with f_0F2, and the virtual heights corresponding to the above fractional-frequency marks are noted; this is the normalization. Because of the logarithmic frequency scale of the ionograms the same card has been used with all the records. The sets of values of virtual heights so obtained are then averaged. The average values are next plotted against the appropriate fractional frequencies while the index frequency is made to correspond to the average value of f_0F2 determined at the beginning. The result is the average normalized h'–f curve for the given hour. The curve is then reduced to true-height electron-density profile. The set of twenty-four such hourly N_e–h curves constitute the "mean F-layer" for the selected groups of days.

The true-height analysis has been made by the method of Schmerling and Ventrice (1959) as elaborated by Wright and Norton (1959). The method is very much similar to that of Kelso (1952) but unlike the latter takes due account of the influence of the earth's magnetic field. The method of true-height analysis however, has the following limitations:

(a) The electron density has been assumed to increase monotonically with height.

(b) The h'–f curves were analysed down to the minimum virtual height in the F-layer ($h'F$) and any possible group retardation by a lower layer (like E during the day or the low-lying electrons with plasma-frequency less than f_{lim} during the night) has not been allowed for.

It is to be mentioned that the results obtained by the Cambridge group of workers, with which we shall compare ours, also suffer from both these limitations.

3. Results and Discussions

3.1. *Diurnal variation of electron density in the* F*-layer*

The diurnal variations of electron density at a series of heights (N_e–t curves) as noted from the "mean quiet F-layers" for Haringhata are shown in Fig. 1 along with those for Slough and Maui as obtained by Schmerling and Thomas (1956); and Thomas (1959). It will be noted that the variations at Haringhata are characterized, firstly, by the presence of large and irregular fluctuations and secondly, by the regular appearance of two prominent peaks around 0200 hours and 1800 hours. These two features are in sharp contrast with the results for Slough (January 1950) which, incidentally, were among those obtained earliest by the method of "mean quiet F-layer". The first of the features indicates the effects of random movements. It may be suggested that the presence of these irregular fluctuations is due to the fact that while these results have been obtained by averaging over

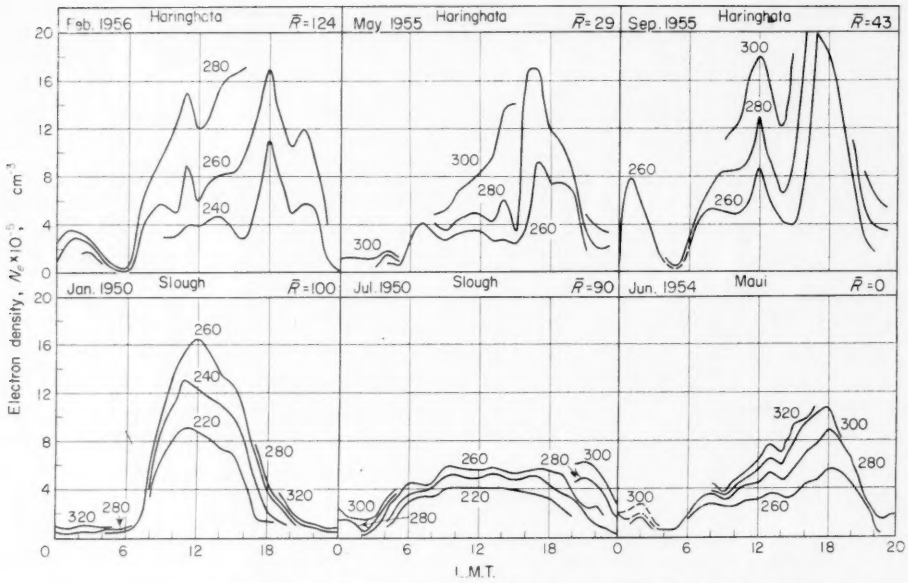

Fig. 1. Average variation of electron density with time at different heights for i.q.d.s. R is the average relative Zürich sunspot number.

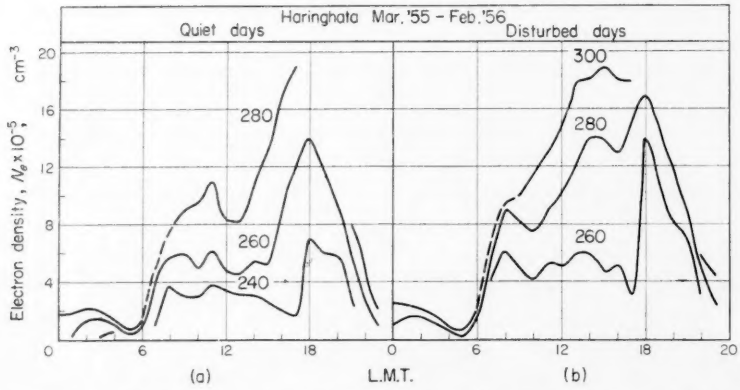

Fig. 2. Average variation of electron density with time at different heights for i.q.d.s and i.d.d.s.

five i.q.d.s only, the Slough results are the average of ten such days. But according to SCHMERLING and THOMAS (1956) averaging on five i.q.d.s alone in any one month is sufficient to remove most of the effect of random variations and the smooth curve for one set of five i.q.d.s in a month is quite similar to that of the other set. Since our results for none of the months examined agreed with this, we felt the necessity of constructing a "mean quiet F-layer" from as many i.q.d.s during a year as possible. The 1 year period finally chosen, suiting the availability of good records, was March 1955 to February 1956 and, as mentioned already, data on three i.q.d.s in each month were examined. The results obtained, shown by the curves in Fig. 2(a), may be compared with those of Fig. 1. It will be found that the two sets of

curves do not show any marked difference in character. The observed irregular fluctuations are, therefore, not due to averaging on insufficient number of days.

The second distinguishing feature of our results, the peaks in the N_e–t curves, no doubt represent effects of regular movements. Compared with the January 1950 results of Slough these are also unexpected, since the Slough (January 1950) results are quite smooth and free from such effects. However, more recent evidence, such as the July 1950 results from Slough or the results from Maui,

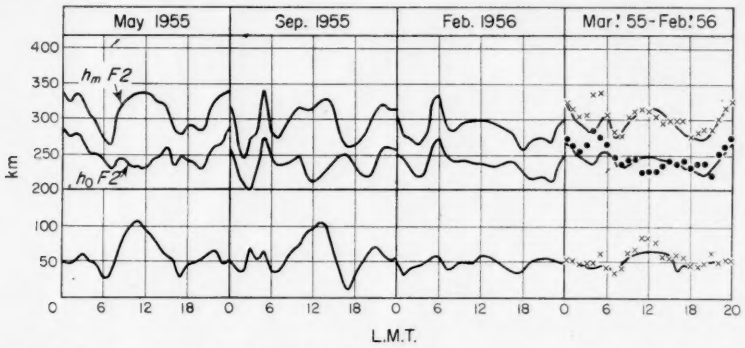

Fig. 3. Average variation of h_mF2, h_0F2 and $T(= h_mF2 - h_0F2)$ for i.q.d.s. Dots and crosses show the corresponding quantities for i.d.d.s.

seem to suggest that none of the two features of our results is exceptional. The results from Maui (28°48′N, 156°30′W) are particularly interesting. Situated at about the same latitude as ours, the N_e–t curves for this place also exhibit two peaks around 0200 hours and 1800 hours though less prominently.

Regarding our results on disturbed days one finds from Fig. 2(b) that these do not show any marked difference from those for quiet days (Fig. 1a).

3.2. *Heights of the peaks of* F2- *and* F1-*layers and the thickness of the* F2-*layer*

Fig. 3 shows the variations of the heights of the peaks of the $F2$- and $F1$-layers (h_mF2 and h_mF1, respectively) and the thickness T of the $F2$-layer, given by $T = h_mF2 - h_0F2$ where h_0F2 is the height of the "bottom" of the $F2$-layer (during the day $h_0F2 = h_mF1$). The crosses and dots show the values of these parameters determined from the "mean disturbed F-layer". For comparison, is shown in Fig. 4 the average variations of h_mF2 at Slough and Maui for i.q.d.s. in a month as given by Thomas (1959). The following features may be noted from these figures.

(a) The values of h_mF2 at Haringhata for the i.d.d.s are greater than those for the i.q.d.s. This is a well-known behaviour of the parameter at a temperate latitude station during a geomagnetic disturbance.

(b) The variation of h_mF2 at Haringhata again, has close similarity to that at Maui. The Slough values, on the other hand, show an opposite variation particularly during the midday period.

(c) With the exception for the maximum at about 0600 hours (Fig. 3, March 1955–February 1956 curve) in the variation of h_mF2 at Haringhata on quiet days, the curve shows marked semi-diurnal periodicity. Fig. 5 shows a comparison between this curve for Haringhata with the hump removed (the dotted portion indicating the probable shape of the curve in the absence of the hump) and a

similar curve (broken line) for Calcutta (28 miles from Haringhata). The latter curve was obtained by MITRA (1951) from an analysis of 4 years' data (1946–1950) to study solar tidal effects. The close similarity between the curves strongly suggests the presence of tidal effects in the "mean quiet F-layer" here.

As to the origin of the hump nothing can be said definitely. It may be due to group retardation by low-lying electrons with plasma-frequency less than f_{lim} or some other phenomenon.

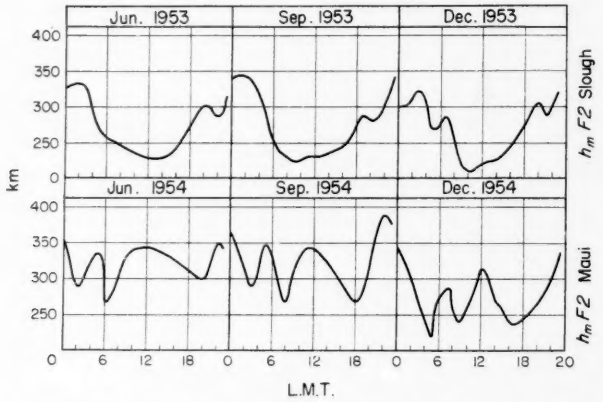

Fig. 4. Average variation of $h_m F2$ at Slough and Maui for i.q.d.s.

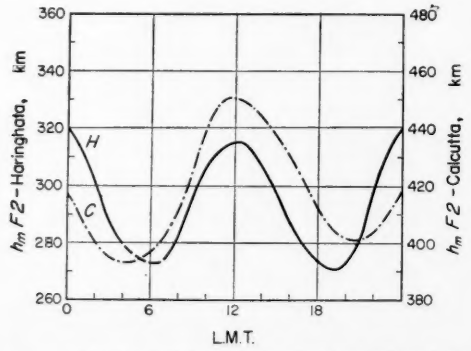

Fig. 5. Average variation of $h_m F2$ at Haringhata (marked H) and Calcutta (marked C). Dotted portion of the curve for Haringhata indicates the probable shape of the curve in absence of the hump around 0600 hours (Fig. 3, March 1955–February 1956 curve).

3.3. *Peak electron density in the* F2*-layer* ($N_m F2$) *and the sub-peak electron content* (n_T)

The variations of the peak electron density in the $F2$-layer ($N_m F2$) and the total electron content (n_T) in a unit column in the F-layer up to the level of $h_m F2$, in the ionosphere over Haringhata, are shown in Fig. 6. The crosses indicate the corresponding values on disturbed days. It will be seen that there are no significant differences between the values of the two parameters on quiet and disturbed days.

3.4. *The loss-coefficient model*

Assuming that the processes of electron loss in the F-layer are attachment-like,

the continuity equation for a given height, during the night hours, can be written as

$$\frac{\partial N_e}{\partial t} = -\beta N_e + M \tag{1}$$

where β is the coefficient of electron loss and M a probable movement term. When movement effects are negligible and the last term omitted, the equation can be

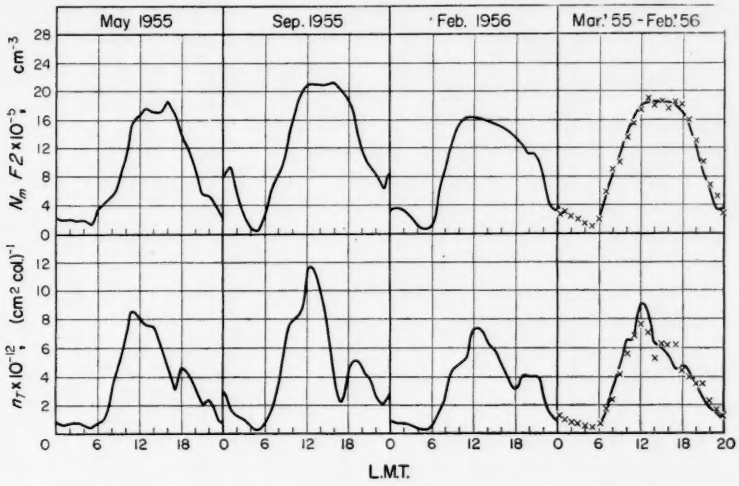

Fig. 6. Average variation of N_mF2 and n_T for i.q.d.s. Crosses show the corresponding quantities for i.d.d.s.

solved easily to yield the value of β. RATCLIFFE *et al.* (1956) have found that movement effects are negligible when the N_e–t curves show a steady decrease at all heights with the advancing of the night. The January 1950 curves for Slough illustrate this kind of behaviour. The loss coefficient model that the above workers have derived under such condition is

$$\beta = 10^{-4} \exp\left[\frac{300 - h\,(\text{km})}{50}\right] \text{sec}^{-1}. \tag{2}$$

Unfortunately, the "mean quiet F-layers" for Haringhata (Figs. 1 and 2) do not exhibit the above behaviour. Accordingly, these curves cannot be analysed by the above method to yield true values of the loss coefficient. We have, however, used selected portions of the curves (i.e., those around 1900 hours and 0400 hours where the curves show a steady decrease with the advancing of the night) for finding values of the loss coefficient. These values are given in Fig. 7 (filled circles for values derived from the yearly curves of Fig. 2(a) and open circles for those obtained from the monthly curves in Fig. 1 for Haringhata). It will be noted that while the filled circles fit the model of RATCLIFFE *et al.* (indicated by broken line in Fig. 7) better, the majority of points define a different model (full line curve in Fig. 7) given by

$$\beta = 0{\cdot}84 \times 10^{-4} \exp\left[\frac{300 - h\,(\text{km})}{30}\right] \text{sec}^{-1}. \tag{3}$$

VOL. 18 1960

Equations (2) and (3) differ significantly only in the values of the effective scale height (50 in equation (2) and 30 in equation (3)). It may be mentioned in this connexion that our value 30 is in better agreement with the more recent value 35 of SCHMERLING quoted by MITRA (1959).

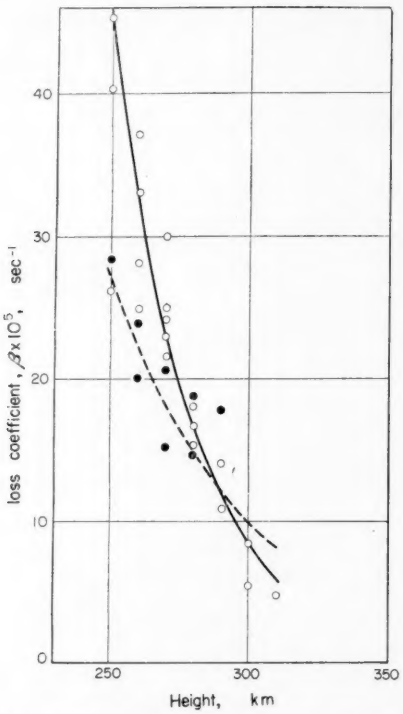

Fig. 7. Loss coefficient models. (Full line, model found for Haringhata; Broken line, model proposed by RATCLIFFE *et al.*, 1956).

Acknowledgements—This work was carried out as part of the programme of Radio Research Committee and was supported by a grant from the Council of Scientific and Industrial Research, Government of India. The writer is indebted to Professor S. K. MITRA, F.R.S. for guidance, to Professor J. N. BHAR, for advice and to Dr. A. P. MITRA of the National Physical Laboratory of India for helpful discussions.

REFERENCES

KELSO J. M.	1952	*J. Geophys. Res.* **57,** 357.
MITRA A. P.	1951	*J. Atmosph. Terr. Phys.* **1,** 286.
MITRA A. P.	1959	*J. Geophys. Res.* **64,** 733.
RATCLIFFE J. A., SCHMERLING E. R., SETTY C. S. G. K. and THOMAS J. O.	1956	*Phil. Trans.* A. **248,** 621.
SCHMERLING E. R. and THOMAS J. O.	1956	*Phil. Trans.* A. **248,** 609.
SCHMERLING E. R. and VENTRICE C. A.	1959	*J. Atmosph. Terr. Phys.* **14,** 249.
THOMAS J. O.	1959	*Proc. Instn Radio Engrs, N.Y.* **47,** 162.
WRIGHT J. W. and NORTON R. B.	1959	Report No. 6031, NBS, U.S.A.

Journa of Atmospheric and Terrestrial Physics, 1960, Vol. 18, pp. 135 to 146. Pergamon Press Ltd. Printed in Northern Ireland

Hydromagnetic wave propagation in the ionosphere

J. A. FEJER
Radio Physics Laboratory,
Defence Research Telecommunications Establishment,
Defence Research Board, Ottawa, Canada

(*Received* 8 *December* 1959)

Abstract—The dispersion equation of hydromagnetic waves, including the effects of collisions, is obtained for an arbitrary angle between the direction of propagation and the direction of a primary magnetic field, assuming certain approximations usually valid in the terrestrial ionosphere. Special cases of the general dispersion equation are considered and some well-known results are regained. Expressions for the dissipated power are derived. The propagation of hydromagnetic waves in a horizontally-stratified ionosphere is discussed, by analogy with the propagation of very-low-frequency radio waves.

1. INTRODUCTION

NUMEROUS extensive theoretical investigations of hydromagnetic wave propagation have been carried out since its discovery by ALFVEN (1942), but these have all been more restrictive in some respects and more general in others than is appropriate to the ionospheric problem. For example no expressions of sufficient generality have yet been given for the susceptibility tensor or for the dispersion equation. The approximations which have been made are not applicable for all frequencies of interest at ionospheric heights and the more accurate treatments do not consider all directions of propagation with respect to the earth's magnetic field.

The main purpose of the present paper is to fill this gap and to provide fairly general expressions for the susceptibility tensor and for the dispersion equation of hydromagnetic waves taking advantage only of approximations which are valid at the heights and frequencies of interest in the terrestrial ionosphere. The method of deriving these expressions is taken over with very little alteration from papers on radio-wave propagation. This similarity of treatment may be helpful to the ionospheric physicist who is familiar with the ionospheric propagation of radio waves but to whom hydromagnetic waves are a new concept.

There is a particularly close mathematical analogy between hydromagnetic waves and very-low-frequency (v.l.f.) radio waves in the ionosphere on account of their large wavelengths. In both cases the validity of the geometrical optical approximation is questionable and the solution of the differential equations of propagation is desirable. The differential equations of hydromagnetic wave propagation have been solved numerically for a horizontally-stratified ionosphere by DUNGEY (1954) in the case of a vertical dominating magnetic field and vertical incidence. Numerical methods for the solution of the differential equations of propagation of v.l.f. radio waves in a horizontally-stratified ionosphere have been given by BUDDEN (1955) under more general circumstances. The application of such methods to the study of hydromagnetic wave propagation is discussed briefly in the present paper.

In Section 2 of this paper some results of previous investigations of hydromagnetic waves are reviewed. In Section 3 the approximations used in subsequent sections are justified in outline and compared with some approximations made

by previous workers. Section 4 contains the derivation of the susceptibility tensor and the dispersion equation. Important special cases are discussed and some well-known results are derived. In Section 5 expressions for the power dissipated per unit volume by hydromagnetic waves are derived in terms of the current density or the electric-field intensity, assuming a sinusoidal variation of the latter quantities with time. Section 6 discusses the numerical solution of the differential equations of hydromagnetic propagation for a horizontally-stratified ionosphere.

2. Previous Work on Hydromagnetic Waves

Initial theoretical work on hydromagnetic waves by Alfven (1942) and Walen (1944) assumed an incompressible liquid. Van de Hulst (1949), Astrom (1950), Ginzburg (1951), Lundquist (1952) and Gershman *et al.* (1957) assume either a fully-ionized gas or an isotropically-conducting compressible liquid.

A fairly complete review of work on the dispersion equation of a fully-ionized gas is given by Gershman *et al.* (1957). There are generally four characteristic waves in a fully-ionized gas in the presence of a dominating magnetic field. Only two of these waves remain if partial pressure terms are neglected. At frequencies well below the ion gyro-frequency these two waves are usually termed hydromagnetic waves. Generally only one of the other two characteristic waves, arising from the partial-pressure terms is non-evanescent; it has the nature of an acoustic wave in the hydromagnetic frequency range. In the special case of transverse propagation three of the characteristic waves are evanescent leaving only one of the two hydromagnetic waves non-evanescent.

The velocity of the hydromagnetic waves is almost independent of frequency. If this velocity is much greater than the velocity of sound, then the effect of the pressure terms on the dispersion equation of the hydromagnetic waves is small. In the special case when the direction of propagation is parallel to the dominating magnetic field (longitudinal propagation), the pressure terms are altogether absent from the dispersion equation of the hydromagnetic waves.

Hines (1953), Dungey (1954), Piddington (1954a, b, 1955, 1956) and Akasofu (1956) assume a partially-ionized gas. Hines (1953) neglects collisions between different types of charged particles and derives the dispersion equation for propagation in the direction of the dominating magnetic field.

Dungey (1954) extends Hines' treatment by taking collisions between ions and electrons into account. He only treats propagation in the direction of the field in detail but indicates briefly the modifications required for waves travelling obliquely to the magnetic field. Dungey (1954) also shows that in the ionosphere the neglect of pressure terms, collisions between ions and electrons, and the motion of neutral particles, is justified if v.l.f. waves are excluded. The range of validity of these approximations, which are adopted in the present paper, is further examined in the following section.

Piddington (1954a, b, 1955) has used a quasi-stationary type of treatment. He assumed that the medium may be described by a conductivity tensor which is independent of frequency. This type of treatment is always a good approximation in a fully-ionized gas. It is valid in weakly-ionized gases only if the circular wave-frequency is much smaller than the collision-frequency of an ion with neutral

VOL
18
196

particles. Thus at the peak of the *F2*-region the approximation is valid for wave-periods well over 10 sec. At greater heights the period would have to be correspondingly longer.

AKASOFU (1956) derives two very general equations, his equation of motion and his generalized Ohm's law, for the mass velocity and the current density in a partially-ionized gas. He only applies these equations in their general form to propagation in the direction of the magnetic field and recovers DUNGEY (1954) results. He makes approximations similar to those of PIDDINGTON (1954a, 1955) in the treatment of transverse propagation.

3. APPROXIMATIONS OF THE PRESENT INVESTIGATION

The approximations used in this paper involve the neglect of partial-pressure terms, collisions between ions and electrons and the motion of neutral particles. The justification of these approximations is now discussed.

Since the motion of neutral particles is neglected for reasons to be given shortly, only the neglect of the forces due to the partial pressures of ions and electrons has to be justified.

In a homogeneous medium this justification is relatively simple if the velocity V of the hydromagnetic wave is much greater than the velocity C of sound in the gas (see for example SPITZER, 1956, p. 57.) This condition is usually satisfied in the ionosphere as for example the results of Section 4 of the present paper show.

In a stratified medium the characteristic length z_0 of the stratification tends to take the place of the reciprocal wave-number k^{-1} of the hydromagnetic wave in the determination of the perturbation pressure gradient if $z_0 \ll k^{-1}$. In this case it would appear that the neglect of the pressure terms is still justified if $V \gg Ck^{-1}/z_0$ or

$$t_0 \ll 2\pi z_0/C \tag{1}$$

where t_0 is the wave-period. This would restrict the application of the results of Section 6 of the present paper to wave-period of less than about 1 min in the terrestrial ionosphere.

The two remaining assumptions of the present approximations are best examined with the aid of DUNGEY's (1954) equation (15) which is valid for propagation in the direction of the field; examination of the general case leads to similar results. DUNGEY's equation (15) shows that the neglect of collisions between ions and electrons is justified if

$$\nu_{ei} \ll \Omega_e\Omega_i\nu_i/2\omega(\omega^2 + \nu_i^2/4)^{1/2} \tag{2}$$

and that the neglect of neutral particle motion is justified if

$$\omega \gg \nu_i\delta/2\rho \tag{3}$$

where ν_{ei} is the collision frequency of an electron with ions, ν_i is the collision-frequency of an ion with neutral particles (it is assumed that all the ions are positive and that their mass is equal to the mass of the neutral particles), Ω_e and Ω_i are the electron and ion gyro-frequencies taken with the positive sign, δ is the density of charged matter and ρ the density of neutral matter.

Substituting into condition (2) the numerical values $\Omega_e \sim 10^7\ \mathrm{sec}^{-1}$,

$\Omega_i \sim 300$ sec^{-1}, $\nu_i \sim 1$ sec^{-1}, $\nu_{ei} \sim 10^3$ sec^{-1} representing conditions near the peak of the $F2$-region and taking the highest frequency of interest as 1 c/s, one obtains

$$\Omega_e\Omega_i\nu_i/2\omega(\omega^2 + \nu_i^2/4)^{1/2} \sim 4 \times 10^7 \text{ sec}^{-1} \gg \nu_{ei} \sim 10^3 \text{ sec}^{-1}.$$

The above assumptions correspond to a neutral-particle density about a thousand times greater than the density of charged particles; condition (2) would thus still hold if the charged particle density were greater by a factor of 10 than the neutral-particle density. One is safe to assume that condition (2) remains satisfied below a height of 1000 km but it is not known whether there are enough neutral particles to satisfy it at still greater heights, or whether it is necessary to consider electron–ion collisions.

Considering condition (3) DUNGEY (1954) estimates that the largest value of $\nu_i\delta/\rho$ is about 10^{-3} sec^{-1} in the ionosphere and thus condition (3) demands that the wave period should be considerably less than $4\pi \times 10^3$ sec $\cong 3$ hr. This is not a very severe restriction.

Although waves of such very-low frequency are not discussed in the subsequent parts of this paper, it is instructive to consider briefly the full dispersion equation which takes them into account. It is convenient to consider the case where the wave-frequency is well below the gyro-frequencies and where the collision-frequency of an ion or an electron is well below its gyro-frequency. HINES obtains for this case and propagation in the direction of the field (HINES' equation (47) with the displacement current neglected)

$$\frac{\omega^2}{k^2} = \frac{B_0^2}{\mu(\rho + \delta)} \frac{\omega\rho - i\delta\nu_i/2}{\omega\rho\delta/(\rho + \delta) - i\delta\nu_i/2} \tag{4}$$

where B_0 is the induction of the dominating magnetic field and μ the permeability. The m.k.s. system of units is used throughout the present paper. HINES uses a differently-defined collision-frequency K_i which corresponds to $\nu_i/2$ in the present notation.

For frequencies well below $\omega_1 = \nu_i\delta/2\rho$ equation (4) results in $\omega^2/k^2 \cong B_0^2/\mu(\rho + \delta)$. Thus ω^2/k^2 is nearly real in this case and its square root $B_0[\mu(\rho + \delta)]^{-1/2}$ is the velocity of the wave as given by ALFVEN's formula.

For frequencies well above $\omega_2 = (\nu_i/2)(\rho + \delta)/\rho$ equation (4) results in $\omega^2/k^2 \cong B_0^2/\mu\delta$ and thus ω^2/k^2 is again nearly real but the velocity of the wave $B_0(\mu\delta)^{-1/2}$ is obtained by substituting into ALFVEN's formula the density of charged matter only.

A wide intermediate-frequency range $\omega_1 \ll \omega \ll \omega_2$ exists in the ionosphere below the height of about 500 km but not at very great heights in the outer ionosphere. Within it ω^2/k^2 is very nearly pure imaginary. Waves in this frequency range are heavily attenuated and are similar to evanescent waves. (For a truly evanescent wave k^2 would be negative.)

The approximation used in the present paper is valid for circular-frequencies much higher than ω_1 while PIDDINGTON's (1954a, 1955) quasi-stationary approximation is valid for frequencies well below ω_2. If the intermediate range $\omega_1 \ll \omega \ll \omega_2$ exists, both approximations are valid within it.

VOL.
18
196

4. Hydromagnetic Waves in a Homogeneous Weakly-ionized Gas

It has been pointed out in the Introduction that, using the approximations of the previous section, the mathematical techniques required for the treatment of hydromagnetic waves are readily available. These known techniques are used in this section to derive the dispersion equation of hydromagnetic waves for an arbitrary angle between the wave-normal and the magnetic field.

One well known method (Ratcliffe, 1959) of describing an ionized medium uses the polarization vector $\mathbf{P}$ that such

$$\mathbf{D} = \varepsilon_0 \mathbf{E} + \mathbf{P} \tag{5}$$

where $\mathbf{D}$ is the displacement vector and ε_0 the dielectric constant of free space. This polarization vector can be calculated from the equations of motion (Chapman and Cowling, 1955, p. 415) for ions and electrons. The result may be written in the form

$$\mathbf{P} = \varepsilon_0 \mathfrak{M} \mathbf{E} \tag{6}$$

where $\mathfrak{M}$, the susceptibility tensor may be written as the sum

$$\mathfrak{M} = \mathfrak{M}_e + \mathfrak{M}_i \tag{7}$$

of an electric term $\mathfrak{M}_e$ and an ionic term $\mathfrak{M}_i$. The electronic term is known from the magneto-ionic theory and is given (Ratcliffe, 1959) by

$$-\frac{X_e}{U_e(U_e^2 - Y_e^2)} \begin{pmatrix} U_e^2 - Y_{xe}^2, & -iU_e Y_{ze} - Y_{xe}Y_{ye}, & iU_e Y_{ye} - Y_{xe}Y_{ze} \\ iU_e Y_{ze} - Y_{ye}Y_{xe}, & U_e^2 - Y_{ye}^2, & -iU Y_{xe} - Y_{ye}Y_{ze} \\ -iU_e Y_{ye} - Y_{ze}Y_{xe}, & iU_e Y_{xe} - Y_{ze}Y_{ye}, & U_e^2 - Y_{ze}^2 \end{pmatrix} \tag{8}$$

while the ionic term $\mathfrak{M}_i$ is given by a similar tensor obtained by replacing the subscript e by the subscript i and changing the sign of each Y symbol. The symbols used in (8) are defined by

$$\begin{aligned} \mathbf{Y}_e &= e\mathbf{B}_0/m_e\omega & \mathbf{Y}_i &= e\mathbf{B}_0/m_i\omega \\ U_e &= 1 - iZ_e = 1 - i\nu_e/\omega & U_i &= 1 - iZ_i = 1 - i\nu_i/2\omega \\ X_e &= Ne^2/\varepsilon_0 m_e\omega^2 & X_i &= Ne^2/\varepsilon_0 m_i\omega^2 \\ Z_e &= \nu_e/\omega & Z_i &= \nu_i/2\omega \end{aligned}$$

where m_e is the mass and e the charge (taken with a positive sign) of an electron, m_i the mass of an ion and N the number density of electrons (or ions). The time factor $\exp(i\omega t)$ is understood in all time-varying quantities in the above equations.

It is convenient to write equation (5) in the form

$$\mathbf{D} = \varepsilon_0 \mathfrak{K} \mathbf{E} \tag{9}$$

where $\mathfrak{K}$ is the dielectric tensor. By suitable orientation of the axes such that $B_{0x} = B_{0y} = 0$, this tensor can be put into the simple form

$$\begin{pmatrix} K_1, & -K_2, & 0 \\ K_2, & K_1, & 0 \\ 0, & 0, & K_0 \end{pmatrix} \tag{10}$$

where

$$K_0 = 1 - \frac{X_e}{1 - iZ_e} - \frac{X_i}{1 - iZ_i} \tag{11}$$

$$K_1 = 1 + \frac{X_e(1 - iZ_e)}{Y_e^2 - (1 - iZ_e)^2} + \frac{X_i(1 - iZ_i)}{Y_i^2 - (1 - iZ_i)^2} \tag{12}$$

$$K_2 = -\frac{iX_eY_e}{Y_e^2 - (1 - iZ_e)^2} + \frac{iX_iY_i}{Y_i^2 - (1 - iZ_i)^2} \tag{13}$$

The refractive index n of a hydromagnetic wave, propagating in a direction which forms an angle θ with the magnetic field, is then given (HINES, 1951, 1957) as a solution of the equation

$$\alpha_4 n^4 + \alpha_2 n^2 + \alpha_0 = 0 \tag{14}$$

where

$$\alpha_4 = K_0 \cos^2\theta + K_1 \sin^2\theta \tag{15}$$

$$\alpha_2 = -[K_0K_1(1 + \cos^2\theta) + (K_1^2 + K_2^2)\sin^2\theta] \tag{16}$$

$$\alpha_0 = (K_1^2 + K_2^2)K_0 \tag{17}$$

The roots of the quadratic equation (14) for n^2 give the squares of the refractive indices of the two characteristic hydromagnetic waves for frequencies below the gyro-frequencies. For sufficiently high frequencies the roots are well approximated by the Appleton–Hartree equation, which can be obtained from (14) by setting $m_i = \infty$.

Equations describing the polarization of the characteristic waves, corresponding to the roots of equation (14) can be obtained from equations (24), (25) and (26) of HINES (1951) in conjunction with equation (9) of HINES (1957) if the expressions (11), (12) and (13) of the present paper are substituted for the corresponding components of the dielectric tensor.

Some special cases of the general dispersion equation (14) are now considered. In the simplest case of longitudinal propagation ($\theta = 0$) the roots of (14) are

$$n^2 = K_1 \pm K_2 \tag{18}$$

while for transverse propagation ($\theta = \pi/2$) the two roots n_1^2 and n_2^2 are

$$n_1^2 = K_1 + K_2^2/K_1 \tag{19}$$

$$n_2^2 = K_0 \tag{20}$$

Equation (20) confirms the well-known result that in transverse propagation the ordinary wave is not influenced by the magnetic field.

A very important approximation is expressed by the conditions that the collision-frequencies are smaller than the corresponding gyro-frequencies, or $Z_e \ll Y_e$, $Z_i \ll Y_i$ and that the circular-frequency is well below the ion gyro-frequency and therefore $Y_e \gg 1$, $Y_i \gg 1$. Equations (12) and (13) then take the form

$$K_1 = 1 + X_e(1 - iZ_e)/Y_e^2 + X_i(1 - iZ_i)/Y_i^2 \tag{21}$$

$$K_2 = 0 \tag{22}$$

and the two solutions of (14) are

$$n_1^2 = K_1 \tag{23}$$

$$n_2^2 = K_0 K_1/(K_0 \cos^2\theta + K_1 \sin^2\theta) \tag{24}$$

with K_0, K_1 and K_2 given by (11), (21) and (22). Insertion of numerical values shows that

$$|K_0| \gg |K_1| \tag{25}$$

and therefore for angles not too near to 90°

$$n_2^2 = K_1/\cos^2\theta. \tag{26}$$

If the approximation is carried one step further by neglecting losses and noting that $m_i \gg m_e$, one obtains

$$K_0 \cong -\omega_e^2/\omega^2,\ K_1 = 1 + N(m_i + m_e)/\varepsilon_0 B_0^2. \tag{27}$$

where $\omega_e = (Ne^2/\varepsilon_0 m_e)^{1/2}$ is the electron plasma-frequency. The mode indicated by (23) has a velocity independent of ω and given by

$$(\varepsilon_0\mu_0 K_1)^{-1/2} = [\mu_0\varepsilon_0 + \mu_0 N(m_i + m_e)/B_0^2]^{-1/2} \cong B_0[\mu_0 N(m_i + m_e)]^{-1/2}. \tag{28}$$

This is the well-known formula for the velocity of a hydromagnetic wave propagated by the charged particles only. The mode indicated by (24) has the velocity given by (28) for $\theta = 0$ and is evanescent for $\theta = \pi/2$ since K_0 is negative. For angles sufficiently removed from $\theta = \pi/2$ equation (26) gives for the velocity

$$(\mu_0\varepsilon_0 K_1)^{-1/2}\cos\theta \cong B_0[\mu_0 N(m_i + m_e)]^{-1/2}\cos\theta. \tag{29}$$

This mode is guided along the magnetic lines of force in the same way as whistlers (Storey, 1953). With the present simplified assumptions the wave-velocity vanishes for $\theta = \tan^{-1}(|K_0|/K_1)$ and according to (25) this angle is very close to 90°. For angles θ nearer to 90° than this critical angle the waves are evanescent. In practice pressure terms modify the behaviour of the waves near $\theta = 90°$ because the wave-velocity given by (29) is not greater there than the velocity of sound. The velocity (28) is, however, several orders greater than the velocity of sound in all parts of the ionosphere and thus our approximation only breaks down for one of the modes (the one, whose energy is guided along the field lines) in the vicinity of $\theta = \pi/2$.

If losses are taken into account, then the refractive indices of the two modes are given by equations (23) and (26) together with (21). The attenuation is mainly determined by the ionic term in (21) which is much greater than the electronic term. If the circular-frequency is much greater than the collision-frequency of an ion with neutral particles, or $Z_i \ll 1$, then the refractive index is almost real; if $Z_i \gg 1$, then the square of the refractive index is almost pure imaginary. If the circular-frequency is lowered below the collision-frequency of a neutral particle with ions $\nu_i\delta/\rho$ then, as explained in Section 3, the present approximation breaks down and the refractive index becomes real again, but has a much greater value corresponding to the substitution of the density of the whole gas, neutral particles included, into Alfven's formula.

The assumptions leading to (21) and (22) are usually valid in the F-region but not in the E-region, in parts of which the collision-frequency is greater than the gyro-frequency for ions but not for electrons and thus $|K_2| \gg |K_1|$. In this case the refractive indices given by (18) for longitudinal propagation and (19) for transverse propagation differ greatly. The situation is very similar to that found in the dynamo theory of magnetic variations, where the "effective conductivity" at E-region heights at moderate latitudes is given approximately by the Hall conductivity σ_2 but near the equator the "Cowling conductivity" $\sigma_1 + \sigma_2^2/\sigma_1$ becomes effective while at F-region heights the effective conductivity is of the order σ_1 at all latitudes.

5. The Dissipation of Hydromagnetic Waves

The dissipation of hydromagnetic waves has been suggested (DESSLER, 1959) as a possible cause of ionospheric heating. It has been pointed out in the Introduction that a solution of the differential equation of hydromagnetic waves is usually necessary before the dissipation can be properly calculated.

It is assumed in this section that such a solution has been obtained and expressions are developed for the power dissipated per unit volume in terms of either the electric field intensity or the current density.

The mean dissipated power P_D per unit volume is given by

$$P_D = \mathrm{Re}(\tfrac{1}{2}\mathbf{E} \cdot \mathbf{j}^*) \tag{30}$$

where Re stands for "real part of", $\mathbf{j}$ is the current density, $\mathbf{E}$ and $\mathbf{j}$ are complex vector quantities and the asterisk denotes the conjugate complex value. The magnitudes are equal to the peak values of the sinusoidally-varying quantities.

In the formation of Section 4 it was convenient to treat the ionized medium as a dielectric. For the purposes of equation (30) it is more convenient to regard the medium as possessing conductivity (this is the more usual formulation in magneto-hydrodynamics), the current density being given by

$$\mathbf{j} = i\omega(\mathbf{D} - \varepsilon_0\mathbf{E}) = i\omega\mathbf{P}. \tag{31}$$

It is convenient to consider the parallel and normal components with respect to the magnetic field $\mathbf{E}_\parallel$, $\mathbf{E}_\perp$ and $\mathbf{j}_\parallel$, $\mathbf{j}_\perp$ of $\mathbf{E}$ and $\mathbf{j}$ separately. Then in terms of the dielectric tensor (9)

$$P_D = \mathrm{Re}(\tfrac{1}{2}\mathbf{E}_\parallel \cdot \mathbf{j}_\parallel^*) + \mathrm{Re}(\tfrac{1}{2}\mathbf{E}_\perp \cdot \mathbf{j}_\perp^*) = \tfrac{1}{2}\omega\varepsilon_0|E_\parallel|^2\,|\mathrm{Im}(K_0)| + \tfrac{1}{2}\omega\varepsilon_0|E_\perp|^2\,|\mathrm{Im}(K_1)| \tag{32}$$

or writing (32) in terms of the current densities given by

$$|j_\parallel| = \omega\varepsilon_0|K_0 - 1|\,|E_\parallel|, \qquad |j_\perp| = \omega\varepsilon_0(|K_1 - 1|^2 + |K_2|^2)^{1/2}|E_\perp| \tag{33}$$

one obtains

$$P_D = |j_\parallel|^2\,|\mathrm{Im}(K_0)|/2\omega\varepsilon_0|K_0 - 1|^2 + |j_\perp|^2\,|\mathrm{Im}(K_1)|/2\omega\varepsilon_0(|K_1 - 1|^2 + |K_2|^2). \tag{34}$$

Equations (32) and (34) are quite general. In practice the second is the more important of the two terms on the right of these equations. In the special cases of

vertical incidence with the magnetic field vertical or horizontal the first term can be shown to be negligibly small.

For circular-frequencies well below the ion collision-frequency the quantities $K_1 - 1$ and K_2 are almost pure imaginary so that $|\mathrm{Im}(K_1)| = |K_1 - 1|$, $|\mathrm{Im}(K_2)| = |K_2|$ and thus in terms of the conductivities defined by $\sigma_1 = \lim_{\omega \to 0}(\omega\varepsilon_0|K_1 - 1|)$, $\sigma_2 = \lim_{\omega \to 0}(\omega\varepsilon_0|K_2|)$ one may rewrite (34) with the first term omitted in the form

$$P_D = \tfrac{1}{2}|j_\perp|^2/\sigma_3 \tag{35}$$

where

$$\sigma_3 = \sigma_1 + \sigma_2^2/\sigma_1 \tag{36}$$

is usually called the Cowling conductivity. This result has been derived previously by COWLING (1956) and PIDDINGTON (1954a). Its validity depends partly, as COWLING has pointed out, on the neglect of pressure terms and partly, as will be seen shortly, on the assumption that the circular-frequency is much smaller than the ion collision-frequency or more concisely that $Z_i \gg 1$.

If the contrary is true and $Z_i \ll 1$, then from equation (12) for $Y_e \gg Y_i \gg 1$

$$P_D \cong \tfrac{1}{2}Z_i|j_\perp|^2/\sigma_3 \cong \tfrac{1}{2}Z_i|j_\perp|^2\, Y_i^2/\omega\varepsilon_0 X_i \tag{37}$$

which is smaller by a factor Z_i than the value given by (35).

In the special case of a single hydromagnetic wave propagated in a homogeneous medium the two approximations (35) and (37) may be expressed in terms of the perturbation induction $\mathbf{b}$. Neglecting the displacement current one has

$$\mathrm{curl}\,\mathbf{b} = \mu_0\mathbf{j} \tag{38}$$

and in our two special cases of vertical incidence, vertical field and vertical incidence, horizontal field this simplifies to

$$|k|\,|b| = \mu_0|j_\perp|. \tag{39}$$

Equation (37) thus leads to

$$P_D = |j_\perp|^2\, B_0^2\nu_i/4\omega^2 N m_i = |k|^2\, B_0^2\nu_i|b|^2/4\omega^2\mu_0^2 N m_i \tag{40}$$

or, since for $Z_i \ll 1$ one may write $\omega/k = B_0(\mu_0 N m_i)^{-1/2}$, equation (40) becomes

$$P_D = \nu_i|b|^2/4\mu_0. \tag{41}$$

Equation (35) can be modified in a similar manner remembering that k^2 is pure imaginary so that the phase velocity V_{HM} of the wave is

$$\omega\sqrt{2}/|k| = V_{HM} = \omega|b|\sqrt{2}/\mu_0|j_\perp|. \tag{42}$$

Equation (35) may then be written in the form

$$P_D = \omega^2|b|^2/\mu_0\sigma_3 V_{HM}^2. \tag{43}$$

Equations (41) and (43) differ only by small numerical factors from corresponding expressions of DESSLER (1959). Presumably DESSLER was only interested in orders of magnitude. DESSLER's formula corresponding to equation (41) of this paper gives a value too low by a factor of 4 while his formula corresponding to equation (43) gives a value too low by a factor of 2·5.

VOL. 18 1960

It must be kept in mind that equations (41) and (43) are only valid for a single hydromagnetic wave in a homogeneous or slowly-varying medium. In general it is safer to use equations (32) and (34) for the calculation of dissipation.

6. Hydromagnetic Waves in a Horizontally-Stratified Partially-ionized Gas

The propagation of hydromagnetic waves through a homogeneous medium was considered in Section 4. The results could be applied fairly directly to a horizontally-stratified medium if a ray treatment was justified, i.e. if the variation of the refractive index within distances of the order of a wavelength were not too great. Unfortunately, even for relatively high frequencies such as 1 c/s, the wavelength in the ionosphere is generally greater than 100 km and thus the variation in the properties of the medium with height is quite large in a wavelength. A technique was developed by Budden (1955) to deal with this type of situation by numerical integration of the differential equations of wave-propagation in a horizontally-stratified medium, using an electronic computer.

The differential equations were given in a form suitable for numerical integration by Clemmow and Heading (1954). They expressed these in the form of four simultaneous first-order differential equations which are given in matrix notation by

$$\mathbf{e}' = -ik\mathfrak{T}\mathbf{e} \tag{44}$$

where $\mathbf{e}$ is a vector with the four components E_x, $-E_y$ Z_0H_x, Z_0H_y, where Z_0 is the impedance of free space, the x- and y-axes are parallel to the planes of stratification and the x- and z-axes are parallel to the plane of incidence. $\mathfrak{T}$ is a three by four matrix given by equation (15) of Clemmow and Heading in terms of the components of $\mathfrak{M}$ which in our problem is the susceptibility tensor given by equation (7). The prime in $\mathbf{e}'$ on the left of equation (44) indicates differentiation with respect to z (height).

If some value (or distribution with depth) of ground conductivity is assumed then the boundary conditions are determined at ground-level apart from the arbitrariness in polarization. The general solution is then a linear combination of two solutions obtained by starting with two arbitrary but different states of polarization from the ground and integrating upward step by step through the ionosphere. Some assumed conditions about the state of polarization at great height then determine the coefficients of the linear combination.

There is here a difference between the propagation of long radio waves and hydromagnetic waves in practice. The latter usually come down through the ionosphere and are reflected from the ground while the former usually start from the ground and are reflected from the ionosphere. Apart from this difference, which changes the direction of integration, the reader is referred to Budden's (1955) paper for further details of the method.

The differential equations are greatly simplified in the two special cases of (a) vertical incidence, vertical magnetic field and (b) vertical incidence, horizontal magnetic field.

In case (a), previously discussed by Dungey (1954), the differential equations may be written in the form of two separate simple wave equations for the two

VOL
18
196

circularly-polarized components of the electric field intensity, with the refractive indices given by (18). Alternatively the two pairs of first-order simultaneous differential equations (60) and (70) for two variables each of CLEMMOW and HEADING (1954) may be used.

Case (b) is still simpler as there is only one propagating mode and it is not coupled to the evanescent mode. The differential equation may then be written either in the form of a wave-equation in the component of the electric field in the direction of propagation, using the refractive index given by (19) or in the form of the pair of first-order simultaneous differential equations (64) of CLEMMOW and HEADING (1954) for $\theta = 0$.

Numerical solutions of the nature just outlined would lead, in the writer's opinion to a better understanding of the process of ionospheric shielding of magnetic disturbances.

It may be argued that at very-low frequencies a treatment using plane stratification fails to take into account that the boundary conditions must be satisfied over a sphere rather than a plane. An approach similar to that used in the dynamo theory of magnetic variations (see for example FEJER, 1953; MAEDA, 1957) could then be a more appropriate method of treating the shielding of magnetic disturbances by the ionosphere. A greatly-enhanced conductivity along a narrow equatorial strip in the ionosphere may well play an important part in the shielding process and could produce enhancement instead of shielding on the ground in the vicinity of the equator.

VOL. 18 1960

7. CONCLUDING REMARKS

It has been demonstrated that the general equations governing hydromagnetic propagation in the ionosphere for wave periods of less than about 1 hr are in many respects very similar to the equations governing the propagation of radio waves. In view of the very large wavelengths of hydromagnetic waves it is further concluded that some of the mathematical techniques used in the study of the propagation of v.l.f. radio waves in the ionosphere would be necessary for the study of ionospheric shielding and dissipation of magnetic disturbances.

In an investigation of dissipation it was found that at circular wave-frequencies well below the ion collision-frequency dissipation caused by the component of the current density normal to the magnetic field may be calculated from COWLING's formula $|j_\perp|^2/2\sigma_3$ but that for frequencies well above the ion collision-frequency the modified formula $(\nu_i/2\omega)|j_\perp|^2/2\sigma_3$ must be used.

Acknowledgements—The writer would like to acknowledge many helpful discussions held with Dr. C. O. HINES, Dr. R. E. BARRINGTON and other colleagues. The work was performed under Project PCC No. D48–95–11–01.

REFERENCES

AKASOFU S.	1956	*Sci. Rep. Tohuku Univ.* Ser 5, **7**, 24.
ALFVEN H.	1942	*Nature, Lond.* **150**, 405.
ASTROM E.	1950	*Ark. Fys.* **2**, 443.
BUDDEN K. G.	1955	*Proc. Roy. Soc.* A **227**, 516.

CHAPMAN S. and COWLING T. G.	1955	*The Mathematical Theory of Non-Uniform Gases.* Cambridge University Press.
CLEMMOW P. C. and HEADING J.	1954	*Proc. Camb. Phil. Soc.* **50,** 319.
COWLING T. G.	1956	*Mon. Not. R. Astr. Soc.* **116,** 114.
DESSLER A. J.	1959	*J. Geophys. Res.* **64,** 397.
DUNGEY J. W.	1954	Pennsylvania State University Scientific Report No. 57.
FEJER J. A.	1953	*J. Atmosph. Terr. Phys.* **4,** 184.
GERSHMAN B. N., GINZBURG V. L. and DENISOV N. G.	1957	*Usp. Fiz. Nauk, Mosk.* **61,** 561 (Translation by U.S. Atomic Energy Commission).
GINZBURG V. L.	1951	*Zh. Eksp. Teoret. Fiz.* **21,** 788.
HINES C. O.	1951	*J. Geophys. Res.* **56,** 63.
HINES C. O.	1953	*Proc. Camb. Phil. Soc.* **49,** 299.
HINES C. O.	1957	*J. Atmosph. Terr. Phys.* **11,** 36.
HULST H. C. VAN DE	1949	IAU Symposium.
LUNDQUIST S.	1952	*Ark. Fys.* **5,** 297.
MAEDA H.	1957	*J. Geomagn. Geoelect., Kyoto.* **9,** 86.
PIDDINGTON J. H.	1954a	*Mon. Not. R. Astr. Soc.* **114,** 638.
PIDDINGTON J. H.	1954b	*Mon. Not. R. Astr. Soc.* **114,** 651.
PIDDINGTON J. H.	1955	*Mon. Not. R. Astr. Soc.* **115,** 671.
PIDDINGTON J. H.	1956	*Mon. Not. R. Astr. Soc.* **116,** 314.
RATCLIFFE J. A.	1959	*The Magneto-Ionic Theory.* Cambridge University Press.
SPITZER L.	1956	*Physics of Fully Ionized Gases.* Interscience, New York
STOREY L. R. O.	1953	*Phil. Trans. Roy. Soc.* A **246,** 113.
WALEN C.	1946	*Arkiv Mat. Astron. Fys.* A **30,** No. 15.

Journal of Atmospheric and Terrestrial Physics, 1960, Vol. 18, pp. 147 to 151. Pergamon Press Ltd. Printed in Northern Ireland

Incoherency of pulse echoes and the measurement of ionospheric absorption

J. TAUBENHEIM
Heinrich-Hertz-Institut der Deutschen Akademie der Wissenschaften
Berlin–Adlershof

(*Received* 8 *December* 1959)

Abstract—The presence of incoherently scattered energy in the h.f. pulse echoes from the ionosphere gives rise to errors in the absorption value determined from the median echo amplitude. These errors are larger for the second-order than for the first-order echo. The calculations are confirmed by experimental results.

THE formulae commonly used for the determination of ionospheric absorption L (expressed in decibels) from the amplitudes E_1 and E_2 of pulse echoes reflected once and twice, respectively, at a virtual height h' in the ionosphere, are

$$L_1 = -20 \log \rho_1 = 20 \log \left(\frac{C}{2h'E_1} \right) \tag{1}$$

$$L_2 = -20 \log \rho_2 = 10 \log \left(\frac{C\rho_g'}{4h'E_2} \right) \tag{2}$$

where ρ is called the apparent reflection coefficient of the ionosphere, C is an instrumental constant and ρ_g is the reflection coefficient of the ground. These formulae are based on a very simple geometrical model, assuming reflection from a homogeneous layer. Under this condition it is to be expected that the echo amplitude varies relatively slowly, according to the variation of absorption.

In fact, however, the echo amplitudes show rapid fluctuations, even after the interference between the magneto-ionic components of the echo has been eliminated. These fluctuations are interpreted as the interference between a regularly-reflected wave and a number of incoherent waves scattered by inhomogeneities in the reflecting layer (RATCLIFFE, 1948), so that the probability distribution of the resulting amplitude R is a Rice-distribution

$$p(R)\,dR = \frac{2R}{a\zeta} \cdot \exp\left[-\frac{R^2 + a^2}{a^2\zeta} \right] \cdot I_0\left(\frac{2R}{a\zeta} \right) dR \tag{3}$$

where a^2 is the regularly-reflected energy and ζ the ratio of scattered energy to regularly-reflected energy (see, e.g., ALPERT, 1953). I_0 is the Bessel function with imaginary argument. Then the mean square amplitude of the received echoes is the sum of reflected and scattered energies, or

$$\overline{R^2} = \int_0^\infty R^2 p(R)\,dR = a^2(1 + \zeta). \tag{4}$$

Usually the rapid fluctuations are eliminated from the determination of ionospheric absorption by inserting in the equations (1) and (2) appropriate mean values for the amplitudes E_1 and E_2, though the conditions of these formulae are not really fulfilled. The distribution (3) shows that all mean values will be influenced by the parameter ζ, representing the "degree of incoherency", which has already been suggested by PIGGOTT (1953). In particular, it is to be expected, that the degrees

of incoherency are different for the first- and second-order reflections, respectively.

It is possible to estimate the error in absorption measurement introduced by neglecting incoherency, using the equations recently derived by ATAEV (1957) from a simple model consideration. For the mean-square amplitude of the first-order echo, ATAEV got

$$\overline{R_1^2} = \frac{E_0^2}{4h'^2}\rho^2\alpha^2(1+\xi) \tag{5}$$

where ξ is the value of ζ for the first-order echo, E_0 is a constant, and α is an effective reflection coefficient for the reflecting layer, which is determined by the scatter mechanism. For the second-order echo, however, he got

$$\overline{R_2^2} = \frac{E_0^2}{16h'^2}\rho_g^2\rho^4\alpha^4(1+4\xi+2\xi^2) \tag{6}$$

if the inhomogeneities are large compared with the sounding wavelength, or

$$\overline{R_2^2} = \frac{E_0^2}{16h'^2}\rho_g^2\rho^4\alpha^4(1+1{\cdot}78\xi+0{\cdot}5\xi^2) \tag{7}$$

if the inhomogeneities are small compared with the sounding wavelength. Thus, if the degree of incoherency is ξ for the first-order echo, and η for the second-order echo, we have the relations

$$\eta = 4\xi + 2\xi^2 \tag{8}$$

for "large" inhomogeneities, and

$$\eta = 1{\cdot}78\xi + 0{\cdot}5\xi^2 \tag{9}$$

for "small" inhomogeneities. The influence of ionospheric absorption, however, is contained only in the factor before the parentheses in equations (5), (6) and (7).

Now it is clear that the presence of random components in the ionospheric echoes gives rise to errors in the absorption measurement, which are different for the first- and second-order echoes. If we denote the real absorption by L_0, while L_1 and L_2 are defined by (1) and (2), we derive from ATAEV's formulae

$$L_0 - L_1 = f_1(\xi) + 20\log\left(\frac{E_0}{C}\right) + 20\log\alpha \tag{10}$$

$$L_1 - L_2 = f_2(\xi) - 10\log\left(\frac{E_0}{C}\right) + 10\log\left(\frac{\rho_g}{\rho_g'}\right) \tag{11}$$

where the (E_0/C)-term on the right-hand side results from the fact that the constant C is usually determined from amplitude measurement at night, which also contains an error from incoherency, which may, however, be different from the error in day-time. Similarly, the (ρ_g/ρ_g')-term takes into account the influence of a possible error in the assumed value of ρ_g'. E_0 and ρ_g are the "true" values of C and ρ_g', respectively. The (log α)-term in (10) contains the effective reflection coefficient α of the reflecting layer. If we simply assume that the scatter mechanism is forward-scattering in such a way that the total energy returned in the first echo is the same as in the case of regular reflection only, it follows from equation (5) that

$$\alpha^2 = \frac{1}{1+\xi}. \tag{12}$$

The values of $(L_0 - L_1)$ and $(L_1 - L_2)$ vs. ξ after equations (10), (11) and (12) are represented in Figs. 1 and 2. They have been calculated under the assumptions that the inhomogeneities are large compared with the sounding wavelength, and that *median* amplitudes are used in the formulae (1) and (2). For calculating the medians of Rice-distributions, the numerical tables of NORTON *et al.* (1955) were used. The shaded areas in Figs. 1 and 2 give the range of possible values caused

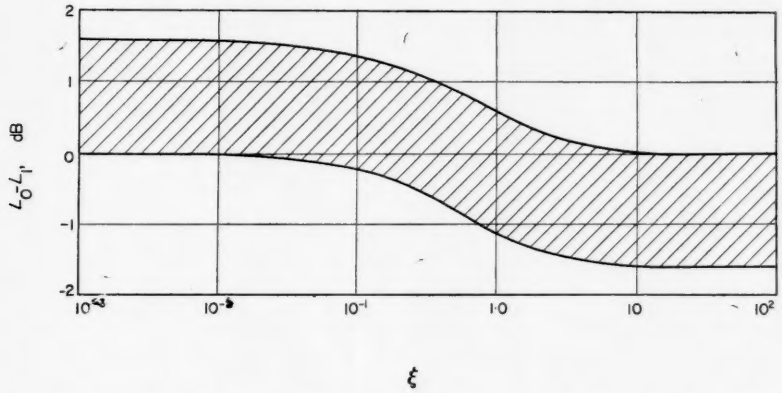

Fig. 1. Difference between true absorption L_0 and measured absorption L_1 from the first-order echo (for "large" inhomogeneities).

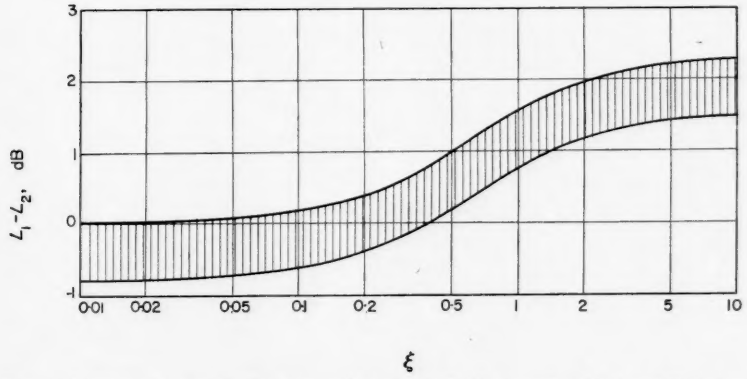

Fig. 2. Difference between the absorption values L_1 (first- order echo) and L_2 (second-order echo) vs. degree of incoherency ξ ("large" inhomogeneities).

by the unknown value of the (E_0/C)-term in equations (10) and (11), the maximum value of which is 1·6 dB.

An experimental verification of equation (11) has been got from the results of routine day-time absorption measurements at Juliusruh/Rügen in winter 1957–1958. The sounding frequency was 3·86 Mc/s, so that the reflection level was in the lower F-region. The histogram in Fig. 3 shows the frequency distribution of the differences $(L_1 - L_2)$, in decibels, for 335 absorption measurements carried out under undisturbed ionospheric conditions. We find that 87 per cent of all differences are positive, like the values of Fig. 2, while the calculation of equation (11)

with "small" inhomogeneities (equation (9)) gives only negative differences for all values of ξ. This shows qualitatively, that the scattering in the lower F-region is caused mainly by inhomogeneities which are large compared with the sounding wavelength of 78 m. Most frequently we have differences between +1 and +2 dB. This is in good agreement with the values of Fig. 2, if the order of magnitude of ξ is 1 and greater. The mean value (about 3 dB) of the histogram distribution in Fig. 3 is slightly greater than the theoretical maximum value of equation (11).

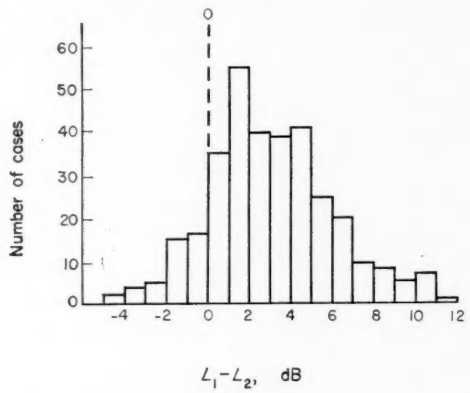

Fig. 3. Distribution of the differences $L_1 - L_2$, from measurements at Juliusruh/Rügen in winter 1957–1958 (3·86 Mc/s).

This might be due to the fact that the degree of incoherency of the second-order echo can be further enhanced by the roughness of the ground, as suggested by PIGGOTT (private communication). Large-scale focusing effects, too, can enhance the multiple-order echo amplitudes more than the first-order amplitude.

Since, for Juliusruh/Rügen, it is assumed that $\rho_g' \approx 1$, the measured differences $(L_1 - L_2)$ would be even too small, if the assumed value of ρ_g' should be in error.

Conclusion—The presence of incoherently scattered energy in the ionospheric echoes gives rise to an error in the absorption value determined from the median echo amplitude. This error is not greater than 1·6 dB, if the first-order echo is used. The absorption calculated from the amplitude of the second-order echo, however, will be always too low. Similarly, it is easily seen that the method of determining ionospheric absorption from the amplitude ratio of first- and second-order echoes after the formula

$$L_{12} = 20 \log (E_1/2E_2) \tag{13}$$

gives incorrect values, which may be 3 dB lower than the correct values. All these conclusions agree well with the experiences of other authors (e.g. PIGGOTT, 1959).

The results of the present consideration are not essentially changed if arithmetic mean amplitudes are used instead of median amplitudes, because for a Rice-distribution the median value is not more than 0·5 dB lower than the mean value.

Acknowledgements—The writer is greatly indebted to Mr. W. R. PIGGOTT, Slough, and Dr. H. SCHWENTEK, Lindau, for their helpful critical remarks on the first form of the manuscript of this paper.

References

Alpert Ya. L.	1953	*Usp. Fiz. Nauk, Mosk.* **49,** 49. (In Russian.)
Ataev O. M.	1957	*Radiotekhnika i Elektronika* **2,** 523. (In Russian.)
Norton K. A., Vogler L. E., Mansfield W. V. and Short P. J.	1955	*Proc. Inst. Radio Engrs, N.Y.* **43,** 1354.
Piggott W. R.	1953	*Proc. Inst. Elect. Engrs,* Pt. III, **100,** 61.
Piggott W. R.	1959	URSI–AGI Meeting, Brussels, September, 1959.
Ratcliffe J. A.	1948	*Nature, Lond.* **162,** 9.

VOL.
18
1960

Journal of Atmospheric and Terrestrial Physics, 1960, Vol. 18, pp. 152 to 159. Pergamon Press Ltd. Printed in Northern Ireland

Sur la détermination des hauteurs réelles de l'ionisation dans les hautes latitudes

D. Lepechinsky et C. Taieb
Groupe Ionosphère du CNET, Bagneux (S), France

(*Received* 15 *December* 1959)

Abstract—The z-trace which often appears on ionograms of high latitude stations is usually much better defined than the o-trace, the latter being rather diffuse. True height determinations including the earth's magnetic field now in use being all based on the o-trace, the writers propose a new matrix method, similar to that of Dr K. G. Budden but applicable to the z-trace. The appropriate matrix has been calculated (for $f_H = 1{\cdot}8$ Mc/s) for frequencies up to 6 Mc/s and the results of a profile determination is presented involving both "o" and z-matrix methods for a typical Terre Adelie ionogram.

1. Introduction

Diverses méthodes ont été mises au point pour la détermination des hauteurs réelles de l'ionisation à partir des ionogrammes ($h'f$) obtenus par les sondages ionosphériques verticaux. Les méthodes les plus simples négligent l'influence du champ magnétique terrestre et celle des chocs entre les électrons et les autres particules (voir par exemple Kelso, 1952).

Les méthodes actuellement les plus complètes tiennent compte de l'influence du champ magnétique terrestre (qui peut être très grande, l'erreur commise en négligeant cet effet pouvant atteindre 20 pour cent sur la hauteur réelle) et n'envisagent pour le profil de la couche que l'hypothèse d'un accroissement monotone de la densité électronique avec l'altitude (voir par exemple Budden, 1954). Toutefois, même ces dernières méthodes négligent complètement l'influence des chocs. Elles sont toutes basées sur la trace ($h'f$) du rayon "ordinaire'. Or l'influence des chocs n'est faible que lorsque le nombre de chocs est faible et que la propagation reste du type "quasi-transversal" (Booker, 1934), c'est-à-dire lorsque la direction de propagation fait un angle suffisamment grand avec celle du champ magnétique terrestre. Elle devient par contre très importante lorsque la propagation passe au type "quasi-longitudinal".

On sait qu'en l'absence de chocs, cette circonstance ne se produit que si la direction de propagation coïncide strictement avec celle du champ magnétique terrestre (inclinaison magnétique $\theta = 90°$); au contraire, si l'on tient compte des chocs, le "niveau de transition" (Lepechinsky, 1956, 1957) de la région inférieure où le nombre de chocs est grand (région-QL) à la région supérieure (région-QT) où il est faible, se situe pour toutes les fréquences émises à la verticale à une altitude telle que:

$$\nu_c = p_H \frac{\cos^2 \theta}{2 \sin \theta} \tag{1}$$

ν_c étant le nombre de chocs par sec et p_H la pulsation de la gyrofréquence f_H, donnée par:

$$p_H = 2\pi f_H = H \frac{e}{mc} \tag{2}$$

où H est le champ magnétique terrestre, e/m le rapport de la charge et de la masse de l'électron et c la vitesse de la lumière dans le vide.

En adoptant pour f_H la valeur moyenne de 1,2 Mc/s, et pour la loi de variation du nombre de chocs ν avec l'altitude une loi exponentielle basée sur les données de la Circulaire No. 462 du National Bureau of Standards des Etats-Unis, LEPECHINSKY, (1956, 1957) a calculé la courbe de variation de l'altitude du niveau de transition QL–QT, répondant à l'équation (1) en fonction de l'inclinaison θ du champ terrestre. D'après cette courbe, la propagation est du type QL, non seulement au pôle magnétique ($\theta = 90°$) mais aussi dans les régions voisines, pour l'ionosphère inférieure, la limite de QL–QT se situant à 200 km lorsque $\theta = 88{\cdot}5°$ et à 100 km lorsque $\theta = 67°$ (la région de propagation QL étant bien entendu celle où $\nu > \nu_c$).

Il est donc bien évident que pour certaines stations de sondage voisines du pôle magnétique—telles que la Terre Adelie ($\theta = 89°$), même la région-F se trouve dans la région-QL.

Or on sait que cette région est caractérisée par *l'absence du rayon "ordinaire"*, théoriquement, la réflexion QL s'effectuant selon les relations:

$$\left.\begin{aligned} X &= 1 + Y \text{ pour le rayon } z \\ X &= 1 - Y \text{ pour le rayon } x \end{aligned}\right\} \tag{3}$$

où $X = 4\pi Ne^2/mp^2$ et $Y = p_H/p$, N étant la densité électronique et p la pulsation de l'onde émise.

Les ionogrammes obtenus en Terre Adelie au cours de l'AGI accusent en effet dans beaucoup de cas, des traces "ordinaires" trop diffuses pour être utilisables, même dans la région-F, de sorte que les méthodes actuellement mises au point pour le calcul des hauteurs réelles, toutes basées comme on l'a vu sur les traces "ordinaires" des ionogrammes sont difficilement applicables à cette station. Lorsque la trace o est présente simultanément en Terre Adelie la trace z est toujours beaucoup mieux marquée et plus facile à dépouiller.

Il nous a donc paru utile de proposer une méthode de calcul convenant à cette catégorie de stations et basée sur les traces z.

2. METHODE DE CALCUL DES HAUTEURS RÉELLES A PARTIR DE LA TRACE z

Pour simplifier les calculs, nous admettrons pour condition de réflexion z la condition ci-dessus, c'est-à-dire:

$$X = 1 + Y$$

qui revient à négliger l'influence des chocs mais à tenir compte du type de propagation. Ne faisant ensuite aucune hypothèse spéciale sur le profil de la couche ionisée, nous admettrons seulement que sa densité électronique augmente de façon monotone avec l'altitude. L'indice de réfraction de phase est alors:

$$\mu^2 = 1 - \frac{X}{1 + Y} \tag{4}$$

avec

$$X = \frac{f_0^2}{f^2}$$

où f_0 = fréquence de plasma ($f_0^2 = Ne^2/\pi m$, N étant la densité électronique);
f = fréquence d'utilisation.

$$Y = \frac{f_H}{f}$$

où f_H = gyrofréquence.

Nous savons qu'entre une hauteur virtuelle (ionogramme) et une hauteur réelle (que l'on veut calculer) il existe la relation:

$$h'(f) = \int_0^{Zr} \mu'(f, f_0)\, dz \tag{5}$$

Zr = hauteur réelle de réflexion.

Nous écrivons, comme le fait BUDDEN (1954) la relation (5) sous la forme:

$$h'(f) = \int_0^{f} \mu'(f, f_0) \frac{dz}{df_0}\, df_0 \tag{6}$$

où $h'(f)$ = hauteur virtuelle (ionogramme);

$\mu'(f,f_0)$ = indice de réfraction de groupe, fonction de f et f_0, quand on s'est fixé la valeur de la gyrofréquence.

Or, μ' est connu à partir de l'indice de réfraction de phase μ, par la formule de Rayleigh:

$$\mu' = \mu + f\frac{d\mu}{df}. \tag{7}$$

La relation (4) peut donc s'écrire $\mu^2 = 1 - \dfrac{f_0^2}{f^2 + ff_H}$. (8)

Dérivons par rapport à f; on a:

$$2\mu \frac{d\mu}{df} = \frac{f_0^2(2f + f_H)}{(f^2 + ff_H)^2}. \tag{9}$$

Entre (7), (8) et (9), on a d'autre part:

$$\mu' = \frac{1 - [f_0^2/(f^2 + ff_H)] + f_0^2(2f^2 + ff_H)/2(f^2 + ff_H)^2}{\sqrt{\{1 - [f_0^2/(f^2 + ff_H)]\}}}. \tag{10}$$

La réflexion a lieu pour $\mu = 0$, soit: $f_0^2 = f^2 + ff_H$, où $f_0 = f\sqrt{[1 + (f_H/f)]}$ La formule (6) s'écrit donc.

$$h'(f) = \int_{f_0=0}^{f_0=f\sqrt{[1+(f_H/f)]}} \mu'(f, f_0) \frac{dz}{df_0}\, df_0. \tag{11}$$

Considérons sur la courbe $h'(f)$ des intervalles de fréquence $\Delta f = 0{,}2$ Mc/s (Fig. 1). A la fréquence Δf correspond la hauteur virtuelle h_1'; à $2\Delta f$ correspond h_2' . . . à $n\Delta f$ correspond h_n'. Lorsque la fréquence d'utilisation est $f = \Delta f$ et si $dz/df_0 =$ constante dans l'intervalle:

$$f_0 = 0 \text{ à } f_{0,1} = \Delta f \sqrt{\left(1 + \frac{f_H}{\Delta f}\right)},$$

l'équation (11) s'écrit:

$$h_1' = \frac{z_1 - z_0}{f_{0,1}} \int_0^{\Delta f\sqrt{[1+(f_H/\Delta f)}} \mu'(\Delta f, f_0)\, df_0.$$

Si la fréquence d'utilisation est $f = 2\Delta f$, (11) s'écrit:

$$h_2' = \frac{z_1 - z_0}{f_{0,1}} \int_0^{f_{0,1}} \mu'(2\Delta f, f_0)\, df_0 + \frac{z_2 - z_1}{f_{0,2} - f_{0,1}} \int_{f_{0,1}}^{f_{0,2}} \mu'(2\Delta f, f_0)\, df_0$$

avec $$f_{0,2} = 2\Delta f \sqrt{\left(1 + \frac{f_H}{2\Delta f}\right)}.$$

D'une manière générale on peut donc écrire:

$$h_n' = \sum_{m=1}^{m=n} \frac{z_m - z_{m-1}}{f_{0,m} - f_{0,m-1}} \int_{f_{0,m-1}}^{f_{0,m}} \mu'(n\Delta f, f_0)\, df_0 \tag{12}$$

avec $$f_{0,m} = m\Delta f \sqrt{\left(1 + \frac{f_H}{m\Delta f}\right)}.$$

On pose: $$M_{n,m} = \frac{1}{f_{0,m} - f_{0,m-1}} \int_{f_{0,m-1}}^{f_{0,m}} \mu'(n\Delta f, f_0)\, df_0. \tag{13}$$

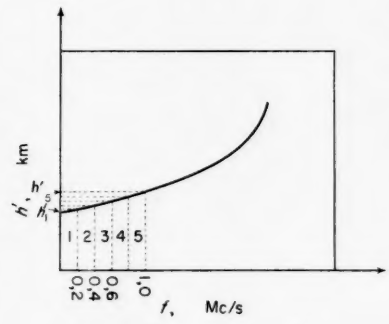

Fig. 1. Hauteurs virtuelles.

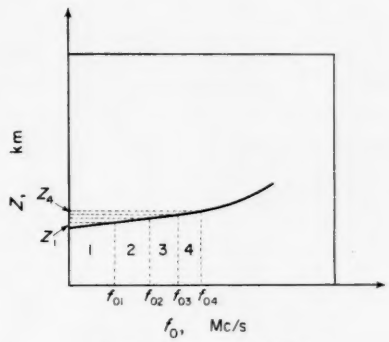

Fig. 2. Hauteurs réelles.

On peut remarquer que $f_{0,m} - f_{0,m-1} > \Delta f$ et que $f_{0,m} - f_{0,m-1}$ tend rapidement vers Δf, comme on peut le voir sur les figures 1 et 2. Prenons un exemple:

$f_H = 1{,}8$ Mc/s $\qquad \Delta f = 0{,}2$ Mc/s

$f_{0,1} = 0{,}63245$

$f_{0,2} = 0{,}93808 \qquad f_{0,2} - f_{0,1} = 0{,}30563$

$f_{0,3} = 1{,}2 \qquad f_{0,3} - f_{0,2} = 0{,}26192$

$f_{0,4} = 1{,}44222 \qquad f_{0,4} - f_{0,3} = 0{,}24222$

$f_{0,5} = 1{,}67332 \qquad f_{0,5} - f_{0,4} = 0{,}2311$

. . . . . .

$f_{0,19} = 4{,}6113$

$f_{0,20} = 4{,}8166 \qquad f_{0,20} - f_{0,19} = 0{,}2053$

VOL. 18 1960

Portons (10) dans l'équation (13):

$$M_{n,m} = \frac{1}{f_{0,m} - f_{0,m-1}} \times$$

$$\times \int_{f_{0,m-1}}^{f_{0,m}} \frac{1 - \{f_0^2/[(n\Delta f)^2 + n\Delta f \cdot f_H]\} + f_0^2[2(n\Delta f)^2 + n\Delta f \cdot f_H]/2[(n\Delta f)^2 + n\Delta f \cdot f_H]^2}{\sqrt{\left|1 - \{f_0^2/[(n\Delta f)^2 + n\Delta f \cdot f_H]\}\right|}} \, df_0$$

Posons:

$$(n\Delta f)^2 + n\Delta f \cdot f_H = \frac{1}{a_n};$$

$$b_n = \frac{a_n^2}{2}[n\Delta f \cdot f_H + 2(n\Delta f)^2] - a_n.$$

On a alors à résoudre une intégrale de la forme:

$$\int \frac{1 + f_0^2 b_n}{\sqrt{(1 - a_n f_0^2)}} \, df_0.$$

Le calcul donne:

$$M_{n,m} = \frac{1}{f_{0,m} - f_{0,m-1}} \left\{ \left(\frac{1}{\sqrt{a_n}} + \frac{b_n}{2a_n\sqrt{a_n}} \right) \left[\arcsin f_0 \sqrt{a_n} \right]_{f_{0,m-1}}^{f_{0,m}} - \right.$$

$$\left. - \frac{b_n}{2a_n\sqrt{a_n}} \left[f_0 \sqrt{a_n} \times \sqrt{(1 - a_n f_0^2)} \right]_{f_{0,m-1}}^{f_{0,m}} \right\}$$

Revenant à l'équation (12) qu'on écrit sous forme matricielle, on a:

$$\begin{bmatrix} h'_1 \\ h'_2 \\ \cdot \\ \cdot \\ \cdot \\ \cdot \\ h'_n \end{bmatrix} = \begin{bmatrix} M_{11} & 0 & 0 & \\ M_{21} - M_{22} & M_{22} & 0 & \\ & & & \\ & & & \\ & & & \\ & & & \\ M_{n,1} - M_{n,2} & M_{n,2} - M_{n,3} \cdots\cdots\cdots & & M_{n,n} \end{bmatrix} \times \begin{bmatrix} z_1 \\ z_2 \\ \cdot \\ \cdot \\ \cdot \\ \cdot \\ z_n \end{bmatrix}$$

soit $$(h'_n) = (M)(z).$$

Ayant calculé l'inverse de la matrice (M) tel que $(L) = (M)^{-1}$ on obtient:

$$(z) = (L)(h')$$

où (L) est la matrice cherchée.

BUDDEN (1954) a calculé les coefficients de cette matrice pour le rayon "ordinaire" et la station de Slough. Nous avons fait le même calcul pour le cas des très hautes latitudes avec $f_H = 1{,}8$ Mc/s et donnons ci-joint (Tableau 1) les coefficients de la matrice (L) correspondante, permettant le calcul des hauteurs réelles avec $\Delta f = 0{,}2$ Mc/s jusqu'à $f = 6$ Mc/s. Rappelons que la hauteur réelle de réflexion de la fréquence $f = n\Delta f$ est donnée par

$$z_n = L_{n,1}h_1' + L_{n,2}h_2' + \cdots\cdots + L_{n,n}h_n'$$

où $L_{n,n}$ est le coefficient de la ne ligne et de la ne colonne du Tableau 1.

VOL. 18 196

Tableau 1. Matrice $[L]$ pour le calcul des hauteurs réelles dans les régions polaires, à partir de la trace z, avec $f_H = 1{,}8$ Mc/s

$f_0 \downarrow$																														
1,8973	1,00																													
2,1166	6941	3057																												
2,3324	5489	1669	2840																											
2,5455	4601	1171	1566	2661																										
2,7568	3991	0912	1108	1479	2509																									
2,9664	3541	0754	0869	1053	1403	2379																								
3,1749	3194	0645	0722	0831	1004	1337	2266																							
3,3823	2915	0566	0620	0693	0796	0962	1279	2168																						
3,5889	2687	0506	0546	0598	0666	0765	0923	1228	2080																					
3,7948	2495	0458	0489	0528	0577	0643	0738	0889	1181	2001																				
4,0000	2331	0420	0444	0474	0510	0558	0621	0712	0858	1140	1931																			
4,2048	2190	0388	0407	0431	0459	0495	0540	0601	0689	0830	1102	1867																		
4,4091	2066	0361	0377	0396	0419	0446	0480	0524	0583	0668	0804	1068	1809																	
4,6130	1957	0337	0351	0367	0385	0407	0434	0466	0509	0566	0648	0781	1036	1755																
4,8166	1860	0317	0329	0342	0357	0375	0396	0422	0454	0495	0550	0630	0759	1007	1706															
5,0200	1772	0299	0309	0321	0333	0348	0366	0386	0411	0442	0482	0536	0614	0739	0980	1661														
5,2230	1693	0284	0292	0302	0313	0325	0340	0357	0377	0401	0431	0470	0522	0598	0720	0955	1619													
5,4258	1622	0269	0277	0286	0295	0305	0318	0332	0348	0367	0391	0421	0459	0510	0584	0702	0931	1579												
5,6285	1556	0257	0264	0271	0279	0289	0299	0311	0324	0340	0360	0383	0411	0448	0498	0570	0686	0910	1543											
5,8309	1496	0246	0252	0258	0265	0273	0282	0292	0304	0317	0333	0352	0374	0402	0438	0487	0558	0671	0890	1509										
6,0333	1441	0236	0241	0247	0253	0260	0267	0276	0286	0297	0310	0326	0344	0366	0393	0429	0477	0546	0656	0871	1477									
6,2353	1390	0226	0231	0236	0241	0248	0254	0262	0271	0280	0291	0304	0319	0337	0359	0386	0420	0467	0534	0643	0853	1447								
6,4373	1342	0218	0222	0226	0231	0237	0243	0249	0257	0265	0275	0286	0298	0313	0330	0351	0378	0412	0458	0524	0630	0836	1418							
6,6393	1298	0210	0213	0218	0222	0227	0232	0238	0245	0252	0260	0269	0280	0292	0307	0324	0345	0371	0404	0449	0514	0618	0820	1391						
6,8411	1257	0202	0206	0209	0213	0218	0223	0228	0234	0240	0247	0255	0264	0275	0287	0301	0318	0338	0364	0397	0441	0504	0607	0805	1366					
								f $\rightarrow$																						
	1,2	1,4	1,6	1,8	2,0	2,2	2,4	2,6	2,8	3	3,2	3,4	3,6	3,8	4,0	4,2	4,4	4,6	4,8	5,0	5,2	5,4	5,6	5,8	6					

Tous les nombres du tableau, à l'exception de la première colonne et des première et dernière lignes, sont en dix-millièmes; ainsi par exemple pour 6941, lire : 0,6941 . . .etc. . . .

Remarquons que les hauteurs réelles z_1, $z_2 \ldots . z_n$ ainsi obtenues sont bien les hauteurs réelles de réflexion des fréquences $f_{0,1}, f_{0,2}, \ldots . f_{0,n}$ dont les hauieurs virtuelles de réflexion (relevées sur la trace z) sont h_1', $h_2' \ldots . h_n'$ correspondantes aux fréquences: f, 2 Δf, ... , n Δf.

Donc, contrairement à ce qui a lieu pour le rayon ordinaire, les densités électroniques situées aux altitudes z_1, $z_2 \ldots . z_n$ doivent être déterminées, non par la relation (QT):

$$f_0 = f$$

où

$$f_0 = \sqrt{\left(\frac{Ne^2}{\pi m}\right)}$$

mais bien par la relation (QL):

$$f_0 = f\sqrt{\left(1 + \frac{f_H}{f}\right)} = \sqrt{\left(\frac{Ne^2}{\pi m}\right)}.$$

3. Exemple d'Application

A titre d'exemple nous avons calculé le profil d'ionisation correspondant à l'ionogramme du 12 novembre 1957 à 0800 TU de la Station de Terre Adelie (Fig. 3).

(1) d'une part à l'aide de la trace z en utilisant la matrice du Tableau 1.

(2) d'autre part à l'aide de la trace o en utilisant la méthode graphique de J. W. Wright et R. B. Norton (cf. N. B. S. Report no. 6031).

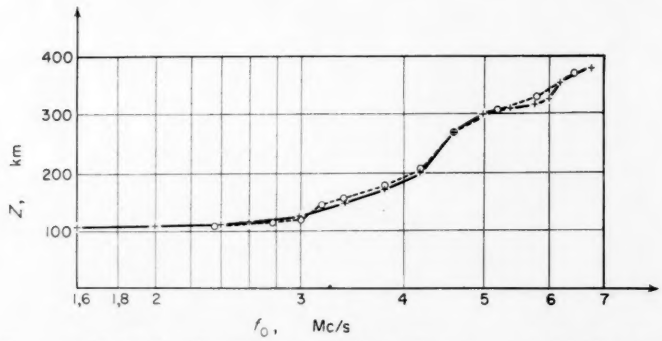

Fig. 4. Hauteurs réelles de réflexion correspondant à l'ionogramme de la Fig. 3, obtenues: (1) à partir de la trace o, + — +; (2) à partir de la trace z, o – – – o.

Les résultats obtenus sont représentés sur la Fig. 4, où le profil obtenu à partir de la trace z est en traits tiretés, celui obtenu par la trace o étant en trait plein.

On constate que les profils sont sensiblement identiques, la différence la plus grande se manifestant entre 3 et 4 Mc/s, où le profil z accuse mieux l'inflexion due à la f_0E.

On remarquera sur l'ionogramme de la Fig. 3 la grande netteté de la trace z et la diffusion marquée, qui, comme à l'ordinaire caractérise la trace o, rendant très approximative la lecture des hauteurs virtuelles de cette trace.

VOL.
18
1960

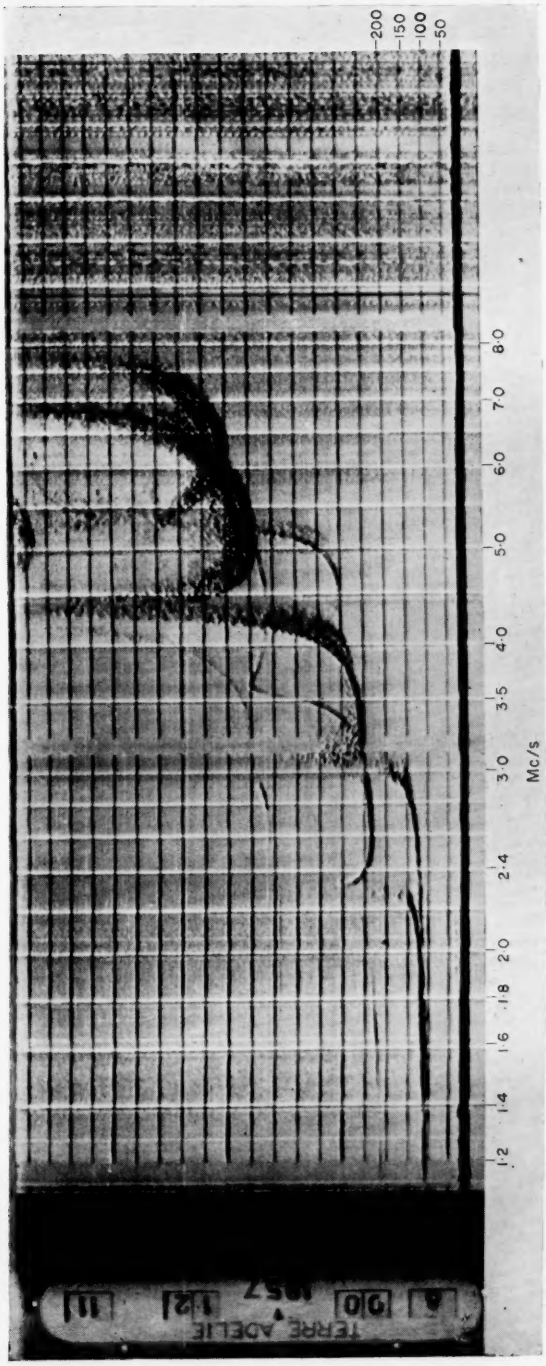

Fig. 3.

VOL
18
196

Sommaire

Les ionogrammes des stations de très hautes latitudes, telle que celle de Terre Adelie, présentent très fréquemment la trace de la troisième composante magnéto-ionique, celle du rayon "ordinaire" étant diffuse ou peu apparente. La détermination des hauteurs réelles de l'ionisation ne peut donc y être faite qu'imparfaitement par les méthodes actuellement mises au point et qui se réfèrent toutes au rayon "ordinaire".

Dans la présente note, une méthode de calcul des hauteurs réelles est proposée à partir de la trace z des ionogrammes. Analogue à celle de K. G. Budden, elle aboutit à une matrice dont les coefficients permettent de trouver la hauteur réelle d'une fréquence f à partir des hauteurs virtuelles de n fréquences inférieures, également réparties de 0 à f.

Bibliographie

Booker H. G.	1934	*Proc. Roy. Soc.* A **147,** 352.
Budden K. G.	1954	*The Physics of the Ionosphere.* Cavendish Laboratory, Cambridge.
Kelso J. M.	1952	*J. Geophys. Res.* **57,** 357.
Lepechinsky D.	1956	*J. Atmosph. Terr. Phys.* **8,** 298.
Lepechinsky D.	1957	*J. Atmosph. Terr. Phys.* **10,** 243.

VOL. 18 1960

Journal of Atmospheric and Terrestrial Physics, 1960, Vol. 18, pp. 160 to 173. Pergamon Press Ltd. Printed in Northern Ireland

On the ionospheric heating by hydromagnetic waves connected with geomagnetic micropulsations

Syun-Ichi Akasofu
Geophysical Institute, College, Alaska

(*Received* 22 *September* 1959; *revised* 11 *January* 1960)

Abstract—The energy dissipation process of the hydromagnetic waves in the ionosphere is studied in detail. It is shown that their heat production and the resulting increase of temperature are negligible.

Introduction

Cowling (1956) has shown that there may be large dissipation of magnetic energy in a partially ionized gas. Piddington (1956) has suggested that the high temperature in the solar corona is due to the dissipation of hydromagnetic energy.

The ionosphere is a partially ionized gas, but the physical conditions are quite different from those of the sun. It is the object of this paper to show that in the *F2*-region the increase of temperature due to this process is less than 5°C in the most favourable conditions.

Fundamental Equations

The ionosphere is treated as a ternary mixture composed of electrons, together with neutral particles and positive ions, each of one kind only. Subscripts e, n and p will indicate reference to these three kinds of particle.

The equation of motion of the ith gas in a mixture (Chapman and Cowling, 1953, pp. 415, 245) is

$$\rho_i \frac{D_i \mathbf{v}_i}{Dt} = \rho_i \mathbf{F}_\mathbf{i} + N_i e_i \mathbf{v}_\mathbf{i} \times \mathbf{H} - \text{grad}\, p_i + \sum_j \alpha_{ij} N_i N_j (\mathbf{v}_\mathbf{j} - \mathbf{v}_\mathbf{i}), \tag{1}$$

where

$$\alpha_{ij} = \frac{8}{3} \sigma_{ij}^2 \left[\frac{2\pi k T m_i m_j}{(m_i + m_j)}\right]^{1/2} \tag{2}$$

and

$\mathbf{v}_\mathbf{i}$ = velocity;
N_i = particle number density;
m_i = mass;
ρ_i = particle mass density = $N_i m_i$;
$\mathbf{F}_\mathbf{i}$ = force per unit mass;
T = temperature;
p_i = particle pressure = kN_iT;
k = Boltzmann constant = $1{\cdot}38 \times 10^{-16}$;
e_i = electronic charge = $1{\cdot}6 \times 10^{-20}$ e.m.u;
$\dfrac{D_i}{D_t} = \dfrac{\partial}{\partial t} + \mathbf{v}_\mathbf{i} \,.\, \text{grad}$;
σ_{ij} = effective collision distance between particles i and j.

It should be noticed that α_{ij} $(=kT/N[D_{ij}]_1)$ relates to the collision frequency ν_{ij} in the following way (CHAPMAN, 1956, p. 12),

$$\nu_{ij} = \frac{\rho_i + \rho_j}{\rho_i \rho_j} N_i N_j \alpha_{ij} = \frac{8}{3} \rho \sigma_{ij}^2 \left[\frac{2\pi kT}{m_i m_j (m_i + m_j)} \right]^{1/2}. \tag{3}$$

Therefore, assuming that $\rho_n \gg \rho_p$ and $\rho_n \gg \rho_e$,

$$\left.\begin{aligned} N_i N_j \alpha_{ij} &= \frac{\rho_i \rho_j}{\rho_i + \rho_j} \nu_{ij}, \\ &\simeq \rho_p \nu_{pn} \text{ (for ions)}, \\ &\simeq \rho_e \nu_{en} \text{ (for electrons)}. \end{aligned}\right\} \tag{4}$$

ν_{ij} calculated by CHAPMAN (1956) is given in Table 1, together with the model of the ionosphere adopted in this paper.

Table 1. Adopted model of the ionosphere (CHAPMAN, 1956)

Height	T(°K)	N_n(cm^3)	N_e(cm^3)	ν_{en}(sec)	ν_{pn}(sec)
80	205	$4{\cdot}38 \times 10^{14}$	10^3	$3{\cdot}39 \times 10^6$	$2{\cdot}11 \times 10^5$
90	220	$8{\cdot}53 \times 10^{13}$	10^4	$6{\cdot}38 \times 10^5$	$4{\cdot}12 \times 10^4$
100	280	$1{\cdot}78 \times 10^{13}$	10^5	$1{\cdot}61 \times 10^5$	$8{\cdot}59 \times 10^3$
125	430	$1{\cdot}23 \times 10^{12}$	$1{\cdot}50 \times 10^5$	$1{\cdot}38 \times 10^4$	$6{\cdot}16 \times 10^2$
150	580	$2{\cdot}16 \times 10^{11}$	$2{\cdot}00 \times 10^5$	$2{\cdot}81 \times 10^3$	$1{\cdot}12 \times 10^2$
175	730	$6{\cdot}03 \times 10^{10}$	$2{\cdot}00 \times 10^5$	$8{\cdot}80 \times 10^2$	$3{\cdot}20 \times 10$
200	880	$2{\cdot}23 \times 10^{10}$	$2{\cdot}00 \times 10^5$	$3{\cdot}57 \times 10^2$	$1{\cdot}21 \times 10$
225	1030	$9{\cdot}98 \times 10^9$	$2{\cdot}25 \times 10^5$	$1{\cdot}73 \times 10^2$	$5{\cdot}53$
250	1180	$5{\cdot}12 \times 10^9$	$2{\cdot}50 \times 10^5$	$9{\cdot}50 \times 10$	$2{\cdot}90$
275	1330	$2{\cdot}92 \times 10^9$	$2{\cdot}75 \times 10^5$	$5{\cdot}75 \times 10$	$1{\cdot}70$
300	1480	$1{\cdot}80 \times 10^9$	$3{\cdot}00 \times 10^5$	$3{\cdot}74 \times 10$	$1{\cdot}08$

Suppose that plane waves of frequency f $(= \omega/2\pi)$ are propagating in the direction of a uniform magnetic field parallel to the axis Oz of a Cartesian system, so that $\partial/\partial x = \partial/\partial y = 0$, $\partial/\partial z \neq 0$. Suppose also that each $\mathbf{v_i}$ $(v_{ix}, v_{iy}, 0)$ is proportional to $\exp(i\omega t)$. Ignoring the body force $\mathbf{F_i}$ (e.g. gravity), (1) for neutral particles takes the form (DUNGEY, 1958, p. 169)

$$i\omega \rho_n \mathbf{v_n} = N_n N_p \alpha_{np} (\mathbf{v_p} - \mathbf{v_n}) + N_n N_p \alpha_{ne} (\mathbf{v_e} - \mathbf{v_n}). \tag{5}$$

As $\alpha_{np}(10^{-32})$ is much larger than $\alpha_{ne}(10^{-35})$ and $\mathbf{v_p} \sim \mathbf{v}_e$ in the $F2$-region (MARTYN, 1953), (5) gives

$$\frac{\mathbf{v_p}}{\mathbf{v_n}} = 1 + i\omega \frac{m_n}{N_p \alpha_{np}}. \tag{6}$$

Under the conditions of (4), equation (1) for positive ions and electrons is

$$\frac{D_i \mathbf{v}_i}{Dt} = \mathbf{F}_i + \frac{e_i}{m_i} \mathbf{v}_i \times \mathbf{H} - \frac{\operatorname{grad} p_i}{\rho_i} + \nu_{in} (\mathbf{v}_n - \mathbf{v}_i). \tag{7a}$$

The dispersion equation, which results from (1) combined with Maxwell's equations, is given (DUNGEY, 1958, p. 170) by

$$K^2 = \frac{\omega^2}{(H^2/4\pi\rho_p)} \frac{[1 - (i\nu_{pn}/\omega)]}{[1 \mp (i\nu_{en}/\Omega_e)][1 \pm (i\nu_{pn}/\Omega_p)]}, \tag{7b}$$

where K denotes the wave number and Ω_e and Ω_p denote the gyro-angular frequency ($=eH/m_i$) of electrons and ions, respectively. The wave number K is *complex* and is expressed by

$$K = K_1 - iK_2. \tag{7c}$$

Therefore any varying field A is expressed by

$$A \exp\{i[\omega t - (K_1 - iK_2)z]\} = A \exp(-K_2) \exp[i(\omega t - K_1 z)]. \tag{7d}$$

INTERACTION BETWEEN IONS AND NEUTRAL ATOMS

A small harmonic motion of neutral atoms, as seen above, can certainly be generated by a harmonic motion of the ions. The result of the interaction between

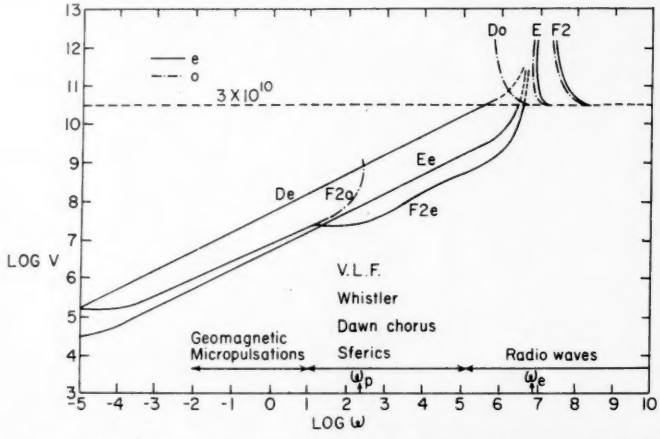

Fig. 1. Dispersion relation (the phase velocity V vs. angular frequency ω) of hydromagnetic waves in the $F2$-, E- and D-regions of the ionosphere. Subscripts o and e refer to ordinary and extraordinary waves, respectively; ω_p and ω_e denotes the gyro-frequencies of ions and electrons, respectively. For various constants used, see Table 1, AKASOFU (1956).

ions and neutral atoms is well shown by (6). A more general treatment gives the main features of the dispersion relation (the phase velocity vs. angular frequency). For the ionosphere this is illustrated in Fig. 1 (AKASOFU, 1956). The theory of propagation of hydromagnetic waves in the ionosphere is an extension of the magneto-ionic theory to the case when the ions can easily move in response to field changes (DUNGEY, 1958, p. 170). The phase velocity varies markedly with frequency, and it is convenient to consider three ranges of frequency.

The highest frequency range ($\omega > 10^5$/sec), corresponding to ordinary radio waves, shows the familiar magneto-ionic behaviour of electrons in the almost immobile positive and neutral background. The middle part of the diagram (ω ranging from 10 to 10^5/sec) is relevant to four distinct phenomena: (1) v.l.f. radio

waves, (2) whistlers, (3) dawn chorus and (4) atmospherics ('sferics). The contribution of the motion of the ions becomes increasingly important (HINES, 1957) in this range.

The part of lowest frequency ($\omega < 10$/sec) shows the dispersion curves for those hydromagnetic waves which are recognized as geomagnetic micropulsations and the other very low frequency phenomena. This range is characterized by the dominant contribution of ions and of neutral atoms. The contribution of neutral atoms can be seen from the "lowering" of the phase velocity. The physical interpretation of this lowering becomes clear from (6), and will be shown by using numerical values for the F-region. The velocity of hydromagnetic waves V is given by

$$V = \frac{H}{(4\pi\rho)^{1/2}}, \tag{8}$$

where ρ in the denominator is the *effective* density.

(a) For the higher frequency range around the gyro-angular frequency ($\Omega_p = eH/m_p$) 2×10^2/sec, (6) gives

$$\frac{\mathbf{v_p}}{\mathbf{v_n}} = 1 + i\frac{2 \times 10^2 \times 2{\cdot}7 \times 10^{-23}}{3 \times 10^5 \times 3{\cdot}3 \times 10^{-32}} \sim i5{\cdot}4 \times 10^5 \tag{9}$$

or

$$|\mathbf{v_n}| \ll |\mathbf{v_p}|.$$

This indicates that the motion of the neutral atoms does not affect the propagation of such hydromagnetic waves, and so in (8) ρ is almost exactly the density of the ionized part of gas, $\rho \sim \rho_p + \rho_e$.

(b) For frequency lower than $\omega = 10^{-5}$/sec, (6) gives

$$\frac{\mathbf{v_p}}{\mathbf{v_n}} = 1 + i2{\cdot}7 \times 10^{-2} \tag{10}$$

or

$$\mathbf{v_n} \simeq \mathbf{v_p}.$$

This indicates that the motion of the neutral atoms fully contributes to the propagation of the waves, and in (8) we must take $\rho = \rho_p + \rho_e + \rho_n$. Therefore for these lower frequencies the velocity of hydromagnetic waves decreases from $H/(4\pi\rho_p)^{1/2}$ and finally converges to $H/[4\pi(\rho_p + \rho_n)]^{1/2}$.

We are particularly interested in hydromagnetic waves connected with geomagnetic micropulsations in the angular frequency range from $\omega = 6{\cdot}38$/sec to $\omega = 0{\cdot}064$/sec (or f from 1 c/s to 0·01 c/s; period from 1 sec to 100 sec). It is clear that in this range the approximate relation

$$\frac{\mathbf{v_p}}{\mathbf{v_n}} \sim i\omega \frac{m_n}{N_p \alpha_{np}} \tag{11}$$

is sufficiently accurate in the *F2*-region.

JOULE HEAT LOSS

The propagation of hydromagnetic waves in a ternary mixture was first

studied by HINES (1953). From (7a) he derived the current and the force equations for harmonic motion of the particles of the partially ionized gas. His current and force equations are

$$\mathbf{J} = \sum_i \left[\frac{N_i e^2 \nu_{in}'}{m_i(\nu_{in}'^2 + \Omega_i^2)}\right] \mathbf{E} + \sum_i \left[\frac{N_i e^3}{m_i^2(\nu_{in}'^2 + \Omega_i^2)}\right] \mathbf{E}\times\mathbf{H} + \\ + \sum_i \left[\frac{N_i e \nu_{in}\nu_{in}'}{(\nu_{in}'^2 + \Omega_i^2)}\right] \mathbf{v_n} + \sum_i \left[\frac{N_i e^2 \nu_{in}}{m_i(\nu_{in}'^2 + \Omega_i^2)}\right] \mathbf{v_n}\times\mathbf{H}, \tag{12}$$

$$\mathbf{F} = \sum_i \left[\frac{N_i e \nu_{in}\nu_{in}'}{(\nu_{in}'^2 + \Omega_i^2)}\right] \mathbf{E} + \sum_i \left[\frac{N_i e^2 \nu_{in}}{m_i(\nu_{in}'^2 + \Omega_i^2)}\right] \mathbf{E}\times\mathbf{H} - \\ - \sum_i \left[N_i m_i \nu_{in} \frac{i\omega\nu_{in}' + \Omega_i^2}{(\nu_{in}'^2 + \Omega_i^2)}\right] \mathbf{v_n} + \sum_i \left[\frac{N_i e \nu_{in}^2}{(\nu_{in}'^2 + \Omega_i^2)}\right] \mathbf{v_n}\times\mathbf{H}, \tag{13}$$

where $\mathbf{F}$ is exactly the right-hand side of (5) and $\nu_{in}' = \nu_{in} + i\omega$.

We now consider the rate of production of heat energy when hydromagnetic waves pass through the ionosphere. Dr. HINES (1959) indicated to me his formulae for a special case, but a more general formulation is presented here. It is seen from Table 1 that important parameters of the ionosphere vary by many orders of magnitude. In order not to limit the application of the equations throughout the ionosphere, we need to develop all the equations in numerical form without any initial approximation.

Substituting (13) into (5) and taking the co-ordinate system such that $\mathbf{v_n}$ lies in the x-direction, we obtain the algebraic simultaneous equations for E_x and E_y. In general, the electric field $\mathbf{E}$ is not perpendicular to $\mathbf{v_n}$, so that there are two components, E_x and E_y. Solving the simultaneous equations, we have

$$E_x = (a\omega^2 + ib\omega)v_n, \tag{14}$$

$$E_y = (a'\omega^2 + ib'\omega)\, v_n, \tag{15}$$

where a, a', b and b' are pure numbers calculated from Table 1 for each level of the ionosphere.

Putting (14) and (15) into (12), we have similar equations for the current components J_x and J_y. The Joule heat dissipation per unit volume per unit time is defined as half the real part of the scalar product $[\mathbf{E}\cdot\tilde{\mathbf{J}}]$, where $\tilde{\mathbf{J}}$ is the complex conjugate of $\mathbf{J}$. This gives the result:

$$Q = \tfrac{1}{2}\mathscr{R}[\mathbf{E}\cdot\tilde{\mathbf{J}}] = \tfrac{1}{2}\mathscr{R}[E_x\cdot\tilde{J}_x + E_y\cdot\tilde{J}_y], \tag{16}$$

where $\mathscr{R}$ signifies real part of [ ].
Substituting from (12), (14) and (15) into the above equation (16,) Q becomes

$$Q = (\alpha\omega^4 + \beta\omega^2)\, v_n^2, \tag{17}$$

where α and β are pure numbers. In the frequency range f from 1 to 0·01 c/s, $a\omega \ll b$, $a'\omega \ll b'$ and $\alpha\omega^2 \ll \beta$, so that we neglect a, a' and α in the later developments.

VOL
18
196

The further relation we need for the determination of Q is one of Maxwell's equations,

$$\text{curl } \mathbf{E} = -\frac{\partial \mathbf{h}}{\partial t}, \tag{18}$$

where $\mathbf{h}$ is the varying part of the magnetic field intensity. Recalling that a varying field is expressed by $A \exp\{i[\omega t - (K_1 - iK_2)z]\}$, (18) gives

$$h^2 = \frac{(K_1^2 + K_2^2)}{\omega^2} E^2, \tag{19}$$

where K_1 and K_2 are already given in (7c), and

$$E^2 = (b^2 + b'^2)\omega^2 v_n^2. \tag{20}$$

From (19) and (20), we have

$$v_n^2 = \left[\frac{1}{(K_1^2 + K_2^2)(b^2 + b'^2)}\right] h^2. \tag{21}$$

Substituting from (21) into (17), we finally obtain

$$Q = \left[\frac{\beta\omega^2}{(K_1^2 + K_2^2)(b^2 + b'^2)}\right] h^2. \tag{22}$$

VOL. 18 1960

The Spectrum of Geomagnetic Micropulsations

In order to calculate from (22) the thermal energy Q produced in the ionosphere, we must know the intensity spectrum (intensity vs. angular frequency), and must have some information about the frequency of occurrence of micropulsations at each level of the ionosphere.

The spectrum of the geomagnetic micropulsations has been obtained by Campbell (1959) at California. His spectrum is reproduced here (Fig. 2). His figure relates to the average amplitude for the daylight hours in a middle latitude during a moderately magnetically disturbed day. We assume that in the auroral zone the intensity will be increased by a factor of 10^2 during geomagnetic storms for the lower frequency end of the spectrum. Fig. 2 shows two distinct maxima; there is a transition from audio and sub-audio waves to geomagnetic micropulsations at frequencies between $0{\cdot}2 \sim 2{\cdot}0$ c/s. The intensity of geomagnetic micropulsations has a maximum at about $f = 0{\cdot}05$ c/s.

Hydromagnetic waves may be generated far above the F-layer. Then a question arises as to whether there is some difference between the spectrum observed at the surface of the earth and that in or above the ionosphere. The dispersion equation involves the *complex* wave number K. Dungey (1958, p. 171; Table 4) gave K^2 for various heights for waves $\omega = 0{\cdot}1$/sec. Similar calculations have been made for K^2 and K, (K_1, K_2), for frequencies $f = 1$, $0{\cdot}1$ and $0{\cdot}01$ c/s (See 7b, c). Then the transmission coefficient T at each level of the ionosphere is evaluated,

$$T = \exp(-dK_2), \tag{23}$$

where d is the thickness of each layer and is taken to be 10 km for a height of 80 or 90 km and 25 km for 100 km and above. The results are shown in Fig. 3.

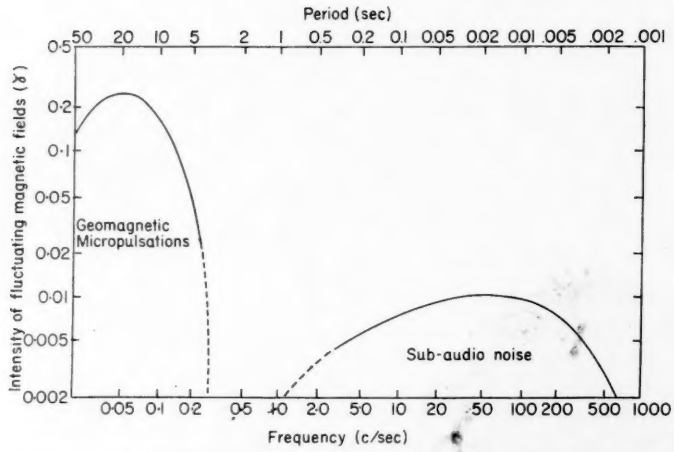
Period (sec)
50 20 10 5 2 1 0.5 0.2 0.1 0.05 0.02 0.01 .005 .002 .001
Intensity of fluctuating magnetic fields (γ)
0·5 0·2 0·1 0·05 0·02 0·01 0·005 0·002
Geomagnetic Micropulsations
Sub-audio noise
0·05 0·1 0·2 0·5 1·0 2·0 5·0 10 20 50 100 200 500 1000
Frequency (c/sec)

Fig. 2. The natural low frequency electromagnetic spectrum in California obtained by CAMPBELL (1959). This figure relates to the average amplitude of the disturbing magnetic field during the daylight hours in middle latitudes during a moderately magnetically disturbed day.

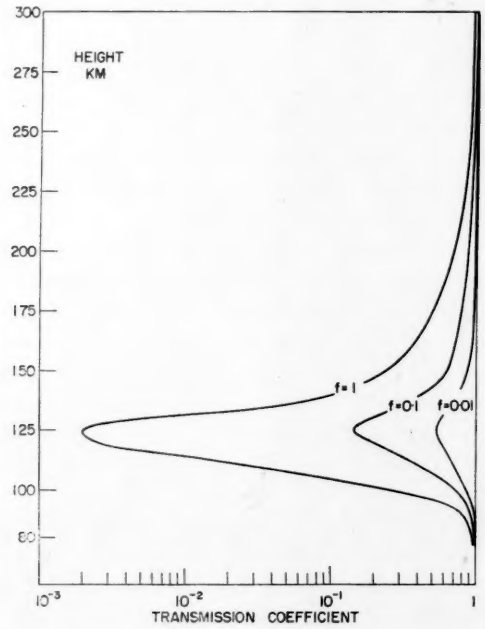

Fig. 3. Transmission coefficient of the ionosphere for frequencies $f = 1$, 0·1 and 0·01 c/s.

Here, $1/K_2$ gives the damping length, in which the amplitude is decreased by the factor $1/e$. Table 2 gives the results of a rough numerical evaluation of the ratio $\exp(-\nu)$ of the wave amplitude at the bottom of the ionosphere to that at the top: here

$$\nu = \int_{h_1}^{h_2} hK_2 \, dh \tag{24}$$

and h_1, h_2 are taken to be 80 km and 300 km.

Table 2. The ratio of the amplitude of hydromagnetic waves at the bottom of the ionosphere to that at the top of the ionosphere for several frequencies

f (c/s)	0·01	0·1	1
ω (/sec)	0·0628	0·628	6·28
Period (sec)	100	10	1
Ratio	0·323	$2{\cdot}83\times10^{-2}$	$8{\cdot}22\times10^{-6}$

From Fig. 3 and Table 2, we can see that for frequencies less than 10^{-2} c/s the ionosphere is nearly transparent. But the E-layer is extremely opaque for higher frequencies around $f = 1$ c/s.

Table 3 shows the intensity $h(\gamma)$ at the ground (taken from CAMPBELL's diagram) and at 300 km calculated from the ratio discussed above. For $f = 1$ c/s,

Table 3. The tentative intensity spectrum of micropulsations at different levels.

Frequency (c/s)	Period (sec)	Amplitude (γ) Ground level (middle lat.)	Amplitude (γ) 300 km (middle lat.)	Amplitude (γ) 300 km (auroral zone)
			(Inferred)	(Adopted)
1	1	$5{\cdot}0\times10^{-3}$*	$6{\cdot}1\times10^{2}$†	1
0·1	10	0·2	7·1	10
0·01	100	0·1	0·31	31·6

* PHILLIPS (1960). † See the following paragraph.

PHILLIPS (1960) reports that in Alaska the maximum amplitude (at ground level) is about $0{\cdot}02\,\gamma$. Using the ratio calculated above, we obtain $h = 2\times10^{-2}\,\gamma/8{\cdot}22\times10^{-6} = 2{\cdot}43\times10^{3}\,\gamma$ as the intensity at 300 km. This would imply an enormous and improbable oscillation of the magnetic field at 7000 km above the ground. It seems more likely that such a sub-audio noise received at the ground is generated in the lower part of the E-layer (below the barrier at about 125 km in height; see Fig. 3).

We are particularly interested in the waves generated above the $F2$-region, for example, by the interaction between the outer atmosphere and the solar

stream. The waves associated with sudden commencements of geomagnetic storms are believed to be of this kind (DESSLER, 1958). Their frequency is about $f = 0{\cdot}01$ c/s or less. A typical amplitude is from 25 to 50 γ. Some inhomogeneity in the stream may produce additional wave motions in the outer atmosphere, but probably with amplitude and frequency not so much different from the above values. Actually, it seems more likely that their amplitude will be less than the above value.*

DESSLER (1959) assumed that during magnetic storms the high frequency end of the wave spectrum will probably be important because of the formation of hydromagnetic shocks. He considered an amplitude of 30 γ for waves of 1 c/s on quiet days, and that this may be increased by a factor of at least 10 on disturbed days. But the amplitude of 30 γ for 1 c/s cannot be attained even on disturbed days. Table 3 gives a tentative model spectrum of the *average* amplitude of geomagnetic micropulsations at the top of the ionosphere in the auroral zone during magnetic storms.

Furthermore, in the magnetograms from the polar regions, one can often see two or three different superposed waves, which combine to give a rather regular sinusoidal variation rather than an irregular change, except on very disturbed days. At present, the only way to check the assumption made in Table 3 is to examine the ionospheric data at times of intense geomagnetic activity. This is done in the last section of this paper.

INCREASE OF TEMPERATURE

The rate of production of thermal energy per unit volume per second is calculated from (22) for $h = 1\ \gamma$ at 300 km for frequencies $f = 1$, $0{\cdot}1$ and $0{\cdot}01$ c/s, taking into account the decrease of amplitude along the path, for vertical incidence. The results are shown in Fig. 4. For later use, some typical values of Q_0 in the *F2*-region and Q at 90 km are also given in Table 4. It is interesting to note that the rate of conversion of electromagnetic energy into heat attains its maximum at about 190–220 km, for the frequencies considered here. Below 170 km the rate of conversion decreases very steeply.

The only further relation we need to determine the change of temperature, which is our main concern, is the equation of thermal conduction. In the steady state the increase of the temperature ΔT at height z satisfies the equation

$$\lambda \frac{d^2 \Delta T}{dz^2} = -Q(z), \tag{25}$$

* CHAPMAN and FERRARO (1931) showed in their theory of sudden commencements of magnetic storms how solar corpuscular streams produce a sudden change of the magnetic field when streams are stopped at several earth's radii. It is now believed that this sudden change is transmitted towards the earth by hydromagnetic propagation into the outer atmosphere, without any change in their basic idea. They also showed how rapidly this happens. The rise time is shown to be about 100 sec which agrees with the observations. A discontinuous change, such as sudden commencements, may be expressed by the Fourier series shown below.

$$f(t) = \frac{4}{\pi}\left(\frac{\sin t}{1} + \frac{\sin 3t}{3} + \frac{\sin 5t}{5} + \ldots\right).$$

This would imply that the amplitude of 1 c/s wave is of order $50\gamma/100 = 0{\cdot}5\gamma$, assuming the amplitude of the first term of order 50γ and the period of 100 sec.

where λ denotes the thermal conductivity of the air and $Q(z)$ the rate of heat production per unit volume per second, as above calculated.

Because of the complexity of $Q(z)$, it is very difficult to infer the exact temperature distribution in the ionosphere. From Fig. 4 it seems reasonable to infer that

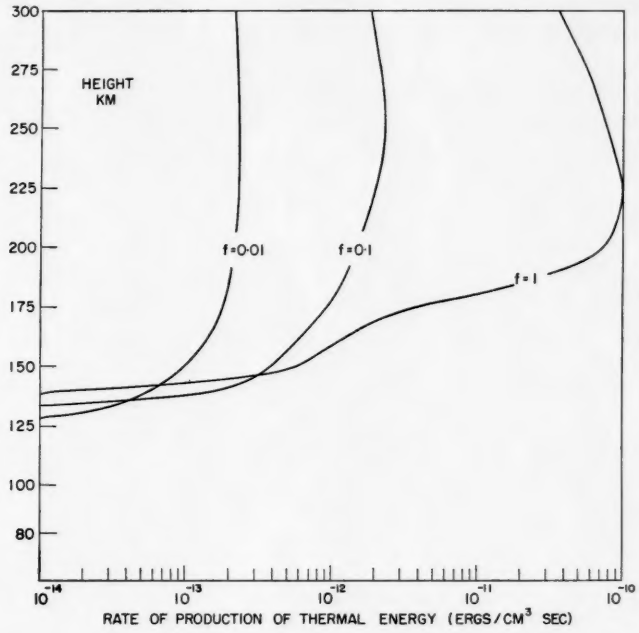

Fig. 4. Thermal energy production rate in the ionosphere (ergs/cm³ sec), for frequencies $f = 1$, 0·1 and 0·01 c/s, for waves of amplitude $h = 1\ \gamma$ at 300 km (vertical incidence).

Table 4. The adopted amplitude at 300 km above the auroral zone, Q_0 and ΔT in the *F2*-region and Q at 90 km

Frequency (c/s)	Period (sec)	**h** (γ)	Q_0 (ergs/cm³ sec)	ΔT (°K)	Q (ergs/cm³ sec)
			F2-Region		90 km
1	1	1	10^{-10}	0·21 (220 km)	$2{\cdot}08 \times 10^{-22}$
0·1	10	10	$1{\cdot}48 \times 10^{-10}$	0·83 (200 km)	$1{\cdot}81 \times 10^{-14}$
0·01	100	31·6	$2{\cdot}30 \times 10^{-10}$	1·18 (190 km)	$2{\cdot}10 \times 10^{-13}$

below the level of maximum heat production, Q decreases rapidly downwards. Let it be taken to be approximately $Q_0 \exp(-az)$, measuring z positive downward; a can be calculated from Table 4.

Hence assuming $d\,\Delta T/dz = 0$ at $z = 0$, where the maximum production occurs, the integral of (25) has the form

$$\frac{d\,\Delta T}{dz} = \frac{Q_0}{\lambda a}[\exp(-az) - 1]. \tag{26}$$

Further integration gives

$$\Delta T(z) - \Delta T(0) = \frac{Q_0}{\lambda a}\left\{\frac{1}{a}[1 - \exp(-az)] - z\right\}, \tag{27}$$

where $\Delta T(z)$ and $\Delta T(0)$ denote the increase of temperature at z and $x = 0$, respectively. I use the thermal conductivity λ given by BATES (1951, p. 815), namely $2{\cdot}4 \times 10^3$ for $T = 500°\text{K}$.

For the frequency $f = 0{\cdot}01$ c/s at 190 km, we may take $Q_0 = 2{\cdot}3 \times 10^{-13} h^2$ ergs/cm^3 sec (if h is expressed in γ). Taking $h = 31{\cdot}6\ \gamma$, $Q_0 = 2{\cdot}3 \times 10^{-10}$ ergs/cm^3 sec at 190 km; as $Q = 2{\cdot}10 \times 10^{-13}$ ergs/cm^3 sec at 90 km (see Table 4), a is found to be 7×10^{-7}/cm.

Therefore (27) becomes

$$\Delta T(z) - \Delta T(0) = 1{\cdot}37 \times 10^7\left\{\frac{1}{7 \times 10^{-7}}[1 - \exp(-7 \times 10^{-7}z)] - z\right\}. \tag{28}$$

The heating effect at 90 km is much less than at 190 km, so that, taking $z = 100$ km $= 10^7$ cm,

$$\Delta T(0) \simeq 1{\cdot}18°\text{C}. \tag{29}$$

A similar calculation for $f = 0{\cdot}1$ and 1 c/s gives $\Delta T(0) \simeq 0{\cdot}83°$C at 200 km and $\Delta T(0) \simeq 0{\cdot}21°$C at 220 km, respectively.

In general, two or three particular frequencies superposed on higher frequency components are seen on the magnetograms in the auroral zone. Therefore, smoothing out the high-frequency waves, of which the heating effect is negligible (see Table 4), we can find these particular waves. However, as the contribution of each wave is at most 1·2°C, according to the above Table 4, the total contribution could not exceed 5°C.

IONOSPHERIC DISTURBANCE ON 11 FEBRUARY 1958

The magnetic storm on 11 February 1958 was accompanied by fluctuations of the magnetic field of a violence exceeding anything observed in the last decade. Therefore it is of great interest to examine whether there was any appreciable heating of the upper atmosphere by hydromagnetic waves, as proposed by DESSLER (1959). The magnetograms from College (gm. lat. 64°.7 N; insensitive recorder) and from Guam (gm. lat, 3°.9 N; sensitive recorder) are shown in Fig. 5 (a,b). Fig. 5(c) shows the ionospheric data (the electron density of the *F2*-layer) from Adak, Alaska (gm. lat. 47°.3 N).

Intense and rapid magnetic fluctuations, of order 100 γ, had begun simultaneously with the sudden commencement at 0126 GMT on 11 February 1958. They were active at least until 0600 GMT. The very abrupt ionospheric storm began at 0215 GMT at Adak, and f_0F2 reached its miminum at 0330. The ionospheric storm quickly subsided at about 0515, while intense fluctuations of the magnetic field were still continuing. Fig. 6 shows the daily variation of the electron density of the *F2*-layer at Adak on the same day. Except for the above mentioned remarkable "bite" out of the normal curve, the ionosphere was rather normal. The same phenomenon was observed at several other places, including Delhi,

VOL
18
196

Singapore, Okinawa, Yamagawa, Kokubunji, Akita, Wakkanai, Maui (Hawaii) and Stanford.

The first difficulty in trying to explain such a phenomenon by hydromagnetic heating is its abrupt beginning. Furthermore, it is altogether impossible to expect such a quick recovery if the upper atmosphere expanded upward *as a whole* and

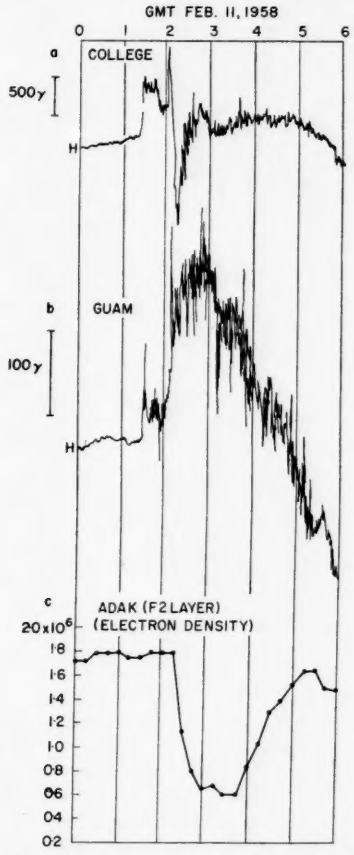

Fig. 5a. Magnetogram (Insensitive recorder), College, Alaska (gm. lat. 64°.7 N), 0000–0600 GMT, 11 February 1958.
b. Magnetogram (Sensitive recorder), Guam (gm. lat. 3°.9 N), 0000–0600 GMT, 11 February 1958.
c. Change of electron density of the *F2*-layer, Adak, Alaska (gm. lat. 47°.3 N), 0000–0600 GMT, 11 February 1958.

heating was still effective (as indicated by the magnetic fluctuations). Such a change of the density distribution by expansion of the upper atmosphere would produce quite a different ion production rate and electron density distribution, although the *F2*-layer may not be an independent ionized layer.

It is interesting to note that at about the commencement of the ionospheric storm, the College magnetogram showed a large polar magnetic disturbance, of order 1000 γ or more (See Fig. 5a). It will be shown elsewhere (AKASOFU, 1960)

VOL. 18 1960

that such a negative polar disturbance is produced by a southward electric field of order 4×10^4 e.m.u. (40 V/km). Such an electric field will produce a vertical upward drift motion of ions and electrons of order 15 m/sec at 210 km at Adak. It may be that only the ions and electrons moved upwards by electric drift, while the neutral background air was little affected; then a new *F2*-layer was formed by solar ultraviolet radiation, after the strong drift ceased.

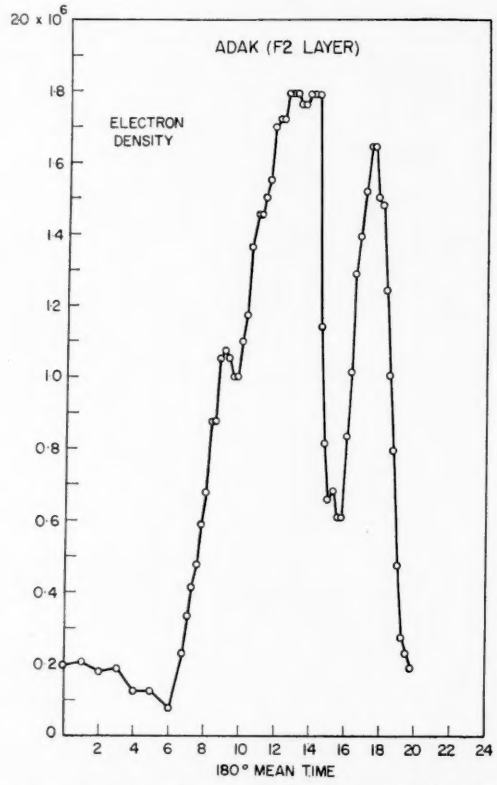

Fig. 6. Daily variation of electron density of the *F2*-layer, Adak, Alaska (gm. lat. 47°.3 N), on 10 February 1958 (180° Mean Time).

CONCLUSION

DESSLER (1959), in a recent paper, discussed ionospheric heating by hydromagnetic waves. He concluded that the increase of $h'F2$ at the time of ionospheric disturbances in the auroral zone may be explained by hydromagnetic heating. It is shown in this paper that the increase of temperature is at most 5°C in the *F2*-region. It seems unlikely that such a small increase of temperature can produce violent upward movement of the upper atmosphere.

Acknowledgements—The writer wishes to express his thanks to Prof. S. CHAPMAN, Dr. C. O. HINES, Dr. A. J. DESSLER and Dr. W. H. CAMPBELL for stimulating discussions during the composition of this paper.

VOL
18
196

References

Akasofu S.	1956	*Rep. Ionosphere Res. Japan*, **10**, 227.
Akasofu S.	1960	In preparation.
Bates D. R.	1951	*Proc. Phys. Soc. Lond.* B **64**, 805.
Campbell W. H.	1959	*J. Geophys. Res.* **64**, 1819; Scientific Report No. 1, NONR 233(47). Institute of Geophysics, University of California.
Chapman S.	1956	*Nuovo Cim.* **4**, 1385.
Chapman S. and Cowling T. G.	1953	*Mathematical Theory of Non-uniform Gases.* Cambridge University Press.
Chapman S. and Ferraro V. C. A.	1931	*Terr. Mag. Atmos. Elect.* **36**, 171.
Cowling T. G.	1956	*Mon. Not. R. Astr. Soc.* **116**, 114.
Dessler A. J.	1958	*J. Geophys. Res.* **63**, 405.
Dessler A. J.	1959	*J. Geophys. Res.* **64**, 397.
Dungey J. W.	1958	*Cosmic Electrodynamics.* Cambridge University Press.
Hines C. O.	1953	*Proc. Camb. Phil. Soc.* **49**, 299.
Hines C. O.	1957	*J. Atmosph. Terr. Phys.* **11**, 36.
Hines C. O.	1959	Private communications.
Martyn D. F.	1953	*Phil. Trans.* A **246**, 306.
Phillips C. A.	1960	Private communication.
Piddington J. H.	1956	*Mon. Not. R. Astr. Soc.* **116**, 314.

VOL. 18 1960

Journal of Atmospheric and Terrestrial Physics, 1960, Vol. 18, pp. 174 to 180. Pergamon Press Ltd. Printed in Northern Ireland

The scattering of 36 Mc/s radio waves by weak auroral ionization

J. S. Greenhow, E. L. Neufeld and C. D. Watkins
Jodrell Bank Experimental Station, University of Manchester

(*Received* 12 *January* 1960)

Abstract—Some observations of weak back-scatter echoes similar in type to the echoes associated with visual aurorae are described. With an equipment of high sensitivity at a frequency of 36 Mc/s, these echoes are present to the north of Jodrell Bank, (lat 53°N, geographic; lat 56°N, geomagnetic), for up to 30 per cent of the observing time. The irregularities in ionization, which are aligned along the earth's magnetic field, have a length scale of 160 m and a scattering polar diagram with a width of approximately $\pm 3°$. The horizontal dimensions of the ionized regions are about 500 km along parallels of geomagnetic latitude, and 50 km at right angles to this direction. Echoes from horizontal layers of ionization, associated with the field aligned irregularities, are also observed.

1. Introduction

Radio echoes from the ionization associated with auroral activity have been observed over the frequency range from a few megacycles per second up to several hundred megacycles per second. Many different types of echoes have been observed (Collins and Forsyth, 1959), one of the most important being direct back-scatter reflections from ionization aligned along the earth's magnetic field. The scattering polar diagram of these irregularities is of particular interest as it determines the angles ψ between the direction of propagation of the radio wave and the normal to the earth's field lines, at which echoes can be observed (Aspinall and Hawkins, 1950; Chapman, 1953; Booker *et al.*, 1955).

At quite low geomagnetic latitudes echoes similar to those associated with visual aurora are of frequent occurrence at frequencies of from 6 to 17 Mc/s, with equipments of moderate sensitivity (Leadabrand, 1955). This paper describes some high-sensitivity observations at a geomagnetic latitude of 56°, where auroral-type echoes appear to be of almost daily occurrence at a frequency of 36 Mc/s. An attempt is made to determine the degree of specularity of the radio reflections with respect to the earth's magnetic field lines.

2. Technique

During the periods 21 March to 14 April, and 17 October to 30 October 1958, while the 250 ft radio telescope at Jodrell Bank was in use for radar observations of the Russian earth satellites, the intervals between transits were used to observe ionospheric back-scatter echoes. These observations were made at a frequency of 36 Mc/s with a pulse repetition frequency of from 18 to 150 per sec, and pulse length from 20 to 300 μsec. The peak transmitter power was 100 kW, but there was a large feeder loss of 10 dB on transmission. The half-power beamwidth of the aerial was $\pm 3\frac{1}{2}°$ in elevation and $\pm 5°$ in azimuth. This is very narrow compared with the usual beamwidths employed at low frequencies, and as the aerial was fully steerable these directional properties enabled a study to be made of the nature of the reflecting regions. The equipment sensitivity was such that an object with a back-scattering area of 0·3 m², could be detected at a range of 300 km. The echoes

were recorded in one of two ways. The first method used a continuously moving film, with an intensity modulated range–time display, while the second method was to photograph a range–amplitude display at $\frac{1}{2}$ min intervals. The range time base was of variable length from 300 to 3000 km. During the periods of observation the telescope was used to perform azimuth scans at fixed elevations between 10° and 20°, or elevation scans between 0° and 30°, at fixed azimuths.

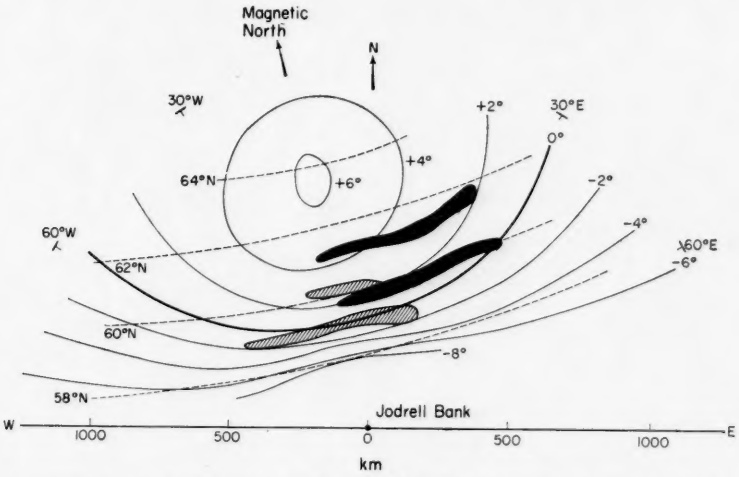

Fig. 1. Locus of points of constant ψ for a height of 115 km, as a function of range and azimuth from Jodrell Bank. Parallels of geomagnetic latitude are shown. The shaded and hatched areas are two examples of the extent of the regions from which echoes are obtained.

3. Results

3.1. *Echoes from field-aligned irregularities*

3.1.1. *Locus of points of constant ψ.* From a knowledge of the earth's local field it is possible to determine the angle ψ between the normal to the field, and the line of sight, for any particular azimuth, elevation or range. Maps can be constructed for different levels in the upper atmosphere, for a given observing station, showing the variation of ψ with range and azimuth. The height of a reflecting region can be determined to within ± 10 km by scanning in elevation, and the mean height for these 36 Mc/s echoes, is found to be 115 km. The actual spread in height is less than the error of a single measurement. The curves of constant ψ for Jodrell Bank for a height of 115 km are shown in Fig. 1, down to the horizon at a range of 1200 km. It can be seen that the $\psi = 0°$ locus is readily observable, and that appreciable areas of the northern sky are enclosed by the curves for angles up to a few degrees. These curves will now be used to investigate the distribution of echoing regions with respect to the earth's magnetic field.

3.1.2. *The distribution of echoing centres as a function of ψ.* From the range and azimuth of any particular auroral echo, the position of the reflecting region in Fig. 1 can be determined. This gives the angle by which the reflection is non-specular with respect to the field lines. The distribution of these angles for all echoes should

VOL. 18 1960

clearly be related to the scattering polar diagram of the irregularities, the most probable angle being 0°. The observed distribution of individual echoes as a function of ψ is given in Fig. 2(a). The scanning speed of the telescope was such that it moved through a complete beamwidth in $\frac{1}{2}$ min, and measurements were therefore made at these intervals. It can be seen that the largest number of echoes are observed near the specular locus, the number falling rapidly for values of ψ of a few degrees. It is, however, necessary to correct this observed distribution for variations in range R, aerial gain G, the different areas of sky enclosed by the

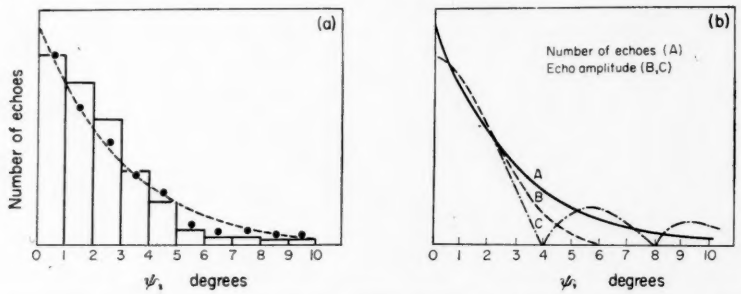

Fig. 2(a). The distribution of weak auroral-type echoes as a function of the angle between the line of sight and the normal to the earth's field lines (ψ). Histogram, observed distribution; – – · – – corrected distribution.

Fig. 2(b). Comparison of the distribution of Fig. 2(a) (curve A) with the scattering polar diagrams of irregularities with a gaussian correlation function of correlation length $2\pi L =$ 160 m (curve B), and a rectangular aperture of length $a = 60$ m (curve C). — observed (corrected) distribution (exp $-(\psi/\psi_0)$ where $\psi_0 = 3°$); – – – – exp $-(\psi/\psi_0)^2$, where $\psi_0 = 3°$; — · — · sin $\bar{n}$ $(\psi/\psi_0)/\bar{n}(\psi/\psi_0)$, where $\psi_0 = 4°$.

various loci in Fig. 1, the different times T spent by the aerial beam in each of these regions and the variation in frequency of occurrence with latitude ($p(\phi)$). This has been done by weighting each small area of sky in Fig. 1 by a factor $R^2/GTp(\phi)$, and summing the weighted areas between each curve of constant ψ. This expression assumes that echo amplitude is proportional to G/R^2, and as the sensitivity of the equipment varies over the observing region, it is necessary to assume some form of distribution for the variation of the number n_A of auroral echoes with amplitude A. Provided the range of sensitivities is kept low the exact form of the assumed distribution is not very critical. A power-law distribution of the form $n_A\,dA \propto A^{-2}\,dA$ has been used, and the variation of G/R^2 limited to a factor of 8. The frequency of occurrence of visual aurorae varies rapidly with latitude. To minimize this effect observations have been limited to a 4° band in latitude. Even so the results of Vestine (1944), show that over this small region the frequency of occurrence varies by a factor of 2 or 3 to 1. A linear variation in $p(\phi)$ with latitude, by a factor of 2·5 over the observing region, has therefore been assumed for the radio-echo data.

The corrected distribution of echoes as a function of ψ is shown in Fig. 2(b). The points fit quite closely to an exponential curve of the form exp $-(\psi/\psi_0)$ where $\psi_0 = 3°$, and this is shown for comparison. There is a 60 per cent probability that echoes will be obtained within 3° of the specular locus, although there is still a significant probability of observing echoes up to 10° off specular.

3.1.3. *The scattering polar diagram and length of the ionized irregularities.* Booker (1956) has considered the case of scattering from inhomogeneities in electron density, elongated along the earth's magnetic field, for the case when the observing frequency is greater than the plasma frequency. Assuming a gaussian correlation curve for the variation of electron density, with correlation distances of T and L perpendicular and parallel to the earth's field, he shows that the back scattering coefficient σ is given by

$$\sigma \propto T^2 L \exp\left(-\frac{8\pi^2 T^2}{\lambda^2}\right) \exp\left(-\frac{8\pi^2 L^2 \psi^2}{\lambda^2}\right) \tag{1}$$

λ is the radio wavelength. The variation of echo amplitude with ψ is therefore given by

$$A \propto \exp\left(-\frac{4\pi^2 L^2 \psi^2}{\lambda^2}\right) \propto \exp -\left(\frac{\psi}{\psi_0}\right)^2. \tag{2}$$

The amplitude falls to $1/e$ in a length scale $2\pi L = \lambda/\psi_0$. This scattering polar diagram is shown for comparison with the observed probability distribution in Fig. 2(b) for $\psi_0 = 3°$. Although the scattering polar diagram of the irregularities need not be identical with the probability distribution, the two curves should be of similar shape for any reasonable amplitude distribution. There appears to be an appreciably higher probability of obtaining an echo from large non-specular angles than would be expected from the gaussian form of equation (2), although the most probable length scale of the irregularities is of the order of that corresponding to $\psi_0 = 3°$. For $\lambda = 8{\cdot}3$ m this gives $2\pi L = 160$ m. The long tail of the observed distribution in Fig. 2 could be due to the presence of a small percentage of irregularities with length scales less than the most probable value of 160 m. If 10 per cent of the irregularities were shorter than approximately 50 m, for example, these would adequately account for the observations. A second possibility is that the irregularities are much more sharply defined than given by equation (2). The diffraction pattern for a uniform rectangular aperture of length 60 m is also shown in Fig. 2(b). Smoothing of the pattern would result for quite a small range in sizes, and the secondary maxima which extend a considerable way beyond the first minimum would easily account for the observed distribution. Such a well-defined ionized column is unlikely to exist, however, unless the ionization exceeds the critical electron density. The question as to whether radar echoes from aurorae arise from underdense or overdense ionization is as yet unresolved.

3.1.4. *The horizontal extent and time variation of the ionized regions.* At a given time echoes from a given patch of ionization, presumably composed of a large number of field-aligned irregularities, may be traced over a fairly wide range of azimuths. The spread in elevation at a given azimuth, on the other hand, is usually smaller than a beamwidth. Because of the good range discrimination, and the directional properties of the aerial, it has been possible to plot the shape of the reflecting regions in the horizontal plane. Two examples are shown in Fig. 1. It can be seen that echoes are received from arcs up to approximately 500 km in length and 50 km in width. The arcs lie very nearly along parallels of geomagnetic latitude. Frequently two or more arcs are present simultaneously, separated by

VOL. 18 1960

about 100 km, in the north–south direction. It is possible of course that arcs may be even longer than 500 km, and that echoes have disappeared near the ends because of the increasing values of ψ. This is unlikely, as arcs are observed which lie entirely within the $\pm 2^\circ$ loci (Fig. 1), whereas from the echo amplitudes and the observed probability distribution it is known that echoes would be observed at greater values of ψ if the irregularities were present. The duration of an individual arc is of the order of half an hour.

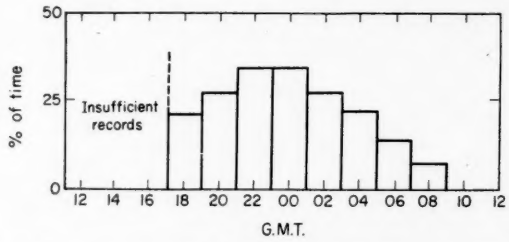

Fig. 3. Diurnal variation in the frequency of occurrence of the weak auroral back-scatter echoes.

The diurnal variation in frequency of occurrence of the echoes is shown in Fig. 3, where the fraction of the total observing time during which echoes were observed is given. In this analysis "observing time" refers only to those periods during which the aerial beam was directed so as to satisfy the condition of near specularity with respect to the earth's field. Intervals when ψ was greater than 3° are not included. Echoes were observed for about 30 per cent of the possible time near 2300 hours, falling to practically 0 per cent after 0900 hours. Insufficient observations were made before 1900 hours to determine fully the corresponding fall off in the evening.

3.2. *Layer-type reflections*

Frequently echoes from the field-aligned irregularities are accompanied by a second series of echoes at almost exactly twice the range. These echoes can be interpreted as back scatter from the ground by double reflection from an ionized layer, closely associated with the field-aligned ionization. Back-scatter echoes of this type have been observed at 6 Mc/s (Leadabrand, 1955), and such an ionized layer probably accounts for some of the forward-scatter echoes observed by other workers (Collins and Forsyth, 1959).

In order to occur at double the range of the specular echoes the ionized layer must not only be at about the same height (to within ± 20 km), but also occur in the same region of sky as the field-aligned irregularities. During vertical scans the range of the ground-scatter echoes does not vary appreciably, showing the horizontal extent of the ionized layers is not great. Considerations of beamwidth and range spread show that the horizontal dimensions of the patches of ionization are only of the order of 50 km. The electron densities involved probably exceed the critical electron density at the equivalent vertical frequency (10 to 15 Mc/s), as reflection at the layer takes place twice and a high-reflection coefficient is required to give a detectable echo.

Ground-return echoes of this type occur at some time on about 10 per cent of the occasions when the direct back-scatter echoes are observed. Long-range echoes which could be of this type are also observed in the absence of specular echoes, when the aerial beam is pointing in directions making appreciable angles with the normal to the earth's field.

3.3. *Magnetic and visual auroral activity during the occurrence of echoes*

The magnetic K-indices recorded at Eskdalemuir, Scotland, have been examined for the period of the observations. This magnetic observatory is located close to the region of the echoes. During the occurrence of echoes K had all values from 1 to 6. It is of particular interest that some echoes were obtained even during magnetically-quiet conditions when K had values of only 1 or 2. Furthermore these echoes displayed the same aspect-sensitive properties as those detected during the moderately-disturbed conditions of $K = 6$.

Visual aurorae were usually reported by observers in the north of the British Isles on the occasions when strong echoes were detected. In general however the visual forms (mainly rays and rayed arcs) were more than 6° of latitude north of Jodrell Bank and thus also north of the location of the echoes. As a rule, during weak echoes no visual forms were situated over the British Isles and any activity was restricted to nearer the auroral zone.

Thus it seems that high-sensitivity radio-echo techniques, using comparatively low frequencies, are capable of detecting weak ionization which is below the threshold of observation as a visual auroral display or as a magnetic disturbance. Such techniques should prove useful for studying the ionosphere during the sunspot minimum.

4. Discussion

A length scale of 160 m has been deduced for the field-aligned irregularities giving rise to weak auroral type radio echoes at a frequency of 36 Mc/s, corresponding to off specular scattering angles of 3°. Observations at Jodrell Bank during intense aurorae show that at 72 Mc/s the reflections are specular to within about 1° (Watkins, 1960). This approximate wavelength proportionality suggests that the irregularities at E-region heights are of the same length during weak or intense activity. The length scale is considerably greater than the figure of 20 m deduced from observations at frequencies of from 216 to 780 Mc/s at College, Alaska, (Presnell *et al.*, 1959), where echoes are observed up to 12° off specular. A 3° scattering polar diagram at 36 Mc/s corresponds to an angle of only 0·15° at 700 Mc/s. However, at College it is not possible to observe any region of sky, at E-region heights, where the line of sight is at right angles to the earth's field. The smallest value of ψ is 1·6°, and echoes from irregularities with a scattering angle of 0·15° would not be observed. It is possible that these high-latitude observations refer only to the long tail of the distribution in Fig. 2 which shows that there is a finite probability of obtaining echoes at quite large values of ψ. In a region of 100 per cent occurrence of strong aurorae, it is not surprising that some echoes are fairly often observed at large non-specular angles, even at very high frequencies. In order to determine the scattering polar diagram at any particular frequency, it is

therefore important to record at a site where the $\psi = 0°$ locus is readily observable, and where there is not a 100 per cent occurrence of aurorae.

A length scale of the order of 40 m at 100 Mc/s has been determined from observations at Cornell (Booker, 1956), and echoes have been observed more than 5° non-specular at a frequency of 55 Mc/s in New Zealand (Unwin, 1958). These observations were made with rather wide-beam aerials, and have not been weighted to allow for the varying probability of detecting an echo at all values of ψ. They indicate length scales approximately one-quarter of the value deduced from the 36 Mc/s observations at Jodrell Bank, and would also be incompatible with the 72 Mc/s observations at this site.

Acknowledgements—The work described in this paper has been carried out at the Jodrell Bank Experimental Station, University of Manchester. The writers wish to thank Professor A. C. B. Lovell, the director of the Station, for his interest in the investigation.

References

Aspinall A. and Hawkins G. S.	1950	*J. Brit. Ast. Assoc.* **60,** 130.
Booker H. G.	1956	*J. Atmosph. Terr. Phys.* **8,** 204.
Booker H. G., Gartlein C. W. and Nichols B.	1955	*J. Geophys. Res.* **60,** 1.
Chapman S.	1953	*J. Atmosph. Terr. Phys.* **3,** 1.
Collins C. and Forsyth P. A.	1959	*J. Atmosph. Terr. Phys.* **13,** 315.
Leadabrand R. L.	1955	Radio Propagation Laboratory, Stanford University. Technical Report No. 98.
Presnell R. I., Leadabrand R. L., Peterson A. M., Dyce R. B., Schlobohm J. C. and Berg M. R.	1959	*J. Geophys. Res.* **64,** 1179.
Unwin R. S.	1958	*J. Geophys. Res.* **63,** 501.
Vestine E. H.	1944	*Terr. Magn. Atmosph. Elect.* **49,** 77.
Watkins C. D.	1960	*J. Atmosph. Terr. Phys.* In press.

Journal of Atmospheric and Terrestrial Physics, 1960, Vol. 18, pp. 181 to 183. Pergamon Press Ltd. Printed in Northern Ireland

The geographical distribution of ionization in the *F2*-layer

C. M. Minnis and G. H. Bazzard
DSIR Radio Research Station, Slough*

(*Received* 10 *April* 1959)

Abstract—For any location the monthly mean *F2*-layer critical frequency, *fF2*, can be expressed as a family of linear functions of an ionospheric index of solar activity. The intercepts of these functions have been determined for sixty-five locations at noon and form a reliable tool for investigating the geographical distribution of *fF2* at minimum solar activity. It has been found that the equatorial trough in *fF2* cannot be conclusively proved to exist in the western hemisphere at certain times of the year.

1. Introduction

The existence of the "equatorial trough" in the ionization at the peak of the *F2*-layer at noon was reported by Appleton (1946) and by Maeda *et al.* (1946) and has since been discussed by many others. In studies relating to the subject, the basic observational data have consisted of monthly mean values of the critical frequencies, *fF2*, measured at ionospheric observatories in various parts of the world. Owing to the small amounts of data available, it has been possible to reach definite conclusions on the distribution of *fF2* only after grouping the data in various ways. It is common, for example, to combine data covering several years, during which solar activity may have changed, so that measurements from two or more observatories may be considered together. Similarly the change of *fF2* with latitude is usually derived by superposing data from locations at all longitudes which lie within one of the "standard" magnetic zones.

The combination of the data in ways such as these has made it difficult to appreciate the exact nature of the geographical distribution of *fF2* and how this varies with season and solar activity.

2. A New Method for Studying *fF2*

Recent investigations into the use of ionospheric indices of solar activity have produced a method of combining all the available basic sets of experimental data relating to *F2*-layer critical frequencies in such a way as to give derived sets of condensed data which are more reliable and more useful, for some purposes, than the basic data. It has been found that for a given observatory, month and local time, the monthly mean values of *fF2* can be expressed as a linear function of the ionospheric index I_{F2}:

$$fF2 = a + bI_{F2}. \tag{1}$$

Thus both the seasonal and solar cycle changes in *fF2* at noon, for example, at any location can be expressed very concisely in terms of the twelve pairs of monthly values of a and b.

These constants have been evaluated for sixty-five locations for which at least 5 years data are available covering both high and low solar activity. Since the

* Official communication.

correlation between $fF2$ and I_{F2} is high, considerable confidence can be placed in the reliability of the statistically determined values of these constants.

The geographical distribution of the constant a is obviously identical with that of $fF2$ at minimum solar activity, when $I_{F2} = 0$. By inserting the appropriate value of I_{F2} in equation (1), the distribution for any other level of activity can easily be obtained.

3. The Construction of the Contours

The local noon values of a have been plotted on maps for each month of the year and contours have been drawn which represent the smooth surface characteristic of each month. In general, there are not enough points to allow these surfaces to be determined unambiguously and hence, before drawing the contours, it is necessary to introduce additional assumptions concerning the form of the surfaces. Two such assumptions have so far been adopted:

Assumption I. The contours drawn should represent the simplest possible surface consistent with the experimental data.

Assumption II. The equatorial trough and the two associated ridges which are found in the eastern hemisphere are also present at all other longitudes and they run almost parallel to the lines of constant geomagnetic dip.

Assumption I leads to the inference that the equatorial trough exists at all seasons in the eastern hemisphere. In the western hemisphere, however, the simplest configuration of the contours, during May, June and July at least, is a single ridge with no equatorial trough, although during the remainder of the year the trough and two ridges continue across this hemisphere. Assumption I appears to be the one on which the contours used for making ionospheric forecasts are based. Fig. 1 shows the change with latitude of the intercept a along the 90°E and 90°W meridians and illustrates the apparent seasonal transition from a single to a double ridge at 90°W.

Starting from assumption II, the locations of the two ridges in relation to the magnetic dip lines are determined fairly closely by the data in the eastern hemisphere. The continuation of these ridges across the Pacific Ocean, keeping them parallel to the dip lines, does not lead to any conflict with the experimental data in this area. The curves for the 90°E and 90°W meridians, resulting from assumption II are shown in Fig. 2 which is directly comparable with Fig. 1.

4. Discussion of Results

It seems unlikely that the physical processes responsible for the distribution of electron density in the eastern and western hemispheres can be so different as to result in the marked differences in the two sets of curves shown in Fig. 1. On physical grounds, therefore, assumption II seems to be preferable; the coincidence that from May to July the peaks of the ridges pass between the few observatories in the Pacific is not an improbable one.

An investigation is in progress, the aim of which is to find an empirical expression, involving such parameters as latitude and the horizontal and vertical components of the earth's field, which is capable of representing all the observed values of the constant a for a given month. If this aim is achieved, it will be possible to use this

VOL
18
196

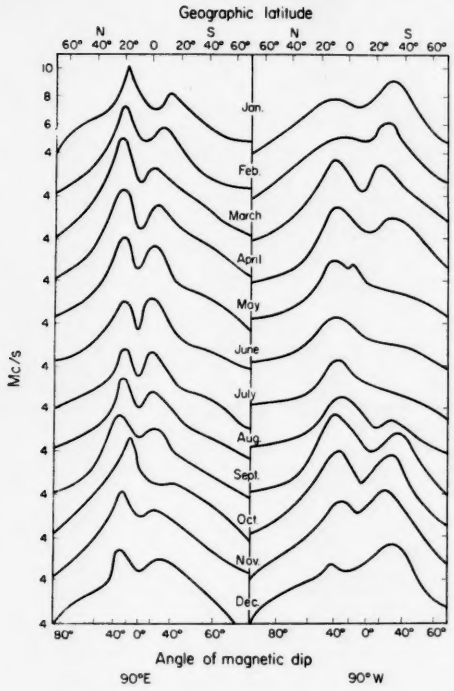

Fig. 1. Latitude variations in f_{F2} at local noon for $I_{F2} = 0$; assumption I.

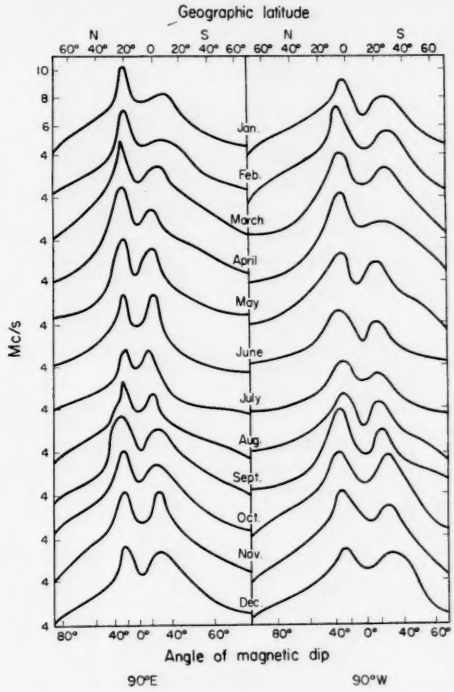

Fig. 2. Latitude variations in f_{F2} at local noon for $I_{F2} = 0$; assumption II.

expression to interpolate the most probable configuration of the contours in areas where this cannot be done satisfactorily given only the data which are at present available.

5. Conclusion

On the simplest interpretation of the experimental data, the equatorial trough which is found to be characteristic of *F2*-layer ionization in the eastern hemisphere is not present during May, June and July in the western hemisphere. It is shown, however, that the available data in the western hemisphere are not sufficient to preclude the existence of the trough and two ridges which can be continued from the western to the eastern hemisphere without conflicting with these data.

Acknowledgements—The work described in the paper was carried out as part of the programme of the Radio Research Board and is published by permission of the Director of Radio Research of the Department of Scientific and Industrial Research.

References

Appleton E. V. 1946 *Nature, Lond.* **157**, 691.

Maeda K, Uyeda H. and Shinkawa H. 1946 *Report on Japanese Research on Radio Wave Propagation* (*U.S. Army Forces*) Vol. I, p. 87.

Journal of Atmospheric and Terrestrial Physics, 1960, Vol. 18, pp. 184 to 191. Pergamon Press Ltd. Printed in Northern Ireland

Low-altitude testing of the rocket-grenade experiment for upper atmosphere temperatures and winds

R. F. Stebbings, G. V. Groves, R. L. F. Boyd and P. J. Bowen
Department of Physics, University College, London

(*Received* 25 *November* 1959)

Abstract—As a preliminary to the British series of rocket-grenade experiments for determining upper atmosphere temperatures and winds, a number of tenth-scale tests using anti-aircraft shells to simulate grenades were carried out at Shoeburyness in 1956. The objects of these trials were to test the widespread array of ground equipment under field conditions, and to check the method of data reduction by comparing the computed temperature and wind results with radio-sonde balloon data. The analysis of sounding data from two night-time trials gave wind speeds which differed in most cases from the balloon values by less than 5 ft/sec. Differences of the order of 10°C in the temperature structures may be reduced by the subsequent inclusion in the method of analysis of second-order acoustic refraction effects.

Introduction

The study of wind and temperature at altitudes of 30–60 km by observing sound waves reflected from these heights has been carried out spasmodically since about 1926. With the advent of upper atmospheric sounding rockets, however, it became possible to operate to greater heights independently of reflection, by exploding grenades in the upper atmosphere. In the United States, the Army Signal Corps carried out experiments of this kind at White Sands, New Mexico (Stroud *et al.*, 1956) and demonstrated the usefulness of the method to heights of about 80 km. During the International Geophysical Year this work has been continued at Fort Churchill, Canada.

At the start of the British Upper Atmosphere research programme in 1954, it was decided to use the velocity of sound method with *Skylark* rockets, and one of us made a study of the theoretical basis of the method (Groves, 1956). As a result of this, it appeared that accuracy could be considerably improved by using a widespread array of microphones and that vertical winds might also be detectable. The price paid for this improved accuracy is the greater complexity and difficulty of operating a widespread array of listening posts and a greatly expanded, though more rigorous process of data reduction. In view of the magnitude of these two parts of the problem it was decided to mount a tenth-scale trial at the ordnance range at Shoeburyness, where the results could be checked against radio-sonde balloon data, and to use the new data to test the programme devised for the Pegasus electronic computer at the Admiralty Research Laboratory.

This paper gives an account of the experiments carried out at Shoeburyness, and compares the results obtained with the radio-sonde figures.

The British Grenade Experiment

The experiment requires ejection from a rocket of a series of grenades filled with a photoflash mixture giving a high light output, in addition to a pressure disturbance which is propagated through the atmosphere. The time of arrival at

the ground of this disturbance is recorded at a number of microphones. The instant of the flash is determined by means of a photoelectric device whilst the burst is photographed by three widely-separated ballistic cameras, and its position in space obtained very accurately by triangulation. The data obtained is in the form of position co-ordinates for the grenade bursts and the microphones, and of travel times of the sound waves between these points. From the measurements corresponding to any particular grenade, the mean values of the three components of the wind velocity and the mean velocity of sound between ground level and the height of the burst may be found. The actual values of the wind-velocity components and the speed of sound between successive bursts may be found by a process of differencing. The temperature is found from the velocity of sound in terms of the mean molecular weight for air, and pressure is obtained from the hydrostatic equation.

Since for each grenade burst there are four unknown quantities, three wind velocities and the temperature, it is theoretically only necessary to use an array of four microphones. However, it is desirable to have a redundancy of microphones so that a least-squares fit may be made to the results and errors examined.

The Shoeburyness Tenth-scale Experiments

During this work the rocket borne grenades were simulated by anti-aircraft shells containing 6 oz pellets of a photoflash mixture and fired to altitudes between 10,000 and 34,000 ft. Standard army sound-ranging equipment was employed, in which the outputs from seven hot-wire microphones were amplified and displayed on a seven-pen moving-paper recorder. Three ballistic cameras were employed together with a flash detector. The former were specially developed for the grenade experiment and will be described in another paper. The layout of the ground equipment used in the Shoeburyness experiment is shown in Fig. 1. Meteorological information in the form of wind speeds and directions, temperatures, pressure and humidity was supplied for altitudes up to 34,000 ft from radio-sonde balloon data for the period of each trial. Survey data for the position co-ordinates of the microphones and cameras were supplied by the range authorities.

Night-time experiments

The initial trials were conducted at night which has the advantage that flash detection is simple and camera shutters may be left open for many minutes. A blue sensitive photomultiplier tube (EMI type 6097) with a 10° field of view was used to detect the flashes. The camera shutters were left open throughout a salvo without undue plate fogging. The output from the flash detector was fed to all seven recorder pens in order that there would be no ambiguity in identification of the flash pulse and that timing errors due to variation in length of the pen arms could be eliminated. Timing for all but the first few trials was effected by means of an accurately-calibrated clock which fed half second pulses to an additional pen. Fig. 2 shows for each microphone the pressure disturbance from a shell bursting at 34,000 ft altitude superimposed on the wind-noise background.

The ballistic cameras used were the prototype version of a series of cameras developed for the grenade experiment, and the Shoeburyness trails provided a

means of testing this type under field conditions. The design requirements for the cameras were that the space co-ordinates of the grenade bursts, obtained from the plate images, should be accurate to within 5 m at 100 km altitude. A Schneider "Xenar" F.4.7 bloomed anastigmat fitted with a Compur Rapid shutter of speed range 1/400 sec to 1 sec was chosen as being adequate for this purpose. The camera body was supported in a rigid framework and capable of full azimuth rotation and

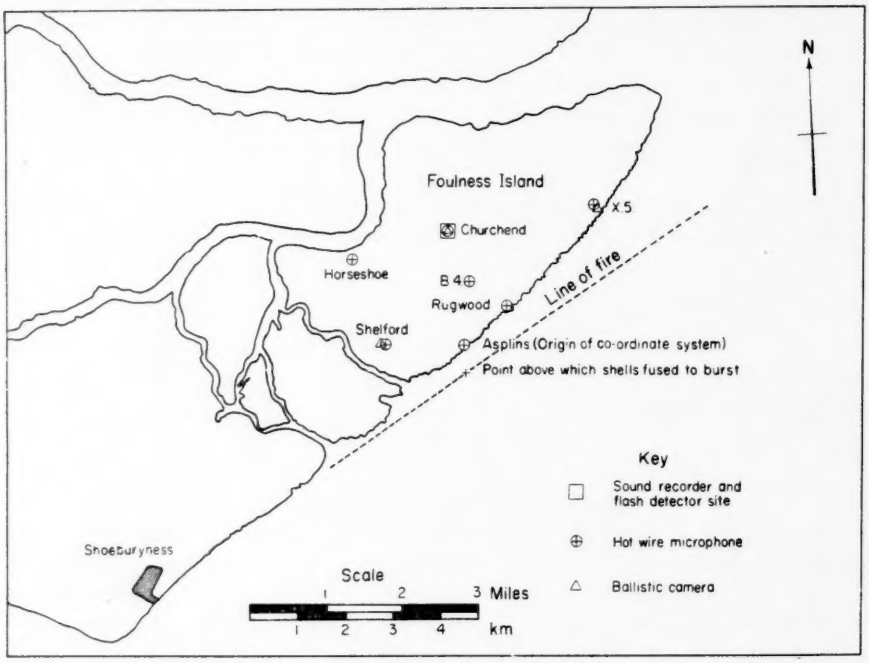

Fig. 1. Layout of the ground equipment used in the Shoeburyness experiments.

of being elevated through 90°. The position of the 12 cm × 9 cm plate was fixed accurately with respect to the lens by three steel-tipped Invar rods, chosen for their extremely low expansion coefficient. These rods were retracted when a camera plate was inserted or removed. In use, the camera was mounted and levelled on a triangular steel frame which was securely pegged into ground.

Day-time experiments

The photography and flash detection of the grenade bursts in the presence of the sky background illumination necessitated certain modifications on the optical side. The photomultiplier was unsuited for operation in these circumstances because of overloading and an alternative system was developed. This employed an infra-red photocell placed in the focal plane of an 8 in. focal length $f2{\cdot}9$ lens. The voltage developed across the photocell load was amplified and fed to the grid of a thyratron, which was adjusted to cut off when only sky noise was present in the system.

VOL. 18 1960

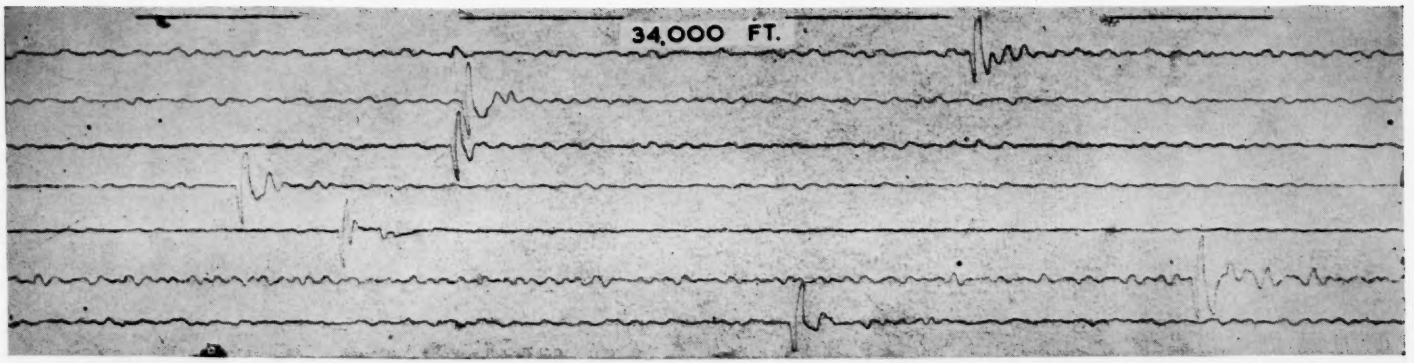

Fig. 2. Portion of sound-ranging record for a shell bursting at 34,000 ft altitude. The $\frac{1}{2}$ sec timing marks can be seen at the top of the record.

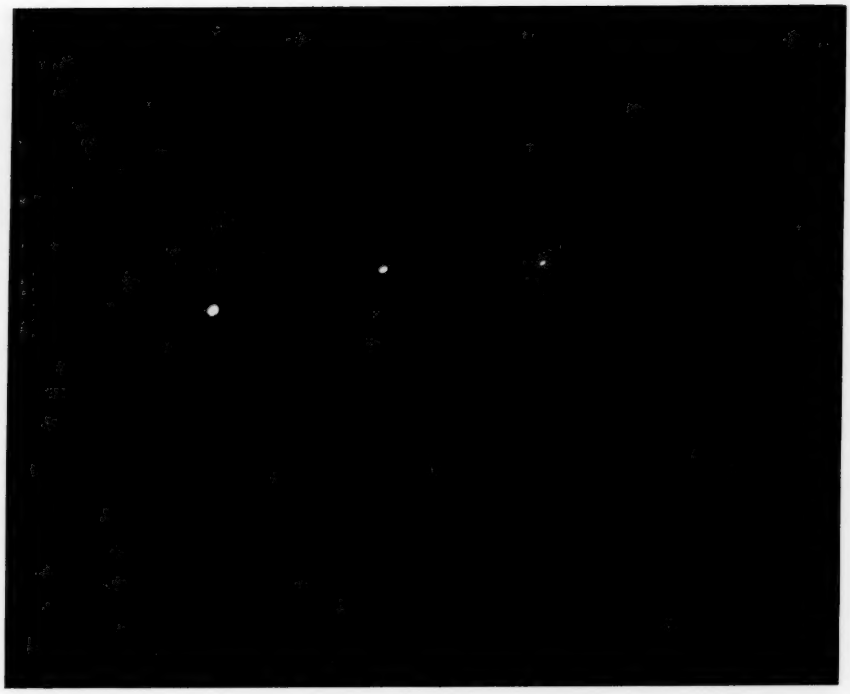

Fig. 3. Ballistic-camera record of three shell flashes at 10,000 ft altitude photographed against the day sky.

VOL.
18
196

The night-time mode of camera operation in which the shutters were left open during the firing sequence would have resulted, in day-time, in severe plate fogging. In consequence a control unit was provided for each camera which would, on command, open the shutter for the correct exposure and then re-set it in readiness for the next operation. The signal developed by the thyratron in the flash detector was transmitted over about $1\frac{1}{2}$ miles of field cable to operate the cameras. These cables were in fact the lines to the recorder from nearby microphones, the signal to the camera being fed from a condenser bridge in parallel with the microphone element.

The overall delay in the system from the instant of burst to shutter fully opening was of the order of 10 msecs. Flashes from three shell-bursts at 10,000 ft photographed in this way are shown in Fig. 3. The output from the flash detector was fed via a d.c. amplifier to an oscilloscope and the shape of the light pulse found (Fig. 4).

Determination of burst co-ordinates

The angular co-ordinates of the camera plates were obtained by photographing the night sky. After a series of shell flashes had been recorded, the camera shutters were closed, and then re-opened for a brief exposure at a given instant of time (accurate to about 1 sec), upon a receipt of a command by field telephone. The resulting star images were used as reference points to determine the plate orientation in terms of nine plate constants, from which the directions of the shell bursts with respect to the camera were found. By employing three ballistic cameras, the space co-ordinates of the bursts were determined by a triangulation method. For day-time experiments, the cameras would normally be left set up in position between the firing and the recording of a star background.

Results

A number of tenth-scale grenade experiments were carried out at Shoeburyness between April and August, 1956. Of these, two night-time trials, conducted on 1 and 14 May, gave complete sets of data on winds and temperatures between 10,000 ft and 34,000 ft. A daylight experiment carried out on 24 August was only partially successful, as insufficient ballistic camera data was obtained to enable the burst co-ordinates to be computed. Details of the successful night-time experiments are given below:

1 *May* 1956. A complete set of data was obtained for a series of five shell bursts at approximately 10, 19, 22, 28 and 34,000 ft. The analysis gave a constant wind over this range and the values obtained are compared in Figs. 5 and 6 with those obtained by meteorological balloon. Fig. 7 shows the corresponding temperature values.

14 *May* 1956. Complete sets of data were obtained from two series of four shells and one series of five bursts. The analysis was carried out with one of the series of four shells giving the curves (A) in Figs. 8 to 10, and with the other two series combined to give the curves (B).

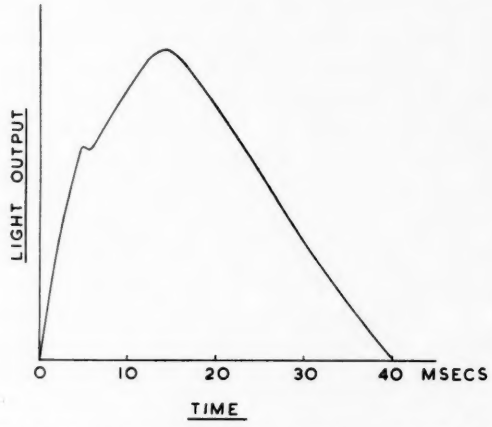

Fig. 4. Typical shape of light-pulse from a shell flash.

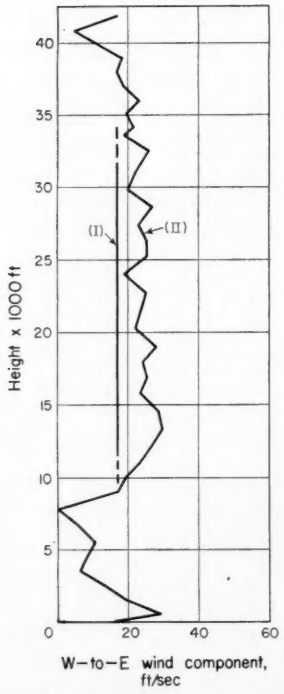

Fig. 5. Shoeburyness 1 May 1956, 2300 hours (approx.). E to W wind component determined by (I) five shells exploding at approximately 10, 19, 22, 28, 34,000 ft, (II) meteorological balloon (unsmoothed).

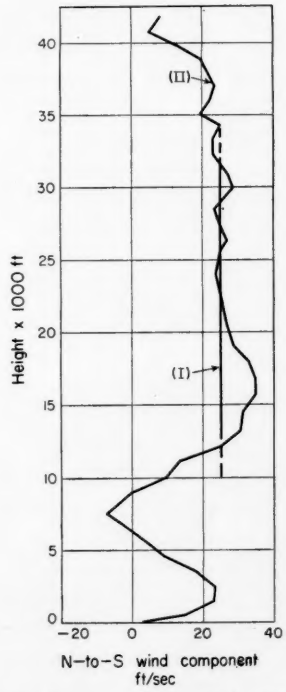

Fig. 6. Shoeburyness 1 May 1956, 2300 hours (approx.). N to S wind component determined by (I) five shells exploding at approximately 10, 19, 22, 28, 34,000 ft, (II) meteorological balloon (unsmoothed).

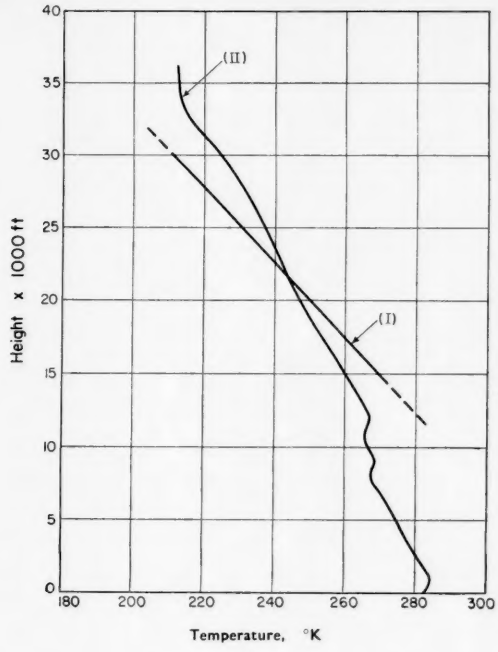

Fig. 7. Shoeburyness 1 May 1956, 2300 hours (approx.). Temperature determined by (I) five shells exploding at approximately 10, 19, 22, 28, 34,000 ft, (II) meteorological balloon.

OL.
18
960

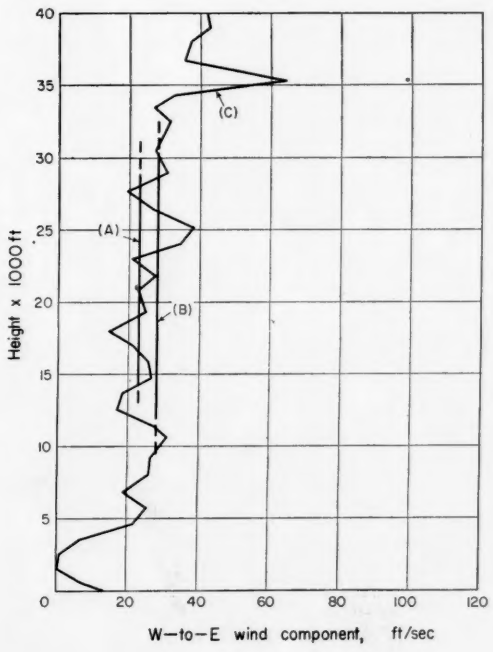

Fig. 8. Shoeburyness 14 May 1956, 2200 hours (approx.). W to E wind component determined by (A) four shells exploding at approximately 13, 19, 22, 31,000 ft, (B) nine shells exploding at approximately 10, 13, 16, 19, 21, 25, 28, 31, 34,000 ft, (C) meteorological balloon (unsmoothed).

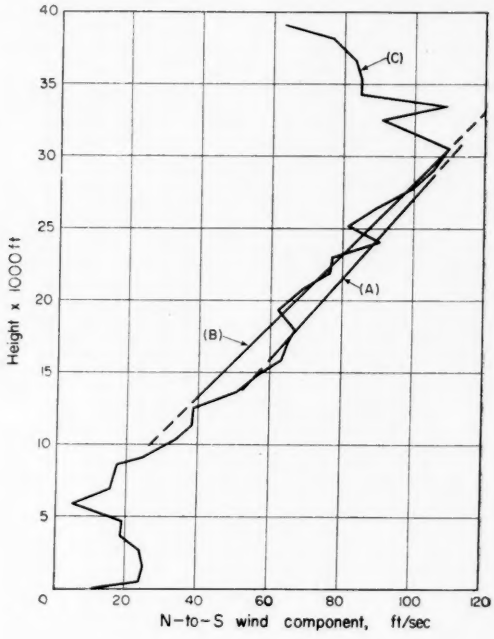

Fig. 9. Shoeburyness 14 May 1956, 2200 hours (approx.). N to S wind component determined by (A) four shells exploding at approximately 13, 19, 25, 31,000 ft, (B) nine shells exploding at approximately 10, 13, 16, 19, 21, 25, 28, 31, 34,000 ft, (C) meteorological balloon (unsmoothed).

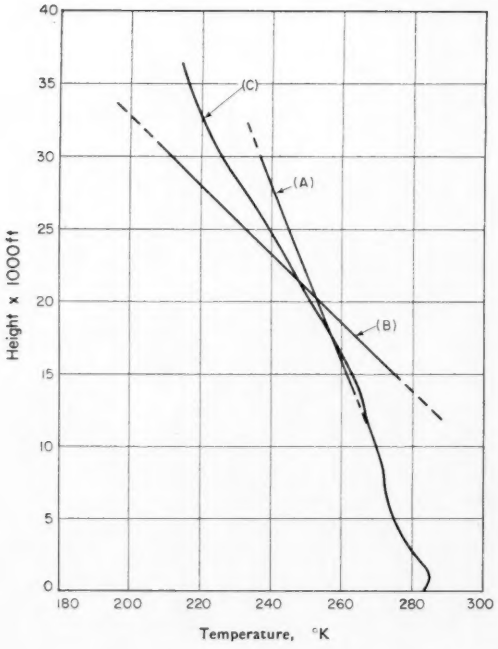

Fig. 10. Shoeburyness 14 May 1956, 2200 hours (approx.). Temperature determined by (A) four shells exploding at approximately 13, 19, 25, 31,000 ft, (B) nine shells exploding at approximately 10, 13, 16, 19, 21, 25, 28, 31, 34,000 ft, (C) meteorological balloon.

Discussion and Conclusions

Over the height range of the experiments, the balloon data gave wind speeds almost constant with height, and Figs. 5, 6, 8 and 9 show that the analysis of the sounding data has led to the same result. The comparison is very close, differences being mainly less than 5 ft/sec. In the temperature structure, Figs. 7 and 10 show that differences amount to the order of 10°C, which is somewhat greater than was expected. Some improvement may still be obtainable from the method of analysis, which so far has not included second-order refraction effects. This is now being investigated. Vertical air motion was not detectably different from zero to an accuracy of about 10 ft/sec.

Acknowledgements—The tests described in this paper were carried out as part of the British upper atmosphere research programme, under the joint sponsorship of the Royal Society and the Ministry of Supply. Acknowledgements are due to the Ministry of Supply Proof and Experimental Establishment, Shoeburyness, for providing the basic facilities for these experiments, and to the Royal Aircraft Establishment for making the initial arrangements concerning the trials. The sound-ranging equipment was supplied by the War Office Technical Stores Organization. Professor C. W. Allen of the University of London Observatory kindly provided facilities for the preparation of ballistic camera-plate data for computing. The programming of the analysis at the Admiralty Research Laboratory was carried out by Mr. G. Owen, and later by Miss M. Thorpe.

VOL. 18 1960

References

Groves G. V. 1956 *J. Atmosph. Terr. Phys.* **8,** 189.

Stroud W. G., Nordberg W. and Walsh J. R. 1956 *J. Geophys. Res.* **61,** 45.

Journal of Atmospheric and Terrestrial Physics, 1960, Vol. 18, pp. 192 to 202. Pergamon Press Ltd. Printed in Northern Ireland

On the current system of solar-flare effects

J. VELDKAMP and D. VAN SABBEN
Royal Netherlands Meteorological Institute, De Bilt

(*Received* 30 *November* 1959)

Abstract—The electric current system responsible for the great solar flare effect (s.f.e.) of 23 March 1958, is compared with the currents of the normal daily variation of the geomagnetic field. Whereas the standard S_q-currents are symmetric with respect to the geographic equator, the pattern of the currents of the s.f.e. as well as that of the currents of the normal daily variation at the time of the s.f.e. are controlled by the magnetic equator. The same result is found by a re-examination of selected s.f.e.s published in the IATME Bulletins nos. 12f and 12h. It is shown that the s.f.e. currents must flow in a region where the disappearance of electrons follows an attachment law. The decrease of the s.f.e. leads to a loss coefficient $\beta = 5 \times 10^{-4}$ sec^{-1}, which compares with the known value for the *D*-layer.

SOLAR flares are generally accompanied by several forms of sudden ionospheric disturbances (s.i.d.), viz. short-wave fade-outs (s.w.f.), sudden cosmic-noise absorption (s.c.a.), sudden phase anomalies of very long radio waves (s.p.a.), sudden anomalies of field strength of very long radio waves (s.f.a.), sudden enhancements of long-wave atmospherics (s.e.a.), and last but not least by typical disturbances of the geomagnetic field (s.f.e. or crochet). The first group of ionospheric disturbances (s.w.f., s.c.a., s.p.a., s.f.a., s.e.a.) is due to the increased ionization and lowering of the *D*-layer. The s.f.e. must be caused by an increased conductivity in the ionosphere; it is generally supposed that the electric currents responsible for this geomagnetic disturbance also flow in the lower ionosphere, e.g. in the *D*-layer.

Several examples of s.f.e.s have been studied by MCNISH (1937) and by BARTELS and VELDKAMP (1951, 1952, 1954); they compared the current vectors responsible for these disturbances with the electric current vectors of the normal daily variation.

On 23 March 1958, a very strong solar flare was observed on the sun; the accompanying s.f.e. was about five times greater than usual. Therefore it offered an excellent opportunity to study the properties of this remarkable magnetic disturbance.

The position of the flare on the sun was 14°S 77°E, the importance was 3+. It commenced at 0950 hours; maxima were observed at 1005 hours, 1010 hours, 1016 hours and 1018 hours; it ended at 1420 hours.

The ionospheric recorder at De Bilt showed a very strong s.w.f., beginning at 0950 hours. From 1005 hours to 1045 hours there was a complete fade-out of all normal ionospheric echoes; after that the *F2*-echo gradually reappeared. However, it lasted till about 1400 hours before the panoramic soundings behaved normally again.

The receiving station NERA of the Netherlands PTT recorded a great outburst in solar radio noise on 200 Mc/s, 545 Mc/s and 2980 Mc/s, beginning between 1000 hours and 1005 hours. Dellinger effects in the field strength of transmitters at Paramaribo and Karachi were recorded at NERA from 0952 hours on.

The magnetic disturbance (s.f.e.) began at 0952 hours, but at 1001 hours a further big sudden increase occurred. The greatest deviation of the magnetic trace was recorded by many stations at 1015 hours.

The magnetic record of this unusually great flare was somewhat spoiled by a polar disturbance which started casually at 1015 hours with a sudden commencement in the stations Si and Co in Northern America, and at the same time in the Antarctic stations Mw and MI.* The magnetograms of the European stations showed a little unrest, following the s.f.e. stations in Central America and in the

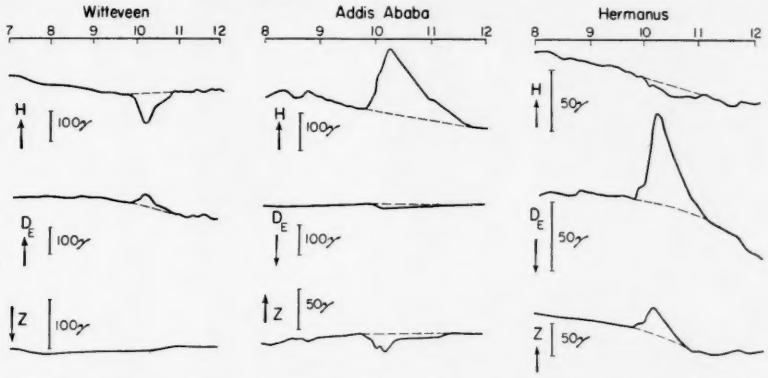

Fig. 1. Magnetograms from the stations Wi, AA and Hr, showing the s.f.e. of 23 March 1958. The arrows indicate the directions of increasing horizontal intensity H, easterly declination D_E and vertical intensity Z.

Pacific recorded a bay disturbance, beginning at 1015 hours, with a maximum at 1100 hours. No (or almost no) disturbance was recorded in the equatorial belt. As in most stations this polar disturbance became visible after the maximum of the s.f.e.; accurate readings of the s.f.e. were quite possible, except for the records of the northern stations Tr, Ai and So. Here the s.f.e., if present, was obscured by the polar storm.

Fig. 1 shows the s.f.e. as recorded by the stations Wi, Hr and AA. The disturbance vector was calculated by measuring the maximum deviations of the horizontal intensity H and the declination D with respect to the interpolated undisturbed traces.

Fig. 2 shows the horizontal electric currents in the ionosphere (heavy arrows with single head), necessary to produce the horizontal components of the s.f.e. during its greatest development, as well as the currents for the normal daily variation at the same time (light arrows with double head).

The components of the daily variation were measured taking the values during the night hours (2200–0200 hours local time) as base values; no measurements were made for those stations where the night hours showed too much disturbance. Scales of γ and A/km are indicated at the bottom of the figure; the relation between the current density in A/km and the magnetic disturbance in γ is

$$i = 0{\cdot}6\,\frac{H}{0{\cdot}2\pi} \qquad (1)$$

* The magnetic observatories are indicated by the two-letter symbol introduced in the IATME (IAGA) Bulletins no. 12.

VOL. 18 1960

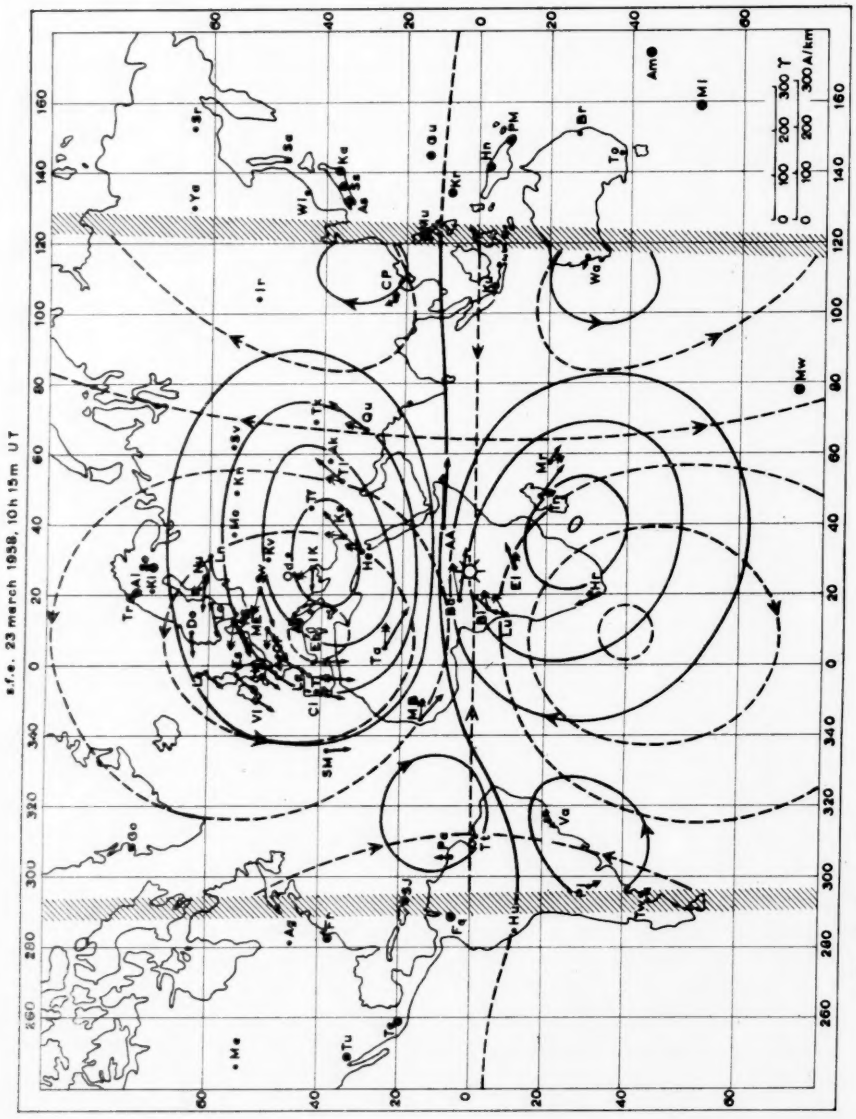

Fig. 2. Map of horizontal electric currents in the ionosphere, necessary to produce the horizontal components of the s.f.e. of 23 March 1958, 1015 hours UT. Heavy arrows with single head represent the s.f.e. currents, light arrows with double head the currents of the normal daily variation at the same time. Heavy dots represent stations where the s.f.e. was not recorded; the star is the sub-solar point. The broken lines are currents of the standard S_c pattern. The partly solid, partly broken line is the magnetic equator. Scale of γ and A/km are indicated at the bottom of the figure.

where the factor 0·6 accounts for the induced currents in the earth (CHAPMAN and BARTELS, 1940). In order to avoid overcrowding the figure, some stations were taken together, e.g. ME shows the mean value of the s.f.e. in the stations Wn, Wi, Ni, Cm, Db, Ma, Pr, Fu, Ti and Hb. A heavy black dot means that no s.f.e. was recorded.

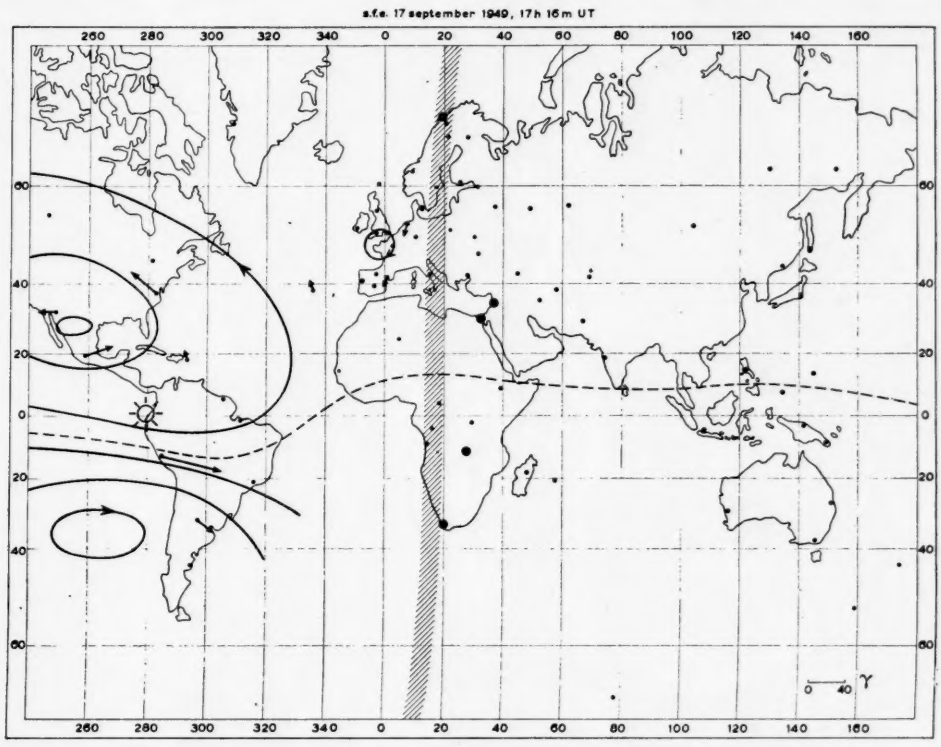

Fig. 3. The current pattern of the s.f.e. of 17 September 1949, 1716 hours UT. The broken line is the magnetic equator. See also IATME Bulletins no. 12e, p. 101.

Roughly speaking, the electric currents responsible for the s.f.e. were twice as strong as the currents of the daily variation.

The solid lines in Fig. 2 show the current pattern of the s.f.e., drawn according to the disturbance vectors. The broken lines are currents of the standard S_q-system for the equinoxes (CHAPMAN and BARTELS, 1940). The star is the subsolar point, the hatched strips indicate the limitation of the daylight hemisphere.

It is quite clear that the current pattern of the s.f.e. is almost symmetric with respect to the magnetic equator (the partly broken line). Consequently, the greatest disturbance (160 γ) was recorded by the station AA which lies nearly on the magnetic equator and under the equatorial electrojet (ONWUMECHILLI, 1959; GOUIN, 1959). The currents of the daily variation at the time of the s.f.e. are in better accordance with the S_q-pattern for the equinoxes; it is, however, clear that in the vicinity of the equator the currents of the normal daily variation are also

influenced by the magnetic equator, and that the centres of the current systems lie easterly from the centres of the standard S_q-pattern, especially in the southern hemisphere. The great vortices of the s.f.e. are accompanied by smaller ones; however, they cannot be drawn accurately for lack of observations.

Compared with CHAPMAN's S_q-system, the current pattern of the s.f.e. is compressed in a north–south direction, especially in the northern hemisphere.

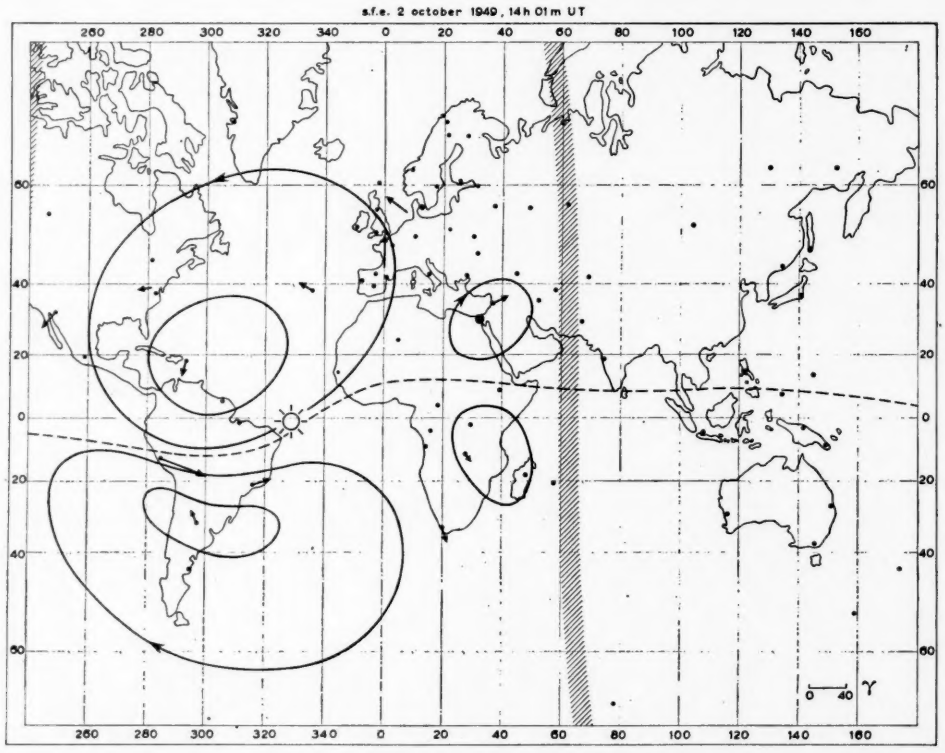

Fig. 4. The current pattern of the s.f.e. of 2 October 1959, 1401 hours UT. See also IATME Bulletin no. 12e, p. 103.

This is apparently due to the fact that the magnetic equator is here north of the geographic equator. Moreover, there is practically no difference in longitude between the centres of the s.f.e. system and the subsolar point, so that the S_q-system is about 1 hr in advance of the s.f.e. pattern.

As for stations lying on the night side of the earth, no s.f.e. was recorded at Fr, Tu, Te, SJ, Fq, Ka, As, Ss, Mm, Kr, Gu, Hn, PM, MI, Mw and Am. The stations Hu and To recorded a small deviation, which may have been caused by the s.f.e. or by the following polar disturbance. Tw, lying in the twilight zone, recorded a small crochet. The s.f.e. was practically confined to the daylight hemisphere.

Formerly it was thought (MCNISH, 1937) that the s.f.e. was caused by the enhanced ionization in the S_q-region, so that the disturbance vectors of the s.f.e.

should have the same direction as the vectors of the normal daily variation. However, the vectors of the solar flare effect and the daily variation generally do not coincide, as is shown by the selected examples in the IATME Bulletins nos. 12e, 12f and 12h (BARTELS and VELDKAMP, 1951, 1952, 1954). An examination of a number of these figures resulted in the current patterns for the s.f.e. disturbance as shown in Figs. 3–6. As the data from these smaller s.f.e.s are generally less

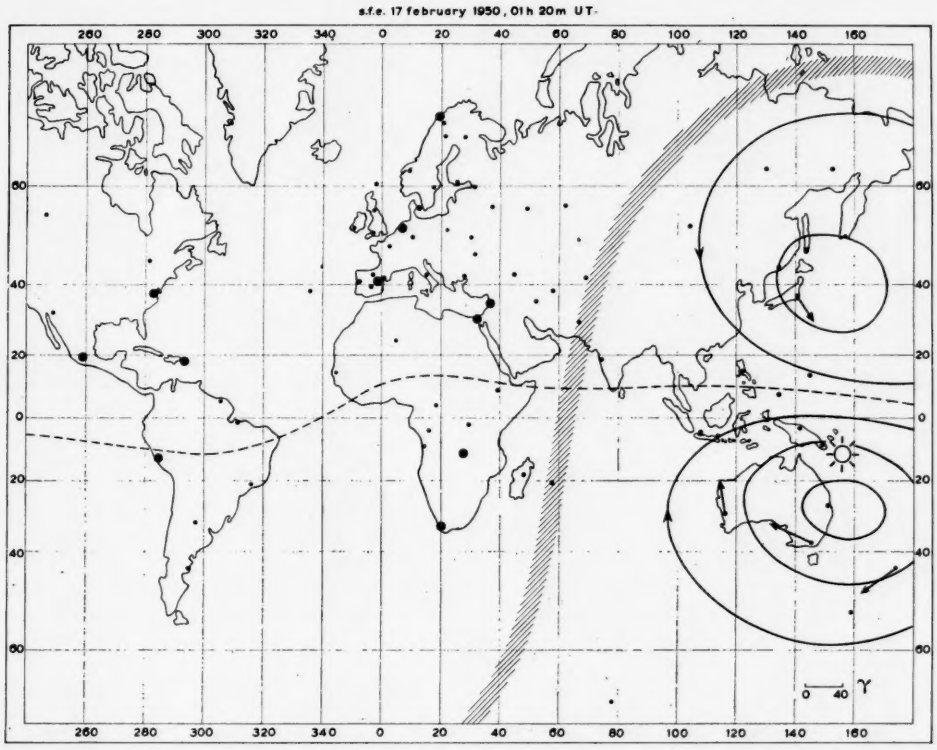

Fig. 5. The current pattern of the s.f.e. of 17 February 1950, 0120 hours UT. See also IATME Bulletin no. 12f, p. 80.

abundant and relatively less accurate, the lines are only drawn with the intention to localize the current vortices and not to give the absolute values of the current densities. The dotted lines represent the magnetic equator for 1945 (VESTINE *et al.*, 1947). From an inspection of these figures it is clear that shape and place of the s.f.e. vortices are related to the magnetic equator, rather than to the geographic equator, just as was found for the great s.f.e. of 23 March 1958. The local times of the centres of the vortices vary from 1000 to 1200 hours. It is reasonable to suppose a dependence on UT, as a consequence of the asymmetry of the magnetic field with respect to the axis of the earth.

GRAFE (1958) has drawn attention to the fact that the occurrence of the s.f.e.s shows maxima during the equinoxes, as do other magnetic disturbances of corpuscular character. His conclusion is that the current system of the s.f.e. is

not an enhanced S_q-system; probably the currents responsible for the s.f.e. flow at a different height to the S_q-currents. VOLLAND and TAUBENHEIM (1958) are of the same opinion. As there appears to be a close correlation between the s.f.e., the s.i.d. and a temporary enhancement of the E-ionization, these authors think that the s.f.e. current system must flow partly in the D-layer and partly in the E-layer, and therefore below the S_q-currents which they suppose to flow above the E-region.

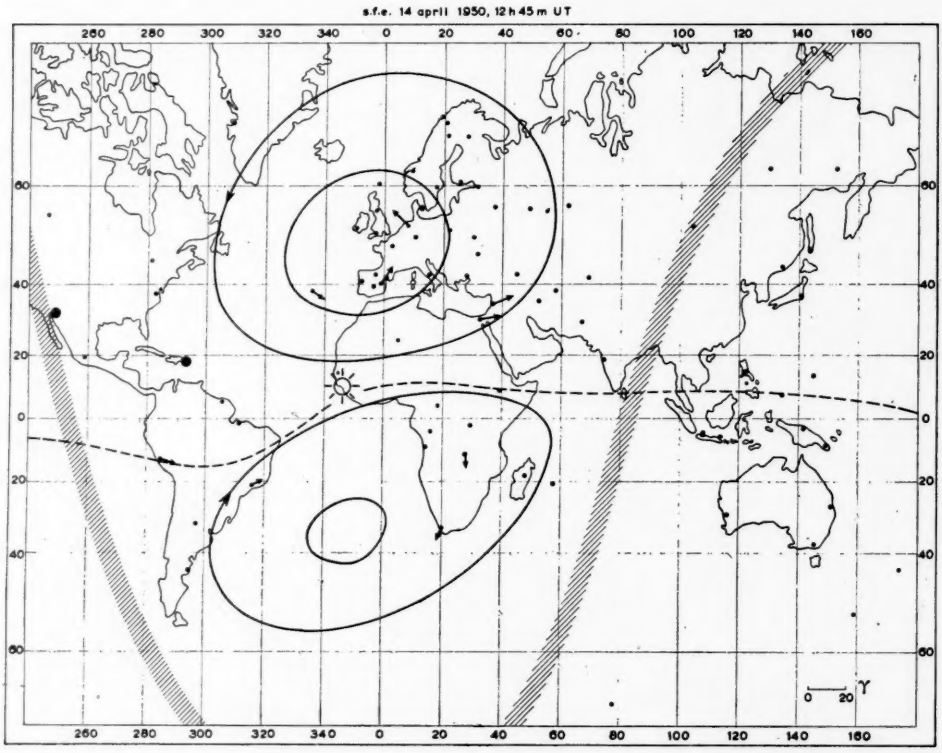

Fig. 6. The current pattern of the s.f.e. of 14 April 1950, 1245 hours UT. See also IATME Bulletin no. 12f, p. 81.

The exploration of the ionosphere by means of rockets (SINGER *et al.*, 1951; CAHILL and VAN ALLEN, 1958) has proved the existence of electric currents flowing in the ionosphere. Supposing an unbounded horizontal sheet current, the change in the geomagnetic field strength in going through the sheet would be twice the geomagnetic variation measured at the earth's surface. It was found that under normal circumstances no appreciable current flows in the D-layer, that a deviation from the inverse-cube law as a function of the altitude was present from 95 to 110 km above the earth, and that a second deviation began at 117 km. The anomaly in passing through the E-layer was less than one-half of the expected value. Therefore the S_q-currents must flow partly in the lower part of the E-layer and partly at a somewhat greater height. Whereas the normal D-layer is formed by Ly α

radiation, which gives a maximum ionization at the height of about 80 km, hard X-rays with wavelengths to 1 or 2 Å are necessary in order to get ionization at levels as low as 65 km. Indeed, rocket measurements obtained during solar flares gave positive evidence of an intense coronal X-ray emission, penetrating below 80 km (CHUBB *et al.*, 1957). This temporary X-radiation accounts for the intense ionization in the *D*-layer which causes the s.i.d. phenomena.

APPLETON and PIGGOTT (1954) have argued that the S_q-currents must flow in the *E*-layer, whereas the absorbing layer must be identical with the *D*-layer. These conclusions are based on the measurements of the recombination coefficient α from the diurnal variation of the electron density N and from the variation of the absorption on normal days and during s.i.d.s. It is supposed that the electron density is controlled by the equation

$$\frac{dN}{dt} = q(t) - \alpha N^2 \tag{2}$$

and it is found that $\alpha N = 4 \times 10^{-4}$ sec^{-1} in the *D*-layer whereas $\alpha N = 12 \times 10^{-4}$ sec^{-1} in the *E*-layer. Moreover they found that in both layers the dissipation of electrons follows the recombination law (αN^2) and not the attachment law (βN).

MITRA and JONES (1954) calculated the following values of α: $\alpha = 10^{-5}$ cm^3 sec^{-1} for 65 km height, $\alpha = 10^{-7}$ cm^3 sec^{-1} for $h = 90$ km and $\alpha = 5 \times 10^{-8}$ cm^3 sec^{-1} for $h = 110$ km. They find that the recombination curve may be explained by attachment and formation of negative ions below 80 km and by dissociative recombination above 90 km.

RATCLIFFE *et al.* (1956) confirm the recombination law in the *E*- and *F1*-layers. In the *F2*-region the disappearance of electrons is according to βN, but here the dissipation by vertical drift introduces considerable uncertainty.

Some new information can be obtained by the investigation of the decrease of the s.f.e. under consideration. Supposing that at some time $t = 0$ after the maximum of the s.f.e. no new extra ionization is formed in the region where the s.f.e. currents flow, and that the electrons disappear by recombination as well as by attachment, the decrease of the electron density with time t is given by

$$\frac{d(N + x)}{dt} = q(t) - \alpha(N + x)^2 - \beta(N + x) \tag{3}$$

where N is the normal electron density and x the extra ionization due to the s.f.e. The solution of (3) is

$$\frac{x}{x_0} = \frac{1}{(\xi_0 + 1)e^{\gamma t} - \xi_0} \tag{4}$$

where $\xi_0 = \alpha x_0/\gamma$ and $\gamma = \beta + 2N\alpha$; x_0 is the excess electron density at the time $t = 0$.

Fig. 7 gives some graphs of x/x_0 for various values of ξ_0. The decrease is exponential for $\xi_0 = 0$, but for values of $\xi_0 > 0$ the extra ionization disappears more slowly at the end.

Now the decrease of the s.f.e. in question is practically exponential, as is shown

by the examples of Fig. 1; this is also the case with many other s.f.e.s (see, for example, the selected examples in IATME Bulletin no. 12h). This means that

$$\alpha x_0 < \beta + 2N\alpha. \tag{5}$$

The current density in the ionosphere is determined by the conductivity

$$\sigma = \frac{eN\nu}{m(\nu^2 + \omega^2)} \tag{6}$$

where N is the electron density, ν the collision frequency and ω the gyro-frequency ($\omega = 7 \times 10^6$ sec^{-1}). In the E-layer N is about 2×10^5 cm^{-3} and ν is between

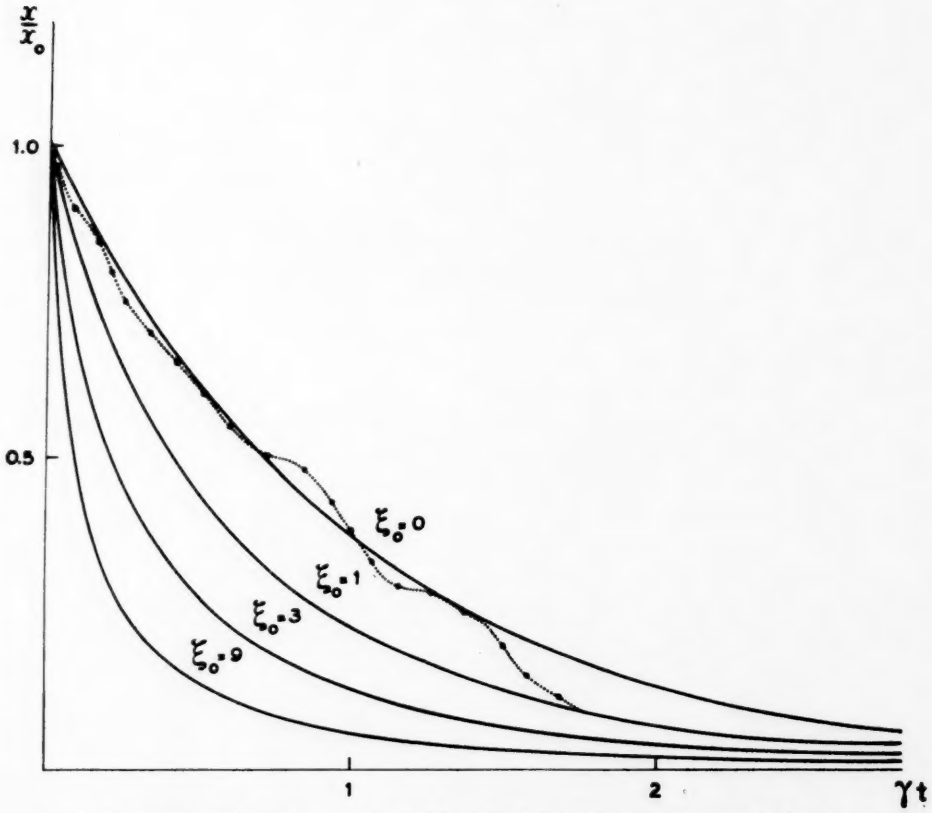

Fig. 7. Graphs of x/x_0 for some values of ξ_0. The dots indicate the decrease of the s.f.e. at Addis Ababa. The irregularities may be ascribed to the polar disturbance which commenced during the s.f.e.

10^4 and 10^5 sec^{-1}; in the normal D-layer N is about 10^3 and ν between 10^6 and 10^8 sec^{-1}. Taking these values we see that σ is only somewhat smaller in the D-layer than in the E-layer; in the F-region the conductivity is much smaller owing to the low value of the collision frequency, which is here between 10^3 and 10 sec^{-1}.

The s.f.e. currents are comparable with the currents of the normal daily variation. If they flow in the D-region where normally the current density is small, it follows that $x_0 \gg N$, so that from (5) $\beta > \alpha x_0$ and therefore $\beta \gg \alpha N$, which means that the s.f.e. currents must flow in a region where the disappearance of electrons is analogous to an attachment process. This might also point to the *F2*-region but it is improbable that here the ionization is enhanced to such a degree as required by the s.f.e. currents.

The following values were found for the half-value time t_1: 20 m (Lo), 15 m (Le), 12 m (Wi), 25 m (TI), 20 m (He), 30 m (Ta), 30 m (AA), 20 m (Qu), 35 m (Ba), 20 m (Mr), 20 m (Hr). There seems to be an increase for t_1 from higher latitudes towards the equator.

Taking $t_1 = 25$ m as a mean value, we obtain $\beta = 5 \times 10^{-4}$ sec^{-1}. This value compares with the value for αN for the D-layer found by APPLETON and PIGGOTT.

Acknowledgements—Copies of magnetograms were gratefully received from Dr. A. ROMANA, Chairman of Committee no. 10, IAGA.

The following stations furnished data: Tromsö (Tr), Kiruna (Ki), Abisko (Ai), Sodankylä (So), Pt. Barrow (PB), College (Co), Dombås (Do), Nurmijärvi (Nu), Lerwick (Le), Lovö (Lo), Sitka (Si), Rude Skov (RS), Eskdalemuir (Es), Wingst (Wn), Witteveen (Wi), Swider (Sw), Helu (Hl), Niemegk (Ni), Valentia (Vl), Collmberg (Cm), Hartland (Ha), Manhay (Ma), Dourbes (Db), Tihany (Ty), Pruhonice (Pr), Fürstenfeldbruck (Fu), Chambon la Fôret (CF), Hurbanova (Hb), Nantes (Na), Istanbul Kandilli (IK), Teheran (TI), Ebro (Eb), Logrono (Lg), Coimbra (Ci), Toledo (Tl), Fredericksburg (Fr), San Miguel (SM), Kakioka (Ka), Aso (As), Shimosato (Ss), Ksara (Ks), Tucson (Tu), Quetta (Qu), Cha Pa (CP), Helwan (He), Tamanrasset (Ta), Honolulu (Ho), Koror (Kr), Guam (Gu), Teoloyucan (Te), Fuquene (Fq), San Juan (SJ), Addis Ababa (AA), M'Bour (MB), Paramaribo (Pa), Bangui (Ba), Hollandia (Hn), Binza (Bi), Luanda (Lu), Elisabethville (El), Kuyper (Ku), Huancayo (Hu), Port Moresby (PM), Apia (Ap), Tananarive (Tn), Mauritius (Mr), Vassouras (Va), Watheroo (Wa), Pilar (Pi), Hermanus (Hr), Toolangi (To), Trelew (Tw), Amberley (Am), Macquarie Island (MI), Mawson (Mw).

The Directors of these observatories are thanked for the readiness with which they supplied us with the necessary data to complete this study. Without their help and kind co-operation this investigation would not have been possible.

REFERENCES

APPLETON E. V. and PIGGOTT W. R.	1954	*J. Atmosph. Terr. Phys.* **5,** 141.
BARTELS J. and VELDKAMP J.	1951	IATME Bulletin No. 12e.
BARTELS J. and VELDKAMP J.	1952	IATME Bulletin No. 12f.
BARTELS J. and VELDKAMP J.	1954	IATME Bulletin No. 12h.
CAHILL L. J. and VAN ALLEN J. A.	1958	*J. Geophys. Res.* **63,** 270.
CHAPMAN and BARTELS J.	1940	*Geomagnetism.* Oxford University Press.
CHUBB T. A., FRIEDMAN H., KREPLIN R. W. and KUPPERIAN J. E.	1957	*J. Geophys. Res.* **62,** 389.
GOUIN P.	1959	*Bull. Geophys. Obs. Addis Ababa* **1,** 1.
GRAFE A.	1958	*Geofis. Pur. Appl.* **40,** 172.

McNish A. G.	1937	*Terr. Magn. Atmos. Elect.* **42,** 109.
Mitra A. P. and Jones R. E.	1954	*J. Geophys. Res.* **59,** 391.
Onwumechilli C. A.	1959	*J. Atmosph. Terr. Phys.* **13,** 222.
Ratcliffe J. A., Schmerling E. R., Setty C. S. G. K. and Thomas J. O.	1956	*Phil. Trans.* A **248,** 621.
Singer S. F., Maple E. and Bowen W. A.	1951	*J. Geophys. Res.* **56,** 265.
Vestine E. H., Laporte L., Lange I. and Cooper C.	1947	Carnegie Institution of Washington, Publ. 578.
Volland H. and Taubenheim J.	1958	*J. Atmosph. Terr. Phys.* **12,** 258.

Journal of Atmospheric and Terrestrial Physics, 1960, Vol. 18, pp. 203 to 214. Pergamon Press Ltd. Printed in Northern Ireland

Diurnal variations of density and scale height in the upper atmosphere

J. S. Greenhow and J. E. Hall
Jodrell Bank Experimental Station, University of Manchester

(*Received* 9 *December* 1959)

Abstract—The radio-echo meteor technique has been used to investigate atmospheric density and scale-height variations between altitudes of 85 and 105 km. A diurnal oscillation of density with an amplitude equal to 13 per cent of the mean density at 96 km is found. The amplitude of this oscillation increases by a factor of 3 over the observed height range. A semi-diurnal density variation approximately half the diurnal oscillation is also present.

VOL. 18 1960

1. Introduction

Meteors burn away between heights of about 80 and 110 km in the upper atmosphere, producing light and ionization by collision processes. Radio echoes are obtained from the ionized trails, enabling the electron densities and meteor velocities to be determined. Observation of the behaviour of the trails after formation also enables the properties of the atmosphere to be investigated. This paper describes measurements of density and scale height in the region 85 to 105 km from the radio-echo observation of meteors. The diurnal variations in density are studied in some detail using two separate methods. The first method depends upon the measurement of the ambipolar diffusion coefficient D (Greenhow and Neufeld, 1955a) which is closely related to echo duration and radio wavelength λ. When the linear electron density α is less than 10^{12} cm^{-1}, the echo amplitude decays exponentially with a time constant

$$T = \lambda^2/16\pi^2 D \text{ (Herlofson, 1948)} \qquad (1)$$

where D is inversely proportional to the atmospheric density.

The second method uses the observed dependence of the height of occurrence of a meteor upon its geocentric velocity (Kaiser, 1954). The basis of this method is that a meteor of given mass and velocity will undergo its maximum rate of evaporation, giving maximum α, after intercepting a constant air mass, thus determining the atmospheric pressure at the height of maximum ionization.

2. Technique

2.1. *Method of height measurement*

The heights of reflection of the radio waves are measured using the split beam technique described by Clegg and Davidson (1950). Two separate aerials are situated at heights of $\lambda/2$ and $\lambda/4$ above a good reflecting surface. Ground reflections modify the vertical polar diagrams of the aerials, and the ratio r in signal strengths received by the aerials varies with elevation E in the manner

$$r = 2 \cos (\pi/2 \sin E). \qquad (2)$$

The transmitter operates at a peak power of 10 kW. with a pulse length of 30 μsec and pulse repetition frequency of 600 per second. The wavelength λ is 8·2 m.

Separate receivers of optimum bandwidths are connected to each of the receiving aerials. A range resolution of 1 km is attained by transmitting every fourth pulse as a pair the second of which is only 7 μsec wide. A third receiver with a bandwidth of 140 kc/s is then used for range measurements. A loss in signal-to-noise ratio is present in this channel but whereas an echo 20 dB above noise is required for elevation measurements, an echo only 6 dB above noise is adequate for ranging.

Each receiving aerial consists of a horizontal folded dipole and reflector, simple aerials being chosen in order that the free space polar diagrams should be as nearly as possible the same. The transmitting system is an array of four Yagi aerials inclined at 45° to the horizontal, with a beamwidth $\pm 20°$ to the first zero in both the E and H planes. This aerial system is designed to restrict the majority of meteor echoes to the central parts of the receiving aerial polar diagrams, where the rate of change of free space gain is small.

2.2. *Photographic recorder*

The display consists of four cathode-ray tubes which show various echo characteristics. A section of film record is illustrated in Fig. 1. A is a range amplitude display which strobes out the region from 100 to 250 km. 10 km and 50 km range markers enable range to be measured to within ± 1 km from visual inspection of the narrow echo pulse.

A slow time base of 0·5 sec duration is displayed as a horizontal deflexion on tube B, while the output of one of the receivers appears as a vertical deflexion. The time base is triggered by the individual meteor echoes when their amplitudes rise above a preset level. Tube B therefore shows the echo amplitude variation for 0·5 sec after the formation of a trail. This time is long enough to include the half-amplitude decay periods of the majority of all decay-type echoes.

The time base on tube C is also triggered by the echo, but has a duration of only 0·1 sec. Successive echo pulses separated by 1·7 msec can be resolved, enabling the diffraction fluctuations which determine meteor velocity to be measured (Davies and Ellyett, 1949). Very rapid amplitude decays are also measured from this tube.

On completion of the slow time-base sweep the camera, which operates without a shutter, winds on 4 mm of 35 mm recording film in readiness for the next echo. The ratio in signal strengths at the receiving aerials is measured from tube D. The outputs of the two receivers are displayed simultaneously on the x- and y-deflexion plates, and a single echo pulse would therefore appear as a line with a slope equal to the required ratio. Bright-up is applied only to the peaks of the pulses on this display, and when an echo of variable amplitude is received a row of points is observed on the screen. The best straight line through these points, the scatter on which is due to noise fluctuations, gives the ratio in echo amplitudes. S is an artificial echo of constant amplitude, radiated from a fixed aerial in front of the receiving aerials, and is used to calibrate the system.

2.3. *Errors in height measurement*

Random errors in the measurement of elevation can arise through noise fluctuations and irregularities in the receiver polar diagrams. An estimate of the

VOL
18
196

VOL.
18
1960

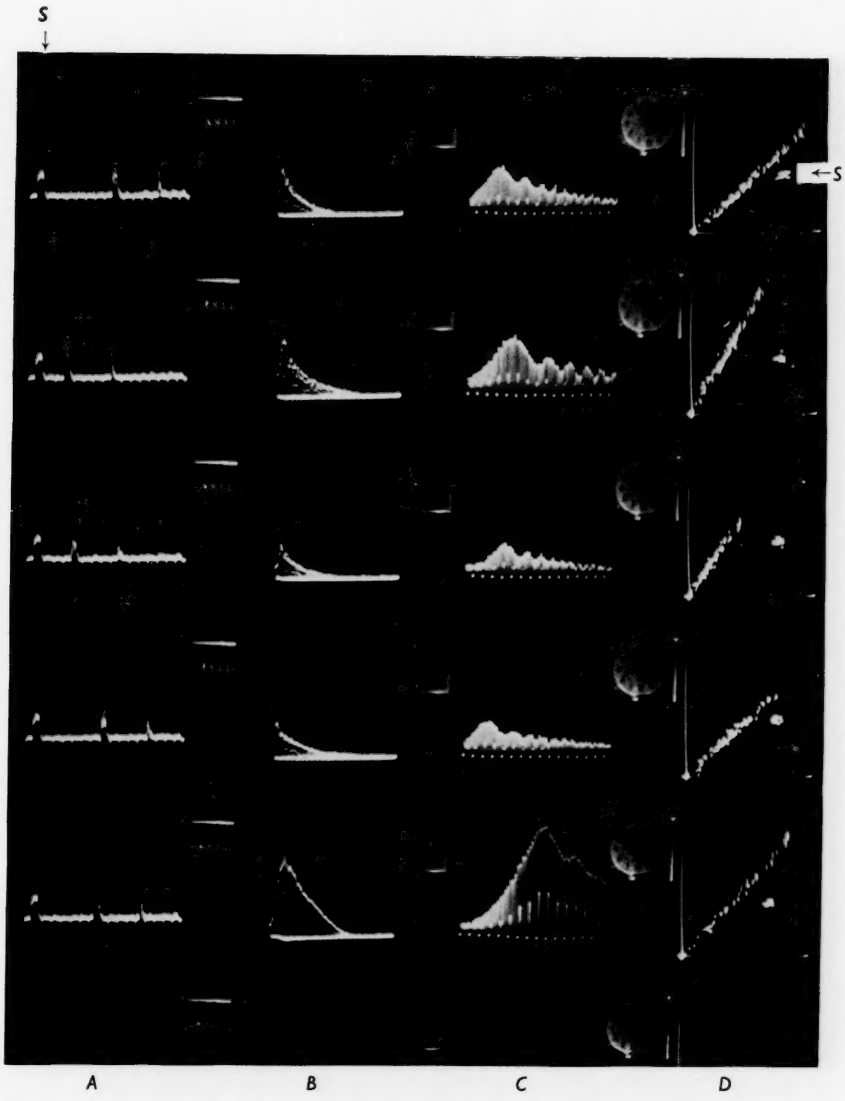

Fig. 1. Section of film record showing a number of meteor echoes. Various echo characteristics are displayed on four cathode-ray tubes *A*, *B*, *C* and *D* (see text).

VOL
18
196

combined errors has been made by observing the departures of amplitude ratios from unity when the aerials are at the same height. The standard deviation of the observed ratio distribution is ± 5 per cent about the mean value, corresponding to a height error of $\pm 3{\cdot}0$ km. This is larger than the error due to noise considerations alone. Further errors may be introduced when the aerials are placed at different heights. The maximum possible error can be found by assuming that echoes with similar decay times occur at the same true height. The width of the height distribution of echoes with similar decay times is found to be 4·5 km. An intermediate value of ± 4 km has therefore been adopted for the accuracy of a single height measurement.

Systematic height errors have been investigated by comparing the calculated values of the artificial echo ratios with the observed values, with the receiving aerials at various heights, when the systematic errors are found to be of the order $0{\cdot}5 \pm 0{\cdot}5$ km.

3. Results

Because of the error of 4 km in each height determination, in order to resolve diurnal variations in atmospheric density of the order of 5 per cent of the mean density, approximately 3000 meteor echoes distributed in a number of intervals throughout the 24 hr are required. These can be obtained in about 10 days observations with the present equipment, and the results obtained during two fortnightly runs in January–February 1958 and 1959 will be compared. The heights, velocities and echo decay times of each meteor have been measured, enabling two independent determinations of the density variations to be made. The first method is through the use of echo decay times to give measurements of the ambipolar diffusion coefficient.

VOL. 18 1960

3.1. *Variation of diffusion coefficient with height*

3.1.1. *Relation between diffusion coefficient, density and temperature.* The ambipolar diffusion coefficient, which determines the rate of dispersal of the ionized matter in a meteor trail, is given approximately by the expression

$$D = \frac{3{\cdot}5\, m}{4\rho A}\left(\frac{kT}{\pi\mu}\right)^{1/2} \tag{3}$$

where m is the mean mass of an air molecule, A the appropriate collision cross-section, k Boltzmann's constant, μ the mean mass of a diffusing particle, ρ the air density and T the temperature (Greenhow and Neufeld, 1955a). The height variation of D is thus determined primarily by the variation of atmospheric density. Second-order effects may be introduced through height gradients of T and m. For an isothermal atmosphere the height/ln ρ relation is a straight line, the slope of which is numerically equal to the scale height $H = kT/mg$ (g is the gravitational acceleration). A height variation of T would cause the straight line to become curved.

Thus measurements of the variation of diffusion coefficient with height enable atmospheric densities and scale heights to be determined.

3.1.2. *The mean diffusion coefficient–height profile.* The heights and corresponding diffusion coefficients, determined from echo-decay times using equation

(1), have been plotted for meteors occurring in 2 or 3 hr intervals for the two series of observations. The method of analysis used in order to derive the curve giving the best fit to the measured values of D and height will be described in another paper.

The results for a number of 3 hr intervals are given in Fig. 2 where least square straight lines have been fitted to the points for each period. The gradients of the lines can be determined to an accuracy of ± 10 per cent, and the values of D at a

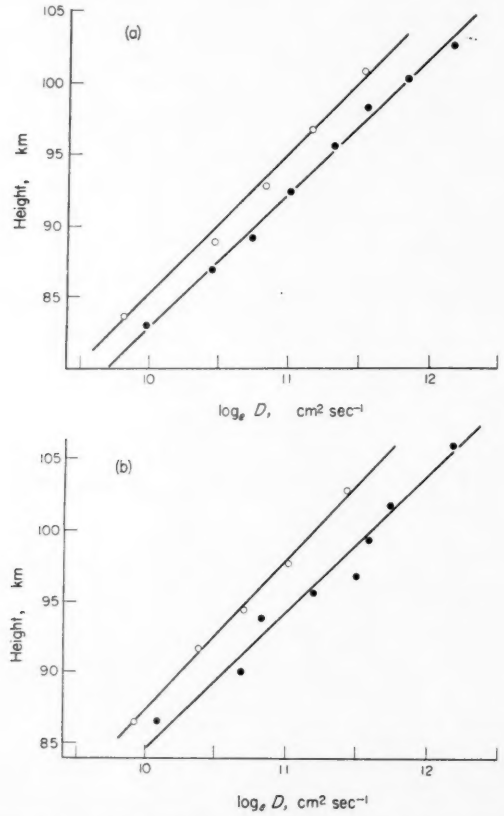

Fig. 2. Variation of diffusion coefficient with height for two 3-hr intervals. (a) ●, 0000–0300 and ○, 1800–2100 hours, January–February 1958. (b) ●, 0000–0300 ○, and 180 –2100 hours, January–February 1959.

given height to ± 5 per cent. No significant second-order terms can be measured using the method of least squares, and no attempt has been made to measure the gradient of scale height. It can be seen from Fig. 2 that quite large variations in diffusion coefficient occur at a given height at different times of the day. The mean curves of diffusion coefficient vs. height for 1958 and 1959, with this daily variation removed (Section 3.1.4) are given in Fig. 3. There is good agreement between the results for the 2 years. The scale heights derived from the slopes of the lines are $8{\cdot}8 \pm 0{\cdot}2$ km in 1958 and $9{\cdot}2 \pm 0{\cdot}3$ km in 1959, and a mean

value of 9·0 ± 0·2 km has been adopted. There is a small displacement of the two straight lines corresponding to a difference in diffusion coefficient of 15 per cent at a height of 96 km. However, the calibration of the equipment in 1958 was not sufficiently accurate to determine whether this is a real variation or a small systematic error of about 1·5 km in the height measurements. The measured values of diffusion coefficient vary from about $2{\cdot}1 \times 10^4$ cm^2 sec^{-1} at a height of 85 km to $2{\cdot}0 \times 10^5$ cm sec^{-1} at 105 km.

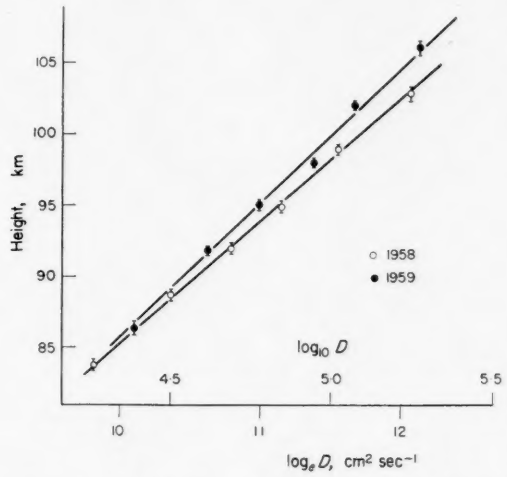

Fig. 3. Mean daily profiles of diffusion coefficient vs. height.

VOL. 18 1960

3.1.3. *The mean density profile*

The measurements of diffusion coefficient described in the previous Section can be converted to atmospheric densities using equation (3). Values of $\mu = 35$ a.m.u., $m = 26$ a.m.u. and $T = 270°$K (determined from the measured scale height), have been assumed. These values are not critical as the largest uncertainty arises in the collision cross-section A. A cross-section of 7×10^{-15} cm^2 has been taken (Ramsauer and Beeck, 1928), but a systematic error of perhaps a factor 2 in ρ may arise because of the uncertainty in this estimate. The mean density profile for the 2 years is given in Fig. 4(i). The measured value of log ρ (g cm^{-3}) varies from −8·2 to −9·2 between 85 and 105 km, with an error of the order of 0·3.

3.1.4. *Diurnal variation in diffusion coefficient and atmospheric density.* The presence of a large diurnal variation in diffusion coefficient at a fixed height is illustrated by the curves in Fig. 2, where the mean profiles for 0000–0300 hours and 1800–2100 hours for 1958 and 1959 are compared.

In 1959 the profiles for the two periods are displaced by 0·4 in ln D at 96 km, corresponding to a change of 1·5 in diffusion coefficient or air density. This daily variation occurs at all heights between 85 and 105 km, and appears to be greater at greater heights. The 1958 results are very similar, with a variation of 0·3 in ln D at 96 km.

The diurnal variation of diffusion coefficient is shown more fully in Fig. 5, where the values of D at a mean height of 96 km are shown for all the 2 or 3 hr groups for both years. In order to reduce the scatter on the individual points in this figure, lines of fixed slope given by the mean $h/\ln D$ relations in Fig. 3 have

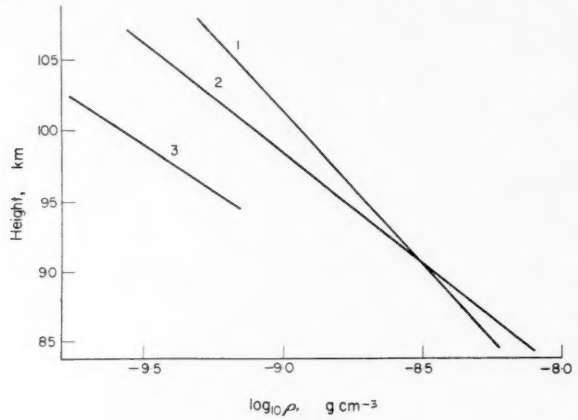

Fig. 4. Density profiles: (1) Meteor radio echo observations. (2) Rocket Panel. (3) Rocket observations (HOROWITZ and LA GOW)

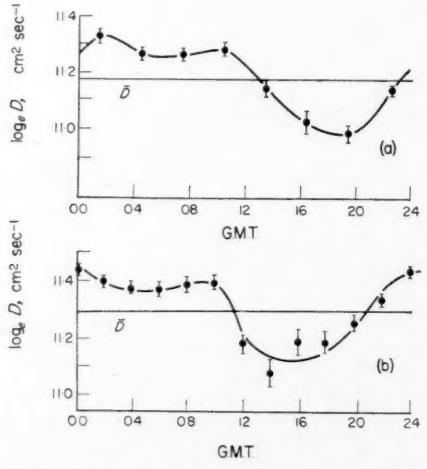

Fig. 5. The diurnal variation in diffusion coefficient at a mean height of 96 km. Smooth curves are drawn through the points. (a) January–February 1958. (b) January–February 1959.

been fitted to the experimental points in each interval. The effects of a possible diurnal variation in slope, suggested by the results illustrated in Fig. 2, will be discussed later. The diffusion coefficient shows a marked diurnal variation with a minimum in the afternoon. A secondary minimum is present in the early morning hours, corresponding to a semi-diurnal variation in D. The results for both years are very similar.

From equation (3), $D \propto \rho^{-1} T^{1/2}$, enabling the curves of Fig. 5 to be converted to curves showing the diurnal variation of $\rho/T^{1/2}$ at a height of 96 km (Fig. 6a,b). If, in the first instance, an isothermal atmosphere is assumed, then these curves show the diurnal variations in density at a fixed height in the upper atmosphere. The peak-to-peak variation in ρ is approximately 30 per cent of the mean density $\bar{\rho}$, and the curves show evidence of both diurnal and semi-diurnal oscillations. A Fourier analysis has therefore been carried out to determine the amplitudes and phases of the 24 hr and 12 hr harmonics of the density oscillation. The

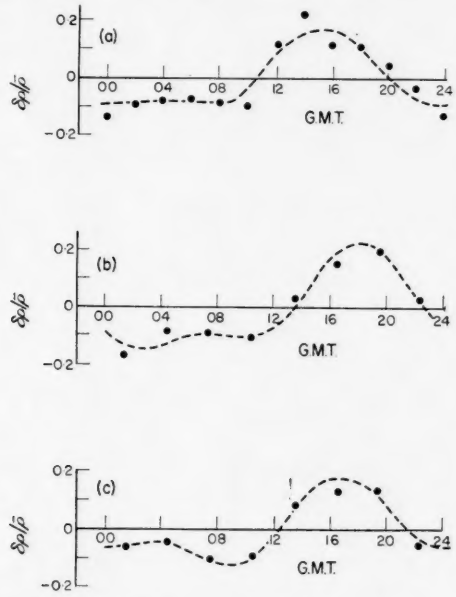

Fig. 6. Diurnal variations in density at a height of 96 km, expressed as a fraction $\delta\rho/\bar{\rho}$ of the mean density $\bar{\rho}$. The broken curves show the sum of the first two terms of the Fourier series giving the 24 hr and 12 hr periodic components (Table 1)

results of the harmonic analysis are given in Table 1 (a) and (b). The amplitude of the 24 hr variation is approximately 15 per cent of $\bar{\rho}$ maximum density occurring about 1630 hours GMT, while the amplitude of the 12 hr harmonic is 6 per cent of $\bar{\rho}$, maximum density occurring near 0450 hours and 1650 hours GMT. The results for the 2 years are in quite good agreement.

3.1.5. *Diurnal variations in slope of the* h/*ln* D *profile and scale height.* The plots of log(diffusion coefficient) vs. height in Fig. 2 show evidence of variations in slope at different times of the day. In order to investigate this effect more fully the gradients of the best straight lines for the results in all the 3 hr intervals have been determined. The gradient is expressed in terms of a scale height H_D over which the diffusion coefficient changes by a factor e, and the results are shown in Fig. 7. The individual points in this figure are weighted means of the measurements during the 2 years. H_D shows a quite marked diurnal oscillation, and harmonic analysis gives the daily variation

$$H_D \text{ (km)} = 9{\cdot}0 + 0{\cdot}9 \sin \pi/12(t - 13{\cdot}4). \qquad (4)$$

VOL. 18 1960

The mean value throughout the day is 9·0 km, while the amplitude of the oscillation is 0·9 $\pm$ 0·3 km. The maximum value of H_D occurs at approximately 1925 $\pm$ 0100 hours. Thus the peak to peak variation of H_D is approximately 20 per cent of the mean value. However, this variation in slope of the h/ln D curve cannot necessarily

Table 1. Diurnal and semi-diurnal variations in atmospheric density at a height of 96 km as a fraction of the mean density $\bar{\rho}$

	Period	Method	Harmonic analysis $\delta\rho/\bar{\rho} = a_1 \sin \pi/12(t - t_1) + a_2 \sin \pi/6(t - t_2)$
(a)	Jan.–Feb. 1958	Diff. coeff. –height	$\delta\rho/\bar{\rho} = 0{\cdot}13 \sin \pi/12(t - 9{\cdot}2) + 0{\cdot}05 \sin \pi/6(t - 0{\cdot}2)$
(b)	Jan.–Feb. 1959	Diff. coeff. –height	$\delta\rho/\bar{\rho} = 0{\cdot}17 \sin \pi/12(t - 11{\cdot}9) + 0{\cdot}07 \sin \pi/6(t - 3{\cdot}4)$
(c)	Jan.–Feb. 1959	Velocity –height	$\delta\rho/\bar{\rho} = 0{\cdot}12 \sin \pi/12(t - 11{\cdot}6) + 0{\cdot}07 \sin \pi/6(t - 1{\cdot}4)$
(d)	Jan.–Feb. 1958 and 1959	Mean curve	$\delta\rho/\bar{\rho} = 0{\cdot}13 \sin \pi/12(t - 10{\cdot}8) + 0{\cdot}05 \sin \pi/6(t - 1{\cdot}8)$

a_1 and a_2 are the amplitudes of the 24 hr and 12 hr components, and t_1 and t_2 their phases. The phases are defined such that the densities are a maximum at times t when the sine terms are unity. t, t_1 and t_2 are measured in hours. t is in GMT. The errors in a_1, a_2 are approximately $\pm$0·02, and in t_1, t_2 approximately 0·5 hr.

be interpreted as a diurnal temperature variation only, as variations of D are a result of changes in both density and temperature. The separation of these two effects will be discussed in detail in Section 4.3.

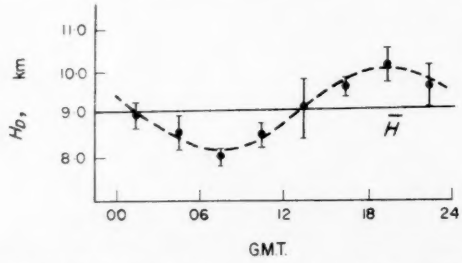

Fig. 7. The diurnal variation in slope of the ln (diffusion coefficient)–height relation, expressed as an apparent scale height H_D.

3.2. *Diurnal density variations from height–velocity observations*

3.2.1. *Method.* The second method for determining diurnal variations in atmospheric density is by observation of the heights of occurrence of meteors with different velocities. Theories of meteor evaporation have been developed which relate the atmospheric density $\rho_{\max}$ at the point at which a meteor undergoes its maximum rate of evaporation, to the meteor velocity V, the linear electron density in the meteor trail $\alpha_{\max}$ and other variables (Kaiser, 1954). In particular

$$\rho_{\max} \propto \alpha_{\max}^{1/3} V^{-2} \beta^{-1/3} T^{-2/3} \qquad (5)$$

where β is the probability that a single evaporated meteor atom will produce a free electron by collision processes. It has been assumed previously that β is independent of velocity, but recent work has shown that $\beta \propto V^3$ so that equation (5) becomes

$$\rho_{\max} T^{2/3} \propto \alpha_{\max}^{1/3} V^{-3}. \tag{6}$$

The observed variation of the height of occurrence of meteors with velocity is shown in Fig. 8, where log V is plotted against the mean heights of meteors in various velocity groups. The slope of the experimental curve varies from that corresponding to $\rho \propto V^{-2}$ for fast meteors, to only $\rho \propto V^{-1}$ for slow meteors. Thus it is clear that serious departures from theory occur, and height–velocity

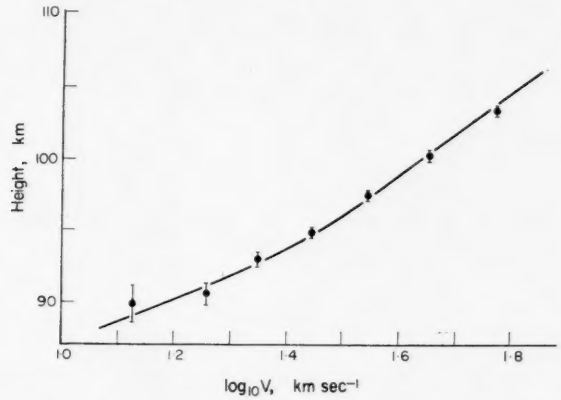

Fig. 8. The variation in mean height of reflection of radio echoes from meteors as a function of meteor velocity.

relationships cannot be used to give absolute measurements of atmospheric density using existing theories. The results are, however, of considerable value if it is required to investigate relative variations of density at a given height only—in particular diurnal and seasonal changes. If it is assumed that

$$\rho_{\max} T^{2/3} \propto f(\alpha_{\max} V) \tag{7}$$

for meteors with a random distribution of radiants and similar constitution, then as a radio equipment detects meteors of similar $\alpha_{\max}$ at all velocities, this expression reduces to

$$\rho_{\max} T^{2/3} \propto f(V). \tag{8}$$

Thus on the average, meteors of given velocity will produce their maximum ionization at a level of constant value of $\rho T^{2/3}$ although the form of the height variation $f(V)$ cannot be predicted. By observing the diurnal variations of heights of meteors of constant velocity, therefore, the diurnal variation of density at a given height can be determined.

3.2.2. *Results.* In order to make full use of the observations, meteors of all velocity groups have been used, and the smooth curve of Fig. 8 has been fitted to the height–velocity results for 3 hr intervals throughout the day. The results for 15 days in January and February 1959 have been integrated to improve the

accuracy of the observations. The results are given in Fig. 9 where the variation in height of occurrence of meteors with constant velocity is shown at 3 hr intervals. This curve may be converted to one showing the density variations at a given height using the known scale height (Fig. 6c). The resulting diurnal density variations refer to a mean height near 96 km (an isothermal atmosphere is again assumed). The shape of the curve in Figs. 9 and 6(c) are very similar to those for the density variations derived from measurements of diffusion coefficient.

Harmonic analysis of the results in Fig. 6(c) shows the presence of both diurnal and semi-diurnal periodic variations in density, and the expression for $\delta\rho/\bar{\rho}$ is

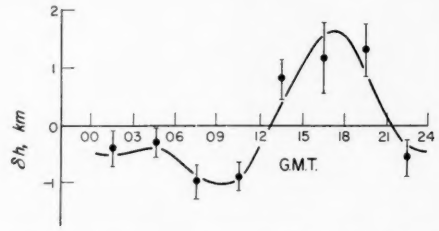

Fig. 9. Curve showing the diurnal variation in height δh of log (velocity)–height curves of the type shown in Fig. 8, for eight 3 hr intervals throughout the day. Displacements δh are measured relative to the mean daily curve in Fig. 8.

given in Table 1(c). The 24 hr density variation has an amplitude equal to 12 ± 2 per cent of the mean density $\bar{\rho}$ throughout the day, with a maximum density at 1735 ± 0030 hours GMT. The 12 hr variation has an amplitude 7 ± 2 per cent of $\bar{\rho}$, with maxima at 0425 ± 0030 and 1625 ± 0030 hours GMT. These values are in good agreement with the results obtained using measurements of diffusion coefficient and height.

4. Discussion

4.1. *The mean temperature and density profile*

The mean density profile determined from measurements of diffusion coefficient is compared with other observations in Fig. 4. The densities are in reasonable agreement with the Rocket Panel measurements (1952) but differ by a factor 2 from the rocket measurements of Horowitz and La Gow (1957). These differences are probably not significant, as systematic errors of this order are present in both the meteor measurements and in the determinations from individual rocket flights. The difference in slope between the profiles is more significant. The scale height determined by the Rocket Panel at latitude 33°N is 6·9 km at a height of 96 km, whereas the meteor observations at a latitude of 53°N give a value of 9 km. This 30 per cent difference may be due to an increase in temperature with latitude. Evidence for such an increase at rather greater heights (about 130 km) is given by rocket flights in the auroral zone (lat. 59°N), where the scale height was found to be almost twice as high as the Rocket Panel determinations (Horowitz and La Gow, 1958).

There is also a possibility that the slope of the $h/\ln D$ curve is artificially increased, because of selection effects which make it difficult to detect meteor

VOL
18
196

echoes with very rapid amplitude decays at the greater heights. This effect is now being investigated.

4.2. *The diurnal density variation*

The diurnal and semi-diurnal variations in upper atmosphere density may be compared with the pressure oscillations required to account for the known upper atmosphere wind systems. These have been extensively studied at Jodrell Bank (GREENHOW and NEUFELD, 1955b, 1956), and Adelaide (ELFORD and ROBERTSON, 1953; ELFORD, 1959).

In the northern hemisphere the semi-diurnal wind is well represented by a vector of constant amplitude rotating in a clockwise direction, such as would be produced by a progressive pressure wave of the form $A(\phi)$ sin $[2(\omega t + \psi)]$; where ψ is the longitude and ω the angular velocity of the earth. Assuming a cos ϕ law for the latitude variation $A(\phi)$ in amplitude of the wave, it is found that a semi-diurnal wind system with an amplitude of 30 msec^{-1} at 96 km, blowing towards the north at 0630 hours (GREENHOW and NEUFELD, 1955b), would be produced by a 3·3 per cent pressure oscillation with a maximum at 0330 hours LT. This is two-thirds the amplitude of the observed variation, while the phase differs by only 1·3 hr from the measured value. As an ideal expression for the pressure wave has been assumed in order to use the equations of motion for a particle in a rotating atmosphere, the agreement between the measured variations and those deduced from the wind system is quite good. The diurnal wind variation on the other hand, is extremely irregular. At Jodrell Bank its amplitude is sometimes equal to that of the semi-diurnal variation, but more usually it is a factor of 3 or 4 times smaller. Also the behaviour of the wind vector is not that which would be expected for a simple progressive pressure wave. At Adelaide, on the other hand, the diurnal wind is the major component and it is generally larger than the semi-diurnal component. Thus in the absence of any well-defined wind structure it is not possible to calculate the nature of the associated pressure variation. As a rough estimate, equal amplitude 24 hr and 12 hr periodic wind systems, such as observed at Adelaide but not at Jodrell Bank, would be produced by pressure oscillations with a ratio 2 or 3 to 1, depending upon the form of the pressure distribution. The observed amplitude ratio is 2·6.

An investigation of diurnal variations in upper atmosphere density has been made by JACCHIA (1957), from the photographic observation of meteors. Least squares analysis of the results gives a semi-diurnal component with an amplitude of 5 ± 5 per cent of the mean density, and JACCHIA only sets an upper limit of $0{\cdot}1\bar{\rho}$ for the amplitude of this periodic variation. As photographic observations can only be made at night-time, they do not enable observations of the larger 24 hr component to be made.

4.3. *Height gradient of the density oscillation and diurnal temperature changes*

In a static, isothermal atmosphere, the slope of the $h/\ln D$ relation gives the scale height H, and if the temperature changes, the slope of the line changes in proportion. Fig. 7 shows the existence of quite large diurnal variations in apparent scale height, equivalent to a peak-to-peak temperature variation of approximately

20 per cent. Such large temperature variations would not be expected in the 96 km region and indeed the similarity of the curves in Fig. 6(a) and (b) which essentially measure the density, to Fig. 6(c) which more nearly measures pressure, show that temperature variations are small. In the presence of an atmospheric pressure oscillation of amplitude δp, however, changes in slope would be produced by an increase in δp with height as well as by temperature variation. For an adiabatic change in pressure $\delta p/p$, there will be a corresponding density variation $\delta\rho/\rho = (1/\gamma)(\delta p/p)$ and temperature variation $\delta T/T = \{(\gamma - 1)/\gamma\}(\delta p/p)$. As there is a pressure oscillation of the order of 10 per cent of the mean daily value, these equations imply that the temperature oscillation will be of the order of 3 per cent about the mean temperature. The rest of the diurnal change in apparent scale height can then be explained by an increase in the periodic density variation $\delta\rho/\bar{\rho}$ with height by approximately 0·007 km^{-1}. As $\delta\rho/\bar{\rho} \sim 0{\cdot}13$ at 96 km, this gradient corresponds to an increase in the fractional diurnal density variation from $0{\cdot}06\bar{\rho}$ at 85 km to $0{\cdot}17\bar{\rho}$ at 100 km. It is interesting to observe that the semi-diurnal pressure oscillation, deduced from the observed wind system, also increases by a factor of 3 between 85 and 100 km during the winter months (Greenhow and Neufeld, 1956).

Acknowledgements—The research work described in this paper has been carried out at the Jodrell Bank Experimental Station, University of Manchester, under the direction of Professor A. C. B. Lovell. The work has been supported in part by the Air Research and Development Command, United States Air Force, under contract no. AF 61(514)-948.

References

Clegg J. A. and Davidson I. A.	1950	*Phil. Mag.* **41,** 77.
Davies J. G. and Ellyett C. D.	1949	*Phil. Mag.* **40,** 614.
Elford W. G.	1959	*Planet. Space Sci.* **1,** 94.
Elford W. G. and Robertson D. S.	1953	*J. Atmosph. Terr. Phys.* **4,** 271.
Greenhow J. S. and Neufeld E. L.	1955a	*J. Atmosph. Terr. Phys.* **6,** 133.
Greenhow J. S. and Neufeld E. L.	1955b	*Phil. Mag.* **46,** 549.
Greenhow J. S. and Neufeld E. L.	1956	*Phil. Mag.* **1,** 1157.
Herlofson N.	1948	*Phys. Soc. Rep. Progr. Phys.* **11,** 444.
Horowitz R. and La Gow H. E.	1957	*J. Geophys. Res.* **62,** 57.
Horowitz R. and La Gow H. E.	1958	*J. Geophys. Res.* **63,** 759.
Jacchia L. G.	1957	*J. Meteor.* **14,** 34.
Kaiser T. R.	1954	*Mon. Not. R. Astr. Soc.* **114,** 39.
Ramsauer C. and Beeck O.	1928	*Ann. Phys., Lpz.* **87,** 1.
Rocket Panel	1952	*Phys. Rev.* **88,** 1027.

Journal of Atmospheric and Terrestrial Physics, 1960, Vol. 18, pp. 215 to 233. Pergamon Press Ltd. Printed in Northern Ireland

Diurnal variation of the electron distribution in the ionospheric *E*-layer

B. J. ROBINSON*
Radiophysics Laboratory, CSIRO, Sydney, Australia

(*Received* 27 *January* 1960)

Abstract—By means of a special sounder $h'(f)$ curves have been obtained with an accuracy sufficient to determine the distribution of the ionization in the *E*-layer. The variation of the scale height in the *E*-region has been deduced from the shape of the layer. The diurnal variation of the ionization has yielded an estimate of the recombination coefficient. It is shown that there may be vertical drift effects comparable with the effects of recombination. The results determined from the layer shapes are compared with the information provided by accurate penetration-frequency measurements.

1. INTRODUCTION

A SERIES of measurements has been made at Cambridge to enable an accurate and detailed investigation to be made of the properties of the *E*-layer above a single station. Height measurements were required with an accuracy considerably greater than provided by routine ionospheric soundings, and a high-resolution sounder was constructed which made it possible to measure group heights with an accuracy of ± 1 km.

Routine measurements of the critical (or penetration) frequency, and of the minimum virtual (or group) height, have shown some small differences from the behaviour of the maximum electron density of an ideal Chapman layer, but have been unable to discriminate between likely non-Chapman effects, such as vertical gradients of the scale height H and recombination coefficient α (see ROBINSON, 1959). From the accurate group-height measurements it has been possible to determine the distribution of electrons with height below the maximum of the *E*-layer. The distribution was computed from the $h'(f)$ records by a numerical method in which allowance was made for the effect of the earth's magnetic field and for the retardation of the waves in passing through the *D*-region. The measured shapes of the layer enable a more detailed comparison to be made with CHAPMAN'S theory than has been possible with penetration-frequency measurements alone. It is possible to deduce values of the scale height at different altitudes, and to estimate the value of the recombination coefficient and the magnitude of vertical drift effects.

Accurate measurements have also been made of the diurnal variation of the penetration frequency, using records taken every 5 min. These measurements have been analysed by well-established procedures, and the results compared with those obtained from the full electron distribution.

2. APPARATUS

In its general principles the sounder used was of conventional design, of the type described by NAISMITH and BAILEY (1951). However, special attention was

* Present address: Radiosterrewacht, Dwingeloo, Netherlands.

paid to those points which limit the accuracy or clarity of the reflections on routine soundings below 4 Mc/s.

Because of the considerable absorption suffered by waves reflected from the E-layer, and the high level of interference at medium frequencies, the transmitter comprised a pulsed oscillator and power amplifier capable of delivering a 70 μsec pulse of 20 kW peak power to the antenna (a horizontal folded-dipole 250 ft long on 60 ft masts). The sounder explored the frequency band 950 kc/s to 4 Mc/s in $2\frac{1}{2}$ min, giving the maximum sensitivity compatible with the changes of the layer with time. Usually soundings were made at 5 min intervals.

The echoes were received on a separate, carefully-balanced, horizontal-folded dipole, with a wide band balance-to-unbalance transformer at the feed point to discriminate against local noise and ground-propagated interference (Piggot, 1955). The receiver intermediate-frequency response was made to decrease very rapidly outside the desired band 30 kc/s wide by means of frequency–selective cathode feedback and overcoupled tuned transformers (Brailsford, 1938; Sturley, 1947). This made it possible to take advantage of any clear bands between interfering stations.

The diurnal change of height of the E-layer is only about 20 km in summer, and less in other seasons, so that an accuracy of ± 1 km is essential for useful height measurements. Lyon and Moorat (1956) have shown that with standard sounders errors of 5 km and more may be introduced by changes in the width of the recorded oscilloscope trace as the echo amplitude changes. Much greater accuracy was achieved here by using fast-acting (within 10 μsec) automatic gain control (van Voorhis, 1948) to make the receiver output pulse independent of the strength of the echo, and by measuring always to the same point on the pulse (the centre was used to minimize dispersion errors). This arrangement is considerably simpler than the alternative of a logarithmic receiver, which Bibl (1951b) has incorporated in an ionospheric sounder to produce records of high resolution. When a single, clean echo was present it was possible to measure group height to within 1 km; if two overlapping echoes were present this accuracy could not be attained, as discussed by Halliday (1936).

Height calibration markers were provided at 10 km intervals, the zero errors due to receiver phase distortion and modulator delay being determined by a method similar to that described by Lyon and Moorat (1956). Frequency calibration marks were provided on the record at intervals of 200 kc/s, using the method of van Berkel (1954).

3. The Shape of the E-Layer

3.1. *Determination of the electron distribution*

The general methods for deducing the variation of the electron density (N) with height (h) have been fully discussed by Becker (1956) and King (1957). Whale (1951) and Shinn and Whale (1952) have shown that, because the E-layer penetration frequency is close to the gyro-frequency, full account must be taken of the effect of the earth's magnetic field. A numerical method based on that described by Jackson (1956) was used. The computational labour required was greatly reduced by reading the $h'(f)$ curve at twenty-five pre-selected values of $\log f$,

so that most of the computations had to be carried out only once for each frequency range considered. These preliminary calculations were kindly performed by Mr. J. E. TITHERIDGE. The refractive index data were taken from the curves published by SHINN and WHALE (1952), assuming that the gyro-frequency was 1·20 Mc/s and that the magnetic dip was 66°41′.

Pulses reflected from the base of the E-layer can be shown to be retarded appreciably in the D-region. Our knowledge of the D-region is growing rapidly (see WAYNICK, 1957) and information about the electron distribution and collision frequencies has been provided by the work of GARDNER and PAWSEY (1953), FEJER (1955) and by rocket flights (SEDDON, 1958). For a 1·25 Mc/s pulse the retardation which would be suffered in passing through FEJER'S D-region is about 3 km (up to 100 km). The retardation in the D-region can also be estimated by comparing the group heights of the ordinary and extraordinary reflections. This was done by computing the $N(h)$ curve from an ordinary wave $h'(f)$ curve on the assumption that there was no D-region, i.e. that the group heights at the lowest recorded frequencies were equal to the actual heights of reflection. The extraordinary wave $h'(f)$ curve corresponding to this distribution was computed, and found to lie about 5 km below the observed extraordinary wave trace. This difference is due to the unrealistic truncating of the ordinary $h'(f)$ curve, the layer computed in this case being thinner than the true layer. An extension of the ordinary $h'(f)$ curve using data from l.f. and v.l.f. measurements greatly modified the lower part of the $N(h)$ curve, and led to much better agreement between the computed and observed extraordinary wave $h'(f)$ curves.

The lack of adequate experimental data about the D-region thus presents a serious problem for the computation of E-layer $N(h)$ curves. The extraordinary wave reflections could not be observed at all times of day in Cambridge and other means of allowing for the retardation had to be devised. It was found that the following approximation gave results which agreed to within the experimental errors with the checks provided by the extraordinary reflections:

(i) The base of the ionosphere was assumed to be the same as the "phase height" of reflection of the 16 kc/s wave received at Cambridge from GBR (Rugby). This "phase height" was measured continuously by the methods described by BRACEWELL *et al.* (1951).

(ii) From this level the electron density was assumed to increase exponentially till it reached the critical density for a wave of frequency 1·2 Mc/s. The scale height of this exponential was calculated to make the group height for a 1·2 Mc/s wave equal to the measured group height (or that extrapolated from a slightly higher frequency when interference obscured the echo on 1·2 Mc/s.) This calculation is described in the Appendix.

3.2. *Diurnal variation of the electron distribution*

On many days the E-region $h'(f)$ curves did not have a simple shape, but were disturbed by scattering or E_s, or showed sudden discontinuities which made it impossible to deduce a reliable $N(h)$ curve. The work described in this paper is restricted to those days when the reflections were clearly defined and showed no sudden discontinuities at frequencies below the penetration frequency. About

VOL. 18 1960

10 per cent of the records fell into this class. The more complex reflections are discussed elsewhere (ROBINSON, 1960).

In Fig. 1 are shown $N(h)$ curves computed for parts of a summer day and a spring day when the $h'(f)$ curves were clearly defined. (In one year of recording there was no occasion when a *complete* day could be analysed.) The layer is seen to follow the sun's elevation in a fairly regular fashion. In summer the retardation is usually limited by an "abnormal E-stratum", and the dashed portion of some of

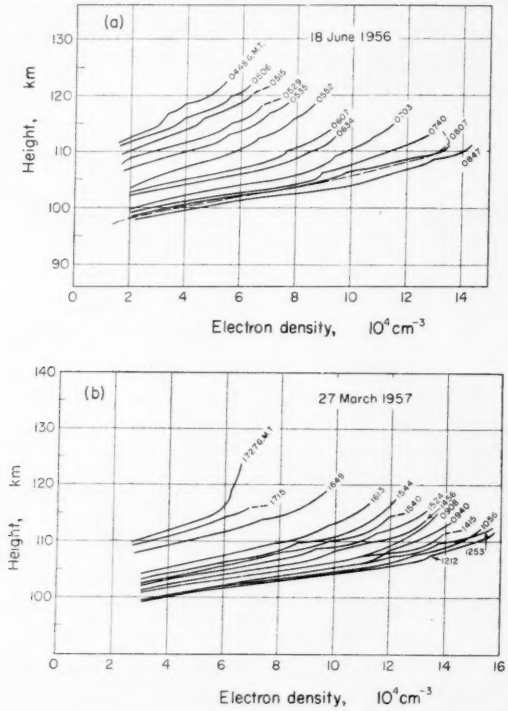

Fig. 1. Variation of the shape of the E-layer on a summer and a spring day at Cambridge (latitude 52°N).

the curves shows the distribution when the analysis was extended onto the falling portion of the $h'(f)$ curve.

3.2.1. *Comparison with ideal Chapman layer.* In Fig. 1(a) the dotted curve is that computed for a Chapman layer in equilibrium with scale height $H = 7{\cdot}5$ km, with N_m fitted to the measured value at 0807 GMT. This curve corresponds adequately to the experimental curve and, by making use of the standard expressions of CHAPMAN, it can be shown that it would correspond to a height (h_0) of the peak for overhead sun of 108 km. With this simple comparison of shapes it is difficult to allow for recombination and for changes of H or α with height, and a more detailed comparison with CHAPMAN's theory will be attempted below.

On the equilibrium approximation the height h_m of the maximum of a Chapman layer is given by (CHAPMAN, 1931):

$$h_m \simeq h_0 + \mathrm{H} \,.\, \ln [Ch(\chi)] \qquad (1)$$

where h_0 is the height of maximum ionization when the sun is overhead, and $Ch(\chi)$ is Chapman's grazing incidence integral (CHAPMAN, 1931; WILKES, 1954). In Figs. 2(a) and (b) the heights of the maxima in Fig. 1 are plotted against ln $[Ch(\chi)]$. The height of the maximum changes in an approximately Chapman fashion, and the slope of a line through the points gives another estimate of the value of H. The dashed lines in the figures show the equilibrium variations for a Chapman layer with $H = 7{\cdot}5$ km and $8{\cdot}5$ km, respectively. We see that there is no sign of a marked recombination lag. The height found for the maximum is not

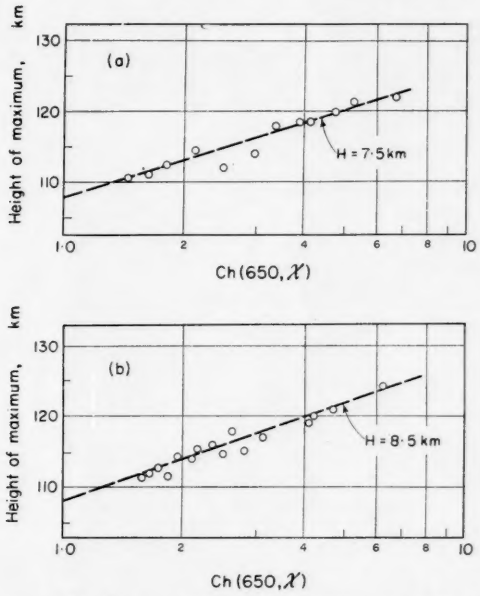

Fig. 2. Dependence of the level of maximum ionization on solar elevation. The dashed lines show the equilibrium behaviour of a Chapman layer.

very reliable, for the errors of measurement are greatest when the echo is greatly retarded and absorbed; or there can be an "abnormal" stratum which makes the penetration of the layer incomplete. Thus the values of h_m provide only approximate values for H and h_0.

GRACE (1951) found that when $h'(f)$ curves measured in Pennsylvania were analysed by the method of KELSO (1952) (neglecting the magnetic field) the height of the maximum remained at a "relatively constant level" for most of the day. The present measurements do not support this observation, and it is difficult to explain the difference. It is unlikely to be due to the fact that GRACE did not allow for the earth's magnetic field; nor is it likely to result from the allowance for D-region retardation in the Cambridge analysis (important only at frequencies well below the penetration frequency, as shown in the Appendix). The difference probably arises in the measurement of the $h'(f)$ curves; in GRACE's manual measurements, at 100 kc/s intervals, it would have been more difficult to recognize disturbances of the $h'(f)$ curve.

The most detailed, and straightforward, comparison with CHAPMAN'S theory can be made by comparing the variation of N with time at a constant height with the computed equilibrium variation. At a constant altitude we have the continuity equation (neglecting drift effects for the present):

$$\frac{\partial N}{\partial t} = q_0 \,.\, \exp\left[1 - z - Ch(\chi).e^{-z}\right] - \alpha N^2 \qquad (2)$$

where q_0 is the maximum rate of electron production for $\chi = 0$ and $z = (h - h_0)/H$.

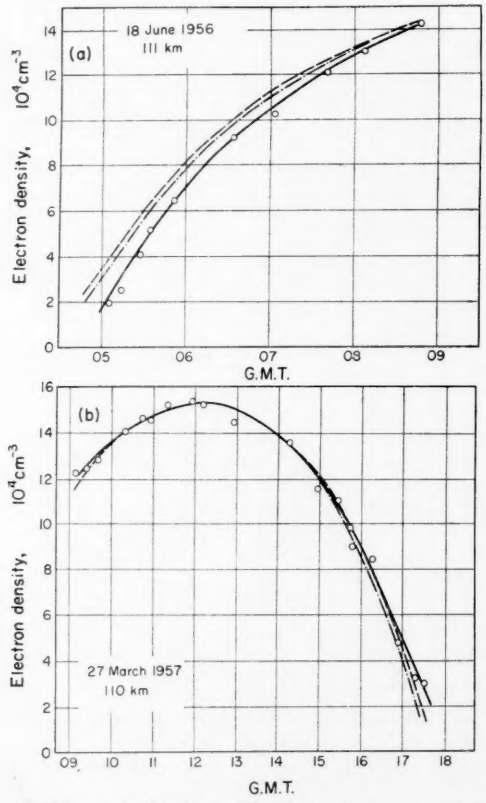

Fig. 3. Variation of E-layer ionization with time at a constant height: ———— equilibrium variation for a Chapman layer with $z = 0{\cdot}4$ in (a), $0{\cdot}15$ in (b); —·—·— equilibrium variation for a layer in an atmosphere with $dH/dh = 0.2$, for (a) $\zeta = 0{\cdot}5$, (b) $\zeta = 0{\cdot}23$.

In Fig. 3(a) the variation of N at a height of 111 km on 18 June 1956 is shown. To compare the curve with equation (2) we must find values for the three parameters q_0, z and α. We can estimate the value of z and q_0/α from the later curves in Fig. 1, which should be close to equilibrium. Comparison of the shape of the later curves with Chapman equilibrium curves gives an estimate of H and h_0, and so of z; at 111 km the value of z found in this way is near $0{\cdot}4$. The dashed line in Fig. 3(a) shows the equilibrium variation for $z = 0{\cdot}4$ with q_0/α chosen to fit the experimental point at 0845 GMT. The variation of N is seen to be reasonably similar to the

shape of the Chapman curve. Thus the loss process is sure to be one of recombination, and from the time lag between the measured and calculated curves we can estimate that the recombination coefficient is about $1{\cdot}2 \times 10^{-8}$ cm^3 sec^{-1}. Fig. 3(b) shows a similar comparison for 27 March 1957; the recombination lag appears to be smaller, corresponding to $\alpha = 2{\cdot}3 \times 10^{-8}$ cm^3 sec^{-1}.

We see from these two examples that the recombination lag is not much greater than the experimental uncertainties. Also a small uncertainty in the value of z is found to lead to a large uncertainty in the value found for α.* But the

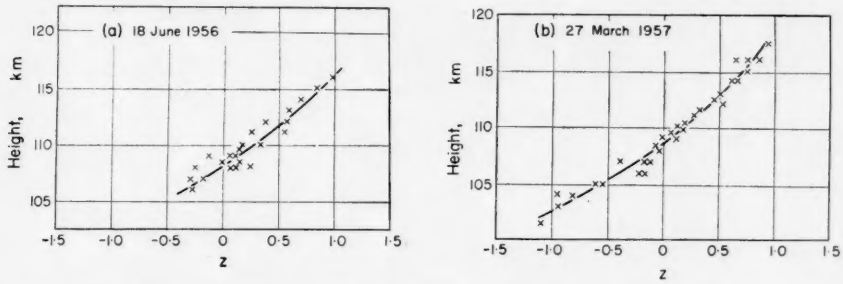

Fig. 4. Variation of Chapman's parameter $z = (h - h_0)/H$ with altitude.

measurements are not accurate enough to enable us to deduce a unique pair of values of z and α from $N(t)$ curves alone, and the simple method of comparison described will lead to errors if the scale height varies with altitude.

The most probable value of z at any height can be found from a comparison of the shape of the $N(h)$ curves at different times, for we have seen that only far from noon do recombination effects become measurable. A method was adopted for a direct determination of z, based on putting $\partial N/\partial t = 0$ in equation (2) and differentiating with respect to z, then:

$$e^{-z} \simeq \cos\chi \left(1 + \frac{2}{N} \cdot \frac{\partial N}{\partial Z}\right). \tag{3}$$

Thus from the slope of the $N(h)$ curves we can find the values of z at different heights. A value of the scale height must first be assumed, as from a simple comparison of shapes or from the variation of h_m with $Ch(x)$, to compute $\partial N/\partial z$. If the values of z are found at different levels the assumed H can be corrected, and the values of z redetermined. The calculations are simple, and the successive approximations for H converge rapidly.

In Fig. 4(a) the values of z determined from the later $N(h)$ curves of Fig. 1(a) are shown. The scale height (dh/dz) near 111 km is about 7·5 km and, although there is quite a scatter of the points about the mean line, the most probable value of z at 111 km is 0·4. The values of z deduced from the midday curves on 27 March 1957 are shown in Fig. 4(b).

For other summer and spring days the results were very similar to the examples discussed above. In Fig. 5(a) the crosses show the values of z determined from the

* In Fig. 3 (a) a change in z from 0·4 to 0·35 increases the estimate of α from $1{\cdot}2 \times 10^{-8}$ to $1{\cdot}5 \times 10^{-8}$.

$N(h)$ curves for 6 days. The scatter in the points is due mainly to errors in the measured group heights (± 1 km under most conditions); there is also likely to be some spread introduced by tidal effects, and by departures of the detailed shape of the layer from a simple Chapman profile. On all days the $N(t)$ curves were similar in shape to Chapman curves; the values of α, corresponding to the values

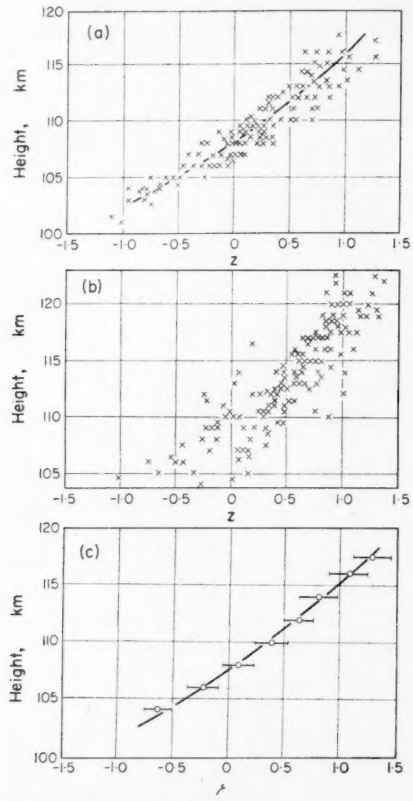

Fig. 5. (a) Values of Chapman's parameter z for summer and spring days. (b) Values of z for winter and autumn days. (c) Mean values of the modified parameter ζ when dH/dh is assumed to be 0·2. Continuous line is theoretical curve for $H_0 = 7$ km at 107·5 km and $dH/dh = 0{\cdot}2$.

of z deduced from equation (3), were found to range from $0{\cdot}8 \times 10^{-8}$ to $2{\cdot}3 \times 10^{-8}$ cm^3 sec^{-1}.

In autumn and winter the behaviour was found to be far less regular. In winter in particular the $h'(f)$ curves had a more complex shape, and the values of z were scattered more widely for the individual days. The results for 4 days are shown in Fig. 5(b). The winter $N(t)$ curves departed somewhat from the Chapman shape. The scatter in the measured $N(t)$ points and the greater uncertainties as to the values of z made it impossible to make a useful estimate of the recombination coefficient.

3.2.2. *Allowance for non-Chapman effects.* The above comparison with the

ideal Chapman theory has shown a moderate agreement and indicated that time-delays due to recombination are very small. But when a more detailed comparison is made definite departures from Chapman behaviour are found. The most striking is that the values of z determined from equation (3) do not increase linearly with height. Also, over the limited height range for which prolonged $N(t)$ curves could be drawn, the values found for α tended to be smaller at the greater heights. However, no comparable change was found in the values of (q_0/α) deduced from the midday points, or from the penetration-frequency measurements discussed in Section 4.2.

It is most likely that in the E-region both the scale height and recombination coefficient vary with altitude, and that the electron distribution is modified by drift effects (see ROBINSON, 1959). A complete description of the behaviour of the layer in such circumstances may require up to seven parameters. In view of the limited experimental accuracy we shall not attempt to include all possible variations or try to deduce these seven parameters. We can, however, set limits to the magnitudes of the height gradients of H and α, and the effect of drifts.

Scale height. Let us first consider the effect of a gradient of scale height within the E-region. If α were constant and drift were small the measurements plotted in Fig. 5(a) would indicate an increase of scale height with altitude. Direct measurements of H using rockets (HOROWITZ and LAGOW, 1957) have shown that H certainly increases with height. In an atmosphere where H is not constant the production of electrons will not follow the simple Chapman expression used earlier for the determination of z. NICOLET and BOSSY (1949), GLEDHILL and SZENDREI (1950), and others have shown that for the case of a linear increase of H with height the production function has the form:

$$q = q_0 \cdot \exp\{(1 + dH/dh)[1 - \zeta - e^{-\zeta} \cdot Ch(\chi)]\} \tag{4}$$

where ζ is defined by $\rho H = \rho_0 \cdot H_0 \cdot e^{-\zeta}$, ρ_0 and H_0 being the density and scale height at the level where ζ is taken to be zero. Equation (3) then becomes:

$$e^{-\zeta} \simeq \cos\chi \left[1 + \frac{2}{N(1 + dH/dh)} \cdot \frac{\partial N}{\partial \zeta}\right]. \tag{5}$$

The values of ζ have been computed from the measurements for various assumed values of dH/dh. At any level the value of ζ from (5) is slightly greater than the value of z from (3), the increase being greatest below the level $\zeta = 0$. In Fig. 5(c) are shown the mean values of ζ found when dH/dh was set equal to 0·2. The continuous line on the figure is a theoretical curve for the case where $dH/dh = 0{\cdot}2$ and $H_0 = 7$ km at 107·5 km. The values of ζ are seen to lie very close to this curve.

In Table 1 the values of H determined from the mean points in Fig. 5(c) are compared with the scale heights determined directly by rocket measurements (HOROWITZ and LAGOW, 1957) and from observations of meteor trails (KAISER and EVANS, 1955). Although we have ignored any gradient of α and any drift effects, the E-layer measurements are seen to be in fair agreement with the rocket measurements, the value at the lowest height appearing to be somewhat smaller. At the lower levels the retardation in the D-region has its greatest effect, and if we have underestimated this retardation the lower parts of the $N(h)$ curves would be too

flat. More extensive measurements of the extraordinary $h'(f)$ curves than those used here would provide a valuable check on the amount of retardation which occurs.

Recombination coefficient. If there is a gradient of scale height the production function given by equation (4) should be used in comparing the measured $N(t)$ curves with calculated equilibrium curves. Equilibrium curves based on (4) have

Table 1. Scale heights in the E-region

Altitude (km)	E-Layer observations* (km)	Rocket measurements† (km)	Meteor observations‡ (km)
100	—	6·3	7·0
102·5	—	6·5	7·3
105	6·3	6·8	7·5
107·5	7·0	7·1	—
110	7·6	7·4	—
112·5	8·0	7·7	—
115	8·5	8·25	—
117·5	9·0	8·9	—
120	—	9·4	—

* All values $\pm$ 0·5 km
† Horowitz and LaGow (1957).
‡ Kaiser and Evans (1955).

been computed with the values of ζ from (5) and with $dH/dh = 0{\cdot}2$. As shown in Figs. 3(a) and (b) the modified equilibrium curves lie closer to the morning measurements and further below the afternoon measurements than when H is taken constant. The values found for α, which spread over a range of 2 : 1 at different times on the same day, are listed in order of increasing altitude in Table 2. For comparison the values found when H is taken constant are also given.

The mean value found for α when $dH/dh = 0{\cdot}2$ is $(2{\cdot}0 \pm 0{\cdot}5) \times 10^{-8}$ cm^3 sec^{-1}, that when H is constant is $(1{\cdot}5 \pm 0{\cdot}5) \times 10^{-8}$. In each case it appears that α might decrease with height, the rate of decrease being the same for each assumption about H. However, because of the limited number of measurements and the great uncertainty in the individual values of α, little significance is attached to this apparent variation of α with height. Recombination effects are so small that drifts or other disturbances in the region could greatly modify the apparent α.

Grace (1951) has determined the values of α from $N(h)$ curves for Pennsylvania, using a direct extension of the method suggested by Appleton (1937). Grace also found that α decreased with altitude, and his measurements for a spring day are shown in the third column of Table 2. They decrease more rapidly with height than is the case for the present measurements.

The non-constancy of the values of α found from the Cambridge measurements reduces the certainty of the scale-height determinations. But till more reliable estimates of any gradient of α can be made it would not be fruitful to recompute the values of H. An increase in α at the lower levels would flatten the base of the

layer and this could well account for the difference between the value found for H at 105 km and the rocket value. A limit to the gradient of α could be set from a comparison of the mean values in the E- and $F1$-layers (MINNIS, 1956b). Another estimate of the gradient will be made in Section 4.2.

Estimate of drift effects. Analysis of routine values of f_0E has lead to results which suggest that vertical transport of electrons is important in the E-region

Table 2. Estimates of recombination coefficient

Altitude (km)	Recombination coefficient ($cm^3\ sec^{-1} \times 10^{-8}$)		
	Cambridge $dH/dh = 0$	Cambridge $dH/dh = 0{\cdot}2$	GRACE (1951)
108	2·0	2·8	1·7
108	2·0	3·0	
109·5	1·1	1·9	
110	2·3	1·9	1·0
111	1·25	1·9	
111	1·0	1·6	
111	1·7	3·0	
112	—	—	0·8
115	1·1	1·5	0·63
115	1·4	0·9	
116	0·8	1·7	
120	—	—	0·57

(APPLETON *et al.*, 1955; BEYNON and BROWN, 1956; SHIMAZAKI, 1957, 1958). Our interest here is that drift effects are likely to modify our estimates of α and, to a lesser extent, of H.

On any one day the values found for α were not independent of time, although there appeared to be no regular dependence of α on t. It is of interest to see how a constant drift velocity, for example, would modify the values of α. In the presence of a constant vertical drift velocity w the continuity equation becomes:

$$\frac{dN}{dt} = \alpha\left[\frac{q}{\alpha} - N^2\right] - w \cdot \frac{\partial N}{\partial h} \tag{6}$$

so that measurements of N, dN/dt and $\partial N/\partial h$ allow α and w to be determined from the computed equilibrium values of q/α. It was found to be possible to describe the time variation of N at a constant height with fixed values of α and w. In the six cases examined the drift term $w \cdot \partial N/\partial h$ was found to be of the same magnitude as the term dN/dt, so that the inclusion of drift could change the value found for α by a factor of 2. The numerical values of w determined from equation (6) ranged from $+3$ m/sec to -5 m/sec.

It can be shown that a constant vertical drift of the order of 5 m/sec has negligible effect on the shape of the layer and so on the scale heights. In Fig. 6 is shown the measured $N(h)$ curve at 0847 GMT on 18 June 1956, and a curve

corrected for a drift $w = 5$ m/sec, using equation (6) with $dN/dt = 0$ and with α taken to be 2×10^{-8} cm^3 sec^{-1}. The change introduced by the drift correction would only modify the values of ζ by an amount of the same order as the experimental uncertainties. A positive drift, as in the case shown, would slightly increase the measured scale heights, while a negative drift would decrease them.

We thus conclude that there are likely to be drift effects in the E-region which are comparable with the effects of recombination. Both are little greater than the

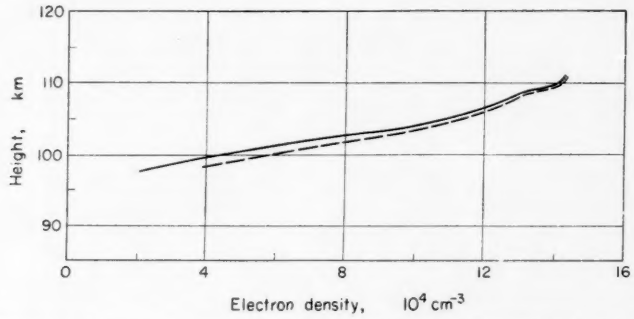

Fig. 6. Measured layer profile (continuous line) and modification (dashed line) by a constant vertical drift of 5 m/sec, assuming $\alpha = 2 \times 10^{-8}$ cm^3 sec^{-1}.

experimental errors in the present investigation and so their numerical values are not reliably known. It appears that drift effects of the order of magnitude found will not greatly modify the shape of the layer, and so are not expected to change the values found for the scale heights. No attempt has been made here to include a *gradient* of drift velocity. It can be shown that in some circumstances a velocity gradient will greatly distort the layer (Robinson, 1960).

4. Accurate Measurements of the Penetration Frequency

The determination of $N(h)$ curves has been seen to yield valuable information about the E-layer, but considerable labour is required to compute each curve. Also disturbances of the $h'(f)$ curve, such as are caused by E_s, made it impossible to deduce the $N(h)$ curve with adequate accuracy on about 90 per cent of the records; but on many of these the penetration frequency could be measured without difficulty. We shall now discuss what information can be gained directly from the $h'(f)$ curves, particularly from determinations of the penetration frequency.

The identification of the true penetration frequency is sometimes very difficult (see Robinson, 1960), and the measurements reported here were confined to those cases where the penetration could be identified unambiguously and where no extrapolation or interpolation was required.

4.1. *Day-to-day variations*

The difficulty of identifying the penetration leaves some doubt as to how great are the day-to-day variations of the maximum electron density of the normal E-layer. To investigate this point the Cambridge records were examined for several periods during the spring of 1957 when a simple penetration was observed on most

days. The measurements were made from records taken within 2 or 3 min of times giving the same solar elevation. From 15 February to 1 April the maximum variation of the penetration frequency was found to be $\pm 2\frac{1}{2}$ per cent. From 13 April to 11 May the maximum variation was ± 3 per cent.

The scatter in these cases, where the penetration is clear, is less than half that found by BIBL (1951a) and RAWER and ARGENCE (1953) when all types of records were considered. It is considerably less than that in the daily values of the routine hourly measurements published by ionospheric observatories. The variation found here for clear penetrations is of the same order as that found by MINNIS (1956a, 1957) when the average value of $f_0E \,.\, \sec^1/n\chi$ was computed from the routine hourly measurements for each day. We are thus led to see what information can be gained from accurate penetration frequency measurements throughout a single day.

4.2. *Diurnal variation of the penetration frequency*

Measurements were made of the penetration frequency for the ordinary ray on those days when the reflections were clear and showed no marked complications. Records were taken at 5 min intervals throughout the day, and measured to an accuracy of 25 kc/s. Examples of the variations found are shown in Fig. 7. Very few of the measured points lay more than 50 kc/s away from smooth curves drawn through them, showing that the diurnal variation is particularly uniform. There is a very flat maximum near noon, but because of the spread in the measurements there is an uncertainty of about 10 min in finding the time of maximum ionization. The centre of symmetry of the diurnal variation can be determined much more accurately. For the 5 months December 1956 to April 1957 the centres of symmetry of the curves lay within ± 3 min of apparent noon.

VOL. 18 1960

For the equilibrium approximation to CHAPMAN's (1931) theory of layer formation, the variation of the penetration frequency (ordinary ray) is described by:

$$\frac{\pi^2 m^2}{e^4} \cdot f_0^4 = N_m^2 \simeq \frac{q_0}{\alpha} \,.\, \cos\chi. \tag{7}$$

The curves corresponding to (7) are shown by the dashed lines in Fig. 7, being fitted to the experimental points at noon. For most of the days studied the measurements lay within 100 kc/s of the dashed curve, being closer in the afternoon than in the morning. This indicates that the quantity (q_0/α) does not vary markedly throughout the day, and confirms that the measurements discussed in Section 3.2.2 do not give the variation of the actual recombination coefficient with height.

A great number of workers have shown (see ROBINSON, 1959) that the monthly median values of penetration frequency published by the ionospheric observatories fit the empirical expression $f_0 \propto \cos^{1/3}\chi$ better than equation (7). All the measurements at Cambridge tended to lie between the curves given by the theoretical and empirical expressions. The measurements for individual days (mean of points equally spaced from apparent noon) were in good agreement with the expression $f_0 \propto \cos^{0.285}\chi$ which HARNISMACHER (1950) has deduced from monthly median routine data for stations near the latitude of Cambridge. The departure of the exponent in these expressions from the Chapman value can be easily accounted for by a variation of the scale height or recombination coefficient with altitude.

However, observation of the penetration frequency alone does not enable any distinction between these two cases to be made.

If H varies linearly with altitude the production function is given by equation (4); if α remains constant the equilibrium variation then has the form:

$$N_m \simeq \left(\frac{q_0}{\alpha}\right)^{1/2} \cdot \cos^{0\cdot5(1+dH/dh)} \chi. \tag{8}$$

The measured variation $f_0 \propto \cos^{0\cdot285} \chi$ would thus correspond to a value of dH/dh

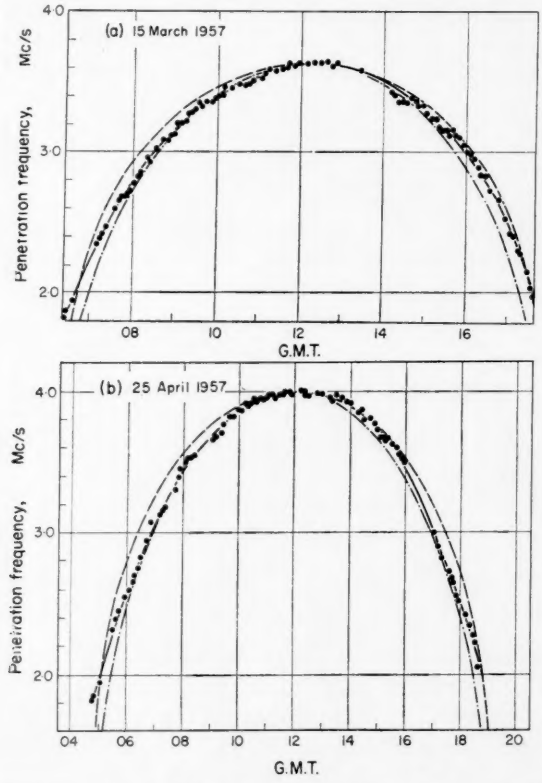

Fig. 7. Diurnal variation of E-layer penetration frequency at Cambridge: ———— equilibrium curve for Chapman layer, $f_0 \propto \cos^{1/4} \chi$; —·—·— empirical expression $f_0 \propto \cos^{1/3} \chi$.

of 0·14. The value determined from the layer shapes when α was assumed constant was 0·20. The difference here may be accounted for by the presence of a gradient of α. If α decreased with altitude the exponent in $f_0 \propto \cos^n \chi$ would be *reduced*. The effect on the determination of ζ from equation (5) would be that $\partial N/\partial\zeta$ would be increased; this would have most effect on the value found for ζ when $\partial N/\partial\zeta$ was large, and would thus lead to a reduction in the values of ζ determined from the lower part of the layer—giving a *larger* apparent gradient for H. If the true gradient of H lies between the values found by the two methods, the measured

values would indicate a decrease in α by about 3 per cent scale height. A variation of this order could easily be accounted for by a change of temperature with height. A temperature gradient must be present to account for the magnitude of the scale height gradient.

The penetration frequency measurements on individual clear days show a high degree of symmetry about noon. HARNISMACHER (1950, 1955) has found a comparable degree of symmetry in monthly median data. The symmetry implies a

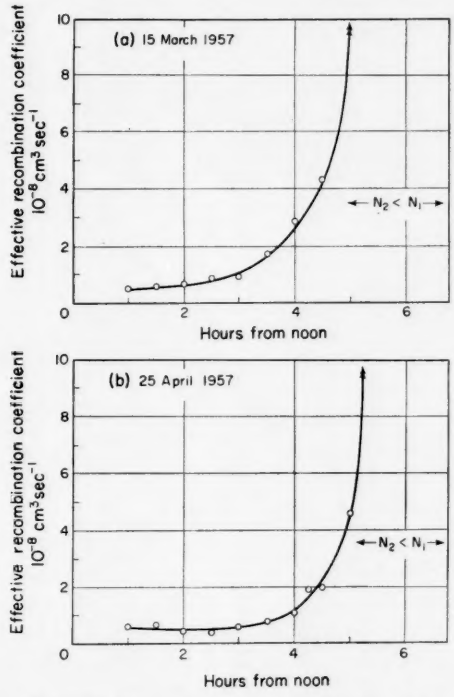

Fig. 8. Values of the effective recombination coffiecient α' determined from Fig. 7.

rapid recombination so that the ionization follows the production function with little time lag. If a time lag can be measured it is possible to estimate the value of α. APPLETON (1937) has shown that α can be estimated from the difference between the ionization at times in the morning and afternoon giving the same values of χ. If morning values are given the subscript 1, afternoon values the subscript 2, the apparent α is

$$\alpha' = \frac{dN_1/dt - dN_2/dt}{N_2^2 - N_1^2}. \tag{9}$$

In Fig. 8 are shown the values of α' determined from the measurements in Fig. 7. Very close to noon no useful estimate of α' can be made because of the errors involved in determining the denominator of equation (9) when $N_1 \simeq N_2$. On all the winter and spring days studied the values of α' were reasonably constant from 3 to 4 hr from noon, being somewhat less than 1×10^{-8} cm^3 sec^{-1}. Farther from

noon the values of α' rose sharply. Instead of N_2 and N_1 separating steadily away from noon they tended to come closer together about 4 hr from noon; farther still from noon the afternoon value of N_m fell below the morning value. The increase in the value of α' for times far from noon has been noted in monthly median data by Seaton (1948) and Appleton (1955). The more frequent and accurate measurements on clear days have revealed that α' is comparatively constant for the central part of the day, and that ultimately the afternoon penetration frequencies become less than the morning values.

The values found for α' over the middle part of the day are smaller than the values of α determined in Section 3, or those deduced from eclipse observations (Piddington, 1951; Minnis, 1956a). Both the $N(h)$ measurements and the dependence of N_m on cos χ show that the actual recombination coefficient does not vary in the way shown in Fig. 8. The negative values of α' show that it does not provide a reliable estimate of the real α. The negative values could betray a drift effect. Appleton and Lyon (1955) show that at the maximum of a layer a drift produces a change:

$$\frac{\partial N_m}{N_m} = -\frac{\partial w/\partial h}{2\alpha N_m} - \frac{1}{4H^2} \cdot \left(\frac{w}{2\alpha N_m}\right)^2 . \tag{10}$$

The observed difference between morning and afternoon values of N_m requires a *change* in the value of w of from 5 to 10 m/sec if $\partial w/\partial h$ is zero. It should be noted that a simple reversal of the sign of w will not produce a differential effect unless there is also a gradient of velocity.

VOL
18
196

4.3. *Seasonal anomaly*

At Slough Beynon (1955) has found that the variation of f_0E as χ changes with the season is accurately described by the Chapman expression (7). The diurnal variation of f_0E observed at Slough and Cambridge is, however, different.

In an attempt to understand the different dependence on cos χ $N(h)$ curves were computed for twenty-four clear days during the year, at times giving the same value of χ. From these curves the scale heights were determined. For the summer months the average value of H was $7{\cdot}8 \pm 0{\cdot}3$ km; for the winter months the value was $7{\cdot}2 \pm 0{\cdot}5$ km. The smaller value of the scale height in winter could explain the difference between the seasonal and diurnal variation of N_m with cos χ. The winter values of the scale height are not very certain, mainly because the occurrence of E_s and greater interference made it difficult to obtain accurate measurements in winter. Some support for a drop in E-region temperatures in winter is provided by recent rocket flights at Churchill (59°N) (LaGow *et al.*, 1958).

5. Conclusion

From accurately-measured $h'(f)$ curves it was possible to deduce the distribution of electrons in the E-layer with moderate accuracy. From the distribution it is possible to obtain information about the properties of the E-layer which cannot be obtained from the most careful penetration-frequency measurements.

To a first approximation the diurnal behaviour of the layer is in agreement with Chapman theory. The height of the maximum follows the changes in the elevation

of the sun during the day, contrary to the result reported by GRACE (1951). A detailed comparison of the measurements with Chapman theory showed that, if the recombination coefficient were constant, the scale height must increase with altitude. Comparison with accurate penetration-frequency measurements showed that the recombination coefficient could not vary by more than a few per cent in a scale height. The scale heights determined from the layer shapes agree closely with rocket measurements. The magnitude of the recombination coefficient was estimated from the variation of the layer shape with time. The recombination lag could be measured only in spring and summer, the mean value of the recombination coefficient in these seasons being $(2{\cdot}0 \pm 0{\cdot}5) \times 10^{-8}$ cm^3 sec^{-1}. Owing to the limited experimental accuracy the variation of the recombination coefficient with height is very uncertain. It is found that there may be drift effects in the E-region which are comparable with the effects of recombination, the drift velocities being of the order of 5 m/s.

Acknowledgements—The work described in this paper was carried out as part of a programme of E-region investigations being conducted at the Cavendish Laboratory, Cambridge. I am very grateful to the Royal Society for the award of a Rutherford Memorial Scholarship to enable me to work at Cambridge. Throughout this investigation I have profited greatly from the guidance and criticism of Mr. J. A. RATCLIFFE and Dr. K. WEEKES, of the Cavendish Laboratory.

VOL. 18 1960

APPENDIX

Group Retardation in an Exponential Layer

If the electron density N increases exponentially from its value N_1 at a height h_1, we have:

$$N = N_1 \,.\, \exp\left(\frac{h - h_1}{H}\right)$$

where the parameter H is a "scale height" for the distribution. Then

$$h - h_1 = H \,.\, \ln\,(N/N_1) \tag{1}$$

The group retardation suffered by a wave of frequency f between the level h_1 and its level of reflection is:

$$h' - h_1' = \int_{h_1}^{h_R} \mu' \,.\, dh \tag{2}$$

and since, from (1), $dh/H = dN/N$,

$$h' - h_1' = \int_{N_1}^{N_R} \mu' \,.\, \frac{H}{N} \,.\, dN$$

If we now write $x = Ne^2/\pi m f^2$,

$$h' - h_1' = H \,.\, \int_{x_1}^{1} \frac{\mu'}{x} \,.\, dx \tag{3}$$

When N_R and N_1 are fixed, we can write

$$\int_{x_1}^{1} \frac{\mu'}{x} \,.\, dx = I(x_1)$$

equations (1) and (3) then give:

$$h - h_1 = \frac{\ln(N_R/N_1)}{I(x_1)} \cdot (h' - h_1') \tag{4}$$

We can apply equation (4) to fit an exponential tail to the E-layer measurements, as discussed in Section 3.1. If N_1 is taken to be 241 per cm^3 (corresponding to the reflection of 16 kc/s), we know that for a wave of frequency 1·2 Mc/s, $h_1' = h_1$ and h_1 will be approximately equal to the "phase height" for 16 kc/s. Then a measurement of h_1 and of the group height h' on 1·2 Mc/s enables us to determine the true height of reflection on 1·2 Mc/s, for:

$$h = h_1 + \frac{\ln(N_R/N_1)}{I(x_1)} \cdot (h' - h_1)$$

For the frequencies concerned, $\ln(N_R/N_1) = 4{\cdot}31$, and the value of $I(x_1)$, found by graphical integration (using the values of μ' given by Shinn and Whale, 1952), is 4·66. With these:

$$h = h_1 + 0{\cdot}925\,(h' - h_1) \tag{5}$$

The point (h, N_R) is then a starting point for the determination of the electron distribution from the rest of the observed $h'(f)$ curve.

It is seen from equation (5) that an error of 5 km in determining h_1 produces a change in h of only 0·4 km. Thus the assumption that h_1 is given by the "phase height" on 16 kc/s is unlikely to introduce a significant error in our determination of h.

References

Appleton E. V.	1937	*Proc. Roy. Soc.* A **162,** 451.
Appleton E. V.	1955	*Proceedings of the Mixed Commission on the Ionosphere, Fourth Meeting,* p. 14. U.R.S.I., Brussels.
Appleton E. V. and Lyon A. J.	1955	*Physics of the Ionosphere,* p. 20. Physical Society, London.
Appleton E. V., Lyon A. J. and Turnbull A. G.	1955	*Nature, Lond.* **176,** 897.
Becker W.	1956	*Alg. Electr. Ubertrag.* **10,** 207.
van Berkel P. L. M.	1954	*Tijd. Ned. Radiogenootsch.* **19,** 305.
Beynon W. J. G.	1955	*Proceedings of the Mixed Commission on the Ionosphere, Fourth Meeting,* p. 31. U.R.S.I., Brussels.
Beynon W. J. G. and Brown G. M.	1956	*Nature, Lond.* **177,** 583.
Bibl K.	1951a	*Ann. Géophys.* **7,** 208.
Bibl K.	1951b	*Ann. Géophys.* **7,** 265.
Bracewell R. N., Budden K. G., Ratcliffe J. A., Straker T. W. and Weekes K.	1951	*Proc. Instn Elect. Engrs* III, **98,** 221.
Brailsford J. D.	1938	*Marconi Rev.* No. 68, 10.
Chapman S.	1931	*Proc. Phys. Soc.* **43,** 26, 483.
Fejer J. A.	1955	*J. Atmosph. Terr. Phys.* **7,** 322.
Gardner F. F. and Pawsey J. L.	1953	*J. Atmosph. Terr. Phys.* **3,** 321.
Gledhill J. A. and Szendrei M. E.	1950	*Proc. Phys. Soc.* B **63,** 427.
Grace C. H.	1951	*J. Geophys. Res.* **56,** 452.

Halliday E. C.	1936	*Proc. Phys. Soc.* **48,** 421.
Harnismacher E.	1950	*C.R. Acad. Sci., Paris* **230,** 1301.
Harnismacher E.	1955	*C.R. Acad. Sci., Paris* **240,** 553.
Horowitz R. and LaGow H. E.	1957	*J. Geophys. Res.* **62,** 57.
Jackson J. E.	1956	*J. Geophys. Res.* **61,** 107.
Kaiser T. R. and Evans S.	1955	*Ann. Géophys.* **11,** 148.
Kelso J. M.	1952	*J. Geophys. Res.* **57,** 357.
King G. A. M.	1957	*J. Atmosph. Terr. Phys.* **11,** 209.
LaGow H. E., Horowitz R. and Ainsworth	1958	IGY Rocket Report Series, No. 1. National Academy of Sciences, Washington.
Lyon A. J. and Moorat A. J. G.	1956	*J. Atmosph. Terr. Phys.* **8,** 309.
Minnis C. M.	1956a	*J. Atmosph. Terr. Phys.* **9,** 36.
Minnis C. M.	1956b	*Solar Eclipses and the Ionosphere*, p. 204. Pergamon Press, London.
Minnis C. M.	1957	*J. Atmosph. Terr. Phys.* **10,** 229.
Naismith R. and Bailey R.	1951	*Proc. Instn Elect. Engrs.* III, **98,** 11.
Nicolet M. and Bossy L.	1949	*Ann. Géophys.* **5,** 275.
Piddington J. H.	1951	*J. Geophys. Res.* **56,** 409.
Piggott W. R.	1955	*Wireless Engr.* **32,** 164.
Rawer K. and Argence E.	1953	*Ann. Géophys.* **9,** 1.
Robinson B. J.	1959	*Rep. Progr. Phys.* **22,** 241.
Robinson B. J.	1960	*J. Atmosph. Terr. Phys.* in press.
Seaton S. L.	1948	*J. Meteorol.* **5,** 204.
Seddon J. C.	1958	*J. Geophys. Res.* **63,** 209.
Shimazaki T.	1957	*J. Radio Res. Lab.* **4,** 37.
Shimazaki T.	1958	*J. Radio Res. Lab.* **5,** 35.
Shinn D. H. and Whale H. A.	1952	*J. Atmosph. Terr. Phys.* **2,** 85.
Sturley K. R.	1947	*Radio Receiver Design* Pt. I, pp. 328–329. Chapman & Hall, London.
van Voorhis S. N.	1948	*Microwave Receivers*, p. 583. McGraw-Hill, New York.
Waynick A. H.	1957	*Proc. Inst. Radio Engrs., N.Y.* **45,** 741.
Whale H. A.	1951	*J. Atmosph. Terr. Phys.* **1,** 244.
Wilkes M. V.	1954	*Proc. Phys. Soc.* B **67,** 304.

VOL. 18 1960

Journal of Atmospheric and Terrestrial Physics, 1960, Vol. 18, pp. 234 to 252. Pergamon Press Ltd. Printed in Northern Ireland

Equilibrium electron distributions in the ionospheric *F2*-layer

H. Rishbeth and D. W. Barron
Cavendish Laboratory, Cambridge

(*Received* 22 *February* 1960)

Abstract—In the *F*-region of the ionosphere, the electron density is controlled by the production of ionization by solar radiation, loss by recombination, and transport of ionization by electromagnetic drift movements and plasma diffusion. This paper is especially concerned with the factors which govern the *F2*-peak of electron density.

An electronic computer has been used to solve the relevant equations for conditions of equilibrium, such as may be approached in the day-time *F*-region. From the numerous examples considered, it is deduced that the maximum electron density, and the height at which it occurs, are such that the magnitudes of the production, loss and diffusion processes are approximately equal. The modifications produced by vertical electromagnetic drifts are discussed.

Most of the work relates to the simple case of an isothermal atmosphere, but the conclusions derived are found to be substantially true for a few more general models which have been considered.

1. Introduction

The density of ionization in the *F2*-layer of the ionosphere is known to be controlled by several processes, which may be listed as production, loss, vertical movement and ambipolar or plasma diffusion. The investigation described in this paper aims to show how the interplay of these processes determines the height distribution of ionization and, in particular, the situation of the peak of electron density.

For this purpose, only equilibrium conditions are considered. This is justified on the grounds that in temperate latitudes the *F*-region is in a state of quasi-equilibrium during most of the day: the rate of change of electron density is considerably smaller than the other terms in the equation of continuity, so that it is permissible as an approximation to neglect it.

It is now generally accepted that the *F1*- and *F2*-layers are formed by the same ionizing radiations, which give rise to a maximum of production in the *F1*-layer: the upward increase of electron density above this level is then supposed to result from a decrease of the loss coefficient. This hypothesis, due to Bradbury (1938), does not of itself account for the *F2*-peak of electron density*, and it was suggested by Yonezawa (1955) and Ratcliffe *et al.* (1956) that diffusion is responsible for the formation of this peak.

The behaviour of the *F2*-layer at night, under the influence of loss processes, diffusion and vertical movement, was discussed by Martyn (1956) and Duncan (1956). The more complicated day-time situation, which includes the production of ionization by solar radiation, was considered by Yonezawa (1958), who solved the relevant equations for a particular model atmosphere which led to solutions in terms of analytic functions. His calculations are important in showing that a

* A peak might be formed at a level where the gradient of the loss coefficient becomes small. This will occur where the rate of direct radiative recombination of electrons and O^+ ions exceeds that of the two-stage mechanism important at lower levels; but this is thought to occur well above the height of the *F2*-peak.

peak is formed by the action of diffusion, but do not reveal any general relationships between the parameters which determine the position and magnitude of the peak.

The equations relating to more general cases do not seem to be soluble in terms of analytic functions, but can be integrated numerically with a digital computer. In the investigation here described, the EDSAC 2 machine at the University Mathematical Laboratory, Cambridge, has been used to determine electron distributions for a series of model atmospheres.

The basic formulae required for this analysis are introduced in the next section. They are first stated in a general form, suitable for use with empirically-determined models of the atmosphere, but can be greatly simplified if certain assumptions are made. Most of the work refers to the special case of an isothermal atmosphere, but in Section 4.3 the more general equations are applied to an atmospheric model which was computed by Dr. K. WEEKES from rocket and satellite data.

The principal conclusions obtained from the work are summarized in Section 6. They do not seem to depend upon the particular atmospheric models employed, and may be applied to the conditions existing in the actual ionosphere. Detailed discussion will not, however, be attempted in this paper.

2. Formulation of the Equations

For conditions of equilibrium the well-known equation of continuity of electron density N may be written:

$$q - \beta N - M = 0 \tag{1}$$

in which q and β represent the production rate and loss coefficient, and M the effect of transport of ionization. Only vertical movements are considered, so that M is given by:

$$M = \frac{d}{dh} N(w + w_D). \tag{2}$$

Here, w is the upward component of the drift velocity due to electromagnetic motions, and is assumed independent of height; and w_D is the vertical component due to plasma diffusion. Motions due to thermal expansion and contraction of the atmosphere are excluded by the assumption of equilibrium.

It is convenient to measure altitude h from a reference level h_0, in terms of a co-ordinate z whose unit is the scale height H of the ionizable constituent of the atmosphere, so that

$$z = \int_{h_0}^{h} \frac{dh}{H}. \tag{3}$$

In subsequent work, the scale height will on occasion be assumed to possess a constant gradient, defined as $\gamma = dH/dh$. More often, this gradient will be assumed to be zero, as in an atmosphere of uniform temperature and composition, so that

$$z = \frac{h - h_0}{H}. \tag{4}$$

Throughout this paper, the level h_0 is taken to be that of maximum production for overhead sun, and is denoted by the suffix 0: the suffix m is used to refer to the level of the electron peak.

2.1 *Production and loss processes*

The production function for monochromatic radiation acting on a single ionizable constituent, of which the concentration is n and ionization cross-section A, is

$$q = S_\infty An \exp(-nAH \sec \chi) \tag{5}$$

where S_∞ is proportional to the flux of solar radiation incident at zenith angle χ at the top of a plane, horizontally-stratified atmosphere. Provided A does not vary too rapidly with wavelength, the equation may be applied to ionization by a finite band of wavelengths. When $\chi = 0$, the peak of production occurs at the level h_0, at which is satisfied the relation

$$n_0 AH_0 = 1 + \left(\frac{dH}{dh}\right)_0. \tag{6}$$

If the gradient $dH/dh = \gamma$ is independent of height, then $n \propto \exp[-z(1+\gamma)]$, and equation (5) reduces to the form (NICOLET, 1951):

$$q = q_0 \exp[(1+\gamma)(1 - z - \exp(-z)\sec\chi)] \tag{7}$$

which if $\gamma = 0$ is the familiar function derived by CHAPMAN (1931).

In accordance with present-day ideas, the ionizable constituent in the *F*-region is supposed to be atomic oxygen, O. Part of the ionizing radiation is absorbed by molecular nitrogen, but the resulting N_2^+ ions decay rapidly by dissociative recombination and do not contribute to the observed ionization. The O^+ ions are lost by a two-stage process involving the formation and subsequent dissociative recombination of molecular ions: the molecular gas participating in this process may be either N_2 or O_2. It is probable that the rate of loss in the *F2*-layer is proportional to the electron density N, the coefficient β depending on the concentration $n(M)$ of the molecular gases, so that

$$\beta = Kn(M). \tag{8}$$

This equation leads to a useful formula if the rate coefficient K is assumed independent of temperature and the scale height gradient is constant. If the scale heights of the molecular gases and of the ionizable constituent are in the ratio $1:k$, then

$$\beta = \beta_0 \exp[-z(k+\gamma)]. \tag{9}$$

If atomic oxygen and the molecular gases are fully mixed in the ionosphere then $k = 1$ in equation (9), but if there is diffusive equilibrium $k = 1{\cdot}75$ for N_2 or 2 for O_2. If the situation is part way between mixing and complete separation intermediate values of k may be appropriate. The "effective" value of k may be modified by temperature dependence of the rate coefficient K.

VOL
18
196

In the lower *F*-region, the two-stage process gives rise to a non-linear loss function which may be written as

$$l(N) = \frac{Kn(M)\alpha N^2}{Kn(M) + \alpha N} \tag{10}$$

(RATCLIFFE, 1956). There is a transition from the βN loss law of the *F2*-region to the αN^2 law applicable in *F1*, which occurs at the level where $Kn(M) \sim \alpha N$. Although most of the work described in this paper is concerned with the linear law, the formula (10) is used in one instance in Section 4.3.

2.2. *Plasma diffusion*

The mathematical formulae relating to plasma diffusion in the ionosphere are based on the equation for the relative velocity of diffusion of a binary gas mixture (CHAPMAN and COWLING, 1952): for a horizontally-stratified atmosphere this is

$$c_1 - c_2 = -\frac{n^2}{n_1 n_2} D_{12}\left[\frac{\partial(n_1/n)}{\partial h} + \frac{n_1 n_2 (m_2 - m_1)}{npp}\frac{\partial p}{\partial h} - \right.$$

$$\left. - \frac{\rho_1 \rho_2}{p\rho}(F_1 - F_2) + \frac{k_T}{T}\frac{\partial T}{\partial h}\right]. \tag{11}$$

Here, the symbols p, ρ, n and m denote pressure, density, concentration or number density, and molecular mass, respectively: with suffixes, they refer to one constituent gas; and without suffixes, to the gas as a whole. T denotes temperature, and F the force per unit mass due to external causes. For gravity, $F_1 - F_2$ vanishes; and although electromagnetic forces would contribute to equation (11), they are in this paper treated separately, and give rise to a vertical velocity w which is distinct from that due to diffusion (cf. equation (2)).

In the present context, one constituent is the plasma and the coefficient D_{12} is the ambipolar diffusion coefficient $D(h)$. The number density N of the plasma is small compared to that of the neutral atmosphere (n); and the last term of equation (11), representing thermal diffusion, is generally neglected. Under these circumstances, the left-hand side of equation (11) is the plasma diffusion velocity, w_D, and the equation becomes (SHIMAZAKI, 1957):

$$-w_D = D(h) \cdot \left[\frac{1}{N}\frac{dN}{dh} + \frac{1}{T}\frac{dT}{dh} + \frac{\mu}{H}\right]. \tag{12}$$

In this equation μ is the ratio of the mean molecular weights of the plasma and the ionized gas: if the two are chemically the same, then $\mu = \frac{1}{2}$. The coefficient D is given approximately by:

$$D = \frac{b\sqrt{T}}{n}\sin^2 I \tag{13}$$

where I is the angle of dip of the earth's magnetic field.

A useful quantity is the diffusion rate, defined as $d = D/H^2$, which has the dimension of (time)$^{-1}$, the same as that of β.

The contribution M_D of diffusion to the term M in the continuity equation may be derived by combining equations (2), (12) and (13). The equations for the most general case are complicated, but are simplified if the scale height gradient and the composition are independent of height, so that γ and μ are constant. In this case $(H/H_0) = (T/T_0) = \exp(\gamma z)$ and $(n/n_0) = \exp[-z(1+\gamma)]$ and so

$$d(z) = d_0 \exp[z(1 - \tfrac{1}{2}\gamma)]. \tag{14}$$

The contribution of diffusion to the movement term in equation (1) is then:

$$M_D = d(z)\left[\frac{d^2N}{dz^2} + (\phi + \psi)\frac{dN}{dz} + \phi\psi N\right] \tag{15}$$

where

$$\phi = \gamma + \mu \tag{16}$$

$$\psi = 1 + \tfrac{1}{2}\gamma \tag{17}$$

These expressions resemble those of SHIMAZAKI (1957). In the simplest case of an isothermal atmosphere with $\gamma = 0$ and $\mu = \frac{1}{2}$, the diffusion term takes a form similar to that derived by FERRARO (1945), viz.:

$$M_D = d_0 \exp(z)\left[\frac{d^2N}{dz^2} + \frac{3}{2}\frac{dN}{dz} + \frac{N}{2}\right]. \tag{18}$$

3. SOLVING THE EQUATIONS

If the forms adopted in the previous sections, for the special case $\gamma = 0$, $\mu = \frac{1}{2}$, $\chi = 0$, are inserted into the continuity equation (1), it becomes the second-order, linear differential equation:

$$d_0 \exp(z)\left[\frac{d^2N}{dz^2} + \frac{3}{2}\frac{dN}{dz} + \frac{N}{2}\right] - \frac{w}{H}\cdot\frac{dN}{dz} - \beta_0 \exp(-kz)N$$
$$= -q_0 \exp[1 - z - \exp(-z)]. \tag{19}$$

At great heights the diffusion terms dominate the equation, and the complementary functions have the asymptotic forms $N \sim \exp(-z/2)$ and $N \sim \exp(-z)$. The former represents diffusive equilibrium of the plasma. The latter represents a situation in which the diffusion velocity w_D is not zero and increases exponentially upwards, and there is an outflow of ionization to a sink at $z = +\infty$. This is not a true equilibrium solution.

Approximations to the complementary functions at the bottom of the layer can be found by the W.K.B. method. For $w = 0$, they have the forms

$$N \propto \exp[(\tfrac{1}{4}k - \tfrac{1}{2})z \pm f(z)] \tag{20}$$

where $f(z)$ itself varies exponentially with z. One of these decreases rapidly to zero as $z \to -\infty$, and resembles in form the lower part of the Chapman function of equation (7): the other is divergent. An acceptable "equilibrium layer" is a particular integral of equation (19) which is proportional to $\exp(-z/2)$ at the top, and convergent at the bottom: the characteristics of greatest interest are the peak electron density N_m, the level z_m at which it is found, and the shape of the function $N(z)$ in this vicinity.

The boundary conditions imposed on the solution are $N \propto \exp(-z/2)$ at $z = +\infty$, and $N \to 0$ as $z \to -\infty$.*

3.1. *Substitutions*

It is desirable to remove the exponential variations of the functions occurring in equation (19) by means of suitable changes of variable, and the considerations of the preceding paragraphs suggest the substitutions

$$x = \exp(-z/2) \tag{21}$$

$$N = xy \tag{22}$$

by means of which equation (19) is transformed into the equation

$$\frac{d^2y}{dx^2} - 2V\left[x\frac{dy}{dx} + y\right] - 4Lx^{2k}y = -4Px\exp(1 - x^2). \tag{23}$$

The parameters in this equation are:

$$P = q_0/d_0, \qquad \text{"production"} \tag{24}$$

$$L = \beta_0/d_0, \qquad \text{"loss"} \tag{25}$$

$$V = w/d_0H, \qquad \text{"vertical drift"} \tag{26}$$

P represents an electron density and the other parameters are dimensionless; the "loss gradient" parameter k of equation (9) is also involved in equation (23).

The boundary conditions in terms of the new variables are:

$$dy/dx = 0 \quad \text{at} \quad x = 0 \quad (z = +\infty) \tag{27}$$

$$y \to 0 \quad \text{as} \quad x \to \infty \quad (z \to -\infty) \tag{28}$$

The equations relating to a constant gradient of scale height may be transformed in a similar way. The solutions have the asymptotic form $N \sim \exp(-\phi z)$, ϕ being defined by equation (16), and the independent variable is accordingly taken as $x = \exp(-\phi z)$. Only solutions with $w = 0$ are considered. The functions given by equations (7), (9), (14) and (15) are inserted in the equation of continuity to yield.

$$\frac{d^2y}{dx^2} - \frac{1}{x}\cdot\frac{dy}{dx}\frac{2\phi - \psi}{\phi} - \frac{y\beta}{\phi^2x^2d} = -\frac{q}{\phi^2x^3d} \tag{29}$$

in which q, β and d are written as functions of x instead of z.

This equation has a singularity at $x = 0$, and so only a special case, in which this is removed by taking $2\phi = \psi$, has been considered. The equation may then be written in terms of quantities analogous to the parameters P, L and k defined previously; apart from slight differences to the right-hand side, the equation resembles (23) and may be solved in the same way.

* Strictly speaking these conditions are too rigorous. The most that can be required is that N shall remain finite at $z = -\infty$. It is, however, evident that in a physically-acceptable solution the stricter condition $N \to 0$ must hold.

3.2. *The computer programme*

Two programmes have been written for EDSAC 2, one to solve the simplified equation for the isothermal atmosphere (23) and the other for the general case of a numerical model of the atmosphere without recourse to analytic transformations of the variables. Although the details of the programmes differ, the basic strategy is the same for both, and this is discussed first.

By taking dN/dz (or dy/dx in the simplified equation) as a second dependent variable the equation can be transformed into a pair of simultaneous first-order

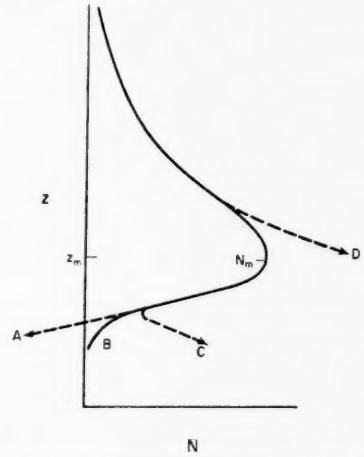

Fig. 1. Types of behaviour of the computed electron density distributions $N(z)$.

equations which can be solved by a stepwise numerical integration. Since the solution proceeds downwards through the atmosphere step by step it is not possible to impose simultaneous boundary conditions at both ends of the range. The boundary condition at $z = +\infty$ can be satisfied by setting $dN/dz = -\frac{1}{2}N$ (or $dy/dx = 0$) at the start of the integration: the initial value of N, say $N(0)$, now has to be chosen in such a way that the solution will be satisfactory at the other end of the range. The only way in which this can be done is by a series of systematic trials. The possible types of behaviour which may arise are illustrated in Fig. 1. Usually either A or C is obtained; if the value of $N(0)$ chosen is very much too large a solution like D is obtained, and B is the desired solution satisfying the boundary conditions. The behaviour of the solution is very sensitive to the value of $N(0)$, and it is possible to change from a solution of type A to one of type C by changing $N(0)$ by 1 part in 10^4. Fortunately, however, the two solutions so obtained are almost identical in the vicinity of the maximum and therefore a good approximation to the required solution can be obtained by finding two slightly different values of $N(0)$, of which one gives a solution like A and the other gives a solution like C. This can be done by starting with two values of $N(0)$, one large, one small, which "bridge" an acceptable solution and arranging for the computer to try values within this range, gradually reducing the difference between the values of $N(0)$ whilst ensuring that they still bridge an acceptable solution.

VOL
18
196

A routine is provided in the programme which will integrate the equation for a specified $N(0)$ until either:

(a) N becomes negative (indicating a solution like A); or

(b) N exceeds a specified limit, usually 10^{10} (indicating a solution like D); or

(c) N attains a minimum having previously attained a maximum (solution like C); or

(d) z becomes large and negative without any of the foregoing conditions being satisfied. (This would indicate an acceptable solution, finite at $z = -\infty$: it is never obtained.)

The routine then records in the store the value of $N(0)$, the position and value of the maximum (if any), and an indication of the type of solution. At any stage in the calculation there are in the machine two values of $N(0)$ which are known to bridge an acceptable solution. The programme takes a value midway between them and by means of the routine just described determines the type of solution obtained: it then replaces the appropriate $N(0)$ by the midway value so that the difference between the bridging values of $N(0)$ is halved. This hunting procedure is continued until the difference between the two values of $N(0)$ is less than a predetermined quantity (usually 1 part in 10^3).

The programme for the isothermal atmosphere starts by reading in the values of the parameters L, P and k, and two values of $N(0)$. At the end of the hunting procedure it prints out, for each $N(0)$ finally obtained, the values of N and z at the maximum and a letter A or C to indicate the type of solution. If required it can also be made to print out a table of $N(z)$ for a range of two scale heights on either side of the maximum for each solution separately. This optional facility was not always used, since the printing of the table occupies an appreciable amount of the total computer time required for the solution.

The programme for the numerical model starts by reading the values of the parameters S_∞, A, χ, K, w and b; and tables of the quantities n, $n(M)$, H, T and μ as functions of geometrical height h. It computes and stores the various quantities required for the most general expressions quoted in Section 2: during the integration values of these expressions are obtained from the tables as required using a three-point interpolation formula. During the hunting procedure the programme stores a table of $N(h)$ for each of the two values of $N(0)$, and when the hunting is finished these tables are printed out. The values of N and h at the maximum are obtained by fitting a parabola to the three points nearest the maximum in the table: this gives more accurate values than the programme for the isothermal atmosphere which merely takes the largest value of N in the table.

4. The Equilibrium Layers

Before the features of the equilibrium layers are discussed, it is useful to consider what values might be taken by the various parameters in the F-region. Some plausible orders of magnitude are presented below: they are generally in accordance with current models of the upper atmosphere (e.g. Ratcliffe *et al.*,

VOL. 18 1960

1956). The numbers of the equations in which the quantities are introduced are shown.

$S_\infty = 10^{10}$ cm^{-2} sec^{-1}	(5)	$h_0 = 180$ km	(3)
$A = 10^{-17}$ cm^2	(5)	$H_0 = 40$ km	(6)
$K = 10^{-13}$ cm^3 sec^{-1}	(8)	$n_0 = 2 \times 10^{10}$ cm^{-3}	(6)
$b\sqrt{T} = 10^{19}$ cm^{-1} sec^{-1}	(13)	$\gamma = 0{\cdot}2$	(3)
$q_0 = 1000$ cm^{-3} sec^{-1}	(7)	$P = 10^8$ cm^{-3}	(24)
$d_0 = 10^{-5}$ sec^{-1}	(14)	$L = 100$	(25)
$\beta_0 = 10^{-3}$ sec^{-1}	(9)		

In the neighbourhood of the *F2*-electron peak, two scale heights above *F1*, β and d are about 10^{-4} sec^{-1}.

The values of the loss parameter actually used range from 1 to 7500. The computed values of N should be directly proportional to the production parameter P; this has been verified in a particular case.

4.1. *Layers with zero vertical drift*

For the simplest situation, with a constant scale height and zero vertical drift velocity, twenty-three computed solutions have been obtained, distributed as follows:

Value of k	1·0	1·2	1·6	2·0	2·6
Total number of solutions	3	8	2	7	3
Number with tabulated $N(z)$	2	5	1	5	1

It is found empirically that the characteristics of the peak are determined by the simple relationships

$$q_m \simeq \beta_m N_m \tag{30}$$

$$\beta_m \simeq d_m \tag{31}$$

The validity of these formulae is demonstrated by the curves of Fig. 2, in which the ratios $(\beta N/q)_m$ and $(\beta/d)_m$ are plotted as functions of L, for different k. Exact fulfilment is represented by the horizontal line whose level represents unity on the vertical logarithmic scale, and deviations from this line indicate the numerical factors which complete the equations. It is evident that equation (30) is well satisfied, especially for $k \simeq 1$, but the factors in equation (31) are rather dependent on k and L. The latter equation is also illustrated by Fig. 3, which shows how the height z_m of the peak depends upon L $(=\beta_0/d_0)$.

The effect of varying the parameter k is illustrated by Fig. 4, in which are plotted equilibrium layers for different values of k but the same value of L. The striking feature is the dependence of N_m upon k: this is, of course, just one aspect of the relationships of equations (30) and (31).

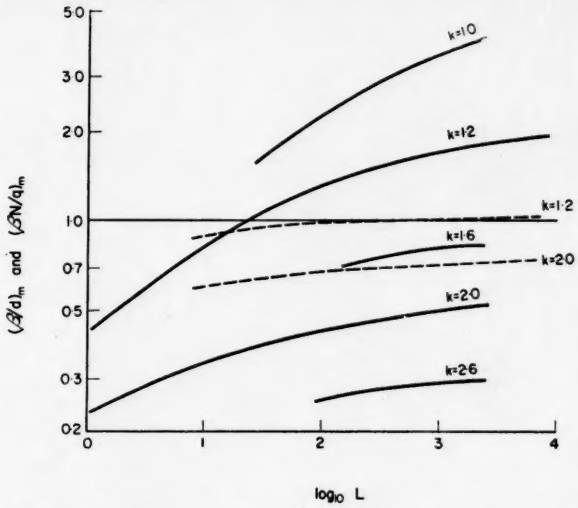

Fig. 2. The relations between production, loss and diffusion rates at the electron peak. Continuous lines show values at the peak of the ratio β/d, for several values of the loss gradient parameter k, as a function of the parameter $L = \beta_0/d_0$. Broken lines show values of the ratio $\beta N/q$ at the peak, for two values of k only: the graphs for other values of k are very similar. See equations (30) and (31).

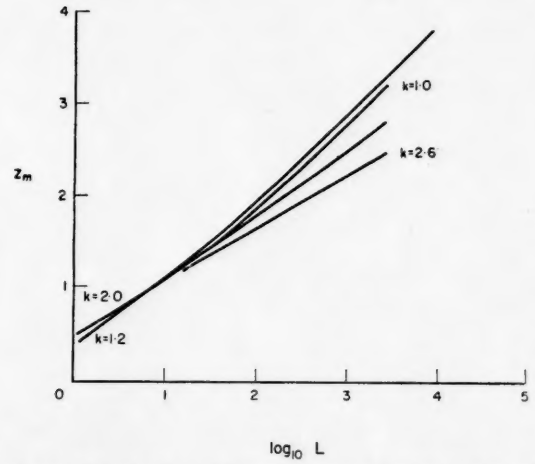

Fig. 3. Dependence of the level z_m of the electron peak upon L, the value of the ratio β/d at the production peak ($z = 0$). Curves for four values of the loss gradient parameter are shown.

Information about the shape of the equilibrium layers is provided by the solutions for which $N(z)$ has been tabulated, between the limits $z_m \pm 2$: the values of N for the two solutions printed begin to differ appreciably near the lower end of this range. The thickness of the layer below the peak is conveniently specified by the quantity z_7: this is defined by an equation in which z is written as a function of N, viz:

$$z_7 = z(N_m) - z(0{\cdot}7N_m). \tag{32}$$

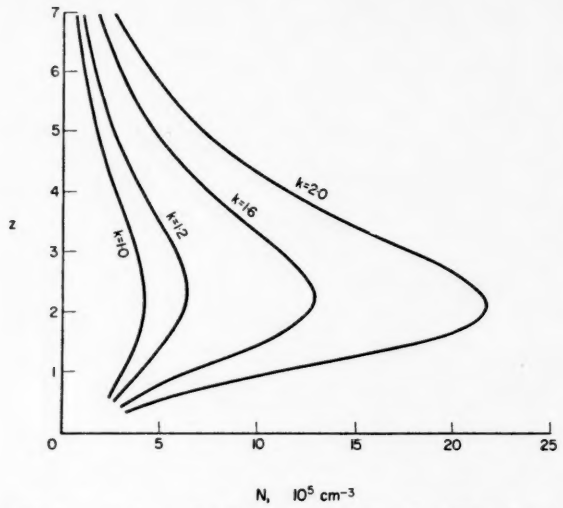

Fig. 4. Equilibrium electron distributions $N(z)$ for $L = 250$, $P = 4 \times 10^7$ cm^{-3}, and values 1·0, 1·2, 1·6 and 2·0 of k.

The equilibrium layers with $L = 250$ and different values of k are plotted again in Fig. 5; in order to display the shapes of the layers the peaks have been brought into coincidence. All the layers resemble the Chapman curve shown, and near the peak they are parabolic. The thickness z_7 depends on the gradient of the ratio $\beta/d \propto \exp[-z(1 + k)]$: it is found empirically that

$$z_7(1 + k) \simeq 2{\cdot}5. \tag{33}$$

For the smaller values of k, the thickness z_7 increases with increasing L; but for $k = 2$, z_7 is almost independent of L.

Equation (29), which includes a gradient of scale height, has been solved with the parameters $\gamma = 0{\cdot}2$, $\mu = 0{\cdot}35$, $L = 370$ and the three values $k = 1{\cdot}0$, $1{\cdot}2$ and $2{\cdot}0$. The values of the ratios $(\beta/d)_m$ and $(\beta N/q)_m$ are the same, to within about 1 per cent, as those for the corresponding solutions for the isothermal case, and the shapes of the layers are very similar. These results suggest that a height-independent gradient of scale height, of a magnitude probably similar to that existing in the *F2*-region, has little effect upon the form of the electron density distribution.

4.2. *Effects of a vertical drift velocity*

Equation (23), which refers to an isothermal atmosphere, includes terms due to a vertical drift velocity which is independent of height. Thirty-four solutions of this equation with non-zero values of V have been obtained, for $k = 1{\cdot}0$, $1{\cdot}2$ and $2{\cdot}0$.

The effect of the drift is illustrated by Fig. 6, in which are plotted the functions $N(z)$ for $k = 1{\cdot}2$, $L = 250$ and a few values of V. These curves are similar to those published by Yonezawa (1958). Qualitatively, an upward drift tends to transport ionization from its level of origin towards a level where the loss rate is smaller,

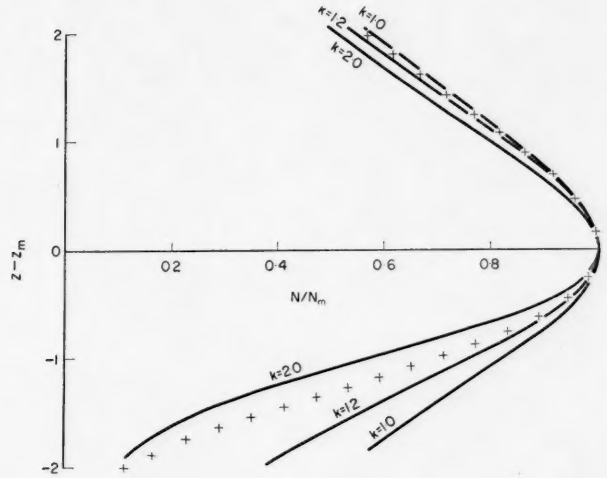

Fig. 5. Equilibrium electron distributions for $L = 250$ and $k = 1{\cdot}0$, $1{\cdot}2$ and $2{\cdot}0$, normalized for comparison of shape. The curve $+++++$ is the Chapman function, given by $N/N_m = \exp \tfrac{1}{2}[1 - (z - z_m) - \exp(z_m - z)]$.

VOL. 18 1960

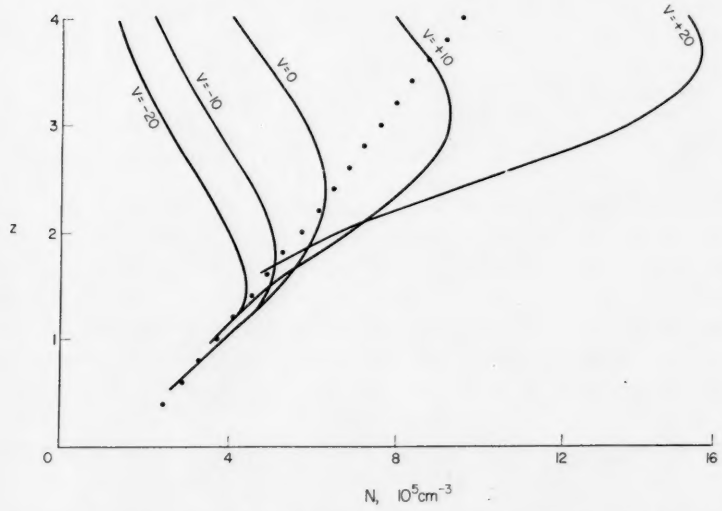

Fig. 6. The effect of vertical drift on the distribution of electron density, for $k = 1{\cdot}2$, $L = 250$, $P = 4 \times 10^7$ cm^{-3}. $N(z)$ curves are shown for values 0, ± 10, ± 20 of the drift parameter V. The electron distribution in the absence of drift and diffusion, given by $N = q/\beta$, is shown by the curve . . . . .

and thus the average lifetime of an ion pair is prolonged and the peak electron density increased. It is apparent that an upward drift produces a greater effect than a downward drift of the same magnitude, but as will be shown in Section 4.3 this feature does not occur when some other atmospheric models are employed.

The changes produced at the peak by a drift w may be summarized by the formulae:

$$\Delta(\log N_m) \simeq \frac{w}{Hd_m} \tag{34}$$

$$\Delta z_m \simeq \frac{w}{Hd_m} \tag{35}$$

in which d_m is the diffusion rate at z_m, the level of the peak when $w = 0$.

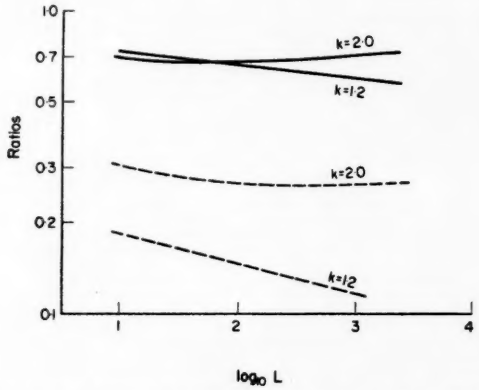

Fig. 7. Changes in peak electron density N_m, and the level z_m of the peak, produced by a vertical drift w, in relation to the diffusion rate at the peak d_m. The continuous lines show values of the ratio $\Delta(\log N_m) . Hd_m/w$, and the broken lines show values of the ratio $\Delta z_m . Hd_m/w$, for $k = 1{\cdot}2$ and $k = 2$, as functions of L. See equations (34) and (35).

The detailed analysis gives numerical factors for insertion into these relations, which hold quite well for drift velocities less than Hd_m: this quantity is of the order of a few metres per second in the *F2*-layer. In Fig. 7 are plotted the ratios $\Delta(\log N_m) . Hd_m/w$ and $\Delta z_m . Hd_m/w$, and their values lie between 0·1 and 1 for the instances shown: they depend somewhat upon k, but for given k are almost independent of L. Moreover, w can be eliminated between equations (34) and (35) to give a relation between $\Delta(\log N_m)$ and Δz_m, which depends upon k but hardly at all upon L.

The shape and thickness of the equilibrium layers are not markedly altered by moderate drifts.

4.3. *Results for the numerical model of the atmosphere*

A programme designed to handle a general model of the atmosphere is clearly capable of endless variation and refinement, of which only a small sample can be dealt with in the computing time available. Consequently, the examples considered have been chosen to show whether the general results obtained from the isothermal

VOL.
18
196(

model, and expressed by equations (30) to (35), are valid for a more complicated model which gives a better representation of the upper atmosphere. As in the previous work, most attention is paid to the parameters N_m and h_m of the electron peak.

The atmospheric model used for this investigation was kindly provided by Dr. K. WEEKES, and is based on the density function shown in Fig. 8. The scale height is also shown in the figure: it possesses a large gradient at the height of the *F1*-layer ($dH/dh \simeq 0{\cdot}4$), but in the *F2*-layer the gradient is only about 0·1 and is even smaller at greater heights.

Two variants of this model are considered. In the first, to be called the "mixed" atmosphere, the gases O and N_2 are supposed to be completely mixed at all

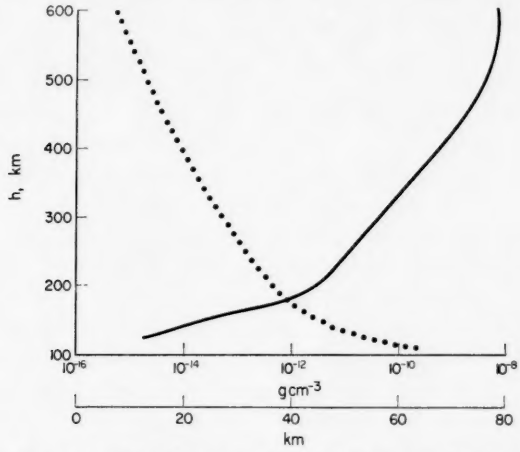

Fig. 8. Atmospheric data, after WEEKES. The dotted curve denotes density, on a logarithmic scale; and the continuous curve the scale height of the neutral atmosphere.

heights, so that $H(\mathrm{O}) = H(\mathrm{N_2})$: this corresponds to the situation $k = 1$ in the isothermal atmosphere. In the other version, referred to as the "separated" atmosphere, these gases are supposed to be diffusively separated at heights above 150 km, so that $H(\mathrm{O}) = 1{\cdot}75H(\mathrm{N_2})$—corresponding to the case $k = 1{\cdot}75$.

The rocket experiments described by JOHNSON *et al.* (1958) suggest that above about 240 km all the positive ions are O^+. In the "mixed" atmosphere, the parameter μ involved in the diffusion velocity (equation (12)) depends upon the relative abundances of N_2 and O, and is about 0·35. In the "separated" atmosphere, μ increases with height and reaches a limiting value of 0·5 at levels where the proportion of N_2 is small. Below 240 km, μ depends upon the ion composition as well as upon that of the neutral atmosphere. In this region, below the *F2*-peak, the term involving μ is not very important and it has been found expedient to estimate this parameter from the results published by JOHNSON *et al.*

These results show a preponderance of NO^+ ions in the lower *F*-region, which suggests that the gas N_2 plays a greater part than O_2 in the loss process. For simplicity, therefore, the presence of the latter gas is ignored in this work, so that $n(M) = n(N_2)$ in the loss formula of equation (8), the coefficient K being chosen empirically.

The peak of the production function is made to occur near 180 km, the height of the *F1*-layer, by suitable choice of the cross-section A (equation (6)). Two refinements have been incorporated into the programme for the "separated" atmosphere: these are a modification of equation (5) to take account of the absorption of part of the solar radiation by N_2, which does not contribute to the observable ionization; and an allowance for the different values of b (equation (13)) which are appropriate to the diffusion in O and in N_2 of O^+ ions (Dalgarno, 1958).

For the solutions with zero vertical drift, the coefficient K has been varied over a range of 100:1. This is analogous to variation of the parameter L in the isothermal case. The computed electron density distributions, $N(h)$, resemble in shape those obtained previously. It has been shown in Section 4.1 that in the isothermal case, the production, loss and diffusion processes are of comparable importance at the peak: the same result is obtained from the computations made with the numerical atmospheric model. The values of the ratio $(\beta N/q)_m$ are the same, to within a few per cent, as those for "isothermal" solutions with similar parameters. The values of (β/d) at the peak are greater by about 20 per cent than for the "isothermal" solutions, but since the gradient of this function is of order 5 per cent per km in the F-region the difference is scarcely significant.

For one example, the non-linear loss formula of equation (10) has been used: the chosen value of $\alpha = 5 \times 10^{-9}$ cm^3 sec^{-1} places the transition level defined by $Kn(M) = \alpha N$ at about 180 km. Although the shape of the $N(h)$ distribution below the maximum is altered by the use of this formula, there is little change at the electron peak: the height h_m, which in the example considered is 250 km, is lowered by 2 km and N_m increased by 7 per cent. Thus the operation of an α-type loss law in the *F1*-layer probably has little influence on the characteristics of the *F2*-peak.

The effects of a height-independent vertical drift on the electron distribution are much the same as those described in Section 4.2, except that the very large increases of N produced by a strong upward drift (cf. Fig. 6) do not occur with the atmospheric model here considered. $N(h)$ curves computed for the "separated" atmosphere are plotted in Fig. 9: they show examples of upward, zero and downward drift.

A useful check between the two types of calculation is obtained by inserting, into the programme for the numerical model, data appropriate to a mixed and isothermal atmosphere. The values of parameters employed are equivalent to those used in previous examples of equilibrium layers with $k = 1$, with zero and non-zero drifts; and the electron distributions obtained by the two methods agree to within the probable accuracy of the calculations.

The results described in this section, for models with a non-uniform scale height, are very similar to those obtained in the idealized case of an isothermal atmosphere. It is thus not unreasonable to suppose that conclusions derived from this work are approximately true for other, more general atmospheric models.

4.4. *Solar zenith angle and magnetic dip*

The analysis of previous sections referred implicitly to a special case of vertical illumination and vertical magnetic field ($\chi = 0$ and $\sin I = 1$). It will now be

VOL
18
196

extended to a more general case, since the matter is relevant to the time of establishment of equilibrium.

Let suffix q refer to the level of the production peak for any value of χ, the

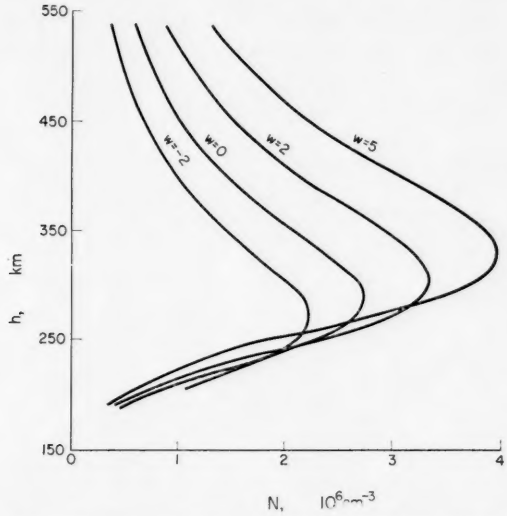

Fig. 9. Electron density distributions computed for the atmospheric model of Fig. 8, with diffusive separation of O and N_2 above 150 km. The production q has a peak value of 275 cm^{-3} sec^{-1} at 200 km. The diffusion and loss functions are given by $b = 1{\cdot}4 \times 10^{17}$ cm^{-1} sec^{-1} $(°K)^{-1/2}$ and $K = 10^{-13}$ cm^3 sec^{-1}, respectively. The numbers attached to the curves are vertical drift velocities in metres per second.

suffix 0 being retained for the level $z = 0$ of peak production for overhead sun. Then, if H is independent of height,

$$z_q = \log \sec \chi \tag{36}$$

$$q_q = q_0 \cos \chi \tag{37}$$

$$\beta_q = \beta_0(\cos \chi)^k \tag{38}$$

$$d_q = d_0 \sec \chi \sin^2 I \tag{39}$$

The expression for d includes the factor $\sin^2 I$ which is generally used to describe the effect on diffusion of the geomagnetic field. Then the production and loss parameters, which must be calculated at the level of the production peak, take the values

$$L_q = L_0 \operatorname{cosec}^2 I \, (\cos \chi)^{k+1} \tag{40}$$

$$P_q = P_0 \operatorname{cosec}^2 I \cos^2 \chi \tag{41}$$

In the absence of vertical drift, the parameters N_M, z_M of the electron peak are related to the values N_m, z_m which refer to the case $\chi = 0$ and $\sin I = 1$, as follows:

$$z_M = z_m + \log \sec \chi \tag{42}$$

$$N_M = (N_m/P) \, . \, P_0 \cos^2 \chi \operatorname{cosec}^2 I \tag{43}$$

In these equations z_m and (N_m/P) are functions of k and L_q only, and are given by the results described in Section 4.1. The resulting values of N_M and z_M are very insensitive to χ, and this is demonstrated by Fig. 10 which shows equilibrium values of N as a function of latitude, for equinox noon conditions and plausible values of P_0 and L_0. This insensitivity is a consequence of the earlier result that $N_m \simeq q_m/\beta_m$, for β is assumed independent of χ and q varies little over a wide range of χ for any given $z > 1$.

The results of the foregoing analysis agree, to within the accuracy of calculation,

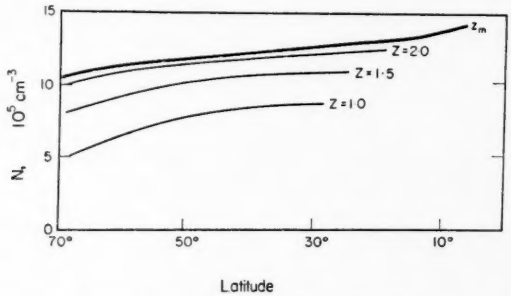

Fig. 10. Equilibrium electron density for equinox noon as a function of geographic latitude, which is assumed equal to magnetic latitude. Values adopted are $k = 1$, $L_0 = 200$, $P_0 = 10^8$ cm^{-3}. The thick line indicates the maximum electron density N_m, and the thinner lines the electron densities at the levels $z = 2{\cdot}0$, $1{\cdot}5$ and $1{\cdot}0$. The increase in low latitudes is due to the factor $\sin^2 I$ in the diffusion coefficient, and the decrease in high latitudes to the large solar zenith angle.

with those of YONEZAWA (1958), who computed electron density distributions for several values of w, for the case $k = 2$ only. It may be shown, by use of equations (40) to (43), that YONEZAWA's deduction that $N_M \cos\chi$ is a function of $\sec\chi$. $(\sin I)^{2/3}$ only is equivalent to the statement that for an equilibrium layer the ratio (N_m/P) depends only upon L_q, valid if V and k are fixed.

5. VALIDITY OF THE ASSUMPTION OF EQUILIBRIUM

At first sight, it appears hazardous to discuss a dynamical system, such as the F-region, in terms of situations from which time variation is excluded. But the neglected term in the continuity equation is seldom dominant, and is often smaller than other terms by a factor of 10 or more. In temperate latitudes, the parameters N_mF2, h_mF2 of the electron peak are often fairly constant for several hours during the day (THOMAS *et al.*, 1958), and this is just what would be expected from consideration of the equilibrium solutions because of the insensitivity of N_M and z_M to the solar zenith angle χ (Section 4.4, and Fig. 10). If production, loss and electromagnetic drifts remain constant, then, in the absence of diffusion, equilibrium is established at any level z in a time of order $1/\beta(z)$. The considerations of SHIMAZAKI (1957) suggest that above the peak, where the situation is dominated by diffusion, the exponential distribution characteristic of diffusive equilibrium is established above any level z in a time of order $1/d(z)$. The approach to equilibrium is then slowest at the peak, where the time taken is comparable to $1/d_m$ $(\simeq 1/\beta_m)$. Numerically, this is about 10^4 sec, or 3 hr, and after the lapse of several

hours equilibrium may be attained, provided the drift has not greatly changed in the meantime. Thus the equilibrium layers described in this paper may be useful for consideration of the actual ionosphere.

6. Conclusions

The use of an electronic computer has made possible the calculation of equilibrium electron distributions for a variety of model atmospheres. It cannot be expected that an empirical approach of the kind employed will establish results with mathematical rigour, but a balance has been struck between the desire for greater certainty and the need for economical use of the computer.

The work described in this paper points towards the following conclusions about equilibrium layers controlled by production, loss, plasma diffusion and vertical drift:

(a) If there is no vertical drift other than that caused by plasma diffusion, then:

(i) the peak of electron density occurs near the level where the loss rate β and the diffusion rate $d = D/H^2$ are equal;

(ii) at the peak, and below it, the electron density is given quite accurately by the expression $N = q/\beta$, just as though there were no diffusion;

(iii) at levels more than one scale height above the electron peak, the electron distribution is controlled by diffusion and takes an exponential form;

(iv) near the electron peak the distribution is approximately parabolic, with a thickness inversely proportional to the gradient of the function log (β/d).

(b) The effects produced by a vertical drift depend on the ratio of its magnitude to the product $H \,.\, d$ at the electron peak. An upward drift for which this ratio is unity raises the peak by about one scale height and increases the peak electron density: a downward drift has opposite effects. The shape of the layer is not greatly altered, and unless the drift is very strong the peak electron density is still given approximately by the relation $N = q/\beta$.

(c) The above conclusions are not materially affected if the scale height of the atmosphere varies with height.

Acknowledgements—This investigation was undertaken at the suggestion of Mr. J. A. Ratcliffe, and it is a pleasure to acknowledge his continual advice and encouragement. We have also benefited from discussions with Dr. K. Weekes and other members of the Cavendish Laboratory.

Our thanks are due to the Director of the University Mathematical Laboratory for permission to use EDSAC 2. We are grateful to the Department of Scientific and Industrial Research for a grant which enabled this work to be carried out, and for a Research Fellowship awarded to one of us (D. W. B.).

References

Bradbury N. E. 1938 *Terr. Magn. Atmos. Elect.* **43,** 55.

Chapman S. 1931 *Proc. Phys. Soc. Lond.* **43,** 26.

Chapman S. and Cowling T. G. 1952 *Mathematical Theory of Non-Uniform Gases,* (2nd Ed.) pp. 140–144. Cambridge University Press.

Dalgarno A.	1958	*J. Atmosph. Terr. Phys.* **12,** 219.
Duncan R. A.	1956	*Aust. J. Phys.* **9,** 436.
Ferraro V. C. A.	1945	*Terr. Magn. Atmos. Elect.* **50,** 215.
Johnson C. Y., Meadows E. B. and Holmes J. C.	1958	*J. Geophys. Res.* **63,** 443.
Martyn D. F.	1956	*Aust. J. Phys.* **9,** 161.
Nicolet M.	1951	*J. Atmosph. Terr. Phys.* **1,** 141.
Ratcliffe J. A.	1956	*J. Atmosph. Terr. Phys.* **8,** 260.
Ratcliffe J. A., Schmerling E. R., Setty C. S. G. K. and Thomas J. O.	1956	*Phil. Trans.* A **248,** 621.
Shimazaki T.	1957	*J. Radio Res. Lab.* **4,** 309.
Thomas J. O., Haselgrove J. and Robbins A. R.	1958	*J. Atmosph. Terr. Phys.* **12,** 46.
Yonezawa T.	1955	*J. Radio Res. Lab.* **2,** 125.
Yonezawa T.	1958	*J. Radio Res. Lab.* **5,** 165.

VOL
18
196

Journal of Atmospheric and Terrestrial Physics, 1960, Vol. 18, pp. 253 to 258. Pergamon Press Ltd. Printed in Northern Ireland

RESEARCH NOTES

Focusing of electromagnetic waves by E_s-clouds

(*Received* 1 *January* 1960)

In measurements of ionic pulse absorption, it is necessary to determine a calibration constant I_0 of the instrument. This is given by the product of the amplitude of the first echo and twice the reflection height.

In this formula it is assumed that the reflection coefficient of the ionosphere is unity.

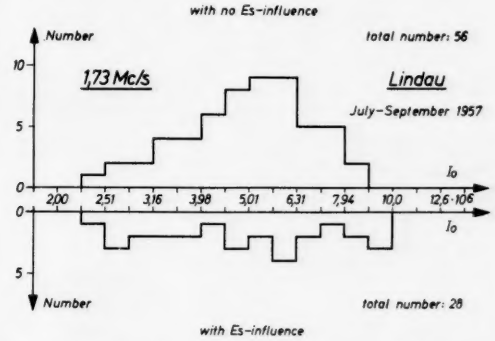

Fig. 1. Histogram of I_0-values with and without influence of E_s for 1·73 Mc/s at Lindau, July–September 1957.

In practice I_0 can be measured as follows: the amplitude of the first echo from the F-layer is measured every 15 sec during the night; mean values for intervals of 15 min are calculated; and these means are plotted in the form of a histogram.

It is usually assumed that the large values are due to focusing effects and the small values to defocusing, both caused by varying curvature of the F-layer. If partial reflections from the E_s-layer are observed, one would expect values for the F-echo amplitudes to be smaller than those without such partial reflections; and hence, from the formula, smaller I_0-values should appear. However, our measurements at Lindau and Tsumeb/SWA occasionally showed larger values under these conditions, provided that the values of the E_s-echo lay within 5–20 per cent of the first F-echo amplitude (Figs. 1–3). This effect is particularly clear in measurements obtained on 16 September 1958 at Tsumeb (lined fields in Figs. 2 and 3).

All attempts to explain this observation by means of focusing effects appear to fail. The objection is that such abnormally high values are never observed in the absence of E_s-echoes, although this is much the commoner condition.

These observations can, however, be explained by a focusing effect of the E_s-clouds. Optical focusing is produced by convex lenses (refractive index $n > 1$). By analogy,

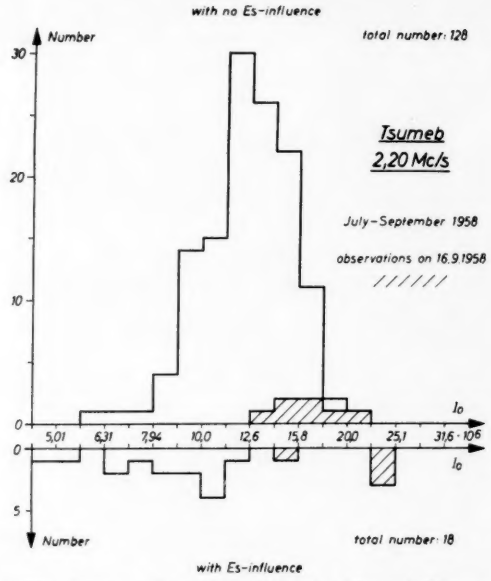

Fig. 2. Histogram of I_0-values with and without influence of E_s for 2·20 Mc/s at Tsumeb, July–September 1958.

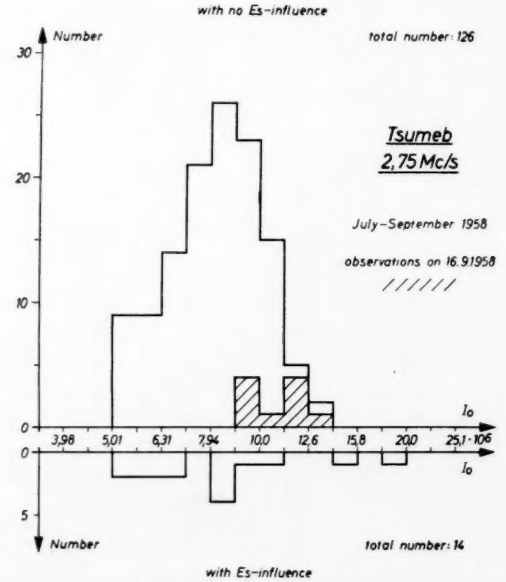

Fig. 3. Histogram of I_0-values with and without influence of E_s for 2·75 Mc/s at Tsumeb, July–September 1958.

focusing can be expected in the ionosphere (refractive index $n < 1$) when there is a concave structure of the level of constant ionization. This analogy is illustrated in Fig. 4.

There is another possible explanation. It seems reasonable to believe that the E-layer sometimes consists of clouds with dimensions of the order of kilometres. The cone from the

VOL.
18
196

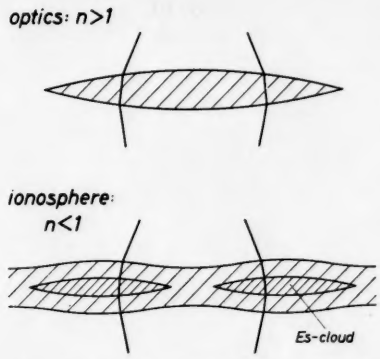

Fig. 4. Analogy between an optical lens and the ionosphere.

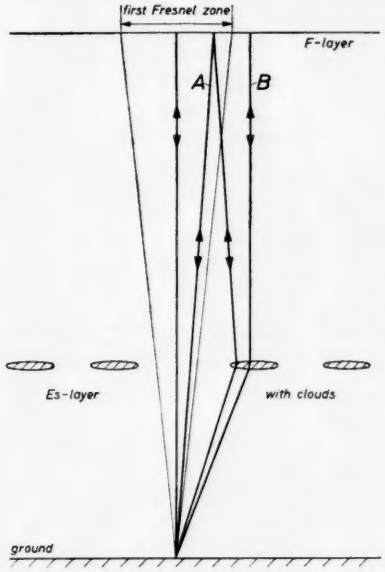

Fig. 5. Raypaths of F-layer-echoes with refraction by E_s-clouds.
(The horizontal scale is expanded).

transmitter to the first Fresnel zone in the F-layer (Fig. 5) may be free from any E_s-clouds for some time, while there are some in the neighbourhood in random positions. The energy within the cone gives normal F-echo amplitudes. But additional energy is reflected from the F-layer within the Fresnel zone and refracted once by the E_s-clouds, as shown by ray A in Fig. 5. This increases the F-echo amplitude. Further additions may come from the energy of rays such as B in Fig. 5. In the absence of E_s-clouds, all of these energy sources would not contribute to the final amplitude of the F-echo.

This theory must be checked by further investigations. It is intended to study the time variation of the effect, and correlate this with the movement of the E_s-clouds.

Max-Planck-Institut für Aeronomie G. UMLAUFT
Institut für Ionospharenphysik
Lindau über Northeim, Hannover

A unified theory of terrestrial and solar magnetization, the outer Van Allen belt and high energy primary cosmic rays

(*Received* 17 *February* 1960)

In a paper in this Journal by Chatterjee (1956) facts and arguments are presented which can supply the basis for an acceptable theory of the Earth's state of magnetization. These may be summarized as follows.

From the accepted facts about the magnetic mineral contents, temperatures and pressures of the upper 25 km of the Earth's crust and from the known facts about magnetic materials, Chatterjee infers that the main magnetization of the Earth may be attributed to a 20 km thick shell in this crust which has temperatures below the Curie point of iron. For he first deduces that "due to the effects of high pressure and temperature, the 20 km shell will behave as a material of high permeability being saturated at a very low field of the order of 0·1–0·01 gauss", then deduces that the average magnetic moment per unit volume of the shell is 11·0 G and finally notes that if the total magnetization of the Earth were confined to a 20 km shell the moment per unit volume would be 8 G.

If we accept his conclusion that a separately produced field of 0·01 G may suffice to account for the known magnetization of the Earth we are then faced with the problem of finding the source of this field and its required direction.

The following considerations appear to indicate that this source is the Sun and its motion with velocity 30 km/sec relatively to that of the Earth in its orbit. For this motion will produce in a non-rotating frame of reference attached to the Earth, at the orbital distance r, a magnetic field H_r which is perpendicular to the Ecliptic, is directed from north to south as required and has the intensity 0·01 G—provided that the Sun carries a net negative electric charge of about $-2{\cdot}2 \times 10^{28}$ e.s.u.

At first sight this conclusion might appear to many theoretical astrophysicists as quite unacceptable on account of its apparent inconsistency with some of their most cherished notions. We shall therefore mention the following facts which very strongly support this conclusion.

If this negative charge were distributed in the Sun in the same way as its mass and if the mass and angular velocity of the Sun were distributed as in Chapman's Model A (1948) then the north polar magnetic field vector of the Sun H_p would be about $-1{\cdot}1$ G. This agrees in order of magnitude and direction with the observations of Hale and Langer who, according to H. W. Babcock (1953), found a mean value for H_p of -4 G. It is also in good agreement with the most recent observations of H. D. Babcock (1959); the temporary reversal, during six years, of the direction of H_p observed by the Babcocks may be provisionally attributed to secondary effects.

Moreover, the field H_r produced by the Sun near the Earth not only magnetizes the Earth but also neutralizes the resulting external terrestrial field in a narrow and approximately toroidal region of radius about 3·3 earth radii which lies nearly in the Earth's magnetic equatorial plane. The magnetic field in and near this toroidal region is such that it could act as a "magnetic bottle" which is partly accessible to fast charged particles from regions much further out. These facts point strongly to the possibility that the outer Van Allen belt (which has a maximum density at about 3·6 earth radii from the Earth's centre) is produced by the same cause as that which produces the Earth's state of magnetization.

Lastly, it should be noted that the Sun's charge produces at the Earth's orbit an electric field of potential $V = -4{\cdot}4 \times 10^{17}$ V which is such that it can attract protons and other nuclei from distant space. The maximum kinetic energy imparted to nuclei of charge Ze would be $4{\cdot}4 \times 10^{17}\,Z$ eV and for an iron nucleus this amounts to about 10^{19} eV. This

VOL
18
196

result is in good agreement with the fact that the maximum energy ever determined for a primary cosmic ray particle lies between 5×10^{18} and 10^{19} eV. Also a high proportion of the attracted nuclei would describe orbits round the Sun which are randomly distributed and so they would reach the Earth isotropically.

It would be a remarkable coincidence if these four phenomena, pertaining to the solar system, were all explained correctly in their orders of magnitude and their related directions by means of a single hypothesis which happened to be completely false. The probability that this is not a mere coincidence is considerably increased if we note that our hypothesis can also lead to simple qualitative explanations of the occurrence in the Sun's corona of relativistic electrons, strong radio noise, fast magnetized clouds of ionized hydrogen and very high temperatures, and of the main events in the Earth's atmosphere which follow strong solar flares. This probability is increased further if we regard the Sun as an average star and extend our hypothesis to the stars, for such an extension leads to simple qualitative explanations of many facts concerning magnetic stars, novae, supernovae and the Galaxy and can even explain, in principle, the recession of the galaxies; it also yields a simple quantitative explanation of the fact, pointed out by BLACKETT (1949), that the ratio P/U of the magnetic moment of the Sun to its angular momentum is approximately the same as the average of the corresponding ratios for the stars in a particular group of five magnetic stars.

A more complete discussion of all these consequences of our hypothesis and two suggestions concerning the possible origin of the steller net charges are in the course of publication elsewhere (BAILEY, 1960).

V. A. BAILEY

University of Sydney
Australia

VOL. 18 1960

REFERENCES

BABCOCK H. D.	1959	*Astrophys. J.* **130,** 364.
BABCOCK H. W.	1953	*Mon. Not. R. Astr. Soc.* **113,** 361.
BAILEY V. A.	1960	*Nature, Lond.* and *Proc. Roy. Soc. N.S.W.* In press.
BLACKETT P. M. S.	1949	*Phil. Mag.* **40,** 125.
CHAPMAN S.	1948	*Mon. Not. R. Astr. Soc.* **108,** 236.
CHATTERJEE J. S.	1956	*J. Atmosph. Terr. Phys.* **8,** 233.

Geomagnetic and sunspot influences on spread-*F* in Baguio

(*Received* 27 *February* 1960)

IT has been shown (LYON, SKINNER and WRIGHT, 1958) that magnetic activity tends to reduce the frequency of occurrence of spread-*F* at Ibadan, Nigeria. This tendency is also observed at Baguio, Philippines (latitude 16·4°N).

A count was made of the presence of spread-*F* on Baguio ionograms, the norm being a spread-echo intensity sufficient to make the scaling of $(M3000)F2$ uncertain. The ionograms studied were the hourly ionograms from 1900 to 0800 hours local time, for five international quiet days, for five international disturbed days, and for all days, of each of the 72 months from January 1953 to December 1958. The counts were transformed to

percentages and averaged for each of the two 3-year groups, 1953–1955 being years of low sunspot count and 1956–1958 of high sunspot count. The results are illustrated in Fig. 1.

It is seen (1) that the tendency of magnetic activity to reduce spread-*F* occurrence is

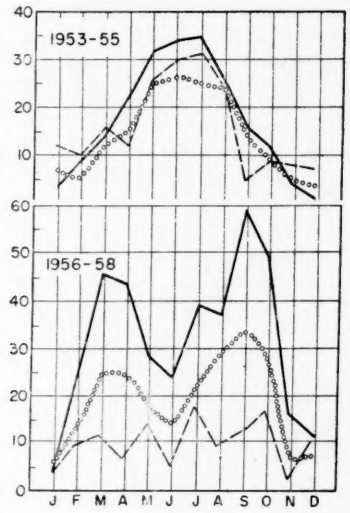

Fig. 1. Percentage occurrence of spread-*F* in Baguio. ——— for five quiet days; – – – – for five disturbed days; o o o o for all days.

greater and more consistent in years of high sunspot count than in years of low sunspot count, and (2) that the pattern of seasonal variation of spread-*F* occurrence changes with the solar cycle independently of magnetic activity.

V. Marasigan, S.J.

Manila Observatory
Baguio, Philippines

Reference

Lyon A. J., Skinner N. J. and Wright R. W. 1958 *Nature, Lond.* **181,** 1724.

Journal of Atmospheric and Terrestrial Physics, 1960, Vol. 18, pp. 259 to 263. Pergamon Press Ltd. Printed in Northern Ireland

Indices of geomagnetic activity

of the Observatories HARTLAND (*Ha*), ESKDALEMUIR (*Es*) and LERWICK (*Le*) November 1959 to March 1960

The figures given on pages 259 to 263 represent the K-indices for three-hour intervals, beginning with 00–03 hrs for the first and ending with 21–24 hrs for the eighth figure.

November 1959

Day	*Ha* Range for $K = 9 : 500\gamma$		*Sum*	*Es* Range for $K = 9 : 750\gamma$		*Sum*	*Le* Range for $K = 9 : 1000\gamma$		*Sum*	*Day*
	K-Indices			*K-Indices*			*K-Indices*			
1	3453	4344	30	3453	4334	29	4444	4344	31	1
2	4544	4565	37	4554	4565	38	6644	5778	47	2
3	5333	4554	32	4334	4555	33	7533	3555	36	3
4	2133	3364	25	2233	4454	27	1233	4564	28	4
5	4343	3232	24	4333	3232	23	5433	3232	25	5
6	4233	3335	26	4333	2234	24	4423	2234	24	6
7	1321	1343	18	1321	1243	17	1322	2243	19	7
8	1312	3231	16	0323	3231	17	1322	2232	17	8
9	0101	2353	15	0102	2343	15	1102	2244	16	9
10	3222	2214	18	3223	2223	19	3112	2123	15	10
11	2202	2111	11	2111	2112	11	2101	1111	8	11
12	2211	2233	16	2212	1233	16	2201	1133	13	12
13	2112	4224	18	2112	3224	17	2112	3224	17	13
14	4334	4443	29	4333	4443	28	5323	3343	26	14
15	2121	1102	10	3111	1002	9	2011	1102	8	15
16	0011	2333	13	1011	2333	14	1012	1433	15	16
17	2422	3101	15	1322	3112	15	2332	2101	14	17
18	2122	3252	19	1212	2352	18	1212	2261	17	18
19	2222	3201	14	2232	3212	17	1122	2201	11	19
20	3101	1001	7	3111	0012	9	3111	0001	7	20
21	1212	3433	19	1212	3433	19	0212	4434	20	21
22	3433	3233	24	3333	3232	22	4332	2233	22	22
23	5444	3253	30	4444	3353	30	5443	4353	31	23
24	3112	2222	15	2211	3222	15	2311	2222	15	24
25	3112	3224	18	3112	3224	18	2111	3325	18	25
26	3123	3123	18	2123	3223	18	3122	2113	15	26
27	3222	2234	20	3222	2234	20	3122	1233	17	27
28	5765	3344	37	4655	4345	36	5764	3355	38	28
29	3213	2232	18	3113	3232	18	4413	3232	22	29
30	2244	4644	30	2144	4544	28	2234	5756	34	30

VOL. 18 1960

December 1959

Day	*Ha* Range for $K = 9 : 500\gamma$			*Es* Range for $K = 9 : 750\gamma$			*Le* Range for $K = 9 : 1000\gamma$			*Day*
	K-Indices		*Sum*	*K-Indices*		*Sum*	*K-Indices*		*Sum*	
1	4333	3332	24	4333	3332	24	4433	3332	25	1
2	3334	3444	28	3334	3444	28	3333	3444	27	2
3	5434	4645	35	4433	4545	32	4444	4635	34	3
4	3322	2233	20	3322	1133	18	3311	1233	17	4
5	1034	5676	32	0033	5696	32	0033	6886	34	5
6	3323	3232	21	2333	3232	21	2322	3232	19	6
7	3212	2102	13	3211	1202	12	3200	1102	9	7
8	1112	1332	14	1112	2322	14	1110	1232	11	8
9	1123	3202	14	1122	3222	15	2122	2212	14	9
10	3112	1122	13	3111	1222	13	3110	1123	12	10
11	0112	2211	10	1222	2212	14	1211	1212	11	11
12	2323	2234	21	2312	2233	18	2222	2134	18	12
13	3322	1235	21	3321	1335	21	4211	1235	19	13
14	4444	4553	33	4343	4553	31	6433	3653	33	14
15	3333	3444	27	3333	3444	27	3333	2344	25	15
16	4123	3423	22	3122	3423	20	3222	2424	21	16
17	3122	1113	14	3122	2113	15	3122	1112	13	17
18	2122	3112	14	3222	2212	16	2122	2212	14	18
19	2233	3231	19	2222	3232	18	2222	3331	18	19
20	3221	1222	15	3122	1221	14	3111	1222	13	20
21	2111	1011	8	1111	1112	9	2111	1012	9	21
22	2000	1323	11	2011	1333	14	2010	1223	11	22
23	2222	2545	24	2233	3545	27	2132	2745	26	23
24	4133	3112	18	3133	2122	17	3133	2211	16	24
25	1212	2123	14	2212	1233	16	2211	1122	12	25
26	2323	3345	25	2324	3345	26	2233	3345	25	26
27	5334	4454	32	4334	4443	29	4333	3445	29	27
28	4433	5543	31	4434	4543	31	5333	4644	32	28
29	3333	3313	22	3323	3312	20	3332	3212	19	29
30	2222	2331	17	2223	3331	19	2222	3332	19	30
31	2111	1032	11	2222	1132	15	2221	1032	13	31

January 1960

Day	*Ha* Range for $K = 9 : 500\gamma$			*Es* Range for $K = 9 : 750\gamma$			*Le* Range for $K = 9 : 1000\gamma$			*Day*
	K-Indices		*Sum*	*K-Indices*		*Sum*	*K-Indices*		*Sum*	
1	2001	1001	5	1112	1111	9	2111	1111	9	1
2	1111	2111	9	1113	2121	12	1012	2112	10	2
3	3201	2121	12	2212	2221	14	2202	1211	11	3
4	2133	3312	18	2133	3312	18	2122	2212	14	4
5	3433	3334	26	3432	3334	25	3332	3324	23	5
6	3222	2221	16	3211	2222	15	3211	2121	13	6
7	1122	2211	12	1122	1211	11	1121	1221	11	7
8	2201	1122	11	2211	1222	13	2211	1122	12	8
9	1210	1111	8	1121	1111	9	1110	1001	5	9
10	1244	4465	30	2144	4655	31	1133	4855	30	10
11	3233	5433	26	3244	4433	27	3333	4423	25	11
12	3122	3334	21	3222	3334	22	3212	2334	20	12
13	2211	1133	14	2211	2133	15	2211	2134	16	13
14	4433	3355	30	4433	3354	29	6433	2277	34	14
15	5432	3322	24	5433	3322	25	7522	2222	24	15
16	0210	1113	9	1101	1223	11	1100	1113	8	16
17	3211	4312	17	3322	4322	21	3321	3211	16	17
18	1143	3233	20	2143	3233	21	1143	2123	17	18
19	3101	2122	12	3212	2212	15	4211	1121	13	19
20	2323	3322	20	1324	3322	20	2223	2322	18	20
21	6334	4565	36	6334	4465	35	6333	3564	33	21
22	4234	2313	22	3234	3323	23	3333	2223	21	22
23	2332	3343	23	2332	3343	23	2332	3333	22	23
24	3323	3333	23	2333	3322	21	3322	3322	20	24
25	2212	2331	16	2222	2331	17	2211	2331	15	25
26	1212	2112	12	1112	2222	13	1112	2212	12	26
27	3312	2101	13	3312	2212	16	3211	1111	11	27
28	3001	2131	11	2112	2131	13	2211	2121	12	28
29	2232	3212	17	2333	3222	20	2232	2221	16	29
30	0001	0000	1	0012	1110	6	0012	1110	6	30
31	0001	1100	3	0112	2111	9	0102	1011	6	31

VOL. 18 1960

February 1960

Day	*Ha* *Range for* $K = 9 : 500\gamma$			*Es* *Range for* $K = 9 : 750\gamma$			*Le* *Range for* $K = 9 : 1000\gamma$			*Day*
	K-Indices		*Sum*	*K-Indices*		*Sum*	*K-Indices*		*Sum*	
1	0212	3221	13	0222	3221	14	0112	3221	12	1
2	1202	3443	19	1112	3444	20	1102	3464	21	2
3	2223	3344	23	2223	3334	22	2223	3345	24	3
4	3423	3233	23	3322	2243	21	3332	2244	23	4
5	1024	3323	18	2124	4323	21	1013	3324	17	5
6	4432	2312	21	3431	2322	20	5532	2321	23	6
7	2221	0000	7	2221	1001	9	2211	1000	7	7
8	0022	3311	12	1123	3221	15	0012	2221	10	8
9	3101	1221	11	3111	1221	12	3201	0111	9	9
10	1222	1100	9	1222	2110	11	0112	1110	7	10
11	0012	1233	12	0012	1333	13	0002	1233	11	11
12	3211	2100	10	3121	2110	11	3211	1100	9	12
13	0021	2144	14	0012	2135	14	0021	1136	14	13
14	4322	3353	25	4323	3353	26	5332	3363	28	14
15	2001	3331	13	1011	3321	12	1011	3331	13	15
16	4223	5434	27	4223	5434	27	4223	4425	26	16
17	3232	3344	24	3233	3334	24	4232	3344	25	17
18	4433	2342	25	5433	3342	27	6442	2342	27	18
19	2133	2444	23	2133	2444	23	2122	2445	22	19
20	5332	2313	22	4322	3323	22	5321	2313	20	20
21	2334	3433	25	2334	3433	25	3333	2433	24	21
22	1123	2233	17	1122	2233	16	1122	2233	16	22
23	2222	2321	16	2222	2322	17	1212	2322	15	23
24	0211	1100	6	0210	2010	6	1110	1110	6	24
25	1001	1003	6	1000	1113	7	1012	1112	9	25
26	0002	2221	9	0002	2321	10	1002	1312	10	26
27	4434	3343	28	3433	3333	25	4333	2233	23	27
28	2112	2201	11	2222	2201	13	3122	1110	11	28
29	4232	3233	22	4232	3233	22	3332	2233	21	29

March 1960

Day	*Ha* Range for $K = 9 : 500\gamma$		*Es* Range for $K = 9 : 750\gamma$		*Le* Range for $K = 9 : 1000\gamma$		*Day*
	K-Indices	*Sum*	*K-Indices*	*Sum*	*K-Indices*	*Sum*	
1	2332 3353	24	2332 3353	24	3322 3353	24	1
2	4333 3334	26	4333 3334	26	4333 2334	25	2
3	2333 3334	24	3333 3333	24	3333 3333	24	3
4	2222 4433	22	2222 4434	23	2222 4444	24	4
5	2231 3343	21	2231 3334	21	2231 3234	20	5
6	2322 2232	18	2223 2232	18	3222 2232	18	6
7	0012 1110	6	1112 1110	8	1112 1110	8	7
8	1133 2222	16	0233 2223	17	0122 2222	13	8
9	2223 2222	17	1123 2322	16	2122 2322	16	9
10	2244 2342	23	2234 3442	24	1234 2342	21	10
11	3435 4443	30	3334 3442	26	3334 3553	29	11
12	2221 3312	16	2122 3312	16	3122 2222	16	12
13	2121 1222	13	2121 1322	14	2111 1222	12	13
14	1122 2311	13	1112 2312	13	1121 1301	10	14
15	2011 3455	21	2011 3445	20	1011 2456	20	15
16	5542 3355	32	5533 3354	31	6652 3456	37	16
17	4333 2343	25	3333 3343	25	3333 2343	24	17
18	3332 2103	17	2232 3113	17	2232 2103	15	18
19	2123 3201	14	2123 3311	16	3112 3311	15	19
20	1121 1100	7	1221 2201	11	1120 1101	7	20
21	0112 3200	9	1112 3201	11	1112 3200	10	21
22	0111 2102	8	1112 3112	12	0001 2112	7	22
23	2001 1102	7	2101 1212	10	2101 0103	8	23
24	4222 2433	22	4222 2433	22	4321 1432	20	24
25	0111 2024	11	1122 2123	14	1111 2123	12	25
26	3112 2110	11	3112 2110	11	3112 2111	12	26
27	2212 1000	8	1212 2101	10	1222 1101	10	27
28	0123 2354	20	0113 3444	20	1123 2354	21	28
29	4333 2224	23	4333 2223	22	4432 1214	21	29
30	4222 3444	25	4212 3444	24	4222 3445	26	30
31	4446 5767	43	4336 5888	45	4335 4879	43	31

VOL. 18 1960

Journal of Atmospheric and Terrestrial Physics, 1960, Vol. 18, p. 264. Pergamon Press Ltd. Printed in Northern Ireland

Papers to be published in future issues

P. Dasgupta and K. K. Vij: Statistical analysis of fading of a single down-coming wave

G. H. Bazzard: Short-term differences in the behaviour of two daily indices of solar activity during the IGY

J. W. Wright: Some magnetoionic phenomena of the Arctic *E*-region

C. M. Minnis and G. H. Bazzard: A monthly ionospheric index of solar activity based on *F2*-layer ionization at eleven stations

C. M. Minnis and G. H. Bazzard: A world-wide semi-annual cycle in the *E*-layer of the ionosphere

L. R. Megill, P. M. Jamnick and J. E. Cruz: Seasonal variations in the twilight enhancement of [OI] 5577

Syun-Ichi Akasofu: Large-scale auroral motions and polar magnetic disturbances—I. A polar disturbance at about 1100 hours on 23 September 1957

C. D. Watkins: The height and geometry of auroral radio echoes

R. G. Rastogi: A synoptic study of the *F2*-region of the ionosphere in the Asian zone

I. L. Jones: Further observations of radio stellar scintillation

C. S. G. Setty: Eclipse effects on the *F*-layer at sunrise

C. S. G. Setty: Some studies of bifurcation of the ionospheric *F*-layer into *F1* and *F2*

C. S. G. Setty: A pre-sunrise phenomena and the presence of negative ions in the *F*-region of the ionosphere

C. S. G. Setty: Eclipse effects on the *F1*-layer observed at Cambridge on 30 June 1954

F. Hepburn: Analysis of smooth type atmospheric waveforms

H. J. A. Chivers: Observed variations in the amplitude scintillations of the Cassiopeia (23N5A) radio source

W. A. Cilliers: The fading of low-frequency radio waves reflected from the ionosphere

B. McInnes and K. A. Robertson: Latitude distribution and seasonal variation of aurora over the British Isles during 1957 and 1958

A. J. Lyon, N. J. Skinner and R. W. H. Wright: The belt of equatorial spread-*F*

V. Marasigan, S.J.: Damping coefficient of vibrating electrons

D. R. Currie and K. S. Kreielsheimer: A double field mill for the measurement of potential gradients in the atmosphere

B. J. Robinson: On some disturbances in the *E*-region

V. Agy: Spiral patterns in geophysics

S. N. Mitra, K. K. Vij and P. Dasgupta: Horizontal drift in the ionosphere over Delhi

VOL
18
196

Journal of Atmospheric and Terrestrial Physics, 1960, Vol. 18, pp. 265 to 275. Pergamon Press Ltd. Printed in Northern Ireland

Statistical analysis of fading of a single down-coming wave

P. DASGUPTA and K. K. VIJ
Research Department, All India Radio, New Delhi

(*Received* 21 *November* 1959)

Abstract—The paper deals with the statistical analysis of fading of a single wave reflected (vertically) from the F-region of the ionosphere. These fading records are usually random and their amplitude distribution has been found by other workers to be Rayleigh, Gaussian or log-normal. The present analysis shows that the amplitude distribution is Rayleigh only in the case of rapid fading, whereas for slow and quasi-periodic fading it is found to represent what can be termed as an M-type. The distribution of successive differences in the amplitudes has also been studied; for a Rayleigh amplitude distribution this time analysis gives rise to a Type-VII distribution of PEARSON as originally pointed out by MITRA (1949b) while in the case of M-type amplitude distribution it becomes Gaussian. Following MITRA's analysis, the r.m.s. value of the random velocity, v_0 of the ionospheric irregularities has been calculated from the time analysis. The value of v_0 has also been calculated from the autocorrelation coefficient of the amplitude R following BOOKER *et al.* (1950). The two values of v_0 thus obtained are compared and are found to agree well.

INTRODUCTION

IT IS well known that the fading of a short wave reflected from the ionosphere is caused either by (a) change in absorption, or (b) interference between several components. Under normal conditions the rate of change of absorption is small, thus making the effect of absorption on short period fading negligible.

The interference fading may be due to one or more of the following causes:

(1) Interference between ground and sky waves, when the receiver is close to the transmitter.

(2) Interference between multiply-reflected waves from one or more ionospheric layers.

(3) Interference between waves reflected from different layers (the so-called M-reflection).

(4) Interference between two magneto-ionic components.

(5) Interference between waves scattered from the local irregularities in the ionosphere.

The fading due to the first three causes can be eliminated by using pulse technique of ionospheric sounding and selecting a single echo by means of an electronic gate. Interference between the magneto-ionic components produces a periodic fading (MITRA, 1949a) and can easily be detected from an inspection of the records. Thus, by proper circuit arrangements and by selecting a fading record which is non-periodic, it is possible to obtain a fading curve which is due only to the last effect.

A short-wave signal incident on the ionosphere is often diffractively scattered by the ionospheric irregularities and the signal strength at a point on the ground is the resultant of a large number of vectors representing the amplitudes and phases of many scattered wavelets within a cone. As the irregularities move, the relative phases of the wavelets change and hence the resultant amplitude also changes. The irregularities may have either a steady drift or a random motion or both.

When the fading is due to the interference between the scattered wavelets, two types of fading are generally experienced:

(1) Quick random fading. The cause of this type of fading is assumed to be predominantly due to random motion of the irregularities amongst themselves.

(2) Slow and quasi-periodic fading. This is presumably caused by a steady drift of the ionospheric irregularities.

Assuming that the irregularities are distributed at random in a horizontal plane, the relative changes in phase of the scattered wavelets in both the cases are random, and hence the resultant amplitude should also change in a random manner. For such fading curves we may expect that the amplitude distribution will be a Rayleigh one. It will be shown in the following sections that the amplitude distribution is not always Rayleigh. For rapid fading, it no doubt resembles a Rayleigh but for slow quasi-periodic fading the distribution is what can be termed as M-type. This is rather surprising as most of the earlier investigators on the subject have indicated only Rayleigh, Gaussian and log-normal amplitude distributions.

The random fading of a single wave from the ionosphere is analogous to a similar situation on random electrical noise and Rice (1944, 1945) was the first to develop full statistical theories for such a phenomenon. He also worked out the distribution of successive differences in the amplitudes, called time distribution. Fürth and MacDonald (1947) later extended the analysis and showed, from theoretical considerations, that when the amplitude distribution is Rayleigh, the time-analysis is Gaussian. Statistical analysis of the fading curves has, however, indicated that this is not always the case. Mitra (1949b) found that such a time analysis is better represented by a Type-VII curve of Pearson and also offered theoretical justification as to why it should be so. McNicol (1949), following similar analysis of fading on c.w. transmissions, came to the same conclusions. We have also attempted time analysis of the fading curve; it is found that Type-VII curve is always a better representation when the amplitude distribution is Rayleigh (rapid fading). For M-type amplitude distribution (slow fading), however, the time analysis gives a Gaussian curve.

It is possible to determine the r.m.s. value of the random velocity of the ionospheric irregularities from the time analysis of the fading curve. This can also be calculated from the autocorrelation function of the amplitude in the fading wave (Booker *et al.*, 1955). We have also carried out the autocorrelation analysis and the results obtained are presented in the paper.

Experimental Procedure

The fading records considered are from those obtained in the spaced receiver experiment for studying the horizontal drift in the ionosphere at Delhi (28°35′N, 77°5′E) by Mitra's technique (1949a). The fading curves were taken on a frequency of 6·5 Mc/s. Typical records of the rapid and slow type of fading utilized in this paper for statistical analysis are shown in Figs. 1 and 2. Statistical analysis was made of only one of the three fading curves in each case. For amplitude distribution, successive amplitudes were read off at an interval of 0·05 sec. The interval was varied while analysing the M-type of distribution.

VOL
18
196

Theoretical Considerations

(a) *Amplitude distribution*

Before we come to the various parameters in the amplitude distribution, it is considered worth while to briefly discuss the basic theory.

The resultant amplitude of the received signal at a point at any instant is the sum of a large number of vectors, each having a random phase. Each vector here corresponds to a wave scattered from a scattering centre moving in a random manner. Lord Rayleigh (1899) has given the mathematical expression for the probability $P(R)$ of the amplitude R for a completely random phenomenon, and a similar situation arises in the problem of random fading. $P(R)$ is given by

$$P(R) = \frac{R}{\psi} \exp\left(\frac{-R^2}{2\psi}\right) \tag{1}$$

where $\int_0^\infty P(R)\,dR = 1$ and $\psi = \int_0^\infty W(f)\,df$

$W(f)$ being the density in the power spectrum. ψ is related to the mean value $\bar{R}$, the mean squared value $\bar{R}^2$ and R_m, the value of R for which $P(R)$ is maximum by the following equations:

$$\bar{R} = \int_0^\infty P(R) R\,dR = \left(\frac{\pi\psi}{2}\right)^{1/2} \tag{2}$$

$$\bar{R}^2 = \int_0^\infty P(R) R^2\,dR = 2\psi \tag{3}$$

$$R_m = \psi^{1/2} \tag{4}$$

ψ can also be calculated from a plot of $\log P(R)/R$ against R^2 which is a straight line and is given by the equation:

$$\log \frac{P(R)}{R} = \log \frac{1}{\psi} - \frac{R^2}{2\psi}.$$

The intercept on $\log P(R)/R$ axis is $\log 1/\psi$ and the slope of the straight line is $1/2\psi$.

(b) *Time analysis*

It is assumed that the scattering centres, whose motion causes the fading, are in continual random motion in such a way that probability distribution $P(v)$ of the line-of-sight velocity v is given by a normal law:

$$P(v) = \frac{1}{\sqrt{(2\pi)}\,v_0} \exp\left(-\frac{v^2}{2{v_0}^2}\right) \tag{5}$$

where $\int_{-\infty}^{\infty} P(v)\,dv = 1$

v_0 = r.m.s. value of the random velocity.

These scattering centres, by their motion produce Doppler shift of frequency, the modified frequency f being given by

$$f = f_0\left(1 + \frac{2v}{c}\right) \tag{6}$$

where f_0 is the incident wave-frequency and c is the velocity of light. $P(f)$ is given by

$$P(f) = \frac{1}{\sqrt{(2\pi)}\, v_0} \frac{c}{2f_0} \exp\left[-\frac{c^2(f-f_0)^2}{8f_0^2 v_0^2}\right].$$

Let $$\sigma = \frac{2f_0 v_0}{c} = \frac{2v_0}{\lambda}.$$

Then $$P(f) = \frac{1}{\sqrt{(2\pi)}\,\sigma} \exp\left[-\frac{(f-f_0)^2}{2\sigma^2}\right]. \tag{7}$$

Since the scattering centres are oriented in a random manner, the phases of the scattered waves from the individual centres are also distributed at random. Powers due to each contribution add up and the power spectrum $W(f)$ is given by

$$W(f) = \frac{\psi}{\sqrt{(2\pi)}\,\sigma} \exp\left[-\frac{(f-f_0)^2}{2\sigma^2}\right] \tag{8}$$

where $\psi = \int_0^\infty W(f)\, df$ = total energy in this power spectrum.

The fading of the resultant is, therefore, due to the interference between different frequency components, frequency distribution of which is given by (7). The situation is analogous to what results if random noise were passed through a filter whose band-pass characteristic is given by (8).

Extending RICE's (1944, 1945) theory, FÜRTH and MACDONALD (1947) derived an expression for the probability distribution of v_τ, when the random noise has a Rayleigh amplitude distribution and is passed through a band-pass filter whose power characteristic is given by (8). v_τ is the difference between two successive amplitudes within a small interval of time τ.

The expression for $P(v_\tau)$ is

$$P(v_\tau)\, dv_\tau = \frac{1}{\sqrt{\pi}} \exp(-x^2)\, dx \tag{9}$$

where $$x = \frac{v_\tau}{2\pi\sigma\tau\sqrt{(2\psi)}} \tag{9a}$$

which shows that the probability distribution of v_τ is Gaussian.

We have earlier pointed out that analysis of experimental results has indicated that in actual practice distribution of v_τ is given by a Type-VII curve of PEARSON. This can be tested in the following way:

The v_τ distribution, as found from the analysis of experimental data, is first plotted. Then a χ^2-test (goodness of fit) gives the best fit to a theoretical Gaussian curve or a Type VII-curve of PEARSON. Depending on the value of χ^2, the distribution of v_τ is selected.

The equation for Type-VII curve is given by

$$P(v_\tau) = A\left(1 + \frac{v_\tau^2}{a^2}\right)^{-m} \tag{10}$$

where

$$A = \frac{N}{a} \cdot \frac{\overline{\lfloor m}}{\sqrt{(\pi)}\,\overline{\lfloor m - \frac{1}{2}}}$$

$$m = \frac{5\beta_2 - 9}{2(\beta_2 - 3)}$$

$$a^2 = \frac{2\mu_2\beta_2}{\beta_2 - 3}$$

and N = total number of observations; μ_2 and β_2 are corrected second-order moment about the mean and the coefficient of excess in the distribution respectively; β_2 is given by $\beta_2 = \mu_4/\mu_2^2$, μ_4 being the corrected fourth order moment.

The equation for a Gaussian distribution is given by

$$P(v_\tau) = \frac{1}{\sigma\sqrt{(2\pi)}} \exp\left(\frac{-v\tau^2}{2\sigma^2}\right) \tag{11}$$

where σ = standard deviation $= \sqrt{\mu_2}$. The difference between a Gaussian distribution and a Type-VII distribution of PEARSON is that for Gaussian curve, $\beta_1 = 0$ and $\beta_2 = 3$, where $\beta_1 = \mu_3^2/\mu_2^3$, μ_3 is the corrected third order moment; and for Type-VII distribution, $\beta_1 = 0$ and $\beta_2 > 3$.

Physically, a Type-VII distribution differs from a Gaussian one by that it is narrower around maxima and wider at the skirts.

The goodness of fit or χ^2-test is made as follows:

$$\chi^2 = \sum \frac{(F_1 \sim F_2)^2}{F_1} \tag{12}$$

where F_1 and F_2 are the calculated and observed frequencies of v_τ, respectively. Standard tables are available for $P(\chi^2)$ for different values of degree of freedom, from which the goodness of fit of the observed curve to the Gaussian or Type-VII can be obtained.

(c) *Calculation of* v_0

For normal distribution of $P(v_\tau)$ the value of v_0, the r.m.s. velocity of the irregularities in the line of sight, can be found out as follows: from (9) and (9a)

$$\frac{\overline{|v_\tau|}}{\tau} = \frac{2}{\tau}\int_0^\infty P(v\tau)v\tau\, dv\tau$$

$$= \sqrt{(2\pi\psi)} \cdot 2\sigma$$

$$= 4\bar{R}\sigma = \frac{8v_0\bar{R}}{\lambda} \tag{13}$$

VOL. 18 1960

where $\sigma = 2v_0/\lambda$ and λ is the wavelength of the radio wave used. v_0 can also be calculated from (9) in another way:

$$\overline{v\tau^2} = \int_{-\infty}^{\infty} P(v\tau) v_\tau^2 \, dv_\tau$$

$$= \tfrac{1}{2}\{2\pi\sigma\tau \sqrt{(2\psi)}\}^2$$

$$= \frac{16\pi^2 v_0^2 \tau^2}{\lambda^2} \psi \, . \tag{14}$$

(d) *Calculation of v_0 from autocorrelation function*

The value of v_0 can also be calculated from a knowledge of the autocorrelation function $\rho(\tau)$ of the amplitude R from its temporal variation. Booker *et al.*, (1950) expressed the autocorrelation function $\rho(\tau)$ in terms of the angular spectrum. They studied the problem of diffractive scattering by the ionospheric irregularities from its optical analogy and considered the ionospheric irregularities as constituting a diffracting screen with the transmitter as a point source of radiation situated on the other side of the ionosphere.

In such a case $\rho(\tau)$ is given by

$$\rho(\tau) = \frac{\int_{-\infty}^{\infty} R(t)R(t+\tau)\,dt - \left[\int_{-\infty}^{\infty} R(t)\,dt\right]^2}{\int_{-\infty}^{\infty} [R(t)]^2\,dt - \left[\int_{-\infty}^{\infty} R(t)\,dt\right]^2} \, . \tag{15}$$

The probability distribution of Doppler shifted frequency f is already known from (7). Now applying the well-known Wiener's theorem (i.e. the autocorrelation function is proportional to the Fourier transform of the distribution of power in the power spectrum), it can be shown that

$$\rho(\tau) \propto \exp\left(-\frac{16\pi^2 v_0^2 \tau^2}{\lambda^2}\right) . \tag{16}$$

Thus $\rho(\tau)$ falls to e^{-1} after a time $\tau = (\lambda/4\pi v_0)$. Knowing the value of τ, v_0 can be calculated.

Experimental Results

As has already been mentioned we have concentrated mainly on two types of fading curve, the rapid fading and slow quasi-periodic fading. The analysis of a few representative samples of such fading is given below.

Group 1.—*Rapid random fading*

A typical record is shown in Fig. 1. Statistical analysis has been subjected to the topmost curve only.

(i) *Amplitude distribution.* The amplitudes are read off at an interval of 0·05 sec from the fading record. The probability distribution for the amplitude is shown in Fig. 3. A theoretical curve obtained from equation (1) is also plotted and it is evident that the observed curve satisfactorily follows a Rayleigh distribution.

VOL.
18
1960

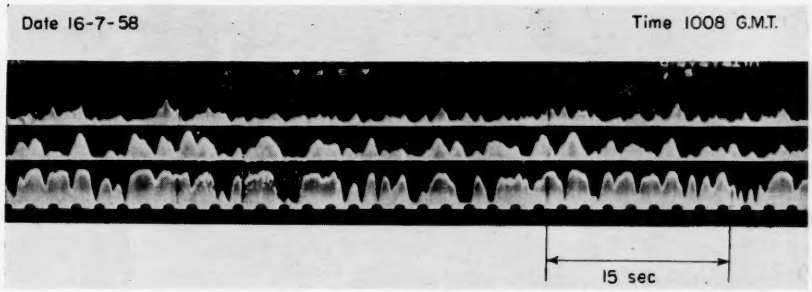

Fig. 1. Rapid fading.

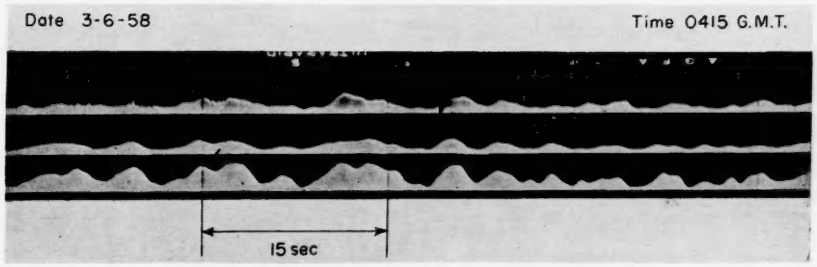

Fig. 2. Slow quasi-periodic fading.

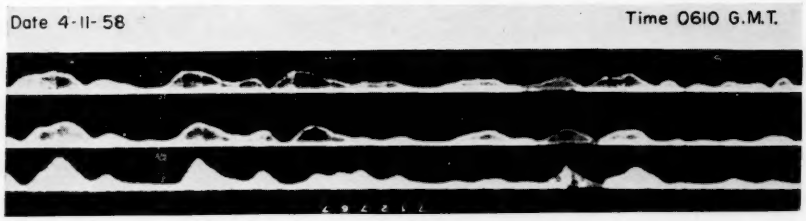

Fig. 7(a). Slow quasi-periodic fading.

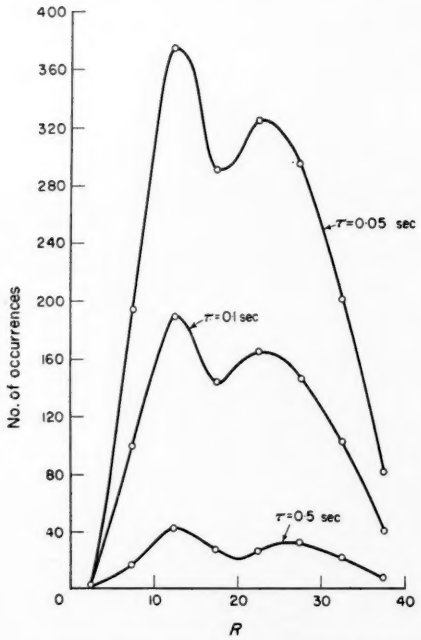

Fig. 7(b). Amplitude distribution of slow fading.

VOL
18
196

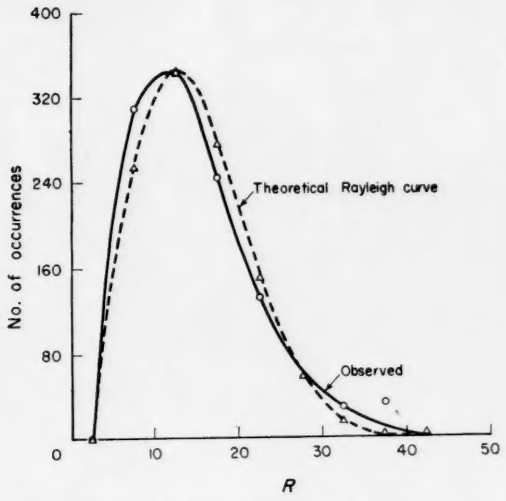

Fig. 3. Amplitude distribution of rapid fading compared with theory.

(ii) *Time analysis.* The probability distribution of v_τ, the difference between two successive amplitudes, is shown in Fig. 4.

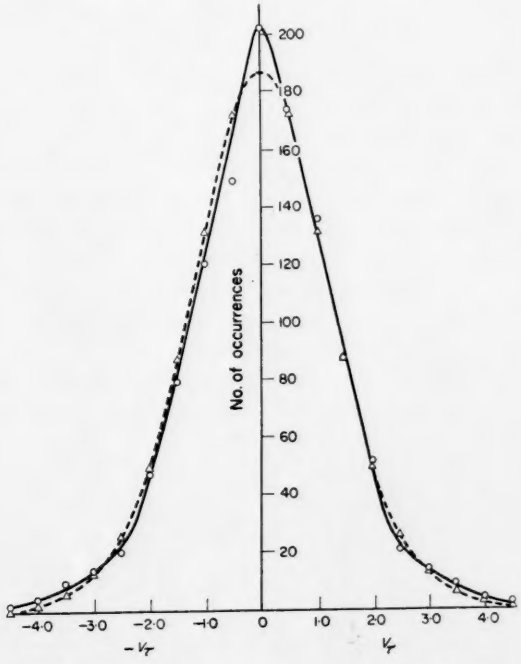

Fig. 4. Statistical distribution of v_τ for $\tau = 0{\cdot}5$ compared with theory. ○ Experimental points. △ Computed points from (10). — Smooth curve through experimental points. - - - - Theoretical Gaussian curve.

To determine the distribution, i.e. whether it is Gaussian or Type-VII of PEARSON, β_1 and β_2 are first calculated. They are

$$\beta_1 = 0{\cdot}000155 \simeq 0, \qquad \text{and} \qquad \beta_2 = 3{\cdot}6$$

$\beta_1 = 0$ and $\beta_2 = 3$ are the conditions for a Type-VII distribution of PEARSON. To test the degree of fitness of the Type-VII curve to the observed one, the theoretical Type-VII curve is also drawn.

The equation of Type-VII curve is given by (10).

Here
$$m = \frac{5\beta_2 - 9}{2(\beta_2 - 3)} = 7{\cdot}5$$

$$a^2 = \frac{2\mu_2\beta_2}{\beta_2 - 3} = 83{\cdot}57$$

whence
$$\frac{1}{a^2} = 0{\cdot}012 \qquad \text{and} \qquad a = 9{\cdot}14$$

$$A = \frac{N}{a} \frac{\overline{\lfloor m}}{\sqrt{(\pi)}\ \overline{\lfloor m - \frac{1}{2}}} = 187{\cdot}5\ .$$

Then the equation for the theoretical curve becomes

$$P(v\tau) = 187{\cdot}5(1 + 0{\cdot}012\ v\tau^2)^{-7{\cdot}5}.$$

The theoretical points are calculated and are plotted in Fig. 4. χ^2 is calculated and percentage $P(\chi^2)$ is found to be 94 per cent. χ^2-test is done for a theoretical Gaussian curve also. $P(\chi^2)$ for the Gaussian distribution is only 2·4 per cent.

The χ^2-test has also been carried out for several other curves of this type and in all the cases the goodness of fit for Type-VII is found to be much higher than that for a Gaussian distribution. In some cases the degree of fitness is found to be as high as 99·9 per cent for Type-VII distribution.

Although $P(v\tau)$ distribution is Type-VII curve of PEARSON, for all practical purposes, where the main object is to calculate the value of v_0, this can be treated as a Gaussian distribution to a first approximation.

The value of v_0 is calculated from (13) and (14) and is found to be 9·7 m/sec.

(iii) *Calculation of v_0 from autocorrelation function $\rho(\tau)$ of* R. Autocorrelation function $\rho(\tau)$ is calculated for various values of τ and Fig. 5 gives the plot of $\rho(\tau)$ against τ. The value of τ for which $\rho(\tau)$ falls to e^{-1} is 0·36 sec.

Therefore
$$v_0 = \frac{\lambda}{4\pi\tau} = 10{\cdot}2 \text{ m/sec } (f = 6{\cdot}5 \text{ Mc/s}).$$

This value of v_0 agrees well with the value calculated by the previous method.

Group 2.—Slow and quasi-periodic fading

A typical record of this type is shown in Fig. 2. Statistical analysis has been carried out only on the lowermost curve.

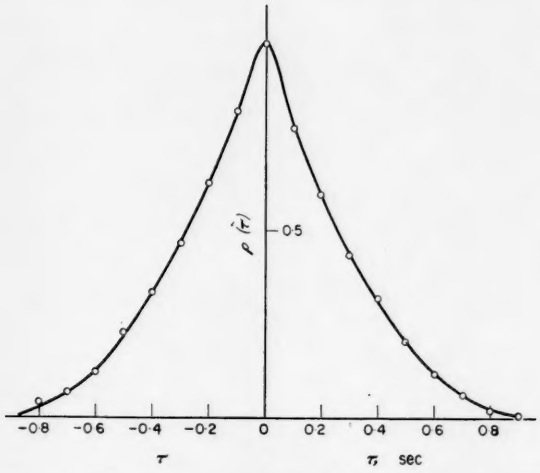

Fig. 5. Autocorrelation of rapid fading.

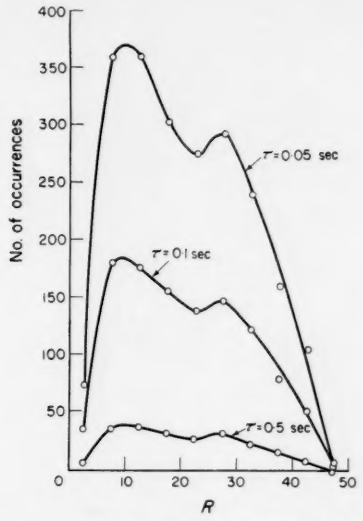

Fig. 6. Amplitude distribution of slow fading.

(i) *Amplitude distribution.* The amplitudes are read off at an interval of 0·05 sec from the fading record and the probability distribution for the amplitudes is shown in Fig. 6.

Unlike the rapid fading, where the amplitude distribution is Rayleigh, the distribution in this case is found to be what can be termed as an M-type. The effect of increasing the time interval between the successive amplitudes is also studied and curves are drawn for different values of τ in Fig. 6. It is evident from the figure that the amplitude distribution is independent of τ and is M-type in the range of τ considered.

The M-type distribution, as obtained from the analysis of slow fading records, has not been observed by other workers. We have carried out statistical analysis of a large number of slow-fading records to ensure that the M-distribution is truly representative. In all the cases, M-distribution is evident. Fig. 7(b) showed another typical example where curves are plotted for $\tau = 0{\cdot}05$, $\tau = 0{\cdot}01$ and $\tau = 0{\cdot}5$ and the distribution of $P(R)$ is identical (M-type) in all the cases. Fig. 7(a) is the corresponding fading curve.

(ii) *Time analysis.* It is not known why the slow fading curves should consistently give an M-type amplitude distribution. We have, however, carried out time analysis of these fading curves in the conventional manner and Fig. 8 shows the distribution of v_r. Surprisingly enough, this distribution fits in extremely well with Gaussian curve, In this case

$$\beta_1 = 0{\cdot}002$$
$$\beta_2 = 2{\cdot}8$$

A theoretical Gaussian curve has also been plotted in Fig. 8 (dotted line) and close correspondence between the observed and theoretical curves is very evident. $P(\chi^2)$ comes out to be 98 per cent for the Gaussian curve.

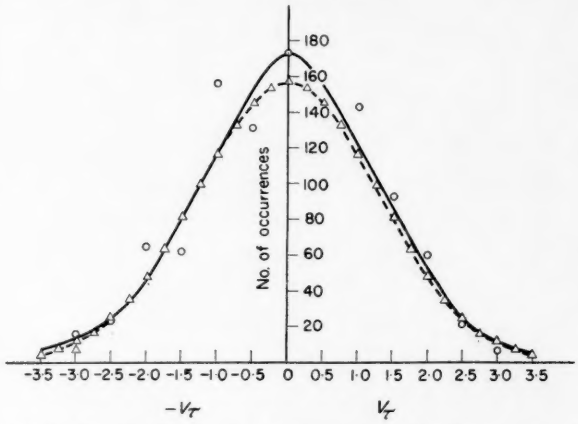

Fig. 8. Statistical distribution of v_T for $v = 0{\cdot}1$ sec compared with theory. ○ Experimental points. Δ Computed points from (11). — Smooth curve through experimental points. - - - - Theoretical Gaussian curve.

Since $P(R)$ distribution is of M-type, it is not possible to calculate the value of v_0 from (13) and (14) which hold good only for Rayleigh distribution. The value of v_0 can, however, be calculated from the autocorrelation function $\rho(\tau)$ assuming that the power density spectrum is also Gaussian.

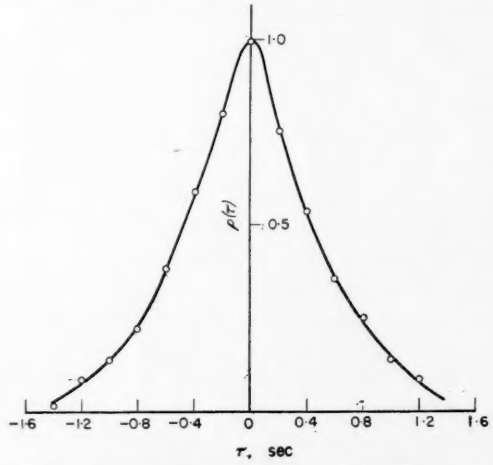

Fig. 9. Autocorrelation function of slow fading.

(iii) *Calculation of v_0 from autocorrelation function $\rho(\tau)$ of* R. $\rho(\tau)$ is found out for different values of τ and plotted in Fig. 9. The value of τ for which $\rho(\tau)$ falls to e^{-1} of its maximum is 0·59 sec. Thus $v_0 = 6{\cdot}2$ m/sec. In the case of rapid fading the value of v_0 has been found to be much higher.

CONCLUSION

From the experimental results, it is evident that the probability distribution of the resultant amplitude does not follow a Rayleigh distribution always, as thought

so far. The amplitude distribution is Rayleigh in the case of rapid random fading only, whereas in the case of quasi-periodic fading, it is usually M-type.

The time analysis shows that the distribution for the case of a Rayleigh distribution is of Type-VII curve of PEARSON. For M-type distribution, the v_τ distribution follows a Gaussian law. It is, however, not clear why the M-type amplitude distribution occurs and gives rise to a Gaussian curve for v_τ.

The values of the random velocity, v_0, calculated from (13) and (14) and from the autocorrelation coefficient agree well. For rapid fading, the value of v_0 is of the order of 10 m/sec, and for quasi-periodic fading it is about 6 m/sec (when the wave-frequency is 6·5 Mc/s).

Acknowledgements—The work described in the paper forms part of a programme of ionospheric research of All India Radio for the International Geophysical Year.

The authors wish to express their gratitude to Mr. S. N. MITRA, Assistant Research Engineer, All India Radio, New Delhi, for suggesting the problem and constant guidance all through the preparation of the paper. Thanks are due to the Council of Scientific and Industrial Research for financial assistance. The paper is published by permission of the Chief Engineer, All India Radio, New Delhi.

REFERENCES

BOOKER H. G., RATCLIFFE J. A. and SHINN D. H.	1950	*Phil. Trans.* A **262,** 579.
FÜRTH R. and MACDONALD D. K. C.	1947	*Proc. Phys. Soc. Lond.* **59,** 388.
MCNICOL R. W. E.	1949	*Proc. Instn Elect. Engrs* **96,** Pt. III, 517.
MITRA S. N.	1949a	*Proc. Instn Elect. Engrs* **96,** Pt. III, 441.
MITRA S. N.	1949b	*Proc. Instn Elect. Engrs* **96,** Pt. II, 505.
PEARSON K.	1931	*Mathematical Tables for Mathematicians and Biometricians.* Cambridge University Press.
RAYLEIGH, LORD	1899	*Collected Works*, vol. **1,** p. 495. Cambridge University Press.
RICE S. O.	1944	*Bell Syst. Tech. J.* **23,** 282.
RICE S. O.	1945	*Bell Syst. Tech. J.* **24,** 46.

VOL. 18 1960

Journal of Atmospheric and Terrestrial Physics, 1960, Vol. 18, pp. 276 to 289. Pergamon Press Ltd. Printed in Northern Ireland

Some magnetoionic phenomena of the Arctic *E*-region

J. W. WRIGHT
National Bureau of Standards,
Boulder Laboratories, Boulder, Colorado

(*Received* 27 *January* 1960)

Abstract—Several unusual phenomena of *E*-region ionogram echoes obtained at Thule, Greenland (mag. dip 85·5°) are described. They are explained as the effects of electron collisions on the propagation of radio waves at high-magnetic latitudes. The third magnetoionic component (*Z*-echo) is explained in this way and several of its distinguishing features are explained and illustrated. New phenomena demonstrate the existence of an *E*-pause (valley above $h_{\max}E$), and permit the measurement of electron densities and collision frequencies therein.

1. INTRODUCTION

THE double-refraction of radio waves in an ionosphere with a static magnetic field is described by the well-known refractive index equation of Appleton–Hartree (APPLETON, 1932). In its complete form including the effects of electron collisions it was shown by APPLETON and BUILDER (1933) that the shape of the dispersion curves and correspondingly, the nature of the propagation, could be classified into two forms, quasi-longitudinal (q.l.) or quasi-transverse (q.t.), according as the ratio

$$\left[\frac{\pi f_H}{\nu}\frac{\sin^2\theta}{\cos\theta}\right]$$

is greater than or less than unity. It may be noted that whether the propagation be q.l. or q.t. depends not only upon θ, the direction of propagation relative to the magnetic field (of electron gyro-frequency f_H), but also upon the relative magnitude of the electron collisional frequency, ν. Fig. 1 shows how the ionosphere along the

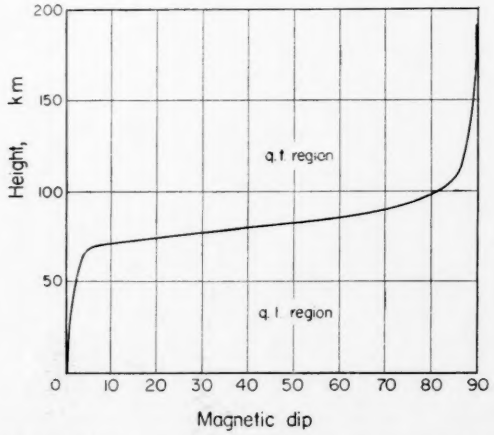

Fig. 1. Level of critical collision frequency in ionosphere separating regions of quasi-longitudinal and quasi-transverse vertical radio propagation. Values of ω_H and dip appropriate to 75°W geographic meridian.

75° W geographical meridian is divided into q.l. and q.t. regions, according to the above expression, and recent estimates (NICOLET, 1956) of collision frequency.

The significance of the terms q.l. and q.t. may be seen by inspection of Figs. 2(a, b) and 3(a, b), showing separately for the ordinary and extraordinary

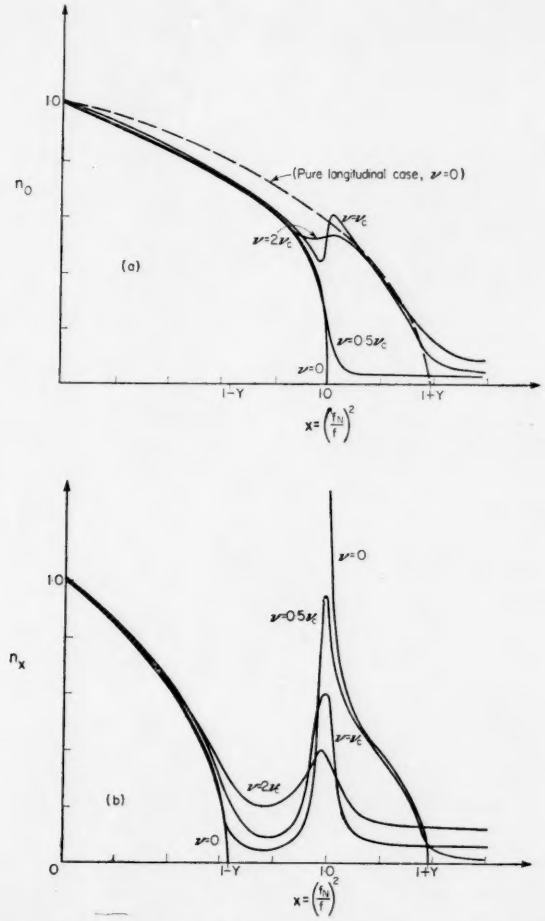

Fig. 2. Ionospheric refractive index for "ordinary" mode (a), and "extraordinary" mode (b). Illustrates the effect of variation of collision frequency (ν) about the critical value.

components the similarity between q.l. and q.t., and purely longitudinal or transverse propagation. These curves show the refractive and absorption indices (the real and imaginary parts, respectively, of the complex refractive index) as a function of $X = f_N^2/f^2$ (proportional to electron density, $N(\text{el/cm}^2) = 12{,}400\, f_N^2$), and $Y = f_H/f$; the curves are parametric in ν/ν_c, where $\nu_c = \pi f_H(\sin^2\theta/\cos\theta)$, the "critical" collision frequency. It may be seen that the change from $\nu = 0{\cdot}5\nu_c$ to $\nu = 2\nu_c$ considerably alters the shape of the dispersion curves for values of $X \geqslant 1$. While those for $\nu > \nu_c$ correspond more closely to the purely longitudinal case,

those for $\nu < \nu_c$ correspond more closely to the purely transverse case; hence the terms q.l. and q.t.

Another important feature illustrated by the curves is the way the transverse extraordinary branch above $X = 1$, becomes continuous with the *ordinary* branch,

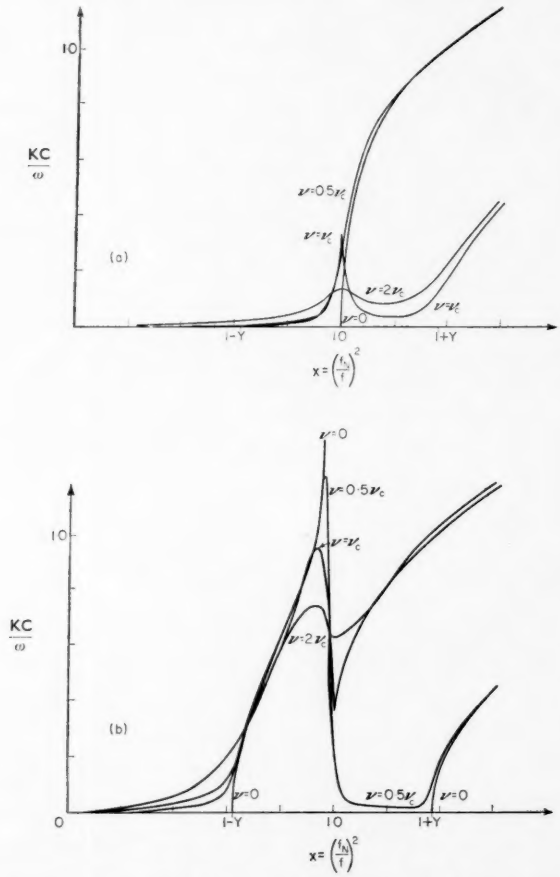

Fig. 3. Ionospheric absorption index for "ordinary" mode (a), and "extraordinary" mode (b). Illustrates effect of variation of collision frequency about the critical value.

as ν/ν_c increases through unity. This takes place via an identity* of both modes at $X = 1$, when $\nu = \nu_c$. This phenomena has been discussed quantitatively in terms, of mode coupling; detailed analyses (RYDBECK, 1950) show that coupling between modes occurs near $X = 1$ for ν near ν_c, and that it is especially strong in the "critical" coupling case $X = 1$, $\nu = \nu_c$.

It may be seen from Fig. 1, that the level $\nu = \nu_c$ remains at about 70–80 km except near the equator where it is well below the ionosphere and is of no interest,

* In Figs. 2 and 3, the identification of "ordinary" and "extraordinary" modes above $X = 1$ in the special case $\nu = \nu_c$, is purely arbitrary. We have chosen the representation shown here, in order better to illustrate the transition from q.t to q.l. conditions as ν/ν_c passes through unity.

VOL. 18 196

and above 80°, where it is located in the E-region. The possibility of observing effects due to transitions across this level in vertical soundings at high latitudes was suggested by LEPECHINSKY (1956) but the particular effects he envisaged do not seem to occur.

It is the purpose of this paper to show some examples of unusual E-region phenomena observed at high geomagnetic latitudes. These phenomena seem to be associated with the existence of the critical level, which should occur at these latitudes at an altitude of about 112 km. For several of the phenomena, a complete and quantitative explanation must await calculation using a full wave treatment, and this may be necessary to justify certain practical exploitations suggested below. However, an adequate phenomenological explanation may be based upon the propagation conditions described above.

2. PARTICULARS OF THE E-REGION AT THULE, GREENLAND

Although there is evidence that most of the phenomena to be described can be observed at other ionosphere sounding stations (for example, at Resolute Bay, Canada, and at one or two of the IGY stations in the Antarctic), the examples and explanations to be offered below refer specifically to conditions at the U.S. Army Signal Corps' station at Thule, Greenland. Table 1 gives pertinent data about the location and the E-region overhead.

Table 1. The E-region over Thule

Geographic co-ordinates	N 76°33′, W 68°50′
Geomagnetic latitude	N 88°6′
Magnetic dip (epoch 1955)	85°36′
Gyrofrequency (epoch 1955)	1·434 Mc/s
Critical collision frequency	$2{\cdot}66 \times 10^4$/sec (NICOLET, 1956)
Height of critical collision frequency	112 km (NICOLET, 1956)
Scale height, H (for collisions, at 112 km)	7 km (NICOLET, 1956)
Height separation between levels $\nu/\nu_c = 0{\cdot}5$ and $\nu/\nu_c = 2{\cdot}0$. $\left(= H \ln\left(\frac{2{\cdot}0}{0{\cdot}5}\right)\right)$	10 km
"Subsolar" f_0E (value implied for overhead sun from observed diurnal variation for 1958)	3·8 Mc/s

3. THE THIRD MAGNETOIONIC COMPONENT (Z-TRACE)

The first, and most striking observation to be made of Arctic E-region vertical soundings, is the occurrence there of the third magnetoionic component or Z-trace. Whereas Z-reflections from the F-region are occasionally seen at lower latitudes, the E-region Z-trace appears to be distinctly a polar phenomenon. The Z-trace corresponds to reflections at the third, or highest zero* of refractive index (at $X = 1 + Y$ of Fig. 2) and may be termed either the "second transverse extraordinary" level, or the "longitudinal ordinary" level. Both terms have been employed, and there seems to be little upon which to base a choice. The term

* In the presence of collisions, the refractive index cannot become zero (as illustrated by Fig. 2) and the condition for reflection to be applied is that dn/dX be large. This is the case near the conventional reflection levels $X = 1 - Y$, 1, and $1 + Y$.

"Z-trace" will be used here, as it can always be discerned from O and X on the surroundings.

Two different explanations have been offered for the E-region Z-trace, and it has not been clear whether either is exclusively the appropriate one. RYDBECK (1950), in an elaborate and meticulous study, showed that the coupling mechanism should produce this echo in the Arctic E-region. At about the same time SCOTT (1950) suggested that simple longitudinal propagation could explain all observations, and there the matter has rested. In fact both explanations probably apply, sometimes simultaneously, as will be seen below. A short review of these two explanations is desirable:

(1) SCOTT based his argument on the hypothesis that appreciable radio energy will be scattered back from the direction of the (nearly vertical) magnetic field in sounding the ionosphere at high magnetic latitudes. Waves proceeding exactly in the direction of the field are propagated (according to the curve in Fig. 2(a) for purely longitudinal propagation) to the $1 + Y$ level and there reflected. The only other reflection level for this particular case is the ubiquitous extraordinary level $1 - Y$, but reflections from the usual ordinary level ($X = 1$) would also be observed coming from other directions of propagation. The essential observational evidences in favour of this mechanism are the following; they are illustrated in the characteristic example of Fig. 4.

(a) Waves producing the Z-trace by purely longitudinal propagation proceed to their level of reflection independently of the other modes. Each magnetoionic component is therefore recorded throughout the frequency range, and no evidence of interaction between modes is observed.

(b) Even when O and X traces show considerable "spread echo" (presumably resulting from off-vertical scattering), the corresponding portions of the Z-trace are quite well defined, suggesting that it returns from a single direction.

(c) Multiple echoes of the F-region Z-trace are not seen, and none would be expected if the energy returns obliquely from the ionosphere.

(d) By the suggested mechanism, the Z-mode should be especially strong in certain favourable cases of layer tilt, or horizontal gradient, in the direction of the magnetic field. In this case estimates of magnetic field strength by measurement of $fx - fz$ would be in error by the gradient-imposed variation of the critical frequencies.

SCOTT produced evidence illustrating (d) and concluded, on the basis of each of these points, that longitudinal propagation was a sufficient explanation of the Z-trace. Additional work by ELLIS (1953) has verified that the angle of arrival of F-region Z-echoes is consistent with the hypothesis that the propagation is longitudinal.

(2) RYDBECK developed the conditions for coupling in the Arctic E-region and concluded that coupling *must* occur near the level of reflection of the ordinary wave, when the collision frequency nears the critical value. Lower in the layer where $\nu > \nu_c$ the propagation would become essentially quasi-longitudinal anyway, so that for ordinary waves reflected near the $\nu = \nu_c$ level and below, reflections from the Z-level should always be seen.

Qualitatively, in terms of the refractive index variations depicted in Figs. 2

VOL.
18
196

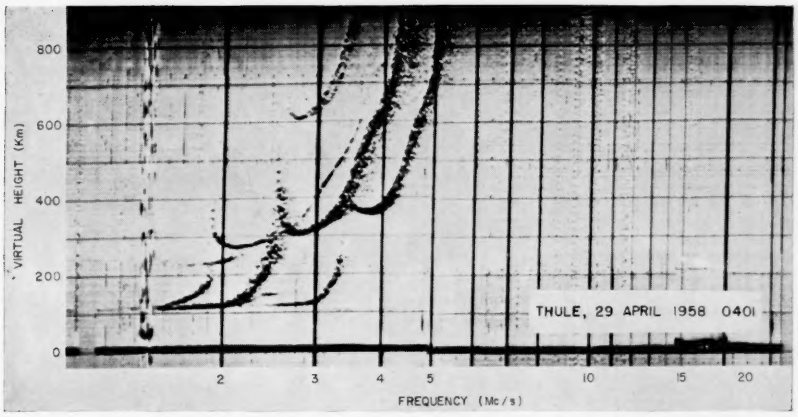

Fig. 4. Ionogram illustrating E- and F-region Z-echoes produced via longitudinal propagation.

OL.
18
960

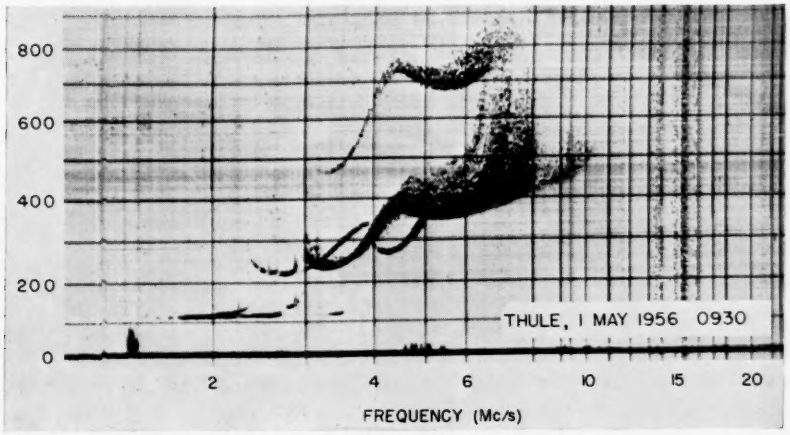

Fig. 6. Examples illustrating virtual height variations in the F-region penetration Z-trace imposed by the shape of the E-layer, through coupling.
(a) Retardation of penetration Z-trace at f_0E.

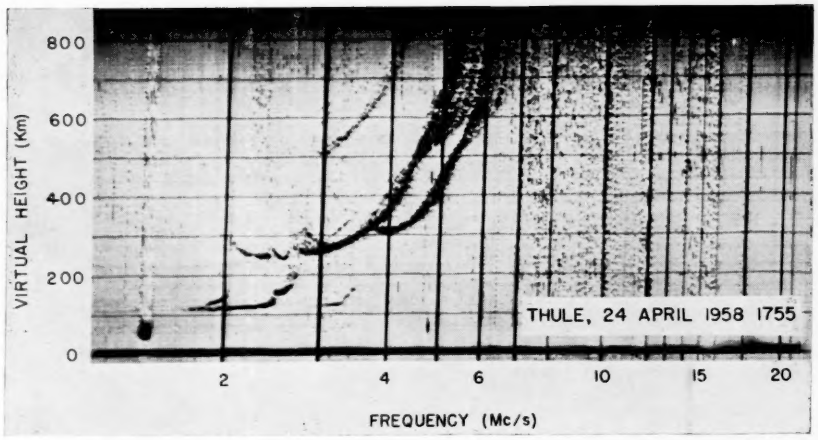

Fig. 6 (b) Effect of E-region stratification on penetration Z-trace.

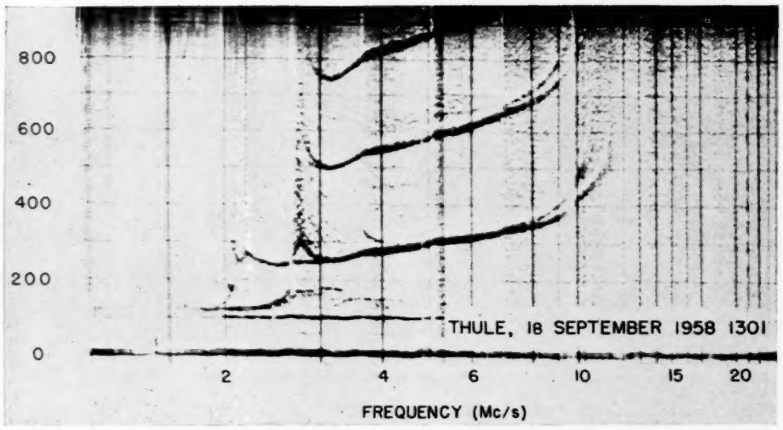

Fig. 6 (c) Simultaneous occurrence of two penetration Z-traces through coupling and longitudinal propagation.

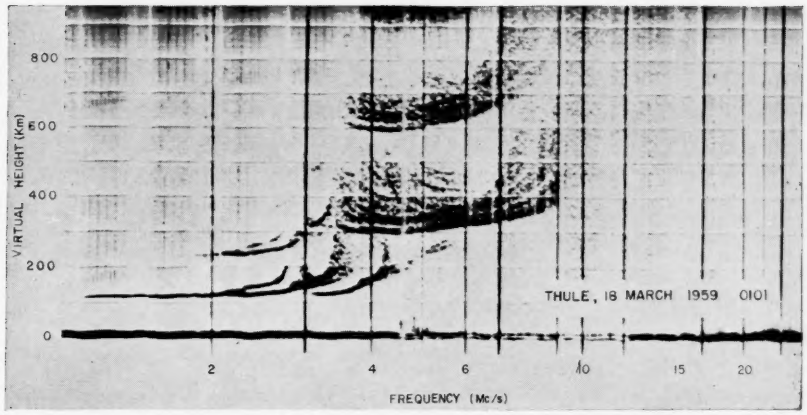

Fig. 7. Virtual height relationship of multiply-reflected E-region echoes requires that coupling be responsible for the observed Z-reflections.

VOL.
18
1960

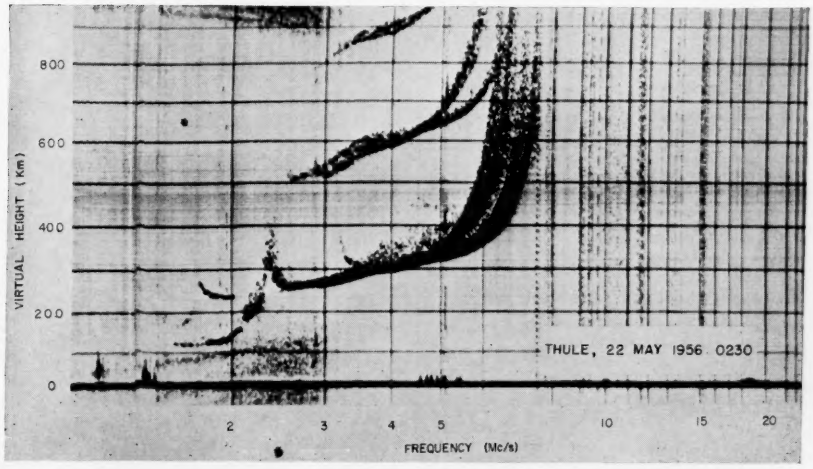

Fig. 10. The limiting upper frequency of the penetration Z-trace (2 Mc/s in this example), is a measure of the minimum ionization between the E- and F-regions.

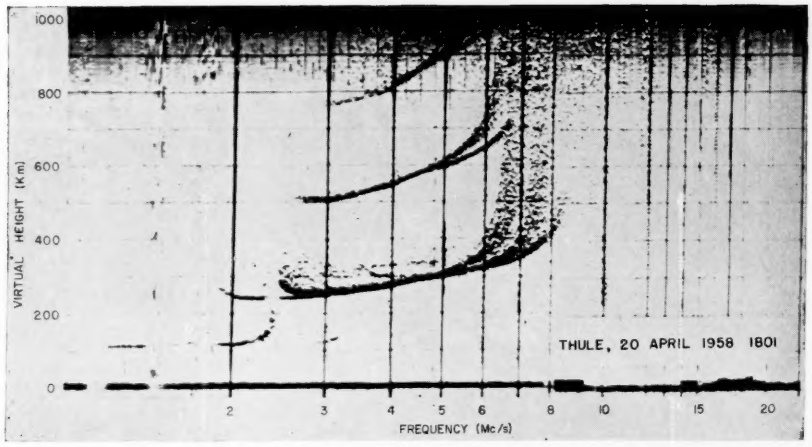

Fig. 11. Absorption gap in penetration Z-trace at f_0E.

VOL
18
196

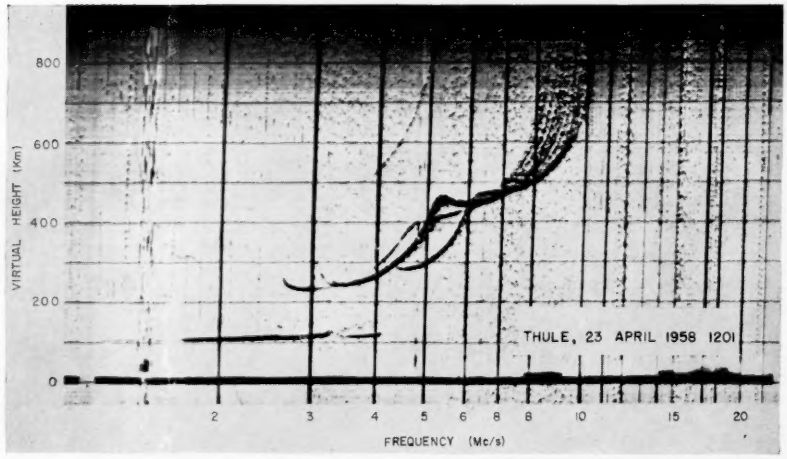

Fig. 12. Ordinary-wave F-region reflections are observed above a frequency of 3·0 Mc/s, although f_0E is 3·2 Mc/s. Note also the small cusp and increased echo strength of the F-region ordinary trace above 3·2 Mc/s.

and 3, we may conclude* that part of the energy will be reflected from the level $X = 1$ (due to the large value of dn/dX there), the remainder passing upwards to be reflected near $X = 1 + Y$.

When this occurs, a unique phenomenon to be seen on vertical soundings is predicted: at frequencies above f_xE the Z-reflection level occurs in the F-region (producing the so-called "penetration Z-trace"). This is the case at the frequency f_1 in Fig. 5. Since the group paths of the Z and O echoes are identical up to the level

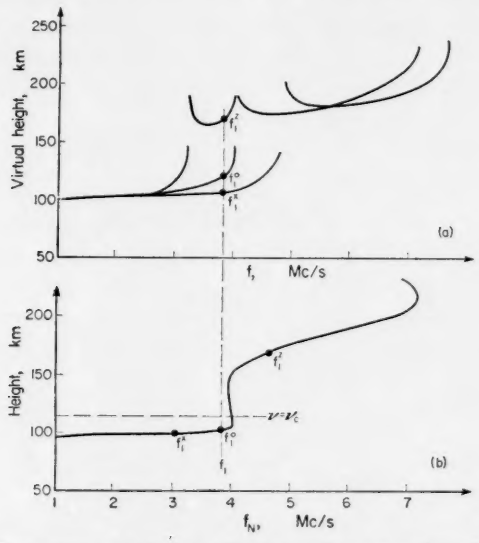

Fig. 5. (a, b). The group retardation affecting a frequency f_1, reflected at its ordinary level of reflection $f_1{}^o$, also affects a coupled Z echo of frequency f_1 reflected at $f_1{}^z$.

$X = 1$, *any group retardation showing in the ordinary trace will be similarly evident in the Z-trace.* Furthermore the Z-trace should cease at the Ordinary critical frequency of the E-layer. These characteristics of the Z-trace were recognized by RYDBECK: he offers one example (his Fig. 23), an example which, unfortunately, is not very convincing because the shape of the F-region is such that the F-region retardation near f_1 could be interpreted as the sole cause of the observed penetration Z-trace retardation.

Other than RYDBECK's, however, it appears that no examples of this phenomenon are to be found in the literature. Three examples from the many available in high-latitude soundings are illustrated in Fig. 6 (a, b, c). Fig. 6(b) is especially interesting; a stratification in the E-region, quite marked in the ordinary-wave reflections, causes a similar variation in the virtual height of the penetration Z-trace. There are also occasions where Z-reflections due to both mechanisms, longitudinal propagation and coupling, appear simultaneously, probably along different propagation paths. Fig. 6(c) is one such example.

* The description of the following phenomena will proceed by a qualitative discussion of the refractive index variations, rather than from the "coupling" point of view. The term "coupling" will be retained, however, as it concisely describes the conditions under which the qualitative discussion is valid.

4. Observation of Multiple Reflections of Coupled Echoes

An unusual ionogram is illustrated in Fig. 7, where strong multiple echoes of the *O*- and *Z*-trace from the *E*-region have been recorded. Generally, second, third, order, etc., multiple echoes are found precisely at two or three times, etc., the virtual height of the first echo (except, of course, where oblique reflections occur; these are not of interest here). However, the ionogram of Fig. 7 discloses that the second *Z*-trace reflection is not found at twice the virtual height of its first echo, but in the same relationship to the ordinary multiple reflection as in the first reflection. Obviously, the energy producing the *Z*-trace multiple echo has been once reflected at the ordinary level, indicating that the respective ray-paths are indistinguishable below the ordinary level of reflection.

5. Observations of a Limiting Upper Frequency of the Penetration *Z*-Trace

Consider the diagram of Fig. 8, and the frequency marked f_1. Part of this energy is reflected at the ordinary level of reflection, (point f_1°; here $\nu > \nu_c$) and

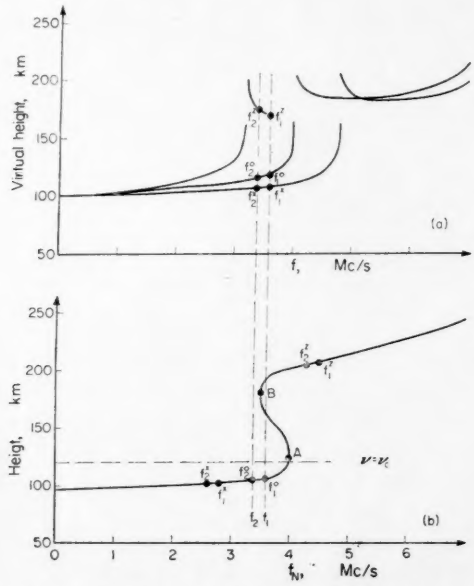

Fig. 8. Virtual height curves (a) produced by electron density distribution (b). Penetration *Z*-trace disappears through absorption if a sufficiently deep valley exists between *E*- and *F*-layers.

part proceeds upward through the *E*-region, passing as it goes, into increasing, then *decreasing*, electron densities bound for the *Z*-reflection level (point f_1^z). At the same time. the collision frequency is decreasing steadily, to values $\nu < \nu_c$.

The dispersion curves for this case are illustrated in Fig. 9. The *Z*-wave has proceeded into the *E*-layer along the "ordinary" curve for $\nu > \nu_c$ to the region *A* on the dispersion curve corresponding to plasma frequency *A*, the peak of the

VOL.
18
1960

E-layer in Fig. 8. The dispersion curves for $\nu > \nu_e$ and $\nu < \nu_e$ are nearly identical in this region. Proceeding to higher levels in the E-layer and to decreasing electron densities we must imagine the wave to follow the curve for $\nu < \nu_e$. If the electron density decreases sufficiently (i.e. if the "valley" between the layers is deep enough), the wave will find itself in a region of rapidly-increasing refractive index, and rapidly-increasing absorption. This region is what exists of the infinity of the

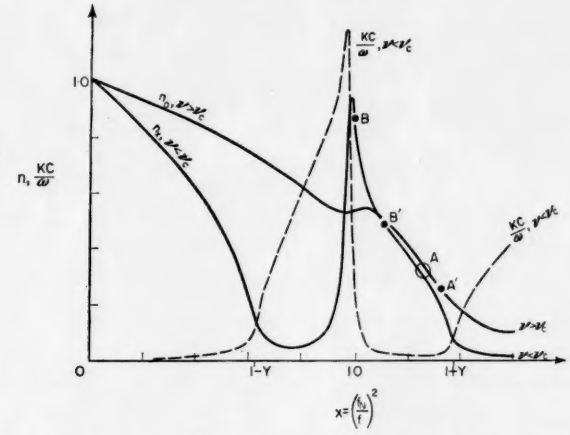

Fig. 9. Dispersion (n_0, n_x) and $(ck/\omega)_x$ curves illustrating absorption of penetration Z-echo when "valley" exists between E- and F-layers. Compare with Fig. 8.

no-collision refractive index, found at $X = (1 - Y^2)/(1 - Y^2 \cos^2 \theta)$. Thus the frequency f_1 never reaches the level of reflection $f_1{}^z$, being absorbed somewhere in the valley between the layers. A lower frequency, f_2 in Fig. 8 reaches the point A' on Fig. 9, at the peak density of the E-layer; its subsequent travel to higher levels through the "valley" does not bring it into the region of strong absorption, but only to the point B', Fig. 9. Past the minimum electron density B, the wave proceeds again into increasing electron densities to its reflection point ($f_2{}^z$ in Fig. 8) and by reversing the entire process, passes out of the ionosphere and appears as a Z-echo on the sounding. A typical ionogram illustrating this is Fig. 10. The upper limiting frequency of the penetration Z-trace therefore measures the minimum density in the valley (a plasma frequency of 2 Mc, or 30 per cent below $N_{\max}E$ in this example).

That this phenomenon could give information regarding the existence of a minimum of ionization, was pointed out by LANDMARK and LIED (1957). It should be noted that the qualitative argument presented here does not indicate exactly how the electron density at the valley minimum is related to the upper limiting frequency of the penetration Z-trace. This relation depends in a complex way upon the gradient of ionization near the minimum, the exact variation of reflectivity with frequency (which in this case demands a full wave treatment), and upon the sensitivity of the ionosonde. However, it appears from the observations that the limiting frequency is overtaken quite rapidly; the minimum electron density is therefore slightly underestimated, but probably only by an insignificant amount.

6. A "GAP" IN THE PENETRATION *Z*-TRACE

A common type of *Z*-trace is that illustrated in Fig. 11. No evidence of coupling such as that described in Section 3.2 can be observed; that is, there is no evident retardation of the penetration *Z*-trace near f_0E. However, the "gap" observed in the penetration *Z*-trace at f_0E appears to be evidence for an interaction between modes in the following way:

We presume that the observed *Z*-echoes are produced in this case not by coupling, but by purely longitudinal propagation of the kind described in Section 3.1. Supporting evidence for this is the fact that the present phenomenon is more prevalent:

(a) At moderately high, but not highest, magnetic latitudes where the critical collision level (hence the level of strongest coupling) is found well below 100 km (of Fig. 1), and therefore *E*-region coupling is weak.

(b) In the early and late hours of the day at the highest magnetic latitudes, at which time the *E*-layer is found at a greater height than midday, hence at a level well above the critical collision level where again, coupling is weak.

In either of these cases, longitudinal propagation will suffice to explain the production of the *E*-region *Z*-echo, the penetration *Z*-echo, and all of the *F*-region *Z*-echo. As discussed in Section 3.1, continuous *Z*, *O* and *X* traces throughout the *E* and *F* regions may be explained by simultaneous propagation of the type q.l. (for the *X* and *Z*), and q.t. for the *O* and *X*). Any coupling occurring at the ordinary level of reflection may be weak due to the small value of ν/ν_c. So long as the wave is reflected in the *E*-layer where the gradient dN/dh is large, the wave spends little time near the ordinary reflection level $X = 1$, and weak coupling has imperceptible effect. But conditions are different at the peak of the *E*-region. There, the gradient of ionization is zero; $X = 1$ over a finite interval of height (which will be an especially large interval in the case (b), above, when the *E*-layer peak is relatively broad). Thus for waves penetrating to the peak of the layer, i.e. just in the vicinity of f_0E, coupling *does* become predominant; the energy travelling as a longitudinal ordinary wave is transformed into the q.t. ordinary mode which is strongly absorbing near $X = 1$. The width and sharpness of the gap therefore depend upon the broadness of the *E*-region peak and the efficiency of the coupling mechanism.

Again, the phenomenon may be discussed qualitatively in terms of the refractive index variations of Figs 2(a, b). Exactly in the direction of the magnetic field, the curve for purely longitudinal propagation (Fig. 2a) applies; at slight angles to the field (small θ) the curve for $\nu < \nu_c$ is appropriate. Considering only the penetration *Z*-trace, it is clear that there exists a range of θ over which appreciable energy can pass the level $X = 1$ provided that level is traversed suddenly. When the level $X = 1$ occurs at the *E*-layer peak, this is no longer true; attenuation (large anyway in the *E*-region) occurs at $X = 1$ for all but a very much smaller range of θ and little energy is able to penetrate further to the level $X = 1 + Y$. In effect, the situation is similar to that considered in Section 5, but with a "valley" completely filled in to the density at f_0E, giving a broad region in which attenuation can take place.

VOL.
18
1960

7. Partial Transparency of the E-Layer to the Ordinary Mode

It is characteristic of radio reflections from the usual thick ionosphere layers (i.e. not sporadic-E) that, for a given mode, reflection is essentially total up to the corresponding critical frequency. That is, higher layers are totally occulted for probing frequencies below the critical or "penetration" value. This conclusion also follows from ray theory. From a wave point of view (Rydbeck, 1944) it is clear that particularly in the E-region some energy penetrates beyond the reflection level at frequencies below f_0E; however, long experience with E-region soundings has demonstrated that this effect is rarely, if ever, observable with ordinary equipment.

Consider the ionogram of Fig. 12: the frequency f_0E is observed to *overlap* the minimum ordinary frequency from the F-region, $f^\circ_{\min}F$, by about 0·2 Mc. That is, the E-layer is evidently partly transparent to the ordinary wave in this frequency range; no such overlap is observed at f_xE or f_zE. Careful inspection of Fig. 12, will also show, in the F-region trace just at f_0E that another slight penetration "cusp" appears, which quickly coalesces at higher frequencies with the overlapping echo to form one F-region ordinary-wave trace.

It is instructive to consider the diurnal variations of these characteristic frequencies. In Fig. 13, the quantities f_zE, f_0E, f_xE and $f^\circ_{\min}F$ are plotted, as indicated, for Thule, 23, 24 April 1957. It may be noted that the overlap between f_0E and $f^\circ_{\min}F$, does not exist when f_0E is less than approximately 2·8 Mc, but occurs for higher values of f_0E (local times between about 0600 and 1700 at this season). The magnitude of the overlap varies considerably, but it appears that $f^\circ_{\min}F$ remains nearly constant while f_0E goes through its normal diurnal variation in accordance with the varying solar zenith angle.

To advance an explanation of this phenomenon, we will assume that at about 0600 local time at this season at Thule, the peak density of the E-layer comes down through the level at which $\nu = \nu_c$, and that this happens when f_0E is about 2·8 Mc. During the middle part of the day, the entire sub-peak E-layer (plus some of the supra-peak portion of the layer) is then in a region where $\nu > \nu_c$, that is to say, a q.l. region. Now consider Fig. 14(a,b) which represents the situation at, say, 1200.

A frequency f_1 arrives at its ordinary reflection point (f_1° in Fig. 14 a, b). Here $X = 1$ and although $\nu > \nu_c$, we must suppose that sufficient variation in refractive index occurs at this level to reflect some energy and thus account for the observed ordinary-wave echoes. The refractive index curve appropriate to the wave in this case is the curve for $\nu > \nu_c$ in Fig. 15. Part of the energy of f_1 passes beyond the level $X = 1$, and on into increasing, then decreasing, electron densities. At the same time, the form of the refractive index curve is changing as ν changes, ultimately becoming similar to that for $\nu < \nu_c$ in Fig. 15. These changes in refractive index occurring above $X = 1$ are slight, and do not appreciably affect the propagation of the energy. However, near the upper level where $X = 1$, and where $\nu < \nu_c$, the energy will be strongly absorbed, due to the large value of the absorption index which develops there. Thus no reflection from the F-region will be observed at f_1. It should be noted that if the valley between the E- and F-layers were "filled in" sufficiently that X could not approach unity for this frequency, then F-reflections would be observed, as a penetration Z-trace at f_1. This is precisely the situation discussed in Section 3.2.

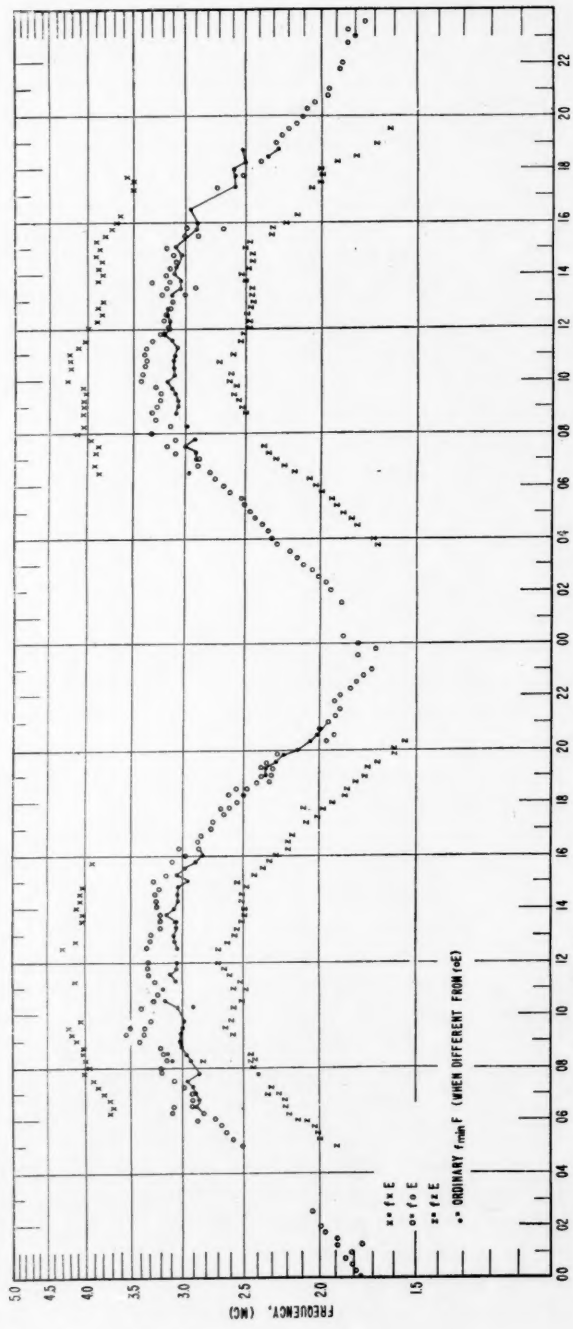

Fig. 13. Diurnal variation of E-region critical frequencies, illustrating transparency of E-region to ordinary-wave near f_0E at midday, 23–24 April 1957, Thule, Greenland.

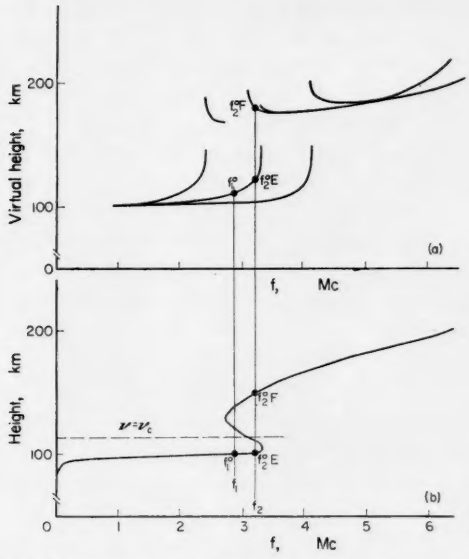

Fig. 14. Virtual height curves (a) produced by electron density distribution (b). Transparency of E-region to ordinary mode occurs for frequencies near f_2 but not f_1.

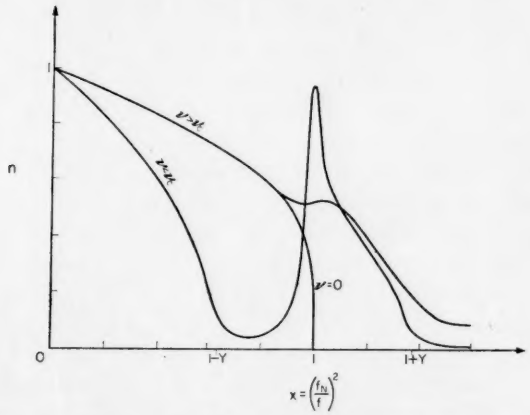

Fig. 15. Dispersion curves accounting for transparency of the E-region to ordinary-wave echoes below f_0E.

Now consider the frequency f_2. Its behaviour up through the E-region peak will be the same as f_1: part of the energy will be reflected at f_2 °E, and part will pass on to increasing, then decreasing, densities in accord with the curve for $\nu > \nu_c$ in Fig. 15. However, the frequency f_2 is such that on the topside of the E-layer, it traverses its second level $X = 1$ where ν is still greater than ν_c. Thus no strong absorption takes place at this level, as it did for f_1; this portion of f_2 passes on through the valley and on into increasing densities in the F-region. However, ν has been decreasing rapidly with height, so that as f_1 enters increasing F-region

densities it follows essentially the Ordinary $\nu = 0$ curve of Fig. 15. It is reflected at $X = 1$ in the F-region (point $f_2{}^\circ F$ in Fig. 14 a, b) and by reversing the entire process appears on the ionogram as an ordinary F-region echo below f_0E. The small additional "cusp" in the F-region reflection at f_0E of course represents the usual F-region minimum frequency.

For a quantitative comparison of this hypothesis with observed E-region diurnal behaviour, it is necessary to know with some accuracy the diurnal variation of $h_{\max}E$ and to have some idea of the shape of the E-region profile above this level. Unfortunately, E-region $N(h)$ profiles are exceedingly difficult to obtain with sufficient accuracy from the usual vertical soundings, especially in the Arctic. However, we may attempt to estimate the magnitude of the present phenomenon under the assumptions that:

(a) The E-layer behaves as a simple Chapman layer of 7 km scale height near its peak.

(b) When the present phenomenon first develops, the height of the peak (0600 in April) is precisely the height of the critical collision level. This is 112 km according to the best present estimates of collision frequency, magnetic dip, and gyro-frequency given in Table 1.

The Chapman layer is given by

$$f_N/f_{N\max} = \exp \tfrac{1}{4}(1 - z - \sec \chi e^{-z}) \qquad (1)$$

where z is measured from $h_{\max}(\chi = 0)$ in units of scale height (H). Also for a Chapman layer,

$$z = \ln \sec \chi.$$

For the mean value of χ appropriate to Thule, April noon, this gives $z = 1{\cdot}67$ at a height of 112 km. When inserted in equation (1), this gives $f_N/f_{N\max} = 0{\cdot}75$. Thus $f_N = 2{\cdot}9$ Mc/s at 112 km at noon, based upon the Thule subsolar $f_0E(= f_{N\max})$ given in Table 1. This seems slightly too low by comparison with the observations of Fig. 13, suggesting that the topside of the E-region may be slightly thicker than a Chapman region. This is not unexpected, in view of the fact that frequently no evidence for a valley may be observed at all.

8. Applications

The phenomena described above appear to offer several opportunities for unique and precise measurements of Arctic E-region collision frequencies and electron densities above $h_{\max}E$. Measurement of the upper limiting frequency of the penetration Z-trace gives an estimate of the depth of an E-region valley. Observation of the quantity $f^\circ{}_{\min}F$, when different from f_0E, gives another point on the valley electron density distribution, the height of which is known quite accurately if the height of the level $\nu = \nu_e$ is known. If an applicable "true height" method is available (and also E-region soundings of high accuracy), then the height of the level $\nu = \nu_e$ may be determined as the height of $h_{\max}E$ at the diurnal beginning or end of the "overlap" phenomenon. This may be used to locate accurately a point on the $\nu(h)$ distribution, provided f_H and θ are known. Finally, amplitude measurements of coupled echoes are capable of providing further collision frequency data. An investigation of Arctic and Antarctic ionograms by these methods is now in progress.

VOL.
18
196(

Summary

Abundant evidence exists to demonstrate that magnetoionic coupling can occur in the E-region at high latitudes, and is manifest by several unique phenomena. A qualitative inspection of the applicable dispersion curves can account for most of these phenomena, but much useful and interesting work remains to be done on their variable time occurrence. Several of the phenomena will permit new information to be obtained regarding the existence and extent of an E-pause, and of the magnitude of E-region collision frequencies.

Acknowledgements—The writer is indebted to Drs. K. Davies and J. Wait of this laboratory for several useful discussions, and to Mr. W. R. Piggott for suggestions regarding the concepts of Section 6.

References

Appleton E. V.	1932	*Proc. Instn Elect. Engrs* **71,** 642.
Appleton E. V. and Builder	1933	*Proc. Phys. Soc.* **45,** 208.
Ellis G. R.	1953	*J. Atmosph. Terr. Phys.* **3,** 263.
Landmark B. and Lied F.	1957	*J. Atmosph. Terr. Phys.* **10,** 114.
Lepechinsky D.	1956	*J. Atmosph. Terr. Phys.* **8,** 297.
Nicolet M.	1956	*J. Atmosph. Terr. Phys.* **3,** 200.
Rydbeck O. E. H.	1944	*Chalmers Tek. Högsk. Handl.* **34.**
Rydbeck O. E. H.	1950	*J. Appl. Phys.* **21,** 1205.
Scott J. C. W.	1950	*J. Geophys. Res.* **55,** 65.

OL.
18
960

Journal of Atmospheric and Terrestrial Physics, 1960, Vol. 18, pp. 290 to 296. Pergamon Press Ltd. Printed in Northern Ireland

Short-term differences in the behaviour of two daily indices of solar activity during the IGY

G. H. Bazzard
DSIR Radio Research Station, Slough*

(*Received* 27 *January* 1960)

Abstract—The variations in the daily values of the flux of solar radio noise at λ 10·7 cm (Φ) and the E-layer character figure (J_E) have been studied for the period of the IGY. It is found that Φ lags behind J_E by about 14 hr. The ratio J_E/Φ fluctuates above and below its normal value and the reasons for these changes have been examined. Troughs in J_E/Φ are attributed partly to increases in geomagnetic activity which cause a decrease in J_E, and partly to the presence of active regions on the sun's disk which tend to emit relatively more radio noise than the quiet sun. Peaks in J_E/Φ are associated with the absence of these active areas.

1. Introduction

The close correlation between monthly mean values of solar radio noise flux at λ 10·7 cm, as measured by Medd and Covington (1958), and the intensity of the ionizing radiation causing the E-layer, as indicated by the character figure $(f_0E)^4$ sec χ, has been demonstrated by Denisse and Kundu (1957) and Minnis and Bazzard (1958). More recently, Kundu and Denisse (1958) have shown that this correlation also exists for daily values of these two indices of solar activity. The rather low accuracy of the E-layer data available to Kundu and Denisse limited the conclusions which could be drawn from their analysis which was restricted to the use of 5-day mean values of the E-layer index for 2 months in each of a number of years.

For the period of the IGY (July 1957–December 1958), Minnis and Bazzard (1959a) have produced a daily E-layer index (J_E) which is probably more accurate than that available to Kundu and Denisse. This index has allowed a more detailed examination to be made of the relation between the daily values of the flux of solar radio noise at λ 10·7 cm (Φ) and of the E-layer ionizing radiation as represented by J_E. Whilst, in general, the findings of Kundu and Denisse were confirmed, some deviations from the normal relation between the two indices were found and are discussed below. The existence of these deviations is of importance because it is sometimes asserted that, since the behaviour of all solar indices is similar, it is necessary to use only a single index of solar activity for all purposes

2. The Phase Difference between J_E and Φ

A visual examination of the day-to-day variations in the two indices suggested that there was a short-term phase difference between them: Φ lagging behind J_E by about 1 day. In order to test this possibility the method of superposed epochs was employed.

* Official communication.

2.1. *Method of analysis*

The erratic fluctuations in J_E are estimated to have an s.d. of about 2 per cent. Throughout this analysis, 3-day running means of J_E and Φ were used to smooth the day-to-day fluctuations. From the 18 months data available, twelve well-defined peaks in Φ were selected. Taking the day of the peak value as a reference, the mean value of Φ for that day and the values for each of the three preceding and the three succeeding days were found for the twelve occasions. The corresponding mean values of J_E and of the daily sunspot number (R) were also determined using

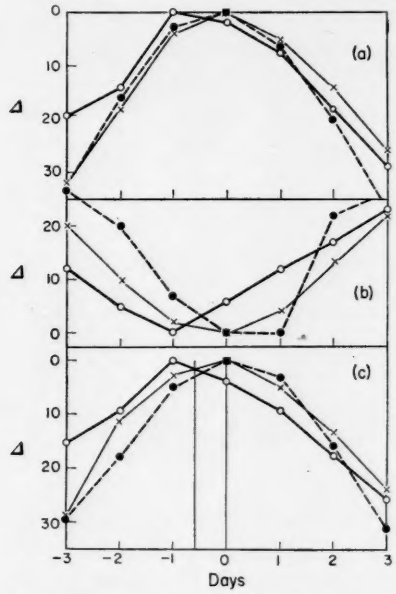

FIG. 1. Superposed epoch diagrams for Φ, J_E and R centered on days characterized by peaks or troughs in Φ: (a) 12 peaks in Φ; (b) 13 troughs in Φ; (c) peaks and troughs combined; Δ difference from maximum value; —×—×— Φ; —○—○— J_E; —●—●— R.

the same reference day and the curves thus obtained are shown in Fig. 1(a). A similar process was applied to the periods of 7 days centred on thirteen troughs in Φ. The curves obtained in this way are shown in Fig. 1(b). The appearance of Figs. 1(a) and 1(b) indicates that the phase differences obtained using both peaks and troughs in Φ are probably very similar and it seems reasonable to combine both sets of data. The resulting curves, derived from the superposition of twenty-five epochs, are shown in Fig. 1(c).

In order to estimate more accurately the phase difference between J_E and Φ, a best-fit parabola was fitted to each set of points using a formula due to AITKEN and quoted by APPLETON and LYON (1957). The time at which the maximum of the fitted parabola occurs in each case is indicated by a vertical line in Fig. 1(c). It was possible to fit two slightly different parabolas to the points for J_E, depending on whether the seven points selected were centred around the reference day for Φ,

or around the day on which the peak value of J_E occurred. The best estimate for the position of the maximum in J_E was assumed to be the mean of the maxima given by these two parabolas.

The conclusion resulting from this analysis is that there is a phase difference between J_E and Φ with J_E leading by 0·60 days ($\simeq$14 hr). There is no significant phase difference between Φ and R.

3. The Relative Magnitudes of J_E and Φ

While examining the relation between daily values of Φ and J_E, it was often found that, for periods of a few days, the ratio J_E/Φ differed considerably from the

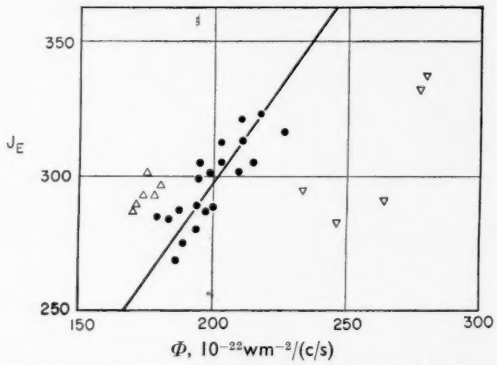

Fig. 2. Relation between 3-day mean values of E-layer ionization index (J_E) and solar radio noise flux (Φ) at λ 10·7 cm for August 1957. Values of J_E/Φ: ● typical; △ high; ▽ low; —— $J_E/\Phi = 1{\cdot}49$.

values typical of the rest of the same month. This is illustrated for August 1957 in Fig. 2 where 3-day mean values have been plotted in order to reduce the scatter and to make the divergencies clearer. Two isolated groups of points are clearly discernable; these lie, respectively, above and below the line representing the approximate average value of J_E/Φ for the month. These divergences cannot be the consequence of the phase difference described in Section 2 because displacement of one of the indices by 1 day produces the same result.

From an investigation of the whole period of the IGY, it has been found that the variations in the ratio J_E/Φ cannot be attributed to a single cause. It appears likely that peaks in the ratio may be due to solar effects while troughs in the ratio may be due to a combination both of solar and terrestrial controls. These differences are discussed in Sections 3.1 and 3.2.

3.1. *Troughs in* J_E/Φ

A trough in the ratio J_E/Φ was defined as a sequence of at least 4 days during which there was a decrease in the value of the ratio of about 10 per cent referred to the values before and after the trough. Using this definition, thirty-one troughs were identified during the period of 18 months under consideration.

3.1.1. *Association of troughs with magnetic activity.* A cursory examination of the dates of occurrence of the troughs suggested some association with magnetic

activity. Disturbed magnetic periods were selected to test this supposition, a disturbed magnetic period being defined as a sequence of 1 or more days which had an Ap figure at least ten units above the normal level for the period being considered.

The occurrences of the J_E/Φ troughs and the Ap peaks are combined in Table 1 in which the expected frequencies of occurrence of the four categories of events are indicated in parentheses.

On applying the χ^2-test of significance to these figures, it was found that the probability that the observed distribution could have occurred by chance was less

Table 1. Occurrence of troughs in J_E/Φ and peaks in Ap

		Troughs in J_E/Φ		Total
		Present	Not present	
Peaks in Ap	Present	26 (15·4)	29 (39·6)	55
	Not present	5 (15·6)	51 (40·4)	56
Total		31	80	111

than 0·001. It is concluded, therefore, that the troughs in J_E/Φ are associated with periods of high magnetic activity.

3.1.2. *Association of troughs with solar active regions.* In order to examine the possibility of an association of troughs in J_E/Φ with the passage of active regions across the sun's disk, a crude daily index of active regions was constructed using data given by TROTTER and ROBERTS (1958, 1959), each of whose classifications of the intensity of active regions (a to e) was allocated a numerical value in the range 1 to 5. A daily index figure was then calculated by taking the sum of the numerical

Table 2. Occurrence of troughs in J_E/Φ and peaks in the active region index

		Troughs in J_E/Φ		Total
		Present	Not present	
Peaks in active region index	Present	13 (8·1)	7 (11·9)	20
	Not present	13 (17·9)	31 (26·1)	44
	Total	26	38	64

values allocated to the active regions where they overlapped and assuming that each area remained uniformly active for 7 days on each side of the date of CMP.

Using this index of active regions as a guide, all periods were extracted which had an index figure above the normal level. These periods were designated as periods of high activity and again a 2 × 2 table (Table 2) was constructed showing coincidences of troughs in J_E/Φ with these periods. The amount of data available for this analysis was less than for that in Section 3.1.1 because the observations on

VOL. 18 1960

active regions were available only up to September 1958. The probability that the observed distribution could have occurred by chance is less than 0·01. It is concluded that troughs in J_E/Φ are also associated with a high degree of activity on the sun as indicated by the intensity and number of active regions present.

It should be mentioned here that no significant association could be found between the presence of solar-active regions and disturbed magnetic conditions for the period of observations which has been used in the above analysis. The results obtained above are, therefore, statistically independent and it is concluded that troughs in J_E/Φ may be associated both with certain solar events and with terrestrial magnetic disturbances.

Table 3. Occurrence of peaks in J_E/Φ and troughs in the active region index

		Peaks in J_E/Φ		Total
		Present	Not present	
Troughs in active region index	Present	10 (6·0)	8 (12·0)	18
	Not present	7 (11·0)	26 (22·0)	33
	Total	17	34	51

3.2. *Peaks in J_E/Φ*

A peak in the value of J_E/Φ was defined in a manner analogous to the definition of a trough. The dates of occurrence of such peaks in the ratio during the period under examination were noted.

3.2.1. *Association of peaks with magnetic activity.* It has been shown in Section 3.1.1 that troughs in J_E/Φ are associated with high values of the magnetic-activity index. It might be assumed, conversely, that peaks in J_E/Φ would occur when magnetic activity was low. This assumption, however, was not supported by the data available for days when peaks in J_E/Φ occurred. It is concluded, therefore, that peaks in J_E/Φ are due to causes other than very low magnetic activity.

3.2.2. *Association of peaks with solar-active regions.* The occurrence of peaks in J_E/Φ during periods when active regions were absent from the sun's disk, or only of low intensity, was examined in a manner analogous to that employed in Section 3.1.2. The distribution of coincidences obtained is shown in Table 3. The probability that this distribution could have occurred by chance is 0·014 and it is concluded that peaks in J_E/Φ tend to occur when active regions are absent from the sun's disk or only of low intensity.

4. Discussion

4.1. *The phase difference between indices*

It has been shown in Section 2 that there is a difference in phase between the ionizing radiation producing the E-layer and solar radio noise at λ 10·7 cm, while there is no difference in phase between radio noise and sunspot number. The reason for this phase difference is not readily apparent.

If the E-layer ionizing radiation is generated at a lower level in the sun's atmosphere than the solar noise at λ 10·7 cm, then an upward-moving disturbance of the type described by WILD (1950) would cause an increase in J_E followed by an increase in Φ. This explanation, however, does not appear to be applicable to the phase difference of 14 hr referred to in Section 2; a very much shorter delay would be expected from the velocities deduced from radio spectrograms.

It is interesting to note that ALLEN (1948) has reported that E-layer ionization lags behind sunspot number by about 13 days while KIEPENHEUER (1946), using a different method of analysis, found a lag of between 2 and 5 days. These results are not necessarily inconsistent with the 14 hr phase difference described here since the long-and-short-time differences could arise from long- and short-term changes in J_E and Φ which result from different mechanisms.

4.2. *Short-term changes in the ratio* J_E/Φ

It has been shown in Section 3 that periods of a few days frequently occur during which the ratio J_E/Φ is greater or less than its normal value. The peaks in J_E/Φ appear to be associated with periods when the number or intensity of active regions on the sun's disk is small, while the troughs tend to occur when the active regions are large in number or intensity. The troughs in the ratio are also independently associated with disturbed terrestrial magnetic conditions.

VOL. 18 1960

It is suggested that the association of troughs in J_E/Φ with magnetically-disturbed conditions is probably due to a decrease in J_E without a corresponding decrease in Φ. This is possible because it has been shown by BEYNON and BROWN (1959) that during disturbed magnetic conditions the noon value of f_0E at temperate latitudes is depressed; such a depression would have a corresponding effect on the value of J_E.

The occurrence of peaks and troughs in J_E/Φ in association with the incidence of active areas on the sun's disk may be explained by assuming that the characteristic value of J_E/Φ for the quiet sun is greater than that for the localized active areas. Such an explanation implies that the monthly mean value of J_E/Φ would show similar changes over a solar cycle since the number and degree of activity of active regions is much greater at the maximum of the cycle than at its minimum.

There is some support for this suggestion in the long-term relation between monthly mean values of an E-layer index (I_E) and of Φ which has been given by MINNIS and BAZZARD (1959b),

$$I_E = 1{\cdot}55\Phi - 1{\cdot}0 \times 10^{-3}\Phi^2 + 14. \qquad (1)$$

In the present context I_E may be regarded as approximately equivalent to the monthly mean value of J_E. Substitution in this equation of typical values of Φ for minimum and maximum phases of the solar cycle leads to values of I_E/Φ which show a reduction in the ratio similar to that observed in the daily variations of J_E/Φ for the period of the IGY (Table 4). The larger range of the ratios of the daily values is to be expected considering that the monthly values are approximate means of the daily values.

5. Conclusions

The relation between daily values of solar noise flux at λ 10·7 cm (Φ) and the intensity of ionizing radiation of the E-layer (J_E), as measured by $(f_0E)^4$ sec χ, has been examined. It has been shown that while, in general, there is a close correlation between the two quantities, there are some short-term systematic differences in their behaviour when they are considered in detail.

A phase difference has been found between J_E and Φ, the latter lagging behind the former by approximately 14 hr. The reason for such a phase difference is not apparent.

Table 4. Variations of I_E/Φ and J_E/Φ with solar activity

Phase of solar activity	Ratio of indices	
	I_E/Φ (monthly)	J_E/Φ (daily)
Low	1·59 (1954)	1·65 (peaks)
High	1·30 (1958)	1·15 (troughs)

It has also been shown that the ratio J_E/Φ frequently departs from its normal value for short intervals of a few days. It is suggested that these departures are the result partly of solar and partly of geomagnetic controls. The value of J_E/Φ characteristic of active areas on the sun may be different from the value for the quiet sun with the result that peaks and troughs are produced in J_E/Φ depending on the incidence of active areas. In addition, troughs may also be produced in J_E/Φ owing to a reduction in the value of J_E resulting from a depression of E-layer ionization during magnetic disturbances.

Acknowledgement—The work described was carried out as part of the programme of the Radio Research Board. The paper is published by permission of the Director of Radio Research of the Department of Scientific and Industrial Research.

References

Allen C. W.	1948	*Terr. Magn. Atmos. Elect.* **53,** 433.
Appleton E. V. and Lyon A. J.	1957	*J. Atmosph. Terr. Phys.* **10,** 1.
Beynon W. J. G. and Brown G. M.	1959	*J. Atmosph. Terr. Phys.* **14,** 138.
Denisse J. F. and Kundu M. R.	1957	*C. R. Acad. Sci., Paris* **244,** 45.
Kiepenheuer K. O.	1946	*Mon. Not. R. Astr. Soc.* **106,** 515.
Kundu M. R. and Denisse J. F.	1958	*J. Atmosph. Terr. Phys.* **13,** 176.
Medd W. J. and Covington A. E.	1958	*Proc. Inst. Radio Engrs, N. Y.* **46,** 112.
Minnis C. M. and Bazzard G. H.	1958	*Nature, Lond.* **181,** 1796.
Minnis C. M. and Bazzard G. H.	1959a	*J. Atmosph. Terr. Phys.* **17,** 57.
Minnis C. M. and Bazzard G. H.	1959b	*J. Atmosph. Terr. Phys.* **14,** 213.
Trotter D. E. and Roberts W. O.	1958	University of Colorado Report HAO Nos. 39, 40 and 42.
Trotter D. E. and Roberts W. O.	1959	University of Colorado Report HAO Nos. 43 and 44.
Wild J. P.	1950	*Aust. J. Sci. Res.* A **3,** 399.

Journal of Atmospheric and Terrestrial Physics, 1960, Vol. 18, pp. 297 to 305. Pergamon Press Ltd. Printed in Northern Ireland

A monthly ionospheric index of solar activity based on *F2*-layer ionization at eleven stations

C. M. MINNIS and G. H. BAZZARD
DSIR Radio Research Station, Slough*

(*Received* 29 *January* 1960)

Abstract—A monthly index has been constructed, for the period 1938 to date, using monthly mean or median noon values of f_0F2 at eleven widely-distributed stations. The correlation between f_0F2 at noon and this index is significantly greater than that between f_0F2 and either the 3 month weighted mean sunspot number or the monthly mean solar radio noise flux at 2800 Mc/s. Numerical estimates have been made of the errors incurred in forecasting noon and midnight f_0F2 several months ahead using these three indices as guides to the trend of solar activity.

1. INTRODUCTION

A METHOD for deriving an index of solar activity based on the ionization in the *F2*-layer has been described by MINNIS (1955). If f_M represents the monthly mean or median f_0F2 at noon at a given station and $R_3 = \frac{1}{4}(R_{n-1} + 2R_n + R_{n+1})$ represents the weighted mean Zurich sunspot number for the month n, the method requires the derivation of the linear regression coefficients relating f_M and R_3. Having obtained regression lines of the form:

$$R_3 = \alpha f_M - \beta \qquad (1)$$

for each month of the year for a given station, the measured values of f_M are substituted in equation (1) to give a series of values R_3'.

The index I_{F2}, tabulated by MINNIS (1955) and revised by MINNIS and BAZZARD (1959), is defined as the mean value of R_3' for the three stations: Slough, Huancayo and Watheroo. Since only three stations were used, the value of I_{F2} for some months was often affected to a fairly large extent by unusually large or small values of f_0F2, and hence of R_3', at one of the stations. Moreover, if a measured value of f_0F2 was not available for a particular month, the value of I_{F2} based on the remaining two stations could not be regarded as reliable.

In view of these considerations, it seemed advisable to construct revised tables of I_{F2} using the same method but including data from a much larger number of stations. It was decided to include not less than nine stations for which data were available back to 1945 or earlier and which were located in such a way as to give a sample of data over a wide range of latitude and longitude. It was later found that these minimum conditions could easily be met and that, in fact, data for twelve representative stations were available back to 1942.

2. CONSTRUCTION OF THE NEW INDEX I_{F2}

It has been noticed that, during the recent periods of very high solar activity, the median values of f_0F2 at Watheroo are much lower than would be expected from past experience; for this reason, Watheroo has not been included among the

* Official communication.

VOL. 18 1960

stations used in constructing the new index. For the remaining eleven stations the values of R_3' were determined using equation (1) with the coefficients α and β obtained from analysis of the data for the years 1942–1957. The median value of R_3' for each month of this period was then determined and adopted provisionally as the new index I_{F2}.

It seemed preferable to exclude any stations which consistently tended to give values of R_3' which lay far above or below the median value for the eleven stations. A test was devised to find whether any stations ought to be excluded on these grounds. The number of months (N_a,N_b) in which each station was responsible for

Table 1. Variability index (N_b/N_a)

Station	N_b/N_a
Washington	2·23
Tokyo	1·89
Churchill	1·54
San Francisco	1·34
Slough	1·25
Fairbanks	1·18
Puerto Rico	1·15
Delhi	1·07
Huancayo	0·96
Canberra	0·94
Christchurch	0·93

(a) one of the two highest or two lowest values of R'; (b) one of the two values with the smallest positive departures from the median or one of the two with the smallest negative departures. The ratio N_b/N_a was adopted as a variability index which seems relevant to the particular requirement mentioned above. The values of this index are shown in Table 1 for the eleven stations.

It is evident that N_b/N_a does not decrease rapidly for the stations in the lower half of the table and hence no advantage would be gained by omitting a few of the stations with the lowest values. In view of this it was finally decided that all the eleven stations referred to in Table 1 should be retained and that the median value of R_3' for these stations should be used as the new index. The median value of R_3' was adopted in preference to the mean in order to minimise the effect of occasional very high or low values. The final values of I_{F2}, determined in this way, cover the period January 1942 to date.

The standard deviation (s) of the differences between I_{F2} and the corresponding values of R_3' has been calculated. When solar activity is low ($\bar{I}_{F2} = 9$), $s = 11{\cdot}5$; when it is high ($\bar{I}_{F2} = 161$), $s = 17{\cdot}3$. Minnis and Bazzard (1959) have shown that the fluxes of E-layer ionizing radiation and of solar radio noise probably reach negligibly-low levels when $I_{F2} \simeq -160$. Thus $I_{F2} + 160$ may be regarded as very approximately proportional to the flux of $F2$-layer ionizing radiation. With this assumption, the two values of s just mentioned are both close to 6 per cent of the flux. Since eleven values of R_3' are used to determine I_{F2}, the standard error of I_{F2} as a measure of radiation flux is approximately 2 per cent at all levels of solar activity.

VOL
18
196

The old three-station values of I_{F2}, given by MINNIS and BAZZARD (1959), and the eleven-station values are related by the expression:

$$I_{F2}\,(\text{new}) = 1{\cdot}09[I_{F2}\,(\text{old}) - 1].$$

The values of I_{F2} (new) for 1938–1941 have been calculated using this relation since there are not sufficient data to determine I_{F2} (new) directly for this period. Copies of tables of I_{F2} from 1938 to date may be obtained by applying to The Director, Radio Research Station, Ditton Park, Slough, Bucks., England.

COMPARISON OF I_{F2} WITH OTHER INDICES

3.1. *Applications of indices*

During investigations of the behaviour of the *F2*-layer over a long period, it is often necessary to reduce the measured characteristics of the layer to a constant level of solar activity to facilitate the study of variations due to causes other than changes in solar radiation. This reduction can only be carried out if an index of solar activity is available to which the ionospheric parameters can be referred. In another field, the forecasting of future values of f_0F2, and of other ionospheric characteristics used in planning radio communications, requires the use of an index of solar activity.

Several indices besides the index I_{F2} are already available for applications of the kind mentioned. The Zurich sunspot number, R, is important because it is available for a much longer period than any other index. Since 1947, the solar noise flux, Φ, at frequencies near 2800 Mc/s has been measured regularly in Canada using techniques described by MEDD and COVINGTON (1958). This flux has been shown to be closely related to the ionization in the *E*-layer by DENISSE and KUNDU (1957) and by MINNIS and BAZZARD (1958).

KUNDU and DENISSE (1958) have made tentative comparisons between an *E*-layer index, solar radio noise, and the values of I_{F2} based on data from three stations. Their conclusions cannot be compared directly with those discussed in Sections 3.2 and 3.3 because they made no direct comparisons with f_0F2.

3.2. *Correlation coefficients*

Some criterion for assessing the relative merits of the indices I_{F2}, R_3 and Φ is necessary. For *F2*-layer studies and for ionospheric forecasting, the most important criteria seem to be that the index should be as closely correlated as possible with f_0F2 and that it should be available over as long a period as possible.

Data from only the stations in Table 1 were used in constructing I_{F2} and it seemed possible that the correlation between I_{F2} and f_0F2 might be considerably less for other stations. To test whether this was so, two groups of stations were selected: data from Group A (Washington, Slough, Huancayo and Christchurch) had been used in deriving I_{F2} but data from Group B (Ottawa, Lindau, Madras and Capetown) had not. For each of the stations in Group A and for each month of the year, the linear correlation coefficient, r, was calculated for monthly mean or median values of f_0F2 and the corresponding values of I_{F2}. The same procedure was then applied to Group B for alternate months.

Since the correlation coefficients for both Groups were high, their distribution was very skew and it was necessary to use Fisher's transformation of r to obtain approximately normal distributions to which the usual tests of significance could be applied. These tests showed that there was no significant difference between the distributions for the two groups and it was, therefore, considered legitimate to

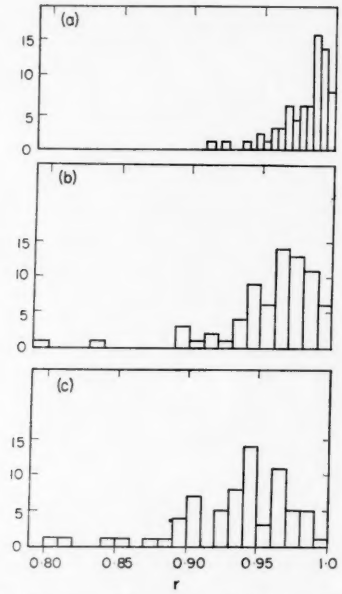

Fig. 1. The distribution of linear correlation coefficients at noon.
(a) f_0F2–I_{F2}; (b) f_0F2–R_3; (c) f_0F2–Φ.

regard the seventy-two values of r for the combined groups as a sample taken from a single parent population (Fig. 1a).

Figs. 1(b) and 1(c) show the frequency distributions of r for the same stations but related to R_3, the 3-month weighted mean sunspot number, and Φ, the monthly mean solar radio noise flux at 2800 Mc/s.

Table 2. Coefficient of correlation (ρ) of f_0F2 and three indices

Index	ρ	$\rho \pm$ s.e.
I_{F2}	0·986	0·989 — 0·982
R_3	0·967	0·974 — 0·959
Φ	0·945	0·956 — 0·930

The data included in each histogram may be regarded as a sample taken from a parent population. The estimated values of ρ for the populations represented by the three histograms, and also their standard errors, are given in Table 2. The standard errors of the differences $\rho(I_{F2}) - \rho(R_3)$ and $\rho(I_{F2}) - \rho(\Phi)$ have been

VOL. 18 1960

calculated and it is concluded that the correlation between f_0F2 and I_{F2} is significantly greater than that between f_0F2 and either of the other two indices. Although $\rho(R_3) > \rho(\Phi)$, there is a probability of 0·1 that this difference may be due to chance and the difference cannot be regarded as significant.

3.3. *Standard error of estimates of* f_0F2

It is important to consider how the magnitude of ρ controls the errors incurred when an index is used to estimate f_0F2. If the regression equation of y on x is used

Table 3. Standard error of estimates of f_0F2 based on three indices (per cent)

Index	S.D. of f_0F2		
	Minimum	Mean	Maximum
I_{F2}	2·6	4·2	6·0
R_3	3·8	6·1	8·8
Φ	5·0	8·1	11·5

to provide estimated values of y for a given set of values of x, the standard error of the estimates, S_E, is given by:

$$S_E = s_y(1 - r^2)^{1/2} \tag{2}$$

where s_y is the s.d. of y;
r is the correlation coefficient for (x,y).

If y represents the monthly mean noon f_0F2, and r the correlation coefficient for a solar index, S_E will provide a figure which can be used for judging the relative merits of different alternative indices in practical applications.

The s.d. of f_0F2 over the full range of solar activity varies with season and the location of the station, but the mean and the minimum and maximum values have been determined using the monthly data for the eight stations in Groups A and B (Section 3.2). To obtain S_E for I_{F2}, R_3 and Φ, these three values of the s.d. of f_0F2 have been associated with the three estimates of ρ quoted in Table 2. The values of S_E are shown in Table 3 and illustrate, more clearly than do the correlation coefficients, the relatively higher accuracy of estimates made using I_{F2} as compared with those using R_3 or Φ.

4. The Use of I_{F2} in Ionospheric Forecasting

4.1. *Origin of errors in forecasts of critical frequencies*

The process of forecasting a critical frequency, such as f_0F2, for a date several months ahead must be carried out in two stages. For the date in question, it is necessary: (a) to forecast the future value of an index of solar activity, such as I_{F2} or R_3; (b) to convert the forecast value of the index into the corresponding series of hourly critical frequencies. In both these stages, errors will be incurred and the error in the final forecast will be a combination of these component errors.

4.2. *Magnitudes of component errors*

The errors arising in stage (b) for forecasts of f_0F2 can be obtained from the standard errors of estimate which are given in Table 3. Those occurring in stage (a) have also been investigated and numerical values for them are given below.

Stage (a) implies the extrapolation of an index from the date of its last-measured value to the future date for which the forecast is required. During the interval between these dates, solar activity will change, partly owing to the long-term 11-year solar cycle and partly as the result of short-term fluctuations in solar activity which often have a quasi-period of about 1 year.

Ionospheric forecasts usually refer to dates about 6 months ahead. In consequence, errors due to inaccurate estimates of the long-term trend will usually be much less than those arising from the short-term fluctuations already mentioned. The magnitude of these fluctuations has been estimated by calculating the standard deviations of the departures of the monthly values of I_{F2} and R_3 from their respective 12 month running mean values; the s.d.'s are $\sigma_1 = 12{\cdot}5$ for I_{F2} and $\sigma_2 = 17{\cdot}8$ for R_3. It seems reasonable to suppose that the variations of I_{F2} above and below its running-mean value represent variations in the solar ionizing radiation which lead to corresponding changes in the ionosphere. The much larger variations which are characteristic of R_3 are assumed to be due to changes in the sunspot number which are not associated with ionospheric changes. The s.d. of this "non-ionospheric" component of the variations in R_3 is, therefore, given by $(\sigma_2{}^2 - \sigma_1{}^2)^{1/2} = 12{\cdot}7$. An estimate of the s.d. of this component was made by Minnis (1955) using a different method and the value obtained, s.d. $= 13{\cdot}3$, is in good agreement with the above figure; the same method gave s.d. $= 1{\cdot}1$ for I_{F2}.

The variations in I_{F2} and R_3 represented by σ_1 and σ_2 can be converted into variations in the critical frequency of the *F2*-layer using the expression

$$\sigma_{F2} = \frac{100\,\sigma}{f}\,\frac{df}{dI} = 100\,\sigma m \qquad (3)$$

where

σ_{F2} = s.d. of variations in f_0F2 (per cent);

σ = s.d. of variations in the index I above and below its running mean;

f = *F2*-layer critical frequency (f_0F2);

I = solar activity index;

$m = (df/dI)/f$.

The magnitudes of df/dI will be the same whether I_{F2} or R_3 is used because both indices are expressed in the same units. The values of m have been determined for a representative sample of points which includes all months of the year and latitudes between 60°N and 60°S, and for low, average and high solar activity as indicated by $I_{F2} = 0$, 90, 180. The mean, maximum and minimum values of m have been substituted in equation (3), together with the values of σ_1 and σ_2 already discussed, and the resulting values of σ_{F2} are given in Table 4.

VOL.
18
196

4.3. *Magnitude of total error*

It is assumed that, for the usual short-term forecasts, the error incurred in forecasting the long-term trend in either I_{F2} or R_3 will be small. Hence the maximum total error in a forecast of f_0F2 will be the sum of the component errors arising in stages (a) and (b) (Section 4.1); the s.d.'s of these errors are given for various circumstances in Tables 4 and 3, respectively. The maximum, mean and

Table 4. S.D. (per cent) of errors in f_0F2 due to errors in forecasts of solar activity

m	Solar activity					
	High		Average		Low	
	I_{F2}	R_3	I_{F2}	R_3	I_{F2}	R_3
Maximum	4·5	6·4	6·6	9·4	12·5	17·8
Mean	3·3	4·7	4·3	6·1	6·2	8·9
Minimum	2·2	3·1	2·6	3·6	3·1	4·5

minimum values of the component errors in each of these tables have been extracted and added together for three levels of solar activity to give Table 5 which illustrates the range of values within which the s.d. of the error in forecasting f_0F2 can lie.

The conclusion drawn from Table 5 is that although the total error may vary over a wide range, the s.d. of the errors incurred in using R_3 is about 45 per cent greater than that which would occur if I_{F2} were used for forecasting f_0F2.

Table 5. S.D. (per cent) of total error in forecasts of f_0F2

Component errors	Solar activity					
	Low		Average		High	
	I_{F2}	R	I_{F2}	R	I_{F2}	R
Minimum	4·1	5·9	3·7	5·2	3·4	4·9
Mean	7·5	10·8	6·0	8·6	5·3	7·7
Maximum	13·9	19·8	8·9	12·9	7·5	10·9

The errors in Table 4 are greater than those which would actually occur in the extrapolation of the indices because when using a monthly index, rather than a 12 month running mean index, it would be possible to estimate approximately the trend of the short-term fluctuations in solar activity. Hence the s.d. of the extrapolation errors would be expected to be less than the s.d. of the fluctuations about the 12 month running mean. If this is so, the total errors given in Table 5 are greater than would be expected in practice.

5. Correlations at Night

Only the correlation of f_0F2 at noon with I_{F2} has been used to derive the results quoted in Section 3. The corresponding correlation for f_0F2 at midnight has also been investigated for all the stations in Groups A and B except Madras. It has been found that although all the noon values of r exceed 0·89, only 82 per cent of the midnight values lie above this limit. In general, the lower correlation at night must necessarily reduce the accuracy of forecasts of f_0F2 but a quantitative estimate of the loss of accuracy can best be gained by calculating the standard error of estimate, S_E (equation (2)) and comparing the related midnight and noon values. The mean value of the ratio S_E (midnight)/S_E (noon) in the sample was 1·4 and it was less than 2·5 in 90 per cent of cases.

The index I_{F2} is based on f_0F2 at noon when the sensitivity of f_0F2 to changes in wave radiation is much greater than it is to particle radiation. Hence I_{F2} may be regarded as primarily a wave radiation index. At night the relative importance of particle radiation in controlling f_0F2 is greater than during the day and this leads to a reduction in the correlation between f_0F2 at night and I_{F2}. To increase the accuracy of forecasts of f_0F2 at night, it would be necessary to use a particle index in addition to I_{F2}.

There appears to be a correlation between the midnight values of r and the s.d. of f_0F2 which can be represented by the rough empirical relation: s.d. = $0{\cdot}4/[(1 - r^2)^{1/2}]$ Mc/s. The substitution of this expression for s_y in equation (2) leads to the conclusion that the standard error of estimate at midnight is approximately 0·4 Mc/s even when r is small. Capetown provides an extreme instance of this compensation for low correlation: $r = 0{\cdot}015$, s.d. = 0·17 Mc/s and hence $S_E = 0{\cdot}17$ Mc/s.

Conclusions

The construction is described of a monthly mean index (I_{F2}) which is based on monthly median or mean noon values of f_0F2 at eleven widely-spaced locations. The correlation between noon f_0F2 and this index ($\rho = 0{\cdot}986$) is significantly greater than that between f_0F2 and either the 3 month weighted mean sunspot number ($\rho = 0{\cdot}967$) or the solar radio noise flux at 2800 Mc/s ($\rho = 0{\cdot}945$). The standard errors of estimate of noon f_0F2 made using I_{F2}, R_3 and Φ are approximately 4 per cent, 6 per cent and 8 per cent, respectively. The fluctuations of I_{F2} above and below its 12 month running mean value have a standard deviation of 12·5 units as compared with 17·8 units for the 3 month weighted mean sunspot number (R_3). The errors incurred in forecasting f_0F2 several months ahead using I_{F2} and R_3 have been calculated; representative values of the s.d. of these errors are 6·0 per cent for I_{F2} and 8·6 per cent for R_3 but the s.d.'s may vary from half to twice these values depending on circumstances. The standard error of estimate of f_0F2 at midnight is approximately 1·4 times as great as at noon.

Acknowledgements—The writers acknowledge the assistance of Miss F. P. Coward who was responsible for most of the numerical work described. The work described above was carried out as part of the programme of the Radio Research Board and is published by permission of the Director of Radio Research of the Department of Scientific and Industrial Research.

VOL
18
196

References

Denisse J. F. and Kundu M. R.	1957	*C.R. Acad. Sci., Paris* **244,** 45.
Kundu M. R. and Denisse J. F.	1958	*J. Atmosph. Terr. Phys.* **13,** 176.
Medd W. J. and Covington A. E.	1958	*Proc. Inst. Radio Engrs, N.Y.* **46,** 112.
Minnis C. M.	1955	*J. Atmosph. Terr. Phys.* **7,** 310.
Minnis C. M. and Bazzard G. H.	1958	*Nature, Lond.* **181,** 1796.
Minnis C. M. and Bazzard G. H.	1959	*J. Atmosph. Terr. Phys.* **14,** 213.

OL.
18
960

Journal of Atmospheric and Terrestrial Physics, 1960, Vol. 18, pp. 306 to 308. Pergamon Press Ltd. Printed in Northern Ireland

A world-wide semi-annual cycle in the *E*-layer of the ionosphere

C. M. Minnis and G. H. Bazzard
DSIR Radio Research Station, Slough*

(*Received* 10 *February* 1960)

Abstract—A study of the *E*-layer character figure for eight stations in the north and south hemispheres has disclosed an unexpected semi-annual cycle the variations in which have the same sign in both hemispheres. The amplitude of the cycle is about ±15 per cent near the maximum of the solar cycle but vanishes at the minimum. Its origin has not yet been discovered but several possibilities are discussed.

If it is assumed that the *E*-layer of the ionosphere is a Chapman layer, the relation between the intensity (S) of the incident solar ionizing radiation, the solar zenith angle (χ) and the critical frequency (f) of the layer near noon can be written:

$$S \propto f^4 \sec \chi = Ch_E.$$

The quantity $f^4 \sec \chi$ is usually referred to as the *E*-layer character figure (Ch_E) and it is nominally proportional to the flux of the ionizing radiation which gives rise to the layer.

Since 1947 the flux (Φ) of the solar radio noise at 2800 Mc/s has been measured regularly at Ottawa by Medd and Covington (1958). Comparisons have been made by Minnis and Bazzard (1959) between the monthly mean values of Φ at Ottawa and Ch_E at Slough. These comparisons show that the slopes of the linear relations connecting Φ and Ch_E vary with the time of year and also that these variations have their origins in the ionospheric data and not in the solar noise measurements.

The comparisons of these two indices have now been extended to include the values of Ch_E derived from data from eight stations covering a wide range of latitudes: Lindau, 51·7°N; Slough, 51·5°N; Washington, 38·7°N; Ibadan, 7·5°N; Singapore, 1·3°N; Watheroo, 30·3°S; Godley Head, 43·6°S; Port Stanley, 51·7°S. The lines representing the Ch_E–Φ relations for each month were drawn for each of the eight stations. The values of Ch_E corresponding to $\Phi = 70$ and 200 (in units of 10^{-22} W m^{-2} per c/s) were then read from these lines.

For all the stations considered, the value of Ch_E corresponding to $\Phi = 70$ units (the minimum of the solar cycle) remains constant throughout the year. On the other hand for $\Phi = 200$ units (near the maximum of the solar cycle) there is a semi-annual cycle in the magnitude of Ch_E. Hence the value of Ch_E for $\Phi = 200$ units may be regarded as consisting of two components: a constant background component (Ch_{Eb}) corresponding to the value of Ch_E when $\Phi = 70$ units, and a variable component (Ch_{Ev}) such that $Ch_E = Ch_{Eb} + Ch_{Ev}$. For each of the stations the ratio ρ_v of the monthly mean value of Ch_{Ev} ($= Ch_E - Ch_{Eb}$) to its annual mean value has been plotted in Fig. 1(a). Figs. 1(b) and 1(c) show the median values of ρ_v and ρ_b for the eight stations. The median values have been corrected to allow for the annual variation in the distance of the earth from the sun. The

* Official communication.

characteristic features of the variations in Ch_{Ev} at all the stations are the two maxima which occur in January or February and in July or August, and the two minima which occur in May and near the end of the year.

It is important to note that the variations in Ch_{Ev} have the same sign in both the northern and southern hemispheres. It is difficult, therefore, to attribute them to seasonal departures from the simple Chapman layer behaviour which is implicitly assumed in calculating Ch_E. The variations seem more likely to be due to an extraterrestrial influence or to some other cause which affects the northern and southern hemispheres in the same way.

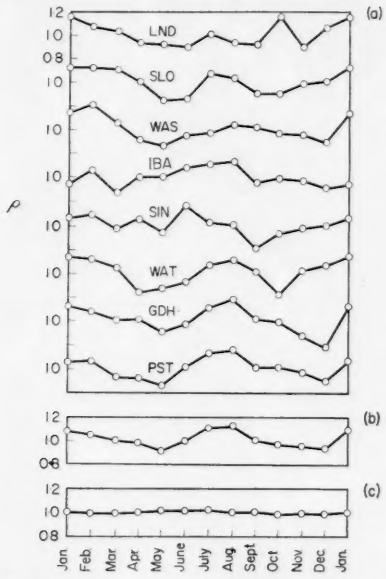

Fig. 1. The semi-annual cyclic variation in the E-layer character figure: (a) eight stations, high solar activity ($\Phi = 200$ units); (b) median values of (a); (c) median values for eight stations, low solar activity ($\Phi = 70$ units).

The fact the variations in Ch_{Ev} have an amplitude which is proportional to the sunspot number, and which is zero when the sunspot number is zero, suggests that the sun may be responsible for them and, in particular, that they may be linked in some way with the existence of visible active areas on the sun which are strong emitters of corpuscular and photon radiation. The flat peaks in geomagnetic activity which occur in March and September are sometimes attributed to increases in the incidence of the corpuscular radiation in these months. The corpuscles are assumed to be emitted, in a direction normal to the sun's surface, from two belts centred north and south of the sun's equator. This mechanism would result in a high intensity of incident corpuscular radiation in March and September when the earth's heliocentric latitude is high and a low intensity in June and December when the earth crosses the sun's equator.

There are two main objections to the suggestion that the same mechanism may be responsible for the variations in Ch_{Ev}. These variations vanish at the minimum

of the solar cycle while the March and September peaks in geomagnetic activity remain. Further, the phases of the Ch_{Ev} and the geomagnetic cycles differ by about two months and it would be necessary, for example, to associate the May minimum in Ch_{Ev} with the March peak in geomagnetic activity.

It might also be suggested that the semi-annual peaks in Ch_{Ev} were due to beams of photon radiation coming from localized active areas which occur much less frequently near the minimum of the solar cycle. Here again, the phase of the Ch_{Ev} cycle is not what would be expected if this hypothesis were valid. If such photon beams existed, they ought to be detectable as changes in the daily values of Ch_E, but a superposed epoch test designed to show this effect did not yield a significant result.

It is at least conceivable that the variations in Ch_{Ev} may be an atmospheric tidal phenomenon. The atmosphere has a period of free oscillation near 12 hr and, at the equinoxes, when the day is 12 hr in length at all latitudes, a resonance might occur which could ultimately lead to changes in the characteristics of the atmosphere at E-layer heights. GREENHOW and NEUFELD (1956) have discussed the relation between atmospheric tides and the semi-annual changes in the E–W component of the wind velocity at heights of about 100 km and it is interesting to note that these changes are very similar to those in Ch_{Ev}.

It is probably worth pointing out that the variations in Ch_{Ev} are also similar to those in the equation of time, and that the appropriate allowance for this anomaly has already been included in the values of $\cos\chi$ used in calculating Ch_{Ev}. Since the Ch_{Ev} variations have an amplitude which varies with solar activity, it is unlikely that there is any connexion between them and the orbital motion of the earth.

The semi-annual variations in Ch_E which have been described above do not appear to have been investigated in detail before. Unexplained anomalies in the E-layer critical frequencies have, however, been referred to by several authors and have been summarized by ROBINSON (1959). These anomalies seem to indicate that the phenomenon was probably present in the data studied by previous authors, but that the methods of analysis used were not capable of isolating the semi-annual cycle from the much larger changes due to month to month fluctuations in solar activity.

Acknowledgements—Some of the original character figures were kindly made available by Dr. Y. Y. MAO of the CCIR Secretariat in Geneva. The work described was carried out as part of the programme of the Radio Research Board. The paper is published by permission of the Director of Radio Research of the Department of Scientific and Industrial Research.

REFERENCES

GREENHOW J. S. and NEUFELD E. L.	1956	*Phil. Mag.* **1**, 1157.
MEDD W. J. and COVINGTON A. E.	1958	*Proc. Inst. Radio. Engrs, N.Y.* **46**, 112.
MINNIS C. M. and BAZZARD G. H.	1959	*J. Atmosph. Terr. Phys.* **14**, 213.
ROBINSON B. J.	1959	*Rep. Progr. Phys.* **22**, 241.

VOL
18
196

Journal of Atmospheric and Terrestrial Physics, 1960, Vol. 18, pp. 309 to 314. Pergamon Press Ltd. Printed in Northern Ireland

Seasonal variations in the twilight enhancement of [OI]5577

L. R. MEGILL*, P. M. JAMNICK* and J. E. CRUZ†‡

(*Received* 22 *February* 1960)

Abstract—Measurements of the twilight enhancement of [OI]5577 were obtained during the period September 1957 to December 1958 at Rapid City, S.D. All these measurements were normalized to the intensity at sunset or sunrise at a height of 100 km. The results obtained indicate that there was a seasonal dependence of the twilight enhancement of [OI]5577 emission. The enhancement occurred most frequently in the autumn and winter months, the maximum occurring about 1 November. The enhancement almost never occurred during the spring and summer months.

THE twilight enhancement of [OI]5577 has recently been reported by MEGILL (1960). In this earlier paper the night of 6/7 January, 1959, was analysed in detail. The present paper is a report of a seasonal variation in this effect, covering the period from September 1957 to December 1958. The regular IGY observing programme for Airglow, conducted by the National Bureau of Standards, used a birefringent filter system which discriminates strongly against the scattered sunlight. This instrument enables one to observe much later in the twilight than is possible with the conventional dielectric filter photometer. During the IGY, observations were carried out with a programme of six almucantars (sweeps at constant zenith distance) at zenith angles of 80°, 75°, 70°, 60°, 40° and 0°. One such programme was executed every 15 min. These measurements were made as early in the twilight, and as late in the dawn, as possible. In looking for an index with which to describe the twilight enhancement, it was decided to use the intensity at the time of sunset at 100 km height, in the part of the sky being observed. In these calculations it is assumed that the sun's rays are screened from the upper atmosphere. The screening height is taken as 35 km. A detailed description of the calculations used may be found in the paper referenced above.

Because the scattered sunlight is the limiting factor in the observations, it is advantageous to use data taken at a large zenith angle. For this reason we have chosen data taken at 75° zenith angle. Since from the previous study it was indicated that the enhanced intensity at all azimuths is essentially the same when normalized to the sunset time, only one azimuth was taken. There is also a moderate amount of computation involved in each sunset time calculation so that it seemed wise to keep the number of points as small as possible. The points used were the west-south-west in the twilight and east-south-east in the dawn. The data for these points in the sky were plotted against time and a smooth curve drawn through the points. The time of sunset, or sunrise, at 100 km was computed for each of these points and drawn in on the curve. An average "night sky" intensity was extrapolated to this sunset, or sunrise time, and both the average or night sky and the enhanced intensities were read off the graph. Two typical

* National Bureau of Standards, Boulder, Colorado.
† South Dakota School of Mines and Technology, Rapid City, South Dakota
‡ Now at Goodyear Aircraft Company, Phoenix, Ariz.

curves are shown in Fig. 1: (a) shows a case in which the enhancement occurs; (b) shows a case in which it does not occur. The data read off are shown in Table 1. Column (1) gives the date, column (2) the night-glow background intensity $\bar{I}$, and column (3) the enhanced intensity I_e. Column (4) gives the quantity $I_e - \bar{I}$ which

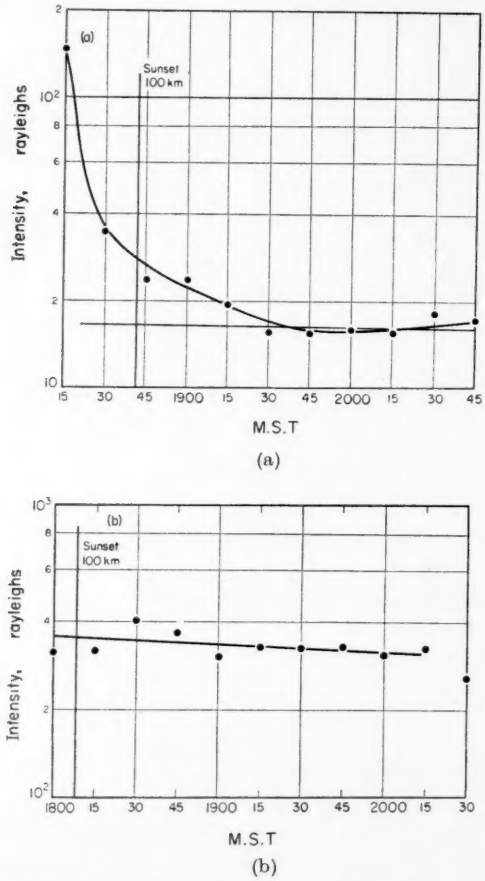

Fig. 1. A plot of the variation of slant intensities, taken at 75° zenith distance, in rayleighs, against local time. The slant intensities are not corrected for scattering or extinction. At the time of sunset at 100 km the amount of enhancement is the difference between the smooth curve drawn through all the points and the heavy straight line giving the average "night-sky" intensity. (a) Evening 21 February 1958. Sunset: $h = 0$; 1763, $h = 100$; 1842. Enhancement occurs. (b) Evening 23 October 1956—100 kΩ. Sunset: $h = 0$; 1702, $h = 100$; 1808. No enhancement occurs.

is the net intensity due to the twilight effect. Column (5) shows the percentage enhancement observed. For reference, column (6) includes remarks about the weather conditions. An attempt was made to include no data which had clouds in the vicinity of the observed region. If clouds were reported anywhere in the sky, the notation partly cloudy is used. For reference, notation is made as to whether or not an aurora was reported at Rapid City on the night of the observations.

Table 1.

Date	$\bar{I}$	I_e	$I_e - \bar{I}$	$\frac{I_e - \bar{I}}{\bar{I}}$	Sky conditions	Occurrence of aurora	A_p
		Evening					
30- 9-57	1750	1960	210	0·12	partly cloudy		—
09-11-57	3980	3980	0	0·00	clear		29
12-11-57	1430	2450	1020	0·71	partly cloudy		17
13-12-57	1660	2000	340	0·20	partly cloudy		22
20-12-57	2000	2300	300	0·15	partly cloudy		20
26- 1-58	1540	1890	350	0·23	clear		16
21- 2-58	492	1060	578	1·17	clear	A	31
24- 2-58	1060	1320	260	0·24	clear		8
05- 5-58	3600	3600	0	0·00	clear		12
10- 5-58	1400	1400	0	0·00	clear		20
09- 6-58	23000	23000	0	0·00	clear	A	32
22- 7-58	1030	1290	260	0·25	clear		20
25- 8-58	670	1230	570	0·85	partly cloudy	A	18
05- 9-58	1060	1530	470	0·44	partly cloudy		71
21- 9-58	1700	2640	940	0·55	clear		4
04-10-58	9800	9800	0	0·00	clear		5
17-10-58	4670	6730	2060	0·44	clear		9
22-10-58	1930	2400	470	0·24	clear	A	47
29-10-58	2260	3060	800	0·35	clear		20
01-11-58	1000	1260	260	0·26	clear		7
21-11-58	2040	2300	260	0·13	partly cloudy		4
		Morning					
27-10-57	380	490	110	0·29	clear		—
10-11-57	3820	7200	3380	0·88	clear		26
11-11-57	1100	2380	1280	1·16	clear	A	21
11-12-57	1300	2300	1000	0·77	partly cloudy	A	41
17- 1-58	1590	2120	530	0·33	clear		22
27- 1-58	1890	2380	490	0·26	clear		8
26- 8-58	2220	2370	150	0·068	clear		14
02- 9-58	2560	2560	0	0·00	clear	A	5
07- 9-58	1990	1990	0	0·00	clear		16
17- 9-58	790	1280	490	0·61	clear		13
10-12-58	1040	2040	1000	0·96	clear		3
17-10-58	4440	6900	2460	0·56	partly cloudy		9
18-10-58	5200	7500	2300	0·44	partly cloudy		8
23-10-58	6590	9190	2600	0·39	clear	A	44
24-10-58	8410	10700	2290	0·27	clear	A	89
08-11-58	1890	2980	1090	0·58	clear		3
22-11-58	2340	3360	1020	0·44	clear		3

On a few occasions the measured intensity was quite high, but no aurora was reported due to the fact that the intensity was fairly uniform over the sky. The last column gives the daily magnetic index A_p taken from the National Bureau of Standards CRPL-F Series reports part B, Compilations of Solar-Geophysical Data.

The intensities reported here are in rayleighs inside the atmosphere, that is, they are uncorrected for extinction and scattering. The increase of the intensity towards the horizon (Van Rijhn effect) is also left in since only a relative study is being made.

Plots of the enhanced intensity, and the fractional enhanced intensity are

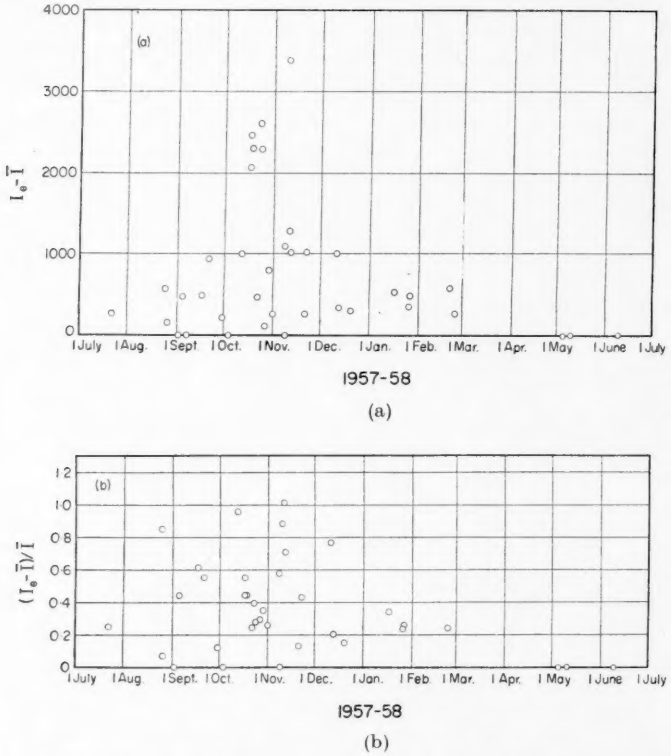

Fig. 2. A plot of the amount of enhancement against day of the year. (a) Ordinate is slant intensity in rayleighs. There appears to be a maximum around 1 November. (b) Ordinate is the percentage enhancement. There still appears to be a maximum around 1 November, although it is not as pronounced as in (a).

shown in Fig. 2. These plots represent all of the available data of this type. It is unfortunate that there are so few points during the spring and summer months. Poor weather during these months prevented the gathering of more data. There were many other nights during this period when observing attempts were made. These nights were eliminated from the formal analysis because of uncertainties regarding the effect of the clouds. However, it is perhaps worth noting that during the months from March to July no case of enhancement of the 5577 Å line was noted upon visual inspection of the records. It will be noted also that there are some cases of no enhancement during the winter months.

Although the small number of points available make the method somewhat suspect, it is of interest to plot the mean enhancement of all the observed points

VOL
18
196

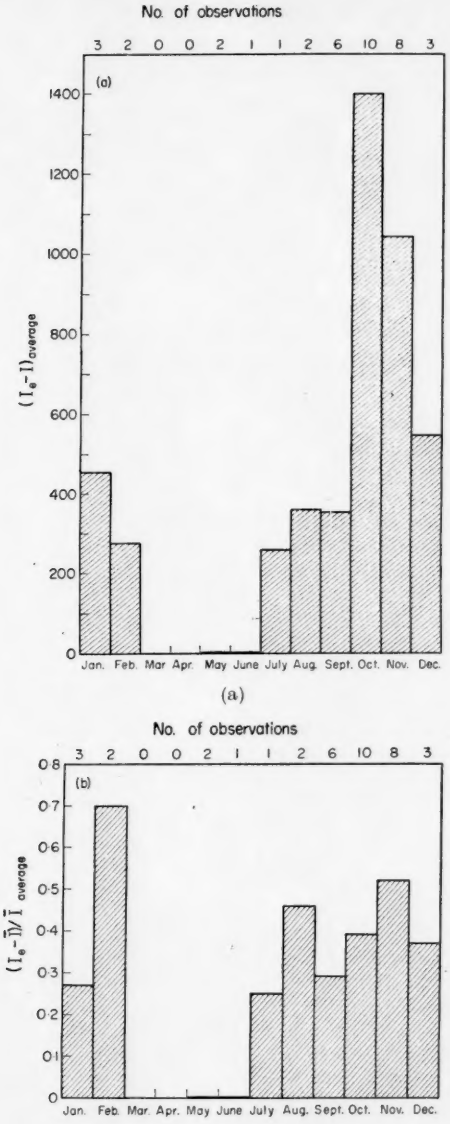

Fig. 3. A graph of average monthly enhancement against month of the year. At the top of the graph are the number of observations made in each month. (a) Ordinate is enhancement in rayleighs. (b) Ordinate is percentage enhancement.

for each month of the year. This is presented in Fig. 3. Fig. 3 (a) shows the mean absolute enhancement of the line

$$\sum_{1}^{n} \frac{I_{ej} - \bar{I}_j}{n}$$

where n is the number of nights observed in the month. Fig. 3 (b) shows the mean relative enhancement

$$\sum_{1}^{n} \frac{(I_{ej} - \bar{I}_j)}{n\bar{I}_j}.$$

When one looks at data from other IGY Airglow stations it appears that there may also be a latitude effect. At Sacramento Peak (32°47′) MANRING and PETTIT have been unable to detect any such effect. At Fritz Peak (39°54′N) the effect has been observed a very few times, while at Rapid City (44°0′N) the effect is as shown here.

There seems to be no clear connexion between the effect and either the daily magnetic index or the occurrence of aurorae. It also appears that there is no clear connexion between the intensity of the airglow and the percentage of enhancement.

The data also indicate a definite seasonal dependence of the twilight enhancement of the [OI]5577 emission from the atmosphere, the maximum enhancement occurring on about 1 November. The enhancement occurs most frequently during the autumn and winter months, and almost never during the spring and summer months. There is a possibility of a latitude effect with the enhancement occurring in the more northerly latitudes.

Acknowledgements—The writers wish to acknowledge the contributions of Dr. F. E. ROACH and the Airglow Group of the National Bureau of Standards to the success of this study. The support for the construction of the equipment and the observational programme came from the National Science Foundation in connexion with the International Geophysical Year effort.

VOL
18
196

REFERENCE

MEGILL L. R. 1960 *J. Atmosph. Terr. Phys.* **17**, 276.

Journal of Atmospheric and Terrestrial Physics 1960, Vol. 18, pp. 315 to 331. Pergamon Press Ltd. Printed in Northern Ireland

A synoptic study of the *F2*-region of the ionosphere in the Asian zone

R. G. RASTOGI
Radio and Electrical Engineering Division, National Research Council, Ottawa, Canada

(*Received* 27 *February* 1960)

Abstract—A detailed study of the variation of f_0F2 at ionospheric stations in the Asian zone shows that the region of maximum f_0F2 varies with the time of the day as well as with the season. The anomalous belt of the *F2*-layer develops at the equator near sunrise and slowly expands with the progress of the day, and is most extended during the afternoon hours.

Multiple splittings in the *F*-region and other abnormal *P'-f* recordings observed at middle latitudes are shown to be associated with some striking features in the synoptic distribution of f_0F2. The abnormal recordings can be explained on the basis of horizontal movements in the ionosphere, being in the east–west direction before sunrise in the morning or after sunset in the evening, and in the north–south direction during the forenoon.

THE ionospheric stations in the Asian zone have provided a very uniform and wide coverage of latitudes between 0° and about 40° N. RASTOGI (1960) has pointed that the meridional transport of ionizations as guided by the earth's magnetic field would have a uniform effect at different stations in the Asian zone. This simplifies the comparison of the ionospheric variations at different stations which do not lie exactly on the same longitude. A synoptic study of the *F2*-layer variations over the Asian zone seemed useful in the understanding of some abnormal features of the *F2*-region.

The co-ordinates of the ionospheric stations of the Asian zone are given in Table 1 and the positions of these are indicated in Fig. 1.

Table 1. Co-ordinates of the ionospheric stations in the Asian zone

Stations	Geographic Latitude °N	Geographic Longitude °E	Geom. lat. °N	Magn. dip °N	Magn. lat. °N
Wakkanai	45·4	141·7	35·3	59·4	40·2
Akita	39·7	140·1	25·7	53·5	34·1
Tokyo	35·7	139·5	25·4	49·3	30·2
Yamagawa	31·2	130·6	20·3	44·3	26·0
Delhi	28·6	77·2	19·2	42·7	24·8
Okinawa	26·3	127·8	15·0	37·0	20·7
Formosa	25·0	121·5	13·7	34·0	18·5
Ahmedabad	23·0	72·6	14·0	34·0	18·5
Calcutta	23·0	88·6	12·5	32·0	17·3
Bombay	19·0	72·8	10·0	24·8	13·1
Baguio	16·4	120·6	5·0	18·0	9·2
Guam Island	13·6	144·9	4·0	14·0	7·1
Madras	13·1	80·2	3·1	10·5	5·3
NhaTrang	12·3	109·2	0·5	8·0	4·0
Tiruchy	10·8	78·7	1·1	4·8	2·4
Kodaikanal	10·2	77·5	0·7	3·5	1·7

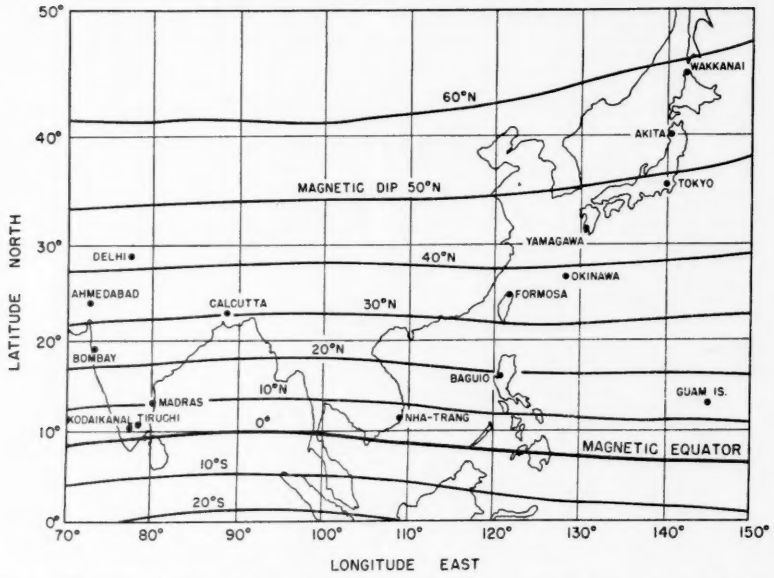

Fig. 1. The map showing the positions of ionospheric stations operating in the Asian zone.

The variations of *F2*-parameters are considered with respect to the magnetic dip as the variations of f_0F2 at low and middle latitudes are controlled more by the real magnetic rather than the idealized geomagnetic latitudes (RASTOGI, 1959a). Magnetic latitude, μ, is derived from magnetic dip, I, according to the relation

$$\mu = \tan^{-1}(\tfrac{1}{2}\tan I).$$

In order to understand the average position of these stations with respect to the region of equatorial geomagnetic distortion of the *F2*-layer, the annual mean

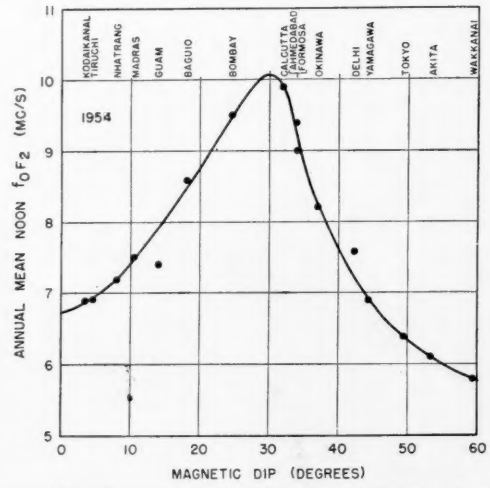

Fig. 2. The variation of annual mean value of noon f_0F2 against the magnetic dip.

value of f_0F2 for the year 1954 at these stations is plotted against the magnetic dip in Fig. 2. The figure shows the well-known geomagnetic control of f_0F2 producing a maximum around the region of 30° magnetic dip. The station nearest to the peak region is Calcutta; Ahmedabad lies just outside and Bombay just inside the so-called equatorial trough of f_0F2. The Japanese stations are all outside the belt of anomalous *F2*-region.

When the variations of f_0F2 with magnetic dip are studied for each month of the year, some significant and consistent changes of the distribution with season are noticed. The region of maximum f_0F2 is found to be farthest from the equator at about 35° dip during the equinoctial months; it lies at about 30° dip during the summer months and is closest to the equator at about 25° dip during the winter months.

This change in the region of maximum f_0F2 can be confirmed on comparing the diurnal variations of f_0F2 at Ahmedabad, Bombay and Calcutta during each of the seasons, as shown in Fig. 3. During the months of June–July 1954, the f_0F2 for

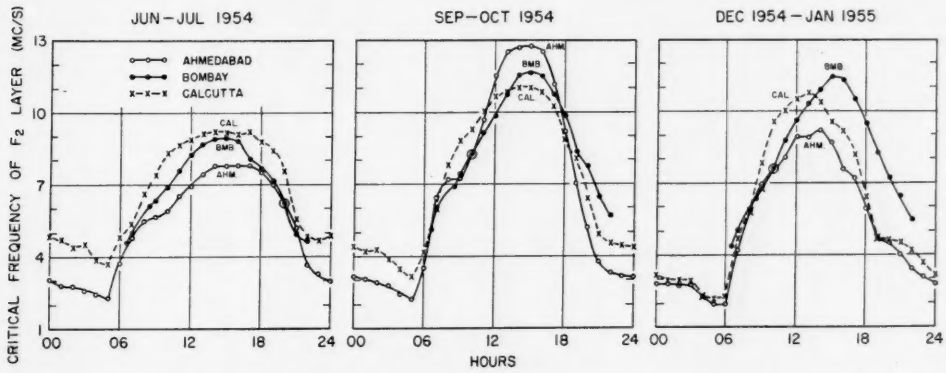

Fig. 3. The diurnal variations of f_0F2 at Ahmedabad, Bombay and Calcutta during the three seasons of the minimum-sunspot year 1954.

any hour is greater at Calcutta than at Bombay or Ahmedabad. Thus the region of maximum f_0F2 is very close to Calcutta during the summer months. During the months of September–October 1954, the highest values of f_0F2 are observed at Ahmedabad, though f_0F2 is slightly greater at Calcutta than at Ahmedabad during the forenoon hours. Thus during the equinoctial months the region of maximum f_0F2 is close to Calcutta during the forenoon hours and close to Ahmedabad in the afternoon hours. During December–January, the highest values of f_0F2 are observed at Bombay; the values at f_0F2 at Ahmedabad being lower than Calcutta or Bombay at any of the hours. Thus during the winter months, the region of maximum f_0F2 is close to Calcutta at the midday hours and close to Bombay in the evening hours. This shows that the region of maximum f_0F2 depends on the time of the day as well as on the season.

The diurnal variations of f_0F2 at these stations during the solsticial months of January and July are compared in Fig. 4. To complete the whole range of latitudes the diurnal variation curves at Sanya during 1942–1943 and at Paramushiro during

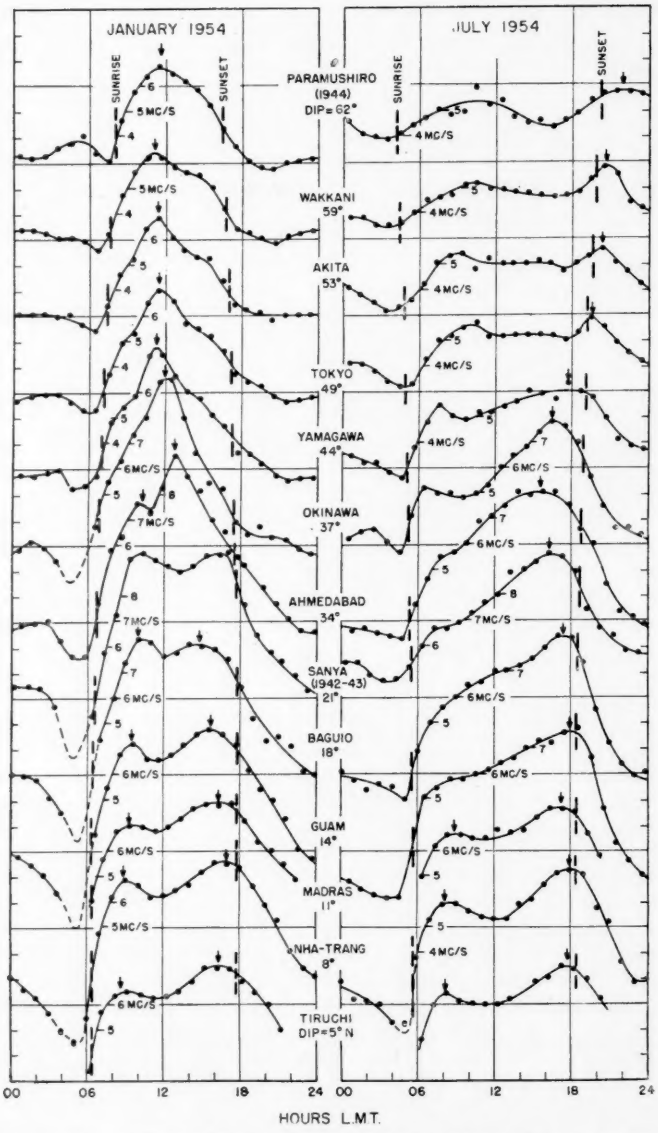

Fig. 4. The diurnal variations of f_0F2 at the ionospheric stations of the Asian zone during the solstices of the minimum-sunspot year.

1944 are also included in the diagram. The years 1942–1944 were close to the period of minimum solar activity, so the variations of f_0F2 at Sanya and Paramushiro can be reasonably compared with the same at other stations during 1954.

Comparing the diurnal variations of f_0F2 at low latitude stations during the equinoctial months, RASTOGI (1959b) has shown that the times of occurrence of the two maxima at these stations get closer with increasing latitude and finally

VOL.
18
196C

converge to a strong single maximum near the latitudes of Bombay. This was interpreted as due to the horizontal motions in the *F*-region of the ionosphere along the meridian towards the poles in the morning and towards the equator in the afternoon.

During winter (January) the diurnal curves at all low-latitude stations show two maxima in the day-time. The morning maximum occurs at about 0800 hours near the equator and later at about 1000 hours at higher latitudes. Similarly, the evening maximum occurs at about 1300 hours at middle latitudes and at about 1800 hours near the equator. Further, the gradual shift of the time of occurrence of these maxima (indicated by the arrows in the figure) is quite evident from these series of curves. At latitudes close to that of Ahmedabad the two maxima occur at the same time giving rise to a very large single maximum near noon. The single maximum at more northerly stations occurs slightly before local noon, which further suggests the dynamic features of the *F2*-layer.

During summer (July) the diurnal variations of f_0F2 are similar to those in winter only for the equatorial stations. At high latitudes f_0F2 shows two maxima during the day, one in the morning and the other in the evening hours. The gradual shift in the time of occurrence of the evening maximum is quite clear, but the morning maximum is absent at few middle-latitude stations. The evening maximum occurs at about 1800 hours near the equator, occurs earlier at increasing latitude being at about 1600 hours near Ahmedabad, again occurring later with increasing latitudes, being at about 2200 hours near Paramushiro.

One finds some important differences in the curves for the two solstices at some of the stations. At low-latitude stations (dip between 14° and 25°), viz. Guam Island, Baguio and Sanya, the noon bite-out of f_0F2 was quite prominent during the winter months, whereas during the summer months the f_0F2 at these stations continued to increase since the time of sunrise up to the evening hours.

The absence of midday bite-out of f_0F2 at low-latitude stations during the summer months can be further noticed in Fig. 5 which shows the diurnal variations of f_0F2 and $h'F2$ at Guam Island during the January and July months of 1950, 1952 and 1954. The variation of f_0F2 during the winter months of any of these years shows the double maxima during the morning and evening hours with a minimum near noon. However, during the summer months of any of these years, the variation of f_0F2 does not show any depression around noon hours.

The midday decrease of f_0F2 at the equatorial stations has been ascribed due to the vertical expansion, thermal or electronic of the *F2*-region (Appleton, 1955). The vertical expansion of the *F2*-region during the midday hours is evidenced by the occurrence of the maximum height of the *F2*-layer at or slightly after the noon. Comparing the curves of the diurnal variation of the minimum virtual height of the *F2*-layer ($h'F2$) at Guam Island, one finds a greater increase of the height during a summer day than a winter one, suggesting a greater vertical expansion of the *F2*-region during the summer. Thus the midday bite-out of f_0F2 is quite prominent during the winter months when the *F2*-region is least expanded and is almost absent in the summer when the *F2*-region is greatly expanded vertically. The theory of the vertical expansion of *F2*-region does not explain the comparative absence of the midday bite-out of f_0F2 at low latitudes during the summer months.

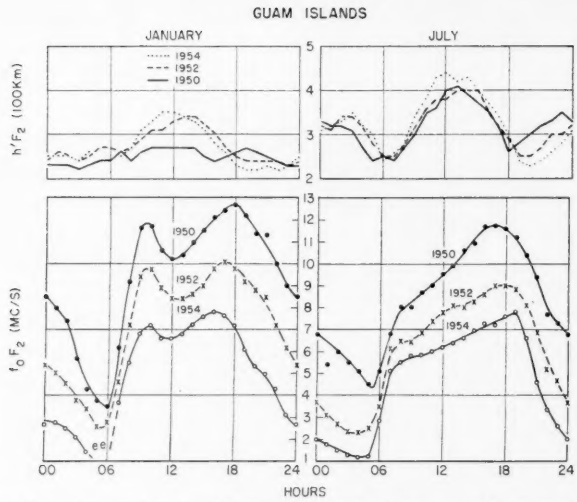

Fig. 5. The diurnal variations of f_0F2 and $h'F2$ at Guam Island during the solsticial months of low-sunspot years.

MARASIGAN (1958) has shown that the percentage occurrence of the bifurcation of the *F*-region into *F1*- and *F2*-layers during the day-time at Baguio is greater during the summer months when there is greatest difference between $h'F2$ and $h'F1$. Thus the greatest bifurcation of the *F*-region at Baguio is accompanied with the least evidence of the midday bite-out of f_0F2. This does not support the theory, that the critical frequency of the *F2*-layer is decreased due to the separation of the *F*-region into *F1*- and *F2*-layers.

These facts indicate some inadequacy of the theory of vertical drifts in the *F*-region to explain fully the anomalous behaviours of the *F2*-layer and suggest that the influence of the horizontal transports of ionizations in the *F*-region are of significant importance.

Synoptic distribution of the critical frequency and height of the F2*-layer*

The general distribution of the *F2*-ionization can be better understood with the contour diagrams showing the lines of constant critical frequency during a particular month on the grid of the local hour and the magnetic dip. Fig. 6 shows such diagrams for the months of January (winter), April (equinox) and July (summer) of 1954. The contour lines of the height of maximum ionization in the *F2*-layer (h_pF2) are also superimposed on the f_0F2 contour diagrams to inter-compare the distributions of the two main characteristics of the *F2*-layer. With such a diagram one can visualize the latitudinal distributions of f_0F2 and h_pF2 at any particular local time or the diurnal variations of these quantities at any particular latitude. Thus the changes in the latitude and the time of occurrence of the maximum f_0F2 during any season and its relation to the variation of the height of the *F2*-region can be easily followed.

A cursory glance at these diagrams shows that during any of the seasons, the height of the *F2*-layer at any place is greatest during midday hours (between 1100–1300 hours) and at any particular time is greatest at the equator.

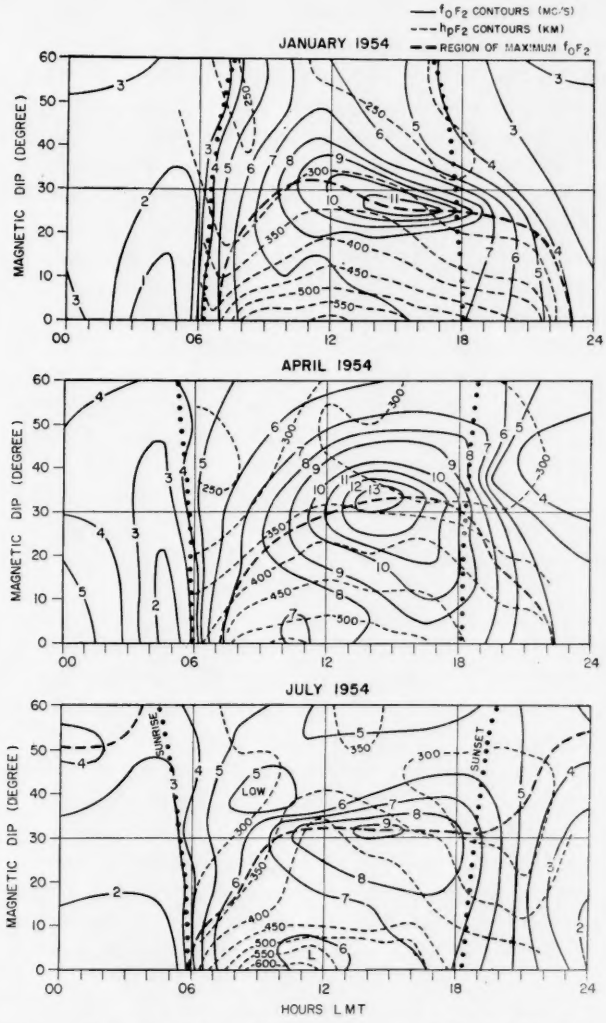

Fig. 6. Contour diagrams of the critical frequency and the height of maximum electron density of the *F2*-layer on the local hour vs. magnetic dip co-ordinates during the months of January, April and July 1954.

During any of the months, the latitude of maximum f_0F2 varies systematically with the time of the day. The region of maximum f_0F2 is near the equator at sunrise, gradually shifts to higher latitudes with time, and is farthest away from the equator at about 1400–1500 hours and this anomaly vanishes by 2100–2300 hours.

The shift of the region of maximum f_0F2 with the time of the day is parallel to the iso-h_pF2 lines at the middle latitudes. There are some important features in these diagrams at some local time and during some seasons, and are discussed hereafter.

Sunrise effect on the F2*-region*

Though the lowest value of f_0F2 in any month is observed at the equator during the pre-sunrise hours, but in the winter months f_0F2 near the equator decreases to a value less than 1·0 Mc/s for a couple of hours. This would result in the absence of the ionospheric reflections on some P'-f records and would indicate the disappearance of the *F2*-layer. BHARGAVA (1952) has reported that at Kodaikanal (geog. lat. 10·2° N) on about 60 per cent of the days during the period March–July 1952, the ionospheric echoes ceased for some time during the predawn period. BONNET (1954) has reported that towards the middle of the night the *F2*-layer at Lwiro (geog. lat. 2·3° S) attained a very low height, sometimes less than 200 km, apparently due to contraction, which was followed by a rapid expansion, frequently coincident with the formation of a layer of density less than measurable.

The phenomenon was observed at Ahmedabad during the winter months but was less frequent than at Kadaikanal. The ionospheric soundings at shorter intervals taken regularly during the early morning hours of December 1954–January 1955 showed that the no-echo condition occurred on only 15–20 per cent of the days. An example of the absence of the echoes at Ahmedabad is shown in Fig. 7. Following the general decrease of f_0F2 and $h'F2$, the echoes vanished at 0500 hours. It is interesting to note that the new *F2*-layer was formed at a height above 275 km.

On some occasions when the night-time *F2*-layer did not die out completely, the critical frequency and height of the *F2* decreased progressively to a very low value followed by the formation of fresh ionizations at much higher level due to the sunrise at those levels. The remnant of the old *F2*-layer at low levels and the new ionizations at higher levels remained simultaneously for some time, the old ionization getting feebler while the new ionization getting stronger with the increasing altitude of the sun. The P'-f records on these occasions resembled the one due to the usual *F1* and *F2*, or the *E2*- and *F2*-layers, and so has been referred to as night *F1*-layer (HAUBERT, 1953), nocturnal *E*-layer (BONNET, 1954) or as night *E2*-layer (RASTOGI, 1956). These designations seem to be based on the minimum height of the old *F2*-layer and the usual heights of the regular *E*-, *E2*- or *F1*-layers during the day-time. Such a development of the *F2*-layer is seen in the sequence of P'-f records taken at Ahmedabad on 30 December 1954 reproduced in Fig. 8. One notices a very fast and gradual decrease of the critical frequency of the *F2*-layer after 0215 hours; by 0315 hours f_xF2 had decreased to 2 Mc/s and the minimum height had dropped to about 175 km. At 0345 hours there appeared fresh ionizations at much higher levels. The new ionizations later strengthened and developed into the day-time *F2*-layer.

On other occasions when the minimum f_0F2 did not drop to very low value during the pre-sunrise period, the formation of fresh ionizations deformed the structure of the overnight *F2*-layer producing the so-called thick *F2*-layer or the ledges in the *F2*-region. SKINNER *et al.* (1954) have described the occurrence of such ledges in the *F2*-layer during the time of layer sunrise at Ibadan.

During the winter of 1956 and 1957, years with greater sunspot number, the morning phenomenon was evidenced mostly by the occurrence of ledges in the *F2*-traces. On many nights, the phenomenon occurred an hour or two before the

VOL.
18
196(

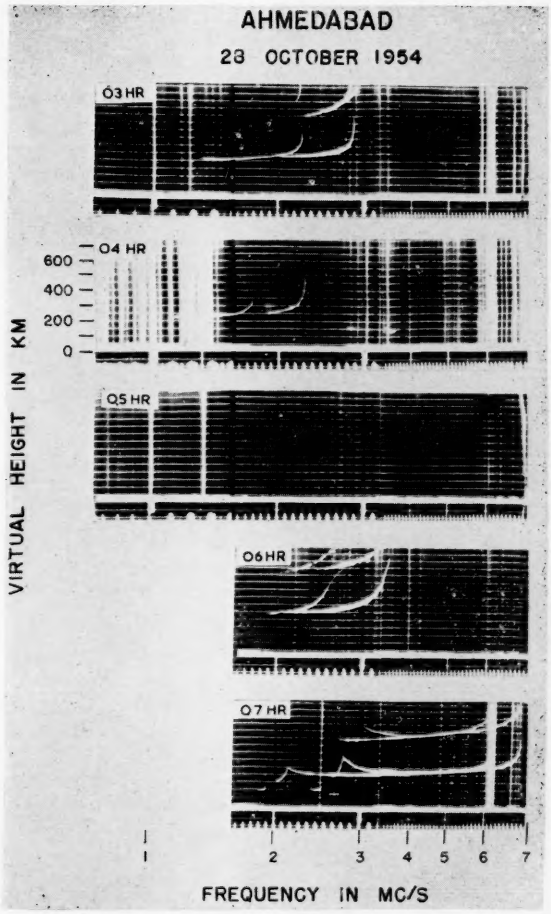

Fig. 7. *P'-f* records observed at Ahmedabad during the pre-sunrise period of 28 October 1954 showing the cessation of the ionospheric echoes.

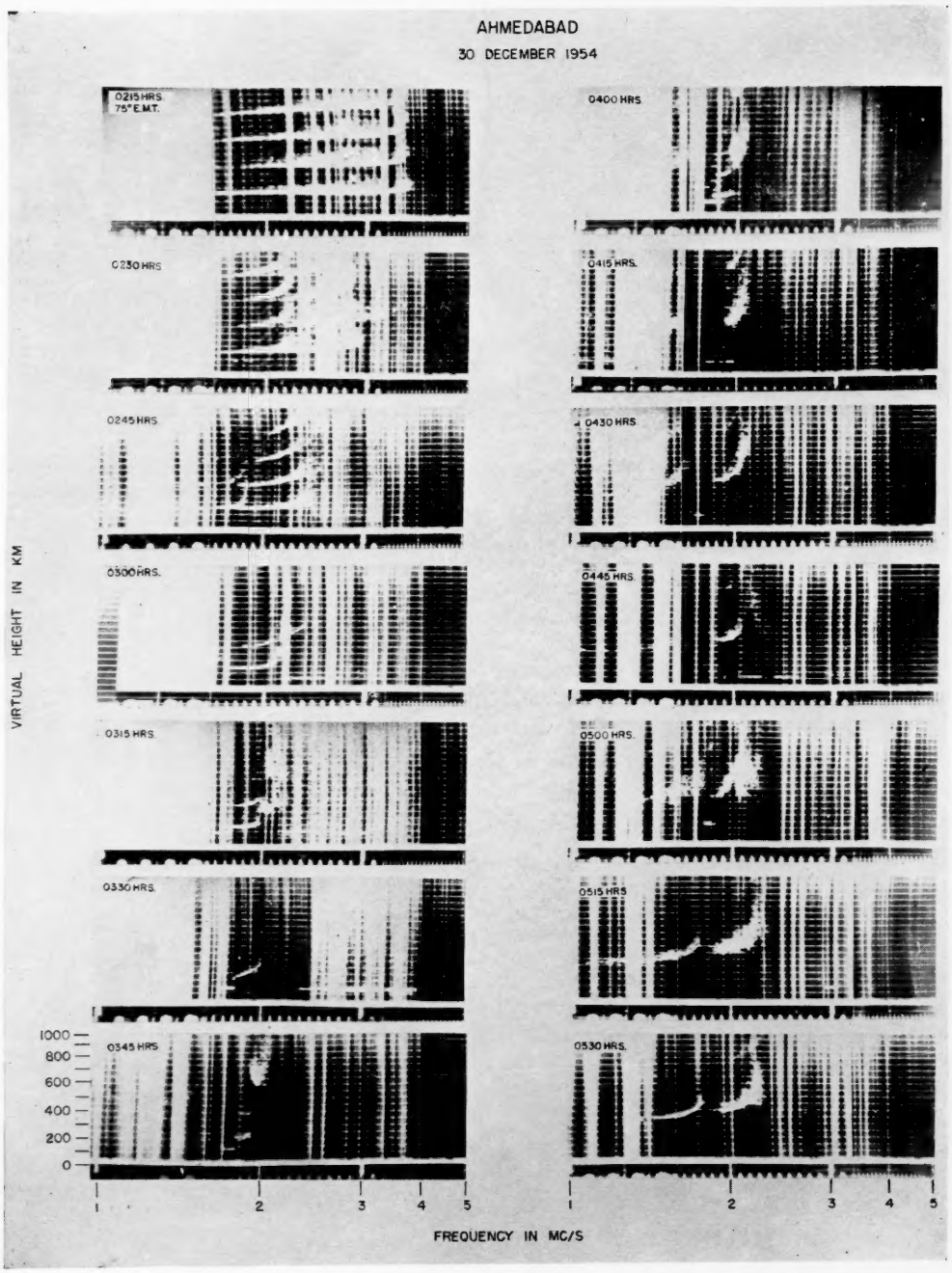

Fig. 8. Sequence of P'-f records at Ahmedabad during the pre-sunrise period of 30 December 1954.

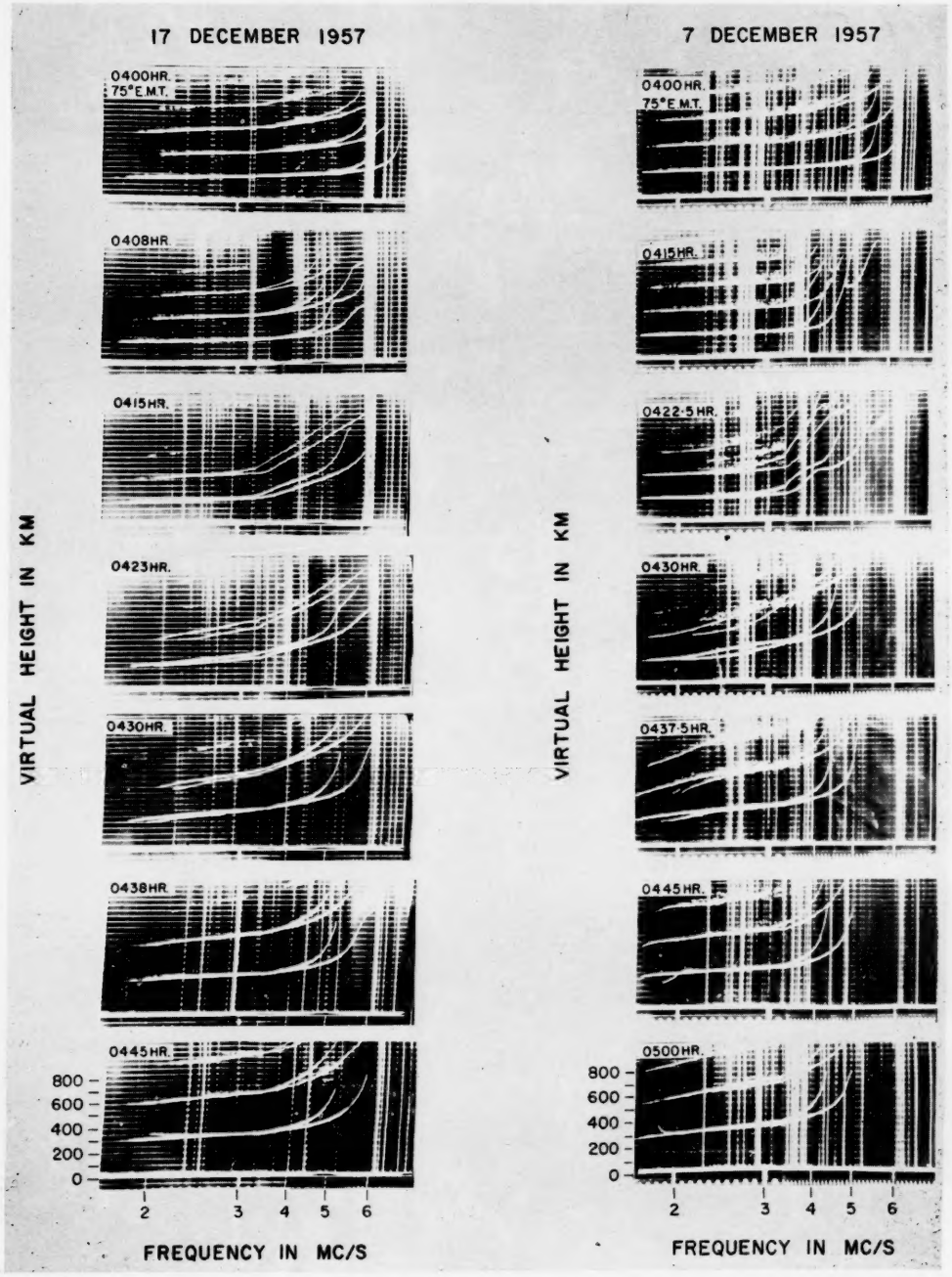

Fig. 9. Sequence of P'-f records at Ahmedabad during the morning hours of 17 December 1957 and 7 December 1957.

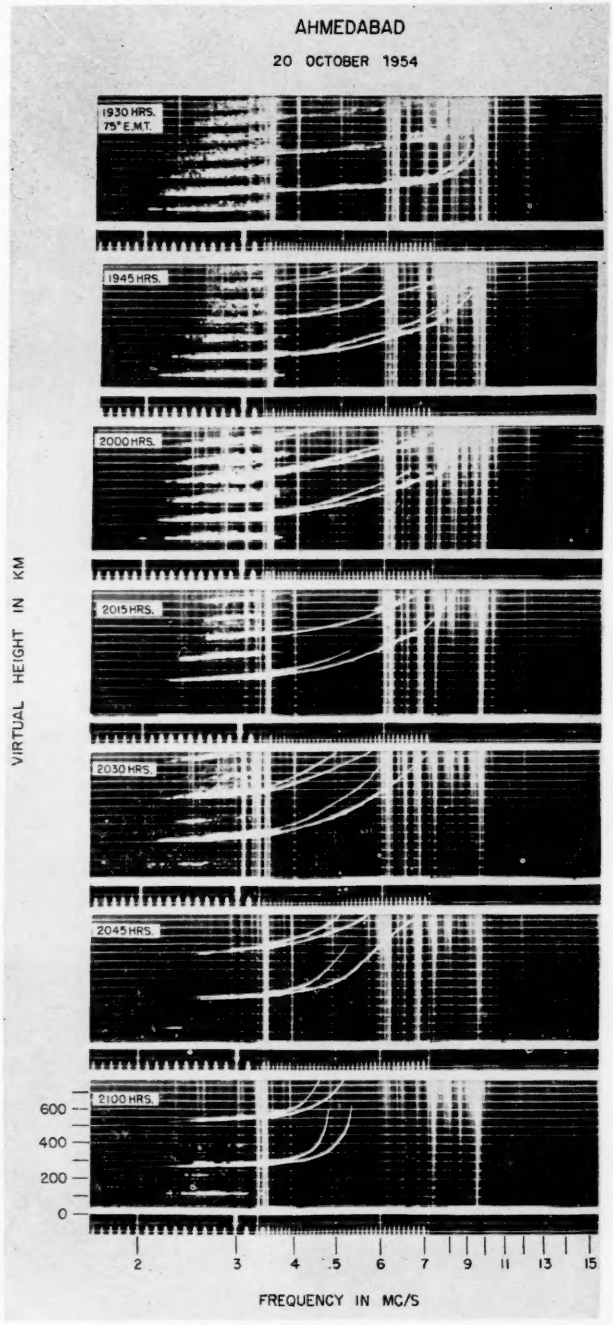

Fig. 10. Sequence of P'-f records at Ahmedabad during the evening hours of 20 October 1954.

VOL.
18
1960

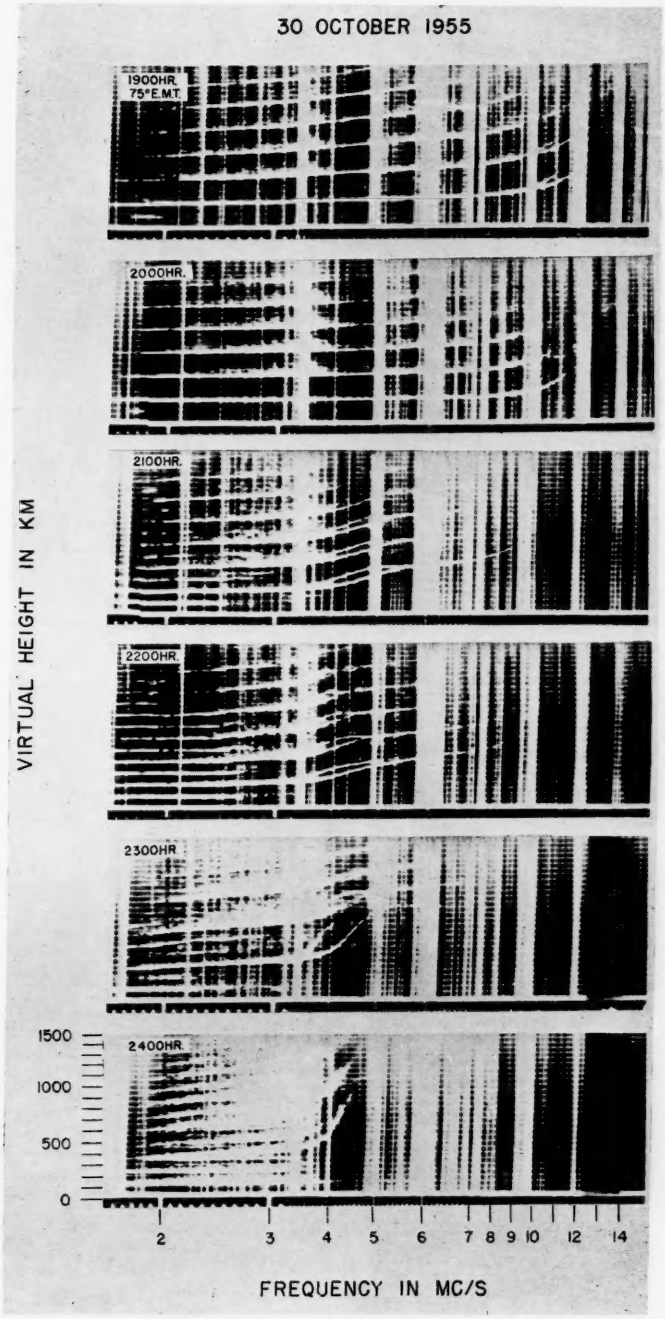

Fig. 11. Sequence of P'-f records at Ahmedabad during the evening hours of 30 October 1955.

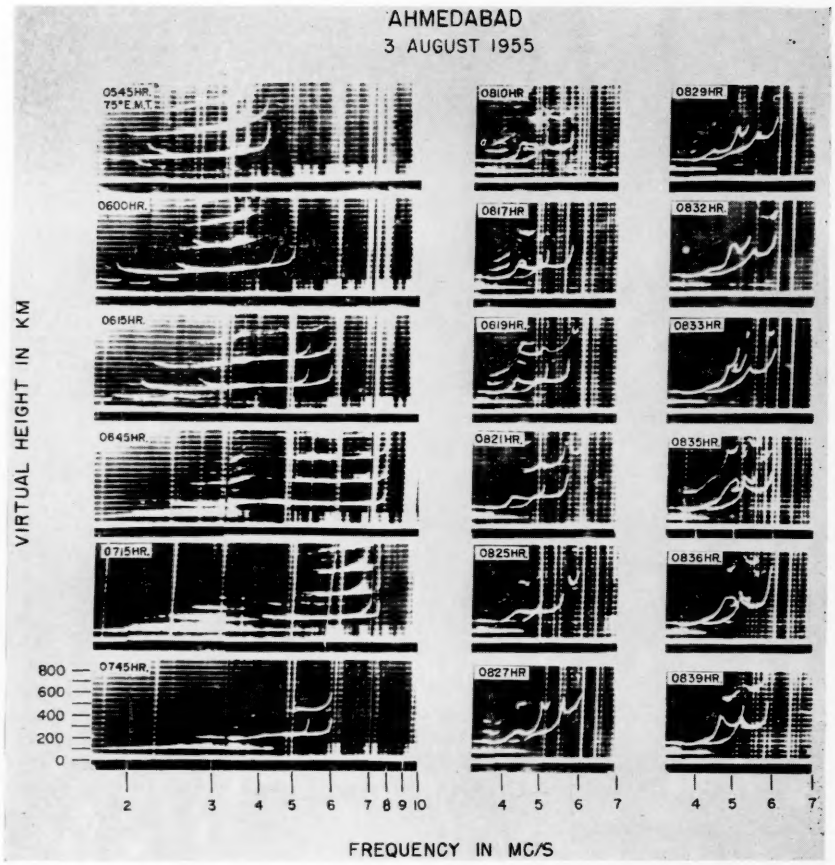

Fig. 15. Sequence of P'-f records at Ahmedabad on 3 August 1955 during the forenoon bite-out of f_0F2.

VOL.
18
196

sunrays illuminated the *F2*-region. The *P'-f* records obtained in quick succession on such occasions were similar to those obtained during the passage of travelling disturbances in the ionosphere (MUNRO, 1950). Examples of such recordings are shown in Fig. 9 where *P'-f* records at Ahmedabad on 7 and 17 December 1957 are reproduced. Referring to the *P'-f* records of 17 December 1957, the *F*-traces at 0400 hours are quite normal. At 0408 hours the kinks develop near the critical frequencies. At subsequent records the kink moves down the frequency scale, till at 0445 hours the *P'-f* traces are again normal. One can notice large discrepancy in the heights of first- and second-order traces for frequencies near the critical frequency between the period 0415 hours to 0438 hours. The second-order reflection height is less than twice the height of first-order reflection at the same frequency Referring to the records of 7 December 1957, one notices the similar features of the phenomenon, except that the disappearance of the kink at the low frequency end is followed by marked group retardation on the beginning of *F*-traces and often *E2*-traces are visible at about 150 km height.

Similar occurrence of splitting in the *F*-layer during the pre-sunrise period at Calcutta has been recently described by BANDYOPADHYAY (1959).

The first- and second-order traces for this period are not similar (0422·5 hours, 7 December 1957) indicating that the two reflections are received from different directions due to great inclinations in the *F2*-layer at that time. After the disturbance the height of the *F2*-layer was generally greater than the original value. This indicates that the early morning phenomenon is due to some kind of moving discontinuity in the *F2*-region preceding the sunrise. The movements in the *F2*-region during the morning hours is further suggested by the occurrence of the very high-order multiple reflections and abnormal height or intensity distribution of the multiple reflections observed slightly before the sunrise (RASTOGI, 1955). As seen from the diagrams, the iso-f_0F2 lines during the early morning hours are parallel to the sunrise line, therefore the discontinuity in the *F*-region should be along E–W direction. Consequently, the direction of horizontal movement in the *F*-region is mainly along E–W directions in the morning hours.

Sunset effect in the F-*region*

Referring to Fig. 6, one notices a greater concentration of iso-f_0F2 contour lines at middle latitudes around the sunset hours indicating a large rate of change of f_0F2 during that period. The very rapid decrease of f_0F2 at Ahmedabad during the evening hours of the equinoctial months can be seen in Fig. 3; f_0F2 decreased from a value of 13 Mc/s at 1600 hours to about 4 Mc/s at 2100 hours, corresponding to a decrease in the maximum electron density of the *F2*-region by about 100 electrons cm^{-3} sec^{-1}.

HAUBERT (1956) has described the appearance of a discontinuity in the *P'-f* records towards 2100 hours at Casablanca. First *h'F* maintains itself for a very long time at a relatively low altitude of about 200–250 km, then the electron density decreases gradually so that the *F*-region appears to divide into two strata one situated at 300–350 km and the other at the original height. The records presented by him show that the lower layer gradually vanishes leaving behind a single "*F2*"-layer at a height of about 300–350 km. Thus the height of the *F2*-layer increases

from 200–250 km to 300–350 km through this sudden jump after the sunset hour.

Similar discontinuities were observed at Ahmedabad around 2000–2100 hours in the form of thick or non-parabolic *F2*-layer or by ledges in the *F2*-region. The most noticeable discrepancy during this period was that the height or the second-order reflection was much smaller than twice the height of the first-order reflection for frequencies near the critical frequency. Such unequal separations between the successive reflection traces has been shown to be due to the reflections from an inclined ionosphere (Uyeda and Nakata, 1954).

Fig. 9 shows a sequence of P'-f records taken at intervals of 15 min during the passage of such a discontinuity over Ahmedabad on 20 October 1954. The traces are quite normal for 1930 hours. At 1945 hours though, the critical frequency has not decreased appreciably but the virtual heights at frequencies close to the critical frequency has appreciably increased suggesting the expansion of the *F2*-region, and consequent thickening of the *F*-layer. The height of the second-order reflection trace is much smaller than twice the height of the first-order one, e.g. the heights of the first- and second-order reflections of 6 Mc/s wave at 2000 hours are 435 km and 660 km, respectively. This distortion in the *F*-region extends to lower frequencies followed by the formation of a ledge in *F2* at 2045 hours. The reflections at 2100 hours are again normal, the critical frequencies being decreased appreciably from those before the disturbance and the height of the *F2*-layer is slightly increased.

At times an extremely large discrepancy was observed in the multiple reflection during the evening hours when P'-f traces are recorded on an extended height range as shown in Fig. 11. At 1900 hours the various traces of *F2*-reflections are normal with f_0F2 equal to 12 Mc/s. At 2000 hours f_0F2 decreases without any appreciable change in the shape of the layer. At 2100 hours there develops a distinct kink in the *F*-traces which shifts slightly to lower frequency at 2200 hours. At 2300 hours the kink is more prominent, the upper portion of the trace is greatly raised in height. A very remarkable fact to be noticed is the anomalous distribution of the heights of the various multiples; these being about 850, 1000, 1200 km for the first, second and third multiples of the upper layer. At 2400 hours the upper reflections have faded out leaving *F2*-layer having critical frequency of only 3·6 Mc/s.

Since in the evening hours, the rapid decrease of f_0F2 is accompanied with changes in the height as well as the thickness of the *F2*-layer, exact explanations of these abnormal reflections is not possible from the study of f_0F2 alone. Therefore, in Fig. 12 are shown the variation with time of the actual height of fixed values of the ionization density in the *F*-region. Assuming the variations with time to be corresponding to the variation with distance along the latitudes, one can estimate the inclination of the surfaces of same ionization in the ionosphere from this diagram. The great slopes in the iso-ionization lines around 2000–2100 hours are clearly seen. The inclination of iso-ionization surface at these times are estimated to be around 5°. On studying the variations in the bearings of short-wave (4 Mc/s) stations in Japan for the period February–March 1954, Kasuya (1954) has estimated the tilts in the equi-electron density surfaces in the *F2*-region to be about 5–6° in the morning and 7–12° in the evening hours.

VOL
18
196

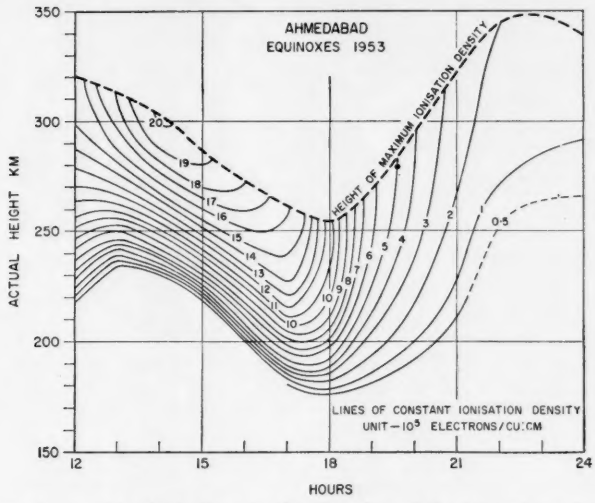

Fig. 12. Contours of iso-ionic lines in the *F*-region of the ionosphere during the evening hours of the equinoxes of 1953 at Ahmedabad.

Forenoon bite-out of f_0F2 *at middle latitudes*

A most striking feature noticed in the contour diagrams is the region of low f_0F2 between 35–45° dip around 0900 hours during July 1954. At the stations within these latitudes, the phenomenon is observed by a decrease of f_0F2 following the regular increase initiated by the sunrise. The decrease of f_0F2 around 0900 hours is very prominent in the curves for Okinawa and Yamagawa in Fig. 4. A cessation of the increase or a decrease of f_0F2 around 0900 hours was often observed at Ahmedabad during the summer months.

The decrease of f_0F2 in the forenoon hours of the summer months is better understood from the contour diagram of the critical frequency of the *F2*-layer at Okinawa (Fig. 13). The maximum f_0F2 are observed during the equinoctial months (April and October), and the minimum midday f_0F2 occurs during January and July. There is a uniform distribution of the contour lines for the morning hours of winter months but there is a significant depression of f_0F2 during the summer months centred at 0900 hours of July.

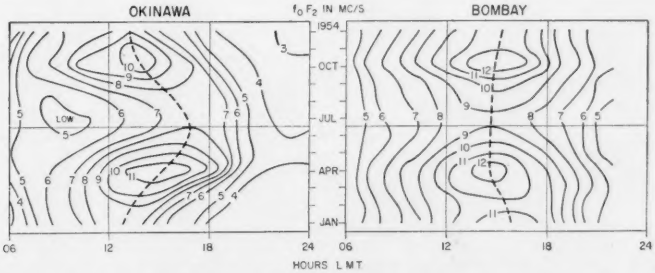

Fig. 13. Contour diagrams of f_0F2 at Okinawa and Bombay during the minimum-sunspot year 1954.

Studying similar contour diagram of f_0F2 at Bombay, a station nearest the region of peak f_0F2 during summer months, one does not notice any significant difference in the diurnal variations of f_0F2 in different months. The time of the

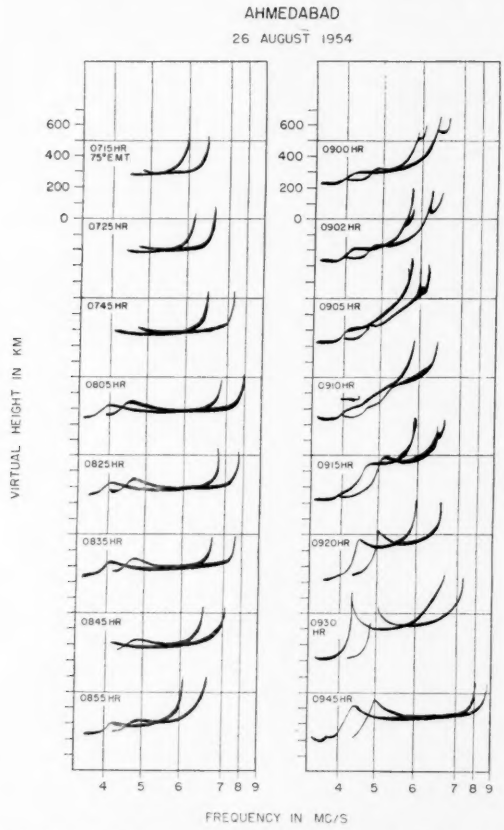

Fig. 14. Redrawn P'-f records obtained at Ahmedabad on 26 August 1954.

diurnal maximum of f_0F2 at Bombay changes very little with season unlike large shifts of the same at Okinawa. The maximum value of f_0F2 is observed during the afternoon hours of April and October.

On comparing the diurnal variations of f_0F2 at Bombay and Ahmedabad on individual days, it was found that on the many days when there was large decrease of f_0F2 at 0900 hours at Ahmedabad, no evidence of the same was noticed at Bombay. This indicated that the forenoon bite-out of f_0F2 at middle latitude during summer was characteristic of the stations just north of the region of maximum f_0F2.

The effect of this phenomenon on the ionospheric records taken at middle latitudes is shown in the P'-f records at Ahmedabad on 28 August 1954 reproduced in Fig. 14. A continuous increase of f_0F2 with time is seen in the initial records due to the increasing intensity of the solar radiations. The f_0F2 remained constant

between 0805 and 0835 hours, but later started decreasing and was followed with the occurrence of multiple splittings in the *F*-region. Abnormal *P'-f* records were obtained between 0900 and 0915 hours showing the ledge between *F1*- and *F2*-layers sometimes called as *F1·5*-layer. Later, the *P'-f* records were quite normal and the steady increase of f_0F2 was resumed.

On some occasions the *P'-f* records obtained during these periods were very complicated and could not be easily analysed. Fig. 15 shows a sequence of *P'-f* records obtained on 3 August 1955 at Ahmedabad. With the sunrise, the f_0F2 increased very fast with the simultaneous development of *F1*-layer. This was later followed by a quick decrease of f_0F2 with the occurrence of abnormal *P'-f* traces. Notice the loop traces at the junction of *F1*- and *F2*-layers during 0810 and 0817 hours. Such traces are described by MUNRO (1950) to be formed by the movement of irregularities in the *F*-region. At 0819 hours a very short cusp was visible at a relatively great height at frequency beyond f_xF2. On successive recordings this cusp got more prominent and moved steady downwards later joining the main curve. The critical frequencies of the original *F2*-layer continued to decrease, and later the *F2*-traces merged with the *F1*-traces. Simultaneously, the new cusp gradually developed into the day-time *F2*-layer trace. It is important to note that the new cusp was observed first on the extraordinary and later on the ordinary trace. Further the cusps on the ordinary and extraordinary components are very dissimilar to each other. This was again followed by the loop traces (0835 hours). Later the critical frequencies started increasing and *P'-f* traces were again normal.

The differences in the time of occurrence and in the shape of the new cusps can be explained on the basis of the divergence of the two components of the wave along the magnetic meridian plane in the ionosphere. In the northern hemisphere, the extraordinary component is deviated southward, i.e. towards the equator while the ordinary component is deviated northward. The occurrence of the cusp earlier on the extraordinary branch of the trace indicates the horizontal movement in the *F2*-region along a direction away from the equator during these periods of the day. This is already suggested from the comparison of the latitudinal variations of f_0F2 at different hours of the day.

The dissimilarities in the nature of the cusps on the ordinary and extraordinary components indicate large differences in the distribution of the *F2*-ionization at the regions of reflection of the two rays which in the Asian zone are very nearly along north–south direction. However, no such dissimilarities were found between the two components of the *P'-f* traces during the morning and evening hours. The horizontal movements during the morning and evening hours is along east–west direction and so the front of any disturbance during these periods would pass through the regions of reflection of the ordinary as well as extraordinary rays at about the same time and the *P'-f* traces due to the two components of the wave would always be similar.

Summing up, the occurrence frequency of the ledges in the *F2*-region at Ahmedabad during the low sunspot years 1953 and 1954 is shown in Fig. 16. The ledges or stratifications are observed more often at 0600 hours (corresponding to the sunrise effect during the winter months), at about 0900 hours (corresponding to the forenoon bite-out of f_0F2 during the summer months) and at about 2000 hours

VOL. 18 1960

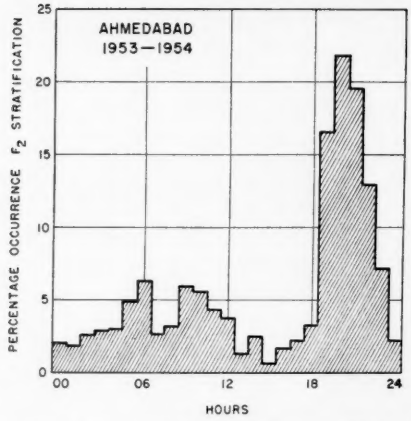

Fig. 16. The occurrence of the stratifications in the *F2*-region of the ionosphere at Ahmedabad during the low-sunspot years 1953–1954.

(corresponding to the sunset effect). The frequency of the occurrence of ledges is about four times greater in the evening than in the morning hours. The times of the occurrence of the ledges in the *F*-region at middle latitudes are associated with the changes in the synoptic distribution of the ionizations in the *F*-region of the ionosphere.

The F2*-region during the maximum sunspot years*

A similar study of the variations in the *F2*-layer during the maximum sunspot year has not been possible due to the lack of data for such periods and partly due to the uncertainty in some of the data. However, some of the changes in the *F2*-layer variations are quite distinct and are briefly described.

During the years with high sunspot number, the region of maximum f_0F2 shifted slightly northward. Highest values of f_0F2 were recorded at Ahmedabad and Formosa (dip 34° N). Any shift in the region of maximum f_0F2 with season could not be determined due to the paucity of the data.

At the equatorial stations, the nature of the diurnal variation of f_0F2 remains the same, though the relative amplitude of the forenoon and afternoon maxima changes systematically with sunspots. During the low-sunspot periods, the forenoon maximum is smaller than the afternoon one, while at the high-sunspot period, the former is greater than the latter (Maeda, 1955; Sarma and Mitra, 1956).

At middle-latitude stations, the diurnal variation of f_0F2 presented some interesting changes with sunspot number. The diurnal variations at few middle-latitude stations during each season of 1956 are shown in Fig. 17. Not only the day-time values of f_0F2 but also the midnight values of f_0F2 at any of these stations were greatest during the equinoxes. Thus the equinoctial effect in f_0F2 was present even in the night values of f_0F2 during the high-sunspot years.

As mentioned earlier, the highest value of f_0F2 was observed at Ahmedabad. The diurnal pattern of the occurrence of *F2*-stratifications at Ahmedabad during 1956 (shown in Fig. 18) was quite different from that in 1953–1954. During 1956,

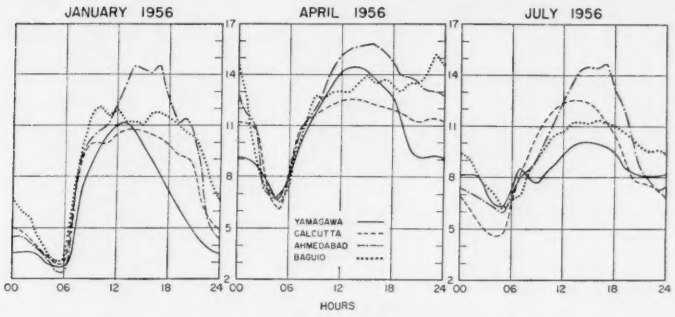

Fig. 17. The diurnal variations of f_0F2 at middle-latitude stations during the three seasons of the high-sunspot year 1956.

the stratifications were most often observed around midday. These stratifications on many occasions were identified as *F1·5* layer, which has been shown to be a common feature at middle latitudes during high-sunspot years (KASUYA, 1957; KOTADIA, 1957). These stratifications seem to be due to great expansion of the *F2*-region during high-sunspot period, rather than due to any changes in the spatial distribution of f_0F2.

The early-morning stratifications were observed during the winter months of high-sunspot years and it is evident by the maximum at 0500 hours in Fig. 18. There is no evidence of the sunset effect and one does not find any quick decrease of the ionizations at sunset hours during the equinoxes of the high-sunspot year. Similarly there is no maximum in the occurrence of *F2*-stratifications around 0900 hours during 1956, corresponding to the absence of any cessation in the increase of f_0F2 during that period.

The diurnal variation of f_0F2 at Formosa too did not show any change around 0900 hours, and a cessation in the increase of f_0F2 around 0900 hours was observed at Okinawa. The diurnal variation of f_0F2 during the summer months at Yamagawa and Tokyo showed a trough of f_0F2 around 0900 hours (refer Fig. 17). On comparing the diurnal variations of the occurrence of *F2*-stratifications at Yamagawa, as indicated by the letter *H* in the tables of the ionospheric data, one finds a sharp maximum in the frequency of *F2*-stratifications around 0900 hours during the summer months of 1957. During other seasons, there was a single maximum of the occurrence of stratifications around midday, very similar to that at Ahmedabad (Fig. 19). Thus the region of forenoon bite-out of f_0F2 during the summer months, seems to have shifted northward during the high-sunspot years, and is associated with similar shift in the region of maximum f_0F2. Thus the forenoon bite-out occurs at places just outside the anomalous belt of *F2*-layer where the f_0F2 decreases very rapidly with increasing latitude.

The diurnal variation of f_0F2 at Baguio and Guam Island presented a unique feature during the equinoctial months. The f_0F2 continued increasing from the sunrise up to about midnight hours, i.e. the ionizations in *F2* were increasing in the evening hours when intensity of solar radiations were decreasing with the setting of the sun and this increase continued well after the sun had set. Very large values of f_0F2 were observed during the first half of the night hours at regions

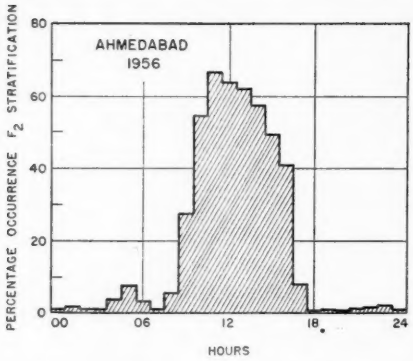

Fig. 18. The occurrence of *F2*-stratifications at Ahmedabad during the year 1956.

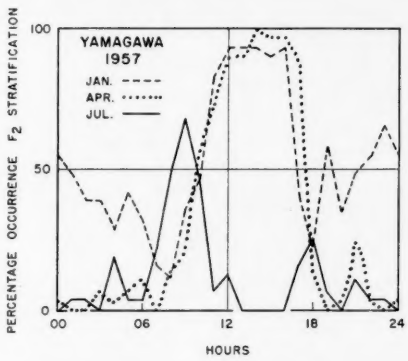

Fig. 19. The occurrence of *F2*-stratifications at Yamagawa during each season of the maximum-sunspot year 1957.

of about 20° dip. APPLETON (1959) found that there are two latitudes within the anomalous belt where the ratio of f_0F2 at sunspot maximum and sunspot minimum exceeds 4 in the late evening hours, and yet the general value of the ratio in high latitudes—where there is little transport—is only 2.

Acknowledgements—The ionospheric records presented in this paper were collected in the course of special observations by the writer at the Physical Research Laboratory, Ahmedabad, India. He is deeply indebted to Prof. K. R. RAMANATHAN for his keen interest and stimulating discussions during the course of the study. Thanks are also due to the Council of Scientific and Industrial Research, India and the National Research Council, Canada for the financial assistance.

REFERENCES

APPLETON E. V.	1955	A note on geomagnetic distotrion in the *F2*-layer. *Proceedings of the fourth meeting, Mixed Commission on the Ionosphere, Brussels*, 16–18 *August* 1954, pp. 113–115.
APPLETON E. V.	1959	Private communication.
BANDYOPADHYAY P.	1959	*J. Atmosph. Terr. Phys.* **16,** 84.
BHARGAVA B. N.	1952	*Nature, Lond.* **170,** 983.
BONNET G.	1954	*Ann. Geophys.* **10,** 348.
HAUBERT A.	1953	*L'ionosphere à Casablanca de Septembre* 1951 *à Mars* 1953. Note préliminaire du laboratoire National de Radio-Électricité, No. 168.
HAUBERT A.	1956	*Ann. Ser. Phys. Globe Met. Sci. Cherifien* **16,** 165.
KASUYA I.	1954	*J. Radio Res. Lab.* **1,** No. 5, 29.
KASUYA I.	1957	*J. Radio Res. Lab.* **4,** 291.
KOTADIA K. M.	1957	*Proc. Ind. Acad. Sci.* **66,** 349.
MAEDA H.	1955	*Rep. Ionos. Res. Japan* **9,** 60.
MARASIGAN V.	1958	*J. Atmosph. Terr. Phys.* **13,** 26.

Munro G. H.	1950	*Proc. Roy. Soc.* A **202,** 208.
Munro G. H. and Heisler L. M.	1956	*Aust. J. Phys.* **9,** 359
Rastogi R. G.	1955	*Proc. Ind. Acad. Sci.* **41,** 253.
Rastogi R. G.	1956	*Studies in the Physics of the Ionosphere.* Ph.D. Thesis, Gujarat University.
Rastogi R. G.	1959a	*Canad. J. Phys.* **37,** 874.
Rastogi R. G.	1959b	*J. Geophys. Res.* **64,** 727.
Rastogi R. G.	1960	*J. Geophys. Res.* **65,** 585
Sarma N. V. G. and Mitra A. P.	1956	*J. Sci. Industr. Res.* **15** B, 320.
Skinner W. J., Brown R. A. and Wright R. W.	1954	*J. Atmosph. Terr. Phys.* **5,** 92.
Uyeda H. and Nakata Y.	1954	*J. Radio Res. Lab.* **1,** No. 6, 17.

OL.
18
960

Journal of Atmospheric and Terrestrial Physics, 1960, Vol. 18, pp. 332 to 343. Pergamon Press Ltd. Printed in Northern Ireland

RESEARCH NOTES

Observations of non-field-aligned auroral rays

(*Received 5 February* 1960)

DURING the auroral display of 26 October 1956, fifteen colour photographs were taken at St. Andrews Observatory, Scotland, as part of an investigation into the photometric value of colour photography of the aurora (GADSDEN, 1960). The film used was Kodak Daylight Ektachrome Type E-2, and the camera was an ordinary 35 mm commercial camera with a 45 mm F/2·8 lens. The exposures necessary varied from 30 min to 4 min.

Careful examination of the photographs revealed the existence on five of them of an auroral ray of unusual appearance. (These five photographs are reproduced in monochrome in Fig. 1, by the process of printing the colour transparencies in light from a neon lamp onto a panchromatic plate. The resulting negative was then printed in the normal way onto high contrast bromide paper.) Three facts were immediately obvious about the unusual rays: (a) in two cases, they were inclined at an appreciable angle to other rays appearing in the same region of sky; (b) as far as can be determined from a colour photograph, they were uniformly red from top to bottom; and (c) they were not due to spurious effects arising from local, ground level, lighting since, in the first two photographs taken (Fig. 1 a and b), the rays were obscured over part of their length by cloud. The possibility that the ray is due to some defect in the emulsion of the colour film has been eliminated by a visual observation of a similar ray (which was not photographed) during the course of the display and by a black-and-white photograph taken, by chance, of one of the rays at almost the same time, and in almost the same direction, as photograph (c) in Fig. 1. It should be mentioned that the rays are entirely different in appearance to the red rays reported by STÖRMER (1957) on the same evening, and also photographed from St. Andrews.

The colour of the rays suggests that they were at a considerable height in the atmosphere (STÖRMER, 1955) and the question arises whether this accounts for the apparent departure from field-alignment, when compared with the normal auroral rays. That is to say, whether the great range of the rays from the observer would have caused the apparent non-alignment to be due to their being aligned along magnetic field lines at a great distance from the observer. Assuming that the magnetic field of the earth may be represented sufficiently well by that of a geocentric dipole, whose axis intersects the Earth's surface at 78·6°N, 70°W (VESTINE *et al.*, 1947), the apparent angle of intersection of a line of force with the horizon of an observer at geomagnetic latitude ϕ is given by

$$\tan\theta = \frac{3d}{1+d^2}\cot\sigma + \frac{2-d^2}{1+d^2}\tan\phi\,\operatorname{cosec}\sigma$$

where σ is the geomagnetic azimuth of the point of observation;

d is the range of the line of force from the observer in the horizontal direction (in units of earth radii);

and θ is the apparent inclination of the tangent to the line of force to the observer's horizon.

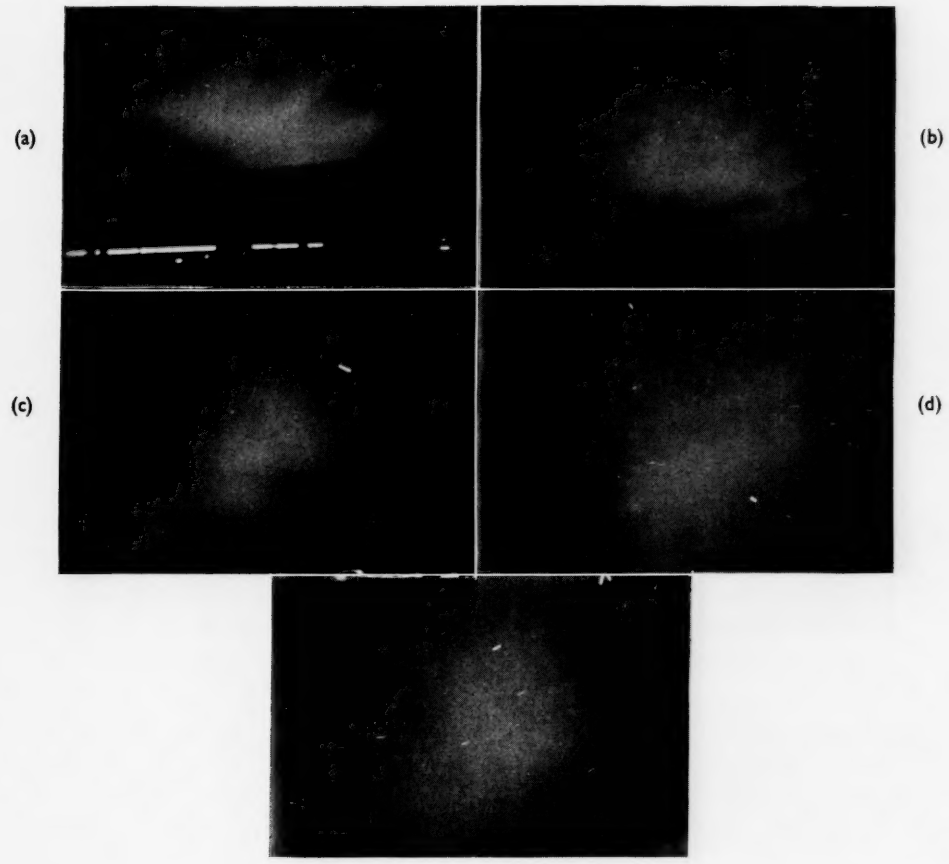

Fig. 1. Photographs of unusual auroral rays taken from St. Andrews, Scotland, on 26 October 1956. The times (U.T.) of the exposures are: (a) 1938–2000; (b) 2034–2054; (c) 2230–2245; (d) 2258–2302; (e) 2321–2329. The unusual rays appear as narrow strips running almost vertically upwards from close to the bottom edges of the photographs.

VOL
18
196

For small d, and σ equal to 90°, this expression reduces to

$$\tan \theta = 2 \tan \phi = \tan D$$

where D is the local angle of dip, calculated on the assumption of a central dipole field.

Fig. 2 shows the variation of θ and σ as a function of d for $\phi = 59{\cdot}4°$, the geomagnetic latitude of St. Andrews. The observed values of θ and σ, measured from the photographs, are listed below and are plotted on Fig. 2 as open circles.

Time of exposure (U.T.)	$\theta°$	$\sigma°$
1938–2000	90	55 E
2034–2054	83	45 E
2230–2245	76	46 W
2258–2302	97	51 W
2321–2329	86	41 E

It will be seen from Fig. 2 that there are no possible values of d corresponding to these values of θ and σ, and that the observed points differ from physically realisable values of

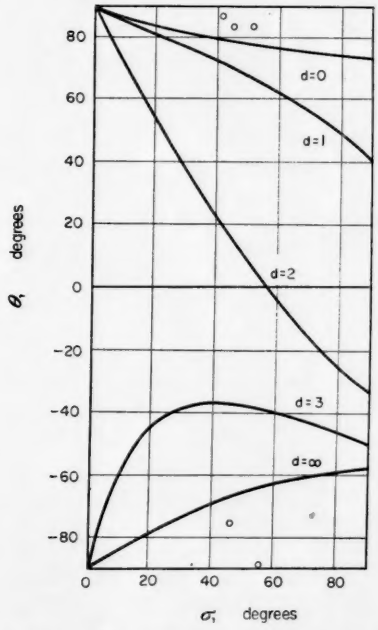

Fig. 2. Variation of θ with σ for various values of d. The open circles are observed values of θ and σ for the non-field-aligned auroral rays.

θ by 5° to 13°. It is unlikely, therefore, that the rays were aligned along a magnetic line of force which had been distorted from the corresponding dipole line during the magnetic disturbance present on 26 October. (The K-index recorded at Eskdalemuir at the time of the exposures was 6.) It should also be noted that the local field at St. Andrews (dip angle = 70·4°) departs from the dipole field (dip angle = 73·5°) in such a way as to make the departure of the ray from field alignment even more marked.

VOL. 18 1960

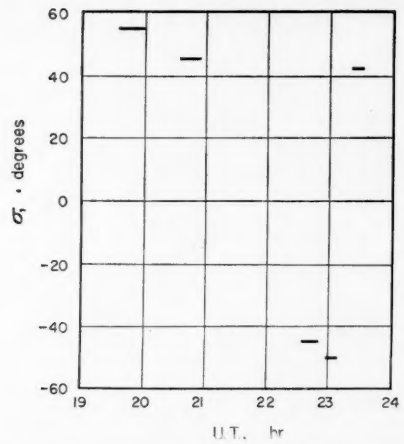

Fig. 3. The observed geomagnetic azimuths σ of the non-field-aligned auroral rays, plotted against the time of observation.

Fig. 3 shows a plot of the observed azimuth of the rays as a function of the time of observation. It is obvious that the rays observed were unlikely to be a single ray showing systematic movement during the evening. This is supported by the small width of the ray—any rapid movement in azimuth of the ray would have caused it to be broadened appreciably during the long exposures made.

The conclusions about these rays may be summarized as follows:

(i) The rays were probably high in the atmosphere, since they appeared to be uniformly red from top to horizon.

(ii) They appear to have been isolated from normal auroral activity, although this may be an effect of range, in that activity close to their bases could have been below the observer's horizon.

(iii) They appeared to be very much longer than they were wide. The ray appearing in the exposure from 2321 to 2329 U.T. extended right across the photograph (a distance of approximately 30°), and was less than 1° wide at all elevations.

(iv) The rays were not field-aligned, as was the case with the normal auroral rays observed on the same evening.

(v) They appear to be fairly rare. (There is no mention of similar rays by Störmer, 1955). A watch has been made from Invercargill, New Zealand, for their appearance during the last two years, without any observed occurrences.

Until more observations have been secured of similar rays, it is fruitless to speculate on their origin. It seems worthwhile to make every effort to observe the occurrence of similar rays, with emphasis on obtaining parallactic photographs of them. Since they may be very high in the atmosphere, a very long base-line would be necessary for successful measurement.

Acknowledgements—One of us (M. G.) wishes to thank Professor W. D. Wright of the Imperial College Technical Optics Section for his encouragement and advice on a research project in the course of which the photographs were obtained. The work described is part of the research programme of the Dominion Physical Laboratory Auroral Station, New Zealand, and stems in part from a project sponsored by the Air research and Development Command, U.S.A.F.

DPL Auroral Station, Awarua Radio
Invercargill, New Zealand

M. Gadsden
C. J. Loughnan

VOL
18
196

REFERENCES

GADSDEN M.	1960	*J. Atmosph. Terr. Phys.* **17**, 347.
STÖRMER C.	1955	*The Polar Aurora* p. 142. Clarendon Press, Oxford.
STÖRMER C.	1957	*Nature, Lond.* **179**, 623.
VESTINE E. H., LAPORTE L., LANCE I. and SCOTT W. E.	1947	*The Geomagnetic Field, Its Description and Analysis.* Publication No. 580, Carnegie Institute, Washington.

Photoionization of atomic oxygen and atomic nitrogen

(*Received* 9 *April* 1960)

IN connection with another problem it was necessary to compute photoionization cross-sections of atomic oxygen and atomic nitrogen for incident radiation down to very short wavelengths. Because of their importance in the interpretation of solar–terrestrial effects and because they differ both qualitatively and quantitatively from the values currently available (NICOLET, 1952a), we present a brief description of the results.

The calculations were carried out initially using the approximate treatment described by BATES (1946a), which is based upon the dipole length formulation. However, a comparison of the derived polarizabilities with those computed more accurately by other methods (DALGARNO and PARKINSON, 1959) showed that the dipole length values were much too large at short wavelengths and the approximate treatment by BATES was therefore extended to the dipole velocity formulation. The derived values yielded much improved polarizabilities and the results shown in Figs. 1 and 2 refer to the dipole velocity cross-sections.

The initial bound state wave functions were taken as the Hartree–Fock functions computed for oxygen by HARTREE *et al.* (1940) and for nitrogen by HARTREE and HARTREE (1948) and the final continuum functions were taken as hydrogenic in a field of unit nuclear charge. All the parameters required have been tabulated by BATES (1946b).

The qualitative differences from the calculations of NICOLET concern the locations of the discontinuities of the cross-sections associated with the ejection of the inner electrons. The most recent observations of the K-absorption spectra of O and N have apparently been made by MAGNUSSON (1938) and of the K-emission spectra by TYRÉN (1940). NICOLET (1952b) has analysed the data and concludes that the edge of the K-absorption continuum for O occurs at 21·5 Å and for N at 29·6 Å We have preferred to adopt the values of 22·8 Å for O and 30·3 Å for N suggested by the Hartree–Fock calculations, but the differences are not significant; it should be noted that for both O and N there are actually two K-absorption edges, which we do not distinguish between.

For the locations of the L_I edges, NICOLET suggests 125 Å for O and 175 Å for N. There are, in fact, two L_I edges for O corresponding to final states $O^+(^4P)$ and $O^+(^2P)$ and two for N corresponding to final states $N^+(^5S)$ and $N^+(^3S)$. From the tables of MOORE (1949) it appears that the edges lie at 435 Å and 310 Å for O and at 608 Å and 367Å for N (the averages of these two pairs of edges are in harmony with those suggested by the Hartree–Fock calculations). Since the resonance line of He^+ is located at 304 Å, the new proposed limits may have important consequences.

The ionization limits corresponding to ejection of a $2p$ electron are well-known and do not require discussion. It should be remarked that many other discontinuities must occur. They may be associated with transitions in which the ion is left in an excited state or with

discrete transitions to highly excited states of the neutral atom followed by autoionization. Our values do not take account of these possibilities.

The derived values of the photoionization cross-sections of atomic oxygen and atomic nitrogen for radiation down to wavelengths of 1 Å are shown in Figs. 1 and 2 and the values

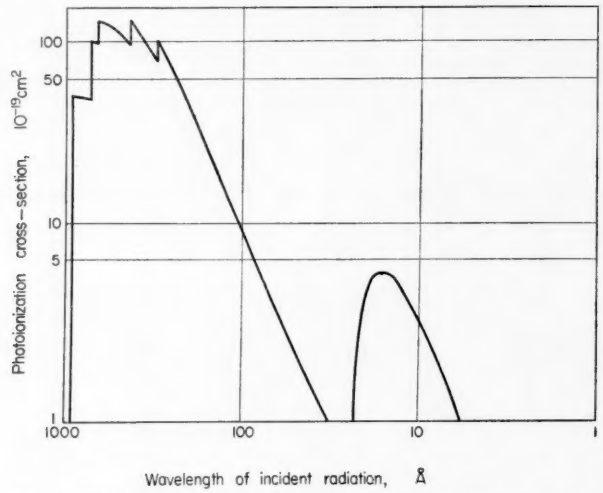

Fig. 1. Photoionization cross-section of atomic oxygen as a function of the wavelength of the incident radiation.

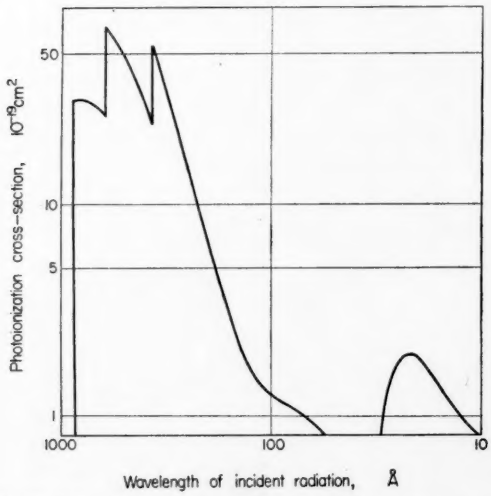

Fig. 2. Photoionization cross-section of atomic nitrogen as a function of the wavelength of the incident radiation.

for two important wavelengths are given in the table. Although the accuracy is not high, the results should be superior to those previously available except in the region of the first ionization limits for which the more refined calculations of BATES and SEATON (1949) are to be preferred.*

* *Note added in proof:* Dr. M. NICOLET has drawn to our attention that accurate measurements at very short wavelengths are available. The values are quoted by M. NICOLET and A. C. AIKEN (*J. Geophys. Res.* **65,** 1469; 1960).

VOL.
18
1960

The K-absorption cross-sections for O_2 and N_2 can be taken, without significant loss of accuracy, as twice those for O and N respectively and a similar doubling should give a useful guide to the L_I-absorption cross-sections.

Table 1. Absorption cross-sections in units of 10^{-17} cm^2 for O and N at 584 Å and 304 Å

λ (Å)		O	N
584	Calculated	1·2	0·7
	Measured*	1·0	1·3
304	Calculated	1·0	0·3
	Measured*	1·0	0·2

* The measurements are for O_2 and N_2; the values given in the table are half the observed values.

Measurements of the absorption cross-sections for incident wavelengths between 1300 Å and 300 Å have been made for O_2 (Weissler and Lee, 1952) and for N_2 (Weissler *et al.*, 1952) and the observed values *per atom* at 584 Å and at 304 Å are included in the table.

Department of Applied Mathematics A. Dalgarno
The Queen's University D. Parkinson
Belfast, N. Ireland

References

Bates D. R.	1946a	*Mon. Not. R. Astr. Soc.* **106**, 423.
Bates D. R.	1946b	*Mon. Not. R. Astr. Soc.* **106**, 432.
Bates D. R. and Seaton M. J.	1949	*Mon. Not. R. Astr. Soc.* **109**, 698.
Dalgarno A. and Parkinson D.	1959	*Proc. Roy. Soc.* A **250**, 422.
Hartree D. R. and Hartree W.	1948	*Proc. Roy. Soc.* A **193**, 299.
Hartree D. R., Hartree W. and Swirles B.	1940	*Phil. Trans.* A **238**, 229.
Magnusson T.	1938	*Nova Acta Soc. Sci. Upsal.* Ser. IV, **11**, No. 2.
Moore C.	1949	*Atomic Energy Levels.* National Bureau of Standards, Washington.
Nicolet M.	1952a	*Physics and Medicine of the Upper Atmosphere* (Ed. by C. S. White and O. O. Benson). University of New Mexico Press, Albuquerque.
Nicolet M.	1952b	*Ann. Géophys.* **8**, 141.
Tyrén F.	1940	*Nova Acta Soc. Sci. Upsal.* Ser. IV, **12**, No. 1.
Weisslær G. L. and Lee P.	1952	*J. Opt. Soc. Amer.* **42**, 200.
Weissler G. L., Lee P. and Mohr E. L.	1952	*J. Opt. Soc. Amer.* **42**, 84.

À propos de la détermination de la hauter vraie du maximum d'ionisation dans la méthode des dix points

(*Received* 16 *April* 1960)

La détermination des hauteurs vraies par la méthode des dix points (Doublet, 1951; Kelso, 1952, 1954; Schmerling, 1958) est maintenant utilisée en de nombreux observatoires ionosphériques.

On sait qu'elle permet de tracer aisément la courbe des hauteurs vraies de réflexion, en fonction de la fréquence, jusqu'à des fréquences très voisines de la fréquence critique, mais que la prolongation de la courbe jusqu'à la fréquence critique, c'est à dire jusqu'à la hauteur du maximum d'ionisation, n'est possible qu'en faisant une hypothèse sur la répartition de l'ionisation en fonction de la hauteur. L'hypothèse la plus satisfaisante est celle d'une répartition obéissant à une loi de la forme:

$$\left(\frac{f}{f_m}\right)^2 = 1 - \left(\frac{h_m - h}{h_m - h_0}\right)^2 \tag{1}$$

où f est la fréquence réfléchie à la hauteur h,
f_m, la fréquence maximum réfléchie (à la hauteur h_m)
h_m, la hauteur du maximum d'ionisation,
h_0, la hauteur de la base de la couche.

Une méthode de détermination de h_m consiste à tracer sur un calque différents modèles de paraboles, calculées avec différentes valeurs des paramètres, et à chercher quelle est la

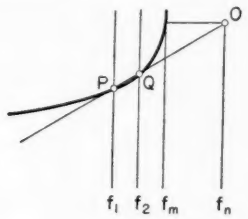

Fig. 1.

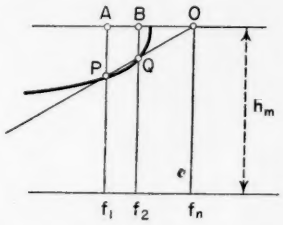

Fig. 2.

courbe qui s'adapte le mieux à la partie déjà tracée pour déterminer les valeurs de ces paramètres. Mais, on peut obtenir directement h_m par la construction graphique décrite ci-dessous.

Prenons un calque que nous superposons au graphique à échelle logarithmique des fréquences et échelle linéaire des hauteurs sur lequel se trouve tracée la courbe des hauteurs vraies, obtenue par la méthode des dix points, jusqu'au voisinage de la fréquence critique.

Traçons sur le calque, Fig. 1, une verticale correspondant à la fréquence critique f_m, puis deux autres lignes verticales correspondant respectivement à:

$$f_1 = K_1 f_m \quad \text{et} \quad f_2 = K_2 f_m$$

enfin une quatrième verticale correspondant à:

$$f_n = \left(\frac{K_2{}^a}{K_1}\right)^{1/(a-1)} f_m ,$$

avec:

$$a = \left(\frac{1 - K_1{}^2}{1 - K_2{}^2}\right)^{\frac{1}{2}} .$$

Exemple: $K_1 = 0{,}96$, $K_2 = 0{,}98$, $a = \sqrt{\frac{784}{396}} \simeq 1{,}4$, $f_n = \left(\frac{(0{,}98)^{1{,}4}}{0{,}96}\right)^{1/0{,}4} f_m = 1{,}032\, f_m$.

La verticale f_m du calque étant placée sur la valeur de la fréquence critique portée sur le graphique, les verticales f_1 et f_2 couperont la courbe des hauteurs vraies tracée, en deux points P et Q. La droite passant par les points P et Q coupera la verticale f_n en un point O

VOL
18
196

qui est à la hauteur du maximum d'ionisation. Il suffira de reporter cette hauteur sur la verticale f_m du graphique et d'extrapoler la courbe jusqu'à ce point en la terminant tangentiellement à la verticale. Bien entendu les fréquences f_1 et f_2 devront être choisies assez proches de f_m.

Nous avons maintenant à justifier cette construction; de (1) nous pouvons écrire:

$$1 - K_1^2 = \left(\frac{h_m - h_1}{h_m - h_0}\right)^2 \tag{2}$$

$$1 - K_2^2 = \left(\frac{h_m - h_2}{h_m - h_0}\right)^2 \tag{3}$$

et enfin:

$$\frac{h_m - h_1}{h_m - h_2} = \left(\frac{1 - K_1^2}{1 - K_2^2}\right)^{1/2} = a. \tag{4}$$

D'après la Fig. 2, nous aurons, le point O étant supposé à la hauteur h_m:

$$h_m - h_1 = AP \quad \text{et} \quad h_m - h_2 = BQ \tag{5}$$

et par similitude des triangles, ainsi que d'après (4):

$$\frac{OA}{OB} = \frac{AP}{BQ} = \frac{h_m - h_1}{h_m - h_2} = a. \tag{6}$$

Or, par suite de l'échelle logarithmique des fréquences:

$$\frac{OA}{OB} = \frac{\log f_n - \log f_1}{\log f_n - \log f_2} = a \tag{7}$$

et nous pouvons écrite:

$$\frac{f_n}{f_1} = \left(\frac{f_n}{f_2}\right)^a \tag{8}$$

d'où:

$$f_n = \left(\frac{f_2^a}{f_1}\right)^{1/(a-1)} = \left(\frac{K_2^a f_m^a}{K_1 f_m}\right)^{1/(a-1)} = \left(\frac{K_2^a}{K_1}\right)^{1/(a-1)} f_m. \tag{9}$$

Centre d'Études Géophysiques
Garchy, Nièvre, France

A. HAUBERT

RÉFÉRENCES

DOUBLET J.	1951	Note préliminaire du L.N.R. No. 149.
KELSO J. H.	1952	*J. Géophys. Res.* **57**, 357.
KELSO J. H.	1954	*J. Atmosph. Terr. Phys.* **5**, 11.
SCHMERLING E. R.	1958	*J. Atmosph. Terr. Phys.* **12**, 8.

Changes in the fading speed of low-frequency radio waves

(*Received* 25 *April* 1960)

THIS paper is concerned with the speed at which low-frequency radio waves fade. When a fading curve appears to be made up of two components with very different correlation times and when different radio frequencies are to be compared, it is not desirable to estimate

fading speed by counting the number of maxima on the fading curve. If, however, it is desired to estimate the way in which fading speed varies with time on one frequency, the counting of maxima gives a simple and satisfactory measure of the speed of the fastest component. Records made on frequencies of 70·8, 113·3 and 200 kc/s were investigated in this way.

Examination of fading records on a single frequency shows that the fading speed, as measured by counting maxima, changes over quite a wide range and in general the fading can be described as either slow, medium or fast. It will here be suggested that the fast

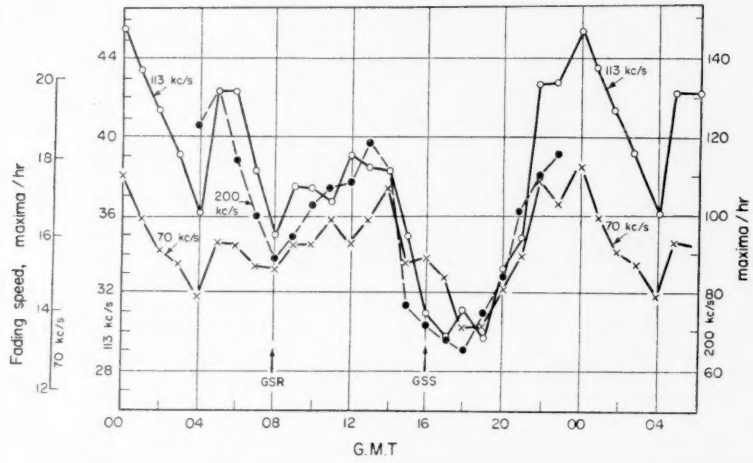

Fig. 1. Hourly average fading speed for three low-frequency waves in December 1957.

fading is associated with the incidence of meteors on the ionosphere. Although it was noticed on many occasions that unusually high magnetic activity was associated with high fading speed, no clear correlation between the two variables was found.

We shall consider fading records of the wave reflected at steep incidence from the ionosphere covering 24 hr periods in winter. In summer the daytime strength of the reflected wave was too weak to be recorded.

The fading speed was measured in terms of number of maxima per hour and the monthly average magnitude was determined for each hour of the twenty-four and denoted by S_m.

The fading speed S_m was compared with the monthly average value (M_m) of the number of meteors (sporadic and shower) which left ionized trails in the atmosphere sufficiently dense to reflect radio waves with a given intensity on a given wavelength. These numbers were kindly provided by Professor A. C. B. Lovell at Jodrell Bank.

In Fig. 1, S_m for each hour of the day is given for the frequencies 70, 113 and 200 kc/s for the month of December 1957. Each point on these curves is the average of between twenty-five and thirty individual values. The shapes of the curves for the different frequencies are very similar, and it is reasonable to suppose that fading on these frequencies had a common origin. Since the speed of the slow component of fading is found to be roughly constant at about eight maxima per hour, these curves are known to represent the changes in the fast component.

Fig. 1 shows that the fading speed is greatest round about 0000 GMT and is least at about 1800 GMT. The curve for M_m against time of day for December 1957 is given in Fig. 2 together with the curve of S_m for 70 kc/s for the same month transferred from Fig. 1.

These curves are remarkably similar and the correlation coefficient was found to be 0·85. Similar curves were evaluated for November 1957 and January 1958 and these confirm the high correlation found for the curves in Fig. 2.

It is known that the number of meteor trails formed decreases quite sharply with height. In the light of the correlation mentioned above, the height of reflection of a particular frequency will then be an important factor determining the fading speed on this

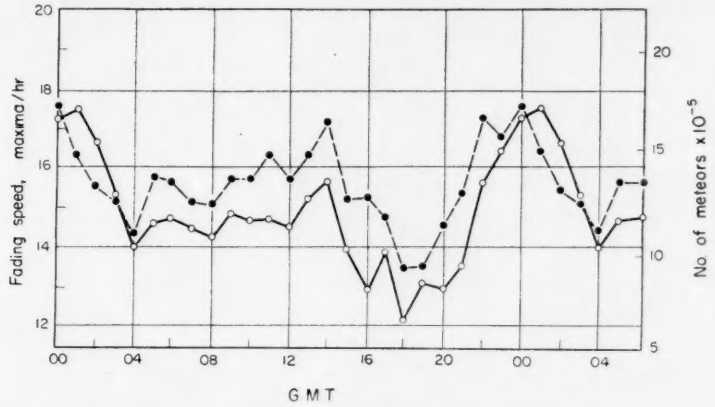

Fig. 2. Mean fading speed on 70 kc/s (taken from Fig. 1) compared with mean number of meteors observed by radio methods, for December 1957. ●– – –● Fading speed (70 kc/s); ○——○ Numbers of meteors.

frequency. Fading speed will change with frequency as a result of the change of wavelength and also because of the change in height of reflection. It is thus not expected to find a linear relationship between fading speed and frequency over a range of frequencies.

It is observed that on frequencies less than about 70 kc/s, the fast component of fading is completely absent for most of the time. One can then, taking the above-mentioned experimental facts into account, perhaps make the statement that at heights where frequencies lower than 70 kc/s are reflected either no (or very few) meteor trails are formed. It may also be that the irregularities present at these heights, are of dimensions smaller than a wavelength of the radio frequencies concerned.

Acknowledgements—The author is indebted to Mr. J. A. Ratcliffe for help and suggestions in connection with this paper. The work was made possible by a grant from the South African Council for Scientific and Industrial Research.

Cavendish Laboratory W. A. Cilliers
Cambridge

An auroral emission in the 2·0–2·2 μ region*

(*Received* 27 *April* 1960)

Infra-red emission near 1·5 μ has been observed by Harrison and Vallance Jones (1959) in very bright active aurora. Two features at 1·46 μ and 1·52 μ were definitely

* Supported by the Geophysics Research Directorate of the Air Force Cambridge Research Center, Air Research and Development Command, under Contract No. AF 19(604)-1831.

identified as the 0,1 and 1,2 bands of the Meinel ($A^2\pi$–$X^2\Sigma^+$) system of N_2^+, while a third feature at 1·59 μ was tentatively identified as the 2,3 band of the same system. Between 1·8 and 2·0 μ atmospheric absorption is virtually complete, while beyond 2·5 μ, NOXON, HARRISON and VALLANCE JONES (1959) have found that the observation of auroral and airglow emissions is precluded by the very intense thermal radiation from the lower atmosphere. Between 2·0 and 2·5 μ the atmospheric transmission is high and the thermal background low; this note reports an attempt to observe auroral emission in the latter region using the new scanning spectrometer previously employed for study of the night sky emission between 1·5 and 4·0 μ.

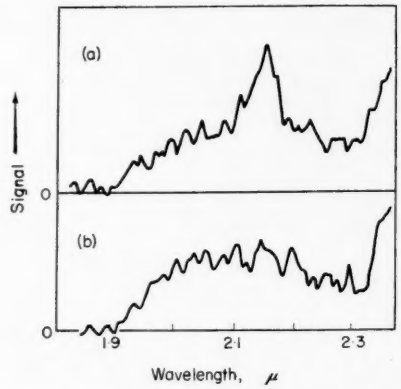

Fig. 1. (a) Spectrum of very bright type-B red aurora. (b) Spectrum of night airglow.

Observations were made during bright active aurora on about a dozen occasions, at a spectral slit width of 300 Å; under these conditions the instrument was capable of detecting a monochromatic emission of brightness greater than about 30 kR. No emission was observed from ordinary active aurora even when the visual brightness corresponded to intensity III. On one occasion, however, during a particularly bright active type-B red display, a feature appeared at about 2·14 μ with a total intensity of about 60 kR. A reproduction of the recorded tracing is shown in Fig. 1a. A tracing of the normal night airglow spectrum is shown in Fig. 1b. The features common to the two spectra are (i) the broad emission between 1·9 and 2·3 μ which is due to the OH bands reported by NOXON *et al.* (1959) and (ii) the rapid increase in emission beyond 2·3 μ which is due to thermal emission.

The only auroral emissions which seem likely to show up in the 2·0–2·5 μ region are further bands of the Meinel N_2^+ system. The most important of these should be the 0,2, 1,3 and 2,4 bands; the origins of these bands fall at 2·13, 2·24 and 2·36 μ respectively. From the $q(v', v'')$ values given by FRASER, JARMAIN and NICHOLLS (1954), and by an extrapolation of the empirically determined dependence of the dipole moment on internuclear separation found by NICHOLLS (1958), one may obtain the intensity ratios: $(0,2)/(0,1) \simeq 0{\cdot}2$; $(1,3)/(1,2) \simeq 0{\cdot}5$ and $(2,4)/(2,3) \simeq 1{\cdot}5$. The mean intensities given by HARRISON and VALLANCE JONES for the 0,1, 1,2 and 2,3 bands are 100, 300 and 100 kR respectively; consequently one might predict intensities of 20, 150 and 150 kR for the 0,2, 1,3 and 2,4 bands.

An identification of the feature observed at 2·14 μ with the 0,2 Meinel band might then seem inconsistent with the absence of even stronger emission at 2·24 μ in view of the predicted relative intensities given above. However, HARRISON and VALLANCE JONES

actually found a considerable variation in the relative intensity of the 0,1 and 1,2 bands between successive 1 min scans; occasionally the 0,1 was observed to be more than twice as bright as the 1,2. Moreover, unlike the 1,2 and 2,3 bands, the 0,1 band falls in a region of high water-vapour absorption; this has resulted in successful observations of the band ordinarily being confined to strong aurora in the zenith. Bearing in mind the effects of water-vapour absorption it appears likely that the 0,1/1,2 intensity ratio could become sufficiently large ($>2{\cdot}5$) on occasion to give a predicted 0,2/1,3 intensity ratio >1, provided the estimated transition probabilities are not seriously in error. In such circumstances it seems possible to identify the $2{\cdot}14\ \mu$ feature as the 0,2 Meinel band and at the same time account for the absence of other bands in the $\Delta v = 2$ sequence.

Apart from the tentative identification of the 0,2 band, the principal conclusion is that only rarely does even the brightest auroral activity lead to an appreciable amount of emission in that part of the spectral region beyond $1{\cdot}8\ \mu$ which is accessible to observation from the ground.

J. F. Noxon
A. Vallance Jones

Department of Physics
University of Saskatchewan
Saskatoon, Saskatchewan, Canada

References

Fraser P. A., Jarmain W. R. and Nicholls R. W.	1954	*Astrophys. J.* **119,** 286.
Harrison A. W. and Vallance Jones A.	1959	*J. Atmosph. Terr. Phys.* **13,** 291.
Nicholls R. W.	1958	*J. Atmosph. Terr. Phys.* **12,** 211.
Noxon J. F., Harrison A. W. and Vallance Jones A.	1959	*J. Atmosph. Terr. Phys.* **16,** 246.

VOL. 18 1960

Journal of Atmospheric and Terrestrial Physics, 1960, Vol. 18, p. 344. Pergamon Press Ltd. Printed in Northern Ireland

LETTER TO THE EDITOR

Fading of satellite transmissions and ionospheric irregularities

(*Received* 31 *March* 1960)

KENT (1959) has recently reported observations at Cambridge of a rapidly fading component on the 40 Mc/s wave radiated from Sputnik I. He has concluded that this fading is due to ionospheric irregularities which disappear in a rather surprising manner south of the observing station. The purpose of this note is to offer the alternative suggestion that the irregularities are present to the south of Cambridge, but are oriented so as to scatter sufficient power for the rapid fading to be observed only when the satellite is in the north.

It seems likely that the irregularities giving rise to the fading are the same as those which cause radio stars to scintillate, and that they are elongated in the direction of the earth's magnetic field lines (SPENCER, 1955). If this is indeed so, their scattering properties may be far from isotropic, as appears to have been assumed by KENT. This view rests on the association, first suggested by PETERSON *et al.* (1955), between the aspect sensitivity of radar echoes scattered back from *F*-region on the one hand, and spread-*F* echoes and radio star scintillation on the other. It is as though relatively large scale anisotropic irregularities, of the sort deduced by SPENCER from widely-spaced receiver observations, have a small-scale filamentary structure capable of scattering metre waves anisotropically. Perhaps, for example, aggregates of field aligned ionization trails produced by charged particles spiralling in along geomagnetic field lines may give both metre-wave aspect senstivity and a relatively large scale diffraction pattern.

In the present case of transmission through the scattering medium the most favourable condition for scattering will occur when the line of sight to the satellite (or radio star) makes a right-angle intersection with a geomagnetic field line. The greater the departure from this condition, the less effective will the irregularities become in scattering the transmitted wave to the observer. On this basis, fading observed at Cambridge ought to cease at a more southerly geographic latitude to the west of Cambridge than to the east. This is because similar geomagnetic conditions occur at a more southerly geographic latitude to the west of Cambridge than to the east. The observations reported by KENT show this behaviour. (In his paper the unconventional course is adopted of referring to magnetic inclination as magnetic latitude).

This suggestion, whilst avoiding the seemingly arbitrary assumption that the irregularities do not occur south of the observer, does not conflict with BRIGGS (1958) who finds in a study of spread-*F* echoes that the degree of spreading is greater at Inverness than at Slough. In fact it is well known that both spread-*F* and radio star scintillation are observed at lower latitudes than Cambridge; and it would be worthwhile to have similar observations to those of KENT at lower latitudes. If the view put forward here turns out to be correct, the scattering geometry may not permit the heights of the irregularities to be deduced so simply as for isotropic scattering.

Department of Scientific and Industrial Research J. MAWDSLEY
Dominion Physical Laboratory
Lower Hutt, New Zealand

REFERENCES

BRIGGS B. H. 1958 *J. Atmosph. Terr. Phys.* **12**, 89.
KENT G. S. 1959 *J. Atmosph. Terr. Phys.* **16**, 10.
PETERSON A. M., VILLARD O. G. JR., LEADABRAND R. L. and GALLAGHER P. B. 1955 *J. Geophys. Res.* **60**, 497.
SPENCER M. 1955 *Proc. Phys. Soc. Lond.* B **68**, 493.

VOL. 18 1960

Journal of Atmospheric and Terrestrial Physics, 1960, Vol. 18, p. 345. Pergamon Press Ltd. Printed in Northern Ireland

BOOK REVIEWS

Electromagnetic Phenomena in Cosmical Physics. Edited by B. LEHNERT. (International Astronomical Union Symposium No. 6.) Cambridge University Press, 1958, 545 pp., 50s.

THE present volume contains the text of some fifty contributions to an International Symposium which was held in Stockholm in the summer of 1956. The papers are arranged, as logically as possible, in a sequence of seven chapters. Apart from the first somewhat general chapter on hydromagnetic phenomena, these deal with solar electrodynamics and theories of solar flares, solar and interplanetary magnetic fields, terrestrial magnetic storms and the effects of interplanetary fields on cosmic rays, and stellar magnetism.

Many of the individual papers had already appeared in scientific journals before the publication of the present volume. However, although readers may be familiar with such papers, they will find much of interest in the very critical and stimulating discussions which followed the presentation of papers at the Symposium and which are printed here in full. Several chapters start with admirable surveys of their respective fields; we mention in particular VAN DE HULST'S introductory paper on magnetic fields in astrophysics, COWLING'S historical account of the development of solar electrodynamics, and FERRARO'S review of the corpuscular theory of magnetic storms. These and some others will be found extremely useful even though our views on questions such as the properties of interplanetary space, the magnetic field of the Sun, or the production of Aurorae, are changing considerably as the result of recent optical, radio and satellite observations. The name and subject index adds much to the value of the volume.

H. A. BRÜCK

F. GODWIN: **The Exploration of the Solar System.** Chapman and Hall, London, 1960, 200 pp., 35s.

TO HAVE started writing this book when he was sixteen years old, and to have published it at the age of nineteen, is a most remarkable feat accomplished by the young author of this book. The text was written when Mr. Godwin was in the United States; he is now back in Britain working for the degree of B.Sc. in Physics at London University. His publishers confidently envisage that, in maturity, he will make distinguished contributions to the subjects of astrophysics and space travel, provided he does not decide to put his present theories to the test in person! Nevertheless the young author shows a remarkable grasp of some of the scientific considerations which must be taken into account in predicting the development of astronautics in the next century and a half. The major criticism which must be made is that certain outstanding difficulties are glossed over. Too readily is it said, for example, that the Martian colony will use solar power while that on Venus will be obliged to use nuclear power—with the laconic addendum that the second requirement will be more difficult to fulfil than the first. Still, as a teen-ager dissertation on space travel, I feel that even the heart of the Astronomer Royal, Dr. R. van der Riet Woolley, would be inclined to melt on reading it. The present reviewer has nothing but admiration for a youngster who, when told that something can't be done, is not inclined to believe it.

E. V. APPLETON

Journal of Atmospheric and Terrestrial Physics, 1960, Vol. 18, p. 346. Pergamon Press Ltd. Printed in Northern Ireland

Indices of geomagnetic activity

of the observatories HARTLAND (*Ha*), ESKDALEMUIR (*Es*) and LERWICK (*Le*)

April 1960

The figures given on this page represent the K-indices for three-hour intervals, beginning with 00–03 hrs for the first and ending with 21–24 hrs for the eighth figure.

April 1960

Day	*Ha* Range for $K = 9 : 500\,\gamma$			*Es* Range for $K = 9 : 750\,\gamma$			*Le* Range for $K = 9 : 1000\,\gamma$			*Day*
	K-Indices		*Sum*	*K-Indices*		*Sum*	*K-Indices*		*Sum*	
1	7766	7986	56	9966	7898	62	9957	8988	63	1
2	6544	4334	33	7545	4333	34	8544	4223	32	2
3	5564	3343	33	6654	3343	34	7763	3332	34	3
4	2332	3334	23	2323	4435	26	2323	3447	28	4
5	4441	4531	26	4432	4532	27	4431	5632	28	5
6	0122	3544	21	1122	3544	22	1122	2444	20	6
7	3320	2354	22	3311	3453	23	3321	2564	26	7
8	3332	2321	19	3322	3322	20	4422	3332	23	8
9	3423	1110	15	3423	2221	19	3332	1210	15	9
10	3322	3345	25	3322	3346	26	2221	3458	27	10
11	4433	3335	28	4423	3334	26	5432	3336	29	11
12	5443	2324	27	5443	2334	28	6543	3435	33	12
13	4442	2233	24	3442	2332	23	4442	2333	25	13
14	3233	2223	20	3233	2223	20	4223	2223	20	14
15	3533	3322	24	3533	3332	25	3642	2322	24	15
16	3222	3543	24	2322	4444	25	3322	5546	30	16
17	5333	3333	26	5333	3443	28	6532	2344	29	17
18	4233	2312	20	4234	2323	23	6433	2322	25	18
19	1211	2100	8	2211	2200	10	2221	2201	12	19
20	0110	1000	3	0111	2101	7	0121	1110	7	20
21	0001	1212	7	1001	1212	8	0111	2212	10	21
22	2011	1200	7	2112	1311	12	2121	2211	12	22
23	2322	1235	20	1222	2235	19	1222	2227	20	23
24	5534	4355	34	7633	4345	35	7743	5477	44	24
25	5444	4445	34	6444	5454	36	8443	5475	40	25
26	4232	2324	22	4232	3334	24	5432	3335	28	26
27	2121	2256	21	2221	2356	23	5212	3258	28	27
28	6554	4453	36	6565	4553	39	8755	5575	47	28
29	5544	3454	34	6544	4454	36	8654	4455	41	29
30	5444	7975	45	6544	8888	51	8844	9976	55	30

VOL.
18
196

Journal of Atmospheric and Terrestrial Physics, 1960, Vol. 18, p. 347. Pergamon Press Ltd. Printed in Northern Ireland

Papers to be published in future issues

SYUN-ICHI AKASOFU: Large-scale auroral motions and polar magnetic disturbances—I. A polar disturbance at about 1100 hours on 23 September 1957

C. D. WATKINS: The height and geometry of auroral radio echoes

I. L. JONES: Further observations of radio stellar scintillation

C. S. G. SETTY: Eclipse effects on the *F*-layer at sunrise

C. S. G. SETTY: Some studies of bifurcation of the ionospheric *F*-layer into *F1* and *F2*

C. S. G. SETTY: A pre-sunrise phenomena and the presence of negative ions in the *F*-region of the ionosphere

C. S. G. SETTY: Eclipse effects on the *F1*-layer observed at Cambridge on 30 June 1954

F. HEPBURN: Analysis of smooth type atmospheric waveforms

H. J. A. CHIVERS: Observed variations in the amplitude scintillations of the Cassiopeia (23N5A) radio source

W. A. CILLIERS: The fading of low-frequency radio waves reflected from the ionosphere

B. MCINNES and K. A. ROBERTSON: Latitude distribution and seasonal variation of aurora over the British Isles during 1957 and 1958

A. J. LYON, N. J. SKINNER and R. W. H. WRIGHT: The belt of equatorial spread-*F*

V. MARASIGAN, S.J.: Damping coefficient of vibrating electrons

D. R. CURRIE and K. S. KREIELSHEIMER: A double field mill for the measurement of potential gradients in the atmosphere

B. J. ROBINSON: On some disturbances in the *E*-region

V. AGY: Spiral patterns in geophysics

S. N. MITRA, K. K. VIJ and P. DASGUPTA: Horizontal drift in the ionosphere over Delhi

M. S. MACRAKIS: A possible long range communications link between ground and low-orbiting satellites

K. MAEDA: Directional dependence of atmospheric temperature effects on cosmic ray muons at sea level

B. HULTQVIST and G. GUSTAFSSON: On the magnetic time dependence on the auroral zone currents

G. S. KENT: The fading of radio waves reflected obliquely from meteor trails

W. G. MATHEWS and L. WALLACE: Auroral temperature determination from $A^2\Pi \rightarrow X^2\Sigma$ bands of the N_2^+ molecule

OL.
18
960